CRANFIELD UNIVERSITY

Mohammed H. Alkhafaji

A Novel Power Management and Control Design Framework for Resilient Operation of Microgrids

School of Water, Energy, and Environment

Thesis Submitted for the Degree of
Doctor of Philosophy

Supervisors: Prof Patrick Chi-Kwong Luk
Dr John Economou

October 2017

CRANFIELD UNIVERSITY

School of Water, Energy, and Environment

Thesis Submitted for the Degree of
Doctor of Philosophy

Mohammed H. Alkhafaji

A Novel Power Management and Control Design Framework for Resilient Operation of Microgrids

Supervisors: Prof Patrick Chi-Kwong Luk
Dr John Economou

October 2017

Abstract

This thesis concerns the investigation of the integration of the microgrid, a form of future electric grids, with renewable energy sources, and electric vehicles. It presents an innovative modular tri-level hierarchical management and control design framework for the future grid as a radical departure from the 'centralised' paradigm in conventional systems, by capturing and exploiting the unique characteristics of a host of new actors in the energy arena - renewable energy sources, storage systems and electric vehicles. The formulation of the tri-level hierarchical management and control design framework involves a new perspective on the problem description of the power management of EVs within a microgrid, with the consideration of, among others, the bi-directional energy flow between storage and renewable sources. The chronological structure of the tri-level hierarchical management operation facilitates a modular power management and control framework from three levels: Microgrid Operator (MGO), Charging Station Operator (CSO), and Electric Vehicle Operator (EVO). At the top level is the MGO that handles **long-term** decisions of balancing the power flow between the Distributed Generators (DGs) and the electrical demand for a restructure realistic microgrid model. Optimal scheduling operation of the DGs and EVs is used within the MGO to minimise the total combined operating and emission costs of a hybrid microgrid including the unit commitment strategy. The results have convincingly revealed that discharging EVs could reduce the total cost of the microgrid operation.

At the middle level is the CSO that manages **medium-term** decisions of centralising the operation of aggregated EVs connected to the bus-bar of the microgrid. An energy management concept of charging or discharging the power of EVs in different situations includes the impacts of frequency and voltage deviation on the system, which is developed upon the MGO model above. Comprehensive case studies show that the EVs can act as a regulator of the microgrid, and can control their participating role by discharging active or reactive power in mitigating frequency and/or voltage deviations.

Finally, at the low level is the EVO that handles the **short-term** decisions of decentralising the functioning of an EV and essential power interfacing circuitry, as well as the generation of low-level switching functions. EVO level is a novel Power and Energy Management System (PEMS), which is further structured into three modular, hierarchical processes: Energy Management Shell (EMS), Power Management Shell (PMS), and Power Electronic Shell (PES). The shells operate chronologically with a different object and a different period term. Controlling the power electronics interfacing circuitry is an essential part of the integration of EVs into the microgrid within the EMS. A modified, multi-level, H-bridge cascade inverter without the use of a main (bulky) inductor is proposed to achieve good performance, high power density, and high efficiency. The proposed inverter can operate with multiple energy resources connected in series to create a synergized energy system. In addition, the integration of EVs into a simulated microgrid environment via a modified multi-level architecture with a novel method of Space Vector Modulation (SVM) by the PES is implemented and validated experimentally. The results from the SVM implementation demonstrate a viable alternative switching scheme for high-performance inverters in EV applications.

The comprehensive simulation results from the MGO and CSO models, together with the experimental results at the EVO level, not only validate the distinctive functionality of each layer within a novel synergy to harness multiple energy resources, but also serve to provide compelling evidence for the potential of the proposed energy management and control framework in the design of future electric grids. The design framework provides an essential design to for grid modernisation

Acknowledgments

All Praise to our almighty **GOD**, Lord of the worlds, for all his blessings and among them enabling me to complete this thesis.

The research journey would not have been as interesting without the fascinating people I met along the way.

I would like to express my deepest gratitude to my first supervisor Prof Patrick Luk for the opportunity to carry out this research project. The patience, support, encouragement, and the useful advice that he has provided throughout the project is very much appreciated.

I would like to express the deepest gratitude to my second supervisor Dr John Economou for his valuable comments and useful discussions. I am most grateful for the encouragement and support that he gave me in writing my thesis.

I would also like to express my sincere gratitude to Dr Maciej Bendyk who helps me to do a 'proper-job' calibre, Dr Akram Bati, Dr Mutaz Shunasi for their valuable assistance, and Prof Philip Longhurst for his insightful recommendations and valuable assistance.

A special thank you goes out to Sam Skears and Heather Simpkins for the perfect understandable, hard activate and nice treatment that they offer to me. I am most grateful for the extensive support Sam gave me along the way of the study and the useful correction Heather gave me in writing my thesis.

I would also express my deepest gratitude to viva examiners: Prof Jun Liang, Dr James Whidborne, and Dr Mark Pawlett for awarded me the PhD degree with useful advices and corrections.

I gratefully acknowledge the financial support of my PhD study from the Iraqi Ministry of Higher Education and Scientific Research (MOHESR) in Baghdad and Cultural Attaché in London.

My sincere thanks are forwarded to my colleagues at Cranfield University for their support, cooperation, and friendly company.

I would also express special thanks to Alison Digger, Joanne Holden, and Chris Binch for teaching, encouraging, and supporting me through the English language course program at Cranfield University.

My sincere appreciation for the tremendous support provided by Cranfield University's technical staff, accommodation office's staff, library's staff, Information department's staff, and all workshop's staff.

My heartfelt appreciation goes out to my precious parents, parents-in-law, my brother (Ali), brothers-in-law, and sister-in-law, my gorgeous daughters for their love, encouragement, and unfailing support.

I owe the greatest debt of gratitude to my Mum and my Dad for their love, patience, support, sacrifice, teaching me the art of transforming imagination into something real, and never forget supplicate to me. I am an extension of both, and proud of it.

Finally,

To my beloved wife, Iman, for tolerating my eccentric ways the past ten years, giving me three lovely kids, and for agreeing to stand by me forever.

Table of Contents

List of Figures

List of Figures in Appendices

List of Tables

List of Tables in Appendices

List of Abbreviations

AC	Alternating current
CPS	Conventional power system
CSA	Charging station agency
CSC	Centralised smart charging
CSO	Charging station operator
CSS	Charging station system
DC	Direct current
DG	Distributed generator
DNO	Distribution network operator
DSC	Decentrlised smart charging
EMS	Energy management shell
EVA	Electric vehicle agency
EVO	Electric vehicle operator
EVs	Electric vehicles
ICE	Internal composition engine
MGO	Microgrid operator
MIQP	Mixed integer quadratic programming
MILP	Mixed integer linear programming
PES	Power electronic shell
PF	Participation factor
PMS	Power management shell
RS	Recharging socket
RSA	Recharging socket agency
SCA	Smart controller agent
SVPWM	Space vector pulse width modulation

Nomenclature

Latin Symbols

A,B,C,D	Generalized circuit constant
A_0, B_0	Generalised line constant
C_d	Degradation cost
$CF(P_i)$	Operating cost of the generating unit i in \$/h
C_i	Fuel costs of the generating unit i in $\$/l$ for DE and $\$/kWh$ for FC and MT
C_k	Treatment cost of the K^{th} type of pollutants emission in \$/kg
C_{nl}	Natural gas price to supply the Microturbine
$C_{rate,pch/qch}$	General active power and reactive power price of charging electricity respectively, for example charging rate is 0.08\$/kWh.
$C_{rate,pdis/qdis}$	General active power and reactive power price of discharging electricity respectively, for example, discharging rate is 1.2\$/kWh.
D	Duty cycle
D	Binary number of the owner choice for either bi-directional power or unidirectional one.
D	Daily electricity demand
$E_b(t)$	State of charge of the battery at the current state.
$E_b(t-1)$	State of charge of the battery at the previous state.
$E_j^{required}$	Battery capacity of the jth electric vehicle
E_n	Energy produced by a generator n
E_{pv}	Photovoltaic energy produced
F	Difference in charging and discharging rate for example charging rate 1 \$/kWh from 00-8 am, 1.2 \$/kWh from 8-16, and 1.1 \$/kWh from15-00.
F_i	Fuel consumption rate of a generating unit i
$F(P_i)$	Operating cost of the generating unit i in \$/h
K	Scale factor to normalise vector ΔQ
G	Solar irradiation in (W/m^3).
G_d	Average daily solar radiation value.
I	Model current (Ampere).
I_0	Saturation current of the diode
I_L	Dc load current
I_L	Light generated current.
I_{or}	Cell saturation current at T_r
I_{os}	Cell reverse saturation current.
I_{SCR}	Short circuit current at 25ºC and 1000W/m^2
J	Jacobian matrix
J_R	Reducible Jacobian matrix
K_0	Current at temperature coefficient (A/K)

K_I	Short circuit current temperature coefficient at $I_{SCR} K_I = 0.0035 A/^o C$
$K_{f.ch/dis}$	Charging or discharging factor from log function of SoC
K_{om}	Proportional maintenance constant of unit i
M	logical number i for grid connected and 0 for grid disconnected
N	Total number of the DG in the microgrid
OM_i	Operating and maintenance cost of a generating unit i in \$/h
P_{G2V}	Net power capacity available to recharge EVs in G2V mode.
P_0	Set point of active power
P_J	Electric power introduces at interval J
P_{V2G}	Aggregated power flow from EVs to grid in V2G mode
$P_{V2G,max}$	Maximum allowed power at ith EVs sources can be discharged.
$P_{ch\backslash dis,ij}$	Power of charging or discharging in a time i for electric vehicle j which is Control variable of the objective function
$P_{cs,dis}$	Power of discharging charging station
P_d	Power demand from non-electric vehicle load
$P_{dg,i}$	Diesel generator (i) output power (kW)
P_{grid}	Output power of the grid
P_i	Decision variables that are representing the real power output from generating unit i in kW.
P_i	Output power of an ith distributed generator
$P_{j,b}^a$	Active power required from MGO
$P_{j,b}^r$	Battery rated charging power used to charge jth electric vehicle during the interval t
$P_{j,sc}^r$	Supercapacitor rated charging power used to charge jth electric vehicle during the interval t
P_{min}, P_{max}	Minimum power and maximum power for charging station that provides from MGO in charging mode or by the state of the electric vehicle in the discharging mode.
P_n	Daily resource energy
$P_{net} = P_s - P_d$	Net power capacity available
P_r	Real power
P_s	Scheduled power
Q_0	Set point of reactive power
Q_j	Rated ampere hour rating (AHR) of the jth battery
$Q_{j,b}^a$	Reactive power required from MGO
Q_r	Reactive power
R_n	Rated power of the generators
R_s	Series resistance (ohm).
R_{sh}	Shunt resistance (ohm).
SC_i	Start-up cost of a generating unit i in \$/h
SoC_B^a	Actual state of charge
SoC_B^d	Desired state of charge by the customer

$SoC^{d}_{b\backslash sc,ij}$	State of charge of battery or supercapacitor at departure time
$SoC_{b\backslash sc,ij}$	State of charge for either battery or supercapacitor in time I for electric vehicle j.
SoC_{max}	Upper limits of the state of charge.
SoC_{min}	Lower limits of the state of charge.
SoC_{req}	Required SoC limit
SoC_t	Current SoC of the jth electric vehicle battery
T	Temperature (^{o}K)
$T_{off,i}$	Time has been off of unit i
T_r	Reference temperature $T_r = 301.18^oK$
V	Model voltage (Voltage).
V_0	Rated grid voltage
$V_{G2V}(t)$	Set of EVs charging at time t
$V_{V2G}(t)$	Set EVs discharging at t time t
V_{tj}	Terminal voltage of the jth battery
V_{pp}	Peak to peak voltage ripple
l	Inductance per kilometre, Henry
I_R	Current at receiving end, ampere
I_S	Current at sending end, ampere
k_d	Shunt compensation
N	Number of generators
P	Measured active power
$P_{R\ critical}$	Critical maximum power at receiving end, Watt
Q	Measured reactive power
V_R	Voltage at receiving end, volt
$V_{R\ critical}$	Critical voltage at receiving end, volt
V_S	Voltage at sending end, volt
Z_0	Characteristic equation
Z_c	Surge impedance loading
b	Susceptance, semens
cf	Capacity Factor
c_{sh}	Shunt capacitance, Farad
$\frac{dV}{dI_{Voc}}$	A slope at V_{oc} and X_V
f_0	Rated frequency
f_s	Effective switching frequency
i	Total number of distributed generator
k	Boltzmann constant $k = 1.38e^{-23} Joule/^oKT$
k	Type of pollutant emission (CO2, SO2, NOx)
ℓ	Line length, meter
m	Slopes tracking for frequency drop
$n = 1.2$	Quality factor of the diode

$p_{G2V,max}$	Maximum allowed power at ith EVs sources can be charged
q	Electron charge $= 1.6e^{-19}$ (coulombs).
q	Slopes tracking for voltage drop
rho	Rho: the density air
s	Binary number either 1 or 0, s_1 refers to charging mode and s_2 refers to discharging mode, where $\|s_1\| + \|s_2\| = 1$
u_a	Binary logic referring Unit commitment applied
u_n	Binary logic referring Unit commitment not applied
t	Set of time interval $t = [t_{arrival}\ ,\ t_{departure}]$
i_r	Receiving end current
$t_{arrival}$	Arrival time
$t_{departure}$	Departure time
t_i^s	Charging duration
t_{j,b_ch}^s	Full charge time duration
v_{cco}	Cut out speed
v_{ci}	Cut on speed
v_{co}	Corner Speed
v_r	Receiving end voltage
v_s	Sending end voltage
$\mathrm{v_r}$	Receiving voltage

Greek Symbols

α	Line-loss factor (attenuation factor), nepers per unit length
$\alpha\ and\ \beta$	Weighting dynamic (delay) coefficient for the charging and discharging power
$\alpha_i\ , \beta_i, \gamma_i$	Coefficients of distributed generator, typically there are given by the manufacturer
β	Phase-shift, radians per unit length
γ	Propagation constant
Γ	Lift eigenvector matrix of reduced Jacobian matrix
$\gamma_{grid,k}$	Coefficient of pollutant emissions of the grid in kg/kW
γ_{ik}	Coefficient of pollutant emissions of the DG named I in kg/kW
θ_{int}	Initial angle of the system
$\Delta(t)$	Sampling time
ΔP	Mismatch active power vector
ΔQ	Mismatch reactive power vector
ΔV	Unknown voltage magnitude correction vector
Δt	Sampling period
$\Delta\delta$	Unknown angle correction vector
δ	Load angle
$\delta_{\mathrm{critical}}$	Critical angular separation, degree

$\delta_{cso,i}$	Binary logic referring charging station operator at discharging mode
δ_{dgi}	Binary logic referring distributed generator operate
δ_i	Cold start-up cost of unit i
δ_{ug}	Binary logic referring utility grid connected
ε	Binary number either 1 or 0, ε_1 refers to active power charging mode and ε_2 refers to reactive power charging mode, where $\|\varepsilon_1\| + \|\varepsilon_2\| = 1$
η_{ch}	Charger efficiency
η_{dis}	Efficiency of the converter
η_{lJ}	Cell efficiency at interval J.
η_{lJ}	Unit efficiency at interval J
θ	Line angle, radian per unit length
Λ	Diagonal eigenvalue matrix of reduced Jacobian matrix
Λ	Wavelength for a line, kilometre
ρ	Priority factor where normally $\rho = 1$ for optimization charging, if $\rho = 1.5$ charge vehicle at maximum current without care of price
σ_G	Standard division
σ_i	Hot startup cost
σ_i	Hot start-up cost of unit i
τ_i	Cooling time constant of unit i
τ_i	Unit cooling time
ϑ	Binary number either 1 or 0, ϑ_1 refers to active power discharging mode at frequency deviation and ϑ_2 refers to reactive power discharging mode at voltage deviation, where $\|\varepsilon_1\| + \|\varepsilon_2\| = 1$
Φ	Right eigenvector matrix of reduced Jacobian matrix
ϕ	Power factor angle
ω = 2πf	Angular frequency in rad/sec

Chapters colouring code

Chapter One	Grey	Chapter Two	Light Blue
Chapter Three	Orange	Chapter Four	Green
Chapter Five	Dark Blue	Chapter Six	Purple
Chapter Seven	Dark Red	Chapter Eight	Red

1. Chapter One: Introduction

1.1 Motivation

1.1.1 Conventional power system

The conventional power system (CPS) consists of three main sectors: generation unit, transmission line, and distribution network. The power is transferred in a single direction from the generation units to a load in the distribution network through the transmission lines. The generation units are large plants that depend mainly on fossil fuel combustion to generate electrical power. The CPS is facing major challenges due to the continuous growth of electricity demand and lack of capital investment in power system sectors [1]. It is a fact that the existing power system in most countries is quite old. On the other hand, powerful trends in technology, policy environments, financing, and business models are driving the evaluating decisions made in power sectors globally, as shown in the pathways that have emerged as viable models for power system transformation presented in Figure 1-1 [2].

The race for a complete electricity system was launched in the Pearl Street Station in New York City in 1882. It was connecting a 100-volt generator that burned coal to power a few hundred lamps in the neighbourhood. By the 1930s regulated electric utilities became well-established, crossing many miles of land, constructing from all three major aspects of electricity: power plants, transmission lines, and distribution, to feed electricity to the end users [3], [4]. On the other hand, due to integrating new mobile loads such as EVs, the demand for the electrical system has grown rapidly during recent years and is expected to increase by 34% by 2035 compared with the electricity in 2014 [5]. However, the existing power system is not capable of covering the rapidly increasing demand using a centralised CPS operation [6]. Moreover, the CPS has recorded high power losses in the transmission line and distribution network for different countries of the world, as presented in the data of World Bank statistics and depicted in Figure 1-2 [7]. According to statistics measured from 1960-2013, annual electricity transmission and average distribution losses worldwide were about 8.36%, as shown in Figure 1-3. The maximum losses recorded in Haiti, for example, were as high as 54.20% due to deep crisis characterised by dramatic shortages and the lowest coverage of electricity which shows an important generation deficit limiting its economic development. However, this reflection must not to only add power but also validate its needs in this area by reduce commercial and technical losses before building new power plants [8]. On the other hand, climate change is a threat to our lives due to increasing the pollution levels which affect our environment, style of life, and the protection of the Earth from outside radiation, and has become a major concern for the diversity of the Earth. The main source of the climate change is carbon dioxide emissions [9]–[11]. Among all sources of carbon dioxide emissions in the world, the energy supply sector and the transportation sector account for about 25% and 14% respectively, as shown in Figure 1-4. Furthermore, most of the generation units that are used in a CPS base their work on fossil fuel energy, as illustrated in Figure 1-5. Thus, the impact of growing electricity demand and the issue of climate change has motivated many countries to modernise their existing power system infrastructure to be used in the more efficient way [12]–

[14]. Growing electricity generation, based on the renewable energy technology, encourages the decentralisation of the CPS to many areas, which has a direct effect on power loss reduction due to installing the generation near the loads.

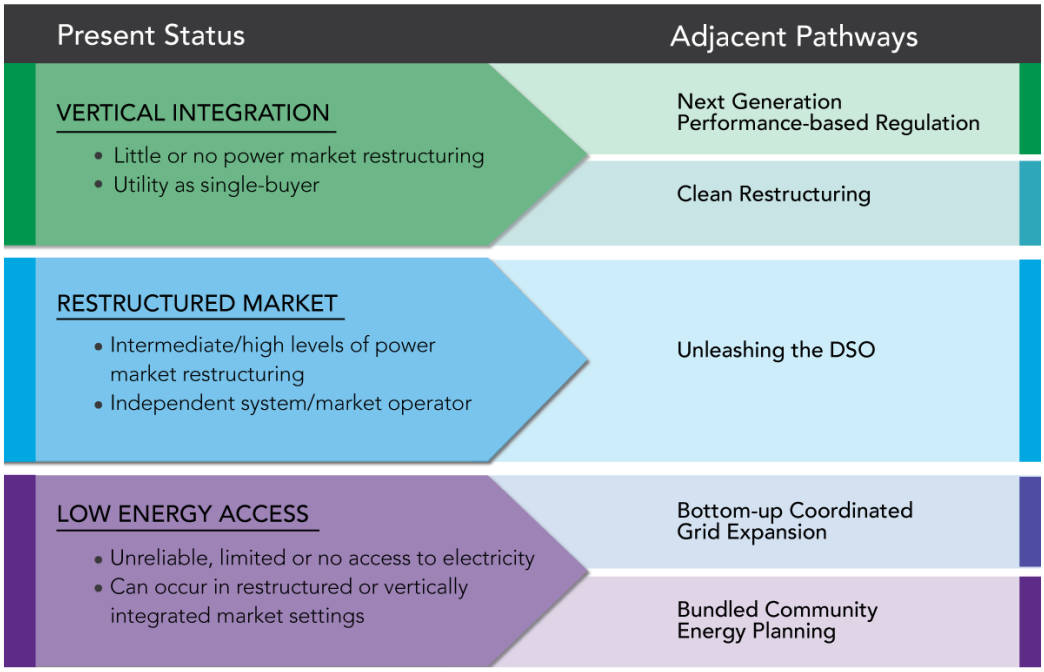

Figure 1-1: Applicability of Pathways based on Present Status of Power Sector Organization [2]

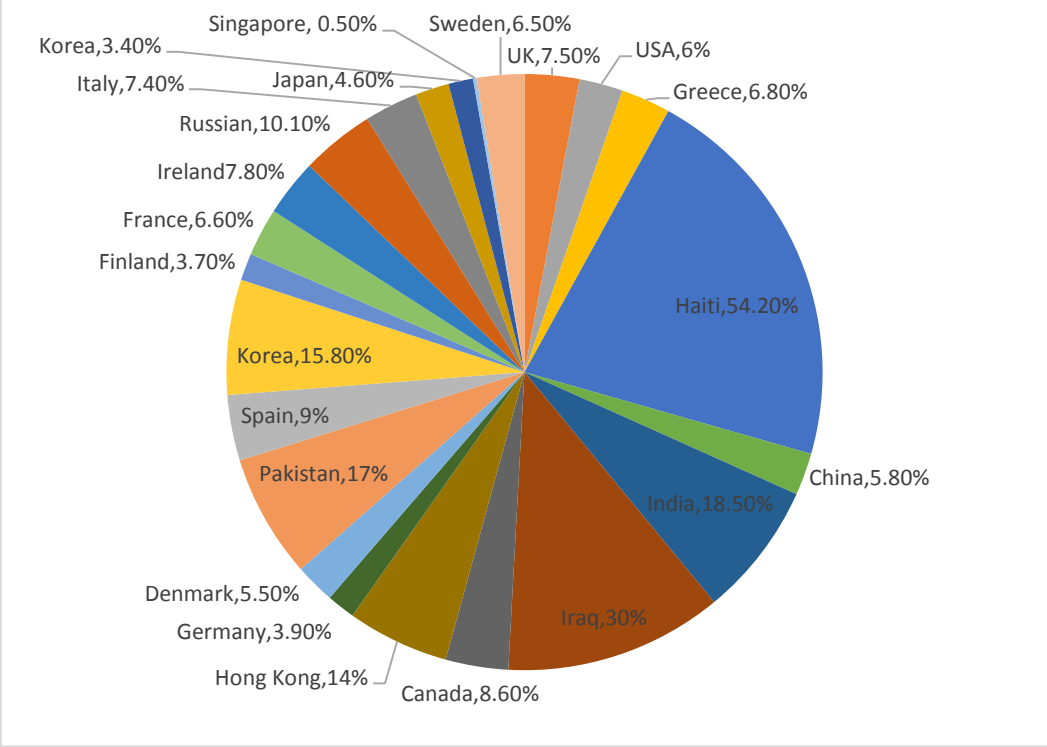

Figure 1-2: Electrical power transmission and distribution losses of various countries in percentage of output for 2013 [7]

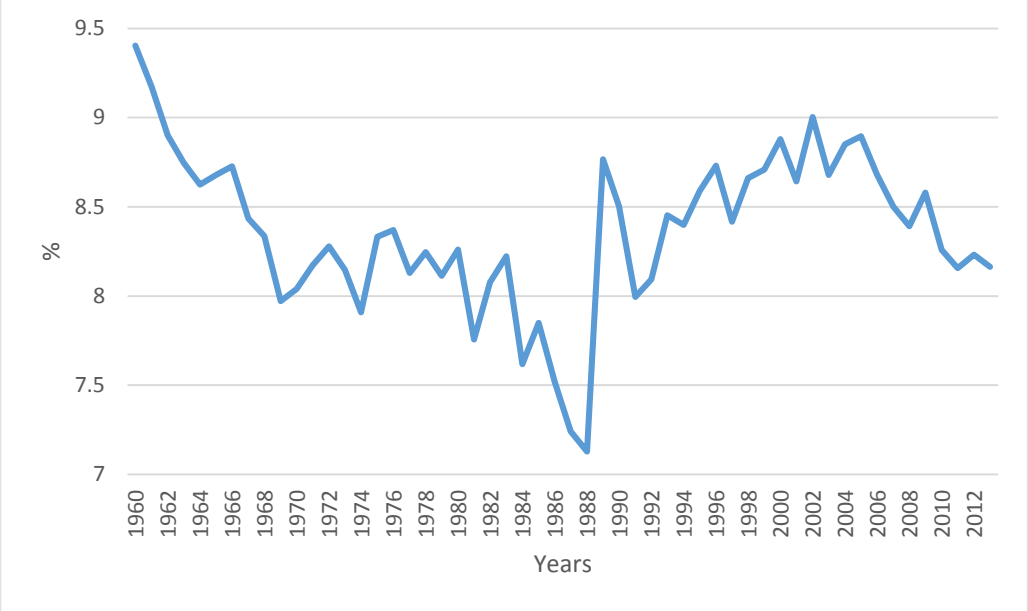

Figure 1-3: Annual worldwide percentage losses[7]

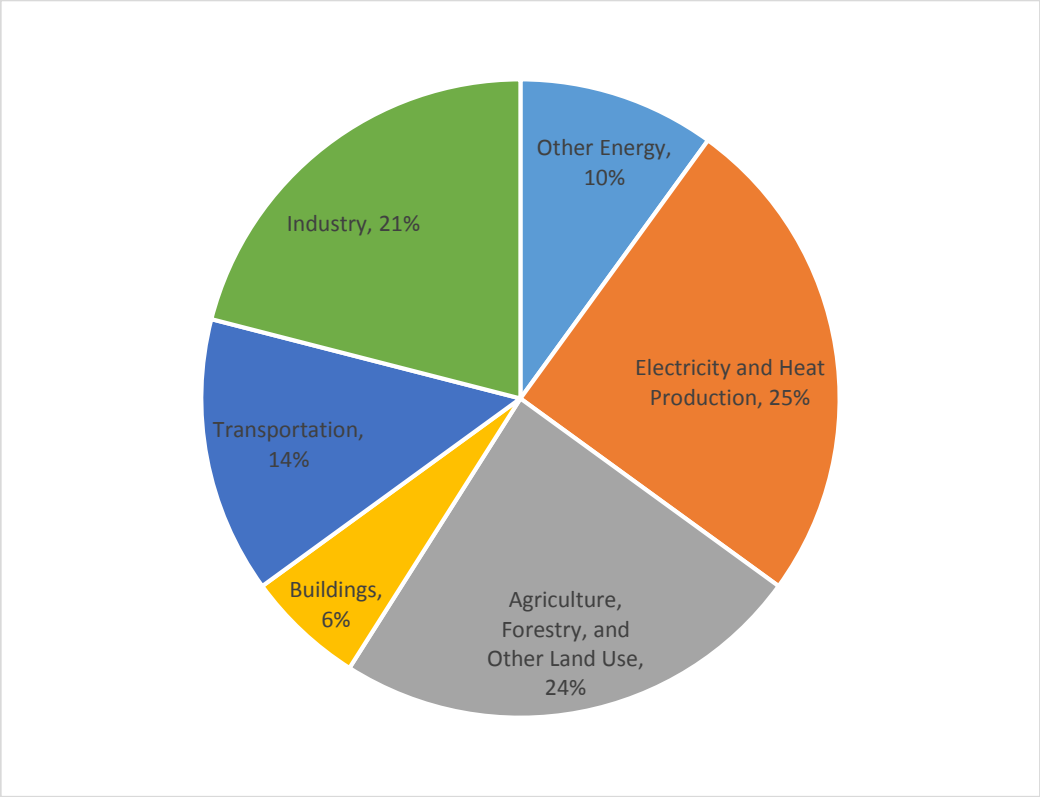

Figure 1-4: Global greenhouse gas emissions by Economic Sector [15]

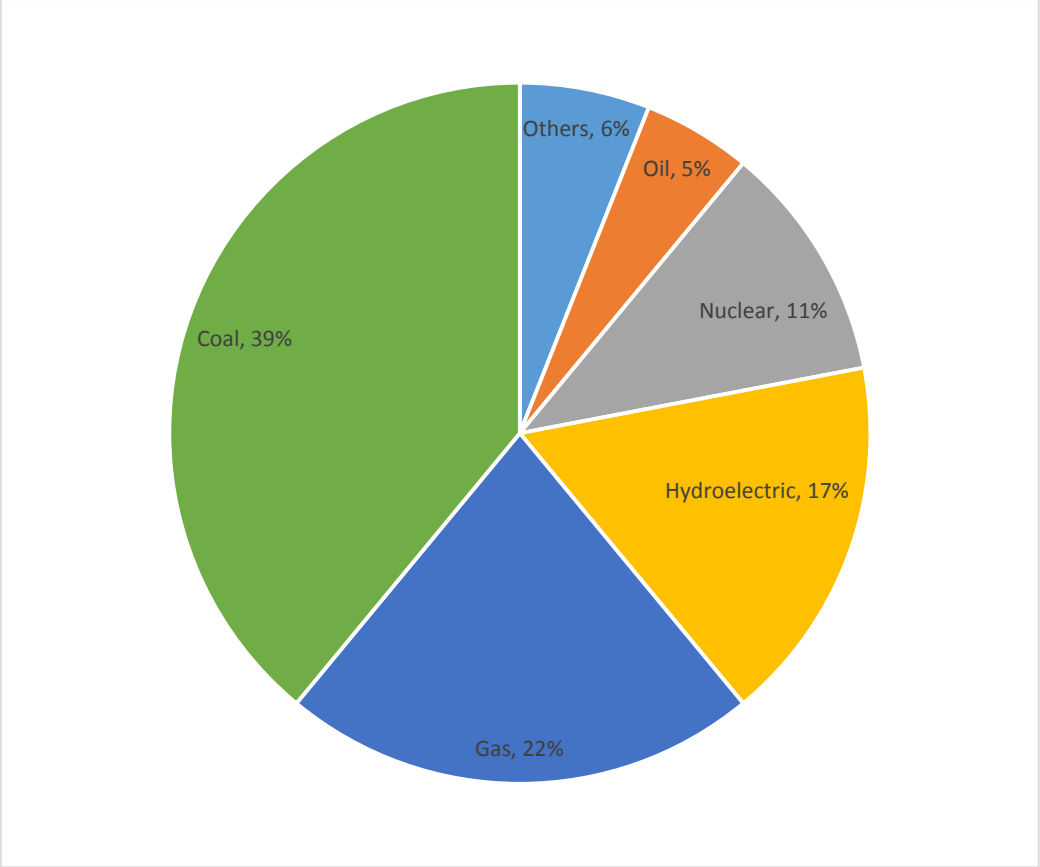

Figure 1-5: World electricity production from all energy sources in 2014 [16]

1.1.2 Conventional power system challenges

Today, electric power is mostly generated centrally in bulk by large generation plants linked by long transmission lines that bring electric power to the end users via the utility grid; for instance the AC and DC high voltage transmission systems of the US, UK, and Iraq transfer power across 157810, 5340, and 10855 miles respectively [17]–[19]. Recently, the utility grid has faced the challenges of a significant increase in demand, threats of climate change, and the security of the power flow. On the other hand, there is increasing pressure for cost reductions on all fronts and maximisation of profits for shareholders and stakeholders.

The centralized power system has been struggling with many issues which affect the efficiency of its functions. Some issues are regarding the growing political instability on the dependence on fossil fuel at the generation and transportation sections. Other issues are regarding the environment situation, such as increasing carbon dioxide and particulates emissions. These issues have led to the use of renewable energy in generation units and electrifying the transportation sector to reduce energy dependency on fossil fuels and achieve decarbonizing objectives. Electrification equipment causes rapid growth in the electrical demand, whereas the infrastructure of the power system that is used today is too old. The nature of the application changes from a single directional power flow to a bidirectional power flow that could connect to the distribution network at any time of a day, with a different number of loads and at various

capacities. At the same time, ensuring the security of supply, working at a high quality, and keeping the power system stable are vital matters in the electric power system operation. However, renewable energy sources are unpredictable and inconsistent due to the intermittency of usage of energy supply [20]–[25]. The power generation from renewable energy sources is much lower than from fossil fuel sources. The current capital cost of constructing renewable energy sources is far greater than the fossil fuel energy sources for the same capacity. Also, renewable energy relies on the weather. Thus, renewable sources construction concentrates on some geographic areas more than others. For example, the wind turbine requires wind to turn the blade; as the speed of the wind on the offshore is higher than onshore, it is normally accepted to install wind turbines in the coastal area. Photovoltaic cells require clear skies and sunshine to generate electricity; therefore, installing them in high strength sunshine areas has a higher efficiency than in a cloudy area. Currently, it is not possible to totally replace the centralised fossil fuel generation units with decentralised renewable generation units to meet total demand of the electricity network, as shown in Figure 1-6. Therefore, the best solution to operate the existing power system is by integrating small-scale renewable resources and distributing generators in distribution areas to work in a synergetic way with the current generation units. This solution could provide power near the load without required transmitting it for long distances using a transmission system. Therefore, the losses on the power system will be reduced significantly, and there would be no need to increase the fossil fuel driven generation unit. Higher utilisation of renewable energy sources can be integrated into the distribution network and could result in the use of fewer fossil fuel generation units, resulting in meeting the decarbonizing environment objectives.

Generating power by using renewable sources in the distribution network and electrifying the transportation sector makes each node in the distribution network capable of absorbing power or generating power in a different situation. Therefore, the power in the distribution network could flow into the node at a time and from the node at another. That means it is hard to anticipate the direction of power within the node because it becomes bidirectional, rather than single directional. At the same time, it is essential to maintain the frequency and voltage characteristics at predefined levels in order to achieve good levels of power system quality. To keep changing the direction of power could affect the waveform characteristics of the power system over or under the limit, leading to a loss in sections, or even all, of the system. Such a system requires precise management, control, and monitoring for each piece of equipment to reach a satisfactory range of operation. Faced with these challenges, the most efficient strategy to deal with these uncertainties has automated the system to maintain the robustness of operation and make it works as a smart grid [13], [26]–[30]. Utility operators have begun to adopt the concept of the smart grid since its first official definition in 2007 [31]. The smart grid is an electrical system that aims to distribute electric power from the producers to the consumers efficiently [12]. As producers and consumers are dominant, sophisticated players in terms of their behaviour in the supply/demand dynamics, the smart grid is a very complex system that deploys different communication protocols to deal with the nonlinearity of user/supplier, hardware, security and bidirectional power flow [32]. Despite recent advances in the modern technology of communication protocols and monitoring devices, supervision of a large complex system still remains very difficult [12], [13], [33]–[36].

The smart grid will enhance the complex monitoring of the system and connection with other components. It increases the interdependency on the power management of demand. A smart grid power infrastructure can be separated into many areas; each area operates either as connected or islanded modes [28], [37]. Its purpose is to reduce the physical and electrical distance between generation units and loads by adding small scale distributed generators, mainly depending on the renewable energy near the electricity demand area. Each island (microgrid) could work alone and cover all the user load requirements within the area, depending mainly on renewable energy sources and distributed generators. Each island area could be connected to the utility grid, in case the generation exceeds the demand, by a point of common coupling where the point of common coupling works as a switch based on the power electronic devices to separate a network into island mode [38], [39].

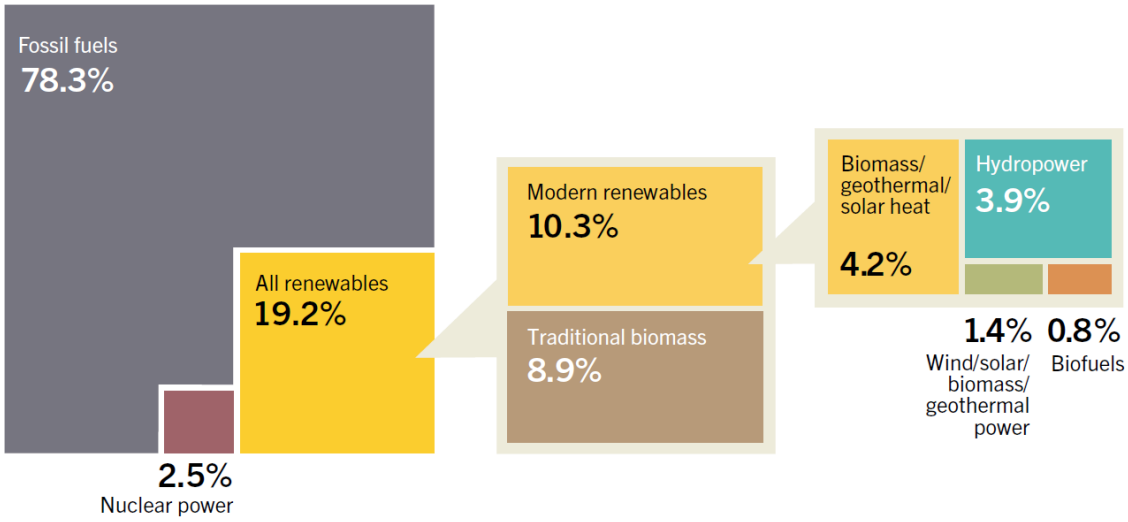

Figure 1-6 Estimated Renewable Energy Share of Global Final Energy Consumption, 2014 [1]

1.1.3 Microgrid

Microgrids are small areas of the smart grid paradigm to provide the flexible and controllable operation of low voltage networks, which then changes the distribution network operation philosophy from passive (single direction power flow) to active (bidirectional power flow). The scale of a microgrid depends on the type of load and network construction. Therefore, the microgrid could be a building or several of buildings. A microgrid is designed to work as a cluster of loads, which are connected to micro sources that deliver power to its local area. To achieve resilient operation, a microgrid should operate as an automated single controllable system to recover quickly in disturbance situation such as demand congestion, load variation, or supply outage which then increases the reliability of the system and reduces the losses and cost of the transmission lines. A distribution network in the microgrid would be changed from passive to active, which is being a real-time infrastructure and dynamically interactive. The system will work in the bidirectional mode rather than the single directional mode used in the traditional operation of the power system. A power congestion may occur in the distribution network. It needs to be handled and controlled accurately by adding an intelligent controller and communication link between the generation units and loads to automate the network operation [40]–[43]. Microgrid operation depends mainly on the power management between load and supply, which could be a sensitive load and sensitive supply.

Voltage and frequency should be limited to the standard system operational settings, depending on the type of operation, in addition to the elimination of harmonics from power electronics devices [26], [44], [45]. However, a system with many small renewable energy sources and variable demand is inherently a weak system, especially considering the effect of the renewable energy sources' intermittency. Electrical power system security is the most important factor to ensure that the system is flexible enough to recover the supply and demand conditions in emerging electricity markets. Voltage instability may happen, which leads to fluctuation or change in the voltage profile at load buses due to either a leak in the reactive power flowing through a line or large circulating reactive power between sources, which causes failure in the system. Therefore, an intelligent controller, to achieve fast response tracking, is required for the resilient operation of a microgrid structure [46].

Micro-sources of the microgrid could play a vital role in the power system in many directions; the distributed generators are regarded as a solution for system security, reliability, stability, and efficiency. Voltage avalanche could occur in a heavily loaded system without balancing between the generation and demand of power. Distributed generators could help in increasing the voltage stability of a system, to prevent causing system blackout, by finding the best location for them. However, distributed generators make no sense without using an energy storage system to cope with the energy balances [47], [48]. However, a combined usage of the different types of distributed generations at various capacities and nature of working in a synergetic arrangement, permit the key attributes of the individual systems to be exploited. The distributed generators require power and energy management to obtain high usage efficiency and to balance the electricity demand in an optimum way.

In general, the smart grid paradigm is best facilitated within a microgrid, which is a relatively small scale localised energy network with the ability to connect to or be isolated from the main grid. The microgrid introduces the distribution network as an intelligent network for self-healing consumers' demand using microsources in a reliable and economical way. A microgrid has the following characteristics [26], [30], [49], [50]:

- Manages sources and demand locally.
- A high-reliability network by lowering the disturbance on the network due to less dependencey on the transmission system and high dependency on the distributed generators.
- Reduction in carbon dioxide emissions by embracing renewable energies rather than fossil fuel sources.
- Economic operation by reducing transmission losses.
- Reduces the expenditure of the whole system by offering economic dispatch and optimal scheduling of demand and microsources.
- Provides a quick interaction response between loads and sources by providing intelligent controller and communication links.

However, microgrids, which are very complex networks, can be highly vulnerable to voltage and frequency variations due to any fault or sudden load changes. A high penetration of intermittent renewable sources in the distribution network will deteriorate the immunity of

network stability during various network contingencies [51], [52]. There are also stability issues arising from using microsources with low inertia. Integration of a new bidirectional load, such as EVs, provides further opportunities and challenges.

1.1.4 Microgrid challenges

A microgrid is a small network with a variety of small capacity distributed generators. Some of them depend on intermittency resources, such as the photovoltaic cell, wind turbine, and energy storage system, and others depend on fuel resources such as a microturbine, fuel cell, and internal combustion reciprocating engine. Due to the intermittency of non-fuel distributed generators, the microgrid cannot be relied on to cover all the demands of the network. A high penetration of small scale distributed generators could cause lower inertia and lower power support of the network which would lead to lower angular stability and lower voltage stability of the network. Furthermore, decentralising the microgrid makes all distributed generators respond to the variation of frequency and voltage, due to dismissing the reference slack that causes low-frequency power oscillation. Energy storage devices have an important function to enhance the efficiency and stability of the microgrid by compensating for the low inertia and slow dynamic responses of the microsources that have a power electronic interface. Nevertheless, various technical and economic problems should be solved to integrate these small scale different types of resources of distributed generators and operate them.

Synchronising a different type, large-scale deployment of distributed generators is an important function to prevent the power imbalance effect due to the power transfer at the transition between the connected mode and isolated mode or connect and disconnect the distributed generators. Therefore, it is a difficult task to balance the power of the microgrid and maintain the stability margins of the network. Many other technical problems arise due to using many power electronic devices in terms of power quality, harmonics, and control. A large number of converters from DC-DC, DC-AC, or AC-AC raise concerns regarding the converters' ability to balance the power demand of the microgrid under stress conditions such as a faulty situation or unplanned demand.

The communication system is responsible for transferring the data of management and control activates the hierarchical structure in addition to monitoring and metering all the processes of the microgrid. Any delays in the communication system and loss of control data could cause distortion of the system which would have an effect on the reliability and protection of the network.

A large-scale deployment of the different type of distributed generators may affect the network's robustness and reliability. Therefore, it is necessary to provide solutions in control, monitoring, and structure, not only to make the concept of the microgrid feasible and commercially viable, but also to keep the microgrid stable and safe to operate.

As a consumer of electricity when hooked up to a charging station, EVs are also classified as a mobile energy storage system that distributes within a microgrid, and as such, produce significant uncertainty for the network [53]. A complete formulation of the optimal microgrid

operation is another issue for the microgrid network, which includes the modelling of distributed energy sources, fixed and mobile storage devices, power exchange with the utility grid, lowest pollution treatment, and losses reduction of the network [54]

1.1.5 Electric vehicles

The first use of the term electric vehicle (EV) dates back to 1902 with the first hybrid EV by Lohner-Porsche [55]. Recently, the evaluation of the combustion engine vehicles, as opposed to the EVs, has been raised due to innovative features and environmental awareness, such as immediate torque, silent ride, fewer maintenance costs, and zero emissions. Therefore, the EVs have been brought to the attention of many customers, which has led to the escalation of a trend for using EVs. The uptake of the EVs market is set to create a considerable amount of loads for the electrical power distribution networks in the near future. In general, EVs will be connected to various locations and numbers of the electrical network at different times of the day for the recharging of their resources. The charging demand of the EVs may tend to coincide with the peak demand of the power distribution network, thus adding extra burdens to the generation capability. On the other hand, the incorporation of microgrids in the existing distribution network not only enables the usage of more renewable energy resources but also allows the EVs to be connected as a mobile energy storage system to balance the load of microgrids, enhance the stability of microgrids, decrease the microgrid usage prices, and reduce the emissions of carbon dioxide and particulate pollutants. The main function of plug-in EVs to the electricity network is to charge the storage systems of the vehicles at the charging operation where the power flows from the network to the EV. However, the microgrid network is less stable than the CPS due to the decentralized operation of the generation units. The EVs could be a versatile operation to discharge the energy storage system on specific occasions, to prevent the microgrid from collapse, and revenue the owners of the EVs money at the discharging operation where the power flows from the EVs to the microgrid. Normally, the discharging tariff is higher than the charging tariff. Therefore, the owners of the EVs could gain money, rather than paying the microgrid operator at the same level of charging and discharging.

Typically, the EV is combined with two resources; overwhelmingly, these resources are a battery and a supercapacitor which operate as the main and auxiliary resources respectively. The main challenge to the EV is to manage the net expenditure power between the multi sources to meet the demand of a motor operation. On the other hand, the EV operates bidirectionally with the microgrid at the bus bar connection; as such a complicated system, power and energy management between multiple resources of the EV and microgrid, which has multiple distributed generators, is essential to strategies and to arbitrate power sharing between them.

Independently from the previous analysis, the transportation sectors account for approximately 31% of the total greenhouse gas emissions, as shown in Figure 1-7 [56], in addition to various pollutant particulates such as Sulphur dioxide (SO_2), Nitrogen oxide (NO_x), Carbon dioxide (CO_2) and more. Recently, the EV technology has been suggested as a solution to synergize the existing generation units and manage a reduction in greenhouse gas emissions to address

the challenges of climate change. The EV is recorded as emissions-free technology. Therefore, many governments around the world encourage the development of EV transportation such as the US, UK, China and others. Recently, researchers proposed the resources of EVs as being a mobile energy storage system that is connected to the distribution network. Normally, EVs are connected to the distribution network for charging resources. In some special cases, such as high voltage variation or high-frequency variation, the resources of the EVs are used to balance the demand of the distribution network. Ideally, the distribution network operator (DNO) should deal with the resources of the EVs as integrated devices within the distribution network. However, the resources of connected EVs may produce different data, such as:

- The initial state of charge of the battery and supercapacitor.
- The capacity of the battery and supercapacitor.
- Time of connection.
- Duration time of parking.
- Required leaving state of charge of the battery by the owner.

Facing these complexity, the EVs require special energy demand management to deal with each EV separatley rather connected to the home park or to the station park as aggregated EVs. Such a system is called the charging station system (CSS) which uses energy demand management to deal with aggregated EVs.

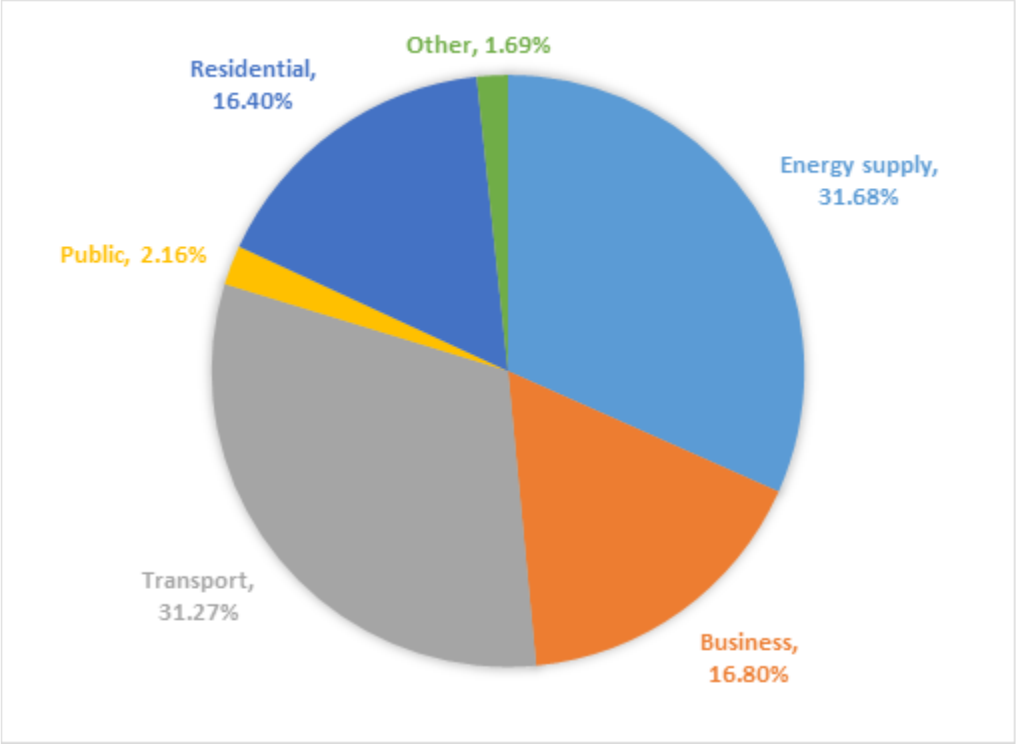

Figure 1-7: Greenhouse gas emissions by sector in UK during Q1 and Q2 of 2016 [56]

1.1.6 Trends of electric vehicles

. According to the International Energy Agency (IEA), about 1.26 million EVs are used on the street today, twice as many as in 2014; the growth of using EVs in many countries over the last ten years is shown in Figure 1-8. It is clear that the number of EV owners has increased significantly during recent years. For example, the accumulated stock in the US increased from fewer than 100 EVs in 2010 to 400,000 EVs in 2015 whereas, in China, it increased from fewer than 100 EVs in 2010 to 300,000 EVs in 2015. Factors relating to ecological impact, safety operation, charging station infrastructures such as service availability and maintenance, and cost of batteries such as driving range, operating cost, and the price of the EV, are the main parameters affecting the decision to purchase EVs. Recent research on battery energy density has enabled the EV to drive a longer range for a lower price, reaching to about 300 km, as shown in Figure 1-9. For example, the cost of the batteries was estimated at 1000 $/kWh in 2008, which decreased to about 280 $/kWh in 2015.

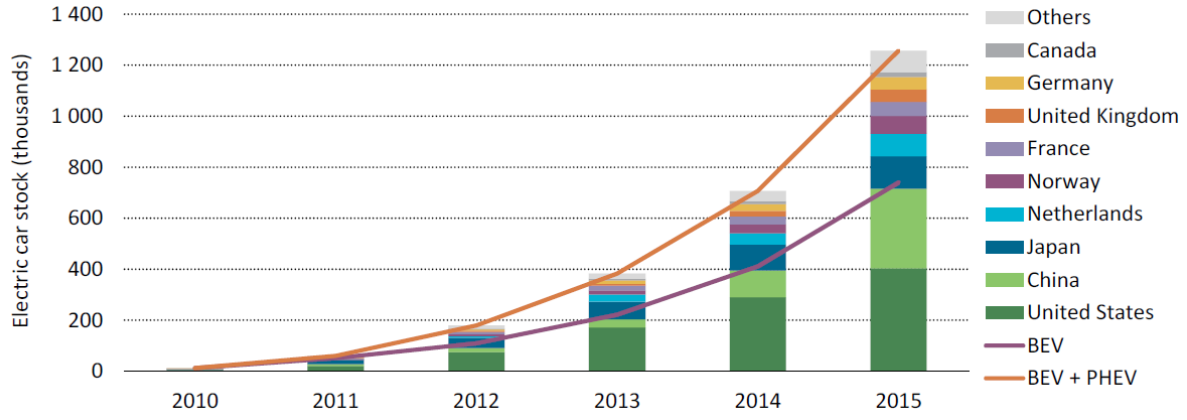

Figure 1-8: Evaluation of the global electric car stock, 2010-2015 [57]

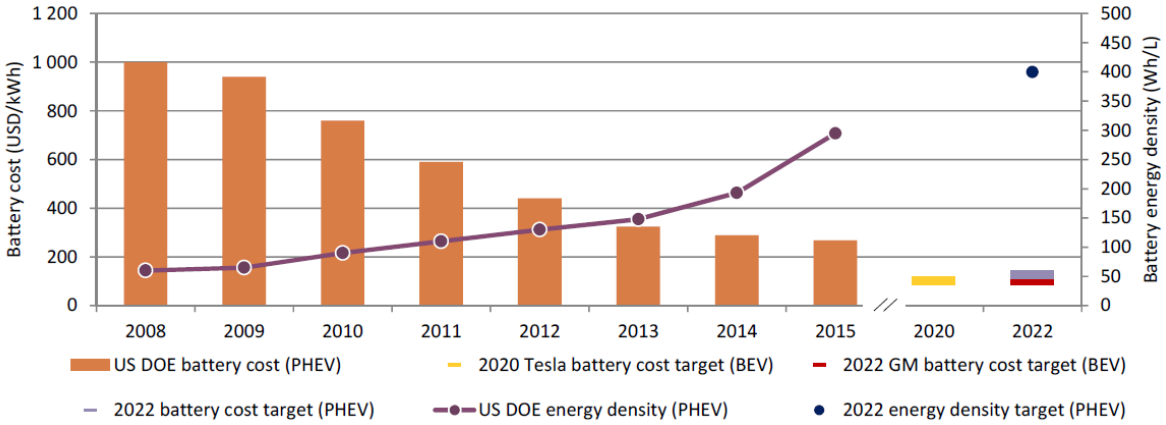

Figure 1-9: Evolution of battery energy density and cost [57]

1.1.7 Main types of electric vehicles

Electric Vehicles (EVs) are a promising technology for drastically reducing the environmental burden of road transport such as air pollutants, especially carbon dioxide emission and noise.

The main electrical resources for EVs are batteries and supercapacitors. There are other resources which could be used, such as fuel cells and flywheels. The battery type, capacity, performance, and cost represent the greatest challenges for commercially deploying the different type of EVs, whereas supercapacitors have a longer lifetime and are less costly compared to batteries. Generally, the other major challenge of large EV usage is recycling resources. Each battery generation is likely to be in production for four to five years, as claimed by battery manufacturers. Both the battery and supercapacitor are modelled with a capacitive characteristic which has a positive impact when connecting to the microgrid in terms of reducing the inductive characteristic of the microgrid elements and therefore enhancing the power factor. Therefore, focusing on the type of EVs that could be connected to the grid is much better from the point of view of adding an extra capacitive characteristic to the microgrid. In practice, EVs can be the dynamic capacitive compensation to the grid because of the capacitive characteristic of the electrical elements of the EVs, such as the battery and supercapacitor.

EVs are classified according to their battery capacity, which correlates directly with the battery mass and performance, and the travelling ranges into hybrid electric vehicles (HEVs) and battery electric vehicles (BEVs). HEVs could be either regular hybrid (RHEVs) or plug-in hybrid (PHEVs), depending on their connectivity to the microgrid.

RHEVs combine a battery-powered electric motor and a gasoline/diesel engine and does not have to be connected to the microgrid . The majority of battery charging comes from the internal compostion engine (ICE) whereas a smaller portion comes from regenerative braking by capturing the kinetic energy of the vehicle. The battery can increase the fuel efficiency of the HEV by 25% when compared with an ICE car [58], [59]. The PHEVs are similar to the RHEVs except for having the ability to plug the vehicle into the power grid for charging batteries to increase the electric driving range of HEVs. The battery of this system has a high capacity that could make it a primary source, whereas petroleum is considered as a secondary energy source for driving a car [58], [59]. The battery charging is obtained from a grid, non-grid sources such as photovoltaic panels, and braking energy. The driving range for such cars depends directly on the battery size and capacity [58], [59]. The BEVs are more efficient than ICE vehicles in terms of noise, local pollutant emission, carbon dioxide emissions, and their interaction with the microgrid; they are also able to reach zero local greenhouse gas and pollutants emissions.

On the other hand, a large number of BEVs will increase the electricity demand of the microgrid substantially. Therefore, the generating grid capacity should be able to meet the additional demand of the BEVs. The power flow in BEVs is bidirectional. Therefore, the microgrid could utilise EVs to allow them to enter the market in short term periods at higher growth rates, when compared to the electricity generation, to keep the system stable without adding extra generation units, whereas the grid capacity needs to grow. Furthermore, the behaviour of the distribution network and the microgrid as part of the distribution network will be modified from a single direction power flow to bidirectional power flow. Such a system is very difficult to control, and congestion could occur affecting elements of the microgrid, which can then result in local power-outages. Uncontrolled charging of BEVs can significantly increase the peak load of the distribution network and thus result in a high cost. Therefore, a hierarchical modular structure is required to manage and control each element of the system,

including EVs similar to those proposed in this thesis, which will then allow a much greater number of EVs in the network. Managing and controlling the EVs may also allow integrating the intermittency of the renewable energy by using EV resources' capacity for mobile storage devices.

The cost of EVs is one of the main barriers to their uptake. In particular, calculation of the total cost of ownership involves a large number of variables such as:

- Cost of batteries.
- Lifetime of batteries.
- Cost of EV use.
- Distance range of EV based on the battery size and cost.
- Electricity use cost per distance units.
- EV taxes.
- Manufacturing age of the EV.

There are many manufacturers competing in the EV market; the EV culture provides a variety of EVs to satisfy each user group which are different in vehicle size and associated battery capacity and lifetime. EVs can be classified into sub compact models, medium sized models, and luxury models. The battery capacity is 12–21 kWh, 22–32 kWh, and 60–90 kWh respectively. The most common EVs are listed in Table 1-1.

In general, the EVs are classified according to their fuel use into partly electrically fueled such as RHEVs and PHEVs or wholly electrically fueled, such as BEVs. The PHEVs and BEVs are the two main technologies which are suitable for grid connection. Depending on the level of sophistication of the vehicle charging process, the EVs may be considered, from the view of the microgrid, as:

- A simple load that draws a continuous current independently from discrete network nodes.
- A flexible load of an aggregation of EVs with coordinated charging.
- Generation units where EVs are using their storage devices to inject power into the grid according to available resources [60]–[62].

Table 1-1: Battery capacity of different types of Electric Vehicle

	Model	**Battery Capacity**
1.	Toyota Prius	4.4kWh
2.	Chevy Volt	16kWh
3.	Mitsubishi iMiEV	16kWh
4.	Smart Fortwo ED	16.5kWh

5.	Honda Fit	20kWh
6.	GM Spark	21kWh
7.	BMW i3	22kWh
8.	Ford Focus	23kWh
9.	Fiat 500e	24kWh
10.	Nissan Leaf	25kWh
11.	Mercedes B	28kWh
12.	Nissan Leaf	30kWh
13.	Tesla S 60	60kWh
14.	Tesla S	70 kWh
15.	Tesla S 85	90kWh

1.1.8 Electric vehicles description from view of microgrids

Microgrid operation depends mainly on the distributed generators and storage energy devices which play a vital role in increasing the power level of the microgrid to balance the demand of the network. In particular, the battery has a high capacity to do work, and normally it has a higher energy density when compared to a supercapacitor of the same volume/size. The supercapacitor delivers energy faster than the battery as it has a higher power density than the battery. A battery-supercapacitor hybrid energy storage system is normally expected to perform better than a battery or supercapacitor alone; in addition, such a system increases the lifetime of both battery and supercapacitor. Typically, the microgrid should use a bank of batteries and supercapacitors connected in series and parallel to meet the voltage level of the network and the power level. The bidirectional converter is required for both to transfer the power from the storage system to the network at the discharging mode or transfer power from the network to the storage system at the charging mode. Such a system is expected to be difficult to implement because it has two different kinds of storage system; each one is constructed from small units connected in series and parallel. Implementation of such a system is expensive, requires a permanent space to install, and requires continuous maintenance. Such system maintenance is difficult due to each unit in the system needing to be tested to identify the replacement flaw units rather than replace the whole the system. Connecting many small units of storage devices with a different response, requires a complex energy management to balance charging and discharging each unit alone.

On the other hand, the EVs deployment has been increased within the electrical system. The main resources of the EV are a combination of multiple energy storage devices such as battery and supercapacitor. EVs are assumed to spend most of a day connected to CSS either at home

or aggregated CSS. The main function of connection of the EV to the CSS is to recharge the EV resources for another journey. Considering some benefits to the owners of the EVs are to encourage him/her to discharge the resources of the EVs which make the EV use the same function as storage energy of microgrid. Therefore, the EVs work as a mobile energy storage system. There is no need to spend the fixed cost of installing, operating, and maintaining a mobile storage energy device to the system when the EV has an owner. The energy management of charging or discharging small resources of the EV is much easier than a large energy storage system with multiple units. However, EVs are distributed in different places with a different state of charge for the battery and supercapacitor. Therefore hierarchical control is applied to manage the power flow between the EVs and the network in two modes: vehicle to grid (V2G) or grid to vehicle (G2V). This is possible because of the large deployment of EVs at different locations, either at private or public CSSs, and due to the bidirectional nature of the power flow of EVs could cause congestion in the microgrid, affecting its stability. Therefore, applying a successful hierarchical management structure to control the charging and discharging process of the EVs becomes vital to obtain a stable operation of connecting EVs within the microgrid.

The EVs' availability has increased significantly. Therefore, there will be millions of EVs spreading across different locations of the microgrids. V2G mode is considered to be a great opportunity for a mobile energy storage system to help the microgrid in disturbance cases or electricity market emergencies, such as generation outage, to balance the demand when the distributed generators are not enough to cover the loads, maintain the voltage and frequency variation on the system, or supply cheaper energy when the energy of the EVs is cheaper than other resources. The EV will play an important role for peak shaving when the demand is high to maintain the voltage stability or frequency stability of the system, and power spinning reserve for an unexpected situation.

This thesis addresses the benefits of: using the microgrid over the CPS, integrating the EV into the distribution line of the microgrid at the connection bus, and the power and energy management of microgrids and EVs in a systematic and holistic manner, by adopting a new perspective approach of functional hierarchical implementation.

1.2 Aim and Objectives

The main goal of this thesis is to improve the stability performance and resilient operation of microgrids through the development of innovative, holistic power management of a microgrid network by addressing a unified, systematic framework, where the power management decomposes into modular blocks in chronological executions. Management consists of the interlocking functions of creating a corporate strategy, policy, and process tiers for organising, planning, controlling, and directing the microgrid and EVs' sources to achieve a robust operation of the microgrid. The main contribution from the proposed functionalities relies on the coordination of power system sources, locally available sources, mobile energy storage systems in EVs, and controllable loads during microgrid autonomous operation. The management and control features are expected to increase the reliability, efficiency and

sustainability of the system, as well as make the system flexible enough to recover the supply and demand conditions in emerging electricity markets, such as after natural disasters, during demand congestion, or grid outage, and to avoid power flow congestion. In order to achieve this major goal, a set of intermediate objectives have been established:

Construct a microgrid from a realistic distribution network of a typical community, considering the advantages of uniform integrating distributed generators based on voltage stability analysis. Several kinds of DGs integrate within the existing distribution network to balance loads of a typical community based on the weakest bus bar analysis to identify the advantages of microgrids over the previous network. Then, the effects of the microgrid on the conventional power system are analysed to determine the voltage stability enhancement of a smart grid over the previous system. To identify the EVs within the power flow analysis of the power system, a set of analytical equations links the EVs' characteristics within the microgrid and determines the effect of integrating EVs on the voltage stability analysis and characteristics of the microgrid.

Design a holistic, systematic management and control framework constructed from several tiers to include the operation of each element connected to the microgrid. In order to balance the electrical sources and demands, and maintain the stability of the microgrid, a chronological structure of the tri-level hierarchical management operation to form a modular power management implementation has been made in order to override the power flow congestion of the bidirectional power flow characteristics in the microgrid. The structure consists of MGO, CSO, and EVO, with the EVO being structured into three modular, hierarchical processes: EMS, PMS and PES.

The objective function of the MGO is the optimal scheduling operation of several types of DGs including renewable energy sources, mobile energy storage of EVs, and controllable loads, to minimise the total combined operation and treatment emission costs of the microgrid. Several scenarios of a typical community case study have been demonstrated including UC strategy, island, and connected operation within this stage of the unified structure.

The objective functions of the CSO either minimise the cost of charging power or maximise the cost of discharging power of aggregated EVs connected to the CSS of the microgrid. EVs can be represented as flexible loads or mobile storage devices to potentially provide frequency and voltage variation regulation during autonomous microgrid operation. A comprehensive case study operating in different scenarios is demonstrated to determine the viability of the proposed energy management concept.

The main objective function of the EVO synchronises the power conversion system of the EV to either provide standard waveforms or consume specific energy, based on the resources state of the EV. The EVO has been structured into three shells, with each shell having a particular objective function and execution period. The EMS is responsible for providing standard waveforms through detecting a positive sequence of an unbalanced waveform nature at a low voltage level network, and controlling it using droop controller and vector controller based on a set of analytical equations emerging from different levels of active and reactive power at different states of resources. The PMS is responsible for arbitrating power between the

resources of EV based on the fuzzy heuristic controller. The PES is accountable for the innovative switching modulation of the multilevel inverter based on a modified SVPWM strategy in order to combine multi-resources operation at minimum losses transition of switches.

The physical model of EV is powered by dual energy resources which are a battery as the main resource and supercapacitors as assistant resources. Power conversion circuitry is an essential part of integrating the DC form of EVs' resources to the AC form of the microgrid. To maintain the voltage balance of the microgrid as well as achieve good performance, high power and high efficiency, a modified three phase, multilevel, H-bridge cascade inverter has been chosen, which is able to operate multiple resources connected in series to synergize each other.

Laboratory implementation and testing of the multilevel inverter operation is necessary to validate the operation of the multilevel inverter by combining the dual resources (battery and bank of supercapacitors). The experimental validation and specification of switching the multilevel inverter are of utmost importance for the deployment of EVs within the microgrid. The fact that the microgrid is a very complex system with hundreds of elements spread over a wide geographical area makes implementing a laboratory microgrid both difficult and expensive, but could be managed by a group of researchers who are generously funded. Therefore, exploited particular implementation part of the system for the development and proof of concept of switching solution envisioning the prototype construction for EVs integration within microgrid. The hierarchical management strategy that will be investigated for the microgrid operation is depicted in Figure 1-10.

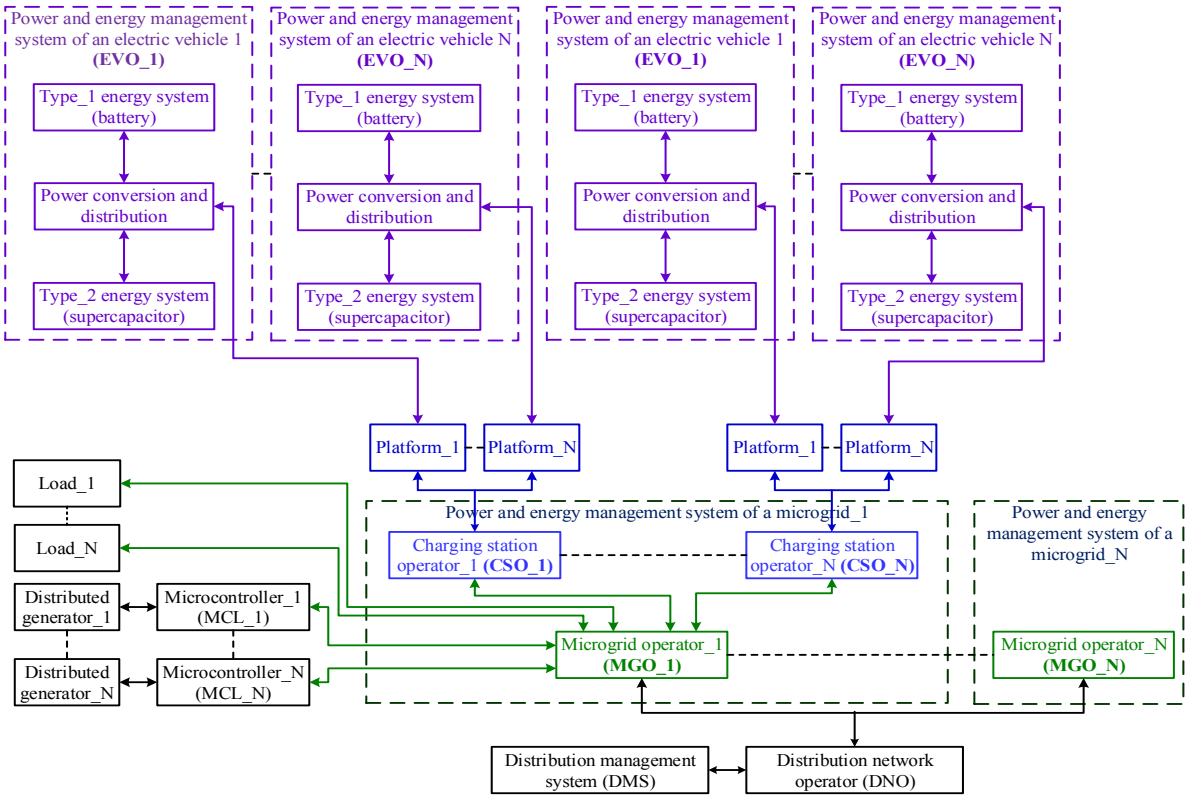

Figure 1-10: Microgrid network architecture

1.3 Methodology

An important aspect of this research that has a direct impact on the research objective is the choice of the system under investigation. A pragmatic approach in this applied research project is adopted to gain and contribute implementation insight to the problem of managing and control balancing between the supplies and loads at minimum cost and high efficiency in the microgrid. The research begins by constructing the microgrid infrastructure and evaluating the advantages of the microgrid from the view of the voltage stability analysis until implementing the signals of the energy storage system of the EV through three levels of hierarchical control strategies. The long-term, medium-term and short-term objectives are the strategy, policy and process of the system, which take place within the MGO controller, CSO controller, and EVO controller respectively.

In this research, an attempt is made to include all relevant components and subsystems to produce results that are directly relevant to the practical design. The practical system is deployed in a geographical location feeding residential, commercial, and industrial demands through the long connection between various distribution network components such as circuit breakers, cables and secondary equipment such as protection relay, distribution automation, and communications equipment. Therefore, it is expected that there is some significant constraint that is not considered using a purely theoretical approach but could be uncovered when the practical system is applied. A realistic distribution network with all cables and load characteristics, a variety of existing EVs, and existing parameters of distributed generators, are considered in control and management aggregated EVs connected to a microgrid in order to mitigate unattainable constraints.

The management and control research of a microgrid begins by constructing the microgrid from the existing distribution network by adding all necessary equipment. The case study investigated integrates some distributed generators into the distribution network to decentralise the distribution network operation and add all necessary power electronic devices and communication links to transfer the distribution network into the microgrid network. The revenue of the microgrid operation is measured by monitoring the voltage stability indicator of the traditional grid compared to the modification grid. Voltage stability model analysis depends on identifying the magnitude of the eigenvalues that provide a relative measurement of proximity to instability and the eigenvectors that present information related to the mechanism of losing voltage stability.

For insight into the effect of the EV on the microgrid, the study proposes appropriate mathematical equations to integrate the EV into a line of the microgrid based on a modification of the characteristic equation of the distribution feeder which carries the EVs. The effective location of the charging station in the microgrid is located using the identification of the most sensitive bus bar to voltage stability analysis in the network compared to the minimum voltage bus bar.

The study proposes a hierarchical management and control strategy from three sections which are MGO, CSO, and EVO to ensure the flexible, stable, and reliable operation of the microgrid and EVs. The MGO sets the objective function to minimise the power cost of distributed

generators and treatment pollutant emissions. The CSO sets the objective function either to minimise the cost of charging the power or maximise the cost of discharging the power of the EV. The EVO function is to operate a smart charger to decentralise charging and discharging the EV. The EV has two energy storage systems: battery and supercapacitors. The baseline design parameters of the energy storage systems are obtained through iterative simulation and reference of literature. The fuzzy logic theory is used to implement the heuristic reasoning of energy management by incorporating the use of battery and supercapacitors in synergistic operations. Modified multi-level space vector modulation control is implemented effectively to design the modified cascade multilevel inverter to control the charging and discharging operation of the battery and bank of supercapacitors with the microgrid. As the modelling platform, the MATLAB environment tools with Matpower and Cplex package are used extensively. The schematic diagrams of the inverter have drawn using Altium designer whereas the LabVIEW software control the laboratory experiment of the inverter. Some graphs are drawn using PSIM simulation software.

The research into power and energy management of a microgrid, including hybrid battery-supercapacitors energy storage systems, is a big challenge because:

- The microgrid has bidirectional power flow in nature.
- It has different distributed generators' characteristics.
- It has different load characteristics.
- It has two modes of working: island and connected mode.
- It has a broad network of the communication system.
- It has many EVs with a different capacity and driving style, whereas each EV has two different storage system characteristics.

All of these uncertainties result in very different energy, power, frequency, voltage, and current characteristics. The interactions between these bidirectional power flow components that have a different dynamic reaction are not obvious without exploration of all components' technologies and performing some empirical verification. This involves adopting a holistic research strategy, embracing all subsystems of distributed generators, EVs, loads, and hierarchical control strategy, rather than narrowly focusing on specific frameworks that adopted other researchers' work. The approach provides a comprehensive perspective and adds value to this applied research topic. Figure 1-11 illustrates the research framework diagrammatically. The operation of a modular, hierarchical controller operates periodically according to predefined times for each term based on the sequential decision process.

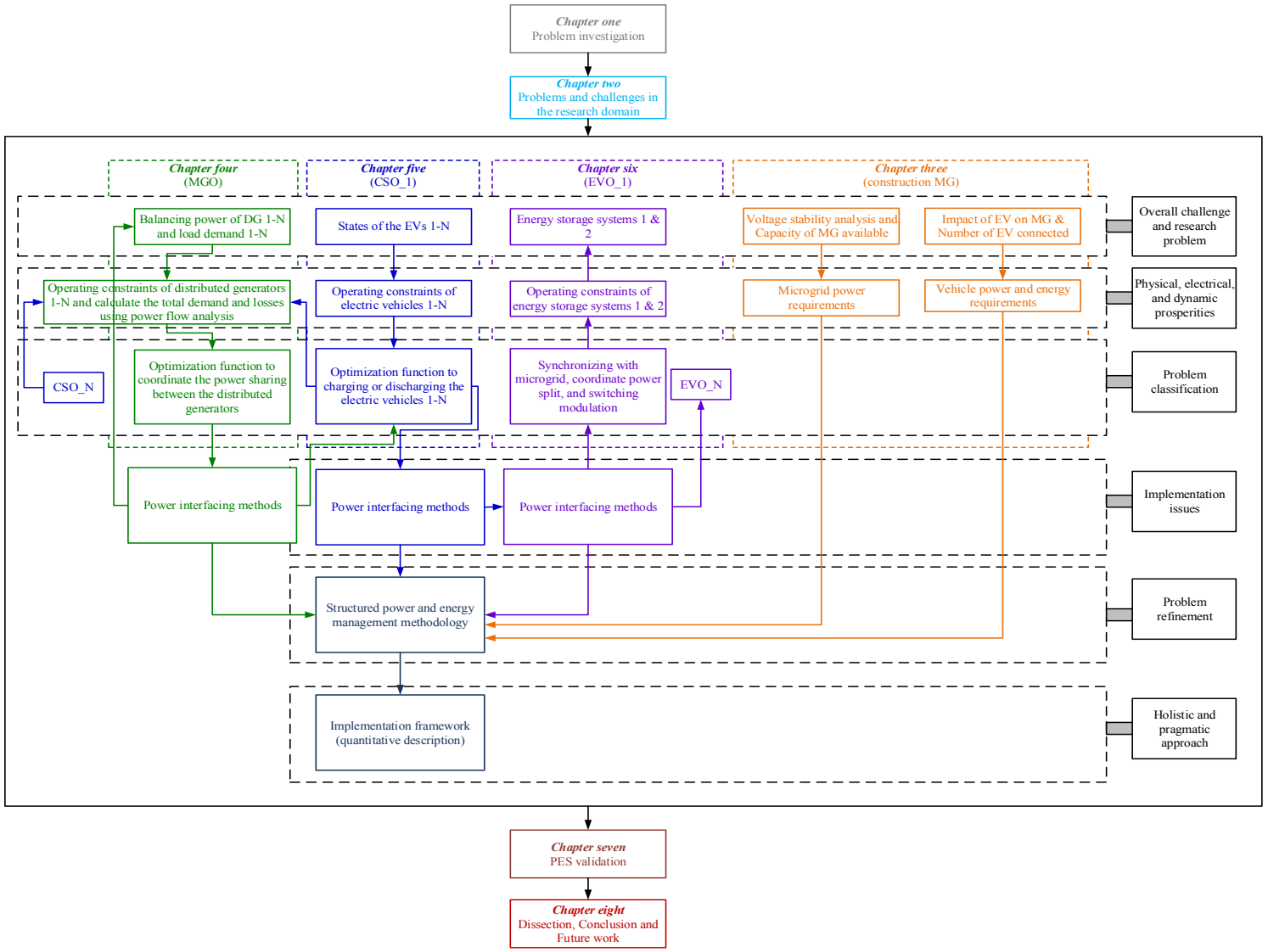

Figure 1-11: Research methodology

1.4 A Novel Structure of the Future Generation of the Electricity System

The smart grid can be defined as an automated power system that balances the generation and load by using an intelligent controller supported by information and communication technology to monitor the generation of the system and load. The smart controller promotes management and control as players (bidirectional or unidirectional) connected to the grid, whereas the communication link monitors the grid using an advanced metering infrastructure to connect the equipment of the grid to the intelligent controller. The operation of the transmission system and distribution networks ensures a fixable power transfer with a secure and stable operation. Distributed energy resources (DERs) and EVs, which are connected at the distribution level, are expected to participate actively in the functioning of the smart grid. Thus, the players (DERs and EVs) connected on the distribution networks would support the transmission system in the grid. Therefore, the deployment of management and control strategies requires extending the monitoring and data acquisition capabilities downstream to the distribution level of the grid, thus, changing the concept of centralised management and control to a decentralised concept and handling the data processing capability of all the control variables and consequent communications. The decentralised management and control network organise the distribution network in small controllable networks called microgrids. Each microgrid operates as a single controllable system that handles and controls the generation units and loads in a coordinated way in grid connected mode and islanded mode. The microgrid is considered to have a self-healing capability which works autonomously to disconnect from the grid, deliver power to its local area, and recover the supply and demand conditions in emerging electricity markets, such as natural disasters, demand congestion, or grid outage. It is possible to restore the service of the smart grid by reconnecting the microgrid to the smart grid in case the demand exceeds the local generation of the microgrid.

Microgrids are small areas of the smart grid paradigm to provide the flexible and controllable operation of low voltage networks, which then changes the distribution network operation philosophy from passive to active. The microgrid is a single controllable network, combining distributed energy sources and controllable loads, connected by a communication system, ensuring the management and control of interconnected elements at autonomous operation mode. The microgrid philosophy improves the system robustness and provides a resilient operation as well as an adequate framework to fully integrate EVs as a new player to the network. Since the largest microgrid problem is maintaining the stability of the system with low inertia and intermittency of microgeneration units, a widely-accepted solution is to use EVs' resources to keep voltage stability, in the short term, in voltage stability oscillation. Extensive deployment of the integration of EVs into microgrids will impose many challenges to the operation and management charging demands of EVs but will assist in avoiding the stability issue.

The EVs will play a major role in microgrid operation. The EVs are new, flexible load or mobile storage devices that are capable of being represented either as a normal load to charge the resources as G2V mode, or providing its power back to the microgrid as a V2G mode. The EVs are often provided with two resources for short operation time storage: seconds to minutes – such as supercapacitor and medium operation time storage; minutes to hours – such as a

battery to meet the performance expectation of the vehicle operator. The energy to power ratio for short operation time storage is less than one second whereas it is between one and ten for medium operation time storage [63]. The energy to power ratio is defined as a division of energy capacity by the power rating to get the operation duration time of the device while delivering its rated power, which is also called discharge time with unit of second. The high-power ratio source (battery) works as a primary energy source while the low power ratio source (supercapacitor) operates as a primary power source. An important feature for short operation time storage is the ability to recapture energy during regenerative braking. Power and energy management of the EV is required to meet the power quality and the stability of the vehicle at running mode and connecting mode.

Hybridization of the battery and the supercapacitor become necessary to achieve high performance and efficiency of EV operation. However, hybridization of multiple energy resources with different characteristics to generate the proportional amount of power and split between them is a big challenge for EV research. Configuring the battery and supercapacitor electrically within the EV power system and within the microgrid network forms the power electronics scope of this research. The multilevel inverter is a good approach to coordinate the multiple resources of the EV in bidirectional operation. This operation requires a high-level control and management scheme to be incorporated by using the battery and supercapacitor in a synergetic way. The charging infrastructure is an essential part of the interfacing between the microgrid and EV. The charging activity could take place at home, work, or through public access as single or aggregated EVs. A CSS could be on board with each EV based on the hardware and energy storage system capability, or outboard when integrated to the microgrid. The outboard charging station is divided into standard charging and fast charging based on the capacity of the charging station and waveform characteristics of the grid. The charging behaviour of the EV depends on:

• The ability of the resources of the EV.	• Period of connection.
• The state of charge of the resources.	• Charging strategies.
• Location and time of connection.	• Microgrid power availability.
• Driving distance and style requirements.	

Widespread integration of the charging stations in the microgrid is a key pillar to reap the wide deployment of EVs and the achievement of their large-scale development. Management of the role of the charging station to mitigate the congestion operation of EVs, apply microgrid constraints, and sophisticate the requirements of the microgrid and owner of an EV, are considered to be the biggest obstacles to the widespread adoption of EVs by customers.

According to complexity of the microgrids' elements, the control system of the microgrids distributes between several operators:

- Distripuation Network Operator (DNO) to mange and control many micorogrids within distribution network.
- Microgrid Operator (MGO) to mange and control balancing the generation and loads of the microgrid.
- Charging Station Operator (CSO) to centralize manage and control aggragated EVs connected at specific bus bar within charging station system on the microgrid.
- Privet-Home Operator (PHO) to mange and control charging and discharging home or private CSS.
- Electric Vehicle Operator (EVO) to either apply the CSO or PHO instructon for charging or discharging the resources of EVs or decentralize mangment and control the resources of EVs.

This new operation increases the reliability, efficiency, and sustainability of the system. The general structure of the CPS and the smart grid system is shown in Figure 1-12.

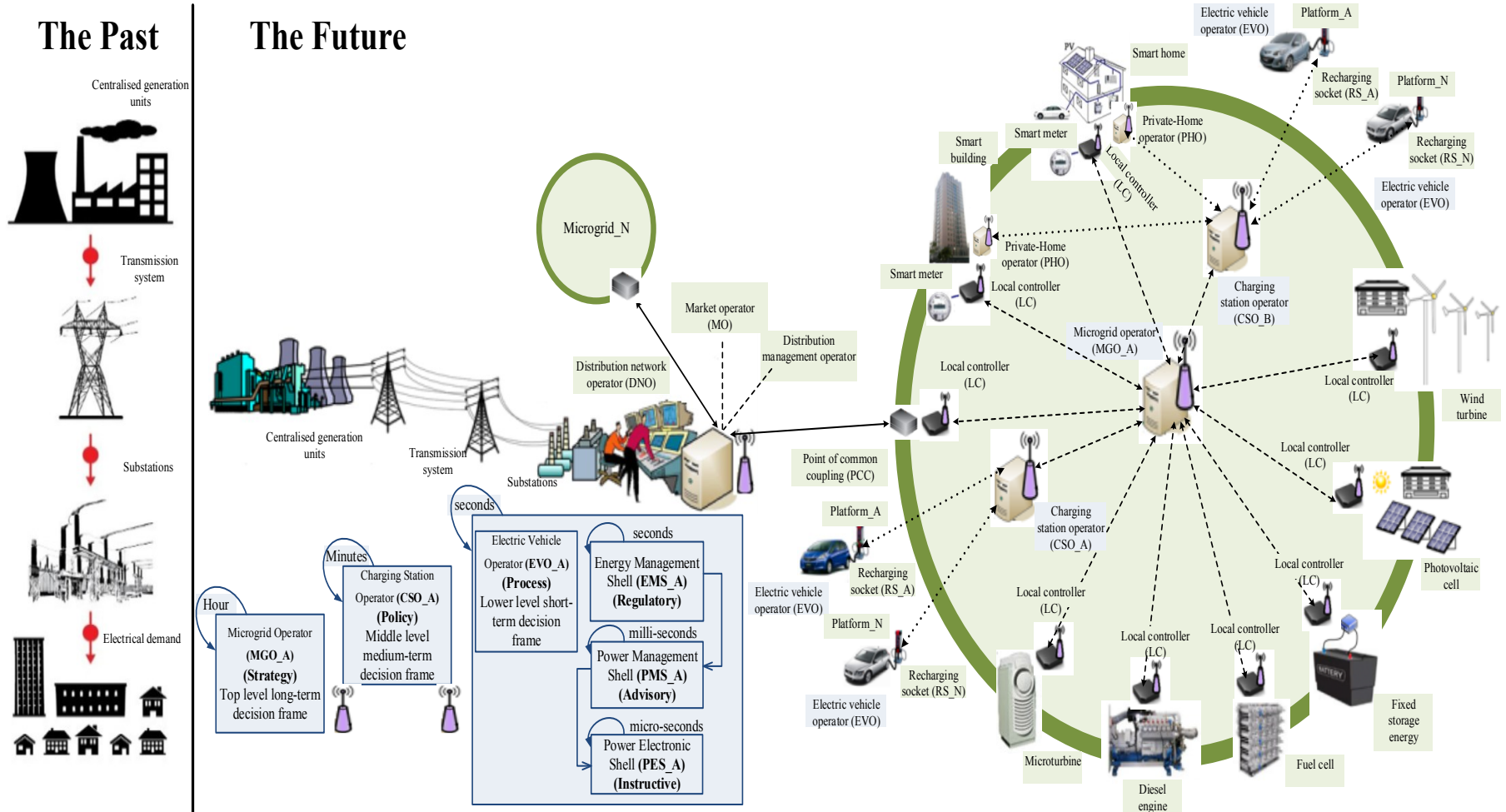

Single failure point could leave us in the dark

A microgrid is a single controllable network that works as a cluster of micro sources which deliver power locally to loads and act as a transceiver with other networks by ensuring communication, management, and control of interconnected elements to achieve autonomous operation mode.

Figure 1-12: The general structure of the conventional power system and the smart grid system

1.5 Optimised Microgrids Model Vision

The power and energy management of the microgrid system within EVs have been addressed through various approaches. In this work, the management structure is classified into several levels or tiers as a demarcation of hierarchy. The levels of hierarchy management collaborate to reach a common objective. The process at each level of the hierarchy management is addressed and different tasks executed within different time scales. The hierarchy is organised at the top, medium and low levels. Each level is responsible for making a decision that influences the specific term targets of the organisation. The framework and decision timeframe of the hierarchical management model are shown in Figure 1-13.

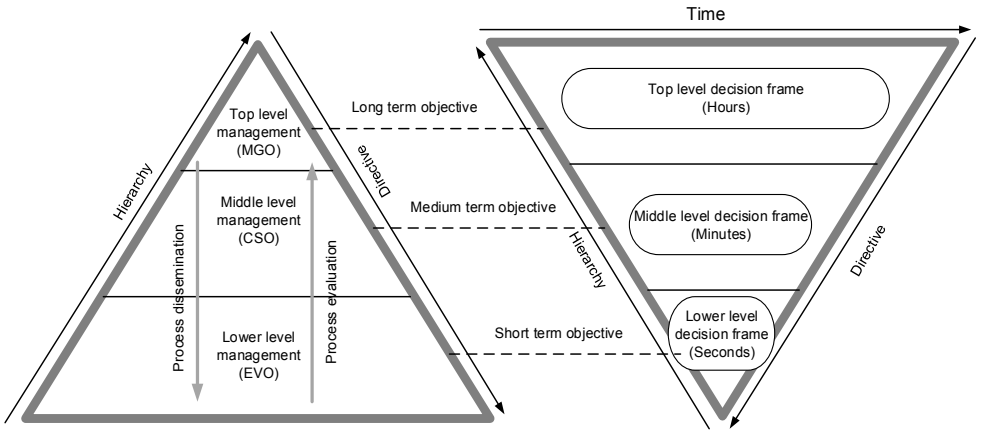

Hierarchical management model Decision time frames of model

Figure 1-13: Hierarchical and decision timeframes of management model

In general, the top level is responsible for long-term goals; the medium level is responsible for medium-term goals; and the low level is responsible for short-term goals of the hierarchy organisation. Each level bears a directive to the next level of the process through communication with each other to enable the levels to carry out the decision-making process successfully. It is not necessary for each level to know detailed information about the other levels. The operation of the short-term level depends on the reference of the medium-term level, whereas the operation of the medium-term level depends on the reference of the long-term level. The tiers operate in a chronological way, with a different time of execution starting from the longest one at the top level to the shortest one at a low level, where the low level executes more frequently than the other levels, and the medium level executes more frequently than the top level. Therefore, the faster time execution level holds the reference of the lower time execution level until the next circle of operation. A change in the internal operation in one level does not affect other levels. Here, the top term level of the hierarchical management system is the microgrid operator (MGO) which handles the information of all micro-sources and loads connected to the microgrid. The middle-term level of the hierarchical management system is charging station operator (CSO) which is responsible for the centralised operation of EVs. The short-term level of the hierarchical management system is the electric vehicle operator (EVO) which is responsible for the decentralised operation of the EVs.

The objective function of the MGO finds the optimum generation of the micro-sources (including EVs) in terms of low pollutant treatment cost and operating cost of the micro-sources. The output of the MGO is the generation required from each micro-source and the charging power available or discharging power required from the CSO according to the state of charge of the EVs. The CSO is more likely to discharge the power of the EVs at low voltage or low-frequency deviations. According to CSO states and the optimisation algorithm, the MGO decides the amount of charging power on offer or discharging power required. The execution time of the MGO is handled longer than other levels and is in the order of tens of minutes of operation.

The input of the CSO is coming from the MGO and each of the electric vehicle agents (EVAs). The MGO parameters are the power required, frequency deviation, and voltage deviation, whereas the EVA parameters are the state of charge, the period of connected time to the CSO, and some controller parameters. The objective function of the CSO concerns the optimisation problem to achieve either a minimum cost of charging EVs or a maximum cost of discharging the EVs, subject to certain constraints. The output of the CSO is charging or discharging the power required from the resources of EVs. The output of the CSO is sent to the EVA of each vehicle to execute the decision taken. The execution time of the CSO is handled in between the MGO and EVO and is in the order of minutes of operation.

The EVO is the cooperative device between the EV and the microgrid. The EVO contains the direct connection of the resources of an EV to the microgrid network via a smart charger and the EVA. The EVO is responsible for the operation between the smart charger of the EV and the EVA. The objective is either to make the EVO recharge the resources of the EV based on the power reference from the CSO, or to make EVO operate as decentralised charging in case of CSO failure to provide the reference power of recharging to the EVA during the operating time. The objective function of the EVO is to manage and control the power flow between the resources of the EV and the microgrid. The output of the EVO provides the real-time simulator for operating the switching of the inverter, which connects the resources of an EV to the microgrid. The EVO has lower execution time than other levels such as within a second. The operation time of the EVO is divided into three shells: the management shell which is handled in seconds; the control shell which is handled in milliseconds; and the power electronic shell which is handled in microseconds.

1.6 A Modular Power Management of the Microgrids Structure

The hierarchical structure of classical management methodology has been chosen as it fits well with the description of problems in this work. The system implementation has been designed as a unified systematic framework where the power management decomposes into modular blocks in chronological executions. The execution of the framework proceeds to demonstrate a reconstruction of the power management problem. Framework management divides the problem into smaller groups to control specific functions, which are the MGO, CSO, and EVO.

Microgrid management focuses on the entire organisation of all available resources and electrical demand from a short-term to long-term perspective to achieve a resilient operation

with maximum efficiency. It includes all equipment of the microgrid network, such as supplies, loads, EVs, conductors, capacitors and reactors, power electronic devices, protective devices, and communication devices. Management consists of the interlocking functions of creating a corporate strategy, policy, and process tiers for organising, planning, controlling, and directing the microgrid resources to achieve resilient operation of the microgrid.

The concept of the modular power management into hierarchical process levels presents an approach to define functionality and interface multidisciplinary objects in a systematic breadth and in-depth manner. This is further illustrated in Figure 1-14. The modular structure involves several processes ranging from long-term period segment decisions of the MGO to very high-speed control of the power electronics to facilitate power management by addressing each major part of the process independently. Then, the modular structure consolidates the multidisciplinary process to form a complete system. The structured format describes hierarchical tiers corresponding to the level of management mission and is seen as the upside-down structure on the left-hand side of Figure 1-13.

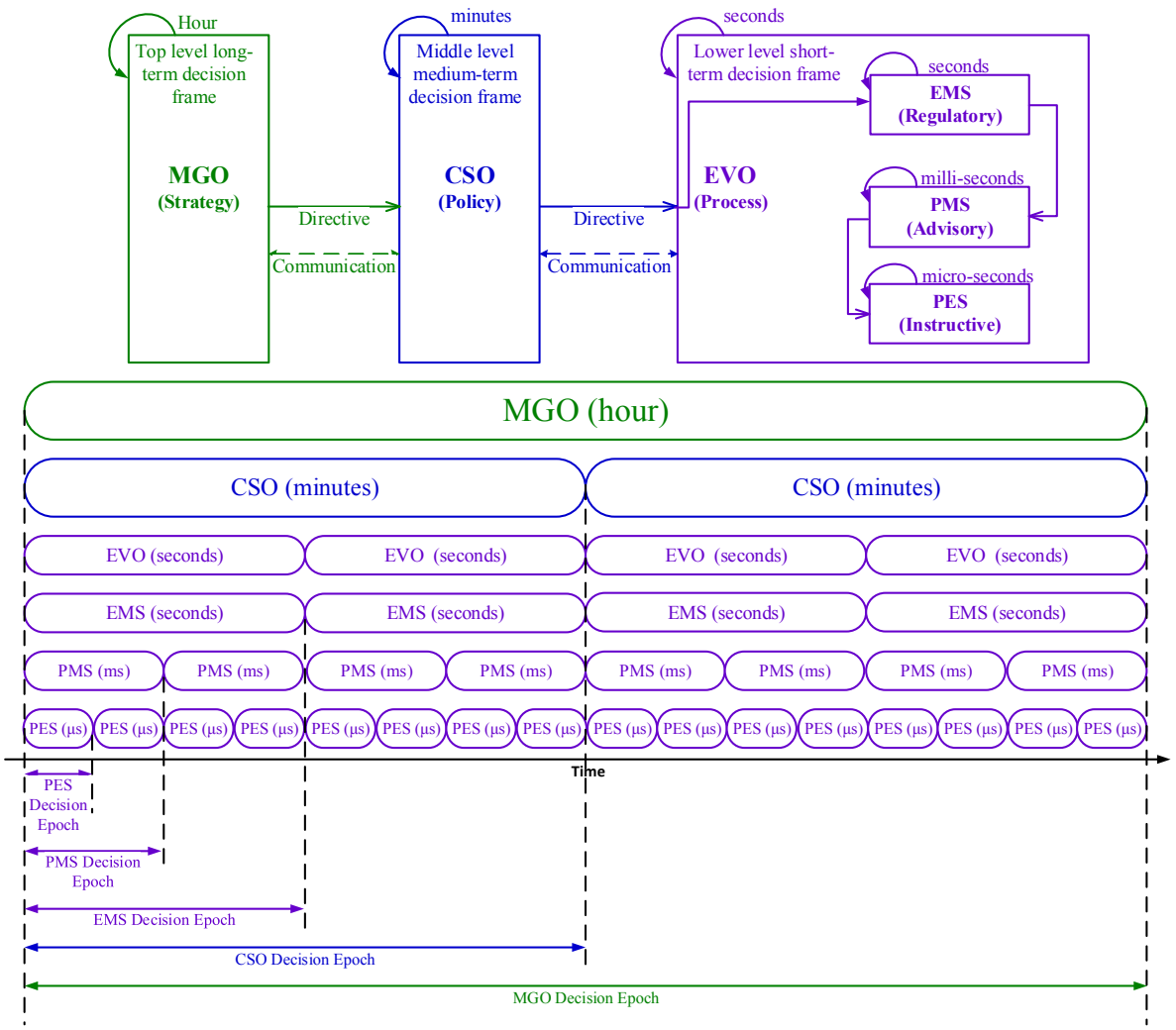

Figure 1-14: Concept of a modular management structure

The breadth of the tier organisation management structure increases lower down the management hierarchy in relation to time execution. The top tier of the modular management structure handles the strategic planning or long-term strategy for balancing of the generation and demand power. The middle tier decides appropriate actions of the policy planning or medium-term policy of the centralised charging/discharging aggregated EV. The decision which has been taken by the middle tier feeds downstream to the lower tier of the execution. The lower tier, which handles the lower-term planning of the EV power management, processes the decision of the middle tier in three stages, which are Energy Management Shell (EMS), Power Management Shell (PMS), and Power Electronics Shell (PES). The EMS involves long-term periodic time segment decisions of the energy expenditure for the process tier due to slow dynamic parameters' responses. The decisions of the energy management are accordingly termed as the regulatory of the system, which provides a regulated periodic manipulation of a set of control parameters to the next stage of the processing tier. The PMS is the next stage of the processing tier which involves medium-term periodic time segment decisions. The PMS is termed as advisory to the processing tier, which is responsible for determining the power split decision for the multiple energy storage systems of the EV. The two objectives of managing energy and power cannot be completely decoupled due to the different objective responses to maintaining the SoC level as well as maximising the usable energy of both resources, and determining the instantaneous power split between the resources.

The dynamic response of the PMS parameters is higher than the EMS parameters. Therefore, the iteration rate of the PMS is several magnitudes higher than the EMS. The final stage in the processing tier is the PES which is termed as being instructive of the process. The PES is responsible for the actual power blending of the energy storage systems of EV using the power split ratio determined by the PMS. The PES decomposes the reference power trajectories into appropriate control switching functions of power electronic devices.

The complete modular structure can be described as a hierarchical decision epoch, as presented in the lower part of Figure 1-14. The MGO-strategy is a plan of action designed to achieve a long-term or overall aim of the power generation from the distributed generators of the MG network to balance the electrical demand. The MGO-strategy is developed to transmit guides and philosophy to all components of the MG network. The MGO-strategy is concise in guiding the framework operation of the power management problem.

The CSO-policy is a mid-term level of the power management framework. It is developed to transmit the strategy guides and philosophy to the EVO-process. CSO-policy should exist to cover almost every aspect of organisational control because the EVs have special requirements to establish the procedure. CSO-policy and EVO-procedure dictate how charging/discharging occurs in each area of the MG. The CSO-policy could be driven either top-down as a centralised charger, or bottom-up as a decentralised charger method of the organisation. Top-down CSO-policy development operates as a central controller for charging/discharging all EVs connected to the CSO. Therefore, the CSO-policy is aligned with the MGO-strategy of the power management; however, it has a slower operation than a bottom-up approach, which requires a substantial amount of time to implement. On the other hand, the bottom-up of the CSO-policy development addresses the privacy concerns of the EV owner because it starts with their

requirement and concerns. It is faster than a top-down approach. However, it has huge disadvantages in the risk of power flow congestion that take off modular management framework leading to a blackout of the entire network. The bottom-up operates in case the chronological sequence of the CSO operation is delayed. Therefore, the EVO responds to the bottom-up policy development. The CSO-policy applies a strong emphasis on the power management framework. It specifies what is expected from the MGO and how management intends to meet the needs of the EVO. The CSO is responsible for security policy, which dictates the commitment of the management to the owner of the EVs, the operation of charging/discharging the resources of the EV, and the flexibility of power flow.

The EVO-process is the lowest level of power management framework that must adhere to CSO guidelines. It addresses the CSO guidelines and implements their philosophy to the energy storage systems of the EV. The EVO-process is more dynamic than the CSO-policy which requires more frequent changes to achieve the CSO and owner of the EV requirements, where they dictate what type of operation the EVO should implement. The EVO-process is implemented by linking three sub-processes involving MES-regulatory for the energy management system, PMS-advisory for the power management system, and PES-instructive for the power electronic interface. Therefore, the holistic power management of the microgrid network is addressed in the proposed methodology. The market operator at the territory control level is responsible for identifying the different rates of the tariff to power direction mode during a day through all operators of the microgrid.

A summary of the microgrid power management modular structure is as follows:

A. **Strategy** – Long term objective – microgrid operator (MGO): decision epoch regarding hours
B. **Policy** – Medium term objective – charging station operator (CSO): decision epoch regarding minutes
C. **Process** – Short term objective – electric vehicle operator (EVO): decision epoch regarding seconds
    1. **Regulatory** – Long term sub-process objective – Energy Management Shell (EMS): decision epoch regarding seconds
    2. **Advisory** – medium term sub-process objective – Power Management Shell (PMS): decision epoch regarding milliseconds
    3. **Instructive** – short term sub-process objective – Power Electronic Shell (PES): decision epoch regarding microseconds

1.7 Contributions

This dissertation deals with the concept of the effect of integrating EVs within a microgrid and applying a hierarchical management applicable to microgrid network application. In particular, the thesis addresses the management of the microgrid, which has a variety of distributed generators and a fleet of EVs connected to a charging station system with hybridization forming the dual resources of an EV. This thesis considered the practical applicability and implementation methodology of managing microgrid components as a holistic, working

system. The majority of the published work is mainly focused on the optimisation of microgrid operation or optimisation of EV operation, as an offline computation and non-physical connection method to obtain the minimum operation cost from the view of optimisation issues. Other researchers limited the research to operating the converter system of the EV to either obtain the optimum power arbitration of dual resources over a predefined load profile, or proposed a topology and switching modulation function to obtain high power quality. Minor researches considered management and control of the microgrid, including the integration of EVs, as a holistic working system. As a result, the contradicting objectives that arise when modifying a distribution network to a microgrid network can be listed as follows:

1- Find the effect of the EVs on the microgrid network.
2- Find the optimum operation of the microgrid that has different characteristics of distributed generators, different kinds of loads, and EVs.
3- Manage and control the centralised charging and discharging operation of the EVs as a supporter of the distributed generator.
4- Compensate the decentralised operation of the EV to manage and control the power flow through energy storage units,including the associated power electronic topology and switching modulation that facilitates the integration of EV into a microgrid.

As a holistic system approach, this thesis contributes to constructing, describing, integrating, and operating the key processes involved in microgrid power and energy management.

This thesis presents the following novelties:

- The positive impact of voltage stability enhancement on the operation of microgrid concept compare with conventional grid.
- The impact of integrating aggregated EV at specific bus bar on the microgrid voltage profile and voltage stability characteristic at discharging operation mode.
- Design a unified systematic framework to implement the power decomposes into modular blocks in chronological execuation for three operators: Microgrid Operator (MGO) to ececute long term desition of management and control couple of distributed generators with loads, Charging Station Operator (CSO) to mange and control aggregated EVs connected at specific bus bar on the microgrid through charging station system, and Elictric Vehicle Operator (EVO) to mange and control operation of duel resources of EV within microgrid in term charging and discharging activity. The holistic Moduler Power Energy Management System (M-PEMS) execuation proceeds to demonestrate a reconsetraction of the power management problem.
- Modified space vector pulse width modulation to do switching an eighten swithes of modified H-bridge multi-level inverter for controlling duel resources of EV.
- Interconnecting the operation of vriaty different dynamic response elements of microgrid at different level to provide reseliance operation of microgrod including EVs through various execution time operators of the modular framework structure, which then makes all the microgrid elements collaborate each other to operate as one compleate system. The EVs integrated into microgrid based on a set of equations to calaculate the power flow and regulate the power level of charging or discharging.

Operating of the M-PEMS has been structured into modular hierarchical process operators. The MGO handles the long-term decisions to optimise minimum cost and minimum pollution of the power usage in the distributed generators at the microgrid. The process within CSO, however, handles medium-term decisions to optimise minimum charging cost or maximum discharging cost of fleet EVs connected at the microgrid. Finally, the EVO handles the short-term decisions that facilitate the power and energy management of EV.

The modified multilevel inverter proposed in this thesis is suitable for EV application that is powered by a dual energy storage system, consisting of the battery connected to a three-phase bridge inverter and three supercapacitors connected in series with each leg of a standard three-leg inverter through an H-bridge converter.

The modular structure approach is oriented to ensure the reliable and stable operation of the microgrid with the objective of contributing completeness of the control and management of the operation of the EVs within the microgrid problem description.

The key contributions as a result of this thesis in order of presenting inside thesis can be summarised as major and minor; the **major** contributions are as follows:

1- The thesis presents a fresh perspective to operating the EVs within the microgrid research arena by introducing a novel approach that provides a modular structure with three distinct hierarchical processes resulting in the following key benefits:
A- Balancing the energy sources and electricity demand within MGO.
B- Managing and controlling the centralised charging and discharging aggregated EVs connected to charging station within CSO.
C- Managing and controlling power flow between the resources of the EV and the microgrid as well as switching to a decentralised charging operation in case any failure happen in the centralised charging station within EVO.
2- The thesis distinguishes the voltage stability enhancement of the smart grid at two modes: i.e. (a) connected and (b) disconnected microgrid operation over the conventional power grid.
3- This work identifies the optimisation requirement and considers all the constraints of the distributed generators and electrical demands to implement and achieve minimum cost operation and minimum cost pollutant treatment for maintaining a balanced operation between the supply and load.
4- The dissertation presents a formulation for the charging and discharging power management with scheduling equations incorporating fleet EVs connected to the charging station at the microgrid to achieve minimum charging cost or maximum discharging cost without a congested power flow. The charging formula constraint is based on several factors: the initial state of charge, a period of connection to the microgrid, desire to leave the state of charge, rated power of the converter, and capacity of the energy storage. The discharging formula is based on owner acceptance, the state of charge of a predefined limit, frequency and/or voltage deviation, in addition to charging formula constraints.

5- It provides a modular structure for decomposing the power and energy management for charging or discharging EV powered by dual energy storage resources within the hierarchical process.
6- The thesis presents a novel formulation of the reference power management by understanding the mathematical equation of integrating EV into the microgrid and the physical constraints of the energy storage technology. The energy management operation illustrates, based on the sequential decision process of control, the power fluctuations at the connection node of the EV to the microgrid to accommodate the process of the management energy shell (EVO-EMS).
7- The method of determining power-split ratios to charge or discharge the battery and the supercapacitors is made using the controlled signal of the EMS to accommodate the process of the power management shell (EVO-PMS).
8- It describes the numerical design and practical validation based on CompactRIO devices and LabVIEW software to modulate SVPWM for operating the multi level inverter under research, and provides technical insight information on the hybridization of the battery and the supercapacitors to accommodate the process of the power electronic shell (EVO-PES).
9- The thesis presents the flexibility of charging or discharging the EV by merging the centralised and decentralised operations of the EV, based on the owner of the EV requirement. The EVA at centralised smart charging implements the instruction of the CSO, whereas a smart agent of the EV is responsible for controlling the charging or discharging intervals of the EV in decentralised smart charging.

The **minor** contributions are as follows

10- It presents a clearly constructed microgrid from an existing distribution system in the form of choosing a suitable type and location of distributed generators and all necessary power electronic equipment. This assists towards reconstructing the existing distribution network into the microgrid concept.
11- It defines clearly the construction of a centralised charging station to connect each EV to its recharging socket, which collects the state of the vehicle and addresses it to the bidirectional power flow meter. The state of the vehicle transfer to the process of the charging station is to apply the optimisation function.

1.8 Publications

The following publications are based on the work completed as part of this thesis. The categories include conferences, Cranfield Events, Journals and poster sessions:

Chapter 1

1. **M. Alkhafaji**, P. C. K. Luk, and J. Economou, “A holistic modular power management framework to achieve resilient operation of microgrid including electric vehicles” Cranfield Science for a Circular Economy . How to tackle the Water , Energy , Food Nexus Conference Proceedings, June 2017 [64].

2. **M. Alkhafaji**, P. C. K. Luk, and J. Economou, "A new modular power management framework for operating a bidirectional vehicle to grid system within microgrid" Cranfield Science for a Circular Economy . How to tackle the Water , Energy , Food Nexus Conference Proceedings, June 2017 [65].

Chapter 3

3. **M. H. Alkhafaji**, P. C. K. Luk, and A. F. Bati, "Integration of electric vehicles within microgrid" *2016 UKACC Int. Conf. Control. UKACC Control 2016*, 2016 [66].
4. **M. Alkhafaji**, P. C. K. Luk, and J. Economou, "Optimising the location of distributed generators in microgrid based on voltage stability analysis" Cranfield Science for a Circular Economy . How to tackle the Water , Energy , Food Nexus Conference Proceedings, June 2017 [67].
5. **M. Alkhafaji**, P. C. K. Luk, and J. Economou, "Impact of integration electric vehicles to the microgrid" Cranfield Science for a Circular Economy . How to tackle the Water , Energy , Food Nexus Conference Proceedings, June 2017 [68].
6. **M. H. Alkhafaji**, P. C. K. Luk, and J. Economou, "Voltage stability analysis of microgrid" to be submitted.

Chapter 4

7. **M. H. Alkhafaji**, P. C. K. Luk, and J. Economou, "Optimal design and planning of electric vehicles within a microgrid" International Conference on Life System Modeling and Simulation, LSMS 2017 and International Conference on Intelligent Computing for Sustainable Energy and Environment, ICSEE 2017 Nanjing, China, September 22–24, 2017, Proceedings, Part III [69].

Chapter 5

8. **M. H. Alkhafaji**, P. C. K. Luk, and J. Economou, "Charging and discharging strategy of electric vehicles within a hierarchical energy management framework" International Conference on Life System Modeling and Simulation, LSMS 2017 and International Conference on Intelligent Computing for Sustainable Energy and Environment, ICSEE 2017 Nanjing, China, September 22–24, 2017, Proceedings, Part III [70].

Chapter 6

9. **M. H. Alkhafaji**, P. C. K. Luk, and J. Economou, M. Bendyk "Optimal design and planning of power and energy management structure for multiple resources of electric vehicle connected to microgrid" to be submitted.

Chapter 7

10. M. Bendyk, P. C. K. Luk, and **M. Alkhafaji**, "Control Strategy for a Modified Cascade Multilevel Inverter with Dual DC Source for Enhanced Drivetrain Operation," *IEEE Trans. Ind. Appl.*, vol. 2, no. 1, pp. 1–10, 2017.
11. **M. H. Alkhafaji**, P. C. K. Luk, and J. Economou, M. Bendyk "Control Strategy for Modified Cascade Multilevel Inverter for Electric Vehicle Application with Multiple Energy Resources" to be submitted.

1.9 Outline

The thesis is organised into eight chapters. The **first chapter** contextualises the problem scope under investigation. The main subjects of this chapter introduce the motivation behind this research, describe the proposed modular structure under investigation, and delineate the thesis aims and set of objectives to achieve these aims. The chapter identifies the main challenges facing the power system grid and suggests decentralising the power system operation towards the microgrid as a solution. The control and management hierarchical strategy main contributions and outlines of this thesis are presented. A brief summary of the contents of the following chapters is given below and explained in Figure 1-15 whereas a brief summary of Thesis' Structure, Aim and objectives, Tasks, and Novelties by chapters are presented in Figure 1-16.

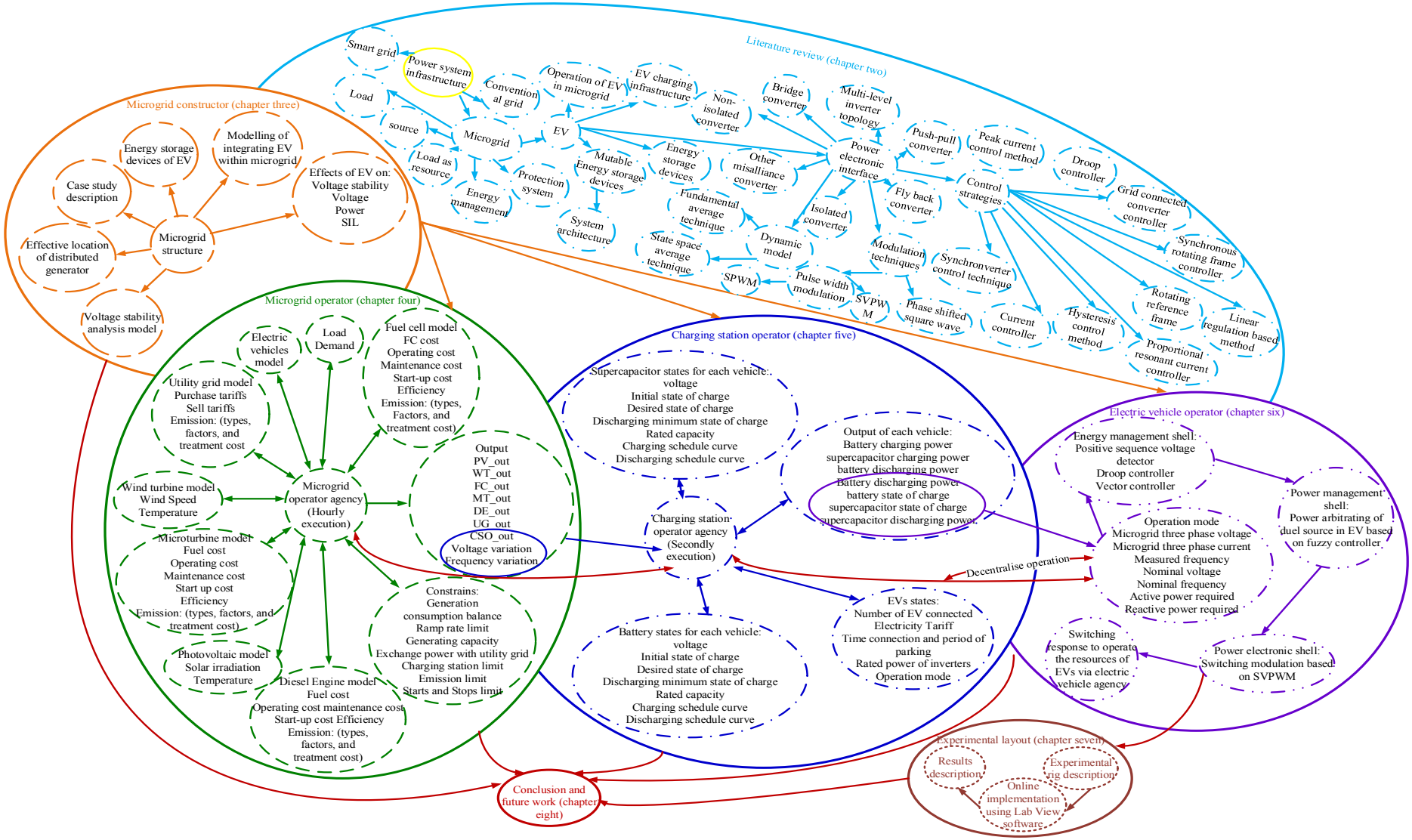

Figure 1-15: Outline of the thesis structure

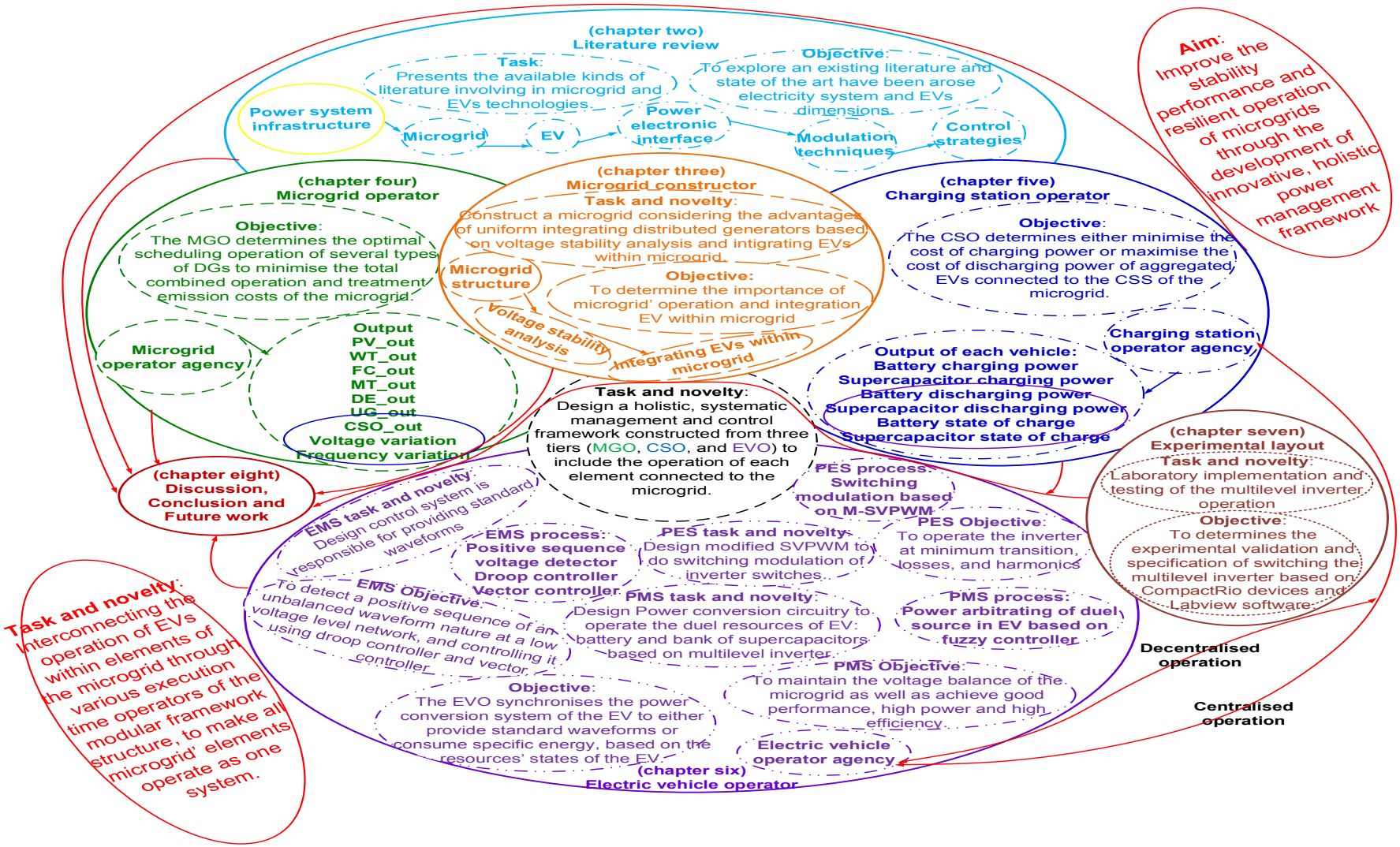

Figure 1-16 Thesis' Structure, Aim and objectives, Tasks, and Novelties

Chapter two provides reviews of the state of art of the power system, smart grid concept, microgrid concept, energy storage system, control of power electronic devices, and topologies of the converters. The research trends focus on the modular framework structure of integrating the EVs into the microgrid. The main components of the microgrid, the impact of the EV operation, and the charging station infrastructure are investigated to gain an understanding of the microgrid and EV. This follows with a review of a charging station infrastructure, and energy storage technologies. The various techniques of power electronic interface including bidirectional isolated and non-isolated converters, switching modulation strategy, and control strategies of the connected converter to the microgrid. A proposed multilevel inverter topology to manage and control multiple energy storage systems in EVs are also presented.

Chapter three discusses the integrating distributed generators and EVs within the microgrid and evaluates the microgrid operation from the view of voltage stability. The chapter determines the effective location of distributed generators in the microgrid based on finding the most sensitive bus to the voltage stability. It also evaluates the microgrid operation in island mode operation compared with the traditional grid, from the view of voltage stability, by using a case study. Furthermore, some obstacles preventing the spreading of microgrids are illustrated. Modifying the electric parameters of a distribution line with the characteristic equations of the energy storage system of EVs is suggested as a solution of the generalised mathematical equations of integrating EVs within a microgrid. This follows studying the effect of EV compensation on the critical receiving end voltage and power values. The impact of the compensation of the EV within the microgrid is discussed using an example of the compensation scheme and numerical analysis of the distribution network case study that has a fleet of EVs connected to the specific bus of the distribution network.

Chapter four focuses on the optimal scheduling of the distributed generators using a mixed integer quadratic programming approach that implements using the MATLAB environment and Cplex package. This chapter discusses the long-term management of the microgrid (MGO) which is responsible for balancing the supply and load to keep the microgrid operationally stable. A multiobjective optimisation algorithm is conceptualised/designed and implemented to schedule the generation of each distributed generator based on the optimisation model, operating cost, set of constraints for each unit, and variable electricity pricing to minimise the operation cost and the emission pollution of the microgrid energy cost. The model of the EVs is implemented as a fleet of EVs connected to the charging station. The medium-term management of the microgrid (CSO) is responsible for informing the MGO about the consumption demand of the EVs and the surplus power that could discharge from the EVs according to the energy storage limit. A case study of the proposed microgrid is analysed using different scenarios of operation that depend on the four parameters to investigate the impact of the MGO. These parameters are status mode (island or connected mode) and unit commitment strategy (applied or not applied).

Chapter five introduces and describes the operation of CSO regarding management charging or discharging the fleet of EVs connected to it. This chapter discusses the medium-term of hierarchical management strategy of the microgrid which should be operated in minutes. The CSO is responsible for satisfying the owner of the EV in terms of several options. These options are charging the EV at minimum cost, reaching the energy storage of the EV to the desired state of charge at the leaving recorded time, metering the charging cost and revenue the discharging cost of each EV. The discharging EVs within CSO are limited to owner choice, frequency deviation, voltage deviation, and a predefined state of charge limit for energy resources. To minimise the charging cost or maximise the discharging cost of the EV, two optimisation algorithms are proposed/designed and implemented to schedule the operation of the inverter of each EV according to the available power from MGO, a period of connection, desired leaving state of charge, and predefined state of charge limit of the energy storage system. Scheduling the charging or discharging operation of the EV is optimised using a mixed integer linear programming approach using the MATLAB environment and Cplex package. Subsequently, charging and discharging many EVs from a different company are tested at the various demands of the MGO. Each EV has two energy resources: the battery as the main energy resource and the supercapacitor as the main power supply.

Chapter six introduces and describes the operation of the EVO regarding management and control of the charging or discharging of the battery and the supercapacitors of the EV. It provides the modelling and application of the battery and supercapacitor for the EV system. A comparison between the traditional bidirectional converter topology and multilevel converter topology of EV application is discussed to find a suitable topology for connecting the EV to the microgrid and hybridization battery with a supercapacitor. The modified algorithm details of a multilevel SVPWM modulation of a suitable inverter for EV application is presented. A decomposition of the energy management and control of the EVO into a structured and modular framework is discussed. The framework of the EVO is accomplished by three sectors: EMS, PMS, and PES. The sectors are then demonstrated in the complete design of processing the charging and discharging dual resources of the EV. An exemplification of the proposed system at the different current range for charging and discharging is discussed along with the simulation results. The power sharing between the battery and the supercapacitor to support the microgrid is also discussed along with the simulation results.

Chapter seven describes the details of the physical experimental setup, the practical circuit diagrams of the rig, and the experimental results to validate the PES operation of the modified cascade multilevel inverter at different output voltages using CompactRio devices and Lab VIEW software.

Chapter eight concludes this thesis. Key areas and some remarks and suggestions that require further investigation are presented in this chapter.

The appendices provide formula derivation details, explanatory tables of chapters, graphs of simulation software, and graphs of practical software.

2. Chapter Two: Literature Review

2.1 Introduction

The prospect of the wide spread of EVs in the future is contingent on the modifying the existing power system to use it in a more effective way to increase the ability to foresee the rapidly increasing demand and the desires of charging/discharging the resources of EVs. It is important to measure the electric system willingness to operate the connected EVs in bidirectional without congestion as well as the EVs willingness to integrate with the electricity system in term of charging or discharging electricity according to the electricity system, resources of EVs, and owners of EVs requirement. Therefore, the electricity community aspects determining an effective strategy to design, management, and control an optimum operation of the electrical system to cover a large deployment of EVs.

In this chapter, the existing literature and state of the art which have risen electricity system and EVs dimensions are explored. However, the main objective of the review is to present the essential parameters of integrating EVs into electrical system effectively and what modelling techniques have been applied to capture this target. In this way, a broad literature survey on electricity system including the conventional system, smart grid, and microgrid research is first presented followed by a review of energy management of microgrid resources. Subsequently, an introduction of linking the electric power system and EVs thus enabling technology is also presented. Therefore, it is possible to illustrate the underlying reasons for modifying the existing power system to smart grid system and the proposed modelling of integrating EVs within microgrid in chapter three. The survey also attempts to overcome reason behind applying the suggested hierarchical modular framework of management and control strategy of operating EVs within microgrid in chapters four, five, and six. Then, the literature of power conversion topologies and control strategies of charging system infrastructure to connect the EVs to electric system are discussed. In this way, it will be possible in chapter six to demonstrate the suggested power conversion topology and proposed management and control multiple resources of EVs. Therefore, all necessary parameters, rules, and factors that might influence the operation of EVs within microgrid are discussed.

2.2 Overview

There are many factors that drive many countries to change their infrastructure of electric system from a traditional system to smart grid system; the main reason is to reduce carbon dioxide emission in addition to depending more on renewable energy than fossil fuel energy. This changing is followed by demand development especially plug and play demand such as electric vehicles (EVs). The EVs are expected to connect to the various location of electricity outlet at the different times of the day; it works as a mobile energy storage system. The electric vehicles produce much lower carbon dioxide than the traditional way of transport during their operation. The target is set for Europe to reduce the carbon dioxide emission from 140.3 gCO_2/km in 2010 to 95 gCO_2/km by 2020 [71], [72]. Among all resources of CO_2 emission in

the UK, the energy supply accounts for about 37% whereas the transportation accounts over 25% as shown in

Figure 2-1[73], the UK target is reducing CO_2 by 80% in 2050 compared with 1990 level [74]. It has set a goal that 30% of the generated electrical energy will be produced from renewable energy resources and 1.7 million of electric vehicles will be used; the renewable energy has produced about 19% from UK generation in 2014 as shown in

Figure 2-2[72]–[75].

BERR concludes that the lifecycle of CO_2 emission for EV will produce less than 50 g/KM; it will produce one-third of petrol-based vehicles [75]. Plug-in Hybrid EVs (PHEVs) and full EVs (BEVs) are mainly two technologies which are expected to represent a load for power distribution system in the forthcoming years [75]. Electric Vehicles could be considered from the view of distribution network as:

- Simple load that draws a continuous current from the electrical outlet.
- Flexible load that could allow an aggregated vehicle to coordinate their charging procedure.
- Energy storage devices that could use the EVs to inject power into the grid according to the available resources of the EVs [76].

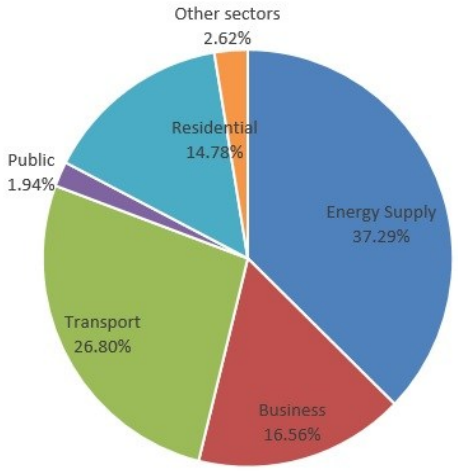

Figure 2-1: Shares of UK greenhouse gas emissions in 2014 [73]

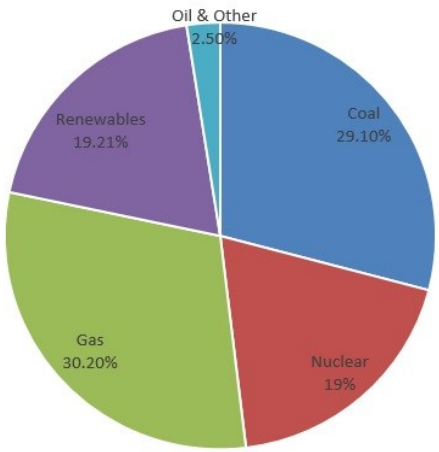

Figure 2-2: Shares of UK electricity generation in 2014 [73]

The invention of the electric vehicle is attributed to various people. In 1828, Ányos Jedlik created a tiny model car powered by an early type of electric motor as shown in Figure 2-3 and Figure 2-4. In 1834, Vermont blacksmith Thomas Davenport operated a small model of EV on a short section of track using a battery powered the DC electric motor. After word, many researchers developed deferent kind or sources to operate the EV paving the way for the later electrification of the transportation sector. In 1902, Dr Ferdinand Porsche took the EVs technology further steps by making a hybrid motor vehicle version of the Lohner electric. After the 1960s, interest in the published work in EVs increased due to environmental awareness and

reduced dependency on imported fossil fuel oil [77]. On the other hand, interest in the published work in microgrid dates back to the early 1990s when rapid development of the renewable energy technology occurred. Since then, the effect of EVs on microgrid was considered the domain of new generation of power system infrastructure and hence not a popular topic of research for electrical engineers until the middle of 2010, where the publication reaches 97 on 2015 as depicted in the histogram of Figure 2-5. Clearly, there is a research gap in understanding the interactions of the microgrid and the EVs and how these can be used to enhance how the operators can benefit together with the consumer. The last few years have shown an increase in publications on EV and microgrid research. It indicates that the integrated EVs into the microgrid and the associated issue of managing power between the resources of EV and microgrid are gaining research interests. EVs are a category as a new plug and play equipment with unique features, The EVs are expected to connect to the various location of electricity outlet at the different time of a day, and it works as mobile equipment with bidirectional power. As such there are many opportunities for contribution in this kind of research. Power management either between the EVs and the microgrid or between virus kind of resources of an EV are one such area of growing research interest as depicted in the histogram of Figure 2-5. Many works focused on the fundamental study of optimal charging EVs, some of them have focused on discharging power of the EVs to the grid. The following sections describe the basis of a microgrid, power electronics of the EV, multiple energy storage systems in the EV, and integrated the EVs into the microgrid.

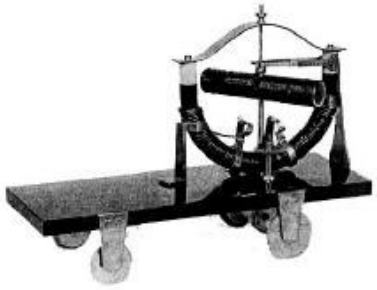

Figure 2-3: The first Electric vehicle model by Ányos Jedlik in 1828.

Figure 2-4: The first Electric motor model by Ányos Jedlik in 1827.

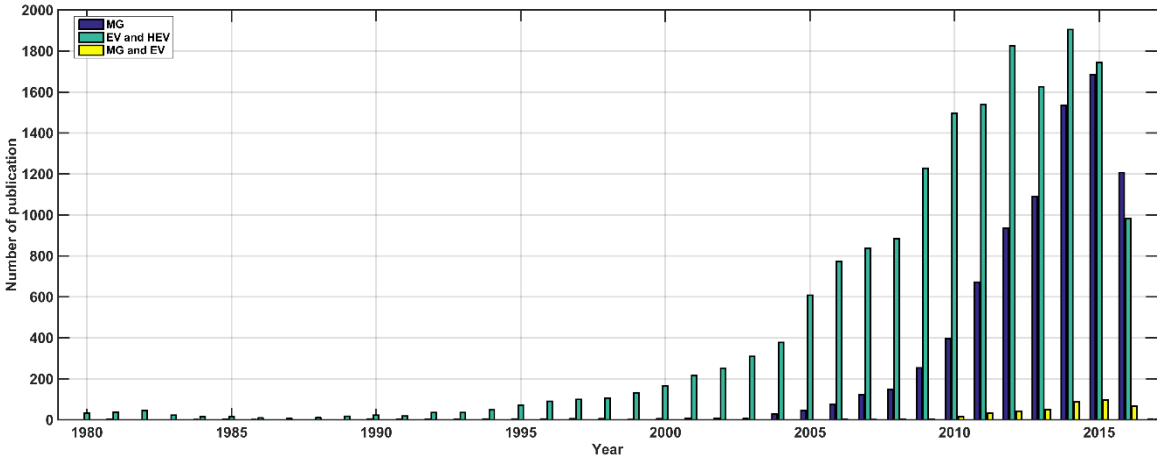

Figure 2-5: Publication on electric vehicle and microgrid extracted from Scopus database

2.3 Power System Infrastructure

The main purpose of the electrical system feeds electricity to consumers, the quality and reliability of electricity within minimum cost and environmental impact are a most important issue for users. Therefore, protection devices keep voltage and frequency within limits, assurance of equipment integrity and operation within fault rating are required. The distribution operator uses supervisory control and data acquisition (SCADA) system for real-time observation, monitoring, and controlling the DN within centralised infrastructure [78, Sec. 1.3], [79].

The conventional power system consists of three levels generation, transmission, and distribution in addition to the protection and metering devices. The power is transferred in a single direction from generation unit to a load in distribution area through the transmission line. The generation unit is a big plant that depends mainly on a fossil fuel to generate the power, for instance, most of the United Kingdom's electricity was produced by combustion of fossil fuels as shown in Figure 2-2 [73], [80].

The power, which is generated at bulk electricity generation, transfers to the demand area through the long transmission line. The transmission line carries high voltage power for long distance thus ensuring minimum transmission line losses. The transmission line connects to the generation area at the grid supply point through high rated supply transformer, for instance the transmission system of UK transfer power through about 25,000 Km and 2,000 Km of high voltage overhead and underground lines respectively, which cover four levels of voltages: 400 kV, 275 kV, 132 kV, and 110 kV [79], [81, Sec. 4.2].

The last stage of power system feeds electricity to the industrial, commercial, and residential customers through different levels of distributed voltages, for instance, the UK distribution levels are 66kV, 33kV, 22kV, 11kV, 6.6kV, 400V, and 230V according to demand [82]. Moreover, there are 14 distribution networks areas operated by eight Distribution Network Operators (DNO) [83].

However, the centralised architecture of traditional/conventional power network may become challenging to meet the development of power system in relation to voltage and frequency regulation for example. climate change, adding new plug and play loads, and growing the renewable energy technology. These concerns, therefore, drive many countries to modernise the existent power system and use the more efficient proposed smart grid concept [84].

2.4 Smart Grid Concept

A definition of the smart grid is still not standardised; there are many definitions to the smart grid such as U.S. Department of Energy (DOE) [85], Independent Electricity System Operator (IESO) [86], and the National Association of Regulatory Utility Commissioners (NARUC) [87]. The DOE definition stated that "A smart grid is an automated, widely distributed energy delivery network, the smart grid will be characterised by a two-way flow of electricity and information and will be capable of monitoring everything from power plants to customer preferences to individual appliances. It will be incorporated into the grid together with the

benefits of distributed computing and communications, therefore, delivering real-time information and enabling the near-instantaneous balance of supply and demand at the device level."

The IESO definition stated that "A smart grid is a modern electric system. It uses communications, sensors, automation and computers to improve the flexibility, security, reliability, efficiency, and safety of the electricity system."

The NARUC definition stated that "The smart grid takes the existing electricity delivery system and makes it 'smart' by linking and applying seamless communications systems that can gather and store data and convert the data to intelligence, communicate intelligence omnidirectional among components in the 'smart' electricity system, and allow automated control that is responsive to that intelligence."

The smart grid will enhance the complexity monitoring of the system and connection with other components using information and communication technologies to gather the information of a component of the smart grid. It increases the interdependency on the power management of demand. The system in smart grid will be separated into many areas; each area called Island to reduce the physical and electrical distance between generation units and loads. Each island is active that is working alone and covering all the demand within the area depending mainly on renewable energy sources. Island area could be connected to the utility grid in case the generation exceeds the demand at the point of common coupling. The point of common coupling works as a switch to separate a network into island mode [38], [39]. This operation increases the efficiency, reliability, and sustainability of the system. The guideline to understand and define the interconnection of an electric power system, a communication system, and an information system of the smart grid are explained in the IEEE 2030 standard on smart grid as shown in Figure 2-6 [88].

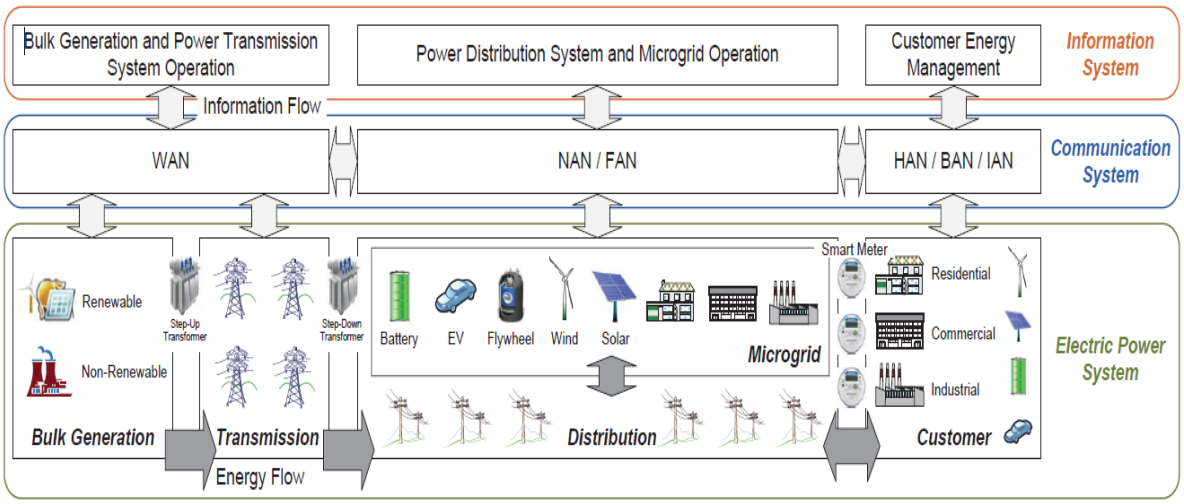

Figure 2-6: Smart grid structure [88]

2.5 Microgrid Concept

The earlier work on a microgrid started by Mukul C. Chandorkar and M. Deepakraj in 1993, they developed a new control method for an inverter to feed real and reactive power to the grid, that is suitable for an island system topology [89]. A definition of the microgrid is still not standardised; there are many definitions to the microgrid, R.H. Lasseter introduced the definition to the micro grid as "a system approach which views generation and associated loads as a subsystem"[44]. Researchers stated other definitions such as Schwaegerl et al., have defined a microgrid as "an integration platform for supply-side (micro-generators) and demand-side resources (storage units and controllable loads) located in a local distribution grid"[52]. C. Marnay et al. have expressed a microgrid as clustering of sources and sinks into semi-autonomous[90]. J.A.P. Lopes et al. have defined microgrid as an LV network plus its loads and several small modular generation systems connected to it, it provides both power and heat to local loads (combined heat and power (CHP)) [37]. The ABB researchers refer to a microgrid as an electrical system that relies on the gathering, distributing, and collecting the information for all electrical components to achieve the best economics, efficiency sustainability and reliability of the scheme. The Consortium for Electric Reliability Technology Solutions (CERTS) assumed microgrid concept as an aggregation of loads and microsources operating as a single system providing both power and heat to its system [91]. U.S. Department of Energy Microgrid Exchange Group identified a microgrid as: ''A microgrid is a group of interconnected loads and distributed energy resources within clearly defined electrical boundaries that acts as a single controllable entity on the grid. A microgrid can connect and disconnect from the grid to enable it to operate in both grid-connected or island mode''[92].

CIGRÉ C6.22 Working Group, Microgrid Evolution Roadmap identified a microgrid as: ''Microgrids are electricity distribution systems containing loads and distributed energy resources, (such as distributed generators, storage devices, or controllable loads) that can be operated in a controlled, coordinated way either connected to the main power network or island mode''[93].

CIGRÉ C6.22 Definition Qualifiers identified a microgrid as:

1- Generators cover all sources possible at the scales and within the context of a microgrid, e.g. fossil or biomass-fired small-scale combined heat and power (CHP), photovoltaic modules (PV), small wind turbines, mini-hydro.
2- Storage Devices includes all of electrical, pressure, gravitational, flywheel, and heat storage technologies. While the microgrid concept focuses on a power system, heat storage can be relevant to its operation whenever its existence affects the operation of the microgrid. For example, the availability of heat storage will alter the desirable operating schedule of a CHP system as the electrical and heat loads are decoupled. Similarly, the pre-cooling or heating of buildings will alter the load shape of heating ventilation and air conditioning (HVAC) system, and therefore the requirement faced by electricity supply resources.
3- Controlled loads, such as automatically dimmable lighting or delayed pumping, are particularly important to microgrid simply by their scale. Inevitably in small power systems, load variability will be more extreme than in utility-scale systems. The

corollary is that load control can make a particularly valuable contribution to a microgrid''. Therefore, microgrid does not have a technical definition which is defined by their function, not by their size. Nevertheless, it has still evolved [26], [37], [90], [91], [94]–[98].

4- The first study for designing energy balance of microgrid in the UK was discussed by Abu-sharkh et al. [49]. They examined the effect of microgrid application on the UK power supply focusing on frequency, voltage control, and power quality. The general conclusion of authors stated that the microgrid has a major contribution to reducing emission. However, a major change should be applied to the electricity market and regularity structure to reconstruct the existing power system to microgrids networks.

A Microgrid is a single controllable network that works as a cluster of micro sources which deliver power locally to loads and act as a transceiver with other networks by ensuring communication, management, and control of interconnected elements to achieve autonomous operation mode. A microgrid is a small-scale power supply network of the smart grid. A microgrid is designed to work as a cluster of loads, which are connected to micro sources that deliver power to its local area. It operates as a single controllable system that provides power and heat to its local area. It increases the reliability of the system and reduces the losses and cost of transmission lines. A distribution network in the microgrid would be changed from passive to active, which is being real time infrastructure and dynamic interactive. The system will work in bidirectional mode rather than single directional mode. A power congestion may occur during the microgrid operation.Therefore,it should be handled and controlled accurately by adding an intelligent controller and communication link between the generation units and loads [40]–[43].

2.6 General Architecture of Microgrids

The microgrid is constructed from three main components which are micro-sources, loads, and managements system in addition to protection system.

2.6.1 Microsources

Distributed generator is an electric source that connects directly to the distribution network at a specific location or to the customer side to balance the demand energy of network. It is characterised by generation capacity ranging from kW to MW level and generation at distribution voltages (11kV or below). The ability to distribute generator that connects to the microgrid is relatively small compared to the conventional grid. Thus they are known as the micro source. Micro sources are classified according to the operating technologies of controllable generators, uncontrollable generators and storage devices. There are two basic classes of the micro source either DC sources such as fuel cell, PV, and battery storage or variable AC sources such as a microturbine, wind turbine and diesel generator. In both cases a power electronic device should interface the micro sources to the network to create an AC waveform of desired magnitude and phase; Table 2-1 shows the distributed generators classification.

Table 2-1: The distributed generator classification

	Distributed generator unit	**Primary sources**	**Power electronic interface**	**Power flow control**
1.	Renewable energy units	Photovoltaic	DC/DC/AC converter	Maximum power point tracking and DC link voltage controls (+P,+/-Q)
		Fixed speed Wind turbine	Induction generator	Stall or pitch control of turbine (+P,-Q)
		variable speed Wind turbine	AC/DC/AC converter	Turbine speed and DC link voltage control (+P,+/-Q)
2.	Non-Renewable energy units	Microturbine	AC/DC/AC converter	Turbine speed and DC link voltage control (+P,+/-Q)
		Combined heat and power	Synchronous generator	AVR and governor (+P,+/-Q)
		Small hydro	Synchronous or induction generator	AVR and governor (+P,+/-Q)
		Internal combustion engine	Synchronous or induction generator	AVR and governor (+P,+/-Q)
		Fuel cell	DC/DC/AC converter	Maximum power point tracking and DC link voltage controls (+P,+/-Q)
3.	Storage units	Flywheel	AC/DC/AC converter	Speed control (+/-P,+/-Q)
		Battery	DC/DC/AC converter	State of charge and output voltage/frequency control (+/-P,+/-Q)
		Supercapacitor	DC/DC/AC converter	State of charge and output voltage/frequency control (+/-P,+/-Q)

Micro source controller is needed for each micro-source to ensure that autonomously regulate the output power and voltage of distributed generators to meet the dynamic requirement of the load. Micro sources can be added to the network immediately at load change based on local voltage and current measurements. The set point of the micro source controller can be independently chosen to regulate a power flow on a feeder, in addition to isolate or connect a microgrid to utility grid smoothly and autonomously.

2.6.2 Load

A load of microgrids is classified mainly to sensitive loads, such as medical equipment and computer servers and non-sensitive load. A sensitive load is a load that should always be supplied; the sensitive load feeder should have at least one micro source to maintain its demand whereas a non-sensitive load is a load that may be shut down if there is a disturbance on the

network. Normally a sensitive load consumes power from micro-sources of microgrid and utility grid. any disturbance occurs in the utility grid; the microgrid is isolated from utility grid by disconnecting point of common coupling in less than a cycle to minimise the disturbance in sensitive load. A microgrid is reconnected to the utility grid in case the sensitive demand exceeds the local generation of the microgrid.

2.6.2.1 Load as resources

Some loads can be classified as normal load or resource at the same time depending on the state of the network and the resources, such as electric vehicle resources

2.6.3 Energy management

The main purpose of the MG energy management is to ensure that the active and the reactive power of resources satisfy the demand of the MG with desired waveform characteristics (frequency, magnitude, phase angle, and power quality). The MG management is responsible for connecting or disconnecting the microsources to the MG or the MG to the utility grid for satisfying the interconnection requirements. The objective functions of the management minimise the operation cost, maximise the operation profit, maximise the operational efficiency of micro-sources, minimise the system emission, or/and minimise the energy losses. Broadly speaking, the MG management could be classified as centralised controller and decentralised controller. The key difference between the centralization and decentralisation controller greatly depends on the location of decision-making power. Constricted decision making responsibility on the high-level power management or dispersal decision making responsibility from a high level to functional level power management is the main difference between the centralization and decentralisation controller respectively. therefore, the centralization controller is more systematic, more formal communication exist, and slower than decentralisation controller [99].

The architecture of **the centralised controller** includes distribution network operator (DNO) which contains distribution management operator (DMO) and market operator (MO), microgrid operator (MGO), charging station operator (CSO), Privet home operator (PHO), electric vehicle operator (EVO), microsource operator (MSO), and load operator (LO), in addition to the communication link between the operators. Figure 2-7 depicts the centralised control levels. A centralised control maintains the entire system. However, this controller could cause multiple communication problems that lead to several disturbances, which could block out the system as a whole.

The decentralised controller enables all devices to control themselves independently when the congestion happens in the system due to bidirectional power flow or mismatch in the communication link between the devices. The construction of the microgrid could be small network or large network based on the nature of the load and operation. On the other hand, decentralisation controller is better for a large system than centralised controller [99]. Therefore, the decentralised controller is applied when the organisation of the system has full control over its management. The decentralised controller is aimed at achieving an operating point of micro sources and load as resources with their power electronic interference without

communication link. The decentralised controller could cause several problems since all decision are made at the MG; the MGO may lose the management of the system and affect the entire MG. Since there is no reference bus in the MG to achieve demand and supply balancing, it is not possible to set an optimisation function within the decentralised controller as all devices respond to any disturbance.

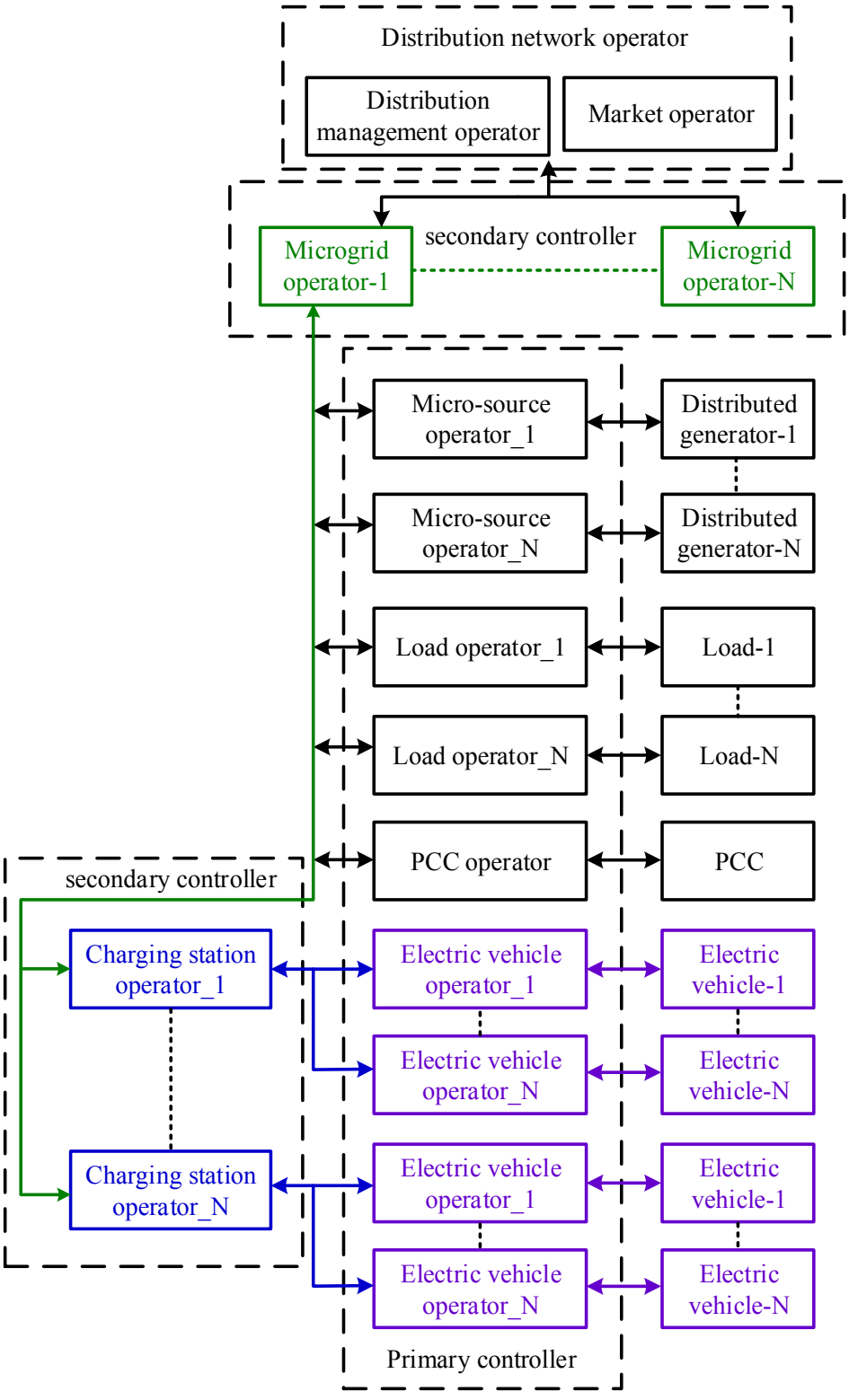

Figure 2-7: The centralised controller levels

Achieving lowest cost, losses, emission, regulating the voltage and frequency of the MG, and balancing the generation and demand of the MG require a well-organised control system. The controller objective can be achieved by either centralised or decentralised controller through three layers.

1- Primary controller which includes distribution network operator (DNO).
2- First secondary controller which includes microgrid operator (MGO)
3- Second secondary controller which includes charging station operator (CSO) and priviate home operator (PHO).
4- Thired secondery controller which includes electric vehicle operator (EVO).
5- Tertiary controller which includes local controller (LC) of micro source operator (MSO) and load operator (LO).

The DNO is necessary to manage and control many microgrids connecting to the same distribution network. The MO and DMO are responsible for market and power management of microgrid respectively. MO and DMO within DNO belong to the main grid, which covers high priority of controller. The second level is divided into two parts; the first part is MGO which has higher priority than the second part which includes CSO and PHO and the third part which includes EVO. The third level of the management system is a LC to manage the power flow through or from the node depending on the nature of the connection either MSO for source node or LO for load node.

Many researchers have studied microgrid optimisation using a different kind of resources. Most of them focused on minimum cost optimisation of resources. Furthermore, due to the complexity of the microgrid optimisation problem and because of the enormous economic benefits that could result from its improved solution, considerable attention is being devoted to the development of better optimisation algorithms and suitable modelling frameworks. The optimisation problem has either nonlinearity characteristics or some important features [100], such as demand side program and neglecting minimum up and down times.

Metaheuristics and heuristics have been proposed to solve the power dispatch problem of the microgrids, such as genetic algorithms [101], [102], evolutionary algorithm [103], particle swarm optimization [104]–[106], Monte Carlo simulation [104], mesh adaptive direct search algorithm [107], shuffled frog leaping algorithm [108], and tabu search algorithms [102], [109], [110]. According to the studies, microgrids can achieve high performance through:

1- Multi-layer controller algorithms based on advanced algorithm accounting for system uncertainty.
2- Deployment of demand response.
3- Optimal use of micro sources to compensate the demand.
4- Applying optimal instead of heuristic based approaches [111]–[114].

Most of the proposed approaches are either computationally intensive and not suitable for real-time applications or can produce locally optimal solutions; further researchers tackled the microgrid optimisation problem by solving several mixed integer linear programming (MINLPs) [115]–[118]. Due to uncertainty and difficulty to predict the generation of renewable

energy, researchers used model predictive control (MPC) to tackle the optimisation problem of the microgrid [119]–[123]. The mathematical solves two optimisation equations for different operators in different execution time for hundreds of equipment. Generally, they are solved minutely in chronological execution way for electrical parts and could be in micro second for power electronic part

The microgrid operation depends mainly on the power management between load demand and the energy sources. The energy flow inside the microgrid network equipped with a micro combined heat and power unit. The microgrid can also buy and sell electricity from/to the utility grid. The electricity could be stored in specific storage devices to compensate the connection and disconnection operation in addition to intermittency resources. Voltage and frequency should be constant at a particular value within a system to maintain the power quality of the microgrid network, in addition to the elimination of harmonics from power electronics device [26], [44], [45] to maintain harmonic quality. However, the distribution network in a microgrid, which is expected to be integrated with many controllable and uncontrolled microsources. Diesel generator (DG), micro turbine (MT), micro combined heat and power (CHP), and fuel cell (FC) are examples of controlled micro sources whereas uncontrolled micro sources that mainly depend on renewable energy sources, such as photovoltaic (PV) and wind turbine (WT). A system with many small distributed generators and variable demands are inherently a weak system, especially considering the effect of the renewable energy sources intermittency. Electrical power system security is the most important factor to ensure that the system is flexible enough to recover the supply and demand condition in emerging electricity markets. Voltage instability may happen which leads to fluctuation or change in the voltage profile at load buses due to reactive power flowing through a line. Voltage instability may cause failure in the system. Unbalanced voltage could be a further issue to microgrid due to most of the distributed generator connecting to microgrid through single phase converter [46], [124].

2.6.4 Protection system

The protection devices should ensure that the microgrid and utility grid work in stable operation where any fault within microgrid should be dealt with internally whereas the microgrid should be disconnected and depend on its resources to balance the load when any fault occurs in utility grid [91][125]. Figure 2-8 shows a schematic diagram example of the microgrid.

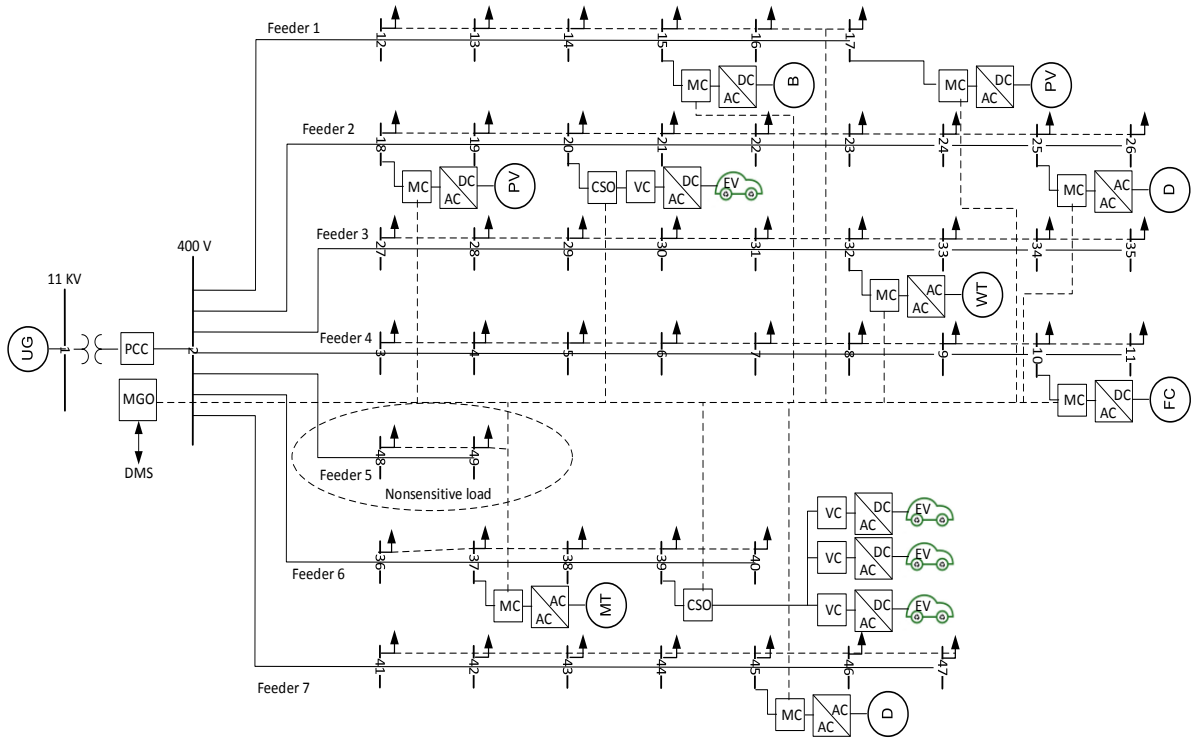

DMS = Distribution management system, MGO = Microgrid operator, PCC = Point of common coupling, MC = Microsource controller, VC = Vehicle controller, AC = Alternating current, DC = Direct current, UG = Utility grid, D = Diesel generator, MT = Microturbine, FC = Fuel cell, WT = Wind turbine, PV = Photovoltaic, B = Battery, EV = Electric vehicle

Figure 2-8: Typical microgrid structure

2.7 Operation of Electric Vehicles in Microgrids

The research on integrated EVs on the power system dates back to the early1980s as a part of the green and sustainable society. The charging demand of the resources of the EVs tends to coincide with the total demand of the system. Therefore, rapidly increasing in the total demand of the network occurs that requires more electricity generation to balance the supply and total electrical demand of the network[126]. Mismatching between the supply and the electricity demand fluctuates the voltage and frequency level from the set point of the system leading to instability issue. On the other hand, the discharging the resources of the EVs or part of them could help the generation units to reduce the gap between the generation and loads to keep the network at stable operation range.

The major change in the power system for an emission-free generation has taken initiatives to encourage the integration of renewable energy sources. However, the reliability of renewable energy sources not guaranteed because they are classified as intermittency sources where the generation cannot be predicted accurately. Therefore, the literature suggested a different solution cope with variability of renewable energies; one solution is using energy storage devices to cover the rest of the demand that renewable energy could not cover it [127]–[133]. The other solution is operating controllable generator as reserved [104], [134], [135]. Recently, using EV resources as mobile energy storage system is proposed [136]–[139]. Normally, the EV is treated as new plug and play load that is connected to the microgrid network to charge its resources. However, the resources of the connected EV could be used to discharge its power

to the network in case any disturbance happens and to accomplish renewable energy intermittency. Ideally, there are many EVs that could be connected to the microgrid at disturbance situation. Therefore, the EV should be integrated in such a way with microgrid to manage easily and control the charging and discharging behaviour resources. Such control system is called energy demand management. Researchers have stated that unmanaged EV could increase energy losses, increase voltage drop of the line, fluctuate the voltage and frequency, and overload transformers and lines [140]–[144]. Moreover, the EV could be used as a microsource to discharge its power to microgrid at frequency regulation, voltage regulation, or active and reactive power compensation. Furthermore, energy demand management could help an owner of the EV to charge his/her vehicle at lower price rate.

The EVs are classified according to fuel using entirely or partly electrical fuel. An electric vehicle system contains an energy storage system, power conversion system, an electric motor for propulsion, and a mechanical transmission, in addition to power control system. Moreover, EV might have an internal combustion engine in case of SoC of battery fade up [58], [145].

The main types of connected EVs to microgrid are either Plug-In Hybrid Electric Vehicle (PHEV) or Battery electric vehicle (BEV). In the PHEV, the petroleum synergies the battery to run the vehicle [58]. The battery could do charging at running mode based on the petroleum. In BEV, the vehicle depends totally on battery energy whereas the driving distance of this car depends directly on the battery size and capacity. The battery charging comes from the microgrid [58].

Typically, researchers treat EVs as a load on the distribution system; PHEV and BEV are considered similar demand on the distribution network. However, they are different regarding their operational characteristics.

There are many researchers have covered the subject of integrated EVs into power system in various ways. Some of the topics are listed below:

The advantages of using EVs together with fixed storage systems for minimising operating cost and minimising harmful gas emission in commercial building are studied in [146], the study indicates that EVs can feed electricity in a high period of energy consumption to reduce the energy cost.

[147], [148] focused on minimising the grid losses, and the total energy cost by using an optimal power flow to EV charging; they have concluded that EVs can have multiple impacts according to the considered objective.

V2G was considered in [149] for developing an optimisation issue to distribute the load profile close to plane load curve. EVs are used as stored energy resources in [150], [151] with a microgrid system, they have concluded that the resources of EVs could be utilised in a V2G mode to support the microgrid network and create income for owners of the EVs.

Improving the grid efficiency through the vehicle to grid interaction with high power factor, minimal current harmonic distortions, and less noise are the main targets for [152], [153]. [152] proposed a multilevel converter to achieve high efficiency and low THD to ensure proper operation of equipment and a longer equipment life span whereas [154] examined the best

optimisation for the grid during off-peak times of changing EVs. A spatial-temporal model to evaluate the impact of EVs on distribution network was developed in [155]
[156], [157], which raised the stability issue for a grid with EVs integration. [156] proposed a set of characteristics equation to reduce the computational complexity whereas [157] proved the possibility of EVs to participate in the primary frequency control to gain a crucial role in the operation of the isolated system. A control strategy of EVs and battery energy storage station to provide regulation frequency coordinate with automatic generation control were studied in [158]. [159] paid attention to the vehicle to grid control participation in power factor correction of the power system. EVs integration based on the hierarchical model predictive control for a smart grid energy management system that provides load frequency control and an economical operation was proposed in [160].

[161] showed a good performance in the implementation peak shaving strategy for EVs charging station and energy storage system in respect of distribution network.

[162], [163] presented an experimental DC charging station methodology to verify design and performance of full EVs.

[164] addressed the integration of a single phase charging devices issue for EVs and low voltage microgrid. The authors in [165] found that there are no major constraints in the integration of EVs with electricity network whereas the capacity is concerned. Furthermore, [166] presented a conceptual framework to integrate EVs into power system successfully. [167] investigated the contribution of EVs to integrate fluctuation of the renewable sources; the study used real-time prices as a control signal and detailed simulation of driving behaviour. Furthermore, [168] studied the control and optimisation the power consumption of residential load for EVs integration with existing photovoltaic system.

In [169] the authors have focused on reducing power system cost at EVs charging scheme with maintaining reliability; the study considered the optimal EVs integration into the New York independent system. In [170] the authors have analysed the effect of different charging and a discharging mode of economic operation of the microgrid; it has presented a mathematical model for microgrid economic scheduling considering the integration of EVs. [171] studied the effect of ramp rate of photovoltaic converter output power whereas integrating EVs with the photovoltaic power system, the ramp rate is reduced with the EVs integration.

Further study for integrated EVs and photovoltaic has been found in [172], it proposed a strategy to improve the predictability of photovoltaic power and reduce the forecast uncertainties by a collaborative working between EVs owners and photovoltaic participant.

EV charging as a linear optimisation issue which takes into account the anticipated and the present constraints on the distribution grid over a finite charging horizon.

During a finite horizon, the anticipated present constraints are taken into account on the distribution grid and modelled as a linear optimisation problem for the charging EVs [141]. This approach in [141] has resulted in sustaining high percentages of EVs uptake for more efficient using of existing networks without any further upgrades.

The potential benefits of using EVs as distributed generator are taken into account on the microgrid to participate in demand side management [151]. This approach in [151] has resulted in operating EVs within microgrid which can reduce peak load and energy consumption. Therefore, the electricity cost for users will reduce.in order to minimise the losses occurring in the existing EV system, [173] verified the efficiency of EV converter and the scheduling process through power flow analysis; the study dealt with an online EV system which utilised the dc power system for reducing loss and the size of the required battery capacity.

For the analytical study, [174] has developed a static load model for the EV loads, the paper revealed the importance of incorporating this model into static voltage studies where integrating fast charging for EVs might significantly reduce the steady state voltage stability of the power grid.

Large scale integration of EVs into the grid to find the optimal placement of charging station for objective of minimising the total transportation distance that is essential to the popularisation of EVs were focused on in [175]. Development a market participation policy for a load aggregator to manage the charging of EVs that plugged in at the same distribution feeder was discussed in [176]. It is used dynamic programming to develop decision support algorithm and participation market policy for a load aggregator

Design methodology for efficient EV charging based on renewable energy supply is the main research target of [177]. It is presented a result of allocating energy from renewable sources to EVs in a cost efficient manner using a stochastic optimal charging scheduling. A unified regulatory framework of electrical protection requirement and earthing arrangements that are applicable to feed EVs was presented in [178]. A distributed EVs charging strategy based on prices of forecasting energy and photovoltaic output as a photovoltaic support policy was evaluated in [179]. This approach in [179] has resulted in fluctuations in real time price of the large scale application of proposed algorithms. Due to simulation the time series power consumption of EVs, a description an interactive mechanism between power system network and EVs in conjunction with a smart charging model are taken into account on [180]. It is proposed a smart charging framework that mimics charging trajectory to control system operation risk. a new stochastic model for EVs was developed in [181] to modify a probabilistically constrained load flow as an optimisation problem that considers Stochastics models of wind power generation. To reduce network losses and improve system voltages, [182] presented the use of battery energy storage system for facilitating the integration of EVs and photovoltaic cells based on probabilistic sizing and scheduling methodology for their system. To minimise the cost of EV charging, [183] performed a multi period optimisation based on utilising unbalanced distribution network load flow and rolling optimisation method. To mitigate the criticality of nodal stresses, [184] constrained on security enhancement of distribution network by a proposed a strategic methodology to integrate EVs into microgrids.[185] proposed a synergistic three level control between EVs and wind energy to mitigate the intermittent wind power generation. The implementation of the proposed control algorithm in [185] figured out that not just the EVs fully charged but also the grid frequency regulation is improved and The synergy operation is achieved substantial cost reduction. EVs with smart charging can contribute towards meeting holistic environmental goals as discussed in [186]. It is performed an examination of the effectiveness of EVs in supporting the achievement of CO_2 reduction by increasing the integration of renewable resources into a grid.

On the other hand, it is examined the advantages and disadvantages of increasing generating of EVs and renewable capacity from requiring electrical demand. Finally, In order to improve the stability of the power system, [187] presented a real-time digital simulator model of aggregated EVs based on wide area controller structure to evaluate the impact of the bulk level charging and discharging transient of EVs to improve the stability of the power system.

2.8 Electric Vehicles Charging Infrastructure

Charging EV can be performed either on AC platform or DC platform. AC platform is more widely used than DC platform[188], [189]. The classification of AC and DC platform depends on the converter location either online converter inside the vehicle or offline converter outside the vehicle. Both of them have to connect to the distribution network by supply equipment of EV which contains: socket outlet, plug in the outlet, secondary cable, EV connector, EV inlet, protection system, and demand side management as shown in Figure 2-10.

Researchers classify the EV charging platform into private or business and ownership platform to cover the variety of owners of EVs requirement . The charging station can be offered either publicly or privately; the EV connects as a single vehicle in privet station or fleet of vehicles in a public station [190]. Figure 2-9 shows the hierarchy management structure of connecting EV to the microgrid

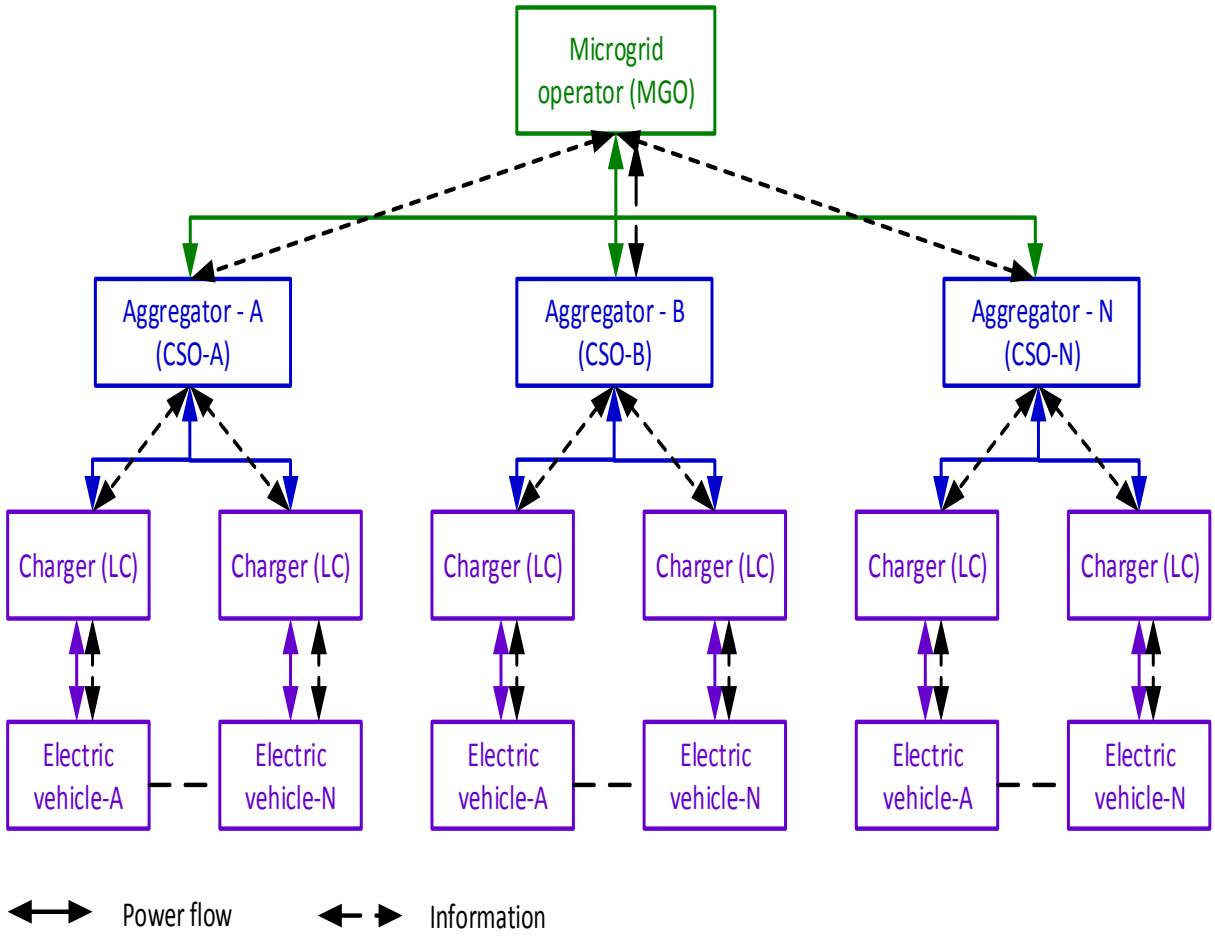

Figure 2-9: EV management structure

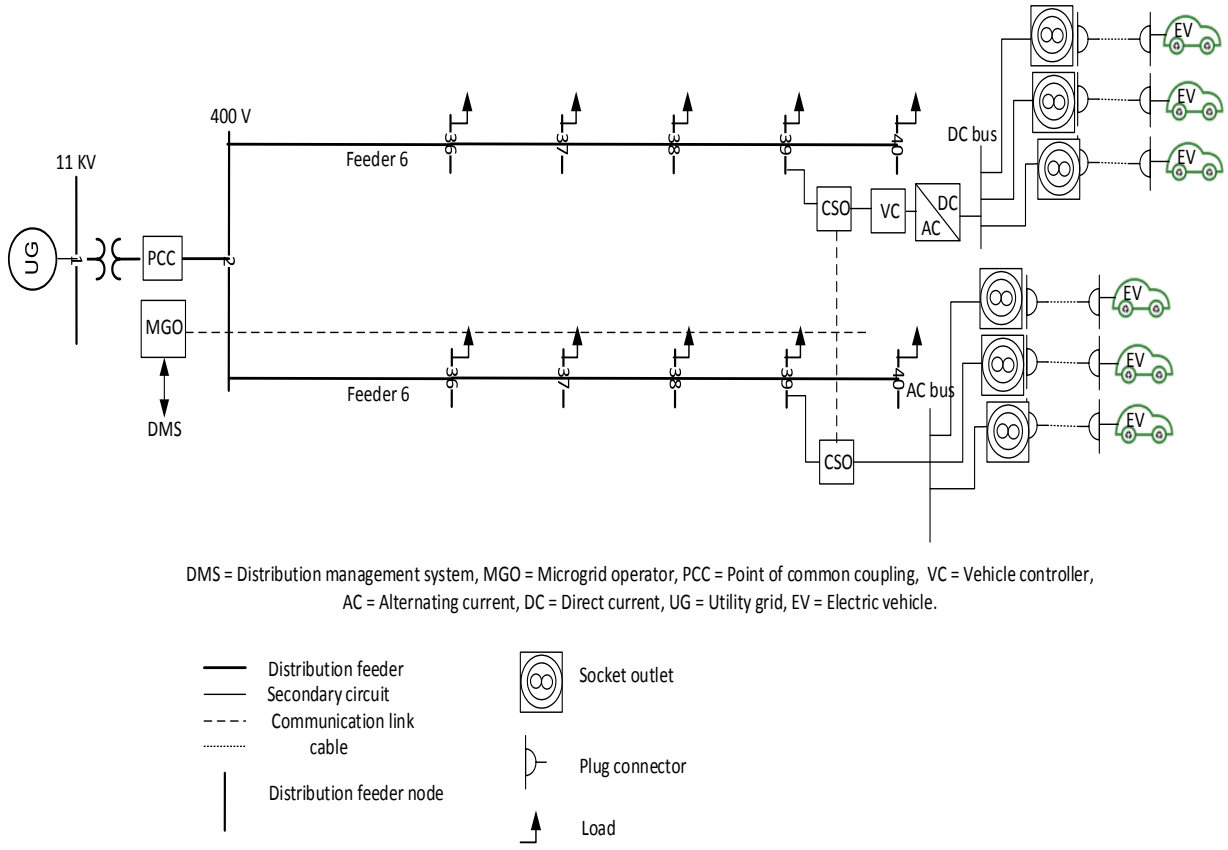

Figure 2-10: Electric vehicle connection platform

2.9 Energy Storage Technologies

Energy storages are devices that store electrical energy from the system at low demand time or low unit cost of generation. They discharge their energy to the network at high demand time or high unit cost of generation to participate actively with the distributed generator supply or to keep the system secure from any fluctuation in voltage or frequency [131], [191]. Since the energy is the daunting prospect of storage in shape, the energy converts to another shape such as kinetic, electrochemical, and electromagnetic energies. Energy storage could be classified into three kinds according to discharge and charge capacity; the long term is for many hours or days, the medium term for minutes or hours, and short term for seconds or minutes. Some examples of stored energy are:

1- Pumped hydro and compressed air, which is long-term storage energy system. They store energy as kinetic energy.
2- Fuel cells and batteries, which are medium term storage energy elements. They store energy as electrochemical energy. The battery is the essential part of the EV. It releases the energy to run the EV motor or to synergize the grid by discharging at low production time.
3- Flywheel, super magnetic, and supercapacitors energy storages work as short term, flywheel stores energy as kinetic energy, super magnetic stores energy as electromagnetic energy, and supercapacitors stores energy as electrostatic energy [131].

2.10 Power Electronic Interface

The bidirectional converter has been optional for many applications in power system, such as EVs, and connection of storage system and renewable energy to the microgrid network. It is used to improve the system performance, reduce the cost, and enhance efficiency.

The power flow from the network to the storage systems (batteries or capacitors) during the charging period. Storage systems should boost the power to the grid during fluctuation or instability period. Therefore, the bidirectional converter has been used to transfer power between sources.

Most of the bidirectional converters are classified into voltage source or current source converter. It depends on the energy storage system as shown in Figure 2-11. Bi-directional energy flow is achieved by a unidirectional semiconductor switch such as MOSFET or IGBT connected in parallel with a diode.

Bidirectional converters are also classified into non-isolated and isolated converters depending on the construction to employ for different applications.

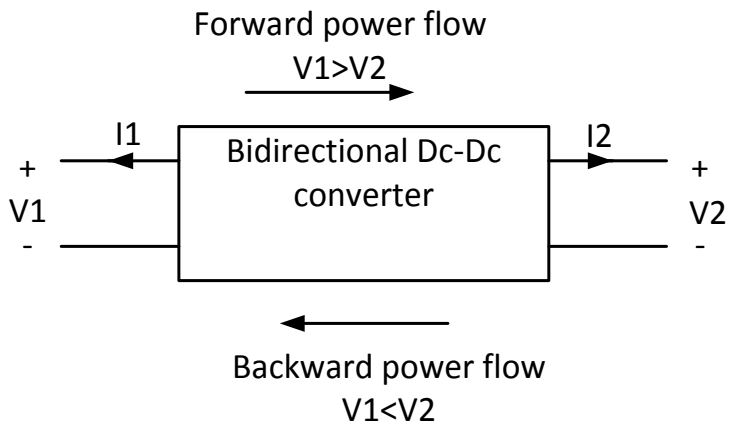

Figure 2-11: Bi-directional power flow

2.10.1 Non-isolated converter:

This converter is constructed without a transformer. Usually, a buck-boost type is used. The buck converter is used to step the voltage down. Meanwhile, the boost converter is used to step the voltage up. The transformerless converter is considered to improve efficiency, cost, weight, and size for the high-power applications. Single phase or multi-phase is presented by the literature according to the power density application. The advantages of the multi-phase converter that is implemented by the device are low current stress, minimising inductance and capacitance on both sides of converter for acceptable voltage ripple, and increasing efficiency [192]–[200].

2.10.2 Isolated converter

Many specifications have been achieved according to the power supply industrial applications such as isolation between supply and demand, high efficiency with low total harmonics, and

high power density to reduce the size and weight of the equipment. However, these devices have many complexities to achieve a design feature and prevent electromagnetic interference [201], [202, Ch. 14].

Isolated bi-directional DC-DC converter, which has been used through the last years by researchers, has a structure as shown in Figure 2-12. The converter works on both sides; the incoming DC voltage is converted to AC waveform then it is transferred to the secondary side through the transformer. The AC waveform is reconverted to the DC waveform again at a different step, which is the output of the converter [203], [204]. Even though the transformer can isolate two voltage sources, it works as impedance matching between them; nevertheless, it adds additional cost and losses.

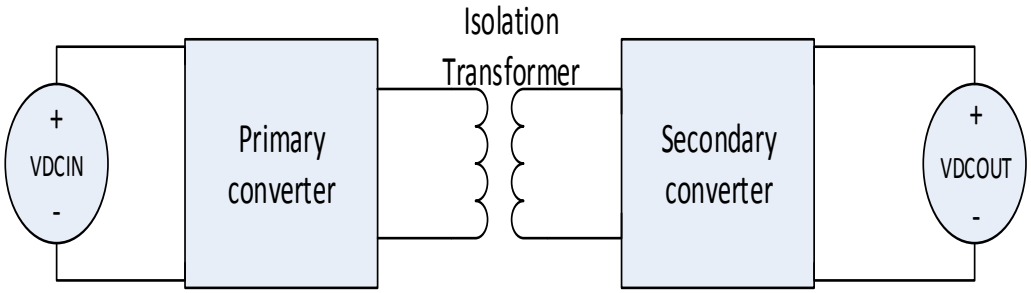

Figure 2-12: Bi-directional topology

Researchers after DeDoncker et.al [205], who patented first dual active bridge (DAB) converter, have identified different topologies for the converter depending on the converter rating, such as the isolated converters of clamped Bi-directional flyback converter; current fed push-pull converter, and bridge converter (Half and full bridge) [206]–[211].

2.10.3 Fly back converter:

A researcher suggested connecting two converters back to back to make them work in the bidirectional mode [212]. MOS1 and MOS2 modulation achieve the bidirectional power flow.

The flyback converter that has a simple topology with fewer components without any output filter supplies a different voltage level by multi-winding transformer [213]. However, the high peak current due to the discontinuous current through this circuit reduces the efficiency. The converter works without any filter. Therefore, the whole energy is stored in the huge transformer magnetisation winding and increases the switching rating for this circuit. Very low leakage inductance design requires transferring energy effectively through transformer [201], [214]. This converter is used for low power applications (less than 100 W) with the high output voltage. The converter is mostly used in discontinuous mode [202, Sec. 14.2.2]

2.10.4 Push-pull converter:

The converter could be bidirectional by connecting a secondary converter to the secondary side of the transformer, which is called hybrid converter. This converter has different primary and secondary voltages [215].

The voltage of primary winding swings between +Vs to –Vs during the complementary switching, the primary voltage is transferred to the output through the secondary transformer and diodes [201], [202, Sec. 14.2.4].

The input current to the transformer, which has grown as a result of the non-ideal modulation signal, could be regulated by the inductor to prevent converter failure due to transformer core saturation as a result of overvoltage event. This saturation is called staircase [201], [216, Sec. 2.2]. However, double input dc voltage should be blocked during each switching cycle. The high blocking voltage makes this converter too expensive. This converter is used in different low voltage applications (less than 400 V) and power levels such as power factor correction, inverter battery charger, supercapacitor connection, fuel cell connected to batteries and hybrid EV [217], [218].

2.10.5 Bridge converter

This converter is classified according to the number of legs to the half bridge (one leg) or full bridge converter (two legs for single phase bridge and three legs for three phase bridge). Each leg operates in complementary switch signal with small delay time to prevent working at the same time. Half-bridge converter is popular for the Isolated DC-DC converter.

The main operation of this converter is to convert DC voltage to AC voltage using the first part (primary side of the transformer) and then to the DC voltage using another part (secondary side of the transformer). This configuration makes the converter work in bidirectional mode at the symmetry construction. Each part can work as a bidirectional power flow from AC to DC or vice versa [219], [220]. The current flow between these two parts can be limited by the inductor, which is connected to them.

Half-bridge converter has less switching than full bridge converter. However, it needs a bulky capacitor to manage a large ripple current amount, which is produced on the AC side. This capacitor can also be used to reduce the oscillation in the power flow. This converter is used for low power application (less than 2 kW) with low voltage level (less than 400V) [202, Sec. 14.2.5,14.2.6], [205], [216, Sec. 3.2]. The full bridge converter is more popular than half bridge converter because the current flow is distributed through more than one leg. Two legs and three legs converters have 180 and 120 phase shift between legs that help to reduce AC component for the power flow through the transformer.

The more the legs, the smaller DC capacitor used, and the less transformed core material is used because the summation of flux is reduced due to the offset between legs. However, the switch modulation complexity increases and the thermal problem appears with the legs increase [221], [222]. Full bridge converter has more flexibility in power rating than others. Thus, the voltage level reaches up to 1KV with high power rating up to 50KW [223].

The converter topology selection depends on the power rating. Fly back, and the push-pull converters are used for rated power up to 100 W and 2 KW respectively. Meanwhile, bridge converter is more appropriate for high power rating. Three phase full bridge converter has more complex construction and switching control than the two-phase full bridge converter. In addition, high cost and heat management are obtained due to the less transformer core.

2.10.6 Multi-Level inverter topology

The multi-level inverter is one of the solutions for high power and high voltage conversion system including a hybrid electric vehicle. The most attractive benefits of the multilevel inverter are generating an output voltage and drawing input current with low distortion in addition to operating with lower switching frequency [224]. There are many existing topologies for multi-level converter; the optimum solution has chosen the topology with less harmonic distortion, and less electromagnetic interface. A modified Cascade H-Bridge Converter has been chosen for this study, due to using a low number of components with separate DC resources. One of them is the battery that connects to the three-leg inverter (one leg for each phase) while the other is a supercapacitor that is connected in series to the battery through H-bridge cascade converter, as shown in Figure 2-13. The modified H-bridge cascade converter works with DC resources separately to be easily accommodated. This topology uses single battery bank and separated supercapacitors that connect in series with the battery for each phase. The supercapacitors work as an active filter.

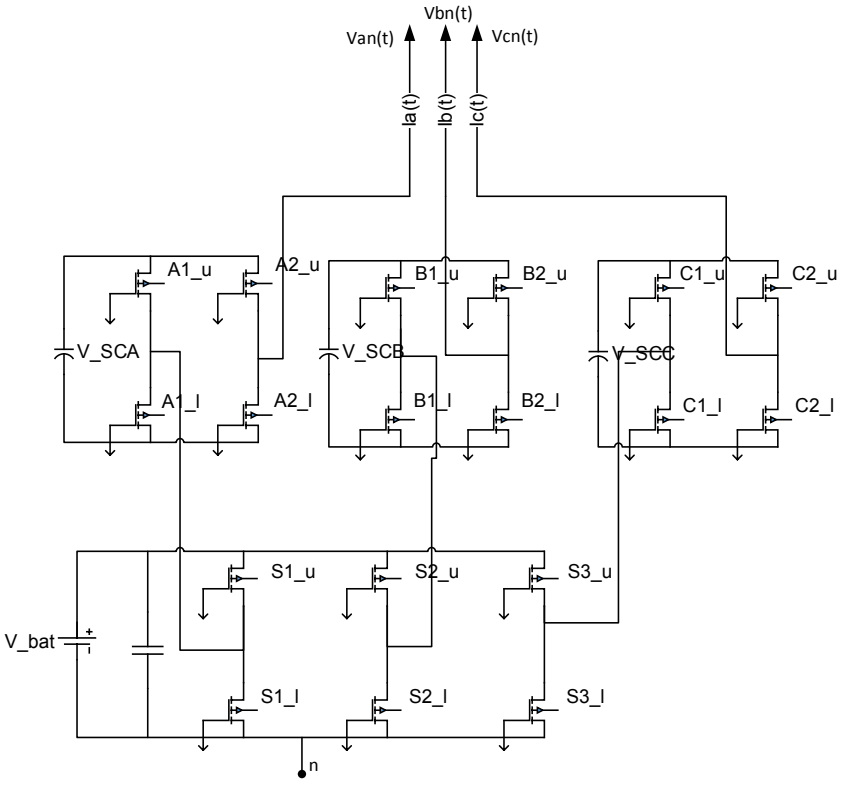

Figure 2-13: Three-phase H-bridge cascade multi-level convert

2.10.7 Other topologies

Power factor correction converters or improved power quality converters are other topologies, which could be used to enhance power quality for a system in both sides; line and load. In addition, it provides a reduction of harmonic distortion, regulating dc voltage, and achieves higher efficiency. Even though, the sudden change of load or source voltage fluctuation occurs. These topologies could be classified according to the power transfer to the following:

1- AC-DC-DC using voltage source inverter, and a half or full wave bridge DC-DC converter.
2- AC-AC-DC using cyclo-converter or matrix converter, and a half or full wave DC-DC converter [219], [220], [225].

2.11 Dynamic Model for Bidirectional DC-DC Converter

A dynamic model is a group of mathematical equations to study and describe the behaviour and the relationship between the output and the input of the system. The model is essential to achieve high-performance of the system. Researchers classified the behaviour of dynamic systems into two groups: state-space averaging technique model and fundamental power flow technique model.

2.11.1 State space averaging technique

This approximation technique is used widely by researchers. It depends on the time signal continuous separation frequency analysis from switching frequency analysis for high switching frequency. Even though the original system is linear, the resulting system from this conversion is nonlinear. This technique is usually taken to represent energy storage component, though each one contributes a system one state space variable [201], [202, Sec. 5.13]. The mathematical representation of nonlinear or linear a model lends itself to several interpretations which aim to deriving models which are practical for systematic control design, as shown in the following.

$$\dot{x} = A(x)x + B(x)u \quad (2\text{-}1)$$

$$y = C(x)x + D(x)u \quad (2\text{-}2)$$

$$\dot{x} = A(x,p)x + B(x,p)u \quad (2\text{-}3)$$

$$y = C(x.p)x + D(x,p)u \quad (2\text{-}4)$$

$$\dot{x} = Ax + Bu \quad (2\text{-}5)$$

$$y = Cx + Du \quad (2\text{-}6)$$

$$\dot{x} = A(p)x + B(p)u \quad (2\text{-}7)$$

$$y = C(p)x + D(p)u \quad (2\text{-}8)$$

A taxonomy of dynamics models [226] is presented in Figure 2-14. The quasi-liner time-varying (QLTV) represents the mathematical description of nonlinear dynamic model which classifies into either quasi-linear time-invariant (QLTI) as represented in equations 2-1 and 2-2 or quasi-linear parameter-varying (QLPV) as represented in equations 2-3 and 2-4. On the other hand, the mathematical description of linear dynamic model is represented as a linear time varying which classifies into linear time-invariant (LTI) as in equations 2-5 and 2-6 or linear parameter varying (LPV) as represented in equations 2-7 and 2-8, where $u = u(t)$, $x(t), and\ y(t) \in R^m, R^n, and\ R^q$ are the vector of inputs, the vector of the states, and the vector of outputs respectively and the $A, B, C, and\ D \in R^{n\times n}, R^{n\times m}, R^{n\times q}, and\ R^{n\times n}$ are matrices with constant real entries. The QLPV and LPV is special case of the QLTV and LTV respectively where the entries of matrices $A, B, C, and\ D$ are no longer constant as in the QLTI and LTI respectively [226].

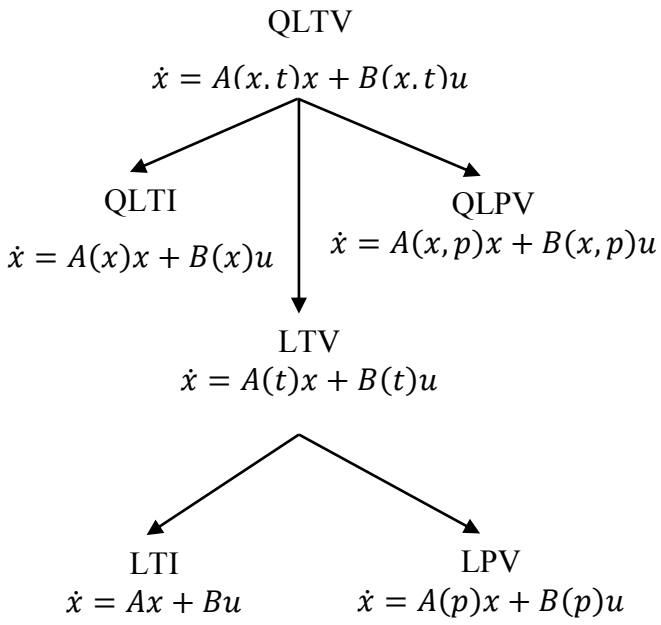

Figure 2-14: General dynamics of a model and their relationships

The difficulty and uncertainty for state space technique lead to the unjustified derivation of a formula. For instance, there is more than one representation for the same model of de donker et al. and krismer et al. The first one derived first order equation to the isolated bi-directional dc-dc converter. Meanwhile, the second one derived fifth order equation [205], [227].

2.11.2 Fundamental average technique model

This technique depends on using a dynamic equation based on a fundamental power expression of a converter [212]. Each bridge for bidirectional converter represents a square voltage source (V_{pri} and V_{sec}). The inductor represents a link between them. It seems that the fundamental component of the square wave dominates, and the high order harmonic can be ignored. Therefore, it is possible to convert the square wave source into sinusoidal one. This approximation makes the system like two synchronous machines connected by a transmission line. The main expression of AC phase theory represented as follows:

$$P_{AC} = \frac{V_1 V_2 sin\delta}{\omega L} \quad 2\text{-}9$$

The converter is assumed to be lossless and operated in steady state; it could be expressed as the output voltage in term of the static RMS value in the time domain expression as shown in the equations below:

$$V_1(t) = \frac{V_{1_{pk}}(t)}{\sqrt{2}} \sin(\omega t) \quad 2\text{-}10$$

$$V_2(t) = \frac{V_{2_{pk}}(t)}{\sqrt{2}} \sin(\omega t + \delta) \quad 2\text{-}11$$

$$P_{DC}(t) = \frac{V_1(t) V_2(t) sin\delta}{\omega L} \quad 2\text{-}12$$

$$P_{DC}(t) = V_{out}(t) V_{in}(t) \quad 2\text{-}13$$

$$\therefore i_{out}(t) = \frac{\sqrt{2} V_1(t) sin\delta}{\omega L} \quad 2\text{-}14$$

2.12 Modulation

Various techniques for trigger modulation are proposed in the literature, such as PWM and PSSW [201], [202, Ch. 6], [228, Sec. 5.5].

2.12.1 Pulse width modulation technique

Many kinds of literature used several types of pulse width modulation techniques for bridge converter modulation to improve the output of the converter such as power factor correction or low harmonic generation. Hysteresis-band PWM control, synchronised carrier modulation, sinusoidal PWM, and space vector PWM are developed throughout the literature. These techniques mainly depend on the comparison between high-frequency triangular waveform with fundamental low-frequency waveform signal; they generate a train of pulses for high-frequency narrow pulses variation in either duty cycle or time range.

In principle, all modulation schemes aim to create the same fundamental volt-second average trains of switched pulses as a target reference waveform at any instant. Identifying which switch on times to great the desired output voltage or current is a primary objective of any PWM scheme whereas determining the effective way of arranging the switching process to minimise the waveform ripple, harmonic effects, the switching losses are classified as the secondary objective of the any PWM scheme. Many researchers have been published wealth material relating to PWM to find useful converter switch ON times based on switching devices at the point of intersection of the reference and the carrier interval. For an instant, the difference between the naturally sampled PWM and the regular sampled PWM for fixed frequency modulation systems are the switching activated either at the intersection of a high-frequency carrier and a target reference waveform or a regularly sampled reference waveform. Researchers stated various development of the PWM for fixed frequency open loop PWM

based on switch pulse width determination, switched pulse position within a carrier interval, and switched pulse sequence within and across carrier intervals [229, Sec. 3.1].

Hysteresis band and synchronised carrier PWM depend on the variable time range technique. Meanwhile, SPWM and SVPWM techniques rely on the variation of the duty cycle [201], [202, Sec. 6.8], [228, Sec. 5.5].

Over multi advantages of PWM, the SPWM and SVPWM switching modulation strategy have been commonly implemented in power electronic applications. The SVPWM generates a reference waveform based on the transition between predefined actives and zeroes switching digital states at different switching period for every switching states rotated in a hexagon diagram as shown in two level hexagon diagram of Figure 2-15. The reference voltage of the SVPWM and the reference of each section can be determined by.

$$\overrightarrow{V_{ref}} = \frac{2}{3}\left(V_a e^{J0} + V_b e^{J2\pi/3} + V_c e^{J4\pi/33}\right) \quad 2\text{-}15$$

$$\overrightarrow{V_k} = \frac{2}{3}\left(V_{dc} e^{J(k-1)\pi/3}\right) \; where \; k = 1, 2, 3, 4, 5, and \; 6 \quad 2\text{-}16$$

On the other hand, the SPWM generates a reference waveform based on a comparison between the triangle carrier waveform with a sinusoidal waveform of required fundamental frequency whereas the relative levels of the two signals determine pulse widths at angular reference position to switch devices of the converter as shown in Figure 2-16. The SVPWM generates less harmonic distortion with proper switching pattern selection, less switching power losses due to a suitable number of switching, and more DC bus utilisation than SPWM. Therefore, many researchers prefer using SVPWM technique according to significant merits of it over its counterparts in terms of easy implementation, maximum transfer ratio and high performance [230]–[238]

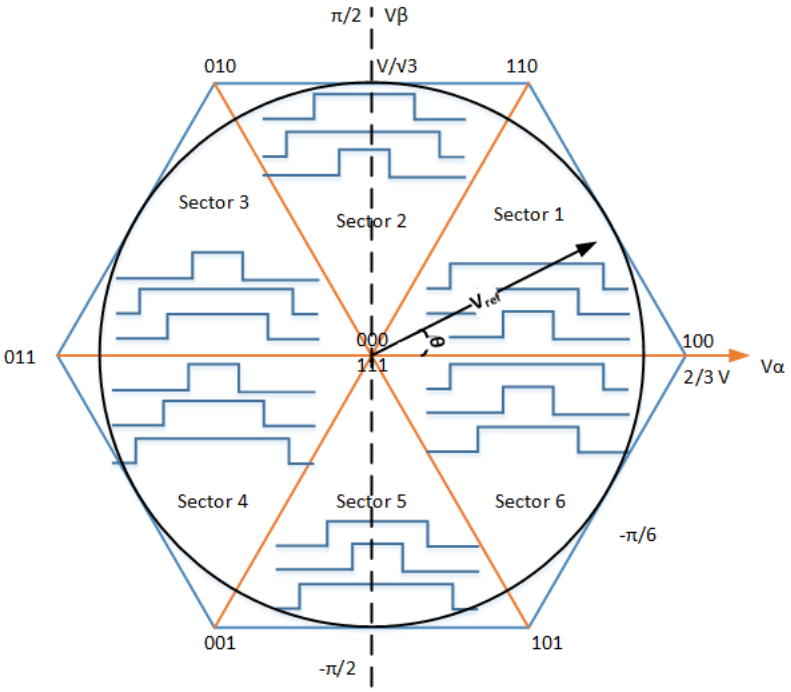

Figure 2-15: Two level rotating reference vector switching states of SVPWM

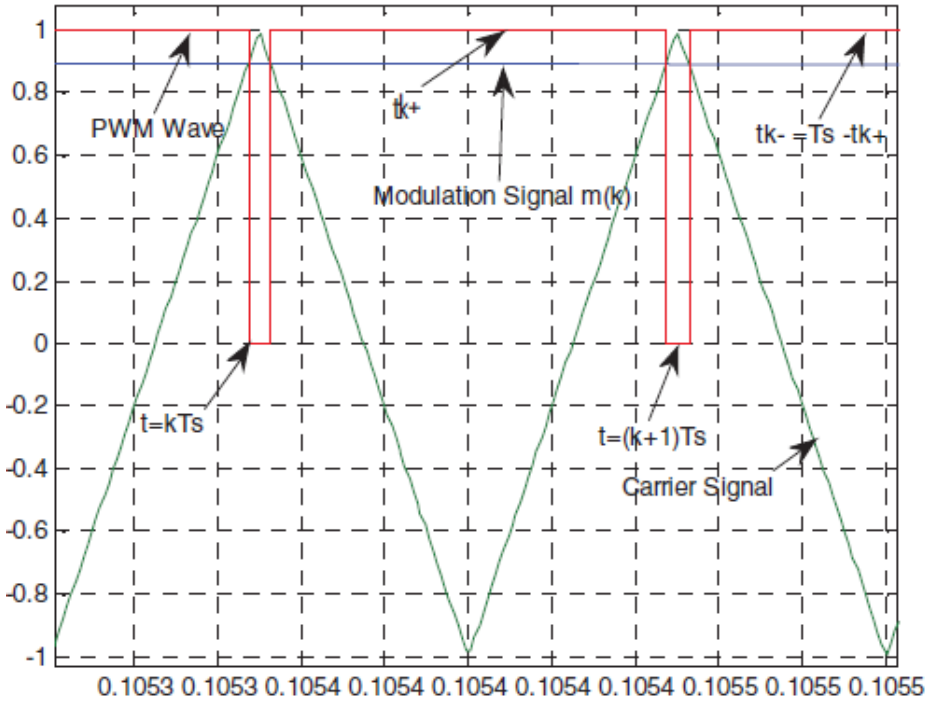

Figure 2-16: Two level carrier based SPWM [239]

2.12.2 Phase shifted square wave (PSSW)

This modulation depends on generating pulses with fixed width. The output for this modulation is either two steps or three steps depending on the phase shift between the two switching modulations. This technique works with high-frequency modulation. Therefore only high-frequency harmonic appears on the output voltage [240], [241].

2.13 Control Strategies

This part of the literature review is related to work that has done in chapter six relating to control the proposed inverter to control charging and discharging multiple energy resources of EV whereas there is different model applied to operate the EVs and each mode has different parameters of the controller. Therefore, this section presents the other researchers work and highlight the proposed strategy to control the inverter.

2.13.1 Current controller

The purpose of the current controller is to tackle the output current for the converter to compact the reference current with specific characteristics such as:

- Generate the reference waveform minimum error.
- Maintain the harmonic distortion as low as possible, and
- Provide a waveform with acceptable transient performance.

The popular current control methods for the converter are:

2.13.1.1 Linear regulation controller

This kind of controller depends mainly on PWM techniques; it tackles the current, using a PI controller. The general scheme is shown in Figure 2-17. This controller operates on constant switching frequency. However, PI controller has some difficulty in tackling a steady state error for the reference. Therefore, the noise is still affecting the current signal. In addition to the system could be slow to get the set point and perturbation response [242], [243], [244, p. 35,36].

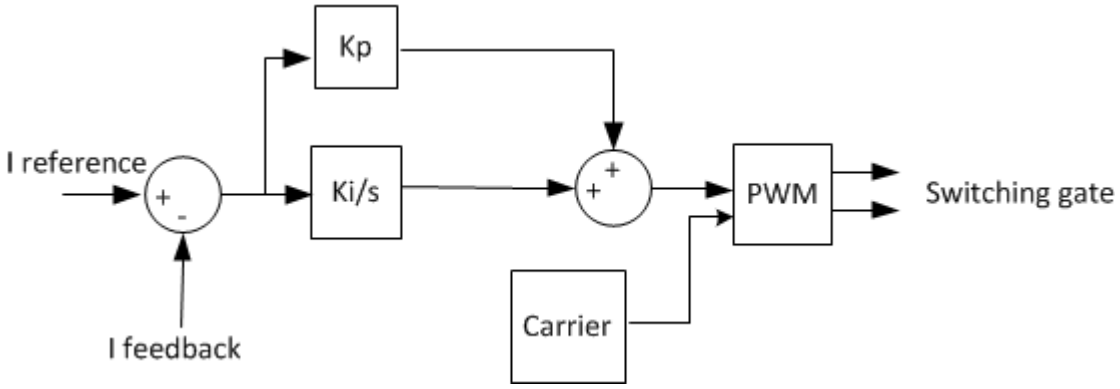

Figure 2-17: Carriers based linear regulation control method

2.13.1.2 Hysteresis controller

The error, which is the difference between reference and output current in this approach, is controlled in hysteresis loop (upper and lower limit). The general scheme is shown in Figure 2-18. During the switching on and off according to the hysteresis limit, the ripple appears on the output waveform due to the variation of the switching signal in addition to increasing THD and switching losses. Some researchers suggested a three-level hysteresis control minimise these losses. Nevertheless, acceptable transient performance could be achieved by this method with less real time calculation [201], [244, p. 37], [245].

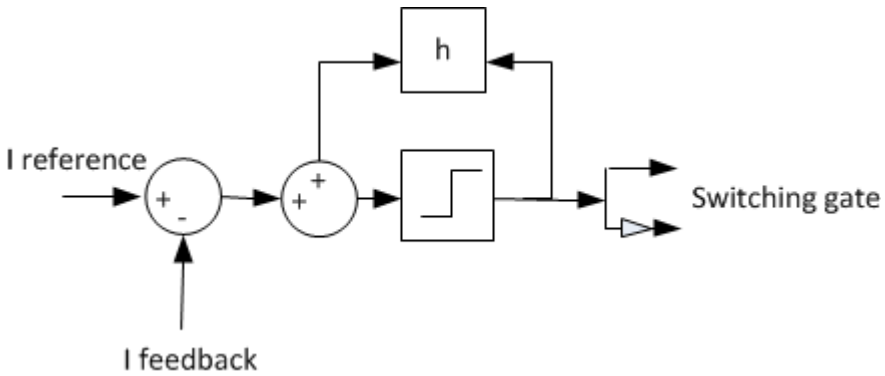

Figure 2-18: Hysteresis control method (Bang-Bang control strategy)

2.13.1.3 Peak current controller

This kind of controller is popular with a DC-DC converter which works with a constant switching frequency. The general scheme is shown in Figure 2-19. The principle depends on comparing a slope inductor current with a certain reference value that makes the switch turn-

on until the error between the reference and inductor current reaches zero. This method could be unstable at a certain time, especially if the duty ratio exceeds 0.5. Therefore triangular signal subtracted from the reference signal is to increase the stability of the controller in addition to eliminating sub-harmonic oscillations [244], [246], [247].

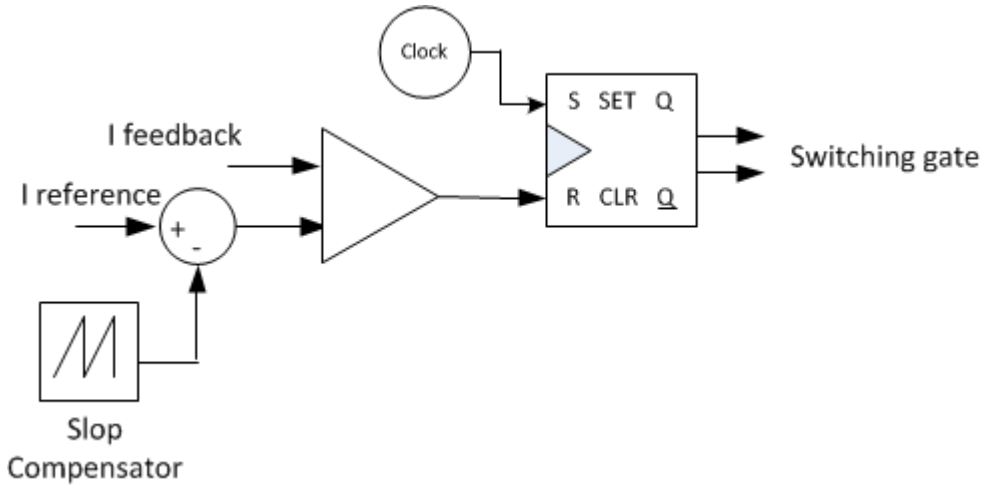

Figure 2-19: Peak current control method

2.13.1.4 Proportional resonant current controller

This controller is common in the DC-DC controller rather than DC-AC because the steady state error harmonic and noise appear in the output sinusoidal current signal. The general scheme is shown in Figure 2-20 [248]. It is revealed that some difficulty exists in implementing this controller on the inverter (DC-AC) because the quality factor cannot be achieved. This controller produces infinity gain which gives infinite quality factor [244, Sec. 2.4.4], [249, Sec. 1.2.7].

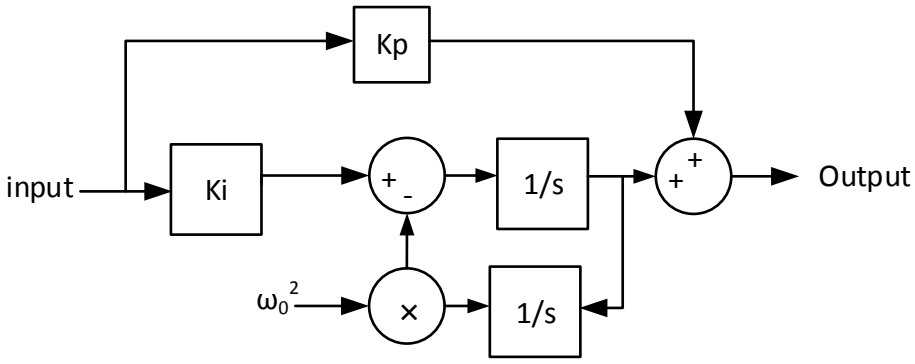

Figure 2-20: Proportional resonant current control method

2.13.2 Synchronous rotating frame controller

This method is popular in the three-phase inverter. The basic principle depends on transforming three phase waveforms on the stator winding (a, b, and c axis time variant) into two phase

stationary axis on the rotor winding (d, and q axis time invariant). The vector transformations and general control scheme are shown in Figure 2-21 and

Figure 2-22 respectively. The transformation depends mainly on the reference frame. They are implementing the Park's transformation or Clarke's transformation which are mathematical tools used in transforming a, b, and c in the stationary frame to the alpha and beta in the stationary orthogonal axis frame then to d and q axis in the rotor axis frame relative to the angular position or vice versa [244, Ch. 4], [250], [251, Ch. 3]. The Clark's transformation, which is an equation to convert the three phase components to α and β components, and the Park's transformation, which is an equation to convert the stationary α and β components to rotating d and q components, can be calculated by.

$$\begin{bmatrix} X_\alpha \\ X_\beta \end{bmatrix} = \begin{bmatrix} 1 & -1/2 & -1/2 \\ 0 & \sqrt{3}/2 & -\sqrt{3}/2 \end{bmatrix} \begin{bmatrix} U \\ V \\ W \end{bmatrix} \quad 2\text{-}17$$

$$\begin{bmatrix} X_d \\ X_q \end{bmatrix} = \begin{bmatrix} cos(wt) & sin(wt) \\ -sin(wt) & cos(wt) \end{bmatrix} \begin{bmatrix} X_\alpha \\ X_\beta \end{bmatrix} \quad 2\text{-}18$$

The Synchronous rotating frame controller makes the proportional resonant controller suitable to be implemented on the three-phase system because the PI controller can tackle the steady state and phase errors for the time-invariant signal. Some researchers apply the PI controller with the stationary reference frame; others apply fuzzy controller; the transfer function for PI controller is defined as [244, Sec. 4.4], [252]–[254]:

$$G_{P-R}^{\alpha\beta}(s) = \begin{bmatrix} K_p + K_i \times \frac{s}{s^2+\omega^2} & 0 \\ 0 & K_p + K_i \times \frac{s}{s^2+\omega^2} \end{bmatrix} \quad 2\text{-}19$$

$$G_{HC}(s) = \sum_{h=3,5,7,\dots} K_i \times \frac{s}{s^2 + (\omega \times h)^2} \quad 2\text{-}20$$

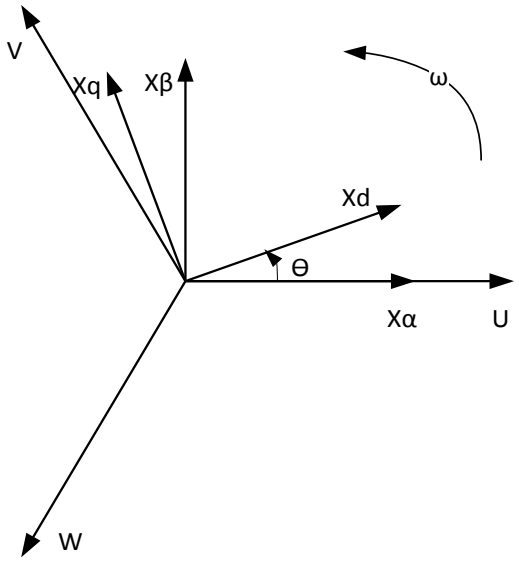

Figure 2-21: Vector transformations

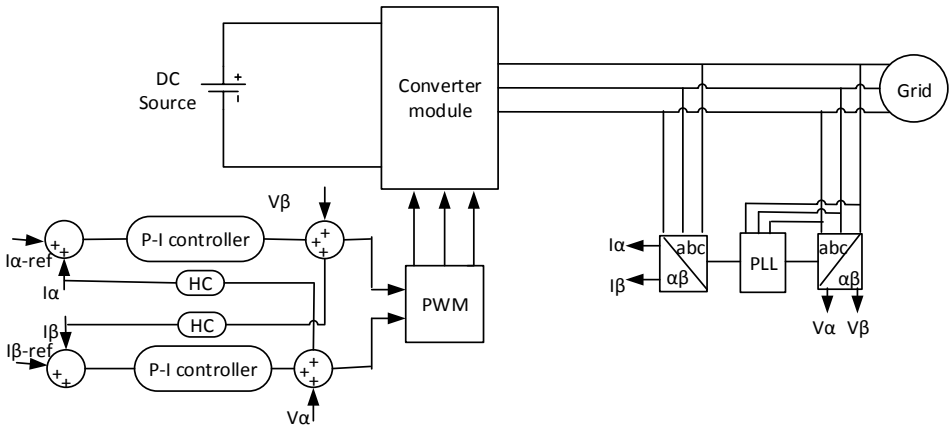

Figure 2-22: Synchronous rotating frame control method

2.13.3 Rotating reference frame controller

This approach depends on transferring the voltage and current measurement for the three-phase system into two orthogonal stationary components (α-β) via Clark's transformation then transferring it again to the two synchronous rotating frame components (d-q) via Park's transformation. The d-q frame rotates synchronously with the grid frequency. The general scheme is shown in Figure 2-23.

The main advantage for this transformation is in producing time-invariant variables. The controller based on this transformation has a fast dynamic response in minimising steady state and phase error.

By using this controller, it is possible to control the voltage and frequency separately by changing amplitude and phase signal. Flexibility in tuning PI controller with the transfer function is shown as

$$G_{PI}^{dq}(s) = \begin{bmatrix} K_{pi} + \dfrac{K_{ii}}{s} & 0 \\ 0 & K_{pj} + \dfrac{K_{ij}}{s} \end{bmatrix} \qquad 2\text{-}21$$

This method has facilitated the use of controllers in the DC-DC converter [253], [255].

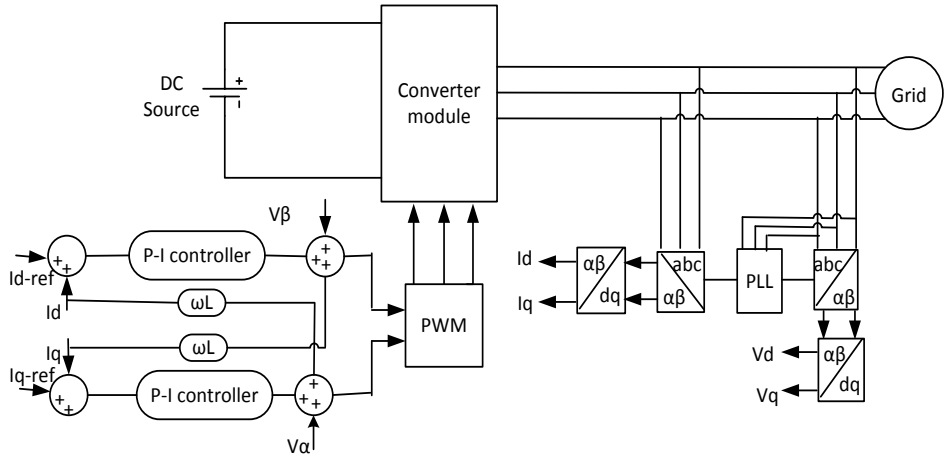

Figure 2-23: Rotating reference frame control method

2.13.4 Synchronverter control technique

This control depends mainly on the synchronous generator theory, which is divided into two parts: power part and electronics part, as shown in Figure 2-25 (A and B respectively) whereas Figure 2-24 shows the structure of idealised three phase synchronous generator [256]. The power section includes the inverter, filters, and a circuit breaker, which connects the converter to the grid. Meanwhile, the electronic part depends on round rotor synchronous generator theory as shown in the following:

$$\begin{bmatrix} \emptyset_a \\ \emptyset_b \\ \emptyset_c \end{bmatrix} = L_s \begin{bmatrix} i_a \\ i_b \\ i_c \end{bmatrix} + M_f i_f \begin{bmatrix} \cos(\theta) \\ \cos(\theta - \frac{2\pi}{3}) \\ \cos(\theta - \frac{4\pi}{3}) \end{bmatrix} \quad 2\text{-}22$$

$$\emptyset_f = L_f i_f + M_f \begin{bmatrix} i_a \times \cos(\theta) \\ i_b \times \cos(\theta - \frac{2\pi}{3}) \\ i_c \times \cos(\theta - \frac{4\pi}{3}) \end{bmatrix} \quad 2\text{-}23$$

$$\begin{bmatrix} V_a \\ V_b \\ V_c \end{bmatrix} = -R_s \begin{bmatrix} i_a \\ i_b \\ i_c \end{bmatrix} - L_s \frac{d}{dt} \begin{bmatrix} i_a \\ i_b \\ i_c \end{bmatrix} + \begin{bmatrix} e_a \\ e_b \\ e_c \end{bmatrix} \quad 2\text{-}24$$

$$\begin{bmatrix} e_a \\ e_b \\ e_c \end{bmatrix} = M_f i_f \dot{\theta} \begin{bmatrix} \sin(\theta) \\ \sin(\theta - \frac{2\pi}{3}) \\ \sin(\theta - \frac{4\pi}{3}) \end{bmatrix} - M_f \frac{d_{i_f}}{dt} \begin{bmatrix} \cos(\theta) \\ \cos(\theta - \frac{2\pi}{3}) \\ \cos(\theta - \frac{4\pi}{3}) \end{bmatrix} \quad 2\text{-}25$$

$$\ddot{\theta} = \frac{1}{J}(T_m - T_e - D_p \dot{\theta_g}) \quad 2\text{-}26$$

$$\begin{bmatrix} P_a \\ P_b \\ P_c \end{bmatrix} = \dot{\theta} M_f i_f \begin{bmatrix} i_a \\ i_b \\ i_c \end{bmatrix} \begin{bmatrix} \sin(\theta) \\ \sin(\theta - \frac{2\pi}{3}) \\ \sin(\theta - \frac{4\pi}{3}) \end{bmatrix} \quad 2\text{-}27$$

$$\begin{bmatrix} Q_a \\ Q_b \\ Q_c \end{bmatrix} = -\dot{\theta} M_f i_f \begin{bmatrix} i_a \\ i_b \\ i_c \end{bmatrix} \begin{bmatrix} \cos(\theta) \\ \cos(\theta - \frac{2\pi}{3}) \\ \cos(\theta - \frac{4\pi}{3}) \end{bmatrix} \quad 2\text{-}28$$

$$T_e = \frac{P}{\dot{\theta}} \quad 2\text{-}29$$

The synchronous machine contains two parts separated by an air gap. The outer part is the stator which contains three windings distributed on the three axes A, B, and C. There is a spatial displacement of 120 degrees between each two adjacent windings. The winding has resistance (R), self-inductance (L), and mutual inductance (M). The inner part is the rotor, which has

direct and quadrature axes. The rotor has a DC field winding on the direct axis. The field winding has a resistance (R_f), self-inductance (l_f), and mutual inductance (M_f) [256], [257].

Synchronverter control technique that mimics synchronous generator has two parts; active power and reactive power control depending on the equation of synchronous generator which is a core for the Synchronverter technique. The active power is controlled by frequency droop control loop while the reactive power is controlled by voltage droop control loop as shown in Figure 2-25.

The frequency control droop loop works by comparing angular velocity ($\dot{\theta}$) with the angular reference frequency, which is normally equal to the nominal angular frequency of the system. It is multiplied by mechanical and frequency droop coefficient (D_p), then comparing the difference with mechanical torque (T_e). The phase angle (θ) is created from multiplying angular velocity ($\dot{\theta}$) by the time. The voltage droop controller loop works similar as the frequency controller droop loop. The field excitation is regulated to the control signal (Q) using the droop coefficient (D_p) [257].

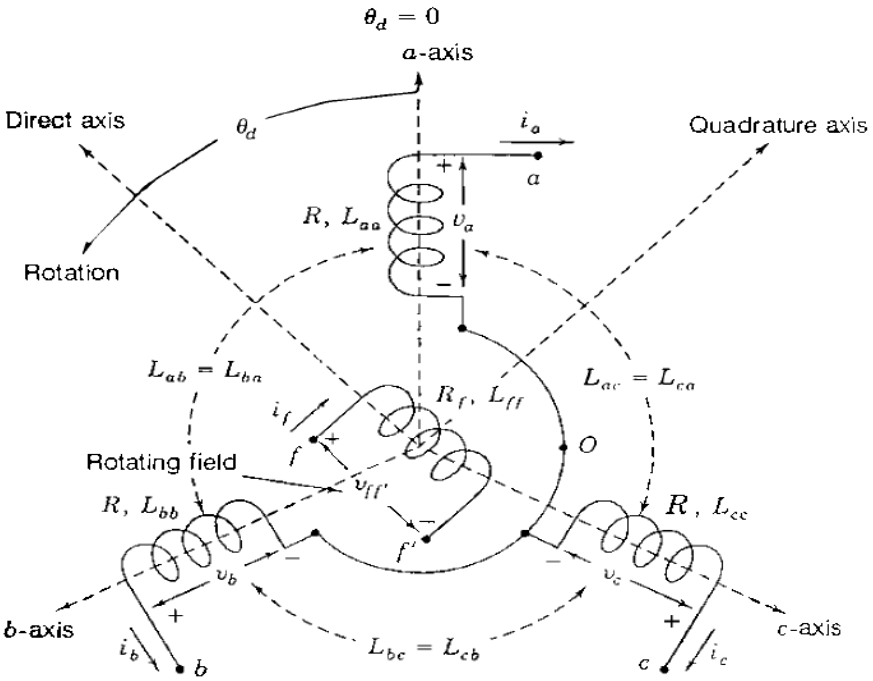

Figure 2-24: Idealised three phase synchronous generator [256]

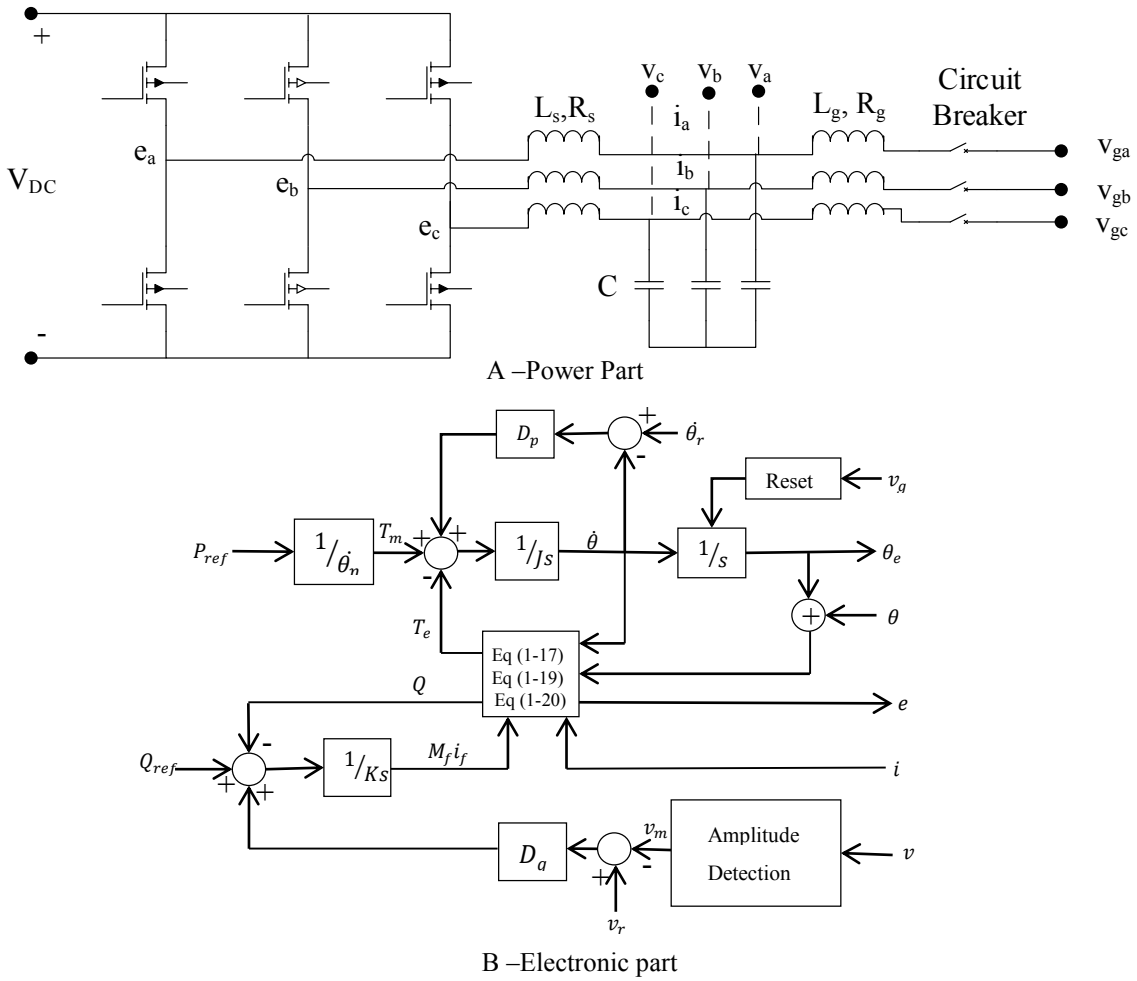

Figure 2-25: Synchronverter control scheme

2.13.5 Grid connected converters controller

The grid-connected converter control depends mainly on the control of DC voltage system and AC voltage system. AC system operation is classified into a connected mode or stand-alone mode. DC voltage could control the voltage variation during power fluctuation through two loops, an outer voltage loop and an inner current loop. The purpose of the outer loop is to achieve better regulation and stability while the purpose of the inner control loop is to achieve short settling time [258], [259, Sec. 9.3.2].

Grid controller can be classified into two types; scalar controller and vector controller. Both have advantages and disadvantages. The scalar controller is cheap well implemented, and simple. However, it is not applicable for controlling dynamic behaviour of the system because the scalar controller controls the magnitude of voltages and frequency instead of controlling the phase and magnitude of currents. On the other hand, the vector controller is better than the scalar controller due to accurate measurement, less steady state error, high performance, and stable control technique. However, the vector controller implementation is complex. [260]

2.13.5.1 Scalar control

The scalar control is described in Figure 2-26. This control has two layers which are an inner loop and outer loop. The inner loop is a current loop. Meanwhile, the outer loop is voltage loop. The outer loop provides a reference current to the inner current loop. The reference current comes from the DC voltage control and sinusoidal three-phase voltage waveform. Three individual current controllers are used to control the difference between the references and the measured current to feed a signal to the switching modulator (PWM). This control does not need delay time that improves the speed response of the system. The application is straightforward in using this method, which can be utilised in an analogue mode. However, constant change reference value is tackled due to inherent error [261], [262].

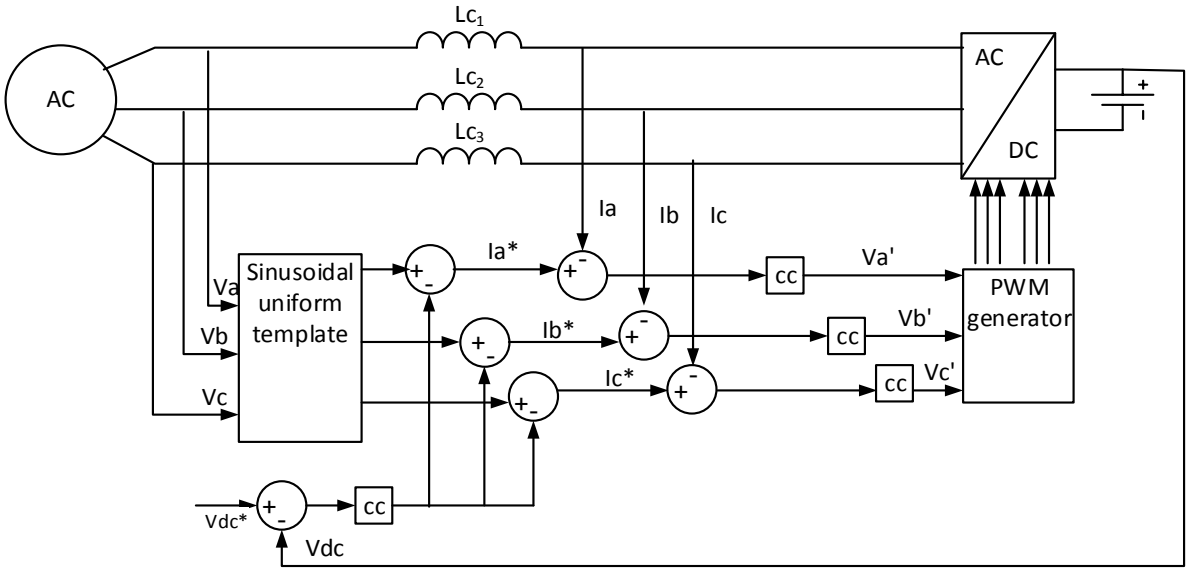

Figure 2-26: Scalar control scheme

2.13.5.2 Vector control

The vector control is described in Figure 2-27. Vector control is an enhancement of the characteristics of scalar control. This control depends mainly on the transformation between rotating a, b, and c reference frame to stationary d and q. The d and q axes can be referred to the active and reactive measurements respectively.

The voltage controller output, which is a comparison between the DC voltage and a reference voltage, is a direct reference current. Meanwhile, quadrature reference current comes from the point common coupling voltage controller, which is a control for a comparator between grid voltage and the reference voltage.

The result of the comparator between reference current and transformation grid current provide a signal to the switching modulation (PWM) through current controller after returning the signal to the rotating a, b, and c reference frame. This system is more complex than scalar control. However, this control is adequate to control active and reactive power and remove the steady state error [258], [263]–[265].

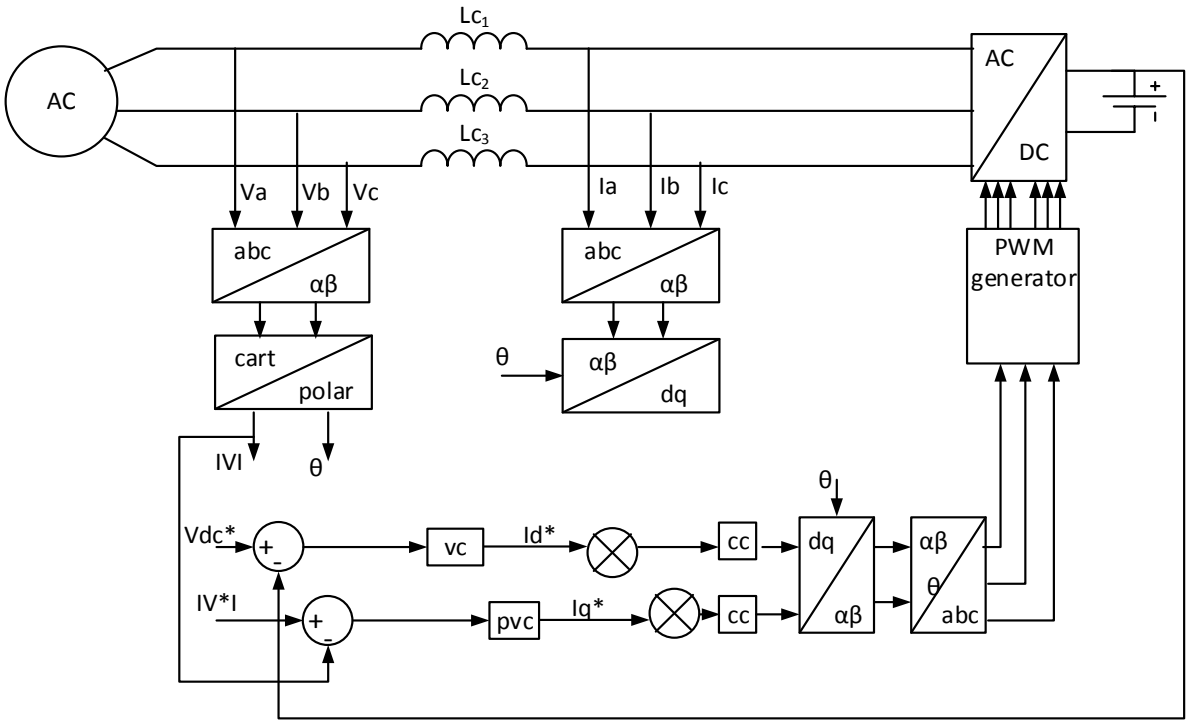

Figure 2-27: Vector control scheme

2.13.6 Droop controller

The power, which flows in a steady state network operation, is described in Figure 2-28 (A and B respectively) and can be calculated by.

$$P + jQ = EI^* = E(\frac{E - V\angle\delta}{Z\angle - \theta}) \quad 2\text{-}30$$

$$P + jQ = [\frac{E^2}{Z}cos\theta - \frac{EV}{Z}\cos(\theta + \delta)] + j[\frac{E^2}{Z}sin\theta - \frac{EV}{Z}\sin(\theta + \delta)] \quad 2\text{-}31$$

$$Z\angle\theta = R + jX \quad 2\text{-}32$$

$$P + jQ = \frac{E}{R^2 + X^2}\{[R(E - Vcos\delta) + XVsin\emptyset] - [RVsin\emptyset + X(E - Vcos\emptyset)]\} \quad 2\text{-}33$$

Assume that $X \gg R$, and δ is very small. Then R may be neglected and $sin\delta = \delta; cos\delta = 1$, therefore:

$$\delta \cong \frac{XP}{EV} \quad 2\text{-}34$$

$$E - V \cong \frac{XQ}{E} \quad 2\text{-}35$$

From the above equation, it is obvious that the power angle and voltage difference depend mainly on the active and reactive power respectively. The frequency and voltage of the grid could be controlled by adjusting the real power and the reactive power respectively, as shown in the following:

$$f - f_o = -K_p(P - P_o) \quad 2\text{-}36$$

$$E - E_o = -K_q(Q - Q_o) \quad 2\text{-}37$$

The droop control characteristics for these equations are shown in Figure 2-29 [244, p. 198], [266]–[268].

In low voltage cable, grid R is no longer neglected while X could be overlooked. In this case, active power and reactive power could be affected by the voltage and frequency respectively. R and X are represented in the mathematical model then active and reactive power could be modified by using transformation matrix and can be determined by[269].

$$\begin{bmatrix}\bar{P}\\ \bar{Q}\end{bmatrix} = T\begin{bmatrix}P\\ Q\end{bmatrix} = \begin{bmatrix}sin\theta & -cos\theta\\ cos\theta & sin\theta\end{bmatrix}\begin{bmatrix}P\\ Q\end{bmatrix} = \begin{bmatrix}\frac{X}{Z} & -\frac{R}{Z}\\ \frac{R}{Z} & \frac{X}{Z}\end{bmatrix}\begin{bmatrix}P\\ Q\end{bmatrix} \quad 2\text{-}38$$

Using Equations 2-34 and 2-35

$$sin\delta = \frac{Z\bar{P}}{EV} \quad 2\text{-}39$$

$$E - Vcos\delta = \frac{Z\bar{Q}}{E} \quad 2\text{-}40$$

The control regulation for frequency and voltage can be calculated by

$$f - f_o = -k_p(\bar{P} - \bar{P_o}) = -k_p\frac{X}{Z}(P - P_o) + k_p\frac{R}{Z}(Q - Q_o) \quad 2\text{-}41$$

$$E - E_o = -k_q(\bar{Q} - \overline{Q_o}) = -k_q\frac{R}{Z}(P - P_o) - k_q\frac{X}{Z}(Q - Q_o) \quad 2\text{-}42$$

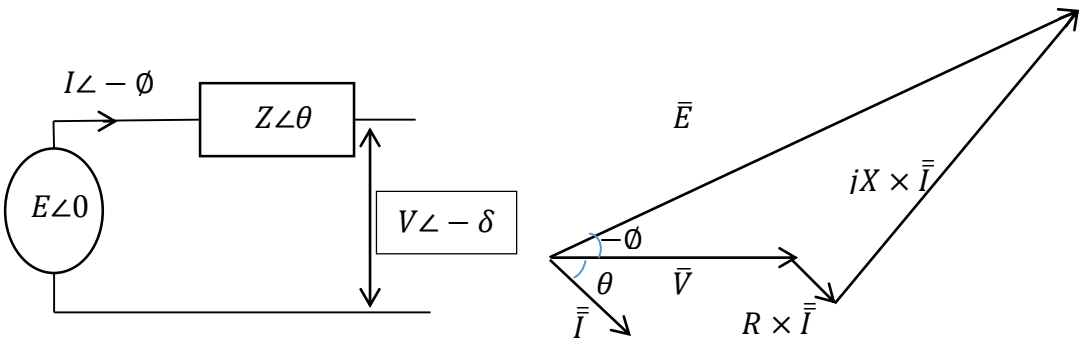

A – Single line diagram B – phasor diagram

Figure 2-28: Transmission line power flow

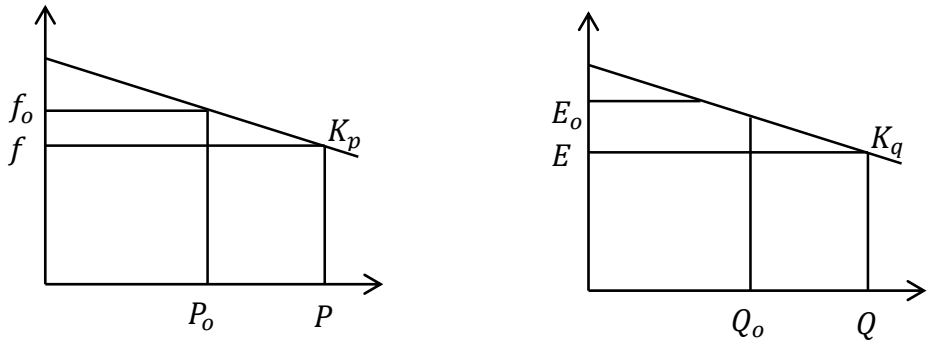

Figure 2-29: Droop characteristic for generator

2.14 System Architecture for Multiple Energy Storage Systems

Researchers proposed many topologies for hybridization of battery and supercapacitor resources. The most common one is a passive hybrid topology as shown in Figure 2-30. The resources in passive hybrid topology are connected in parallel directly to the dc link. The advantages of this topology are the simplicity and the lack of power electronics and control circuitry, and in reducing the overall energy and power density. The disadvantage is the uncontrolled current flow.

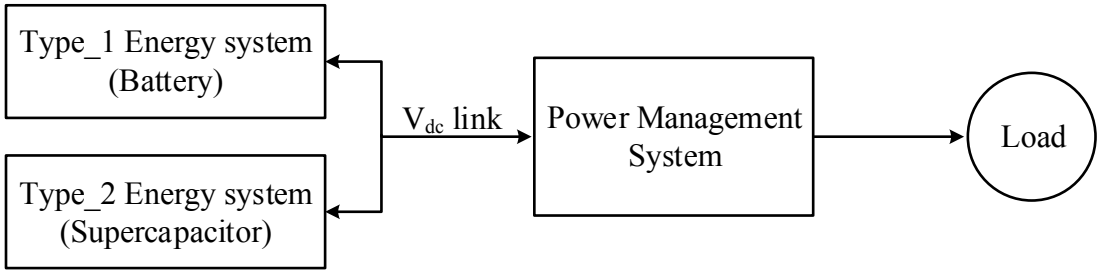

Figure 2-30: Passive hybrid topology

Parallel semi-active hybrid topology improves the characteristics of passive hybrid topology by adding bi-directional converter between the DC link and the load as shown in Figure 2-31. However, the battery in such system still needs to supply part of the dynamic power of the load.

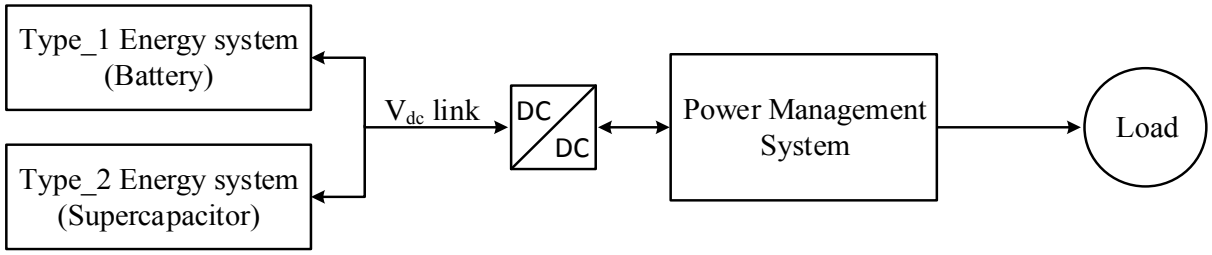

Figure 2-31: Parallel semi-active hybrid topology

Capacitor semi-active hybrid topology allows decoupling between supercapacitor and DC link by DC/DC converter as shown in Figure 2-32.Thus, the impact of supercapacitor energy is improved. However, the battery still provides some dynamic power of the load.

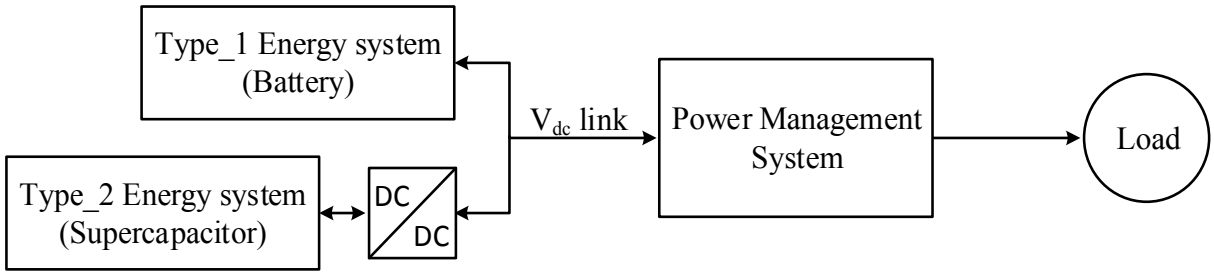

Figure 2-32: Capacitor semi-active hybrid topology

Battery semi-active hybrid topology has significant improvement of the battery performance regarding efficiency, temperature and lifetime, where the DC/DC converter is connected to the battery with DC link side, as shown in Figure 2-33.This topology also reduces battery rated requirement and weight.

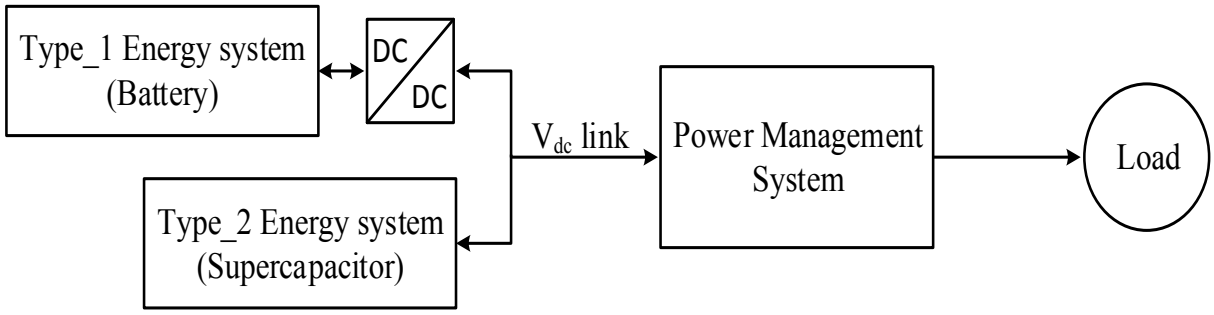

Figure 2-33: Battery semi-active hybrid topology

A further enhancement is proposed in series active hybrid topology, as shown in Figure 2-34, in addition to the advantage of battery semi-active hybrid topology; it solved the supercapacitor voltage variation. However, there are two conversions for battery voltage to DC link connection. Thus, the efficiency is reduced, and full rating of the converter is increased.

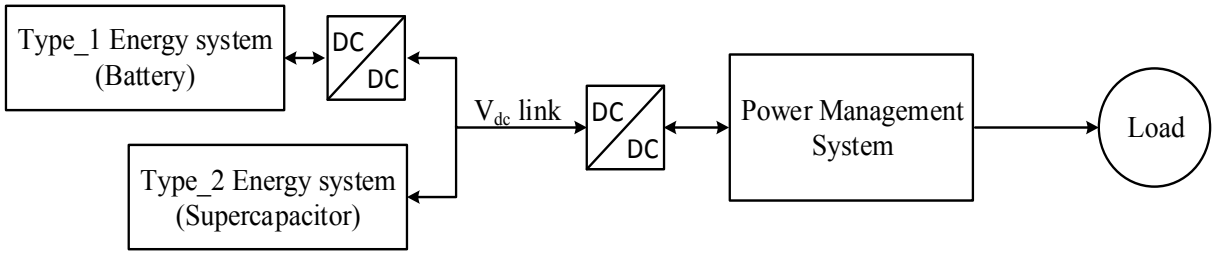

Figure 2-34: Series active hybrid topology

Parallel Active Hybrid topology is the most optimal active hybrid which has been used by researchers. It buffers both battery and supercapacitor from DC link by connecting DC/DC converter, as shown in Figure 2-35. Therefore, it enhances the voltage variation of battery and supercapacitor with a dc link, limiting the dynamic power effect of battery, and limited current

flow from battery and supercapacitor. However, adding two DC/DC converters for each resource increases the complexity control effort and losses of the system.

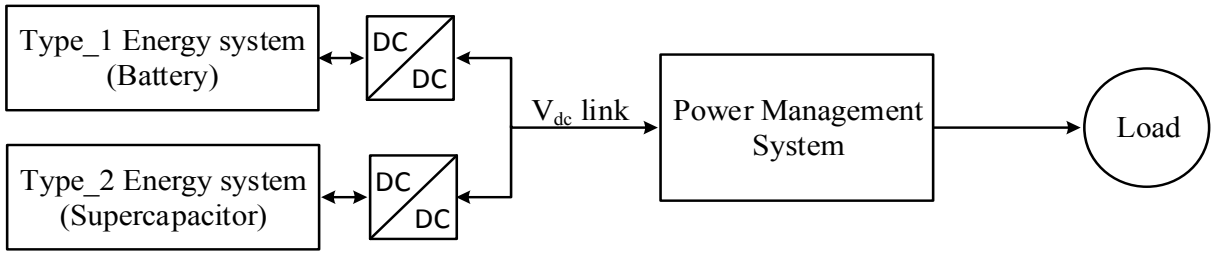

Figure 2-35: Parallel Active Hybrid topology

2.15 Conclusion

This chapter presents the available kinds of literature involving in microgrid and EVs technologies. It is predicted that increasing the electrification of the transportation system and renewable energy resources will change the structure of the electric system from the traditional power system into a smart grid. The area of smart, grid, microgrid, and EVs domain is relatively new and encompasses several different disciplines. At present, microgrids and EVs within the smart grid paradigm are becoming very popular; therefore, there are very active researchers working on new technologies to change the infrastructure of the grid from passive to active and reduce carbon dioxide emissions. Since the largest microgrid problem is maintaining the stability of the system with low inertia and intermittency of micro sources, the widely-accepted solution is to use EVs' resources to keep voltage stability, in the short term, of voltage stability oscillation. Extensive deployment of the integration of EVs into microgrids will impose many challenges to the operation and management charging demand of EVs and will assist in avoiding the stability issue. Furthermore, EVs are expected to represent a load at microgrids in forthcoming years. Therefore, the charging demand of the EVs may tend to coincide with the maximum demand of the network. This work proposes the chronological structure of the tri-level hierarchical management operation to form a modular power management implementation structure: MGO, CSO, and EVO. The proposed system contributes mainly to resolve the rapidly increasing demand on the power system and to the reduction of greenhouse gas emissions.

Primarily, the challenges in the autonomous power system represent managing and control many elements distributed in wide area geographically that have different dynamic response. On the other hand, The EVs are expected to connect to the various locations of electricity outlets at different times of day to work as a mobile load or energy storage system. The challenges in the operating EVs within microgrid, having multiple energy resources, represent managing the charging and discharging variety brand EVs by plugging in at a different location at a different time of a day with unspecific number among many charging station systems. Moreover, EVs are enabling further expansion of renewable energy resources to feed power into the microgrid.

3. Chapter Three: Modelling and Analysis of Microgrids

3.1 Introduction

The previous chapter described the benefits of a restructuring of the distribution network to use the microgrid operation more efficiently for finding a solution to rapidly increasing demand and environmental awareness. However, technically modifying the existing distribution network to a microgrid network indicates many challenges. This chapter presents the development of reconstructing a realistic distribution network in a Baghdad community to use it as a microgrid network from the view of:

- allocating distributed generators on the buses of the distribution network.
- the size of the microgrid, based on the load type, to integrate the point of common coupling for connecting to or isolating the microgrid from other microgrids or with the conventional grid.
- determining the effect of the microgrid operation on the voltage stability level of the system for different operation, such as the conventional grid, smart grid, and microgrid,
- identifying the useful bus on the microgrid to install a charging station system for charging and discharging a fleet of EVs from the view of voltage stability enhancement.
- identifying a set of mathematical equations to integrate the resources of the EVs within the distribution feeder of the microgrid at connection buses to count EVs as part of the distribution network for load flow analysis purposes.

This chapter paves the way for the following chapters to design a modular structure framework to manage and control the operation of the microgrid in a chronological execution. Therefore, the size and location of the distributed generators, the location of the charging station systems, and the mathematical equation for integrating the EVs within the distribution line of the microgrid of the case study for this chapter will be applied in the next three chapters.

3.2 Description of Voltage Stability Issue

Traditionally, loss of voltage stability occurs in the case of imbalance between delivered and consumed reactive power in the electric power system; this refers to the voltage magnitude of the power system declining to an unacceptably low level. The utility grid covers a large area and uses bulk power generators and long transmission lines compared to microgrids. In contrast to the transmission line of the utility grid, low voltage cables in the microgrid network have mainly a resistive and reactance nature. Therefore, adjusting active power affects the voltage magnitude, whereas active power injection could maintain the voltage stability in a microgrid, as well as reactive power injection. There are many reasons for believing that the voltage stability issue in a microgrid is of more concern than in a utility grid [50]. Microsources, storage devices, network parameters, nature of the load, bidirectional power flow, control topology, the communication link between devices parameters could all cause a fluctuation in voltage stability, especially in islanding mode and needs a deep study to make the microgrid work

autonomously and robustly. The main source to recover the voltage stability of a microgrid is an energy storage system that could provide missing active or reactive power in order to balance the consumption and maintain the voltage level of the network. The uptake of the EV market is set to create a considerable amount of loads for the electrical power distribution network in the near future. In general, the EVs will be connected at various locations of the electricity network and at different times of day for the recharging of their batteries. The charging demands of EVs may tend to coincide with the peak demands of the power distribution network adding extra burdens to the generation capacity. On the other hand, the incorporation of microgrids within the existing distribution network not only enables the penetration of renewable energy resources but also allows EVs to be connected as mobile energy storage systems. The EVs may be considered from the view of the distribution network as either load that is drawing current from the microgrid network, or generation units that inject power into the microgrid network.

Recent developments that are key to extending the lifetime and increasing the efficiency of a mobile storage device have focused on the hybridization of the supercapacitors and batteries. The complementary properties of the supercapacitor as a peak power resource and the battery as a base power resource can be fully exploited to enhance the EV performance further, due to the growth in advanced intelligent controller technology. When the EV is connected to the electrical network, the supercapacitor would then become an additional resource of reactive power or voltage regulation of the network. Some studies have suggested that aggregating and coordinating the supercapacitors and batteries of the EVs can significantly improve the short-term voltage stability performance of the network [4-5]. To date, there appears to be no comprehensive analytical modelling that works on the connection of EVs to microgrids. Therefore, this chapter focuses on the analytical development of a line model and a power flow analysis of a distribution network with EV integration. Therefore, the positive impacts of EVs' integration on the voltage stability of the network can be quantified.

3.3 Modelling Analysis of Voltage Stability

The modal analysis depends mainly on the power-flow Jacobian matrix. The Jacobian matrix is square can be written as follows:

$$\begin{bmatrix}\Delta P\\ \Delta Q\end{bmatrix} = \begin{bmatrix}J_{11} & J_{12}\\ J_{21} & J_{22}\end{bmatrix}\begin{bmatrix}\Delta\delta\\ \Delta V\end{bmatrix} \quad 3\text{-}1$$

By letting $\Delta P = 0$ in Equation 3-1:

$$\Delta P = 0 = J_{11}\Delta\delta + J_{12}\Delta V \quad 3\text{-}2$$

$$\Delta\delta = -J_{11}^{-1}J_{12}\Delta V \quad 3\text{-}3$$

$$\Delta Q = j_{21}\Delta\delta + j_{22}\Delta v \quad 3\text{-}4$$

Substituting Equation 3-3 in Equation 3-4

where $$\Delta Q = J_R \Delta V \quad (3\text{-}5)$$

$$J_R = J_{22} - J_{21} J_{11}^{-1} J_{12} \quad (3\text{-}6)$$

J_R is the reduced Jacobian matrix of the system. Equation 3-6 can be written as

$$\Delta V = J_R^{-1} \Delta Q \quad (3\text{-}7)$$

The eigenvalues and eigenvectors of the reduced order Jacobian matrix J_R are used for the voltage stability analysis. Voltage instability can be detected by identifying the modes of the eigenvalues matrix J_R. The magnitude of the eigenvalues provides a relative measure of proximity to instability. The eigenvectors on the other hand present information related to the mechanism of loss of voltage stability. Eigenvalue analysis of J_R results in the following:

$$J_R = \Phi \Lambda \Gamma \quad (3\text{-}8)$$

where J_R is the reduced Jacobian matrix of the system

Φ is the right eigen vector matrix of J_R

Γ is the left eigen vector matrix of J_R

Λ is the diagonal eigenvalue matrix of J_R

Equation 3-8 can be written as:

$$J_R^{-1} = \Phi \Lambda^{-1} \Gamma \quad (3\text{-}9)$$

where $\Phi\Gamma = 1$

Substituting 3-9 in 3-7:

$$\Delta V = \sum_i {\Phi_i \Gamma_i}/{\lambda_i} \, \Delta Q \quad (3\text{-}10)$$

where λ_i is the i^{th} eigenvalue J_R.

Φ_i is the i^{th} of colomun right eignvector J_R.

Γ_i is the i^{th} of row left eignvector of matrix J_R.

Each eigenvalue λ_i and corresponding right and left eigenvectors Φ_i and Γ_i, define the i^{th} mode of the system. The i^{th} modal reactive power variation is defined as:

$$\Delta Q_{mi} = K_i \Phi_i \quad (3\text{-}11)$$

where K_i is a scale factor to normalize vector ΔQ_i so that

$$K_i^2 \sum_j \Phi_{ji}^2 = 1 \quad (3\text{-}12)$$

With Φ_{ji} is the Jth element of Φ_i

The corresponding i^{th} modal voltage variation is:

$$\Delta V_{mi} = {}^{1}/_{\lambda_i} \Delta Q_{mi} \qquad 3\text{-}13$$

Equation 3-13 can be summarised as follows:

1) If $\lambda_i = 0$, the i^{th} modal voltage will collapse because any change in that modal reactive power will cause infinite modal voltage variation.
2) If $\lambda_i > 0$, the i^{th} modal voltage and i^{th} reactive power variation are along the same direction, indicating that the system is voltage stable.
3) If $\lambda_i < 0$, the i^{th} modal voltage and the i^{th} reactive power variation are in opposite directions, indicating that the system is voltage unstable.

The relationship between the system voltage stability and eigenvalues of the J_R matrix is best understood by relating the eigenvalues to the V-Q sensitivities of each bus (which must be positive for stability). J_R must be taken as a symmetric matrix and therefore the eigenvalues of J_R are close to being purely real. If all the eigenvalues are positive, J_R is positive definite and the V-Q sensitivities are also positive, indicating that the system is voltage stable [47], [270], [271].

It is not necessary to evaluate all the eigenvalues of J_R of a large power system because it is known that once the minimum eigenvalues become zeros the system Jacobian matrix becomes singular and voltage instability occurs. The eigenvalues of importance are the critical eigenvalues of the reduced Jacobian matrix J_R. Thus, the smallest eigenvalues of J_R are taken to be the least stable modes of the system. The rest of the eigenvalues are neglected because they are considered to be strong enough. Once the minimum eigenvalues and the corresponding left and right eigenvectors have been calculated, the participation factor, which is the left and right eigenvectors' multiplication, can be used to identify the weakest node or bus in the system. Figure 3-1 is a flow chart diagram of the calculation of the voltage stability level using eigenvalues and the mechanism of voltage stability using eigenvectors.

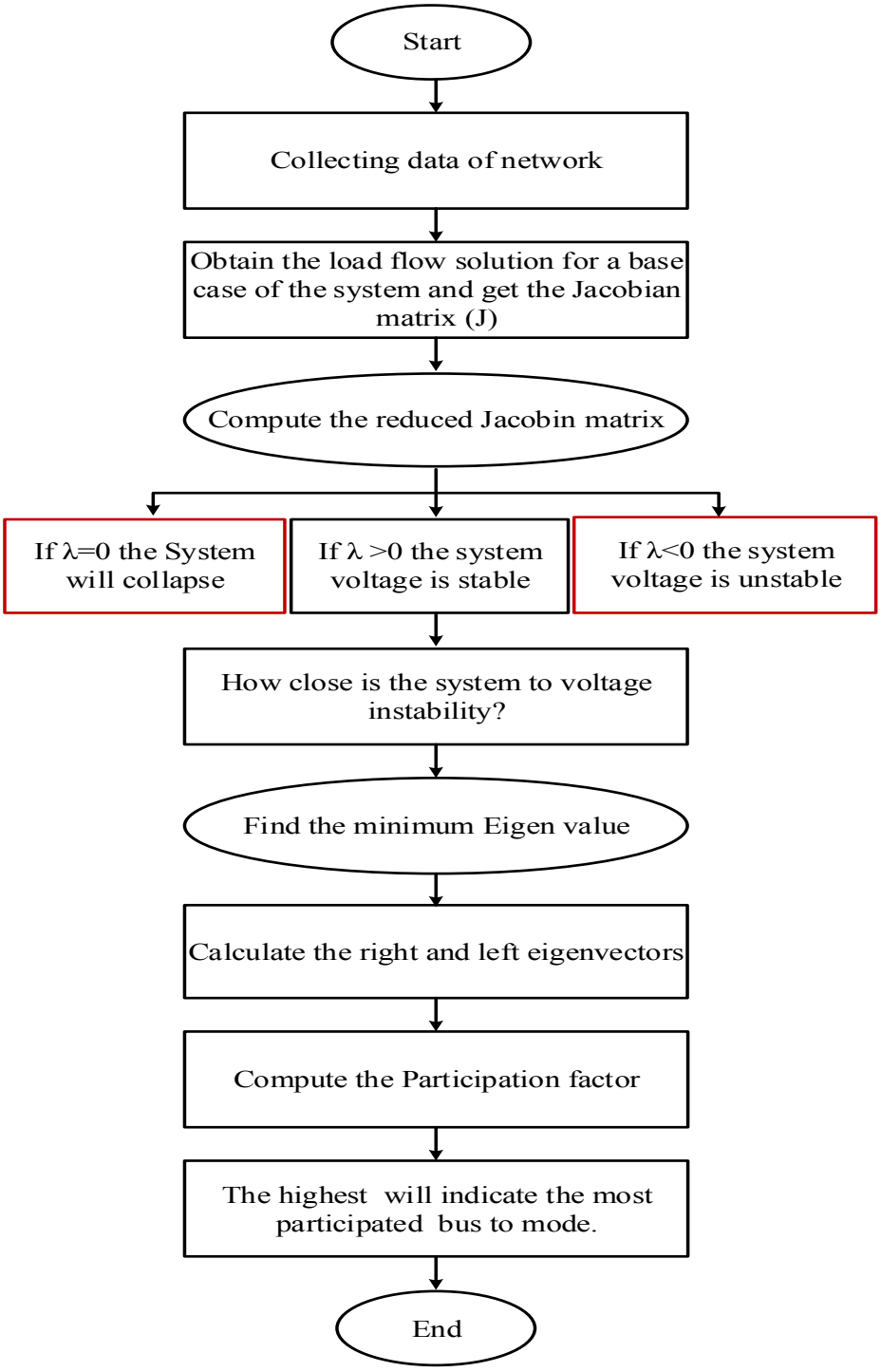

Figure 3-1: Flow chart diagram explaining the voltage stability identification.

3.4 Effective Location of Distributed Generators based on Voltage Stability

Typically, the distribution network is considered to be a radial operation that is fed power by centralising generation units through interconnected transmission lines. The distribution network is considered to be a passive network, where the power is flowing in a single direction. Due to the high voltage ratio of R/X, the distribution network suffers from large voltage drops,

high power losses, and low voltage stability. The suffering of the distribution network is increased by rapidly increasing the demand, especially with a newly integrated load such as EVs. Recently, using distributed generators has become widespread as a solution to the problem of the distribution network, since the rapid growth of Renewable Energy Technologies (RETs) has helped to develop electricity generation and a distribution infrastructure to meet electricity demand requirements. Some of the other non-renewable energy technologies that are widely practised, such as gas turbine, fuel cell, and diesel generator, increase the development of distributed generators. Integrated distributed generators could be used to support a weak distribution network or could be operated in an island mode, which is an approach to the microgrid concept. Since the distributed generators are installed closer to the load demand, the transmission line losses are either avoided in island operation mode or reduced in connected mode.

In order to achieve the high benefits from distributed generators, their size and placement in the microgrid have to be optimised. Researchers have formulated the placement of distributed generators by using many objective functions, such as voltage profile improvement, loss minimization, improvement in reliability aspects, economic revenue, and environmental impact reduction. [47], [112], [272]–[278]. In this study, four types of distributed generators are suggested to be integrated within a distribution network: gas microturbine, fuel cell, photovoltaic cell, and diesel power generator [48], [279]. The average wind speed in the case study environment in this study, which is Baghdad city, is less than three m/s. Normally, the wind turbine is cut off at a wind speed lower than three m/s. Therefore, the wind turbine has been excluded from this study. The distributed generators are formulated according to the voltage stability improvement in two attempts: finding the lowest voltage bus bar or the most sensitive bus bar to the voltage stability (weakest bus bar). The procedure for determining the candidate bus bar in which to integrate the distributed generators is given below:

1- The power flow of the network is analysed using the Newton-Raphson method to obtain the voltage profile, line flow, total power losses (real and reactive), line losses, Jacobian matrix, and reduced Jacobian matrix.
2- According to the attempts, identifying the lowest voltage bus bar or the most sensitive bus bar to voltage stability is approached by using the participation factor based on finding the minimum eigenvalues and eigenvectors of the network.
3- The first specific type of distributed generator is integrated based on the certain capacity of active and reactive power into the candidate bus bar to enhance either the voltage level or the minimum eigenvalue of the network.
4- The system is analysed again to find the next candidate bus bar. In case the next candidate bus bar is the same as the previous candidate, the power of the distributed generator should be increased to a higher level.
5- The second generator is integrated into the second bus bar.
6- The procedure is iterated until combining the objective function that covers all demands of the system.

The flow chart for integrating the distributed generators into the most sensitive bus bar and the minimum voltage bus is shown in Figure 3-2.

The voltage stability indication increased from 0.063 to 0.446 when integrating the distributed generators at minimum voltage bus and most sensitive bus, respectively, for the same number and capacity of distributed generators. The results show that integrated microsources at the weakest bus bar improved the voltage stability much more than integrated microsources at the minimum voltage bus bar, as shown in Table 3-1. The five minimum eigenvalues of the conventional grid without distributed generators, the microgrid at island mode, and the conventional grid (smart grid) at island mode, are shown in Table 3-2.

Table 3-1: Distributed generator arrangement on buses

	Uniform distribution busses	**Type of sources**	**Power rated kW+kVAR**	**Non-uniform distribution busses**
1.	25 (62)	Gas microturbine (MT)	75+35	47
2.	16 (53)	Fuel cell (FC)	50+20	46
3.	10 (47)	Gas microturbine (MT)	75+35	45
4.	34 (71)	Photovoltaic cell (PV)	50+20	35
5.	45 (82)	Fuel cell (FC)	50+20	34
6.	39 (76)	Gas microturbine (MT)	75+35	33
7.	32 (69)	Photovoltaic cell (PV)	50+20	32
8.	15 (52)	Gas microturbine (MT)	75+35	11
9.	20 (57)	Photovoltaic cell (PV)	50+20	26
10.	17 (54)	Photovoltaic cell (PV)	50+20	25
11.	18 (55)	Diesel power generator (DE)	250+175	10
12.	33 (70)	Fuel cell (FC)	50+20	17
13.	42 (79)	Photovoltaic cell (PV)	50+20	16
	Minimum eigenvalue = 0.446		Minimum eigenvalue = 0.063	
	Total demand = 682.1Kw+328.8Kvar			

Table 3-2: The eigenvalue for lowest buses

	Type of connection	**Bus No**	**Eigen Value**
1.	Traditional grid without DG	37	0.071
		74	0.084
		75	0.105
		77	0.116
		66	0.149
2.	Microgrid at isolated mode	70 (33)	0.446
		62 (25)	0.750
		63 (26)	0.955
		71 (34)	0.984
		78 (41)	0.986
3.	Smart grid at isolated mode	17	4.927
		19	10.175
		20	10.621
		24	17.772
		27	19.280

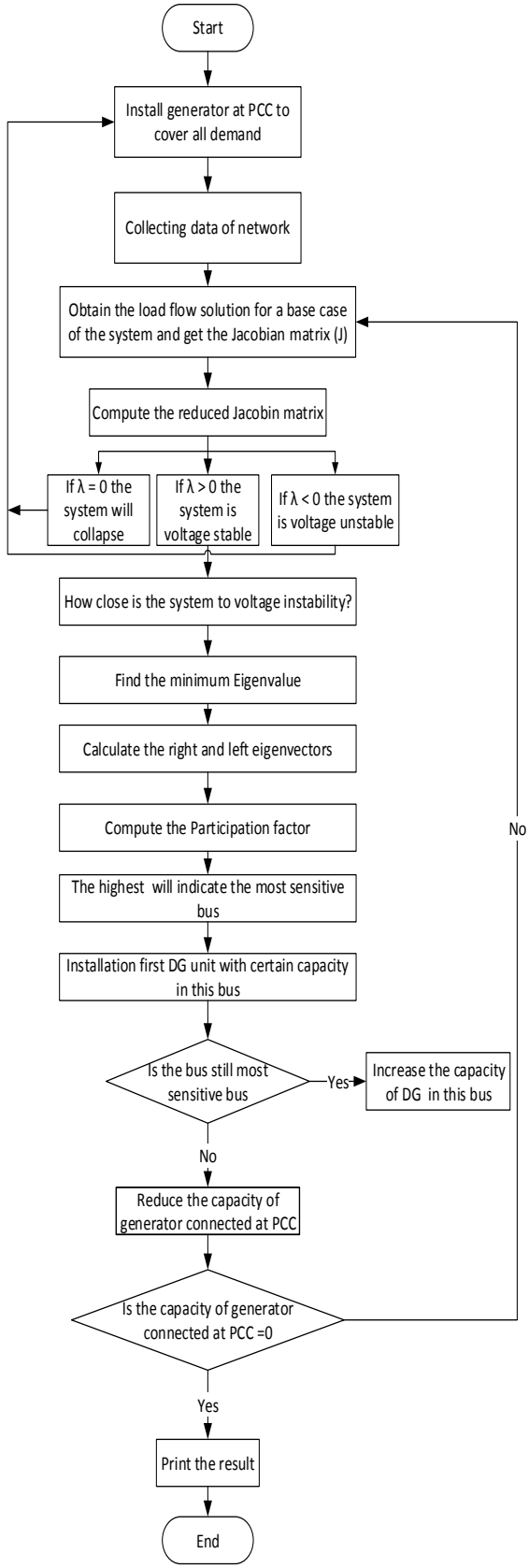

a- integrated DG at weakest bus bars attempt

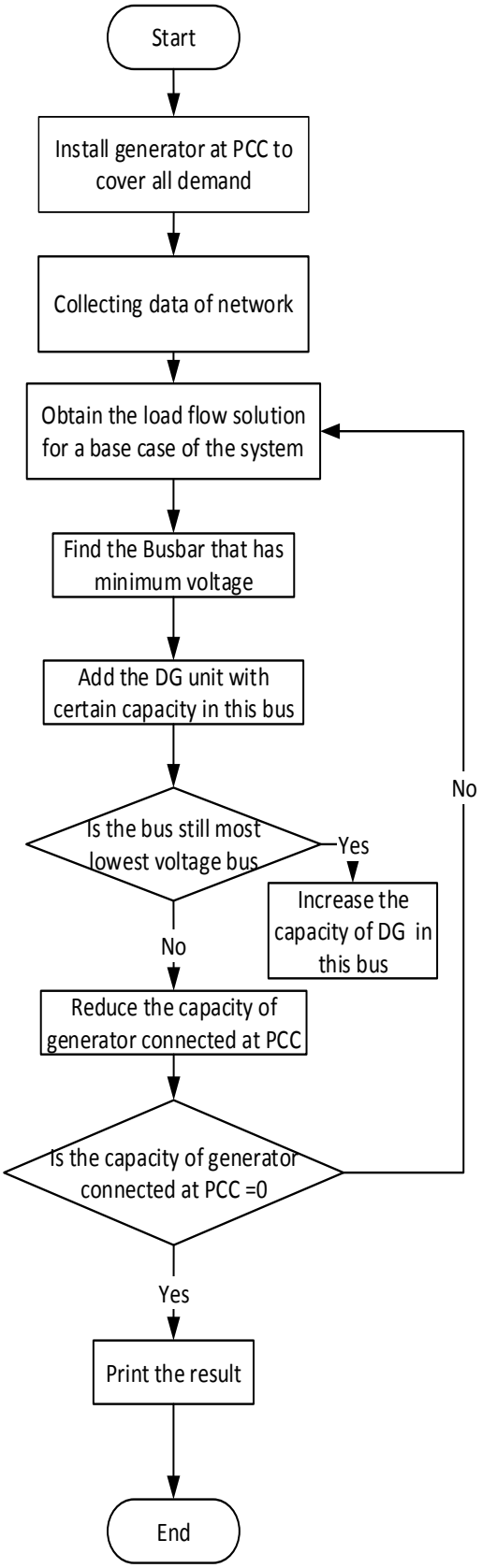

b- integrated DG at minimum voltage bus bars attempt

Figure 3-2: Flow charts of the DG placement algorithms

3.5 Case Study Analysis

This section gives the detail of the case study's architecture connection, generation, and loads. The system operates in four scenarios: a conventional grid, smart grid at connected mode, smart grid at disconnected mode, and microgrid. The reason for operating the case study in many scenarios is to find the voltage profile, participation factor, and voltage stability value at each scenario to determine the best operation for the case study. The illustration of the case study and scenarios operation are described in the next subsections:

3.5.1 Conventional grid

For an academic study, this work proposes a traditional system for a power grid, which consists of generation, transmission, and a distribution network. The transmission system consists of 37 buses, ten generators, 49 transmission lines and transformers [280, Sec. 6.6]. It operates at three voltage levels which are 132 kV, 66 kV, and 11 kV. The distribution network under study consists of 49 bus bars distributed on seven laterals and 48 underground feeders to supply the electrical loads of a typical community in Baghdad. As the typical loading profiles and line impedances of the network are readily available to the author, it presents a realistic case study for the investigation of the integration of EVs. The original distribution network is connected to a conventional power system via the transmission line through substations. A schematic diagram is given in Figure 3-3.

The scale load of Newton-Raphson based on the Matpower program [281] and eigenvalues and eigenvectors for reducing the Jacobian matrix are used in analyses to calculate power flow solutions and monitor voltage stability. A voltage profile of the grid is shown in Figure 3-4. The system is stable according to the calculated minimum eigenvalue, which is positive and equal to 0.071. The multiplication of the right and the left eigenvectors of the system give more details about the sensitivity of buses to stability. Bus bar number 62 is the weakest on the system according to the data presented in Figure 3-5. Bus bar number 13 has the minimum voltage level of the system, which is equal 0.9143 according to the data presented in Figure 3-4.

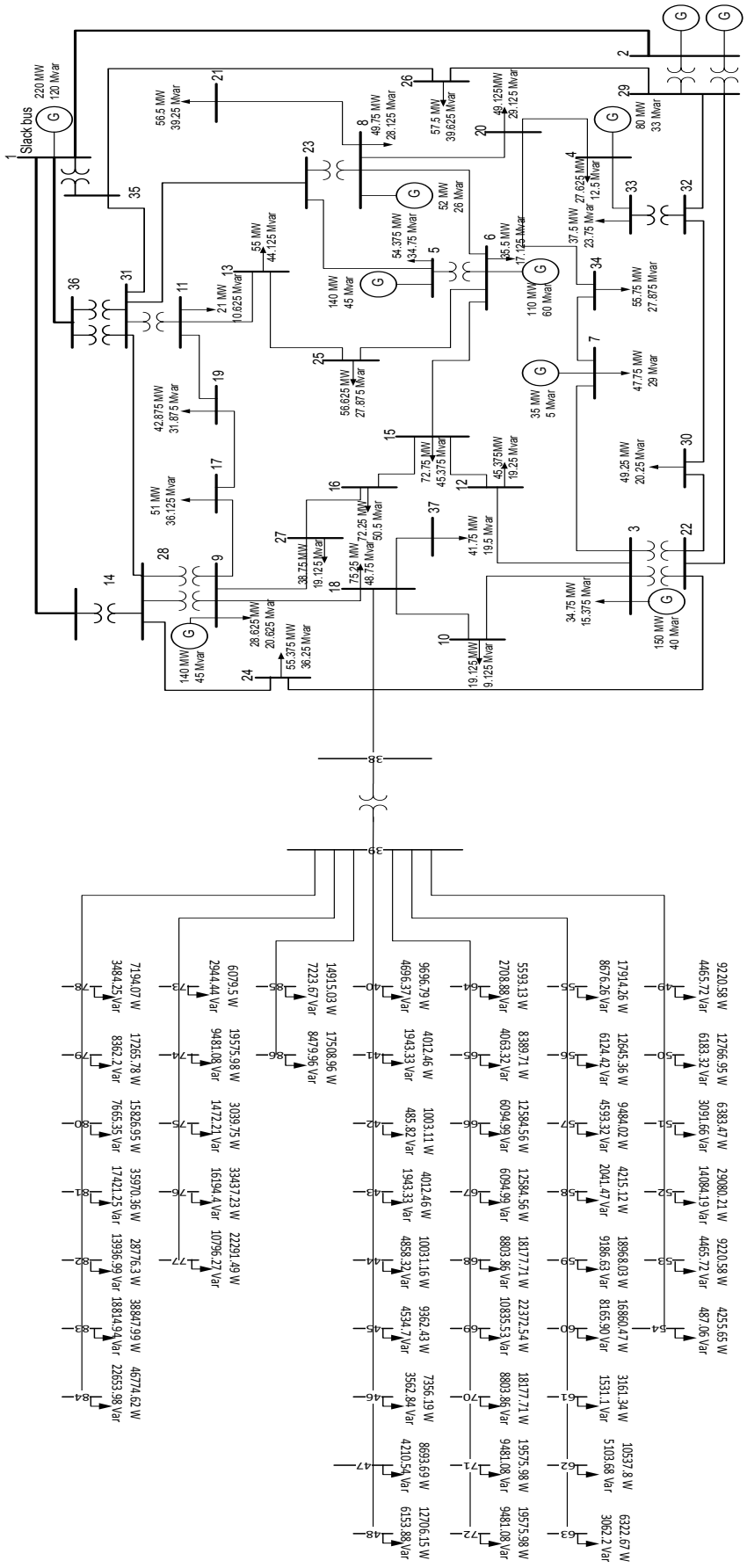

Figure 3-3: Case study

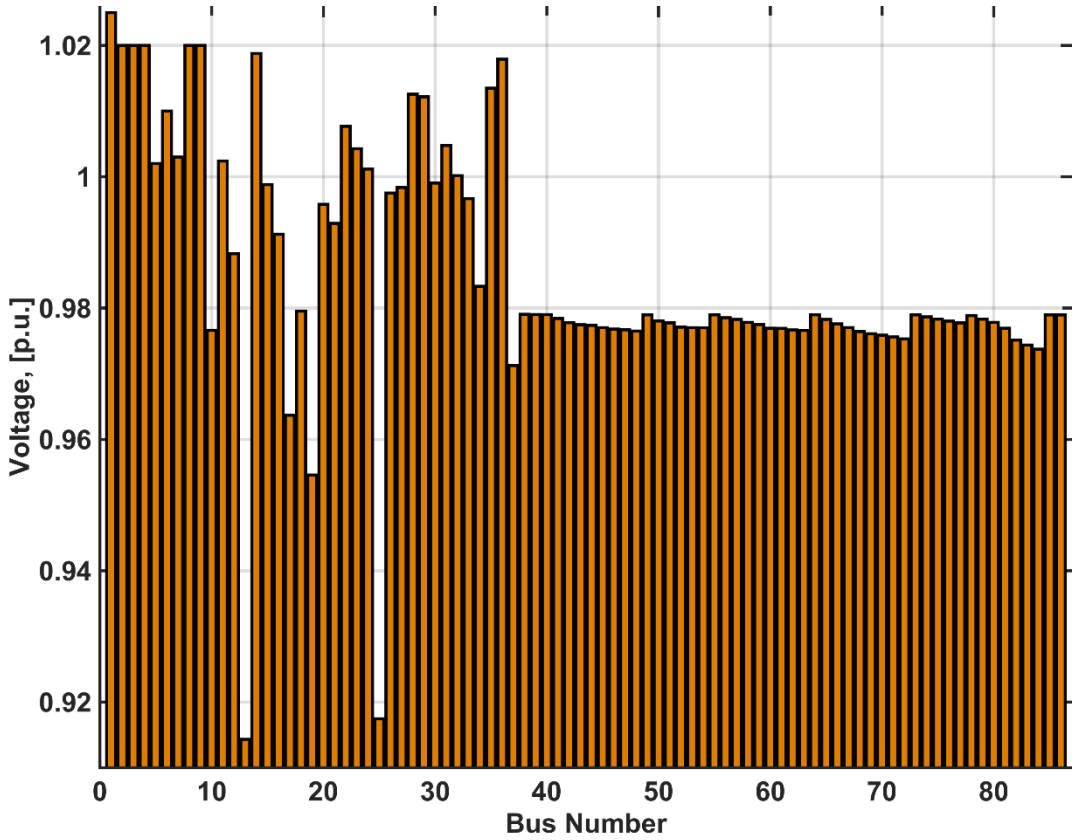

Figure 3-4: Voltage profile for the conventional grid (without DG impact)

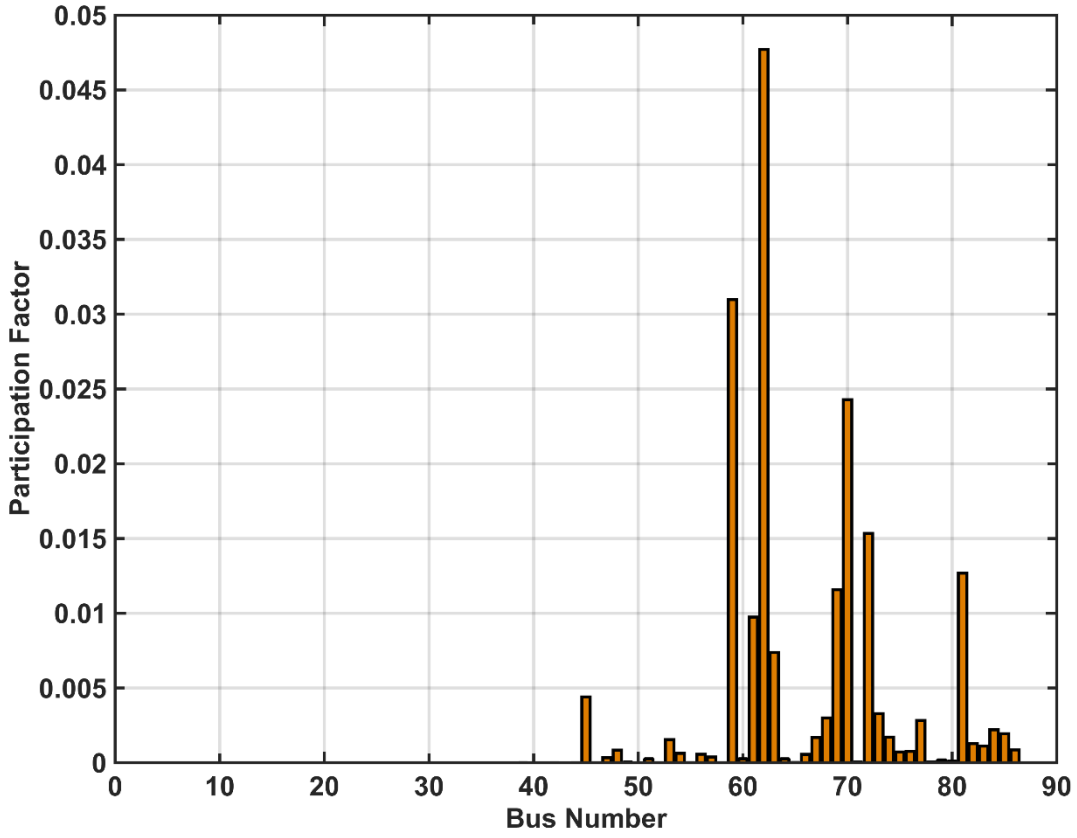

Figure 3-5: Participation factor for the conventional grid (without DG impact)

3.5.2 Distribution network as microgrid

The power in the distribution network is flowing unidirectionally from the generation unit to the load. Some assumptions are made to allow the study of perspective connections of the EVs, distributed generators and renewable energy resources to the existing network:

- Interfacing power electronics, protective devices and communication links allowing bidirectional power flow at the selected nodes are connected with distributed generators.
- A pseudo-isolated operating mode, such that the entire local loads which are 682.1 kW and 328.8 kVAR in this study, are met by several distributed generators located at selected nodes, as shown in the case study depicted in Figure 3-6.

It is noted that the above assumptions have basically transformed the distribution network into a microgrid. Although it is envisaged that many new microgrids will be designed and developed with advanced intelligent controllers and communication links in the future [6-8], the reality is more likely to be a gradual progression from existing networks, such as described in the case study here. While only distributed generators are included in the current study, it should be noted that other energy sources such as wind turbines are likely to be included in a realistic microgrid, which will further increase the interdependence of the resources and loads, and the control complexity of the system [40]–[42].

A microgrid operates as a single controllable network that acts either in an island mode to balance its demand and power generation, or in a connected mode with conventional grid and other microgrids to support the conventional grid.

Typically, the normal operation of the microgrid is as a connected mode to support the transmission system and enhance the efficiency of the transmission system operation. A voltage profile of the connected grid is given in Figure 3-7. The system is stable according to the minimum eigenvalue calculated, which is positive and equal to 0.446. The multiplication of the right and left eigenvectors of the system gives more details about the sensitivity of buses to stability. Bus bar number 59 is the weakest bus on the system according to the data presented in Figure 3-8. Bus bar number 13 has a minimum voltage level of the system which is equal 0.9143 according to the data presented in Figure 3-7.

In emergency electricity markets, such as following natural disasters, demand congestion, or grid outage, the distribution management operator within distribution network operator takes a decision to isolate the microgrid by disconnecting the point of common coupling which makes the microgrid work as a single controllable system. The voltage stability indicates that the minimum eigenvalue of the system becomes 4.927. The transmission system in islanded mode becomes more stable from the view of voltage stability than in connected mode due to the release of some load which is covered by the distributed generators of the microgrid. Bus bar number 25 is the weakest bus on the system according to the data presented in Figure 3-10. Bus bar number 13 has the minimum voltage level of the system which is equal to 0.9143 according to the data presented in Figure 3-9.

At the microgrid side, the voltage stability indicates that the minimum eigenvalue of the network becomes 0.446. Bus bar number 33 is the weakest bus on the network according to the data presented in Figure 3-12. Bus bars numbers 47 and 46 have the minimum voltage level of the system which are equal to 0.9987 and 0.9993 respectively, according to the data presented in Figure 3-11.

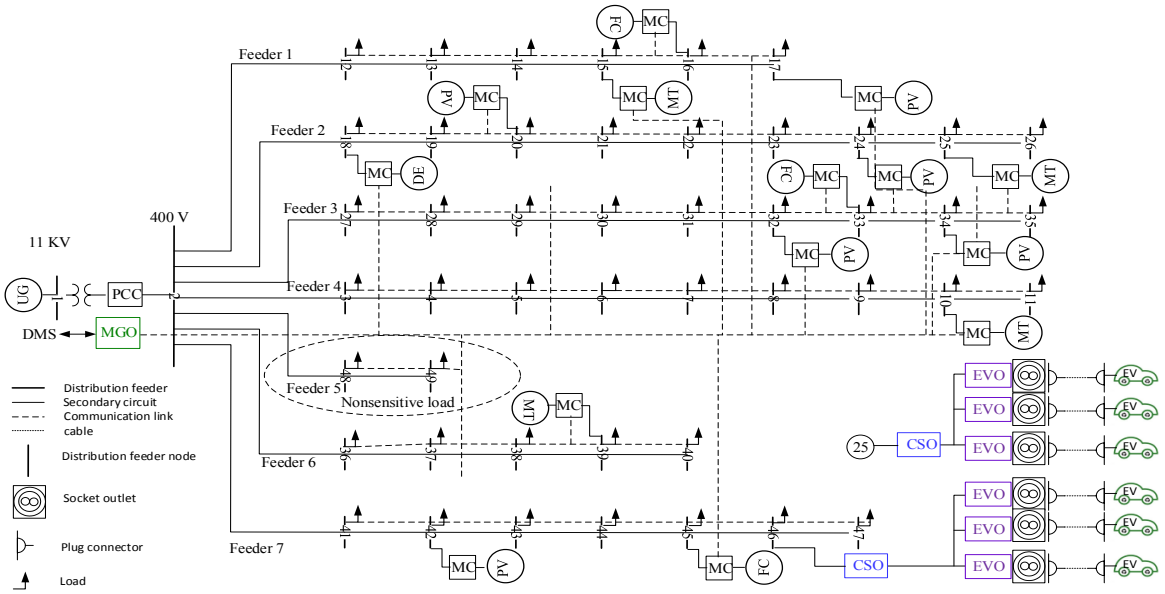

DMS = Distribution management system, MGO = Microgrid Operator, CSO = Charging Station Operator, EVO = Electric Vehicle operator, PCC = Point of common coupling, MC = Microsource controller, AC = Alternating current, DC = Direct current, UG = Utility grid, DE = Diesel generator, MT = Microturbine, FC = Fuel cell, WT = Wind turbine, PV = Photovoltaic, EV = Electric vehicle

Figure 3-6: Microgrid case study

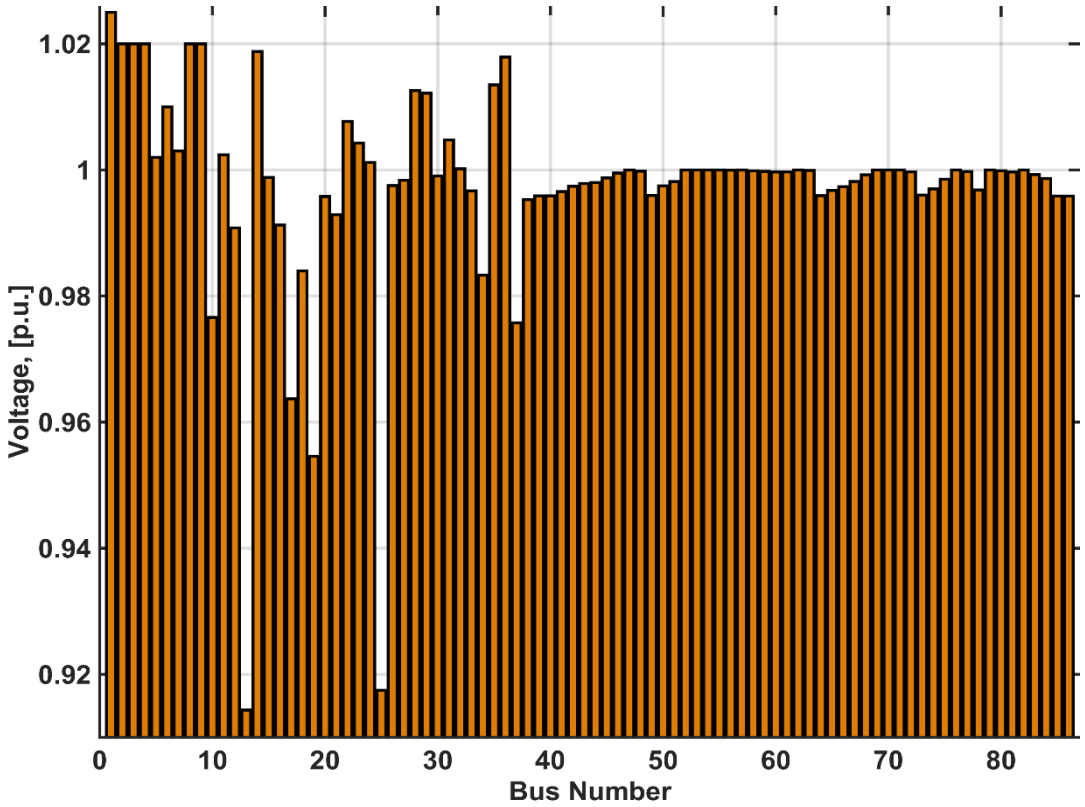

Figure 3-7: Voltage profile for the smart grid at connected mode (with DG impact)

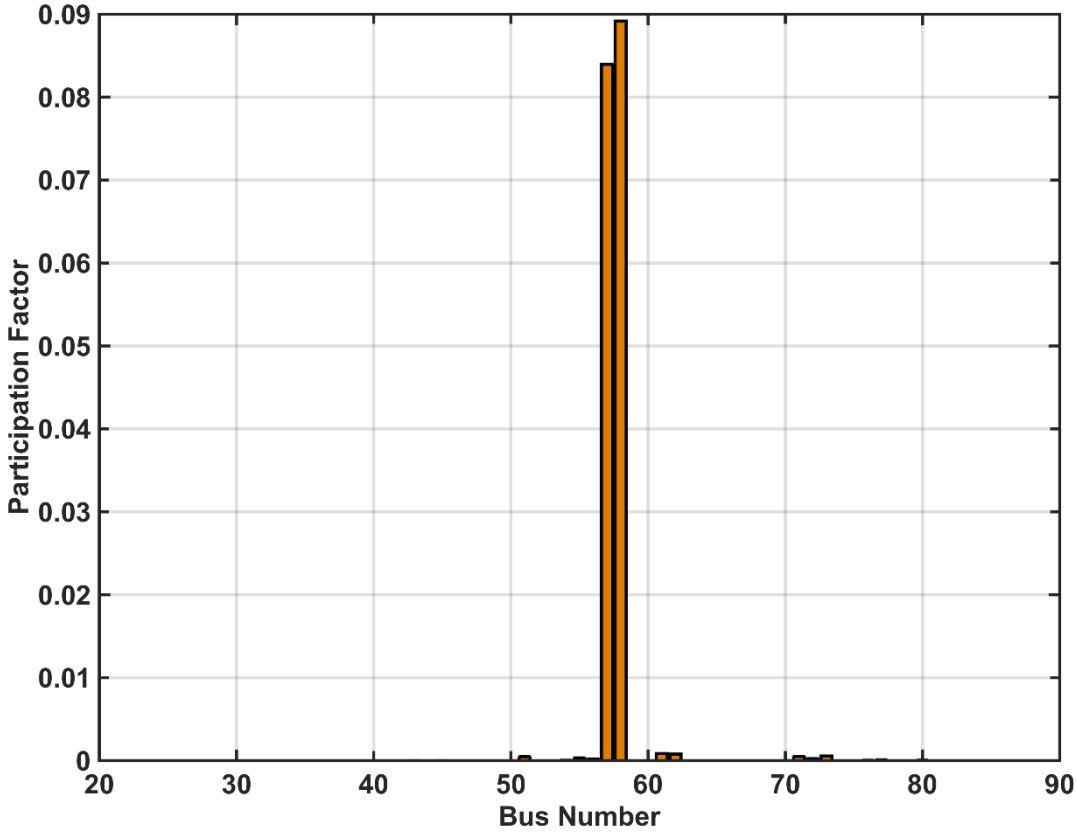

Figure 3-8: Participation factor for the smart grid at connected mode (with DG impact)

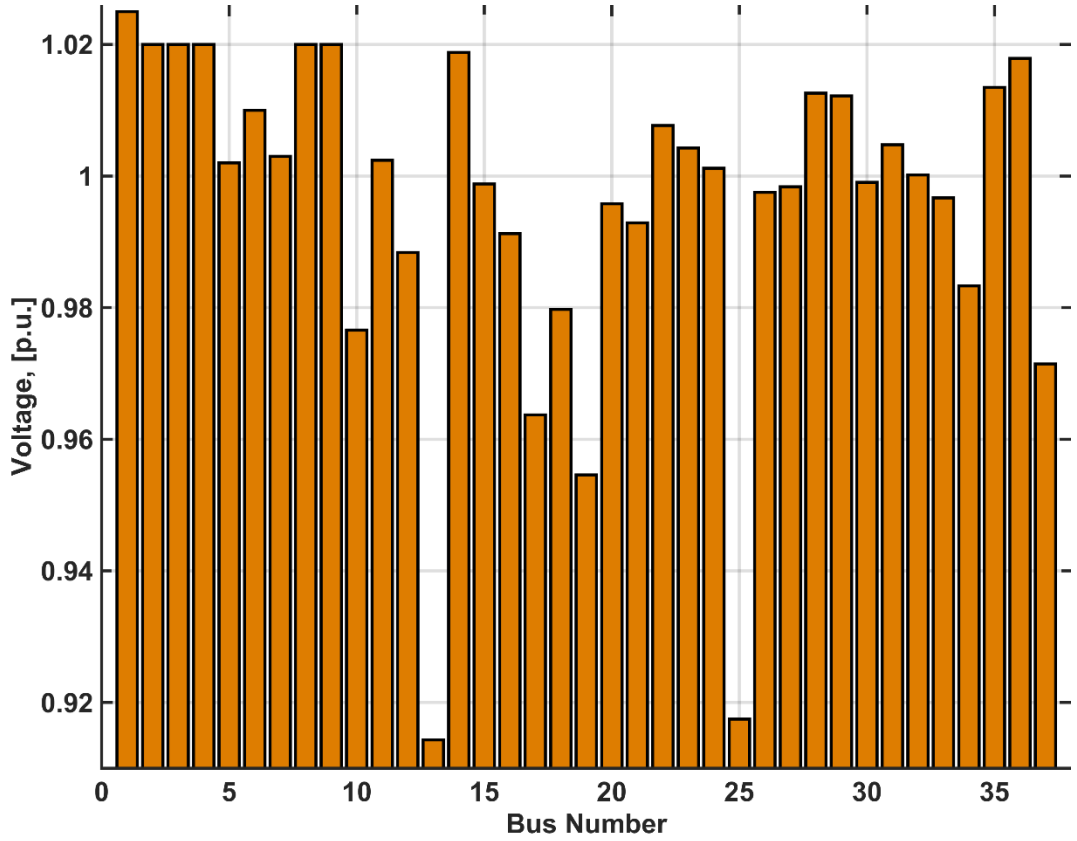

Figure 3-9: Voltage profile for smart grid at isolated mode

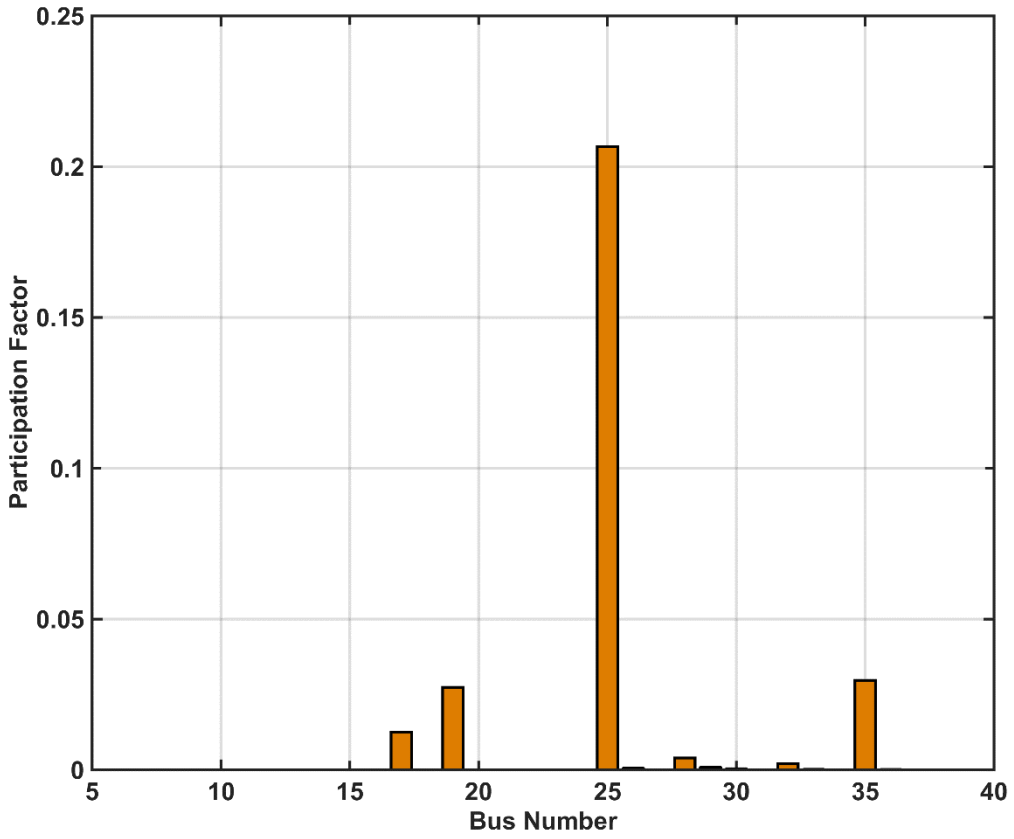

Figure 3-10: Participation factor for smart grid at isolated mode

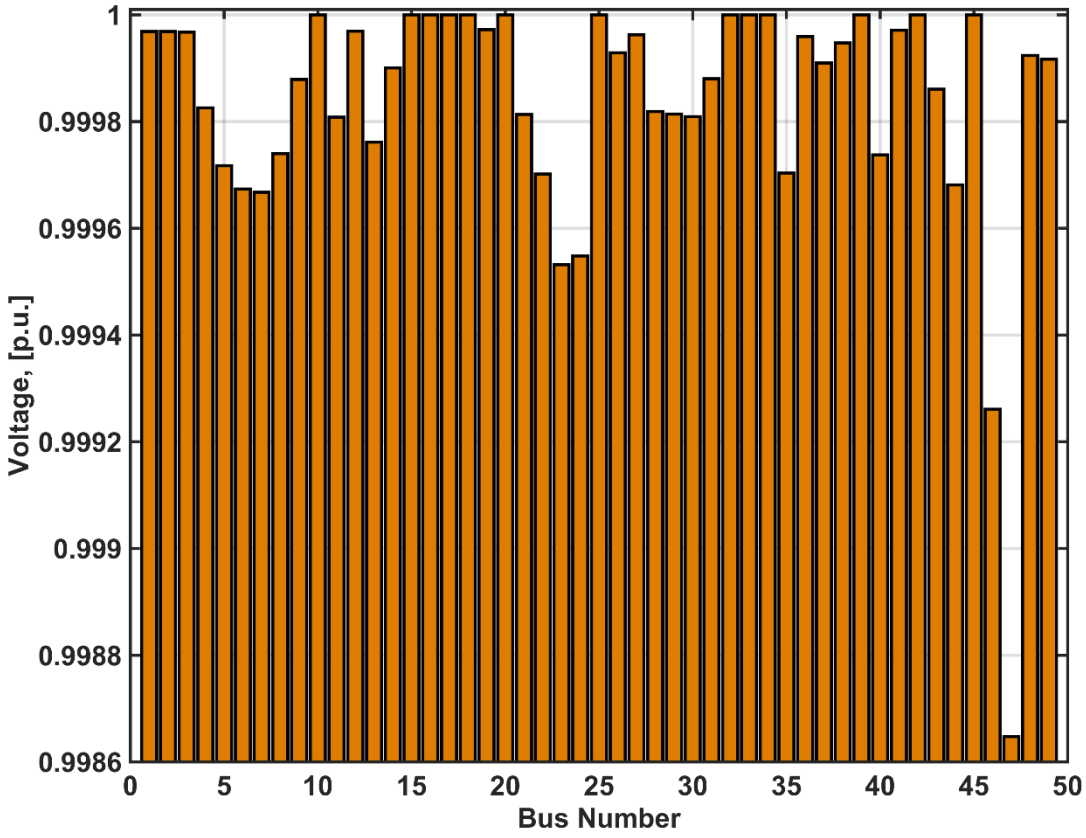

Figure 3-11: Voltage profile for microgrid at isolated mode

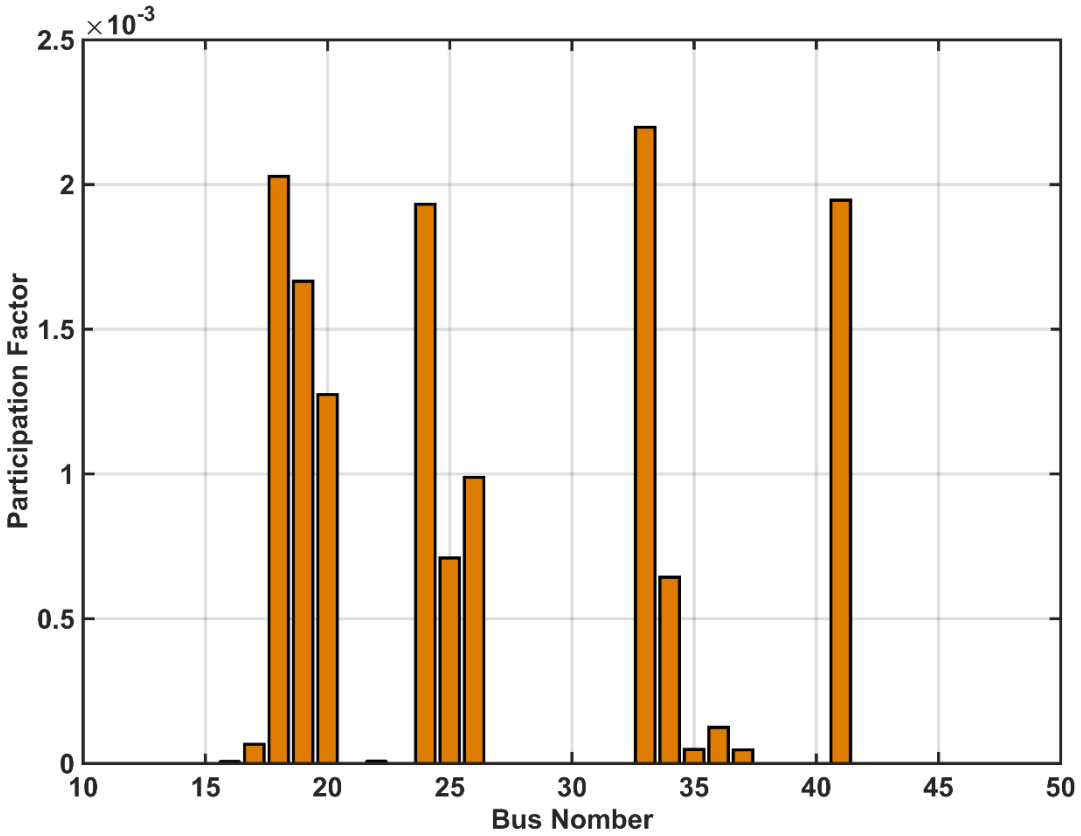

Figure 3-12: Participation factor for microgrid at isolated mode

3.5.3 Discussion of voltage profile results

Figure 3-13 reveals an enhancement in voltage profile for the smart grid at grid connected operation in bus bars 12, 18 and 37 as shown in points A, B and C, whereas the voltage profile at connected smart grid recorded a higher voltage than the conventional grid or isolated smart grid. The points also show that the voltage profile at isolated smart grid recorded a better value than the conventional grid. On the other hand, the distribution network connected to the transmission system at bus bar 18 through the transformer. Therefore, in the smart grid at connected operation, the surplus power from the microgrid moves towards the transmission system to enhance the voltage profile at connected bus and weak adjacent connected bus, depending on the amount of power. Therefore, buses 37 and 12 have an enhancement than the conventional operation due to generating power near the load. Figure 3-14 reveals the voltage profile enhancement in all bus bars of the system during microgrid operation at connected mode or isolated mode. The operation of isolated is better than the operation of connected in all bus bars of the analysis scenarios in terms of voltage profile enhancement. Some bus bars show the same voltage profile level as connected smart grid operation and microgrid operation, as shown in point A of bus bar 10 and 11 in the figure, whereas other bus bars show better voltage levels of the connected smart grid than microgrid operation, as shown at point B of bus bar 21 to 24 in the figure. Furthermore, the voltage profile at the microgrid operation recorded a better value than the voltage profile at connected smart grid operation, as shown in point C of bus bar 47 and 48 in the figure. Figure 3-15 shows the voltage profile for all systems in one graph.

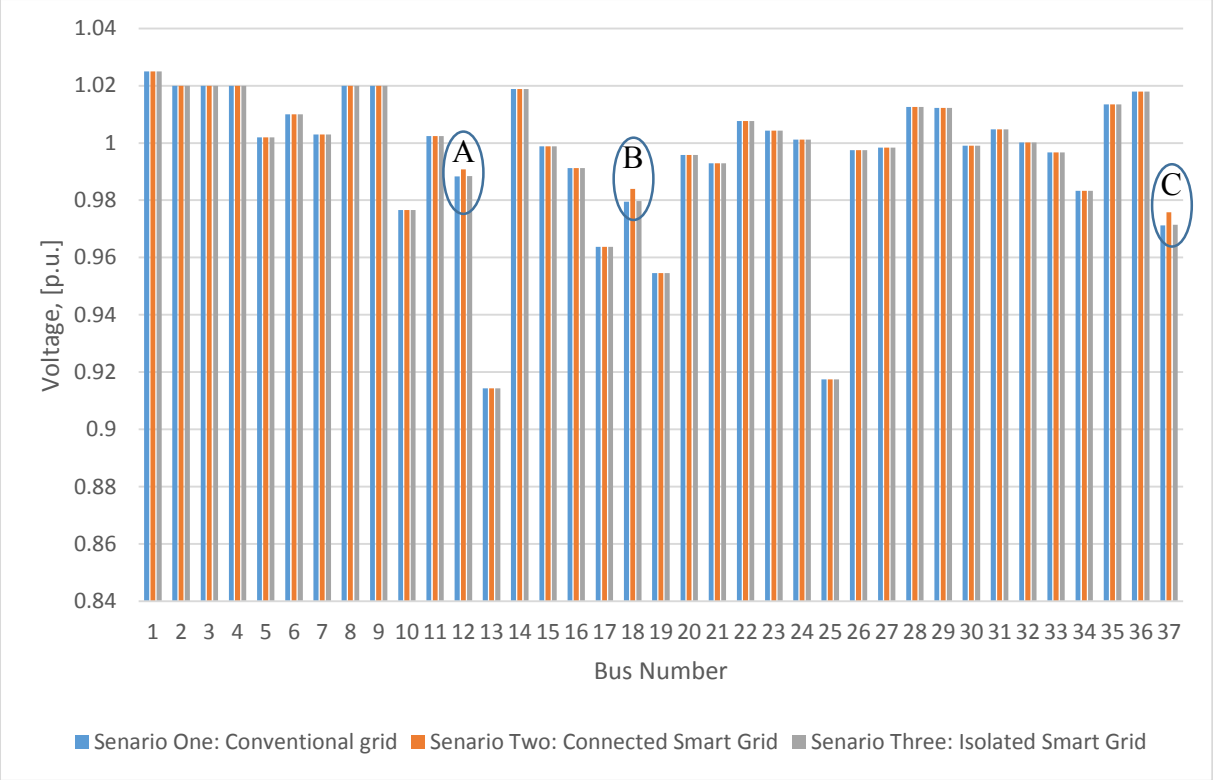

Figure 3-13: Voltage profile comparison of transmission system for all scenarios

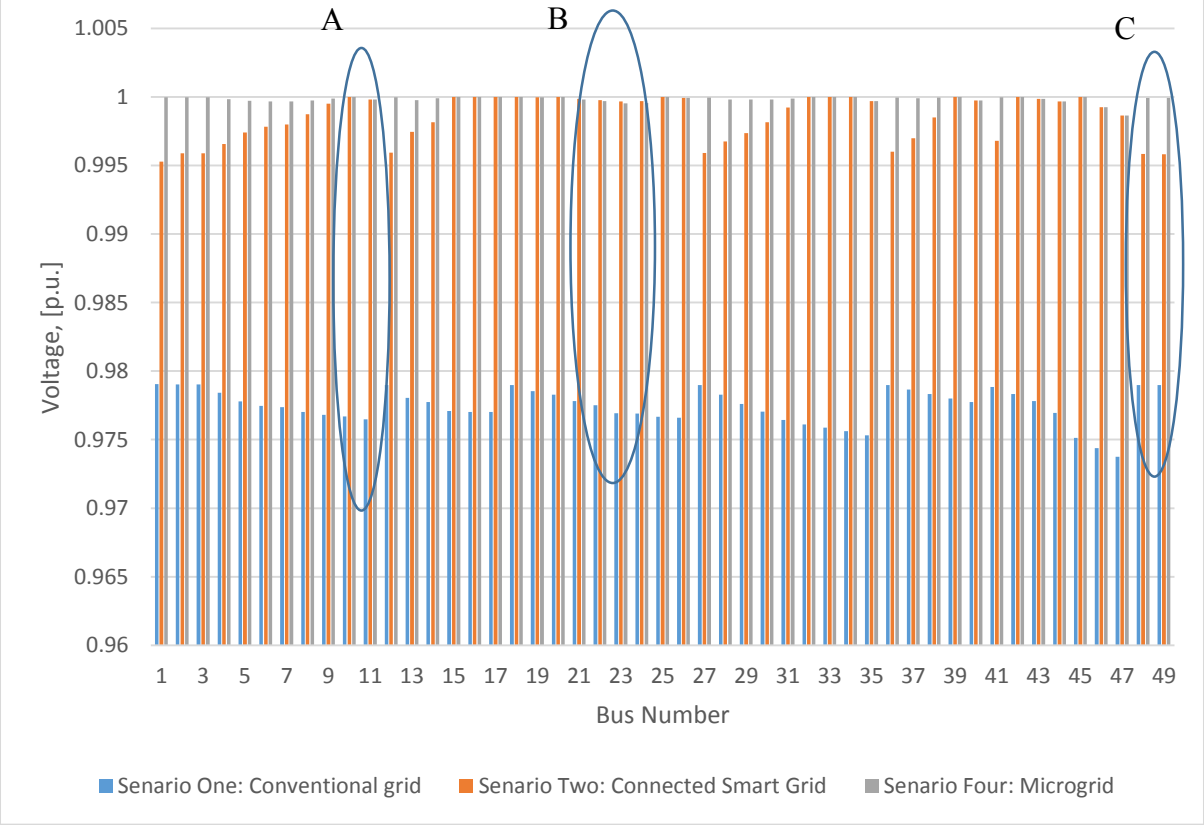

Figure 3-14: Voltage profile comparison of distribution network for all scenarios

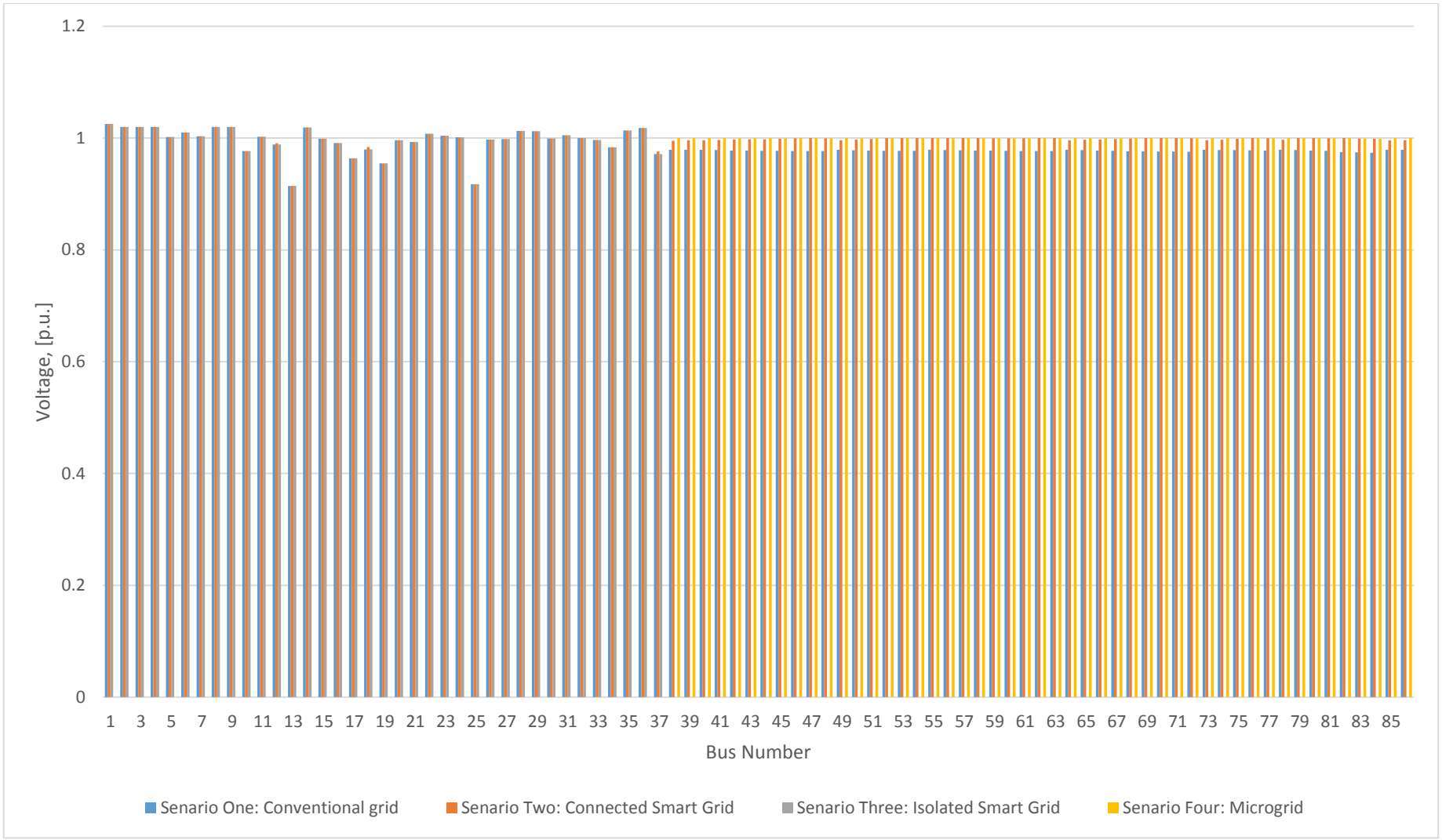

Figure 3-15: Voltage profile comparison for all scenarios

The next sections try to find appropriate equations to integrate the EVs within the distribution line and find their characteristics' effects on the microgrid network; then, in Chapter five the hierarchical strategy of the charging and discharging algorithm of each vehicle will be discussed.

3.6 Electrical Lines Parameters of Microgrid

This section will develop the characteristic equations of the distribution line based on the conventional transmission line model. Four distributed circuit parameters are used to characterise a line model: series resistance (r), inductance (l), shunt conductance (g), and capacitance (c); the lower-case symbols indicate per-kilometer values. All four parameters are a function of the line design, and depend on the conductor size, type, spacing between single conductors, and height above ground, frequency, and temperature. They are classified according to length into short, medium, and long lines. The lines shorter than or equal to 80 km (50 miles) are classified as a short line whereas lines longer than or equal to 250 km (150 miles) are classified as a long line. Otherwise, the line is classified as a medium line. All the mathematical equations for the long line are applicable to the short and medium lines. They also vary according to the number of nearby parallel conductors. Furthermore, different values are obtained for positive-sequence and zero-sequence currents [282, Sec. 2.2.1], [283, Ch. 5]. Here, it is only analysed for positive-sequence nominal values for a short line to simulate the distribution line under study, where shunt conductance is ignored for simplicity. The $ABCD$ constants of the transmission line and the $ABCD$ values can be calculated using the following formulas: [283, Sec. 5.2].

$$\begin{bmatrix} V_S \\ I_S \end{bmatrix} = \begin{bmatrix} A & B \\ C & D \end{bmatrix} \begin{bmatrix} V_R \\ I_R \end{bmatrix} \quad 3\text{-}14$$

$$A = \cosh(\gamma \ell) \quad 3\text{-}15$$

$$B = Z_c \sinh(\gamma \ell) \quad 3\text{-}16$$

$$C = \frac{1}{Z_c} \sinh(\gamma \ell) \quad 3\text{-}17$$

$$D = \cosh(\gamma \ell) \quad 3\text{-}18$$

where $A = D$ and $AD - BC = 1$.

3.7 Modified Line Modelling Including Energy Storage Devices (Battery and Supercapacitor) of the Electric Vehicles

In the analysis, EVs can be connected to any node on the line. The power resources of the EVs are battery and supercapacitor. It is useful to derive certain basic relationships for the ideal case of uniformly distributed compensation. The formulae are driven in most cases approximately for a practical system by focusing on compensation, since the spacing between the compensator

is limited by the same factors that limit the maximum length of the uncompensated line [282, Sec. 2.3.3].

The surge impedance Z_0 of an uncompensated line can be written as follows:

$$Z_0 = \sqrt{\frac{L}{C}} = \sqrt{\frac{j\omega L}{j\omega C}} = \sqrt{X_l X_c} \qquad 3\text{-}19$$

If a uniformly distributed shunt compensating capacitance C_{sh} (farad/km) is introduced, the effective value of the shunt capacitive admittance per km can be described in the following:

$$\overline{j\omega C} = j\omega C + j\omega C_{sh} = j\omega C(1 + K_d) \qquad 3\text{-}20$$

$$K_d = \frac{C_{sh}}{C} = \frac{X_c}{X_{sh}} = \frac{b}{\omega C} \qquad 3\text{-}21$$

Shunt capacitive compensation decreases virtual surge impedance and increases virtual natural load where it is assumed that the voltage remains unchanged, as shown in the following:

$$\overline{Z_0} = \frac{Z_0}{\sqrt{1 + K_d}} \qquad 3\text{-}22$$

$$\overline{P_0} = P_0\sqrt{1 + K_d} \qquad 3\text{-}23$$

The parameter K_d is useful to measure the required reactive power ratings for the compensating equipment [283].

The phase-shift constant (β) and the line angle (θ) are also modified and have a virtual value according to

$$\bar{\beta} = \beta\sqrt{1 + K_d} \qquad 3\text{-}24$$

$$\bar{\theta} = \theta\sqrt{1 + K_d} \qquad 3\text{-}25$$

where $\theta = \beta\ \ell$ and $\bar{\theta} = \bar{\beta}\ \ell$ [282, Sec. 2.3.3].

When the resistance of the transmission line is equal to zero, the line is called a lossless line, and the line loss factor (α) is equal to zero. Otherwise, the line is called a lossy line, and the loss factor α can be determined by [284].

$$\alpha = \frac{R}{\omega L}, \omega = 2\pi f \qquad 3\text{-}26$$

The surge impedance of the lossy line $\overline{\overline{Z_0}}$ can also be represented as

$$\overline{\overline{Z_0}} = Z_0\sqrt{1 - j\alpha} \qquad 3\text{-}27$$

For any degree of shunt compensation, the effect of additional shunt compensation capacitive increases $\bar{\theta}$ and $\overline{P_0}$ and decreases $\overline{Z_0}$, whereas inductive shunt compensation has the reverse effect. The above equations are used in the next sections to develop the mathematical equations

for finding the effect of integrating EV within the distribution line of a microgrid on the critical receiving end voltage and power value.

3.8 Voltage Stability Limits with Electric Vehicles Compensation

In general, the state of an electric power system can be classified as either stable or unstable. The boundary line of stability is any condition for a slight change in the unfavourable direction of any pertinent quality which will cause instability. The voltage instability of a system may occur due to an avalanche voltage process during a period of the light load with minimum plant generation, and low short-circuit level [284].

System voltage stability could be enhanced by adding reactive shunt compensation to the line either as a lumped capacitor or distributed capacitor. The battery and supercapacitor of EVs could be used as a shunt compensation to the line through a converter to match the electricity form between the resources and microgrid which is DC and AC respectively. Participating the resources of the EV as a shunt compensation depends on its state of charge. Due to its superior ability to short burst power, the supercapacitor in the EVs can be charged and discharged very rapidly. Therefore, it is almost possible to maintain a full charge for the supercapacitor before the stoppage of the EV. The EV could be used as effective bulk shunt compensation in an aggregated EV connected to the distributed network.

3.9 Effect of Compensation on Critical Receiving End Voltage and Power Values

The condition of voltage stability for connecting to the critical angular separation $\delta_{critical}$ and the critical receiving end voltage $V_{Rcritical}$ regarding the sending end voltage V_s and a generalized circuit constant $A_0 = a_1 + ja_2$ of the compensated transmission system at constant power factor (PF), is derived and set as

$$V_{Rcritical} = \frac{V_s}{2(a_1 \cos \delta_{critical} + a_2 \sin \delta_{critical})} \qquad 3\text{-}28$$

In addition, the critical transmission angle $\delta_{critical}$ that gives a constant power factor for the load is determined by

$$\delta_{critical} = \frac{1}{2} \tan^{-1}\left(\frac{k_1}{k_2}\right) \qquad 3\text{-}29$$

Finally, The maximum power transfer $P_{Rcritical}$ that limits the compensated system in terms of the SIL of a lossy line corresponding to $V_{Rcritical}$ and $\delta_{critical}$ when the system is operating on the verge of voltage stability, is derived in Appendix (C) and given by [6].

$$k_1 = a_1(b_1 \tan \emptyset + b_2) + a_2(b_1 - b_2 \tan \emptyset) \qquad 3\text{-}30$$

$$k_2 = a_1(b_1 - b_2 \tan \emptyset) - a_2(b_1 \tan \emptyset + b_2) \quad 3\text{-}31$$

$$P_{Rcritical} = \frac{\sqrt{2\sqrt{(1+\alpha^2)}}k_3k_4 - (a_1b_1 + a_2b_2)}{\sqrt{1+\sqrt{1+\alpha^2}}(b_1^2 + b_2^2) \times k_4^2} \quad 3\text{-}32$$

$$k_3 = b_1 \cos\delta_{critical} + b_2 \sin\delta_{critical} \quad 3\text{-}33$$

$$k_4 = a_1 \cos\delta_{critical} + a_2 \sin\delta_{critical} \quad 3\text{-}34$$

The transmission angle $\delta_{critical}$, load voltage $V_{Rcritical}$, and power transfer $P_{Rcritical}$ at the critical condition are evaluated by using equations 3-23, 3-24, and 3-25 respectively. The generalised line constants $a_1, a_2, b_1, and\ b_2$ for a line that plugs in EVs is given in Appendices D and E.

3.10 Example of Compensation Scheme

It may be useful to start with the simple line model without EV compensation. The generalised circuit constants $(ABCD)$ of the uncompensated transmission line are shown in the following [12]:

$$A_0 = \cosh(j\bar{\theta}) \quad 3\text{-}35$$

$$B_0 = \sinh(j\bar{\theta})Z_0R \quad 3\text{-}36$$

$$C_0 = \sinh(j\bar{\theta})\frac{1}{Z_0R} \quad 3\text{-}37$$

$$D_0 = \cosh(j\bar{\theta}) \quad 3\text{-}38$$

The characteristics of shunt compensation are illustrated as an EV connected to simplify the two-bus test system at the receiving end. The sending end produces active power which is transferred through a distribution line to the receiving end with constant power factor. The characteristics of the line under study are as follows [285]:

- Voltage at sending end is 400 V at 50Hz;
- Transmission line length is 300 m;
- Resistance for the line is 0.264 Ω/km; Inductance for the line is 0.071 mil Henry/km.

The generalised circuit constants $(ABCD)$ of the distribution line with EV compensation can be detrmined by

$$A_0 = \cosh(j\bar{\theta}) - j\sinh(j\bar{\theta})K_d\bar{\theta} \quad 3\text{-}39$$

$$B_0 = \sinh(j\bar{\theta})Z_0R \quad 3\text{-}40$$

$$C_0 = \sinh(j\bar{\theta})\frac{1}{Z_0R} - j\cosh(j\bar{\theta})\frac{K_d\theta}{Z_0} \quad 3\text{-}41$$

$$D_0 = \cosh(j\bar{\theta}) \quad 3\text{-}42$$

The numerical results from the line model are shown in Figure 3-16 to Figure 3-19. It is concluded that increasing the degree of shunt capacitive compensation will lead to an increase in the critical load angle, critical voltage and critical power curves at the receiving end bus bar. On the other hand, the results show a decrease in the surge impedance of the line. The reason for that linear increase is the additional shunt compensation which reduces the imaginary part of A and C parameters of the characteristics equation, whereas the B parameters remain the same at the same time the power factor is maintained as constant. Therefore, the *k* factors of the critical angle, voltage, and power influence due to A parameters change, which is reflected in the step increase of the curves. On the other hand, physically increasing the reactive power of the shunt compensation affects positively the voltage magnitude at the point of connection due to couple between the voltage and the reactive power of the Jacobian matrix. The power of the system is in relation to the voltage and current of the system. Thus, increasing the voltage of the system leads to increasing the power. The surge impedance loading has a nonlinear effect due to changing the compensation factor, whereas the K_d is the root square at denominated part of the surge impedance equation. Therefore, changing the compensation factor results in a negative effect on surge impedance loading, even at a constant power factor. On the other hand, adding a capacitive part to the electrical system leads to a reduction in the indicative characteristics of that system. Adding the battery and supercapacitor, both of which have capacitor characteristics, to the distribution line leads to a reduction in the inductive characteristics of that line. Therefore, adding a capacitor to the line is important to increase critical voltage and critical power at any point of the distribution line and reduce the inductive characteristics of the distribution line.

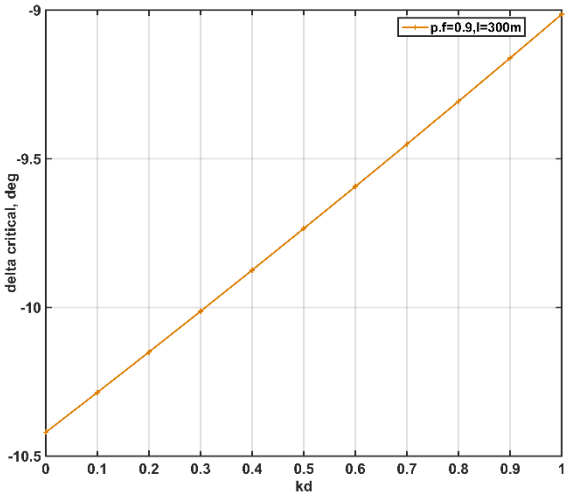

Figure 3-16: Critical load angle against range of capacitor shunt compensation

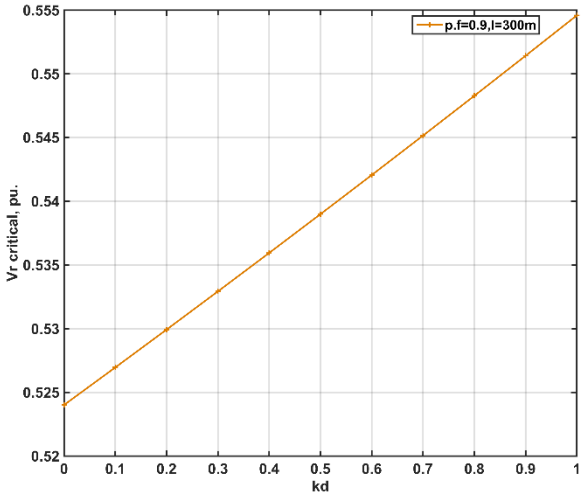

Figure 3-17: Critical voltage at receiving end bus against range of capacitor shunt compensation

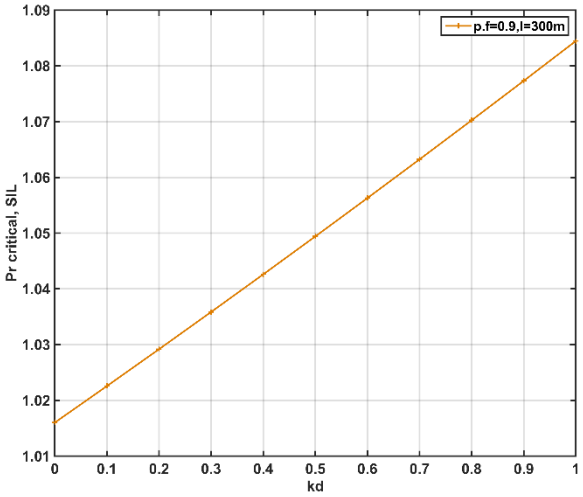

Figure 3-18: Critical power at receiving end voltage against range of capacitor shunt compensation

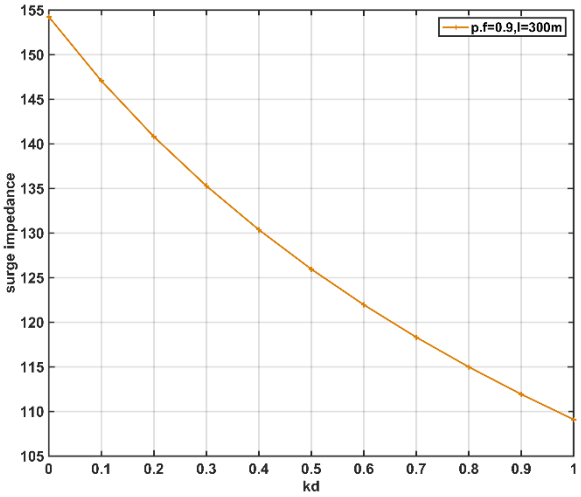

Figure 3-19: Surge impedance loading against range of capacitor shunt compensation

3.11 Numerical Analysis of Distribution Network with Electric Vehicles Compensation

Previous analysis of the microgrid has found that the minimum voltage profile occurs at bus bar number 47 which is about 0.9987 p.u. The minimum eigenvalue recorded is 0.446, which infers that the system is stable, whereas the participation factor analysis refers to bus bar number 33 as the weakest bus in the network. The decision about which selected node(s) the EVs should be connected to is based on the minimum voltage bus bar or the weakest bus bar on the system. It is suggested that reducing the eigenvalue of the system could be obtained by isolating the generator from bus bar 45 to study the effect of EVs on the microgrid. The minimum voltage becomes 0.9955 and 0.9961 at bus bar 47 and 46 respectively as shown in the voltage profile (VP) of the system without compensation at Figure 3-20 whereas the weakest bus bar becomes 49 as shown in the participation factor (PF) of the system without compensation at Figure 3-21. The details of the minimum voltage, minimum eigenvalue, and weakest bus bar of the system are illustrated in Table 3-3. The VPs of ten EVs are connected to the minimum voltage bus bar, weakest bus bar, and each of them, is shown in Figure 3-22, Figure 3-23, and Figure 3-24 respectively. The PF of ten EVs which are connected to the minimum voltage bus bar, weakest bus bar, and at each of them, are shown in Figure 3-25, Figure 3-26, and Figure 3-27 respectively.

The results show that the effect of adding ten EVs at the weakest bus bar (bus 25 from Figure 3-5) or the lowest voltage bus bar (bus 46-47 from Figure 3-4 and Figure 3-20) have a positive impact on the voltage stability and voltage magnitude at the minimum voltage bus bar. It is observable that the system voltage stability enhanced from 0.179 to 0.206 in the weakest bus bar integration case, whereas the voltage stability is still the same at the minimum voltage bus bar integration case. The voltage magnitude has the opposite effect to the voltage stability monitor. The results recorded that the voltage magnitude increased from 0.9955 as shown in Figure 3-20 to 0.9968 as in Figure 3-23 at bus bar 47 for the minimum voltage bus bar

integration case, whereas the voltage is still the same as in Figure 3-22 at bus bar 47 in the weakest bus bar integration case. Consequently, focusing on the enhancement of both parameters of voltage stability and voltage magnitude at the minimum voltage bus bar, the study proposes integrating the ten EVs on both bus bars. The results show that the voltage stability increased from 0.179 to 0.206 and the lowest bus bar voltage level increased from 0.9955 as in Figure 3-20 to 0.9968 as in Figure 3-24. The weakest bus bar is allocated at each analysis which has been moved from bus bar 49 as in Figure 3-21 to 45 as in Figure 3-25 at the weakest bus bar integration case and 40 as in Figure 3-26 at the minimum voltage bus bar integration case. It has become bus bar 21 as in Figure 3-27 for both bus bars integration cases.

Table 3-3: EVs connection detail

	Bus compensation No.	**Minimum voltage**	**Minimum eigenvalue**	**Weak bus**
1.	Without compensation	0.9955 at bus 47 and 0.9961 at bus 46	0.179	49
2.	Ten EVs at bus 25	0.9955 at bus 47 and 0.9961 at bus 46	0.206	45
3.	Ten EVs at bus 46	0.9968 at bus 47 and 0.9969 at bus 46	0.179	49
4.	Ten EVs at bus 25 and 46	0.9968 at bus 47 and 0.9969 at bus 46	0.206	21

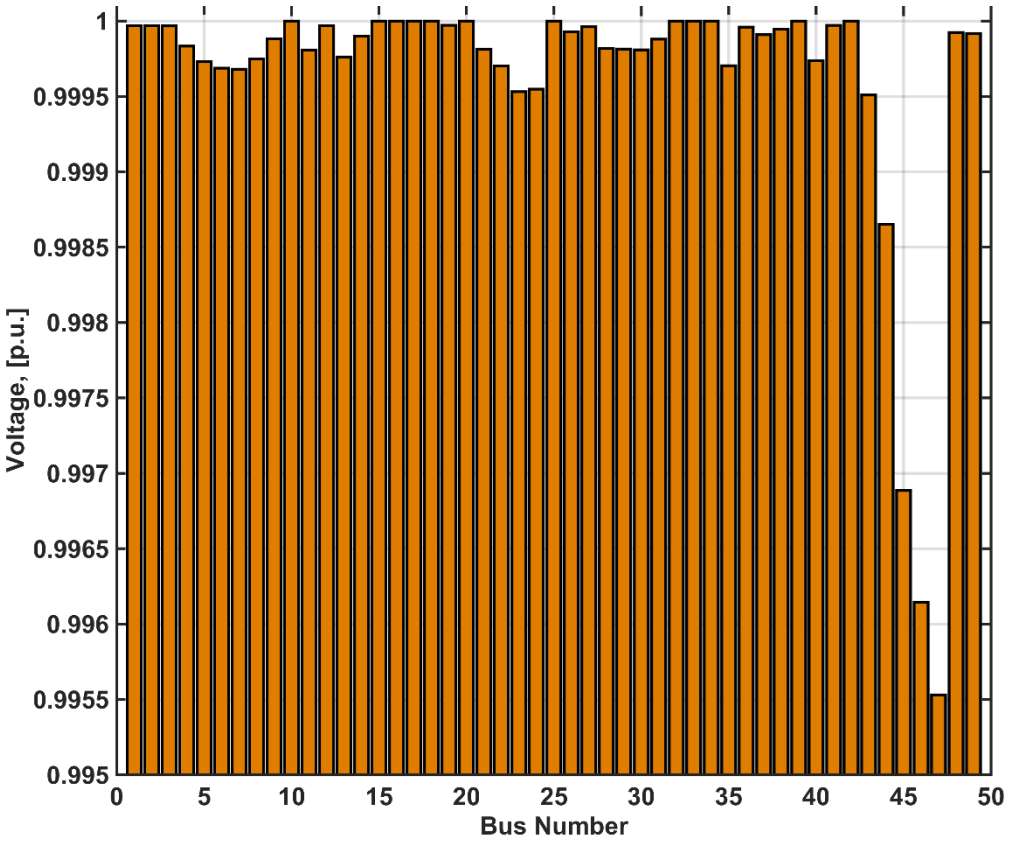

Figure 3-20: Voltage profile for microgrid at isolated mode and isolating the generator of bus bar 45

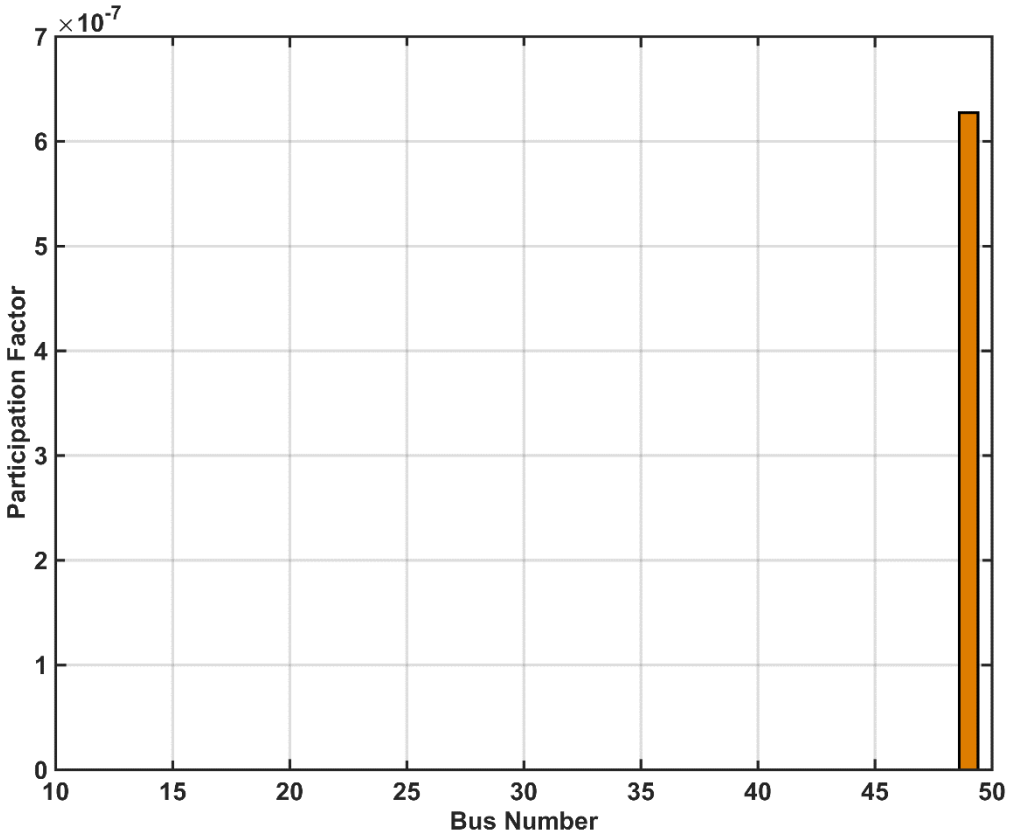

Figure 3-21: Participation factor for microgrid at isolated mode and isolating the generator of bus bar 45

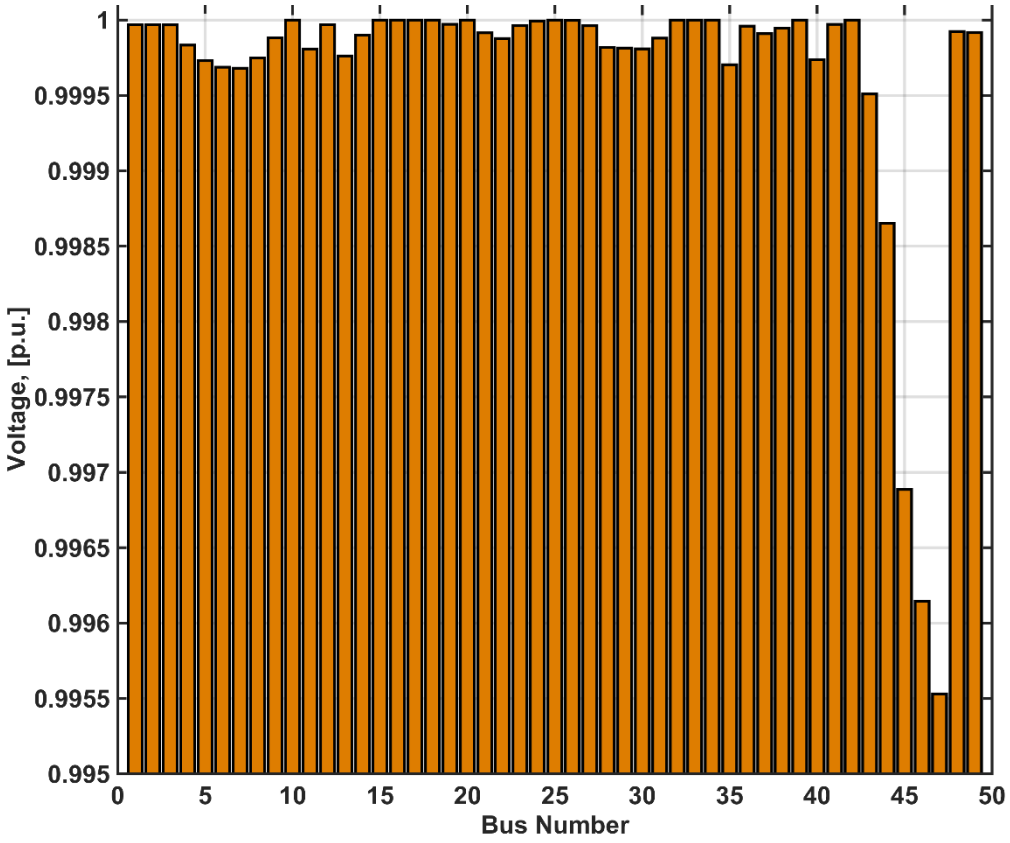

Figure 3-22: Voltage profile for system with ten EV compensation at weakest bus 25

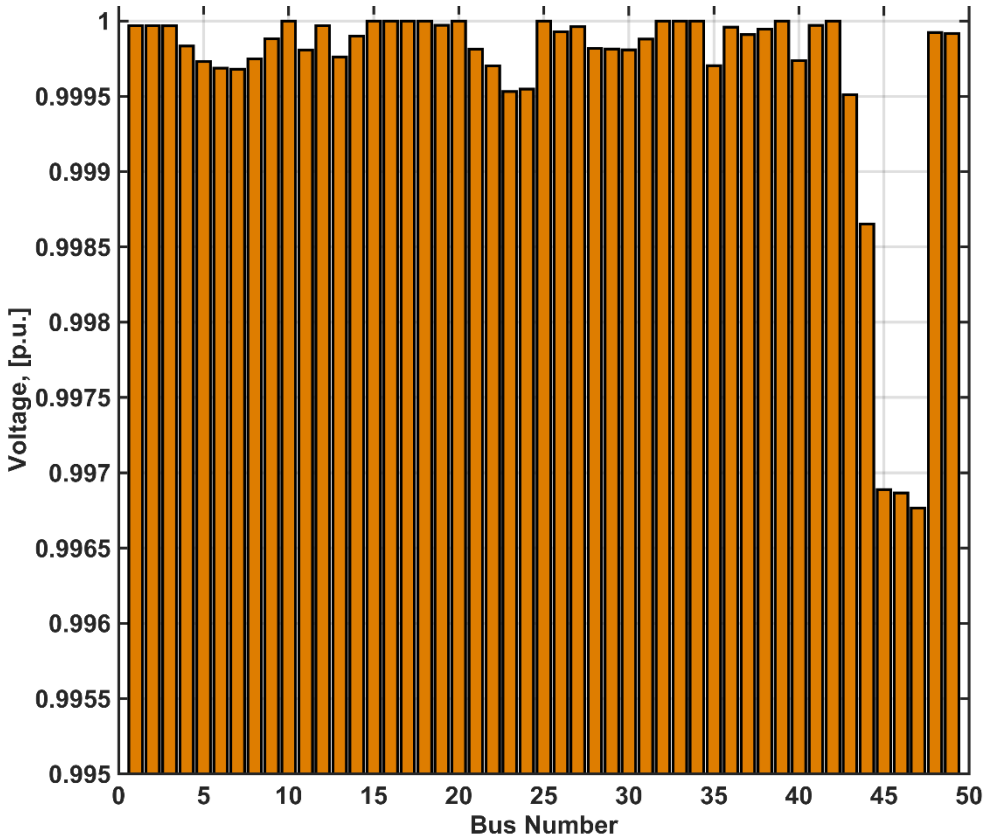

Figure 3-23: Voltage profile for system with ten EV compensation at minimum voltage bus 46

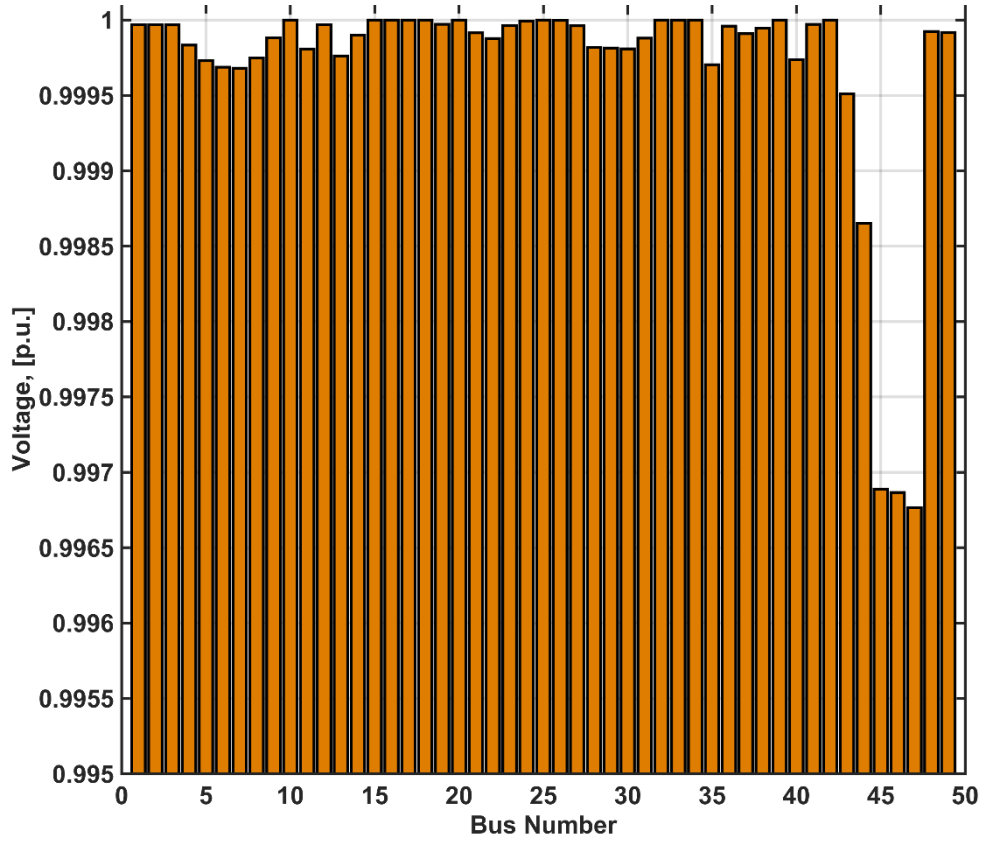

Figure 3-24: Voltage profile for system with ten EV compensation at bus 25 & 46

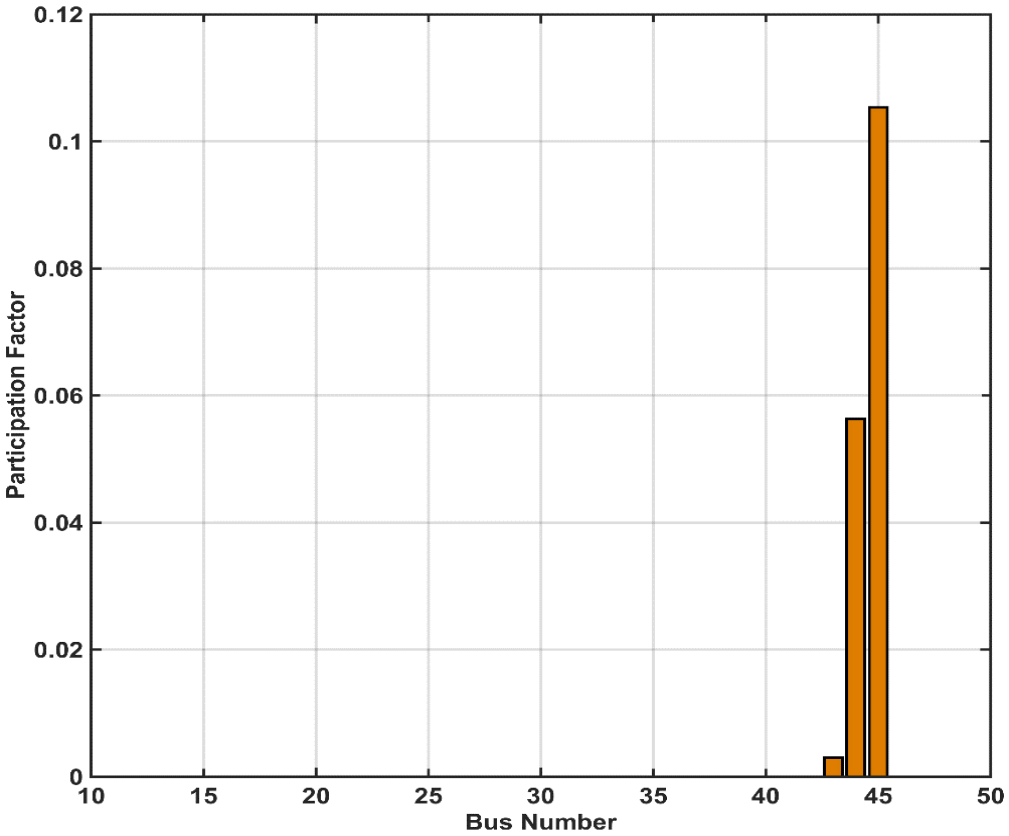

Figure 3-25: Participation factor for system with ten EV compensation at bus 25

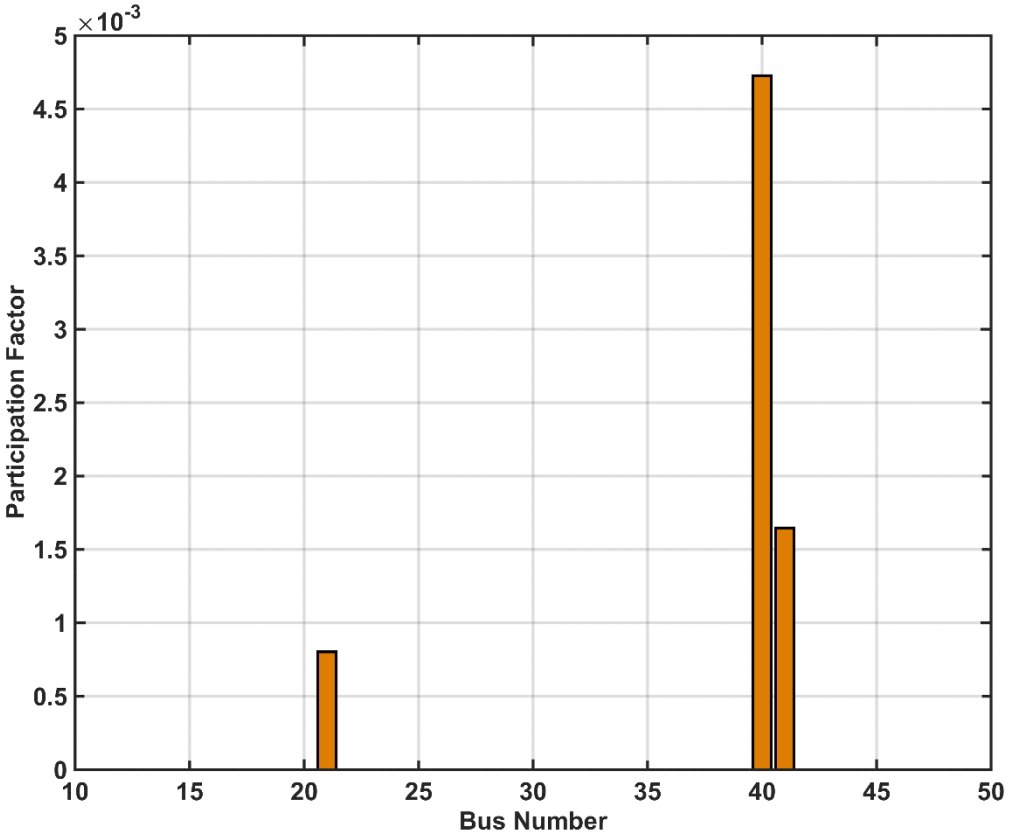

Figure 3-26: Participation factor for system with ten EV compensation at bus 46

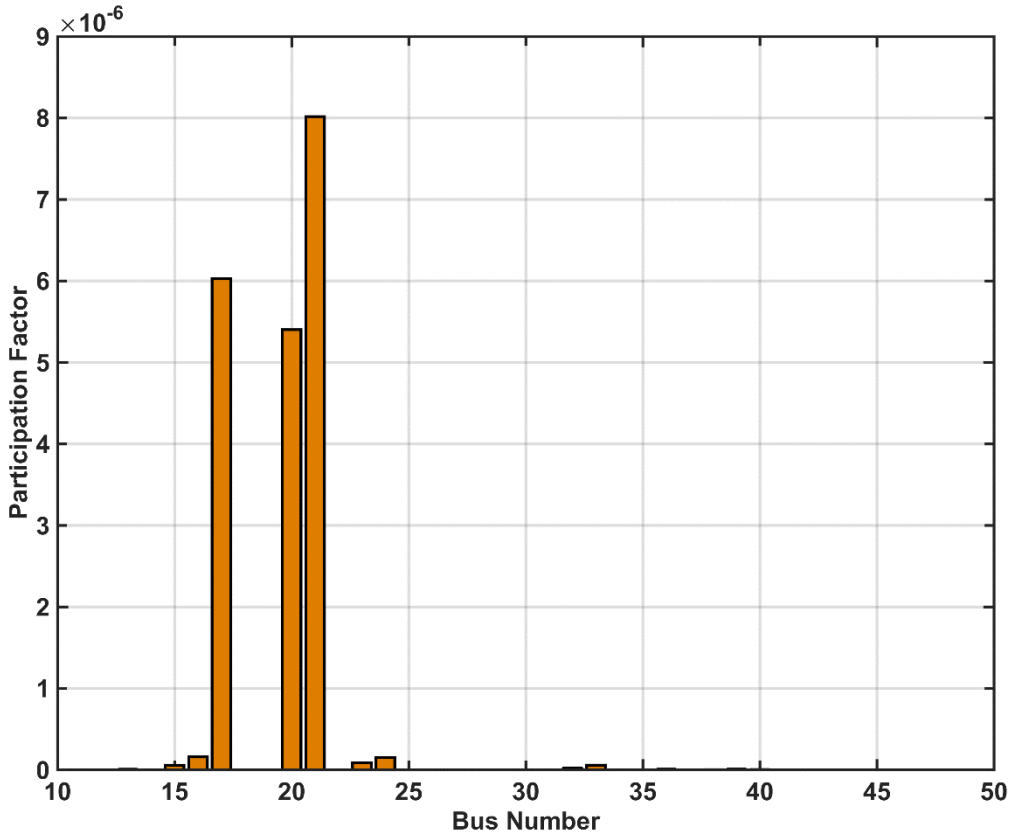

Figure 3-27: Participation factor for system with ten EV compensation at bus 25 & 46

Figure 3-28 shows the comparison of voltage profile for microgrid operation with connecting 10 EVs at different bus bar whereas the blue, orange, grey, and yellow bars refer to voltage profiles of microgrid without EVs, ten EVs connected at 25, ten EVs connected to bus 46, and ten EVs connected to buses 25 and 46 respectively. The voltage profile at some bus bars is not changed as shown in point A of bus bars one, two, and three at the figure. Bus bars 21, 22, 23, and 24 remarks at the point at the figure show better voltage profile value at connected EVs at bus bar 25 than other cases whereas bus bars 46, and 47 show better voltage profile level at connected EVs at bus bar 46 than other cases.

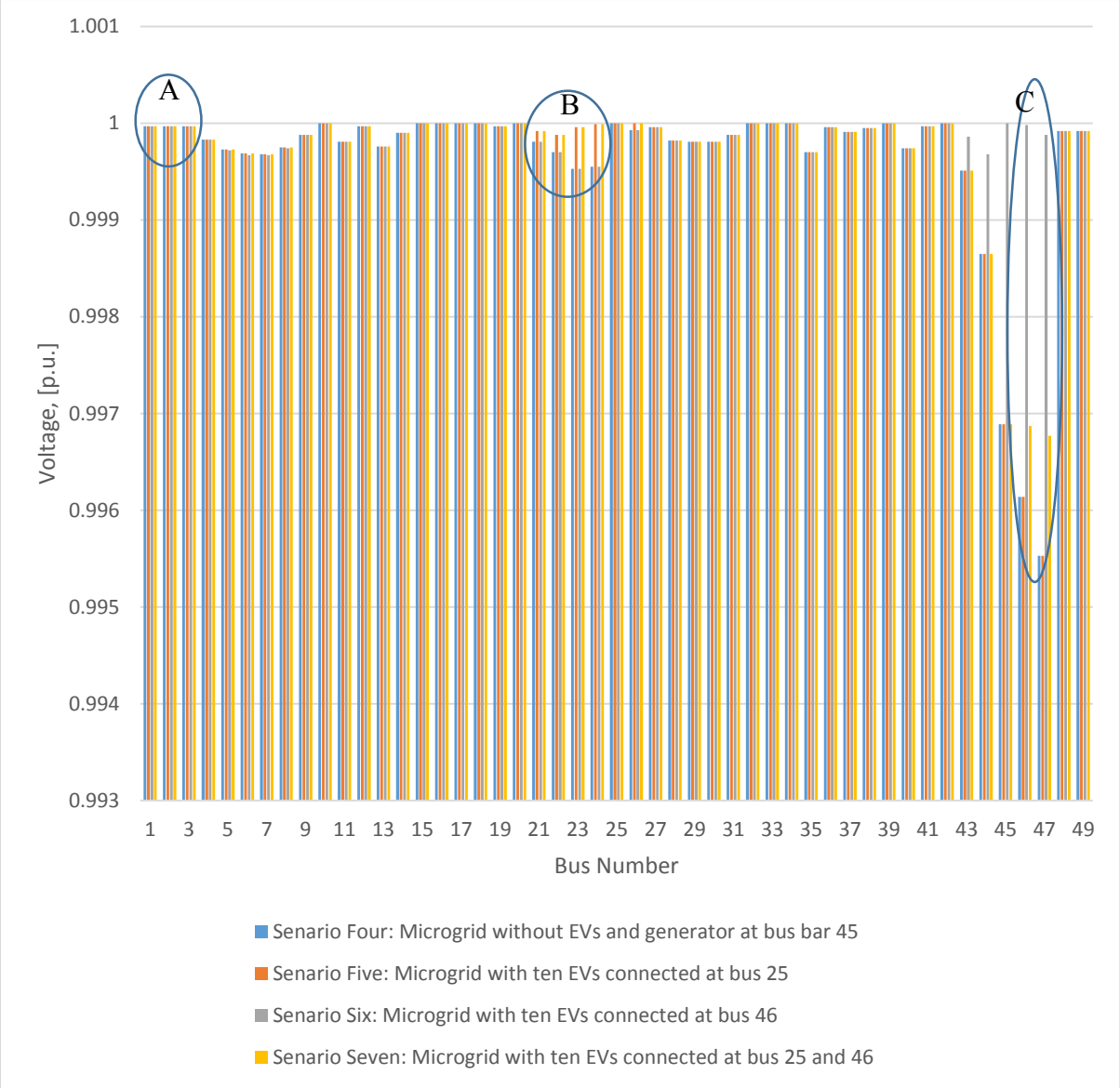

Figure 3-28: Voltage profile comparison of microgrid at different connected EVs buses

3.12 Conclusion

This chapter discusses the constructed resilient microgrid to recover quickly in disturbance situation for local operation in the realistic distribution network of a typical community and the effect of voltage stability and EVs on it. The resiliency index are focused on the development of advanced microgrid management and control functionalities to manage microgrid storage, electric vehicles, and load responsiveness, to operate the microgrid autonomously and in a manner of self-recovery that helps mitigate power grid disturbances which then improves electricity system flexibility, efficiency and stability. The major benefit of the microgrid concept is focused on covering the rapid growth of demand and reducing carbon dioxide emissions and pollutants using the ripeness of integrated distributed generators, especially the renewable energy resources. The resources are integrated near the electrical demand rather than generating the electricity in a large generation unit which mostly depends on fossil fuel located far away from the load. Different kinds of available distributed generators depend on the type of fuel consumed. The type of generator has been chosen based on the fuel cost and sustainability of generation to ensure that there is enough power to cover the demand at all times of a day and night. Some distributed generators are used including photovoltaic cells, microturbines, fuel cells, and diesel generator. The wind turbine is excluded from the study due to the low speed of the wind in Baghdad environment which makes using the wind turbine inefficient. The locations for installing the distributed generators are proposed to strengthen the most sensitive bus bar to voltage stability, which identifies using a participation factor analysis of eigenvectors. The eigenvalues indicate the voltage stability situation, whereas the eigenvectors indicate the mechanism of losing voltage stability in the system. The voltage analysis refers to the voltage stability being enhanced in the system for microgrid operation due to increasing the generation near the load. The microgrid makes the network able to operate in an island mode as a small single controllable system, or in a connected mode with the utility grid. This kind of operation (island and connected modes) leads a reduction in the losses and electrical demand at the transmission system, reduces the generation pressure on the supply units, and reduces the emission of pollutions that are produced at generation units. Therefore, the voltage stability is enhanced not only in the transmission system but also in the microgrid. However, this development makes the distribution network active, and the power flow bidirectional, which increases the possibility of electricity congestion happening in the system. Therefore, the microgrid needs to be controlled and handled properly by adding an intelligent controller and communication link between the loads and generation units.

The intermittent nature of the renewable energy may cause instability on the microgrid, which leads to integrating an energy storage system to compensate for the intermittency and maintain the generation and load balance of the microgrid. The EVs are a new insight to electrify the transportation sector for reducing emissions and pollutants and replace the existing propulsion vehicle with higher efficiency vehicles. There are many types of EVs in existence today; all of them are passive vehicles as power flows from the network to be stored in the energy storage system of the EVs. The future generation of EVs would be active where the power flow is bidirectional rather than unidirectional. Furthermore, the future generation makes the EVs feed energy into the microgrid by absorbing energy from the microgrid at the connection points. Therefore, the EVs could be exploited as mobile energy resources around the microgrid, thus

giving some revenue to the owners of the EVs at the discharging situation. Thus, it becomes essential to design an intelligent smart charger to control the energy storage systems of the EVs and satisfy the owners of the EVs. The location of a smart charger has been chosen as the proposed strategy to synergize the distributed generators.

Connecting many EVs to the microgrid, where power flow is bidirectional, requires mathematical equations to integrate the EVs into the distribution line of the microgrid. The mathematical equations facilitate the power flow analysis of the microgrid within integrating EVs and find the effect of the EVs on the microgrid characteristics. The efficient EV has two energy storage systems: battery as the main energy resource and supercapacitor as the main power resource. The electrical characteristic of the battery could be simplified to a capacitor storage because there is no exact implementation of the chemical reaction of the battery on the electrical characteristics. Moreover, the supercapacitor is a development of the conventional capacitor. Therefore, the electrical characteristics of the battery and supercapacitor are a capacitive load.

The results show that integrating the EVs within a microgrid reduces the surge impedance loading of the microgrid and increases the critical voltage limit and the critical power limit of the microgrid. Furthermore, the results show that integrating a combination of distributed generators and EVs in a particular location of an existing distribution network enhance the voltage stability and keep the system well away from a blackout in the heavily loaded system.

4. Chapter Four: Optimal Operation of Microgrids

4.1 Introduction

The previous chapter describes the benefits of operating the distribution network in a microgrid operation based on voltage stability analysis as either in connected mode with a transmission system or in isolated mode, in emergency electricity markets. Furthermore, a mathematical model is proposed in order to integrate the EVs within the distribution line of the microgrid to easily accommodate the EVs' parameter within the power flow analysis of the system. However, the microgrid operates in a bidirectional rather than a single direction. Therefore, the possibility of electricity congestion becomes a challenge to achieving a resilient operation of the microgrid. The microgrid should be handled accurately by adding an intelligent controller to operate properly each device connected to the microgrid and the communication links between the devices, to communicate with them instantly for a precise decision on balancing the load and generation of the system. Therefore, this thesis proposes a unified systematic framework structure that decomposes the power management of the devices into modular blocks in chronological executions. This chapter describes the top tier of the modular management structure that handles the strategic planning or long-term strategy of the balancing between generation and electrical demand for power. An intelligent technique is designed and simulated, which manages the operation of EVs within the microgrid units. Cplex within the MATLAB environment is used to find the optimal operation setting, depending on the detailed economic and environmental models. The proposed methodology is applied to the realistic network of a Baghdad community operating in four scenarios. The objective function of the intelligent management and control tool is to minimise both the operation costs of the generating units and the pollutant treatments cost by satisfying the load demand and the operating constraints. Moreover, the optimisation problem could be classified as a multiobjective and quadratic programming problem. Therefore, the approach used is mixed integer quadratic programming to solve the multiobjective optimisation problem based on the weighted sum method. The proposed optimisation method considers the operation, maintenance, and start-up costs in the modelling of each generating unit, as well as the emission reduction treatment cost of NO_x, SO_2, and CO_2. The tariff curve of daily operation has been chosen as the variable across a whole day.

This chapter attempts to provide a further understanding of the impact of the management and control of EVs and distributed generators in a microgrid; it focuses primarily on the implementation of the 'microgrid operator'.

4.2 Algorithm Design of the MGO

The hierarchical modular framework structures the microgrid into three operators. MGO is the high strategy level of framework to manage and control balancing sources and loads power flow. The output of the optimisation model is the optimal configuration of the microgrid. The procedure to achieve optimal operation is listed below and depicted in Figure 4-1 whereas the

implementation strategy of microgrid optimisation operation summarises in the flow chart as shown in Figure 4-2.

- Calculate the power output of wind turbines using the wind turbine model based on deterministic wind speed measurement data for the city of Baghdad during July 2015, as depicted in Figure 4-5 [286].
- Calculate the power output of photovoltaic panels using the photovoltaic model based on deterministic sun irradiation measurement data and temperature measurement data for the city of Baghdad during July 2015, as depicted in Figure 4-3 and Figure 4-4 respectively [286].
- Calculate the unmet load demand of a wind turbine and photovoltaic panel to serve it from other distributed generators.
- Calculate either the CSO charging power in a healthy system or the CSO discharging power in an unhealthy system.
- Apply the optimisation algorithm to calculate the optimum fuel cells' power, microturbine power, and diesel generator power that meet the rest of the load demand.
- Calculate either the purchasing power from the utility grid when the sum of the distributed generators power is not enough to meet the load demand or sell power to the utility grid when the sum of the distributed generators power is more than the load demand and cheaper than the power of the utility grid at an hourly tariff.

The decision of the power amount taken from the distributed generators of an optimisation algorithm is based on the fuel price, the maintenance cost, the startup cost, and pollutants treatment cost. The wind turbine and the photovoltaic panels are assumed to generate free emission.

Normally the microgrid operation based on renewable energy sources to cover the main loads for low operation and treatment cost. However, in case of missing the source of renewable energy, different types of distributed generators are used to cover the loads of the microgrid. Therefore, the wind turbine is replaced with the photovoltaic cell in this study because the wind turbine is not efficient to use as the wind speed is very low in the Baghdad area, whereas the output power of the wind turbine is very small or cut off at a wind speed below 3 m/s.

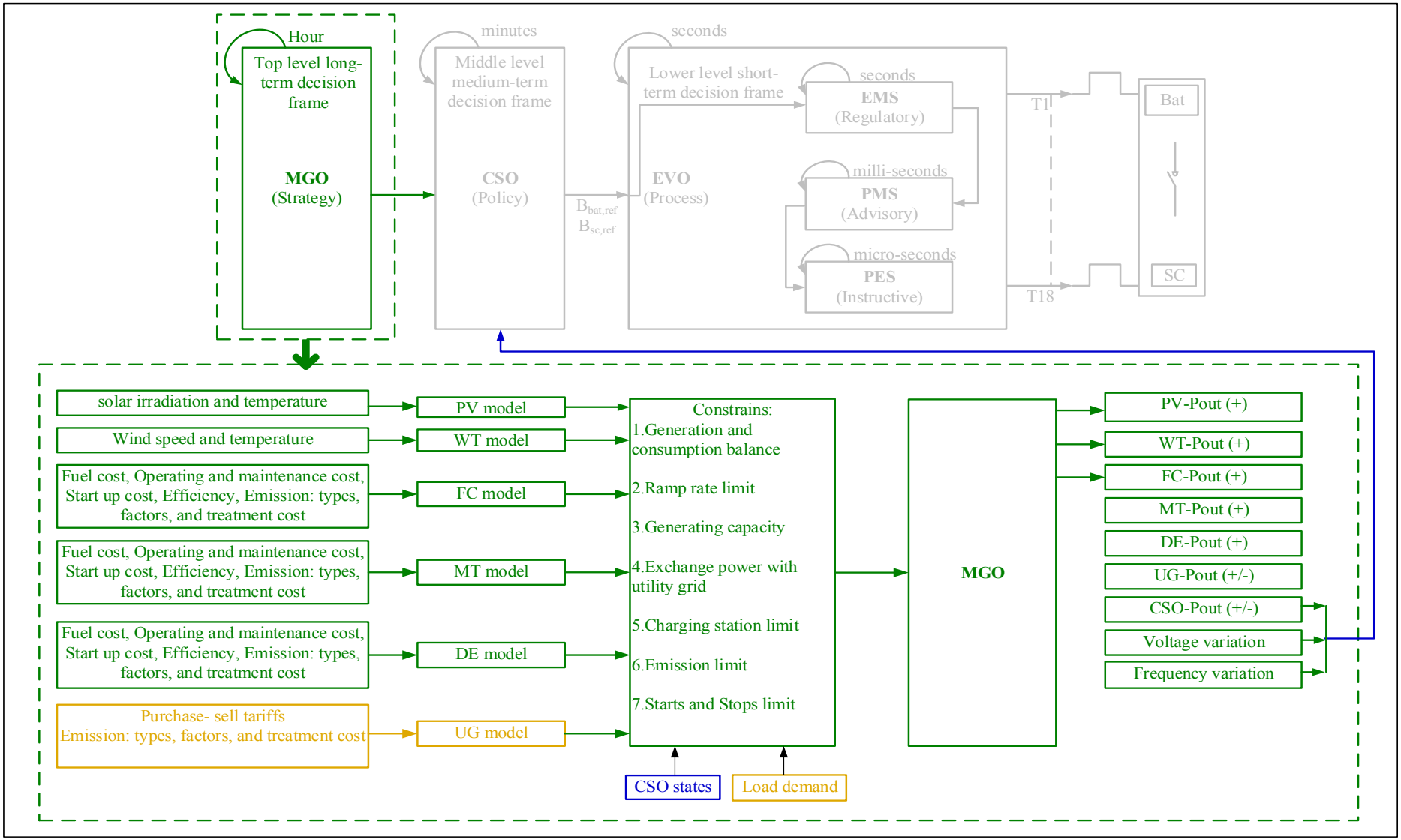

Figure 4-1: The optimisation algorithm

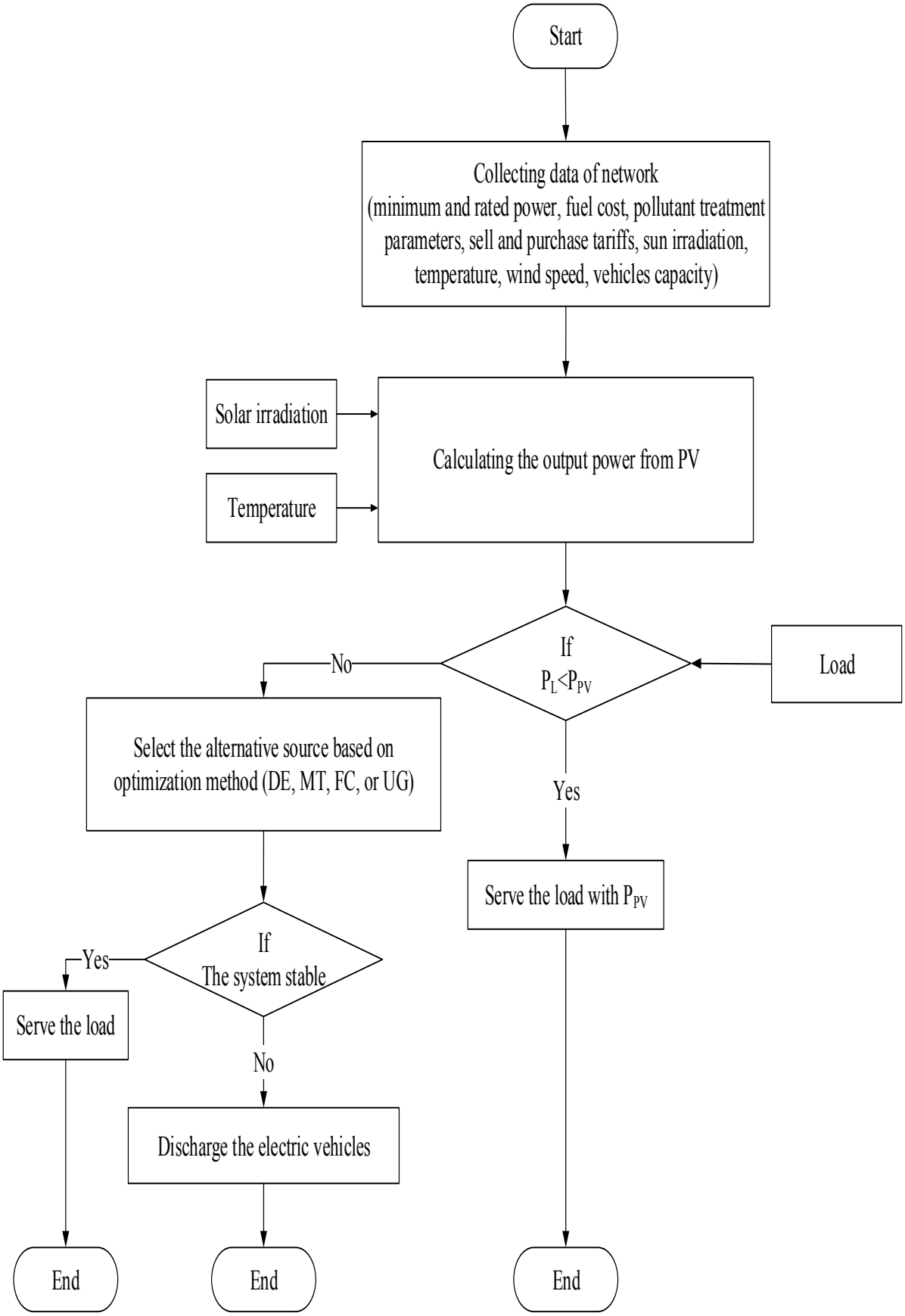

Figure 4-2: Flow chart of microgrid optimisation strategy

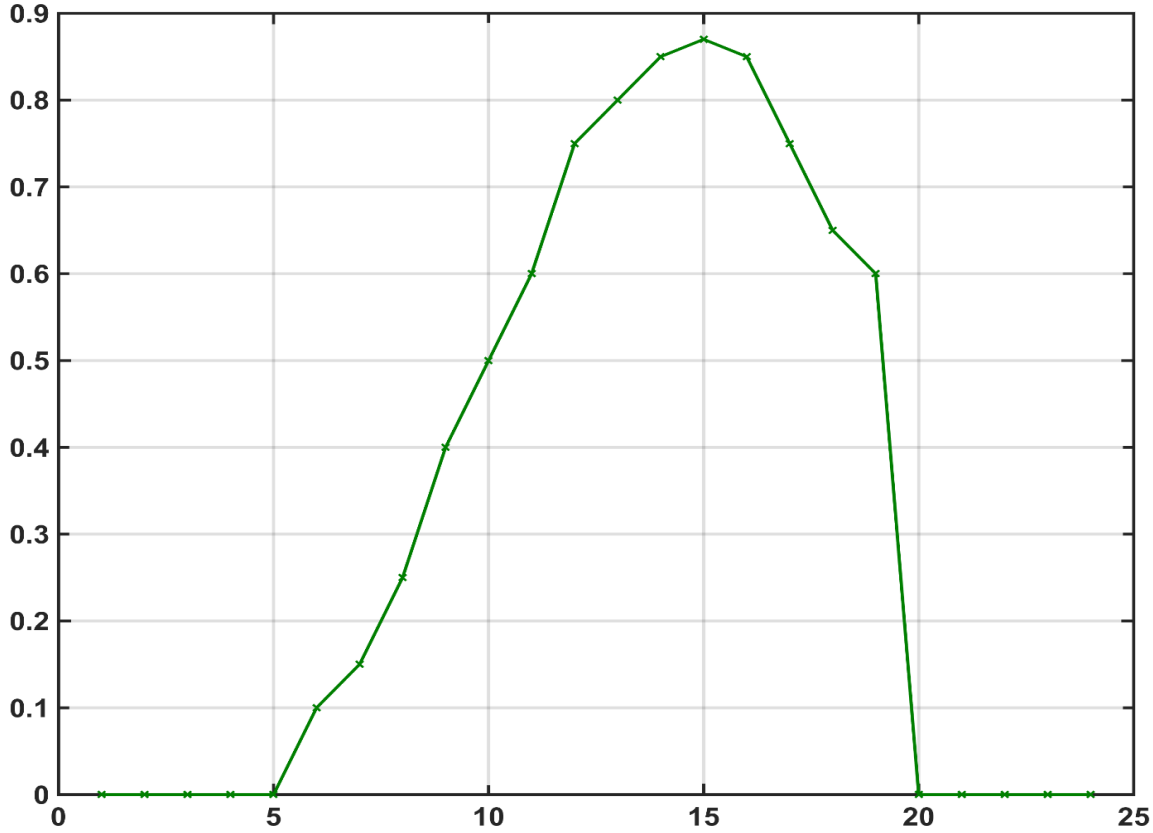

Figure 4-3: The input solar irradiation to the model (Experimental data with linear interpolations) [286]

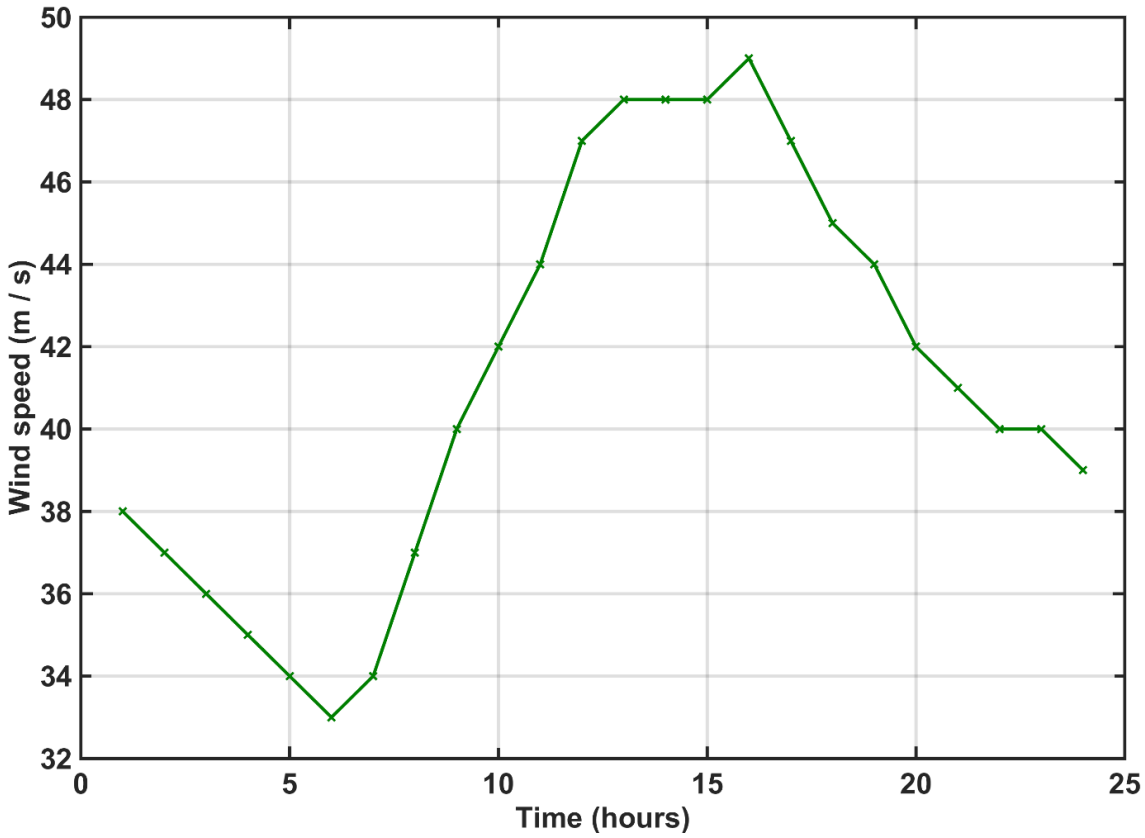

Figure 4-4: The input temperature to the model (Experimental data with linear interpolations) [286]

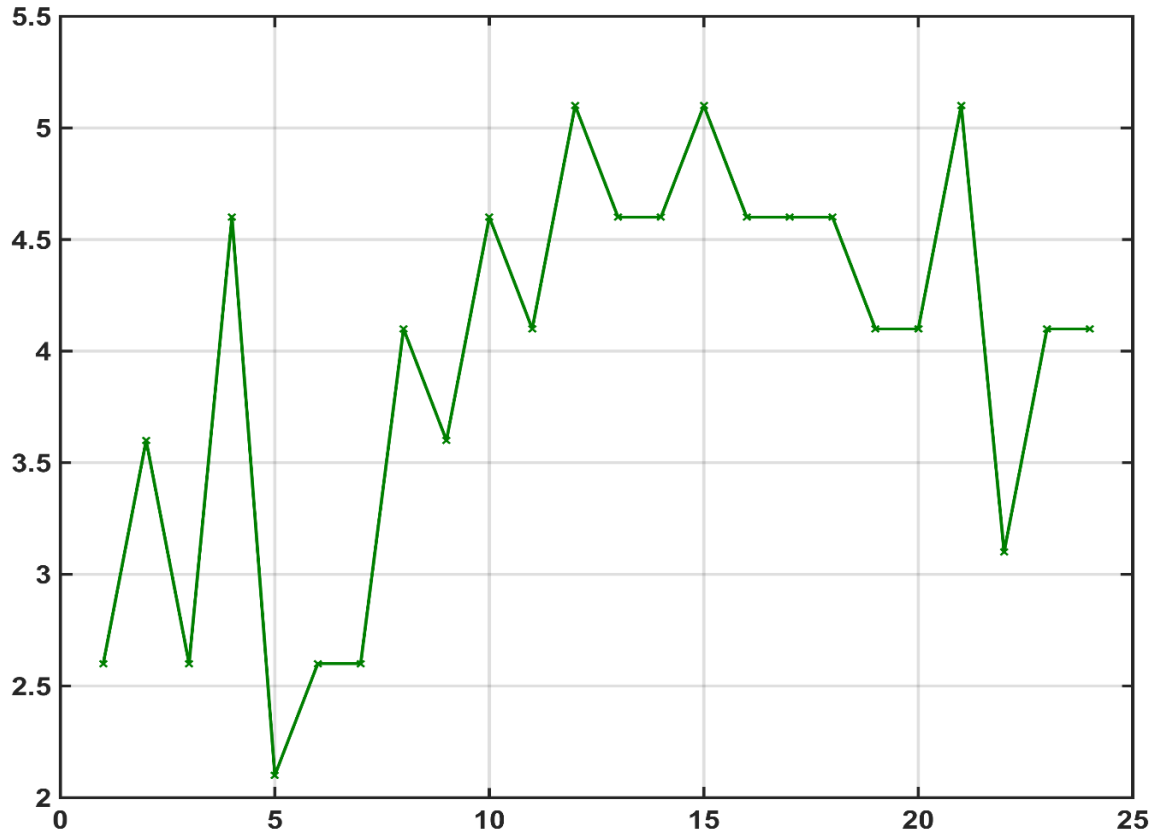

Figure 4-5: The input wind speed to the model (Experimental data with linear interpolations) [286]

4.3 Optimisation Model of Microsources

Energy management of the microgrid sets the active and reactive power output of each of the microsources. It was developed and tailored for the microgrid with the high penetration of distributed generators, including renewable energy sources. The energy management problem amounts to minimising the microgrid social net cost. It affects operation cost, minimises the network losses, reduces greenhouse gas emissions and particulates, and adjusts the value of voltage and frequency in microgrid operation. The economic optimisation of the microgrid regarding costs, losses and greenhouse gases, is implemented using the economic dispatch. The main impact of the economic dispatch is balancing the generation and demand in microgrid operation to maintain the voltage and frequency range. This section focuses on the economic dispatch problem to produce an output power of microsources in a multiobjective function, in both grid connected mode and islanded mode. The objective function introduces multiobjective functions, which are lowest operation cost, lowest pollutants treatment cost and lowest carbon dioxide treatment cost. The output of the optimisation model is the optimal operation of the microgrid when considering all parameters, which include the following:

- Technical performance of available energy sources.
- Fuel cost.
- Operating and maintenance cost.
- Sun irradiation.
- Daily sell-buy power tariff.
- Daily load demand curve.

- Startup cost.
- Wind speed.
- Losses of the microgrid operation.
- Pollutants treatment costs.

Several different kinds of literature have detailed the modelling of various microsources of the microgrid, such as [106], [287]–[291]:

4.3.1 Wind turbines model

Two important factors are considered in the design of the wind turbine model: the wind speed at the specific location and the power curve of the wind turbine. The optimisation wind turbine model, which is used to calculate the output power supplied by the wind turbine generator as a function of wind velocity, density of air, capture area or swept area, and capacity factor, can be calculated by

$$P_W = \begin{cases} 0 & v < v_{ci} \\ 0.5.sa.v^3.rho.cf & v_{ci} \le v \le v_{co} \\ P_{Wr} & v_{co} \le v < v_{cco} \\ 0 & v_{cco} < v \end{cases} \quad 4\text{-}1$$

$$Sweptarea(sa) = \pi\left(\frac{rotordiameter}{2}\right)^2 \quad 4\text{-}2$$

where

Cut on speed $v_{ci} = 3\ m/s$
Corner Speed $v_{co} = 14\ m/s$
Cut out speed $v_{cco} = 25\ m/s$
Rotor Diameter $= 10\ m$
The density air $\rho = 0.1\ kg/m^3$
Capacity Factor (cf): it is actual output to potential output ratio.

The wind speed data for the rated power of 50kW from the wind generator output is obtained from [292] for 24 hours on 26 July 2015, as shown in Figure 4-6.

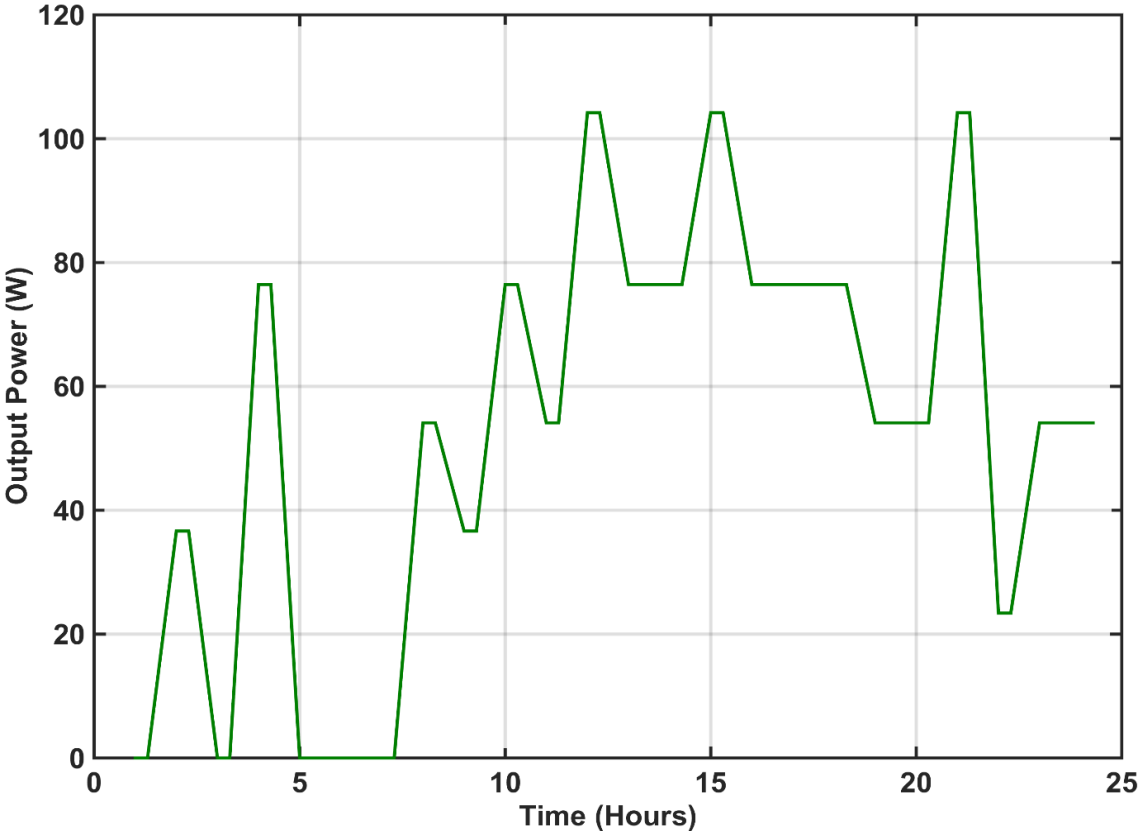

Figure 4-6: Wind turbine power generation (simulated results)

4.3.2 Photovoltaic arrays model

The photovoltaic system is a set of solar cells electrically connected and supported in a mechanical structure. The simple equivalent model of a solar cell is shown in Figure 4-7; it is represented by a diode in parallel with the constant current source and shunt resistance, all of which are connected in series with resistance. The series resistance represents the internal resistance of the current flow, whereas the shunt resistance relates inversely to the leakage current to the ground. Ideally, there is no series loss. Thus, the series resistance is equal to zero, and there is no leakage to the ground where shunt resistance is equal to infinity. The photovoltaic model is very sensitive to any variation in series resistance, whereas it is not sensitive to the variation of shunt resistance. Therefore, any change in series resistance could affect the photovoltaic model output significantly. The output current of a solar cell is proportional to the light falling on the cell. It is necessary to take weather data (irradiance and temperature) as an input variable to draw current, voltage, and power as an output value. The net current of the solar cell, which represents the difference between photocurrent and diode current [293], [294], is explained in the following:

$$I = I_L - I_{os}\left(e^{\frac{q(V+IR_S)}{nkT}} - 1\right) - \frac{V + IR_s}{R_{sh}} \quad 4\text{-}3$$

$$I_L = \frac{G}{100}[I_{SCR} + K_I(T - 25)] \quad 4\text{-}4$$

$$I_{os} = I_{or}\left(\frac{T}{T_r}\right)^{\frac{3}{n}} e^{\frac{qE_{GO}}{nk\left(\frac{1}{T}-\frac{1}{T_1}\right)}} \quad 4\text{-}5$$

$$I_{or} = \frac{I_{sc}(T)}{\left(e^{\frac{q(V_{OC}(T))}{nkT_1}} - 1\right)} \quad 4\text{-}6$$

The series resistance of each cell can be written as:

$$R_s = -\frac{dV}{dI_{Voc}} - \frac{1}{X_V} \quad 4\text{-}7$$

$$X_V = I_0(T)\frac{q}{nkT_1} e^{\frac{q(V_{OC}(T))}{nkT_1}} \quad 4\text{-}8$$

. The net output power of a photovoltaic cell depends mainly on the number of solar cells connected to the model. A photovoltaic system output is typically connected to microgrid via an inverter to convert the output DC power of the photovoltaic system side to AC power at the grid side.

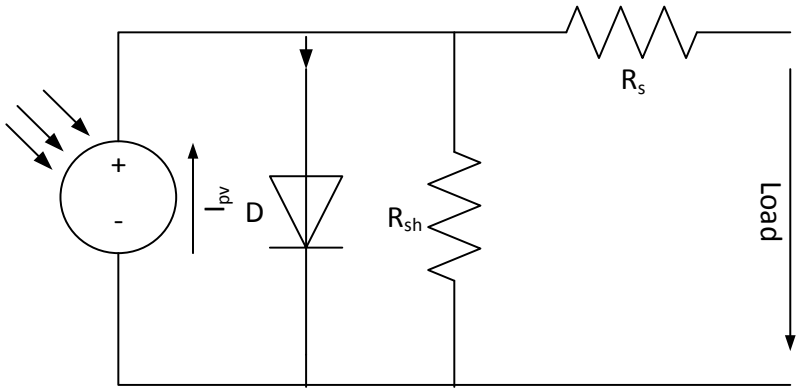

Figure 4-7: Photovoltaic model

The standard output power and maximum output power tracking of the cell are shown in the following:

$$P_{cell} = V_g I \quad 4\text{-}9$$

$$P_m = V_m I_m \quad 4\text{-}10$$

The solar generation data for photovoltaic generation output are obtained from [292] for 24 hours on 26 July 2015, as shown in Figure 4-8. The rated power of the photovoltaic cell is 50 kW and the total surface to combine them can be described by.

Total Power Output = Total Area . Solar Irradiance . Conversion Efficiency 4-11

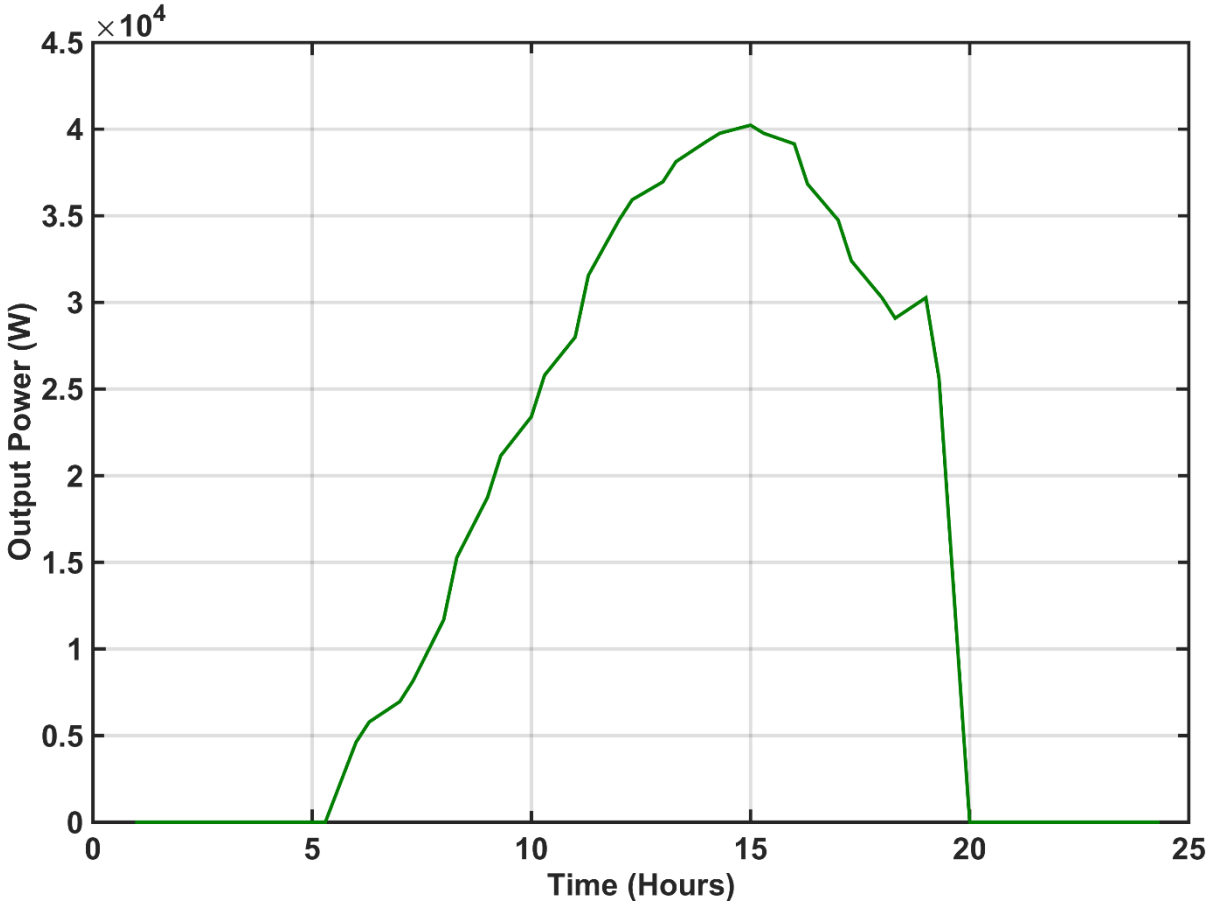

Figure 4-8: Photovoltaic power generation (simulated results)

4.3.3 Microturbines model

The microturbine is a small combustion distributed generator with a power output of 25 kW to 500 kW. The microturbine creates high-speed rotation by burning gaseous and liquid fuel to generate electricity. Typically, the microturbine can ramp up within a short time, estimated to be between 10 seconds and several minutes, to generate electricity based on the size range [289]. Microturbine efficiency increases with the increase of supplied power [295]. The microturbine has the environmental advantage of low emissions as well as fuel cells [296]; fuel cells are quieter than microturbines.

4.3.4 Fuel cells model

A fuel cell is a small electrochemical process distributed generator with a power output of a few kilowatts. The fuel cell produces energy using an electrochemical reaction between oxygen and hydrogen. The fuel cell has a higher efficiency and lower emissions than diesel engines; however, it is too expensive for many applications.

4.3.5 Diesel generators model

A diesel generator is a small combustion distributed generator with various power outputs from small units of 1 kW to large units of several tens of MW. The diesel generator is used in many applications because of its high efficiency and reliability. The diesel generator also has a fast dynamic response for disturbance rejection to cover any sudden changes in demand. However, the power cost and carbon dioxide emissions of a diesel generator are relatively higher than other distributed generators. The fuel cost of diesel generator power can be modelled as a quadratic polynomial according to

$$C_{dg,i} = \sum_{i=1}^{N} \alpha_i + \beta_i P_{dg,i} + \gamma_i P_{dg,i}^2 \qquad 4\text{-}12$$

The comparison between distributed generators is shown in Table 4-1.

Table 4-1: Distributed generators compression [297]–[300]

Criterion	Fuel cell	Gas turbine	Diesel
Efficiency over a wide range of loads	Relatively flat	Best at > 80%, very poor at partial load	Best at > 75%, poor at partial load
Response to load changes	Slow at start-up	Fast	Good
Life	5 years (goal)	20+ years	20+ years
Noise vibration	Low	Medium	High
Power range	20-2500 kW modular	Up to 50 MW	Up to 68 MW
NO_x, CO, HC emissions, CO_2	Very low, reduced CO_2	Medium, no CO_2 benefit	Medium
Life time in operation hours	>2,000	>20,000	~13,000
Moving parts number of units	Blower/pump	Rotor only	>50
Thermal management	Water cooled	Exhaust emission	Water cooled
Onboard fluid storage	Water antifreeze	None	Water antifreeze and lubricating oil
Electrical generation	Yes	Yes	Yes
Emission control treatment	No	Yes	Yes
Freeze tolerant	No	Yes	Yes
>60ºC ambient operation	Not proven	Not proven	yes
Heat to power ratio	1.4	2.6	1.6

4.4 Electric Vehicles Model

The energy storage system is the powertrain of EVs, which have bidirectional power flow characteristics. Therefore, the EVs provide a great opportunity to discharge some power from

the energy storage system to synergize the distributed generators of the microgrid in balancing the net demand under the supervision of the intelligent controller. This feature could encourage the owners of the EVs to charge those vehicles at a low rate tariff, which normally occurs during light demand, and make it ready to discharge at high rate tariff which normally happens during high demand. Therefore, the owners of the EVs could make revenue money from charging and discharging those vehicles where the discharging rate is often higher than charging rate. Discharging the EVs helps the microgrid to maintain the stability and reliability of the system.

The modelling of the EVs is intended primarily to follow the behaviour of drivers. Prediction, the discharging power of the EVs, depends mainly on the spatial characteristics of the EVs, the range of the discharging state of charge of the energy sources, and the required energy for the next journey of the EVs after being unplugged from the microgrid.

The CSO is responsible for the centralised smart charger. The objective function of the CSO is either achieving a minimum charging cost of the EVs where

$$\text{Cost charge} = \sum_{i=t_a}^{t_d} \sum_{j=1}^{N} \alpha . s_1 . \varepsilon_1 . P_{ch,ij} . \Delta t . F . \rho . C_{rate,p,ch} + \alpha . s_1 . \varepsilon_2 . Q_{ch,ij} . \Delta t . F . \rho . C_{rate,q,ch} \quad 4\text{-}13$$

or achieving a maximum discharging cost of the EVs where

$$\text{Cost discharge} = \sum_{i=t_a}^{t_d} \sum_{j=1}^{N} D . \beta . s_2 . P_{dis,ij} . \Delta t . F . C_{rate,p,dis} + D . \beta . s_2 . Q_{dis,ij} . \Delta t . F . C_{rate,q,dis} \quad 4\text{-}14$$

Further information about the operation of the CSO, to optimise the charging and discharging power of EVs is provided in Chapter five.

4.5 Electric Vehicles Charging-Discharging Limits

The total number of EVs are distributed around the grid related to the geographical area based on the chosen location of the charging station system [166]. Two bus bars have been chosen to distribute aggregated EVs according to the effective location calculation based on voltage stability; these bus bars are the weakest bus bar and the lowest voltage profile bus bar. The EVs are considered to be mobile energy storage systems in this chapter, whereas the next chapter describes the status of each EV. Therefore, the EVs are represented as a group of storage energy systems connected to the bus bars.

The amount of power that can be supplied to or from the EVs at a specific time is limited to the power amount stored in the resources of the EVs, which represents the power of the CSO

as one step behind the collective power of the EVs for the resilient process, can be determined by

$$P_{EVs}(t) = P_{cso}(t-1) \quad 4\text{-}15$$

The measurements of charging or discharging are based on the state of charge level and specific rates.

4.6 Cost formulation – Multiple Objective Definition

Each type of distributed generator has a different operating cost based on the type of fuel, maintenance cost, and startup cost as follows:

4.6.1 Microsources operating cost

The operating cost of the microturbine and fuel cell usually includes fuel cost, maintenance cost, and startup/shutdown cost in ($/h) can be calculated as follows [289]**:**

$$CF(P) = \sum_{i=1}^{N} (C_{dg,i}P_{dg,i} + OM_{dg,i} + SC_{dg,i}) \quad 4\text{-}16$$

4.6.2 Fuel costs of Microturbines and fuel cells

The fuel cost of the microturbine and fuel cell is calculated as [295].

$$C_{MT,i} = C_{nl} \sum_{J} \frac{P_J}{\eta_{lJ}} \quad 4\text{-}17$$

4.6.3 Maintenance costs

Maintenance costs of the microturbine, fuel cell and diesel generator are proportional to the supplied power, based on forecasting in a minimal real life situation of microsources. Thus, the maintenance cost of unit i in time interval t, which refers to accumulated power generated by a source time of the maintenance factor of that source, can be written as [287].

$$OM_{dg,i} = K_{om} \sum_{i=1}^{N} P_{dg,i} \quad 4\text{-}18$$

4.6.4 Startup costs

The distributed generator start-up cost depends mainly on the time the unit has been off before it starts up again. The start-up cost of the distributed generators can be described as follows[301]:

$$SC_{i,t} = KSC_i(\delta_{dgi,t} - \delta_{dgi,t-1}) \quad 4\text{-}19$$

where $SC_{dg,i,t} \geq 0$

$$\delta_{dgi} = \begin{cases} 1 & \text{if distributed generator is ON} \\ 0 & \text{otherwise} \end{cases}$$

4.6.5 Pollutants treatment costs

The pollutants treatment cost of the microgrid can be described as two functions: the pollutants treatment cost and the carbon dioxide (CO_2) treatment cost. The pollutants treatment cost includes sulphur dioxide (SO_2) and nitrogen oxide (NO_x). The equations to implement the pollutants treatment cost in the microgrid network are divided into two equations, as explained in the following:

$$E(P) = E1(P) + E2(P) \quad 4\text{-}20$$

$$E1(P) = \sum_{i=1}^{N}\sum_{k=1}^{N}(C_k\gamma_{ik})P_{dg,i} + \sum_{k=1}^{N}(C_k\gamma_{grid,k})P_{grid} \quad 4\text{-}21$$

$$E2(P) = \sum_{i=1}^{N}\sum_{k=1}^{N}(C_{co2}\gamma_{ico2})P_{dg,i} + \sum_{k=1}^{N}(C_{co2}\gamma_{grid,co2})P_{grid} \quad 4\text{-}22$$

Equation 4-21 refers to SO_2 and NO_x pollutants treatment cost whereas equation 4-22 refers to CO_2 pollutants treatment cost. The weight coefficient of each one is different from the other as explained in the judgment matrix in the next section.

4.7 Multiobjective Functions

Multiobjective optimisation is a technique to find the optimum solution between different conflicting objectives, whereas there are no decision variables which can set all the objectives to function simultaneously. The multiobjective function is used to search the efficient decision variables for the optimisation function. A general mathematical formulation of multiobjective optimisation, which has n-dimensional decision variables, is expressed as follows.

$$\min\{f_1(x), f_2(x), \dots, f_k(x)\} \quad 4\text{-}23$$

$$subject\ to \begin{matrix} g_i(x) \leq 0, i = 1,2,\dots,q \\ h_j(x) = 0, j = 1,2,\dots,p \end{matrix} \quad 4\text{-}24$$

where $x = (x_1, x_2, \dots, x_n)$, is the n-dimensional decision variables

$f_k(x)$ is the k-th objective function

$g_i(x) \leq 0$ is inequality constraints

$h_j(x) = 0$ is equality constraints

There are different methods to solve multi-objective optimisation problems. One of them is the weighting method. The general idea of the weighting method is to associate each objective function with a weighting coefficient and minimise the weighted sum of the objectives. The

multiobjective roles in this approach are transformed into a single objective function [302], [303].

Mathematically, the economic dispatch/environmental pollutants of the microgrid problem are considered in this study. The mathematical equation is formulated to find output power of each distributed generator according to the lowest operation cost, the lowest environment pollutions treatment cost (sulphur dioxide SO_2 and nitrogen oxide NO_x), and the lowest carbon dioxide (CO_2) emission treatment cost of the generation unit, as modelled by.

$$\text{Minimise objective function} = \sum_{t} \{w_1(CF(P(t)) + \delta_g P_{grid}(t)) + w_2 E1(P(t)) + w_3 E2(P(t))\} \quad 4\text{-}25$$

where w_1, w_2, w_3 are the weight coefficients of the fuel cost, pollutant treatment cost, and carbon dioxide treatment cost objective functions respectively.

The criteria to calculate the judgment matrix of the objective function are based on the intensity of importance among the various objectives according to the Analytic Hierarchy Process (AHP), analytically proposed in [304], which is shown in Table 4-2. The effectiveness scale of judgment matrix has validated through theoretical justification of what scale one must use in the comparison of homogeneous elements in addition to many applications by a number of people [304, Ch. 1].

Table 4-2: The criteria of the judgment matrix

	Intensity of Importance	**Definition**	**Explanation**
1	1	Equal Importance	Two activities contribute equally to the objective.
2	2	Weak	Two activities contribute slightly equally to the objective.
3	5	Strong Importance	Experience and judgment strongly favour one activity over another.
	Reciprocals of above	If activity x has one of the above values assigned to it when compared with activity y, then y has reciprocal value when compared with x.	A reasonable assumption.
	Rationales	Ratios arising from the scale	If consistency were to be forced by obtaining n numerical values to span the matrix.

The objective function is classified into three levels; operating cost as the first level, carbon dioxide treatment cost as the second level, and pollutants treatment cost as the third level. The rank of the criteria subjective is explained below:

- The operating cost is five time as important as the pollutants treatment cost.
- The operating cost is three time as important as the carbon dioxide treatment cost.
- The pollutants treatment cost is twice as important as the carbon dioxide treatment cost.

The judgment values of the criteria subjective matrix J 4-26 are $w_1 = 0.64833$, $w_2 = 0.22965$, and $w_3 = 0.12202$.

$$J = \begin{bmatrix} 1 & 3 & 5 \\ 1/3 & 1 & 2 \\ 1/5 & 1/2 & 1 \end{bmatrix} \quad 4\text{-}26$$

4.8 Constraint Formulation

The objective function of the optimisation problem is subject to the following:

4.8.1 Generation and consumption balance

The microgrid operator should balance between the total load demand and the total power generation, as represented by

$$\sum_t \left(CF(P(t)) + \delta_g P_{grid}(t)\right) = P_d(t) \quad 4\text{-}27$$

4.8.2 Ramp rate limit

The ramp rate refers to the changing distributed generators output in megawatts per minutes. The ramp rate should be met at each sampling time, as expressed by

$$-DR_i \Delta T \leq P_i(t+1) - P_i(t) \leq UR_i \Delta T \quad 4\text{-}28$$

4.8.3 Generating capacity

For stable operation, each distributed generator should limit the output power according to its capacity, as shown by.

$$P_{i,min}(t) \leq P_i(t) \leq P_{i,max}(t) \quad 4\text{-}29$$

4.8.4 Exchange power with utility grid

The power is exchanged between the microgrid and UG at connected mode bidirectionally where each direction, either purchasing or selling, has its tariff and limits. The market operator at the primary control level is responsible for identifying the different tariff rates of the power direction mode during a day through all operators. It is not possible to purchase and sell at the same time. Therefore, binary numbers $\delta_{ug,b}(t) \in \{0,1\}$ and $\delta_{ug,s}(t) \in \{0,1\}$ are introduced to

selling and purchasing modes where, $\delta_{ug,b}(t) + \delta_{ug,s}(t) = 1$. The exchange power between the microgrid and UG can be represented by

$$\begin{cases} P_{g,smin}(t) \le P_{g,s}(t) \le P_{g,smax}(t) \\ P_{g,bmin}(t) \le P_{g,b}(t) \le P_{g,bmax}(t) \end{cases} \quad 4\text{-}30$$

4.8.5 Charging stations limit

The battery state at each sampling time can be represented based on the state of charge into either the charging, discharging, or not, act. The decision of battery states is made by the CSO depending on how many EVs are connected to the network at a particular time, the resources capacity of each EV, and the state of charge of the resources. The objective function of the discharging mode is formulated to obtain the maximum discharging power cost as follows:

$$P_{EVs,min}(t) \le P_{cso,i}(t) \le P_{EVs,max}(t) \quad 4\text{-}31$$

4.8.6 Emissions limit

The total environment pollutants should not exceed the certain limit for each distributed generator, as follows:

$$\sum_i E_i(P(t)) \le L_i \quad 4\text{-}32$$

4.8.7 Start and stop limit

For the stable operation of the distributed generators, start-ups of each distributed generator should be limited to a certain number based on distributed generator type, as follows:

$$\sum_i N_{start-stop,i} \le N_{start-stop,\max} \quad 4\text{-}33$$

4.9 The Mathematical Model of the Microgrid Optimisation Problem

The optimisation problem of the distributed generators deals with nonlinear, nonconvex, and high dimensional problems; it also deals with the unit commitment problem. The achievement should be a balance between the supply of the 13 distributed generators, CSO operation, exchange power with the UG, and consumer electrical demand, with the lowest cost of operation and pollutants treatment. The cost functions of the microturbine and fuel cell are linear, whereas the cost functions of the diesel generator and UG are nonlinear. Therefore, the cost of power generating is an intersection at some points, i.e. the UG has the lowest cost between 24:00 and 6:00 whereas the microturbine has less cost than the fuel cell below 35 kW.

The main UG is treated as another source connected to the microgrid, with its operation prices and pollutants treatment in the optimisation problem. It also balances the difference between consumer demand and the microsources output power, whenever the distributed generators are

unable to cover consumer demand. On the other hand, the microgrid distributed generators could operate as a stability balance of the UG whenever the voltage and frequency stability oscillates near to collapse point, in order to enhance the stability margin. The microgrid could purchase or sell the power to the UG based on the power availability, and minimum operation cost and pollutants treatment cost of the distributed generators. However, the tariff of selling power and purchasing power could be either variable during the time of day, based on the UG price policy, wherever the selling power is cheaper or more expensive than the purchasing power, or at a similar rate. The states between the microgrid and the UG could be either exchange power from the microgrid to the UG (buying power) or exchange power from the UG to the microgrid (selling power) as formulated in the following:

$$F_{ug,b}(\mathrm{t}) = C_{ug,b}(\mathrm{t})P_{ug,b}(t)\delta_{ug,b}(t) \quad 4\text{-}34$$

$$F_{ug,s}(\mathrm{t}) = C_{ug,s}(\mathrm{t})P_{ug,s}(t)\delta_{ug,s}(t) \quad 4\text{-}35$$

If there is no exchange power between the microgrid or the UG this means that either the point of common coupling isolates both systems from each other or the microgrid covers itself with cheaper operating cost than the UG without penalty of power to sell. The constraint of selling and buying power is stated by

$$\begin{cases} \delta_{ug,b}(t)P_{ugmin,b}(t) \le P_{ug,b}(t) \le \delta_{ug,b}(t)P_{ugmax,b}(t) \\ \delta_{ug,s}(t)P_{ugmin,s}(t) \le P_{ug,s}(t) \le \delta_{ug,s}(t)P_{ugmax,s}(t) \end{cases} \quad 4\text{-}36$$

The binary variable $\delta_{ug,b}$ is activited at the buying mode whereas the binary variable $\delta_{ug,s}$ is activated at the selling mode, as determined by the following:

$$\delta_{ug,b} = \begin{cases} 1 & if\ buying\ mode\ is\ applied \\ 0 & otherwise \end{cases} \quad 4\text{-}37$$

$$\delta_{ug,s} = \begin{cases} 1 & if\ selling\ mode\ is\ applied \\ 0 & otherwise \end{cases} \quad 4\text{-}38$$

To prevent activating both modes at same time, the extra condition of limited $\delta_{ug,b}$ and $\delta_{ug,s}$ to one is activated in the calculation, as follows:

$$\delta_{ug,b}(t) + \delta_{ug,s}(t) = 1\ , \delta_{ug} \in \{0,1\} \quad 4\text{-}39$$

The EVs have dual functions from the view of the optimisation problem, as either electrical demand or resources. The CSOs send the states of the connected EVs to the MGO, such as the total electrical demand required to charge them as well as the available power that could be discharged from them. The MGO collects the information from all CSOs within the microgrid. The discharging decision is taken based on the voltage variation, frequency variation, or both. After activating the discharging option, the MGO treats the CSOs as a source of power. Therefore, the power available on the EVs connected at CSOs competes with other distributed generators according to the objective function. The CSO's formula includes the operation cost where the emission cost is equal to zero, as modeled by

$$F_{cso}(\mathrm{t}) = \left(C_{ug,s}(t)\delta_{cso,d}(t) + C_{ug,b}(t)\delta_{cso,c}(t)\right)P_{cso,i}(t) \quad 4\text{-}40$$

To divert between the charging and discharging operation of the CSO, other binary terms are included in the formula, which are $\delta_{cso,d}$ for discharging operation and $\delta_{cso,c}$ for charging operation, as reveled in the following:

$$\delta_{cso,d} = \begin{cases} 1 & if\ discharge\ mode\ is\ applied \\ 0 & otherwise \end{cases} \quad 4\text{-}41$$

$$\delta_{cso,c} = \begin{cases} 1 & if\ charge\ mode\ is\ applied \\ 0 & otherwise \end{cases} \quad 4\text{-}42$$

whereas the sum of these terms do not exceed one, as follows:

$$\delta_{cso,d}(t) + \delta_{cso,c}(t) = 1\ , \delta_{cso} \in \{0,1\} \quad 4\text{-}43$$

Further detail about CSOs is available in the next chapter.

The fuel consumption rate of distributed generators is expressed by the following:

$$F_{dg}(\mathrm{t}) = C_{dg}(\mathrm{t}) P_{dg}(t) \delta_{dg}(t) \quad 4\text{-}44$$

where

$$\delta_{dg} = \begin{cases} 1 & if distributed\ generator\ is\ ON \\ 0 & otherwise \end{cases} \quad 4\text{-}45$$

$$\delta_{dg} \in \{0,1\}$$

The unit commitment application is applied to schedule the distributed generator operation at every period of the executed optimisation algorithm. It is introduced as a binary variable u_a to express the logical statement of the unit commitment implementation, which is applied as shown in Equations 4-46 and 4-47. It is not logical to implement and not implement the unit commitment strategy at the same time. Therefore, another term implemented to verify one condition of unit commitment is applied by the following:

Where

$$u_a = \begin{cases} 1 & if\ unit\ commitment\ is\ applied \\ 0 & otherwise \end{cases} \quad 4\text{-}46$$

$$u_n = \begin{cases} 1 & if\ unit\ commitment\ is\ not\ applied \\ 0 & otherwise \end{cases} \quad 4\text{-}47$$

$$u_a(t) + u_n(t) = 1\ , u \in \{0,1\} \quad 4\text{-}48$$

According to the previous explanation of microgrid equipment operation, the proposed cost function of the microgrid in connected mode with distributed generators, CSOs, UG, and unit commitment consideration, is formulated to minimise the operation cost and treatment pollution cost of the microgrid as follows

$$CF(P) = w_1\left(\sum_{t=1}^{24}\sum_{i=1}^{N}\left(u_a\delta_{dg,i,t}+u_n\right)\left(F_{dg,i,t}+OM_{dg,i,t}+SC_{dg,i,t}\right)+F_{cso,i,t}+F_{ug,t}\delta_{ug,t}\right) + \sum_{t=1}^{24}\left(\sum_{i=1}^{N}\sum_{k=1}^{N}\left(u_a\delta_{dg,i,t}+u_n\right)\left((w_2C_k\gamma_{ik}+w_3C_{co2}\gamma_{ico2})P_{dg,i,t}\right)+\sum_{k=1}^{N}\left(w_2C_k\gamma_{grid,k}+w_3C_{co2}\gamma_{grid,co2}\right)P_{grid,t}\delta_{ug,t}\right) \quad 4\text{-}49$$

4.10 Case Study

A case study can offer a useful insight to simplify a very complex problem by focusing on the snapshot operation of a typical network. Figure 3-6 shows the distribution network under study. It consists of seven feeders and 49 bus bars to supply the electrical loads of a local community in the City of Baghdad. As the typical loading profiles and line impedances of the network are readily available to the author, it presents a realistic case study for the investigation of the integration of EVs. Thirteen distributed generators are integrated within the case study to cover the local demand. The distributed generators comprise one diesel generator, three fuel cells, four microturbines and five photovoltaic cells, as well as two EV charging stations.

4.10.1 Load curve

The typical aggregated daily load curve pattern of the microgrid network under study and based on appliances ownership is shown in Figure 4-9 [19]. The figure shows that the load demand is minimum at night, then increases during the early morning gradually until reaching daily peaks at 12:00 and 17:00 respectively. There is some fluctuation in demand during the daytime. The range of demand is between 355.5620 kW at 2:30 and 682.1000 kW at 12:30.

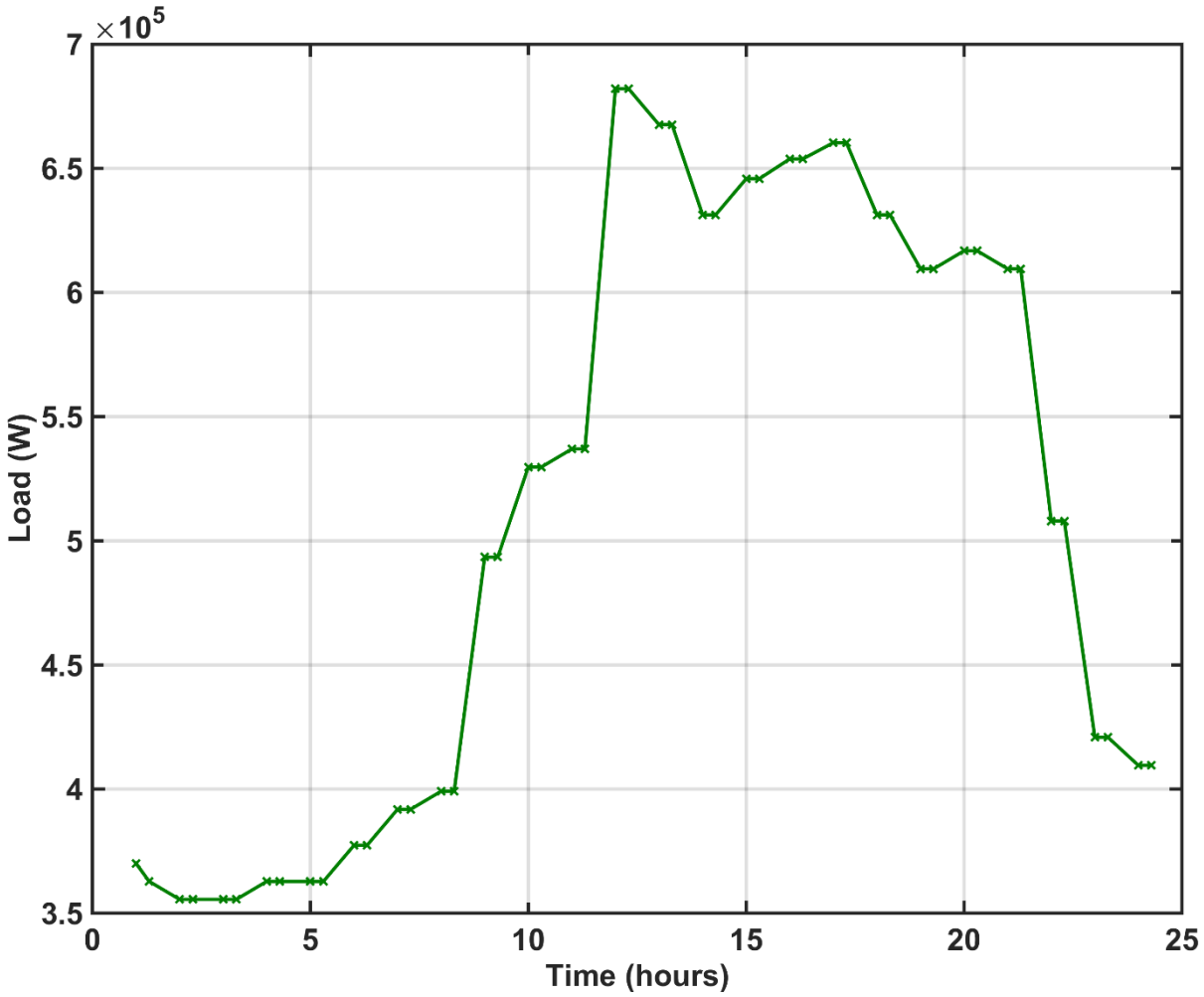

Figure 4-9: Daily load curve (Experimental Data with Linear Interpolation) [19]

4.10.2 Distributed generators selection

Generally, the load of the distribution network is classified into four classes: industrial, large commercial, small commercial, and residential, according to their contracted power. Furthermore, the load in the microgrid can be classified into sensitive and non-sensitive loads, according to power supply reliability. The distributed generator selected should meet the sensitive load in island mode. In the grid-connected mode, the energy sources and exchange power with the UG should meet all the demand (sensitive or non-sensitive). According to Figure 4-10, the solid oxide fuel cell has a much better efficiency than the micro gas turbine for the range of 10-100 kW. The gas and diesel motors work in the range of 90-20,000 kW but with a lower efficiency than the solid oxide fuel cell and a better efficiency than the micro gas turbine. This study is focused on distributing small, differently distributed generators to a specific location to meet the total demand of the microgrid. Because the wind turbine is not efficient in the Baghdad area, it is discarded from this study. The power range location of distributed generators is chosen based on the voltage stability distributed location algorithm, as shown in Table 3-1 and Table 4-3. The parameters of the distributed generators are shown in Table 4-4.

Table 4-3: Distributed generators' type, range, and location

	Type	Power range (kW)	Number of bus bars
1.	Photovoltaic cell	$0 \leq P_{PV} \leq 50$	17, 20, 24, 34, 32
2.	Solid oxide fuel cell	$0 \leq P_{FC} \leq 50$	16, 23, 45
3.	Micro gas turbine	$0 \leq P_{MT} \leq 75$	10, 15, 25, 39
4.	Diesel generator	$25 \leq P_{DE} \leq 250$	18
5.	Utility grid	$-200 \leq P_{UG} \leq 200$	1

Table 4-4: Parameter constant of the grid equipment [104], [287], [288], [302], [303], [305].

		FC parameters	**MT parameters**	**DE parameters**	**UG parameters**	**PV parameters**
Emission type	Pollutant disposal coefficient ($/kg)	Pollutant Emission coefficient (g/kWh)	Pollutant Emission coefficient (g/kWh)	Pollutant Emission coefficient (g/kWh)	Pollutant Emission coefficient (g/kWh)	Pollutant Emission coefficient (g/kWh)
NO_x	9.34	0.01	0.2	9.89	1.6	0
SO_2	2.21	0.003	0.0036	0.206	1.8	0
CO_2	0.032	489	724	649	889	0
Other parameters						
Fuel cost ($/kWh)	/	0.0294	0.0457	$\alpha = 0.4$ $\beta = 0.0185$ $\gamma = 0.0042$	See Figure 4-11	0.024
Kom ($/kWh)	/	0.00419	0.00587	0.01258	/	0.001
KSC_i ($)	/	0.96	1.65	1.75	/	0

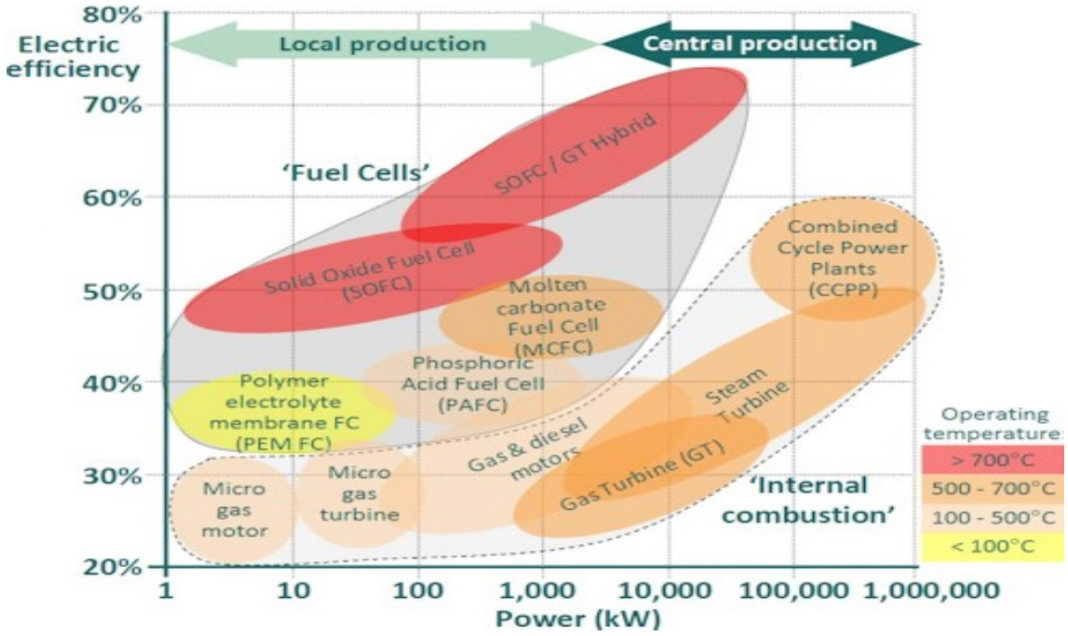

Figure 4-10: Type and efficiency of distributed generator [306]

4.11 Case Study Results

Based on the proposed modelling concept, there are many scenarios which can be considered when studying the microgrid states. However, there are two main scenarios for microgrid operation which are either working at isolated mode or working in connected mode. Both scenarios have two cases: the microgrid operating either with or without unit commitment strategy. The main objective function minimises the operation cost and the treatment pollutant cost of the microgrid with different weight; the operation cost has a higher weight than the pollutants treatment cost. Therefore, the results are classified into two scenarios each with two cases, as described below:

1. **Scenario one:** Isolated mode optimisation including operation and pollutants treatment policy.

(i) Case one: Minimum operational and pollutants treatment policy with unit commitment consideration.

(ii) Case two: Minimum operational and pollutants treatment policy without unit commitment consideration.

2. **Scenario Two:** Connected mode optimisation including operation and pollutants treatment policy.

(i) Case one: Minimum operational and pollutants treatment policy of microgrid with unit commitment consideration.

(ii) Case two: Minimum operational and pollutants treatment policy of microgrid without unit commitment consideration.

The power tariff has been chosen based on the time of the day, which starts with a lower price during the night, then increases rapidly in the early morning. The tariff is increased gradually until reaching a maximum at midday which is 0.286 ($/kWh). After midday, the tariff starts to reduce gradually until reaching a minimum at midnight; then it is kept constant until early morning, as shown in Figure 4-11.

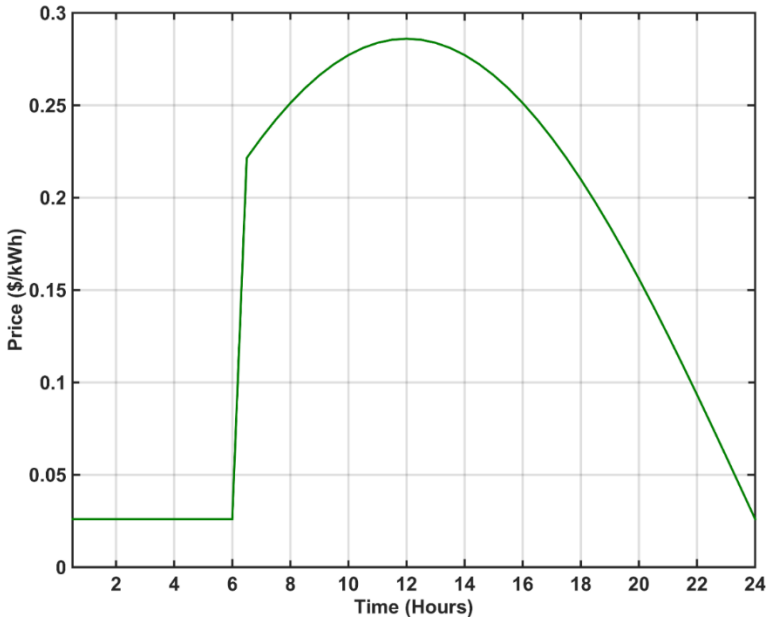

Figure 4-11: Proposed Utility Grid Tariff

4.11.1 Scenario one: Isolated mode optimisation including operation and pollutants treatment policy

This scenario has two cases of operation based on either considering a unit commitment strategy in operating the distributed generators or not considering it, as follows:

(I) Case one: Minimum operational and pollutants treatment policy with unit commitment consideration.

The microgrid in isolated mode should cover all sensitive demands without any exchange power with the UG, where the point of common coupling has isolated the microgrid from the UG. The proposed cost function of the microgrid in an isolated mode with unit commitment consideration is formulated by follows:

$$CF(P) = w_1\left(\sum_{t=1}^{24}\sum_{i=1}^{N}\left(u_a\delta_{dg,i,t}\right)\left(F_{dg,i,t} + OM_{dg,i,t} + SC_{dg,i,t}\right) + F_{cso,i,t}\right) + \sum_{t=1}^{24}\left(\sum_{i=1}^{N}\sum_{k=1}^{N}\left(u_a\delta_{dg,i,t}\right)\left((w_2C_k\gamma_{ik} + w_3C_{co2}\gamma_{ico2})P_{dg,i,t}\right)\right) \quad 4\text{-}50$$

Figure 4-12 shows the hourly optimal power schedule of distributed generators in isolated mode with unit commitment consideration. The photovoltaic panels worked for the period between 6:00 and 19:00 at different power output based on sun radiation; the fuel cells and photovoltaic panels covered the base load of the microgrid, whereas microturbines covered the medium demand of the load curve. The diesel generator covered the peak demand of the load curve to balance the demand and maintain the voltage and frequency at a certain level. Figure 4-13 reveals the hourly operating cost of the distributed generators, pollutants treatment cost, and the carbon dioxide treatment cost of the microgrid in isolated mode with unit commitment consideration. The total operation and emission costs are presented in Table 4-5, whereas the ON-OFF states of distributed generators operation over a day are shown in Apx_Table I-1 in the Appendix I.

The price change is based on the demand and type of the distributed generators. Most of the load is supplied from photovoltaic panels, fuel cells, and microturbines respectively. Due to the intermittent nature of renewable energy sources and considering unit commitment strategy, the voltage has some variations during the peak demand of the load curve. Therefore, either the CSOs or diesel generator should supply power to balance the demand and keep the voltage and frequency at the fundamental limit. The MGO decides which source should operate based on the availability and total cost of operation and emission treatment. The CSOs deliver power cheaper than the diesel generator with zero emission. Therefore, the CSOs have priority to balance the load in case the power from connected EVs is available to discharge. There are 74 EVs at each CSS that could deliver power to the network at voltage deviation times. The CSOs distribute the discharging period among the EVs until maintaining the voltage value of the system. Therefore, the CSOs deliver about 58.355 kW at 12:00 and 52.485 kW at 12:30, whereas the diesel generator is shut down while operating the CSOs. In case the power of the

CSOs is not enough to make the system stable, then the MGO should operate the diesel generator to cover the rest of the demand.

The significant increase in price occurs at 20:00 due to missing the sun's radiation, which leads to use of the diesel generator instead of the photovoltaic cells to supply the demand. Figure 4-13 shows the difference in using the diesel generator instead of the CSOs to compensate the voltage stability, where using the diesel generator recorded a higher price than using the CSOs.

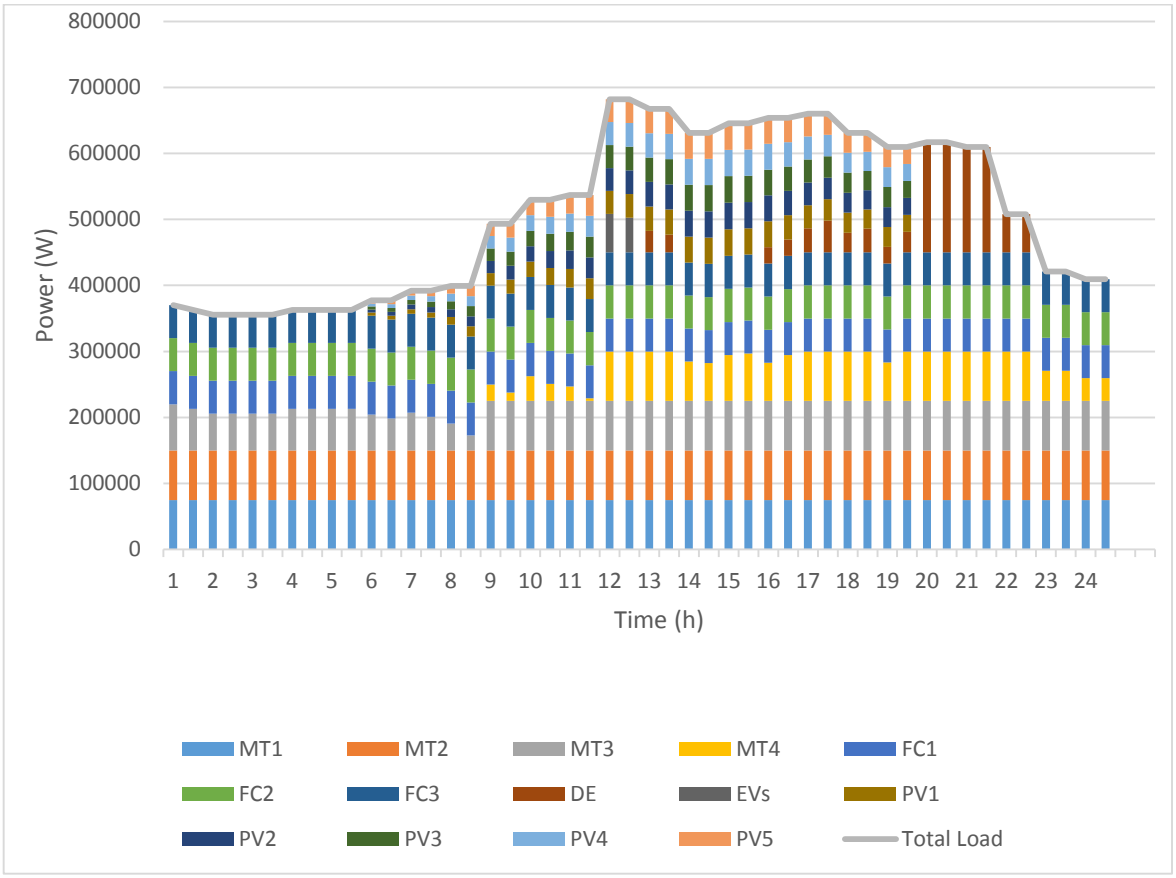

Figure 4-12: Hourly optimal power schedule of DGs under isolated mode with UC consideration (Simulated results).

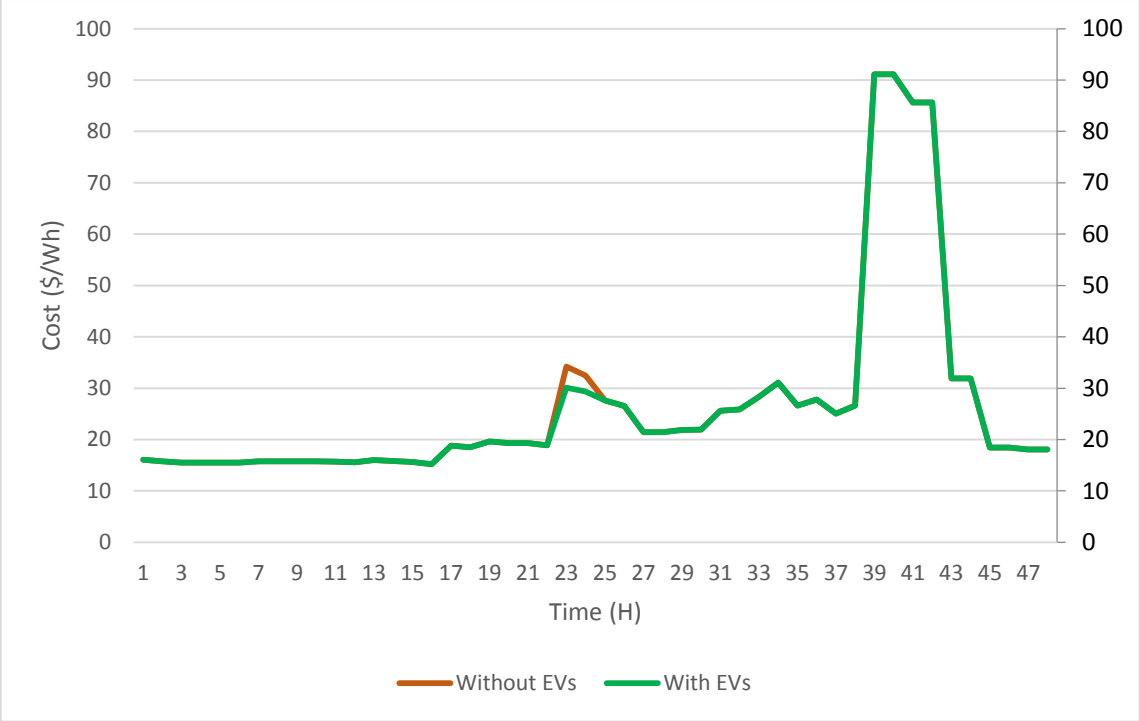

Figure 4-13: Hourly total DGs operating cost under isolated mode with UC consideration (Simulated results).

Table 4-5: Daily cost of total DGs operating cost under isolated mode with UC consideration

	Daily operation cost ($)	**Daily emission treatment cost ($)**	**Daily overall cost ($)**
Without EVs	1000.9424	279.146	1280.088
With EVs	999.9678	272.850	1272.818

(II) Case Two: Minimum operational and pollutants treatment policy without unit commitment consideration.

Without applying a unit commitment policy, all generators should work at minimum generation level. The diesel generator, which is a most expensive distributed generator, could not be run without electricity due to its manufacture. The diesel generator supplies its minimum power, and the rest of the distributed generators cover the residual of the power demand. The proposed cost function of the microgrid in isolated mode without considering unit commitment is formulated by follows:

$$CF(P) = w_1\left(\sum_{t=1}^{24}\sum_{i=1}^{N}(u_n)\left(F_{dg,i,t} + OM_{dg,i,t} + SC_{dg,i,t}\right) + F_{cso,i,t}\right) + \sum_{t=1}^{24}\left(\sum_{i=1}^{N}\sum_{k=1}^{N}(u_n)\left((w_2 C_k \gamma_{ik} + w_3 C_{co2}\gamma_{ico2})P_{dg,i,t}\right)\right) \quad 4\text{-}51$$

Figure 4-14 depicts the hourly optimal power schedule of DGs.

The base demand is covered by a minimum range of the diesel generator, fuel cells and photovoltaic cells, whereas the medium demand is covered by the microturbines. The microturbines and diesel generator supply the peak demand of the load curve. The photovoltaic cells supply power during the sun period, i.e. between 6:00 and 19:00 at varied levels of power output. All the distributed generators worked during the highest power demand which is from 12:00 to 13:30. Therefore, the voltage and frequency are both stable around the fundamental value. Thus, there is no need to use CSOs. Figure 4-15 reveals the total hourly operation and pollutants treatment cost of the islanded microgrid without considering unit commitment operation. The operation, emission, and total cost of the distributed generators are shown in Table 4-6. The daily operating cost of the islanded microgrid without unit commitment operation recorded a higher cost than the daily operating cost of the islanded microgrid with unit commitment operation, due to the obligation of continuous operation of DGs at minimum capacity. The maximum value of the operating and pollutant treatment cost occurs at from 20:00 to 21:30, which is a relatively large demand without photovoltaic cells' generation.

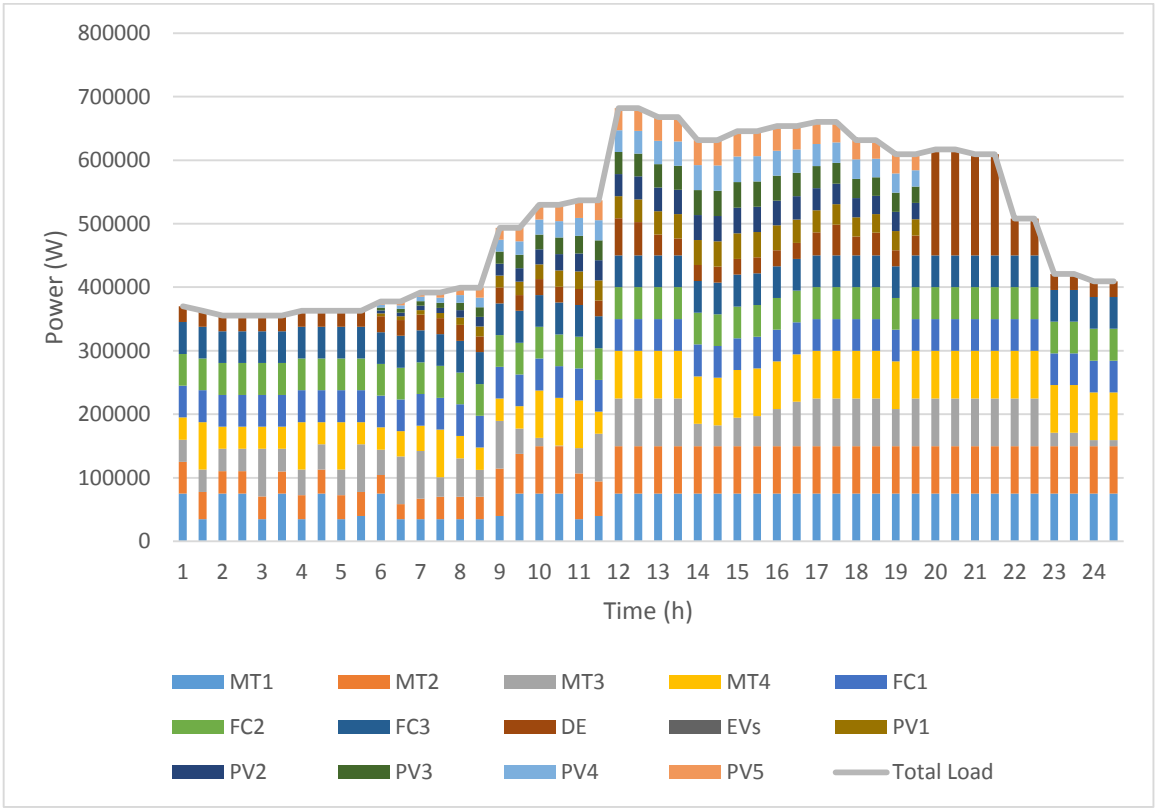

Figure 4-14: Hourly optimal power schedule of DGs under isolated mode without UC consideration (Simulated results).

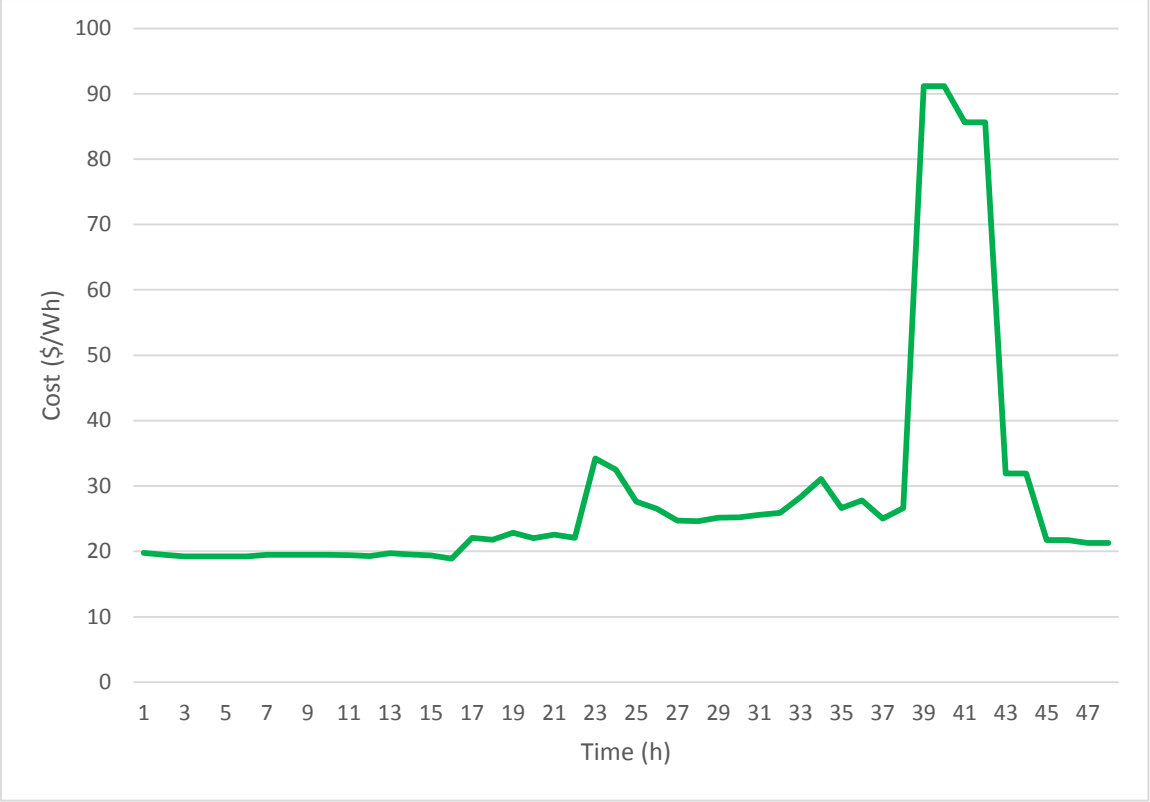

Figure 4-15: Hourly total DGs operating cost under isolated mode without UC consideration (Simulated results)

Table 4-6: Daily cost of total DGs operating cost under isolated mode without UC consideration

Daily operation cost ($)	Daily emission treatment cost ($)	Daily overall cost ($)
1072.063	312.3431	1384.407

4.11.2 Scenario two: Connected mode optimisation including operation and pollutants treatment policy

This scenario also has two cases based on either considering unit commitment strategy in operating the distributed generators or not considering it, as follows:

(I) Case one: Minimum operation and pollutant treatment policy of microgrid with grid connected mode operation and unit commitment consideration.

The operation of the microgrid in connected mode is expressed as the island mode connected to the infinite bus. Therefore, there is a penalty of power which could move bidirectionally between the microgrid and the UG. The direction of power is decided according to the cooperation between the DMS in DNO and MGO and according to availability, requirement and total cost. Monitoring the voltage, frequency and surplus power of the distributed generators are the primary factors to find either the availability or required power. The cost comparison of the objective function determines whether to sell or buy the electricity between the microgrid and the UG. The proposed cost function of the microgrid in connected mode with unit commitment consideration is formulated by follows:

$$CF(P) = w_1\left(\sum_{t=1}^{24}\sum_{i=1}^{N}\left(u_a\delta_{dg,i,t}\right)\left(F_{dg,i,t} + OM_{dg,i,t} + SC_{dg,i,t}\right) + F_{cso,i,t} + F_{ug,t}\delta_{ug,t}\right) + \sum_{t=1}^{24}\left(\sum_{i=1}^{N}\sum_{k=1}^{N}\left(u_a\delta_{dg,i,t}\right)\left((w_2C_k\gamma_{ik} + w_3C_{co2}\gamma_{ico2})P_{dg,i,t}\right) + \sum_{k=1}^{N}\left(w_2C_k\gamma_{grid,k} + w_3C_{co2}\gamma_{grid,co2}\right)P_{grid,t}\delta_{ug,t}\right) \quad 4\text{-}52$$

The equation includes the operation cost, maintenance cost, and start-up cost of DGs which are affected by unit commitment factor and weighted to the first judgment value of the criteria subjective matrix after accumulating the cost of CSO and UG. The pollutant treatment cost and carbon dioxide emission cost of the DG at the microgrid and UG are weighted to second and third judgment values of the criteria subjective matrix, whereas the pollutant treatment cost and Carbon dioxide emission cost of the MG are affected by unit commitment strategy.

Figure 4-16 shows the hourly optimal schedule power of distributed generators and exchange power with the UG. The tariff of the UG is less than other distributed generators between the periods of 1:00 and 6:00. Therefore, the UG covered most of the electrical demand reaching the upper limit of the UG constraint. After 6:00 the UG tariff increased nonlinearly until reaching a maximum at midday. Therefore, the curve cost of the power generation of distributed generations and UG intersect according to the power amount.

The objective function of the optimisation problem decides the sufficient power amount to buy or sell from the microgrid. At peak demand, the tariff of the utility grid is higher than other distributed generators; however, there is not enough power to sell. Therefore, voltage and frequency oscillation could happen in the microgrid. At peak load, voltage variation happens. Therefore, the MGO permits the CSOs to supply power stored in the storage energy system of the EVs. The operation of the supplier is classified according to the UG tariff. The UG is the main supply from 1:00 to 6:00 whereas the fuel cells and microturbines supply the rest of the demand according to the objective function of the optimisation problem. After 6:00 the photovoltaic cells and fuel cells cover the based demand, whereas the microturbines cover the medium demand. Furthermore, the diesel generator cover the peak demand and selling power to the UG. Between 8:00 and 9:00, the UG and fuel cells cover the base demand, whereas the microturbine and diesel generator cover the medium load and peak load respectively. After 9:00, the UG covers the base and medium demand, whereas the fuel cells and microturbines cover the rest of the load according to the objective function of the optimisation problem.

Figure 4-17 depicts the whole hourly operation and pollutant treatment cost of the connected microgrid when considering unit commitment operation. The operation, emission, and total

cost of the microgrid are shown in Table 4-7. The total price of the connected mode is significantly lower than the islanded mode. The highest value of the operating and pollutant treatment cost occurs at between 20:00 and 21:30, which is a relatively high demand without photovoltaic panels and without selling power to the UG. The total cost of the CSOs is slightly better than replacing them with the diesel generator. At high penetration of the EVs, the cost difference between using CSOs and the diesel generator become clear as the diesel generator cost curve is quadratic which increases nonlinearly when power is increased. The ON-OFF states of distributed generators' operation during a day are shown in Apx_Table I-2 in the Appendix I.

Table 4-7: Daily cost of total DGs' operating cost under grid connected mode with UC consideration

	Daily operation cost ($)	**Daily emission treatment cost ($)**	**Daily overall cost ($)**
Without EVs	667.46276	291.488	958.9503
With EVs	666.4882	285.192	951.6803

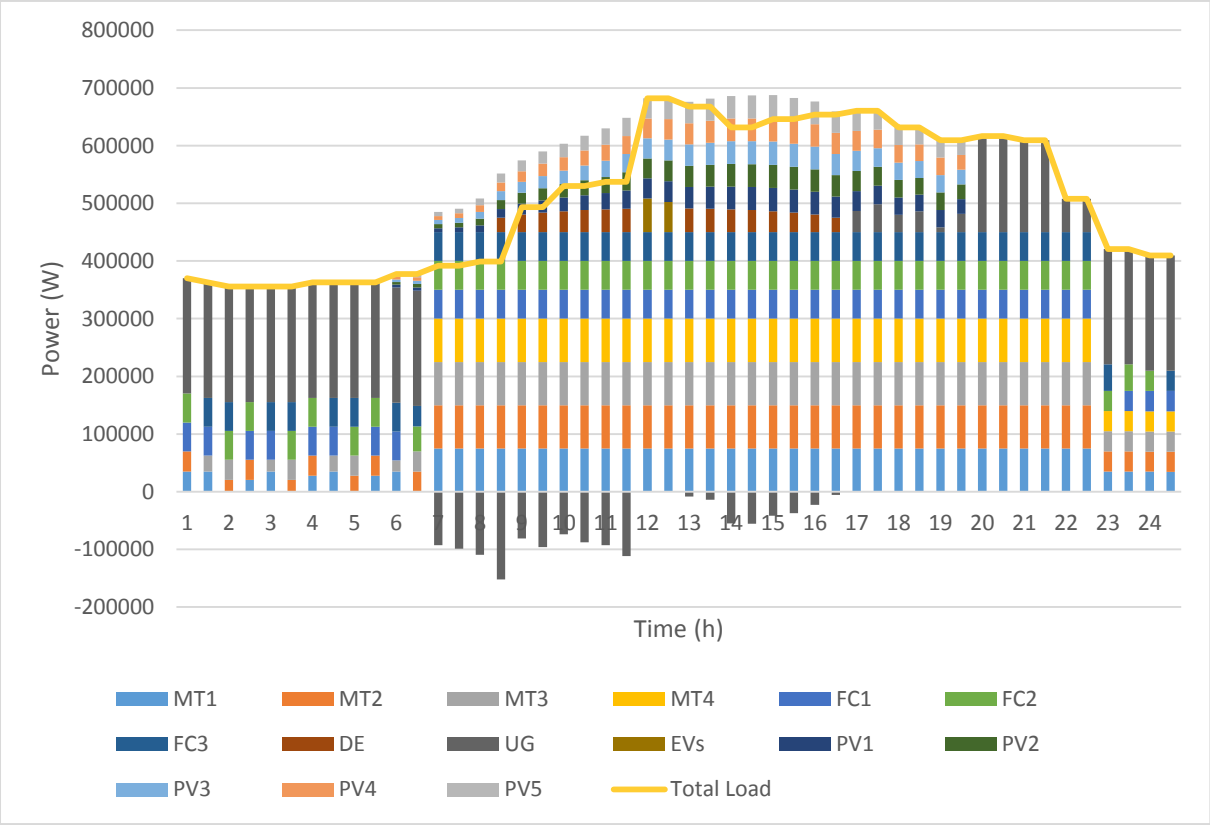

Figure 4-16: Hourly optimal power schedule of DGs and exchange power with UG under grid connected mode with UC consideration and pollutant treatment consideration (Simulated results).

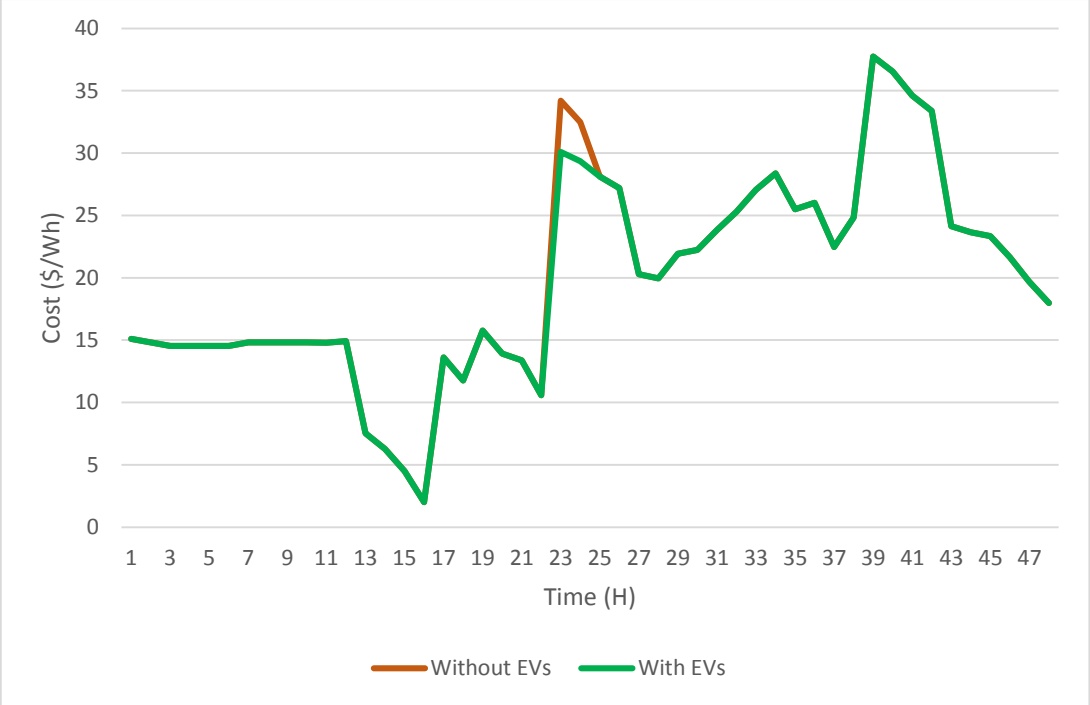

Figure 4-17: Hourly total DGs operating cost under grid connected mode with UC consideration and emission consideration (Simulated results).

(II) Case two: Minimum operational and pollutant treatment policy of microgrid with grid connected mode operation and without unit commitment consideration.

Microgrid operation at the connected mode with discarded unit commitment, make all the distributed generators work at a minimum generation. The proposed cost function of the microgrid in connected mode with unit commitment consideration is formulated by follows:

$$CF(P) = w_1\left(\sum_{t=1}^{24}\sum_{i=1}^{N}(u_n)\left(F_{dg,i,t} + OM_{dg,i,t} + SC_{dg,i,t}\right) + F_{cso,i,t} + F_{ug,t}\delta_{ug,t}\right) + \sum_{t=1}^{24}\left(\sum_{i=1}^{N}\sum_{k=1}^{N}(u_n)\left((w_2 C_k \gamma_{ik} + w_3 C_{co2}\gamma_{ico2})P_{dg,i,t}\right)\right) + \sum_{k=1}^{N}\left(w_2 C_k \gamma_{grid,k} + w_3 C_{co2}\gamma_{grid,co2}\right)P_{grid,t}\delta_{ug,t}\Bigg) \quad 4\text{-}53$$

Figure 4-18 shows the same behaviour from the resources connected at the microgrid of the previous scenario except for the continuous operation of the diesel generator due to the constraint of providing minimum power. Therefore, the total cost of daily operation of the microgrid would be higher than the previous state, as shown in Table 4-8, which is depicted in Figure 4-19. The microgrid is a more stable option due to the penalty of power available. Therefore, there is no permission to operate CSOs as resources in the microgrid.

Table 4-8: Daily cost of total DGs' operating cost under grid connected mode without UC consideration

Daily operation cost ($)	Daily emission treatment cost ($)	Daily overall cost ($)
710.375	322.430	1032.805

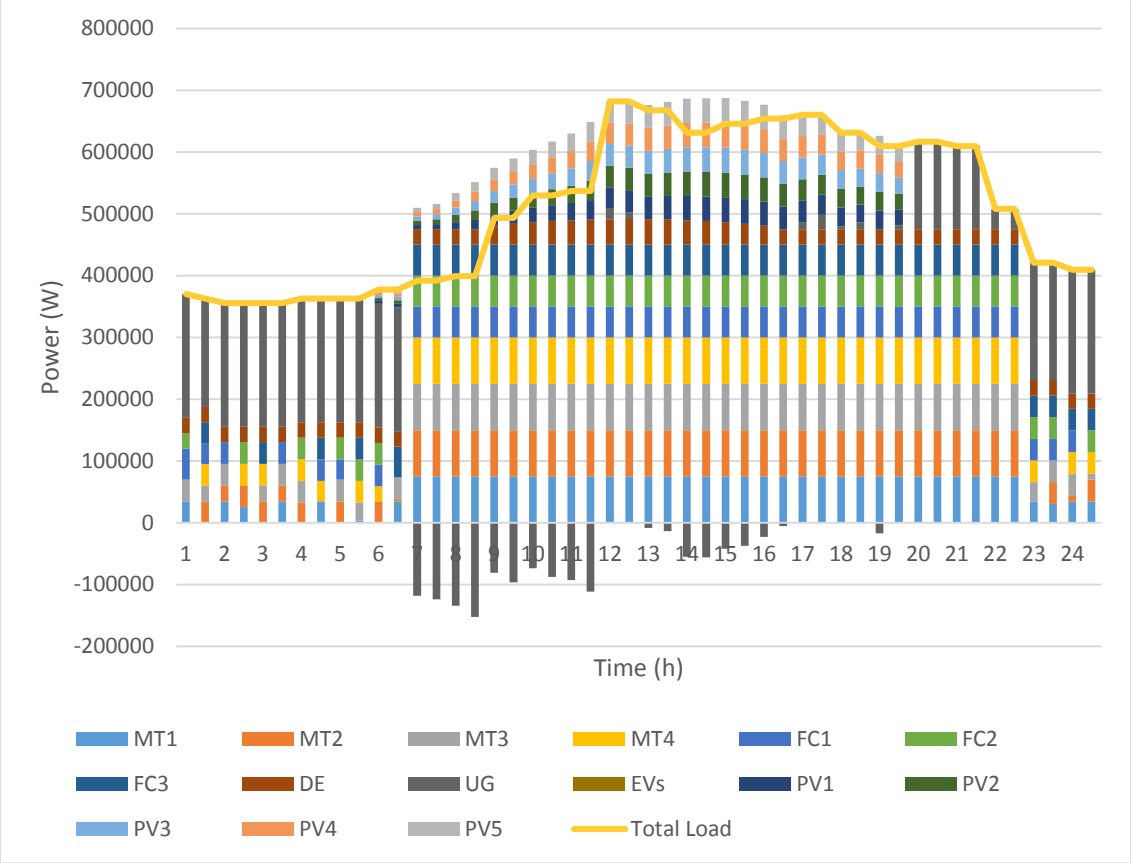

Figure 4-18: Hourly optimal power schedule of DGs and exchange power with UG under grid connected mode without UC consideration and emission consideration (Simulated results).

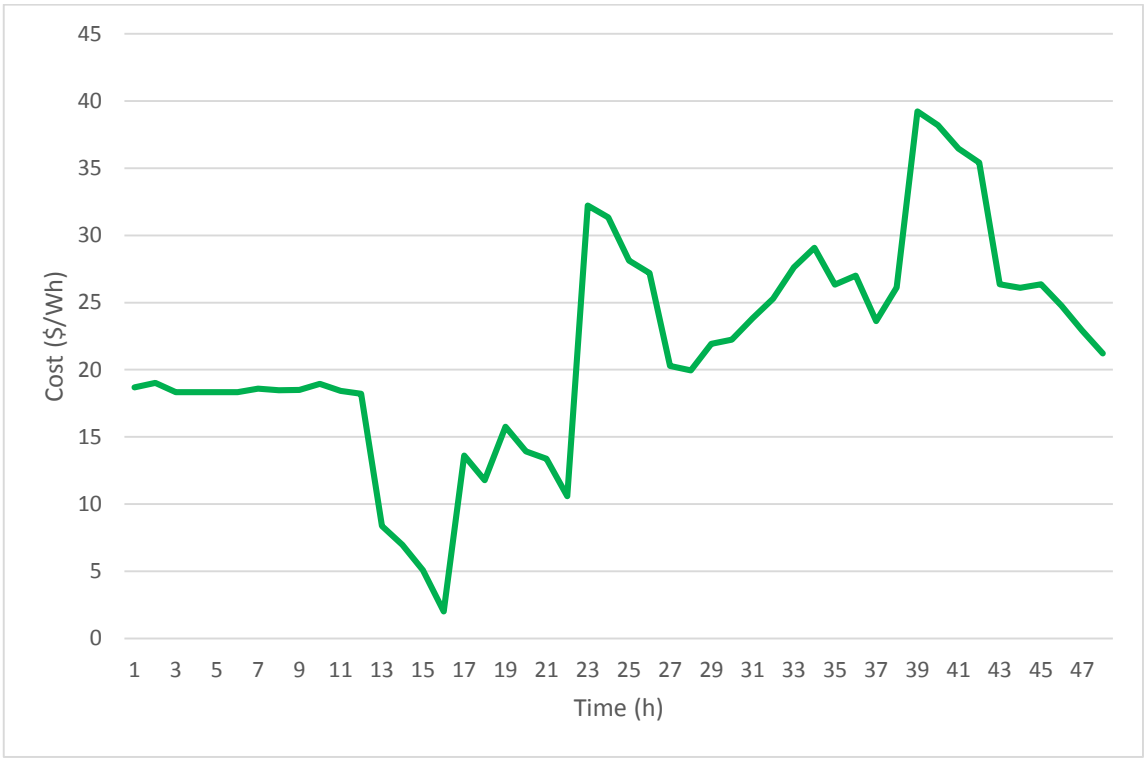

Figure 4-19: Hourly total DGs operating cost under grid connected mode without UC consideration and emission consideration (Simulated results)

4.12 Conclusion

The main function of the microgrids is balancing the electrical generation and load to keep the system stable and reliable. The power generation of the microgrid consists of many distributed generators that use different types of fuel and have different emission levels of pollution. Each distributed generator is implemented as a mathematical model relevant to the optimisation problem. The cost of the electricity unit of the distributed generators is variable depending on the many constraints that limit the operation of the distributed generators. The fuel cost, maintenance cost, start-up cost, and the emission treatment cost for each distributed generator have justified the price of the electricity unit per time. The Nitrogen oxide, Sulphur dioxide, and Carbon dioxide emissions are the major polluting emissions from the distributed generators, which should be treated to save the environment. The cheapest operation resources among the distributed generators are renewable energy, such as photovoltaic panels and wind turbines that have zero emission pollutants. However, the renewable energy could not cover the load over the entire day because of the weather changing situation, such as day or night, windy weather or not windy weather, in addition to the intermittent nature of available sources, such as cloudy weather and low wind speed. Therefore, many distributed generators synergize the renewable energy to balance the load and keep the system stable.

The operation of distributed generators, the multiobjective optimisation function using MATLAB environment, Matpower package, and Cplex software is demonstrated to optimise the power generation of the distributed generators at minimum cost and minimum pollutants treatment. Some distributed generators have quadratic equation characteristics to estimate the fuel consumption cost of the electricity unit. Therefore, a mixed integer quadratic function is used to solve the optimisation problem. The tariff of the electricity unit has been chosen as variable over a day. The results are arranged as in operation mode – either islanding or connecting.

For both modes, two operations of distributed generators are represented, which are operating the microgrid either with or without unit commitment strategy. Generally, the priority of generating power is given to the renewable energy resources as they produce the cheapest energy without emissions. The fuel cells, microturbines and diesel generator produce the rest of the load respectively. The cost of the generation increases rapidly when the diesel generator supplies the load. Due to the described development of the intermittency of photovoltaic cells, there is a voltage deviation happening in the system around midday during the heavy loads period without operating the diesel generator.

EVs are demonstrated as being mobile energy storage to compensate the intermittency of renewable energy at a frequency and/or voltage deviation. At the time of voltage deviation, the CSOs inform the MGO that it has 74 EVs, which have surplus power to discharge, connected to each charging station. The MGO calculates the power ratio of discharging EVs to balance the demand. The CSOs distribute to the power ratio of discharging among the EVs based on the capacity, state of charge, desired leaving the state of charge of energy storage. The result of the generation cost of island mode considering a unit commitment strategy shows that using the surplus power of the EVs reduces the cost of power better than using the diesel generator to balance the load. Excluding unit commitment strategy increases the cost of the microgrid

operation for the same load. However, the system with an applied unit commitment strategy is more stable than without it because the diesel generator covers the intermittency of the renewable energy directly.

Regarding the relationship between power and fuel cost of distributed generators in connected mode, the photovoltaic cells, fuel cells and microturbines have linear characteristics, whereas the UG and distributed generator have nonlinear characteristics. From midnight until early morning the cost of the power generation of the UG is cheaper than other distributed generators; therefore, the microgrid purchases power from the UG. On the other hand, the microgrid may sell power to the UG around midday when the tariff of the UG becomes higher than other distributed generators. The optimisation function evaluates the intersection point between the distributed generators to identify the minimum cost of the power generation from each unit at a particular time of the day.

In the unit commitment operation, the voltage deviation happens at a heavy load. Therefore, the fleet of EVs, connected at charging stations, synergize the distributed generators to balance the load with cheaper power generation than a diesel generator. The microgrid is more stable at discarding the unit commitment strategy from operation than including it, due to the operation of the diesel generator all day. However, the total cost of the power generation at discarding the unit commitment strategy becomes higher than including it.

This chapter describes the development of the objective achievement of management optimisation of balancing the distributed generators, UG, CSOs, and load, to avoid possible overloading of network degradation, at minimum operation cost and pollutants' emission treatment cost. The operation of the microgrid at connected mode with unit commitment activation achieved minimum operation cost and minimum emission treatment cost. Therefore, this strategy is the optimum solution to operate the microgrid at a minimum daily total cost.

5. Chapter Five: Management of Electric Vehicles in Microgrids

5.1 Introduction

The previous chapter describes the top tier strategic planning of the modular management structure to handle the electricity congestion of the microgrid due to the nature of the bidirectional operation. The system has been designed as a unified systematic framework where the power management decomposes into modular blocks in chronological executions. This chapter describes the middle tier of the modular management structure which decides appropriate actions of the policy planning or medium-term policy of the centralised charging/discharging aggregated EV to feed downstream to the lower tier of the execution in the next chapter. The chapter focuses on the centralised charging/discharging aggregated EVs connected to the specific bus bar on the microgrid through the charging station. The control signal for either charging EVs or discharging qualified EVs of the CSO is received from the MGO based on the state of the voltage and frequency level of the network. The MGO delivers either all the required charging power of the charging station system or a part of it, based on balancing available power on the MGO and required power from the CSO without affecting the resilient operation of the microgrid. The discharging operation is activated by the MGO when there is a fluctuation in voltage or frequency beyond the acceptable standard level. The CSO manages and controlsthe constructed resilient microgrid either charging all connected EVs or schedules charging them or discharging some EVs that have a specific state of charge limit of energy storage devices using Cplex software and the MATLAB environment. Minimising the power charging cost or maximising the power discharging cost of EVs are the objective functions of the optimisation problem. Mixed integer linear programming is used to achieve the objective function of the mathematical equations of charging or discharging EVs. Five scenarios of realistic 15 brands of EVs are included to explain the operation of the proposed module of charging or discharging. The tariff curve of daily operation has been chosen as a variable over a day.

This chapter paves the way for the next chapters to design the third tier of a modular structure framework to manage and control the operation of the EV within EVO. Therefore, the power reference of the CSO will be utilised in the next chapter.

5.2 Algorithm Design of the CSO

The hierarchical modular framework structures the microgrid into three operators. CSO is the medium policy level of framework to manage and control aggregated EVs connected at CSS of the microgrid. The output of the optimisation model is the either minimum charging cost of each EV or maximum discharging cost of qualified EV. The procedure to achieve the objective functions is depicted in Figure 5-1 whereas the implementation strategy of CSO summarises in the flow chart as shown in Figure 5-2. Further explanation arranges in next sections.

The CSO uses energy demand management to deal with aggregated EVs. There is a communication link between the CSO and MGO. The CSO sends information to the MGO

about how much power is required to charge the EVs at connection time and the availability of power that EVs could discharge to the network based on the state of charge of each EV. On the other hand, the MGO informs the CSO about how much power could be consumed in order to charge or require to discharge the EVs. The CSO has a faster response than the MGO, which operates hourly; the CSO executes the information in minutes based on the size of the grid and dynamic response of the devices, whereas collecting data from the system and processing them requires more time than by the CSO. It is a preferable online operation but is expensive and difficult, and the possibility of congestion becomes a major issue for the system. The timing of the operators could be ten minutes for MGO, one minute for CSO, and a second for the EVO starting from one second at EMS downstream to a microsecond for PES. However, the amount of data will be considerable, and it is difficult to study and draw it academically, that is why this thesis has chosen the existing distribution time between the operators. In this study, the CSO updates states of connected EVs every ten minutes, whereas the MGO updates states of connected equipment every half hour.

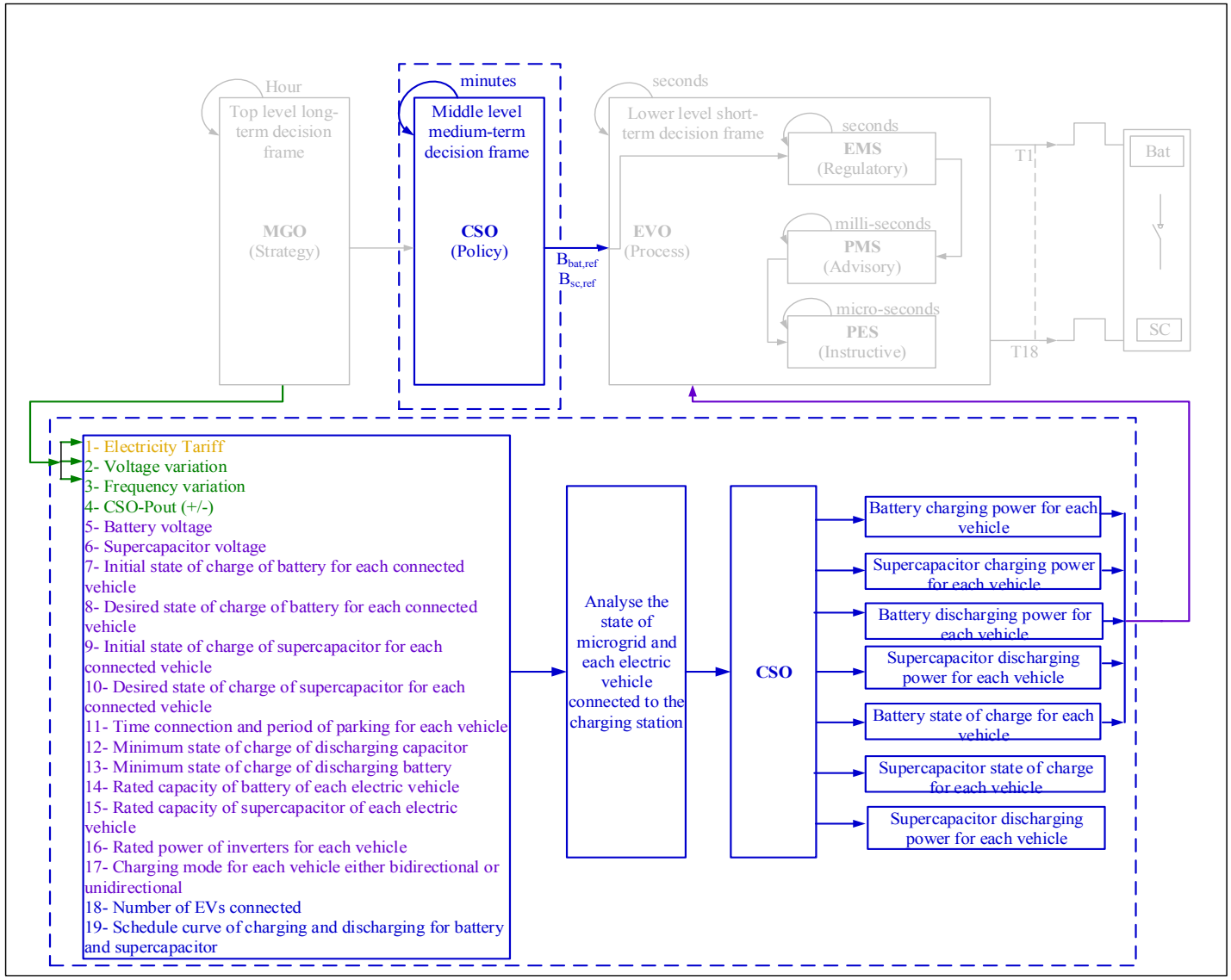

Figure 5-1: CSO optimisation algorithm

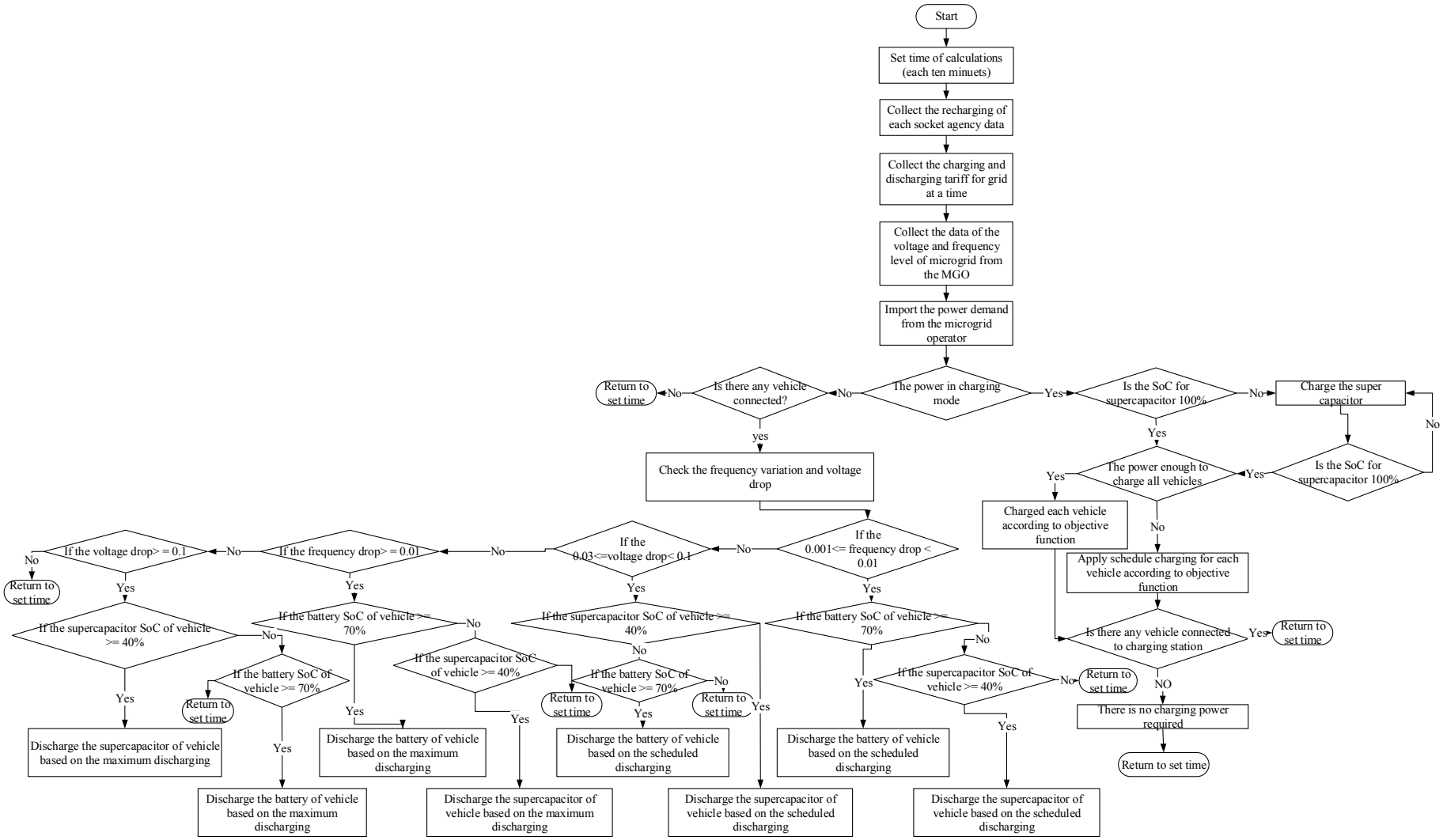

Figure 5-2: Flow chart of CSO optimisation algorithm

5.3 The Effects of Electric Vehicles on the Microgrid

EVs are classified as a new demand for the microgrid which may create multiple challenges for distributed generators of the microgrid. Intelligent controller and communication link between the microgrid utilities are necessary to control charging each EV efficiently as well as controlling the electricity back to the microgrid from the resources of the EV. The ability to predict the spatiotemporal connection of the EV and the state of charge for resources of the EV is required to achieve optimal bidirectional power control between the microgrid and the EV.

There are many methods proposed of charging EVs, either as single or aggregated charging, which are classified in the following:

1. The EV starts charging immediately after being plugged in to ensure fully charging the battery of the EV. The electricity tariff is usually kept fixed for the whole day in this charging strategy [307].
2. The dual tariff charging strategy is that the day tariff is more expensive than the night tariff. The EV starts charging overnight when the demand and the power tariff are lower than the rest of the day. This settling of charging can influence the behaviour of users in terms of scheduling journeys.
3. Scheduling charging of the EVs to achieve a specific objective function which is either a single objective function such as achieving minimum charging cost or maximum operator profit, or multiple objectives such as achieving both previous objectives. This method is further classified into.
    a. **Centralised smart charging (CSC)**; the electric vehicle agent (EVA) collaborates with the plug-in socket outlet to decide to charge or to discharge the EVs [308]–[315].
    b. **Decentralised smart charging (DSC)**; the supplier disperses the EV demands in time and space according to the electricity tariff and the EV states [159], [307], [316]–[318].

The location of the optimisation decision is the main difference between CSC and DSC, whereas the control centre of the aggregator level and EVA are represented as the charging decision in the CSC and DSC respectively. One central point can control many EVs in CSC. In contrast, each EV has an onboard smart control unit in the DSC. Both have an opportunity to reach an optimal solution for charging the EVs; however, the DSC reaches a less optimal solution than the CSC. Furthermore, the optimal solution decision of the CSC is easier than that of DSC because all information from the microgrid network is intensive at the central point, in contrast to the DSC where the information is processed in a distributed way. Therefore, processing the information of the CSC maximises the network capacity to interact with a high number of EVs concurrently. However, the CSC requires a high communication cost, time and effort to achieve the optimisation solution in contrast to the DSC which requires low communication cost for the same purpose. Furthermore, the CSC should have more computational complexity, more implantation flexibility, and more information exchange requirements than the DSC. Connecting a new EV leads to changing the control program of the CSC. On the other hand, the DSC results in improving privacy regarding the choice of charging pattern for the EV. More accurate information provided from the EVA in the CSC

means that a more precise decision can be made because the CSC is more sensitive to errors than the DSC. Figure 5-3 shows the connection schematic diagram of the EVs to the microgrid in terms of CSC and DSC.

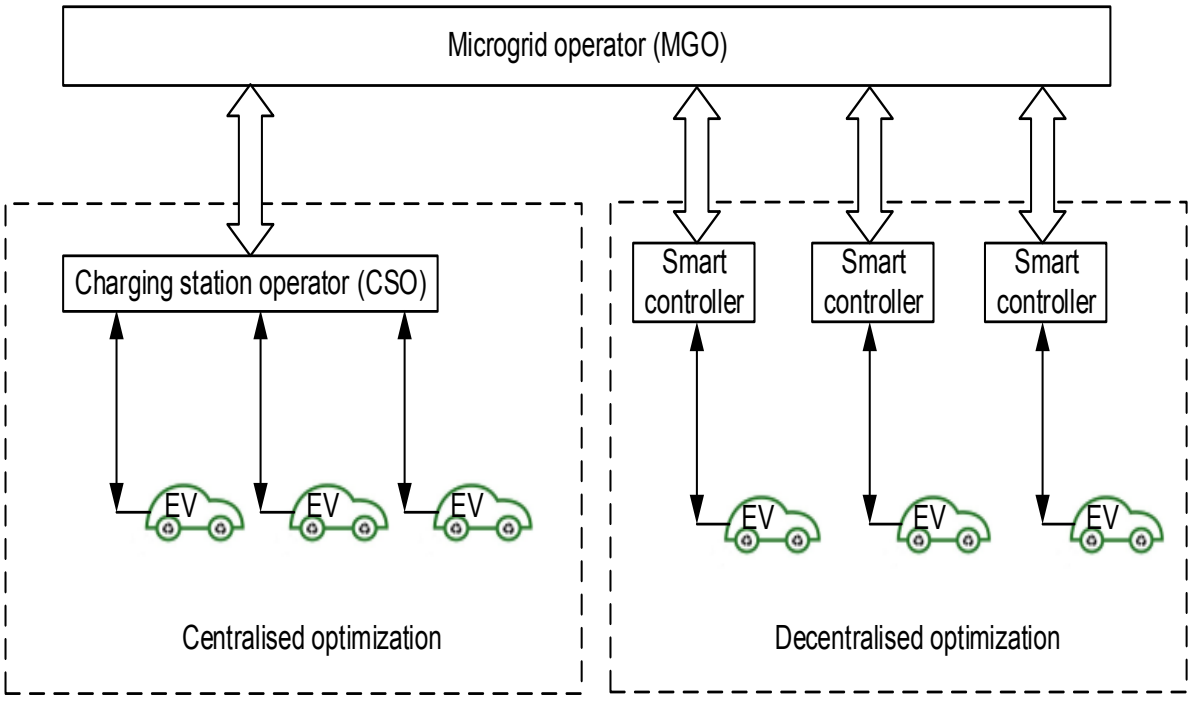

Figure 5-3: Electric vehicles' smart charger architecture

5.4 Charging Station System

Recharging infrastructure is an important part of the interface between the EVs and the microgrid network for managing the charging of the EVs. It is classified according to installation into two modes: either onboard mode or outboard (fixed point) mode. The charger is installed inside the vehicle in the onboard mode which allows the user to plug the vehicle into any standard charger outlet. In contrast, the charger is installed outside the vehicle in the specific charging location in the fixed point mode.

There are three levels of recharging infrastructure proposed by the Electric Power Research Institute (EPRI):

- Level one: classified as the lowest common voltage level which is 120 V, (12 A or 16 A) that can achieve 1.44 kW as maximum power.
- Level two: classified as a primary charging level which is working on single phase 240 V, 40 A.
- Level three: classified as a fast charging level which is working on three phase 400 V.

The specification of a different range of charging station characteristics is shown in Table 5-1.

Table 5-1: Typical characteristics of different charging modes as defined by the IEC [319].

	Maximum power output from EVSE (kilowatts)	Example charging time (hrs: mins)	Input voltage (volts)	Maximum current (amps)	Mode
AC	2.3	8h 20m	230 AC	10	2 / 3
	3	6h 30m	230 AC	13	2 / 3
	3.7	5h 15m	230 AC	16	(2) 3
	7.4	2h 35m	230 AC	32	(2) 3
	14.5	1h 20m	400 AC	21	3
	22	55m	400 AC	32	3
	43	30m	400 AC	63	3
DC	20	1h	400 AC	40	4
	50	25m	400 AC	100	4
	100	15m	400 AC	200	4

5.5 Charging Strategy of Charging Station System

Managing recharging of EVs with different capacities can achieve the optimum schedule operation. However, unmanaged recharging of EVs can cause many problems for the microgrid, which include increasing power losses in the network, voltage and frequency drop, and overload of the equipment of the microgrid such as transformers and cables. It is even possible to black out the microgrid if the recharging demand exceeds the power supply of the network. The benefits of recharging management become vital when multiple charging stations are integrated into the microgrid. In the event that many charging station systems (CSSs) are spread around the distribution network, each CSS should be obeyed by the MGO before managing the connected EVs.

In urban areas, the EV is charged either at home using one charging point or at the specifically designed CSS using multi-charging points. The CSS is an ideal place to monitor charging or discharging aggregated EVs. The main function of the CSO, which is an operator of the CSS, is to manage the charging resources of the EVs to the desired state of charge before departure. The objective function of the CSO is either to minimise the charging cost of each EV or to maximise the discharging cost of the candidate discharging the EV. The schematic diagram of connected aggregated EVs to the microgrid and the architecture diagram of connecting EVs to the CSO are shown in Figure 5-5 and Figure 5-6 respectively, which have been adopted and modified from [320].

The EV is plugged into the recharging socket of the CSS through a cable or by wireless means. The recharging socket has a power flow control meter and a data acquisition part to save the state of the EV into a digital memory. The memory of the recharging socket is labelled in the same way as the EV registration number for metering purposes. A Recharging Socket Agent (RSA), which is a part of recharging socket, and EVA, which is a part of EVO, collaborates to collect the states of the resources of EVs as well as send the order of the CSO to the EVO. The

EVA has an interaction between the owner and other parts of the EV to manage the operation of the power train drive of the EV.
In order to maintain a resilient operation, the CSO should collect data and update them minute by minute, and solve the problem every time that some changes happen such as connecting or disconnecting a new EV. Therefore, the CSO collects the data, analyse them, and solves the optimisation function periodically such as minute by minute. When an EV is parked and connected to the charging station, the recharging socket outlet records the connection time and collects some information from the EVA which is shown in Figure 5-4 and listed in the following:

1- The initial state of charge for battery and supercapacitor.
2- The desired state of charge for the battery whereas the supercapacitor is assumed to be fully charged at departure time.
3- The rated capacity of the battery and the supercapacitor of the EV.
4- The assumed leaving time of the vehicle to calculate the period of parking time.
5- The owner obligation of unidirectional or bidirectional power flow of resources.
6- The converter power limits of the vehicle.
7- The label of the EV to record the electricity bill for this vehicle.

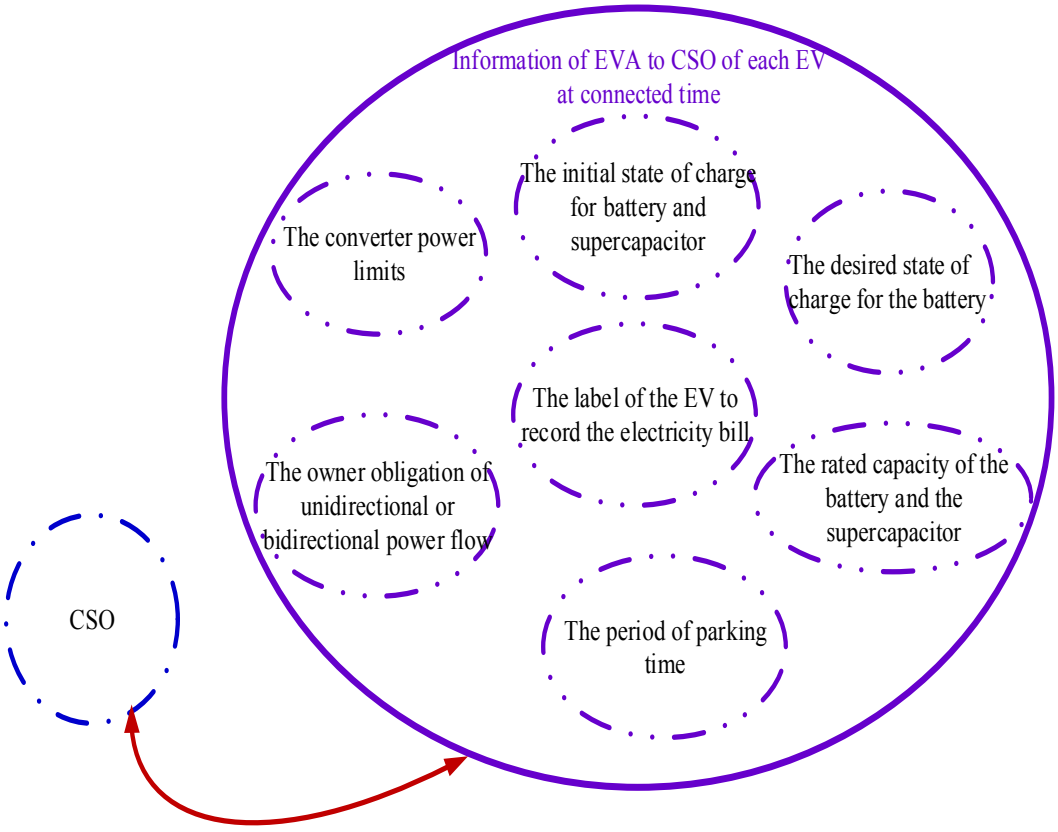

Figure 5-4: Information of EVA to CSA of each EV at connected time

The collected information by the RSA is sent to the central memory of the charging station agent (CSA), which has a direct connection to the processor of the CSA, to analysis the data and send the related information to the MGO and EVO. The related information of the MGO

is the net power required to charge the EVs and the net power available to discharge from the EVs, whereas the related information of the EVO is the reference charging or discharging power. The MGO informs the CSO about the available charging power or required discharging power. The CSO builds the schedule charging or discharging for each EV, based on the input RSA and MGO information.

The data from the recharging sockets are sent to the CSA through a bridge by an internal data bus to actuate the charging and discharging signals, process the states of the EVs, and book slots for each EV regarding charging or discharging based on the solving optimisation function formula, whereas the microprocessor calculates the slots and saves them in the memory of the recharging socket of each EV through the bridge. The main part of the CSA is a microprocessor which interfaces the reconfiguration algorithm software stored in flash memory automatically through a storage controller unit. The available or required power of the CSO and MGO stored inside the storage device interfaces with the microprocessor through the internal data bus. The microprocessor transmits and receives data from the recharging sockets that are stored inside a bridge through the bus interface unit in order to control the power electronic device of the recharging socket. The power electronic device of each recharging socket is responsible for making the power flow into the EV. The interrupt controller is responsible for communicating with the MGO and EVO for any unpredictable situation with the support of the watchdog timer. The watchdog timer, in turn, is responsible for generating a system reset automatically to involve the state of the MGO, which has a high priority to interrupt the operation of the CSO and obligate a new state. The watchdog timer also resets the system when the main program of the CSO fails or hangs because of a software or hardware fault. The schematic diagram of connected EVs to the microgrid, the schematic diagram of CSO, and the infrastructure diagram of the CSO are shown in Figure 5-5, Figure 5-6, and Figure 5-7 respectively.

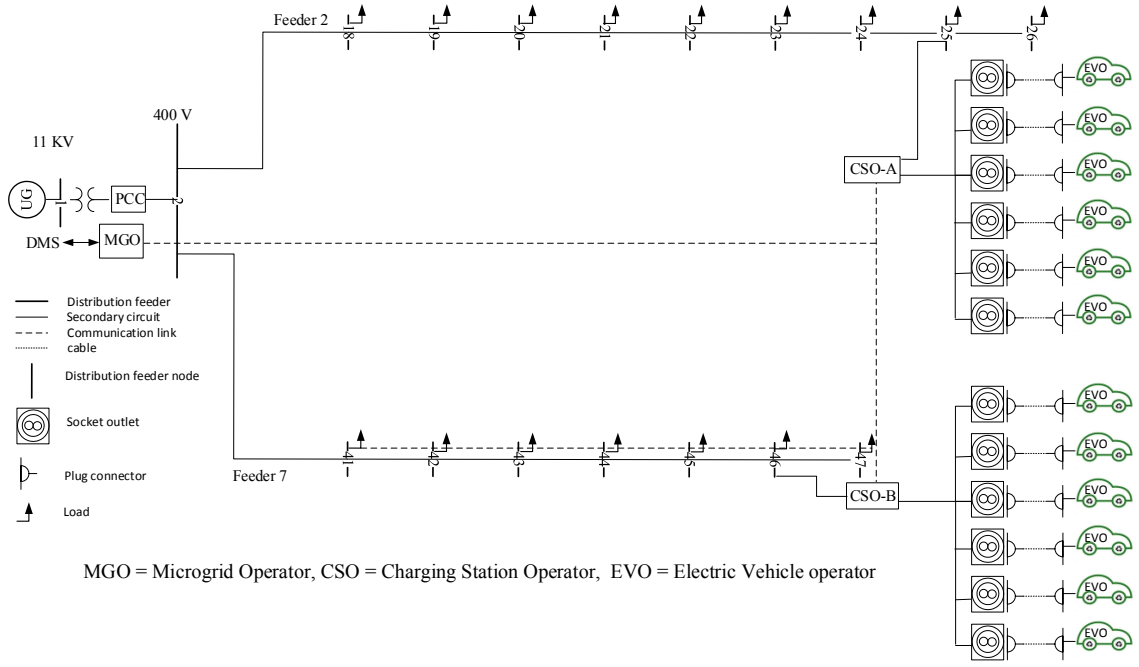

Figure 5-5: Schematic diagram of connected electric vehicles to microgrid

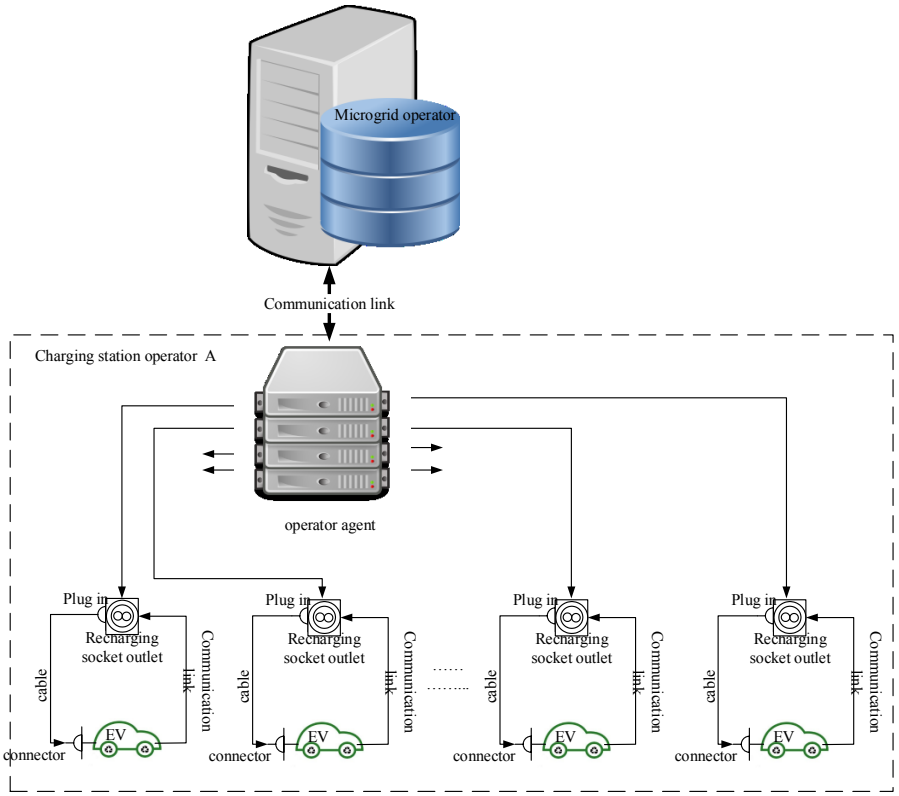

Figure 5-6: Schematic diagram of CSO

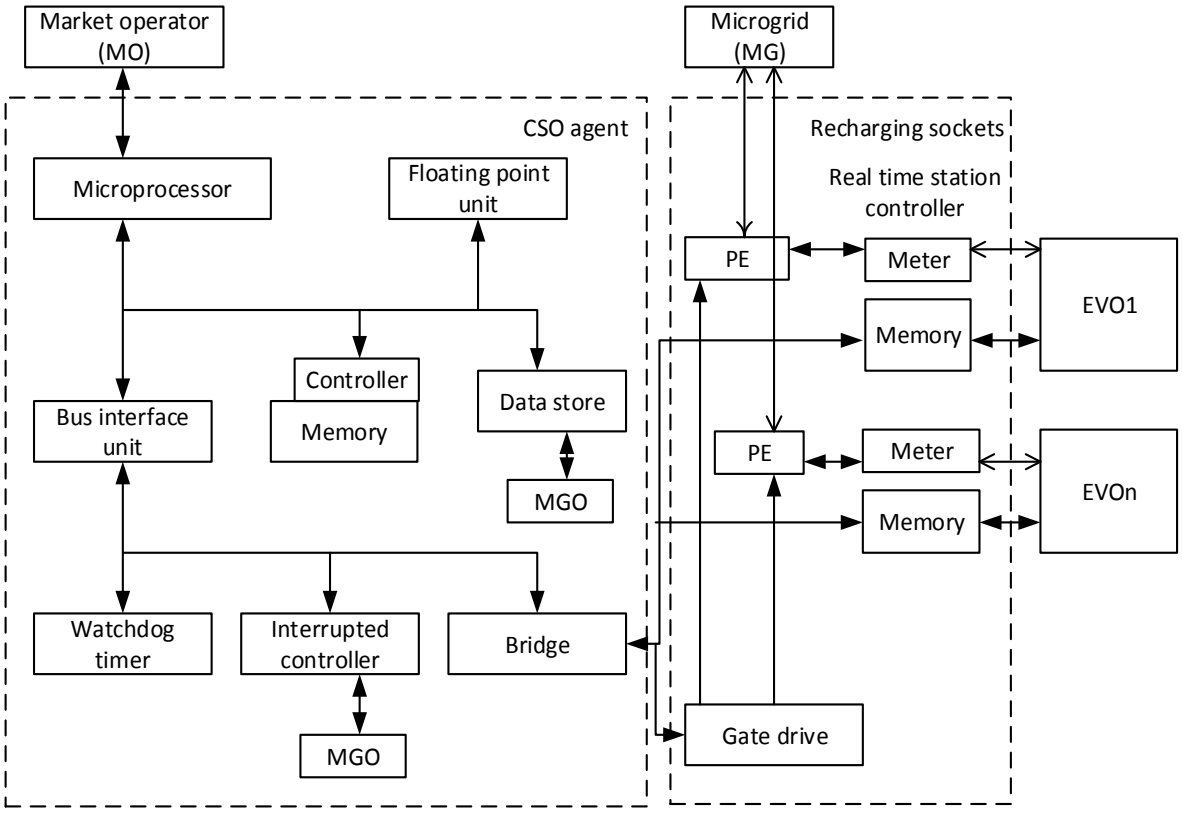

Figure 5-7: CSO infrastructure

5.6 Problem Formulation

The charging system operator may work in two modes:

Mode 1: If $P_{net} > 0$, the electric vehicle works in charging mode (G2V).

Mode 2: If $P_{net} < 0$, the electric vehicle works in discharging mode (V2G).

where $P_{net} = P_s - P_d$

In addition to these two modes, it is possible to discharge the energy of the EVs at $P_{net} > 0$ during a sudden change either in voltage or frequency. According to these two modes, the objective function is arranged, based on the MGO requirement, into charging EVs mode or discharging EVs mode.

The CSO knows the charging and discharging power tariff at each time from the market operator within distribution network operator control level, the frequency deviation, and the voltage deviation by the MGO. The CSO labels all the connected EVs and solves the objective function problem periodically to book slots for charging or discharging each EV. The CSO sends the required power to charge all the connected EVs and the available power that could be discharged from the EVs to the MGO. According to the information provided from the microgrid components, the MGO decides to cover all demand from the charging station or part of it and sends the power reference to the CSO. The power reference provided by the MGO either covers the full or partial demand of the CSS, then the CSS builds the charging strategy.

For charging mode, the CSO sets the objective function of the optimisation problem to achieve minimum power charging cost, as shown in Equation 5-1. There are two states in charging mode; the MGO could either cover all or part of the demand of the EVs. The CSO books charging slots for each EV by solving equation 5-1 based on the information provided from the EVA to cover the full demand state. For part demand, the strategy of charging depends on the voltage and frequency level; either schedule charging applies when the voltage level is at voltage above nominal (VAN) or voltage over above nominal (VOAN) and the frequency level is at frequency above nominal (FAN) or frequency over above nominal (FOAN), or curtail charging of EVs applies when the voltage level is at voltage below nominal (VBN) or voltage over below nominal (VOBN) and the frequency level is at frequency below nominal (FBN) or frequency over below nominal (FOBN), as explained in Table 5-2 and Table 5-3 respectively. The schedule or curtail charging EVs strategies are based mainly on the state of charge of the battery and supercapacitor of the EVs. The CSO predicts the optimum power charging slots of each EV based on the level of power demand and required time to reach the desired leaving state of charge, whereas the low state of charge resources has a high charging priority by applying a k scale factor to equation 5-1, as shown in equation 5-3 and described in Figure 5-8. If the EV does not reach the desired leaving state of charge, the CSO applies the priority charging based on giving priority to the earliest EV departure that has a low state of charge level compared to the desired leaving state of charge. Furthermore, If the CSO predicts that the EV barely reaches the desired leaving state of charge or does not reach it, the CSO informs the owner that the CSO could not charge the EV to selected leaving state of charge and suggests a new level of the desired leaving state of charge to the owner.

Table 5-2: Frequency and voltage range of operation

	Term	Range	
1.	Nominal frequency (NF)	$-0.001f_n \leq f \leq 0.001f_n$	
2.	Nominal voltage (NV)	$-0.03V_n \leq V \leq 0.03V_n$	
3.	Frequency above nominal (FAN)	$0.001f_n \leq f \leq 0.01f_n$	Charging reference
4.	Frequency over above nominal (FOAN)	$0.01f_n < f$	
5.	Voltage above nominal (VAN)	$0.03V_n \leq V \leq 0.1V_n$	
6.	Voltage over above nominal (VOAN)	$0.1V_n < V$	
7.	Frequency below nominal (FBN)	$-0.001f_n \leq f \leq -0.01f_n$	Discharging reference
8.	Frequency over below nominal (FOBN)	$-0.01f_n < f$	
9.	Voltage below nominal (VBN)	$-0.03V_n \leq V \leq -0.1V_n$	
10.	Voltage over below nominal (VOBN)	$-0.1V_n < V$	
11.	The procedure for operating these references is described in Table 5-3. f_n and V_n are the fundumental frequency and voltage of the microgrid respectively. In this thesis the f_n=50 Hz whereas the $V_n = 220$ V.		

In the discharging mode, the MGO sends the information to the CSO to discharge the qualified EVs due to frequency deviation or voltage deviation. Hence no EV could discharge power lower than the predefined state of charge limit. The objective function of the discharging mode would obtain the maximum discharging power cost, as shown in equation 5-2. The priority of discharging is classified according to the voltage deviations at VBN or VOBN or frequency deviations at FBN or FOBN into either discharging the resources of the EV at scheduled discharging for VBN and FBN or at maximum discharging for VOBN and FOBN, as explained in Table 5-2 and Table 5-3 respectively.

The supercapacitor is more efficient than the battery to compensate for voltage deviations whereas the battery is much more efficient than the supercapacitor to compensate for frequency divisions. However, in the microgrid, adjusting the active power influences the voltage deviation, whereas adjusting reactive power influences the frequency divisions. Therefore, a healthy battery starts discharging to compensate for voltage divisions in case the state of charge of the supercapacitor goes below the control limit of 40%. Moreover, the same procedures are applied to discharge the healthy supercapacitor to compensate for frequency divisions in case the state of charge of the battery goes below the control limit of 70%. The battery and supercapacitor of the EV work as controllable resources of power balance. However, both should not discharge fully because of degradation issues and driver planning for the next journey.

Table 5-3: Map range of frequency and voltage deviation

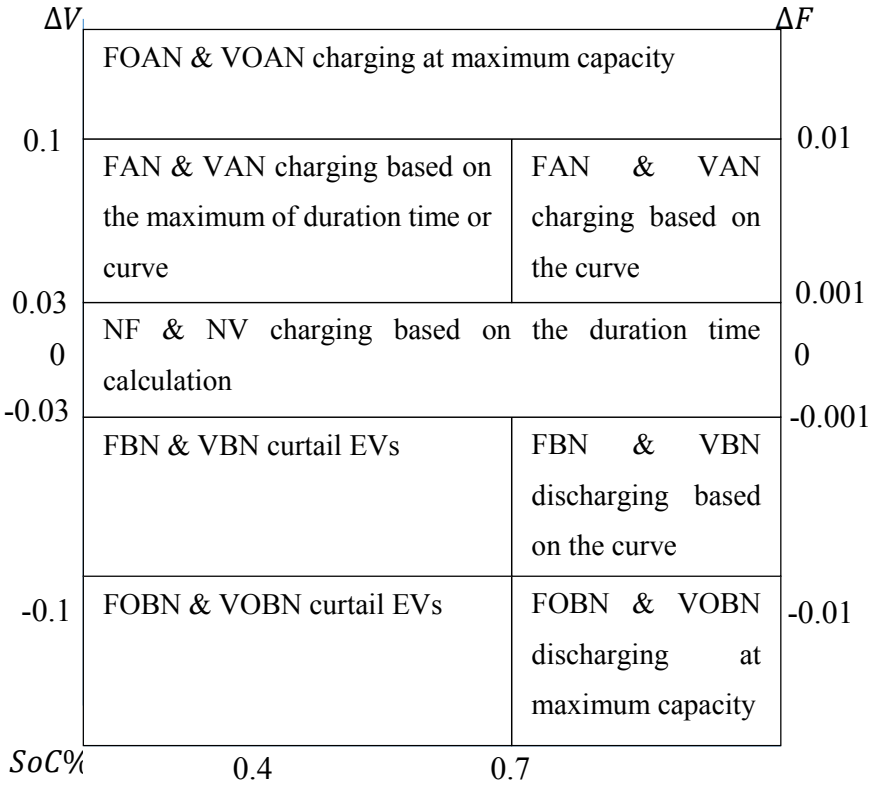

To meet these conditions, there must be a controller limit for the battery and supercapacitor considering the state of the charge level of both. The lower discharge limit of the battery and supercapacitor has been chosen regarding the different characteristics of both, such as the supercapacitor operation being about ten times faster than the battery, and the degradation of the supercapacitor being much less than the battery. Therefore, the reference limit of the supercapacitor could be less than the reference limit of the battery. The lower discharge limit of the supercapacitor has been chosen to be 40% of the state of charge of the supercapacitor, whereas the lower discharge limit of the battery has been chosen to be 70% of the state of charge of battery to meet the convenience of the owners and prevent deep discharging. Hence, no vehicles will be discharged below these limits. According to the lower limit, the schedule discharging factor of the battery is shown in equation 5-4 and explained in Figure 5-9 whereas the schedule discharging factor of the supercapacitor is shown in equation 5-5 and explained in Figure 5-10. The basic idea behind schedule charging or discharging is explained as operating units with a high state of charge level more frequently than a low state of charge units, as explained in the examples below:

- At charging mode: the activated schedule charging of Figure 5-8 flows 0.8 and 0.5 of the required current for vehicles that have 60% and 90% of the state of charge respectively.
- At discharging mode: the activated schedule discharging battery of Figure 5-9 draws 0.95 and 0.7 of reference current from vehicles that have 95% and 80% of the state of charge respectively.
- At discharging mode: the activated schedule discharging supercapacitor of Figure 5-10 draws 0.97 and 0.73 of reference current from vehicles that have 90% and 60% of the state of charge respectively.

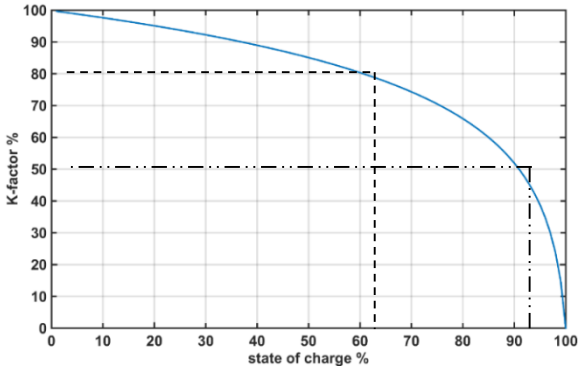

Figure 5-8: Charging schedule factor of battery and supercapacitor

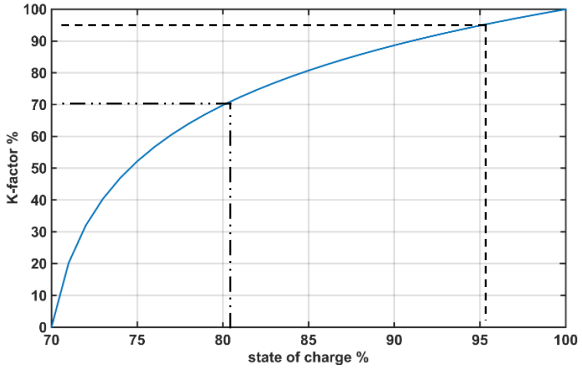

Figure 5-9: Discharging schedule factor of battery

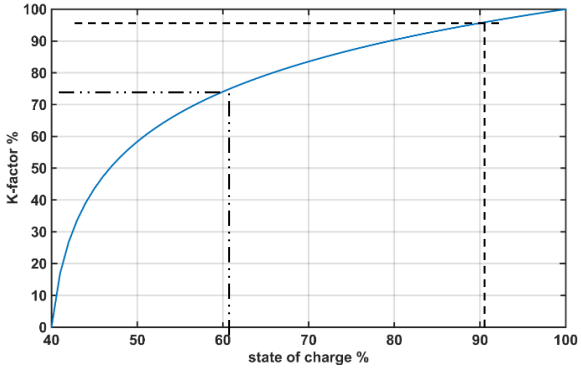

Figure 5-10: Discharging schedule factor of supercapacitor

The detail of calculation required and available energy and power in the battery and supercapacitor are shown in equations 5-6 to 5-12, whereas the control parameters of charging current and discharging current are shown in equations 5-13 to 5-15. Equation 5-1 refers the optimisation function of calculating the minimum cost of charging the active and reactive power of EVs based on a number of parameters: the charging weight dynamic coefficient α, charging binary signals s_1, active and reactive binary signals ε_1 and ε_2 respectively, and charging priority factor ρ. On the other hand, equation 5-2 refers to the calculation of the optimisation function of maximum discharging based on a number of parameters: owner choice D, the discharging weight dynamic coefficient B, charging binary signals s_2, active and reactive binary signals ϑ_1 and ϑ_2 respectively, and the factor of discharging tariff F. The energy available and required of the battery and supercapacitor are calculated in Equations 5-6 and 5-7 respectively based on terminal voltage V_t, rated power Q_j^{rated}, and desired and initial state of charge $SoC_j^{desired} - SoC_j^{initial}$. The active and reactive power required and available power are calculated using equations 5-8 and 5-9 respectively based on energy calculation, period of EV connection, and efficiency of the resources. The required and actual capacity of the resources are calculated using equations 5-10 and 5-11 respectively based on the power calculation, terminal voltage, and rated capacity of the resources. Then, the current of charging or discharging battery at nominal value or scheduling value is formulated based on required and rate capacity, schedule charging, battery schedule discharging, and supercapacitor schedule discharging in the following:

$$Min-Cost=\sum_{i=t_a}^{t_d}\sum_{j=1}^{N}\alpha.s_1.\varepsilon_1.P_{ch,ij}.\Delta t.\rho.T_{P,ch}+\alpha.s_1.\varepsilon_2.Q_{ch,ij}.\Delta t.\rho.T_{Q,ch} \quad 5\text{-}1$$

$$Max-Cost=\sum_{i=t_a}^{t_d}\sum_{j=1}^{N}D.\beta.s_2.\vartheta_1.P_{dis,ij}.\Delta t.F.T_{P,ch}+D.\beta.s_2.\vartheta_2.Q_{dis,ij}.\Delta t.F.T_{Q,ch} \quad 5\text{-}2$$

$$k_{b/sc,ch}=15\times\log_2(SoC-101) \quad 5\text{-}3$$

$$k_{b,dis}=20.18\times\log_2(SoC-69) \quad 5\text{-}4$$

$$k_{sc,dis}=16.86\times\log_2(SoC-39) \quad 5\text{-}5$$

$$E_{j,b/sc}^{required}=V_{t,b/sc}Q_{j,b/sc}^{rated}\left(\left(SoC_{j,b\backslash sc}^{desired}-SoC_{j,b\backslash sc}^{initial}\right)/100\right) \quad 5\text{-}6$$

$$E_{j,b/sc}^{available}=V_{t,b/sc}Q_{j,b/sc}^{rated}\left(\left(SoC_{j,b\backslash sc}^{initial}-SoC_{j,b\backslash sc}^{min}\right)/100\right) \quad 5\text{-}7$$

$$P_{j,b}^{required}=\frac{E_{j,b}^{required}}{\left(t_j^{departure}-t_j^{connected}\right).\eta_{ch}}$$

$$Q_{j,sc}^{required}=\frac{E_{j,sc}^{required}}{t_j^{departure}-t_j^{connected}.\eta_{ch}} \quad 5\text{-}8$$

$$P_{j,b}^{available}=\frac{E_{j,b}^{available}}{\left(t_j^{departure}-t_j^{connected}\right).\eta_{ch}}$$

$$Q_{j,sc}^{available}=\frac{E_{j,sc}^{available}}{\left(t_j^{departure}-t_j^{connected}\right).\eta_{ch}} \quad 5\text{-}9$$

$$C_{rate}^{required}=\frac{\varepsilon_1P_{j,b}^{required}+\varepsilon_2Q_{j,sc}^{required}}{V_{tb/sc}Q_{j,b,sc}^{rated}} \quad 5\text{-}10$$

$$C_{rate}^{actual}=\frac{\varepsilon_1P_{j,b}^{available}+\varepsilon_2Q_{j,sc}^{available}}{V_{tb/sc}Q_{j,b/sc}^{rated}} \quad 5\text{-}11$$

At charging mode, the current equations of the battery and supercapacitor are formulated in 5-12.

$$\begin{aligned}I_{j,b}^{ch}&=Q_{j,b}^{rated}C_{rate}^{required} && if\ s_1=1,\varepsilon_1=1\\ I_{j,sc}^{ch}&=Q_{j,sc}^{rated}C_{rate}^{required} && if\ s_1=1,\varepsilon_2=1\end{aligned} \quad 5\text{-}12$$

At schedule charging mode, the impact of the schedule charging factor at the battery and supercapacitor is considered within their current equations as presented in 5-13.

$$\begin{aligned}I_{j,b}^{sch}&=Q_{j,b}^{rated}C_{rate}^{required}.K_{f,ch} && if\ s_1=1,\varepsilon_1=1\\ I_{j,sc}^{sch}&=Q_{j,sc}^{rated}C_{rate}^{required}.K_{f,ch} && if\ s_1=1,\varepsilon_2=1\end{aligned} \quad 5\text{-}13$$

At discharging mode, the current equations of the battery and supercapacitor are presented in 5-14:

$$\begin{aligned}I_{j,b}^{dis}&=Q_{j,b}^{rated}C_{rate}^{actual} && if\ s_2=1,\vartheta_1=1,D=1\\ I_{j,sc}^{dis}&=Q_{j,sc}^{rated}C_{rate}^{actual} && if\ s_2=1,\vartheta_2=1,D=1\end{aligned} \quad 5\text{-}14$$

At schedule discharging mode, the schedule discharging factors' effect on the current equations of the battery and supercapacitor are shown as::

$$I_{j,b}^{sdis} = Q_{j,b}^{rated} C_{rate}^{actual} . K_{f,dis} \quad if s_2 = 1, \vartheta_1 = 1, D = 1$$
$$I_{j,sc}^{sdis} = Q_{j,sc}^{rated} C_{rate}^{actual} . K_{f.dis} \quad if s_2 = 1, \vartheta_2 = 1, D = 1 \qquad 5\text{-}15$$

The charging and discharging of the normal and scheduled current of the battery and the supercapacitor limitation are revealed in equations 5-16 and 5-17 respectively.

$$I_{j,b/sc,min}^{ch/dis} \leq I_{j,b/sc}^{ch/dis} \leq I_{j,b/sc,max}^{ch/dis} \qquad 5\text{-}16$$

$$I_{j,b/sc,min}^{sch/sdis} \leq I_{j,b/sc}^{sch/sdis} \leq I_{j,b/sc,max}^{sch/sdis} \qquad 5\text{-}17$$

s is the binary number either 1 or 0, s_1 refers to the charging mode and s_2 refers to the discharging mode, whereas the $s_1 + s_2 = 1$. The states of the binary logic s are explained in equations 5-18 and 5-19 respectively.

$$s_1 = \begin{cases} 1 & if \sum_{j=1}^{N} P_{ch,ij} \geq P_{net}(t)\ charging\ mode\ applies \\ 0 & otherwise \end{cases} \qquad 5\text{-}18$$

$$s_2 = \begin{cases} 1 & if \sum_{j=1}^{N} P_{dis,ij} \geq P_{v2g}(t)\ discharging\ mode\ applies \\ 0 & otherwise \end{cases} \qquad 5\text{-}19$$

ε is the binary number which is either 1 or 0, ε_1 refers to active power charging mode and ε_2 refers to reactive power charging mode, whereas $\varepsilon_1 + \varepsilon_2 = 1$. The states of the binary logic ε are explained in equations 5-20 and 5-21. Respectively.

$$\varepsilon_1 = \begin{cases} 1 & if SoC_B^d - SoC_B^a \leq 0 \\ 0 & otherwise \end{cases} \qquad 5\text{-}20$$

$$\varepsilon_2 = \begin{cases} 1 & if SoC_B^d - SoC_B^a > 0\ \&\ SoC_{sc}^d - SoC_{sc}^a \leq 0 \\ 0 & otherwise \end{cases} \qquad 5\text{-}21$$

ρ is the priority factor of charging mode which is equal to either 1 when applying the optimisation algorithm or 1.5 when the EV is charged directly without the applied optimisation algorithm which is activated by the owner of the EV. The explanation of priority charging factor ρ is shown in Equation 5-22.

$$\rho = \begin{cases} 1 & Apply\ optimization\ algorithm \\ 1.5 & Charge\ EV\ at\ rated\ power\ with\ 50\%\ extra\ price \end{cases} \qquad 5\text{-}22$$

D is the binary number of the owner choice for either bidirectional power flow or unidirectional power flow from the EV. The CSO calculates the available discharging power of the EV according to the predefined level of state of charge of resources when D is activated otherwise the CSO hides the EV from any discharge activity for any level of state of charge of resources as shown in Equation 5-23.

$$D = \begin{cases} 1 & if\ bidirectional \\ 0 & if\ unidirectional \end{cases} \qquad 5\text{-}23$$

ϑ is the binary which is either 1 or 0 for discharging either active or reactive power from the resources of the EV number whereas ϑ_1 refers to active power discharging mode at frequency deviation and ϑ_2 refers to reactive power discharging mode at voltage deviation. The sum of binary numbers ϑ_1 and ϑ_2 should not exceed one ($\vartheta_1 + \vartheta_2 = 1$) to prevent overlap, as explained

in equations 5-24 and 5-25 respectively. The system response for frequency variation is stricter than the voltage variation due to the sensitivity of frequency level in the system over voltage level.

$$\vartheta_1 = \begin{cases} 1 & if\ \Delta\omega > 0.001\ and\ SoC_b \geq 70\%\ OR\ \Delta V > 0.3\ and\ SoC_{sc} \leq 40\% \\ 0 & otherwise \end{cases} \quad 5\text{-}24$$

$$\vartheta_2 = \begin{cases} 1 & if\ \Delta V > 0.3\ and\ SoC_{sc} \geq 40\%\ OR\ \Delta\omega > 0.001\ and\ SoC_b \leq 70\% \\ 0 & otherwise \end{cases} \quad 5\text{-}25$$

The degradation cost (C_d) is adapted from [321] to equal 6.5 cents / kWh.

The factor of discharging tariff is represented by F which has been chosen at 10% higher than the charging tariff. It could be variable over a day.

$T_{P,ch}$, $T_{Q,ch}$ refer to active and reactive tariffs of electricity units over a day.

$\alpha\ and\ \beta$ are weighting dynamic (delay) coefficients for the charging and discharging power. They represent the rate of convergence for charging or discharging to an equilibrium point. This is required at high disturbance to reduce the oscillation in frequency or voltage variation by adjusting it to a high value. It could be increasing those values or choosing it to be the minimum at normal state.

5.7 Constraints

The previous model of battery and supercapacitor operation is limited due to manufacturing constraints, whereas the capacities of the battery and supercapacitor are different due to how the vehicles are used. Therefore, the following power, current, and state of charge constraints should be applied for each vehicle to obligate the CSO not to exceed them and avoid damaging the storage units of the EVs. The essential constraints to be considered are as follows:

5.7.1 Power constraints

In charging mode, the MGO should cover all the demands for the EVs, as shown by

$$\sum_{n=1}^{N} P_{EV,n} \leq |P_{net}| \quad 5\text{-}26$$

In case the MGO provides less than the net power of the EVs then scheduled charging should apply based on the SoC and period of parking.

In discharging mode, the EVs should supply the required power to maintain the network stability as represented by

$$P_{min} \leq \sum_{i \in T} \sum_{j \in N} P_{ch\backslash dis,ij} \leq P_{max}, \forall i \in T, \forall j \in N \quad 5\text{-}27$$

where P_{min}, P_{max}= the minimum power and maximum power of the CSO.

In case the total power of qualified EVs is less than the required power of the MGO, then the MGO should use the available power from EVs and search for extra power from the rest of the distributed generators to balance the load. It may be that the MGO is not able to find the surplus power to cover the load, then the MGO applies the curtail strategy starting with non-sensitive demand.

5.7.2 Current constraints

For safe operation of the battery and supercapacitor, the current flow through the energy storage system should be limited. The maximum current flow from the battery depends mainly on the chemical reaction and ambient temperature. Exceeding the maximum current of the energy storage system causes heat, flames and smoke which could cause damage to the devices. Operating the energy storage system beyond the rated value causes overuse of the device leading to degrading their lifecycle, which adversely affects the lifetime of the energy storage system. The limited charging and discharging current are determined by

$$I_{j,b/sc,min}^{ch/dis} \leq I_{j,b/sc}^{ch/dis} \leq I_{j,b/sc,max}^{ch/dis} \quad 5\text{-}28$$

$$I_{j,b/sc,min}^{sch/sdis} \leq I_{j,b/sc}^{sch/sdis} \leq I_{j,b/sc,max}^{sch/sdis} \quad 5\text{-}29$$

5.7.3 State of charge constraints

The state of charge of the battery and the supercapacitor represents the amount of stored energy inside them. To maintain the long life of the energy storage system at charging mode, the state of charge should be limited to prevent degrading their lifecycle. In discharging mode, the discharging power from the energy storage system should be limited to keep the energy of the battery for next journey and increase the lifetime of the devices. The state of charge limitation is defined by the following formula:

$$SoC_{min} \leq \sum_{i \in T} \sum_{j \in N} SoC_{b\backslash sc,ij} \leq SoC_{max}, \qquad \forall i \in T, \forall j \in N \quad 5\text{-}30$$

5.8 Case Study

To explain the implementation of the optimisation algorithm strategy clearly under various circumstances, five scenarios of numerical simulation are explored in this chapter which cover the different scenarios of operation for EVs. There are four scenarios selected to simulate and analyse battery operation, whereas the last scenario is selected to simulate and analyse the supercapacitor operation. The scenarios are justifying the clarity of the methodology proposed for the EVs' operation within the CSS based on the CSO controller. These scenarios are explained below and shown in Figure 5-11:

1- The first scenario concerns the strategy of first connected first charging, where the MGO could cover all demands of the EVs at the CSS.
2- The second scenario concerns charging the EVs according to distributing the time slots of each EV to achieve the objective function where the microgrid could cover all demands of connected EVs at the CSS.
3- The third scenario concerns the predicted charging slots of each EV according to the objective function. If the EV could not reach the desired leaving state of charge, the CSA will apply the priority strategy. The MGO provides 75% of EVs' demands.
4- The fourth scenario concerns charging or discharging the battery of the EVs according to the charging or discharging objective function.
5- The fifth scenario is about charging or discharging the supercapacitor of the EVs according to the charging or discharging objective function.

All scenarios have 150 samples of EVs from different brands with different capacities of battery and supercapacitor connected at different times of the day, as shown in Apx_Table J-1 in Appendix J. the number of EVs could be more or less. However, if more vehicles are used it could be difficult to present the results of the academic study. Similarly, a lower number of vehicles could result in the unrealistic distribution of EVs within the microgrid. Therefore, 150 samples of EVs are about right to validate the proposed methodology of operating EVs within the microgrid based on the CSO controller.

Originally, the EVs have had a battery as their main energy storage system; these have been modified to include a supercapacitor as a power storage system to enhance the battery performance. Table J-1 in the Appendix J shows the related information for batteries and supercapacitors including rated capacity, control reference of the state of charge, the initial and required state of charge, and arrival and expecting to leave time for each vehicle. The supercapacitor charging characteristics are very fast, at about ten times faster than that of the battery. The capacity of the supercapacitor has chosen lower than the capacity of the battery. Thus, the first minutes of processing time are booked to the charging supercapacitor.

The power tariff is the chosen variable based on the time of day, which starts at a lower price during the night. The tariff steps up in the early morning and increases gradually until reaching the maximum at midday. After that, it starts to reduce gradually until reaching its minimum tariff at midnight; then it is kept constant until early morning, as shown in Figure 4-11. The power tariff is stored by the market operator (MO) at a territory control level, which is responsible for providing the tariff rate for all control levels of the system.

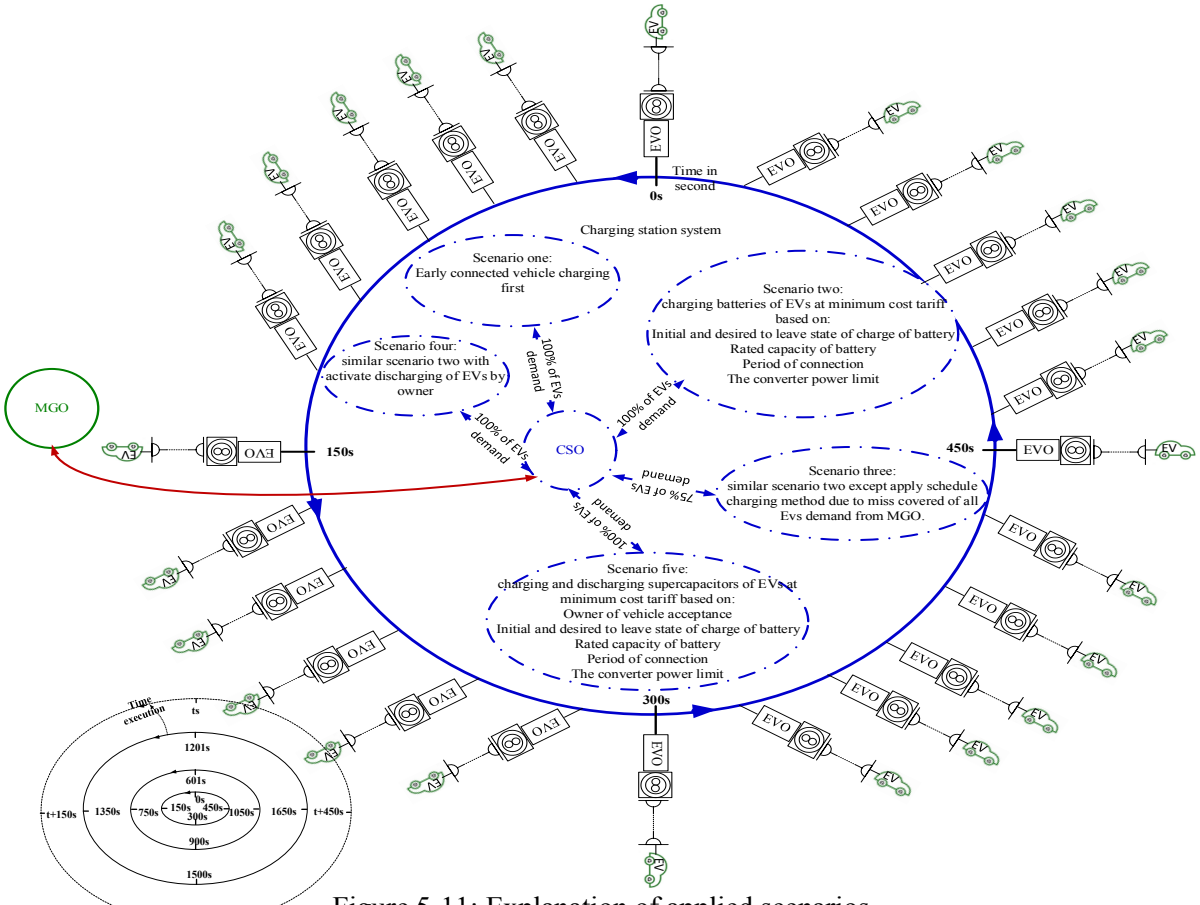

Figure 5-11: Explanation of applied scenarios

5.8.1 Scenario one

In this case, the MGO sends information to the CSO to start charging all connected EVs to the microgrid directly at any time of a day. The microgrid is healthy enough to cover all demands at any time of a day. The performance of each EV out of 150 over a day is in terms of the state of charge and power consumed, as depicted in Figure 5-12 and Figure 5-13 respectively where the curves show the response of initial SoC of EVs at connected time and zero at disconnected time. Figure 5-12 clearly shows that all the EVs reached the desired state of charge before leaving the CSS. All EVs have charged continuously since being connected without interruption due to the available charging power from the MGO and missing optimisation algorithm. The charging current stop flow throws the converter of the EV when the state of charge reaches the desired level, as seen in Figure 5-13.

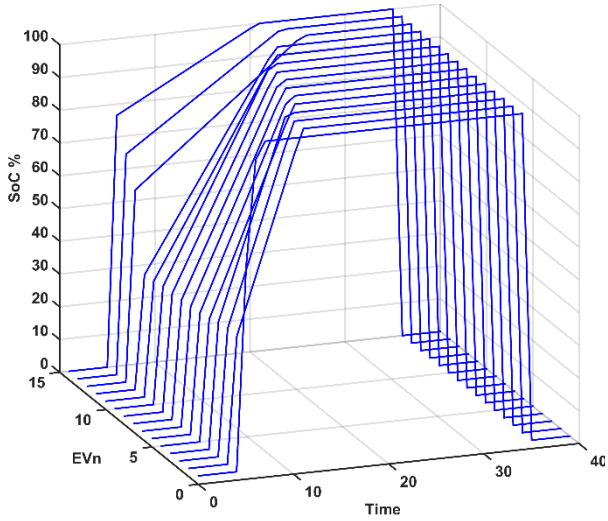

A- State of charge for vehicles number 1-15

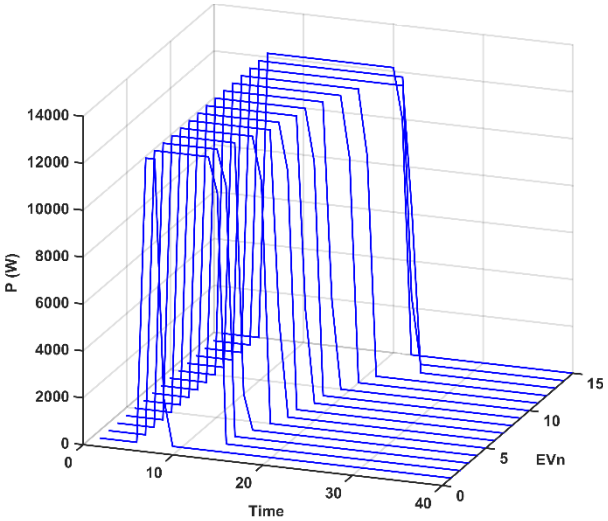

A- Power consumed for vehicles number 1-15

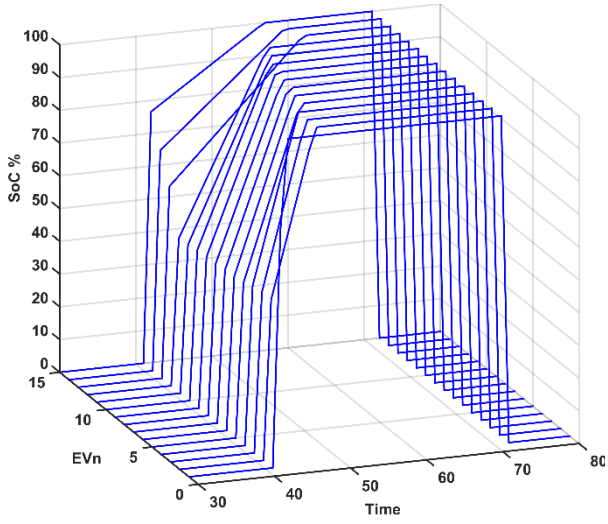

B- State of charge for vehicles number 16-30

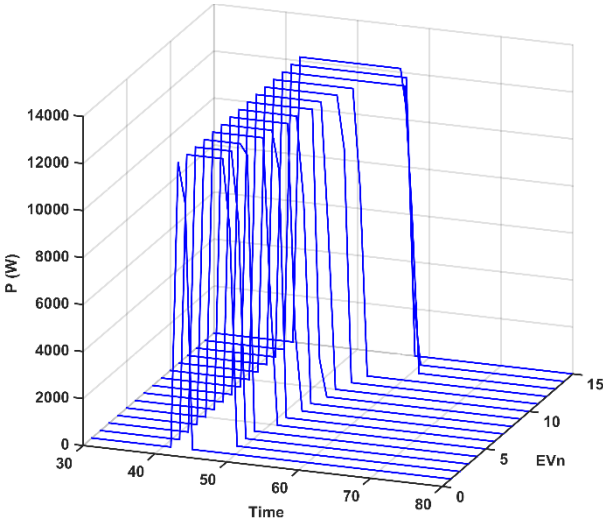

B- Power consumed for vehicles number 16-30

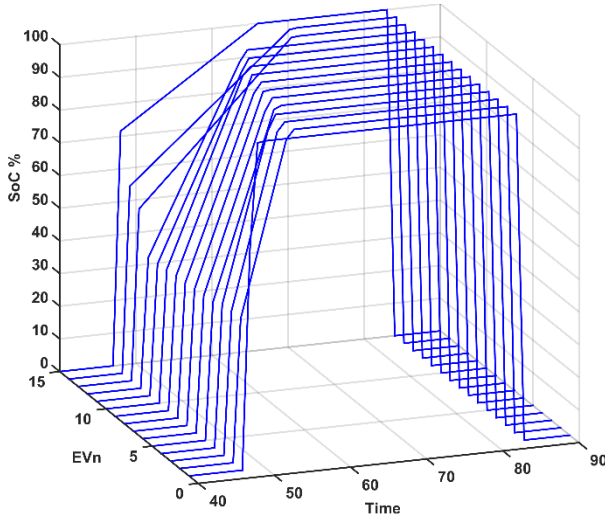

C- State of charge for vehicles number 31-45

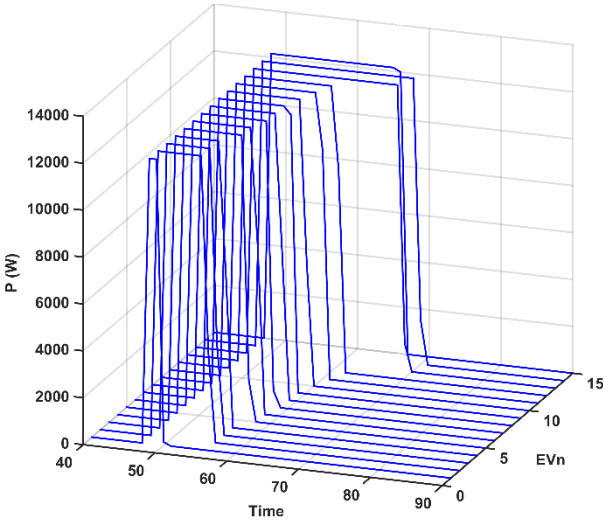

C- Power consumed for vehicles number 31-45

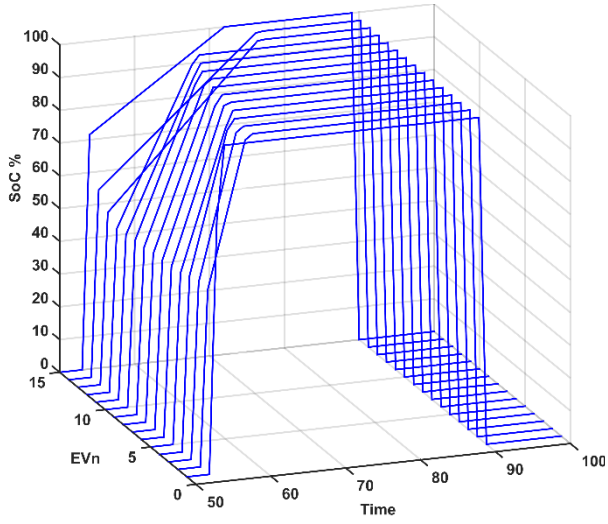

D- State of charge for vehicles number 46-60

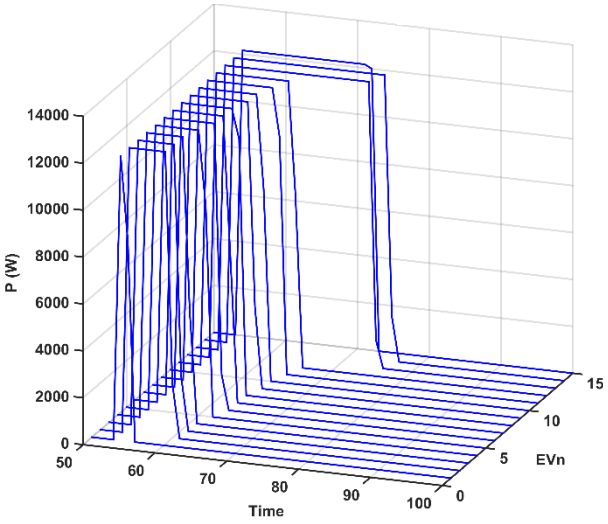

D- Power consumed for vehicles number 46-60

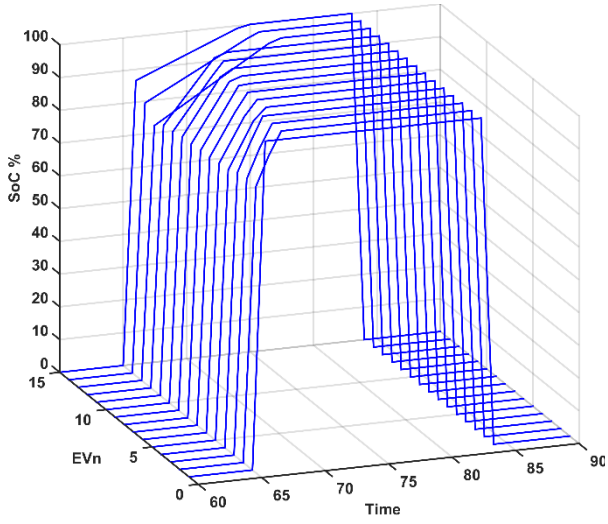

E- State of charge for vehicles number 61-75

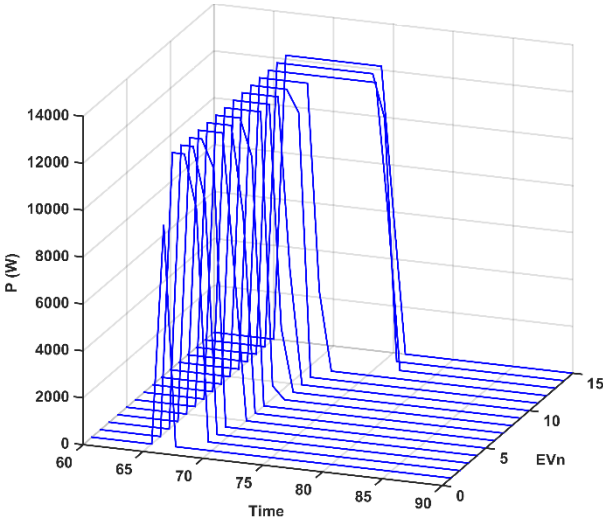

E- Power consumed for vehicles number 61-75

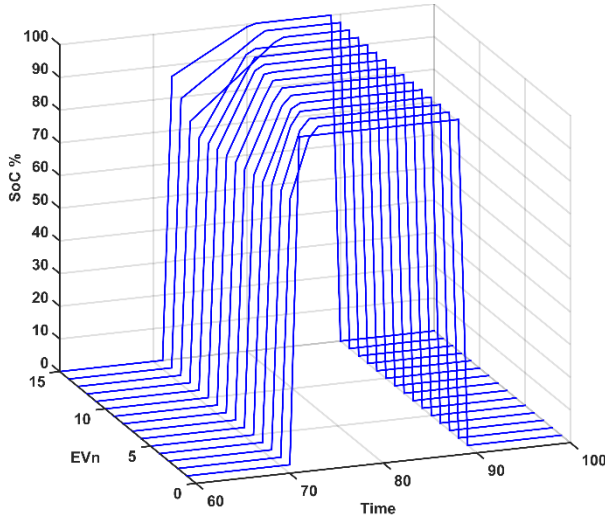

F- State of charge for vehicles number 76-90

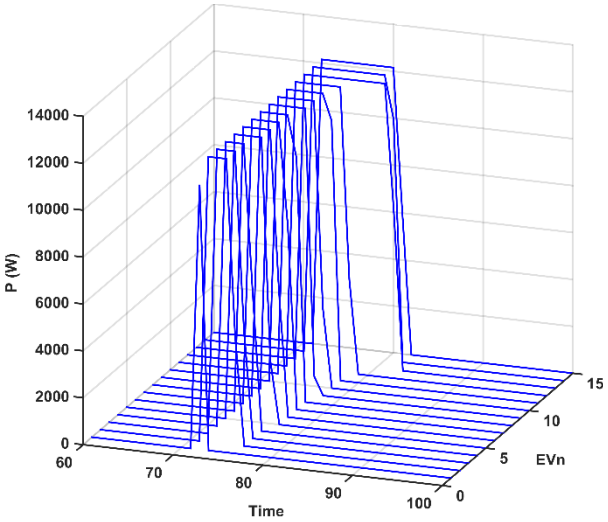

F- Power consumed for vehicles number 76-90

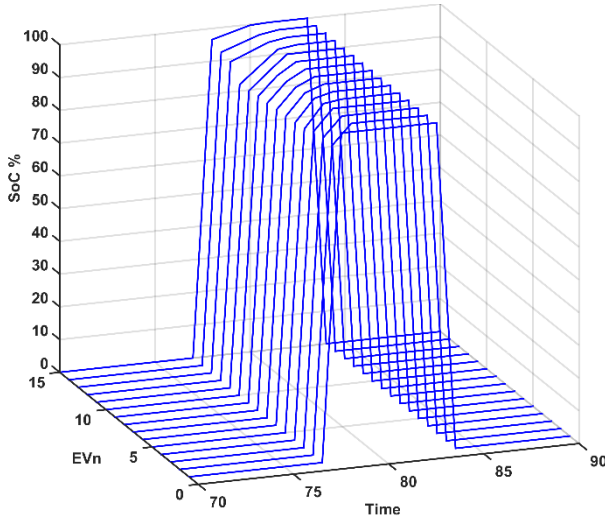

G- State of charge for vehicles number 91-105

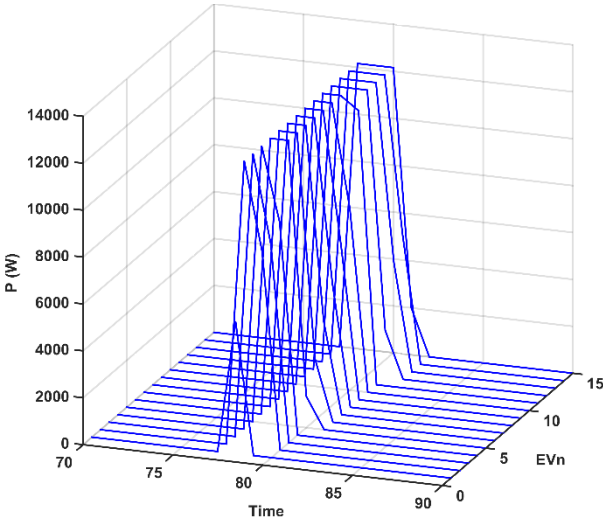

G- Power consumed for vehicles number 91-105

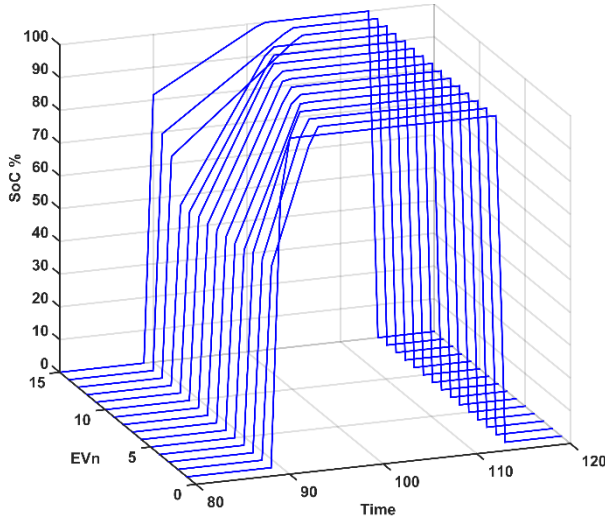

H- State of charge for vehicles number 106-120

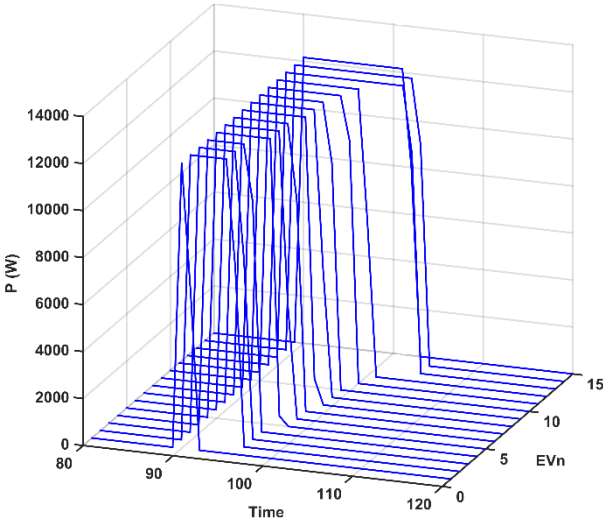

H- Power consumed for vehicles number 106-120

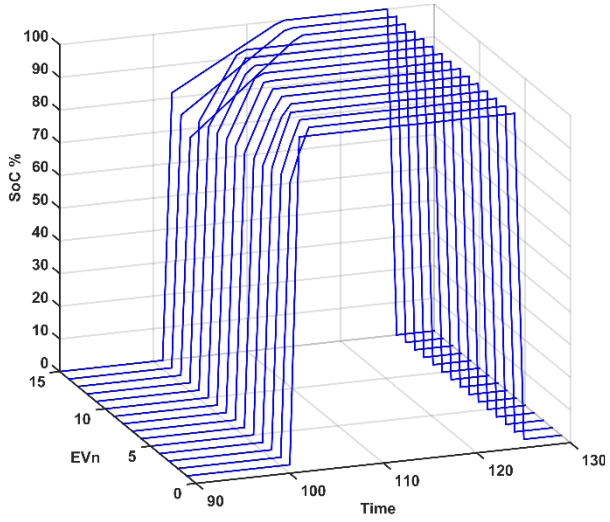

I- State of charge for vehicles number 121-135

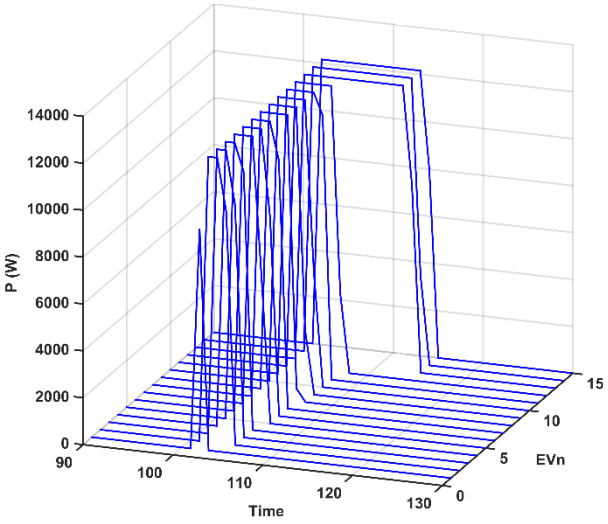

I- Power consumed for vehicles number 121-135

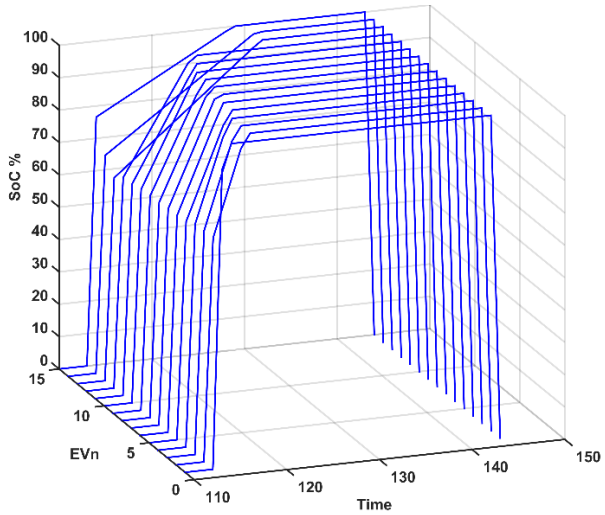

J- State of charge for vehicles number 136-150

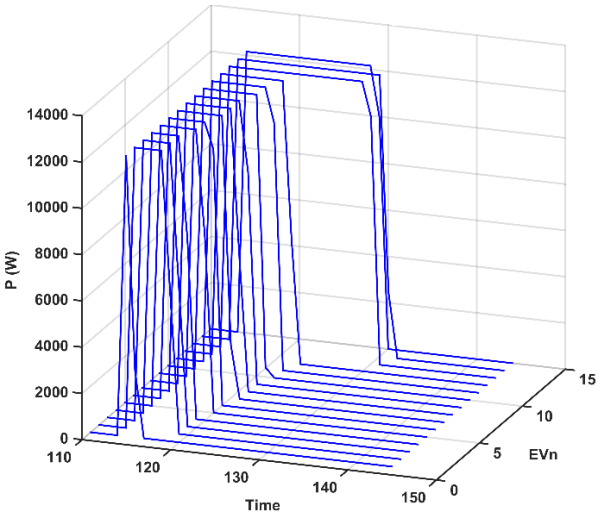

J- Power consumed for vehicles number 136-150

Figure 5-12: SoC of charging EVs with power demand 100%

Figure 5-13: Power consumed of charging EVs with power demand 100%

Figure 5-14 shows the comparison between the numbers of EVs connected to the CSS at time t with the number of EVs that do not reach the desired state of charge at the same time. All 150 samples of EVs start charging directly after connection until reaching the desired state of charge. Therefore, the number of EVs in dark blue bars start reducing until reaching zero before leaving time. Furthermore, the number of EVs that fully reached the desired state of charge is shown in Figure 5-15, where the light blue bars refer to the connected vehicle to the CSS and the dark blue bars refer to the EVs still charging towards the desire to leave state of charge. The cost of power charging for each EV is shown in Figure 5-16 which refers to the higher charging cost for high EV battery capacity.

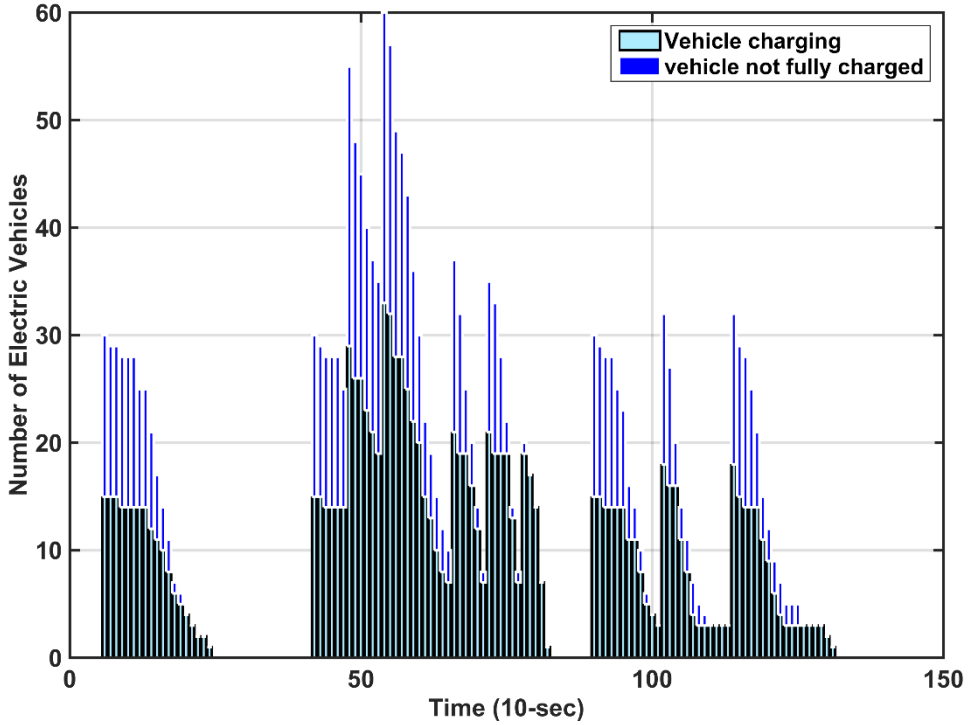

Figure 5-14: Number of vehicles connected vs. number of vehicles that do not achieve the desired SoC at a specific time

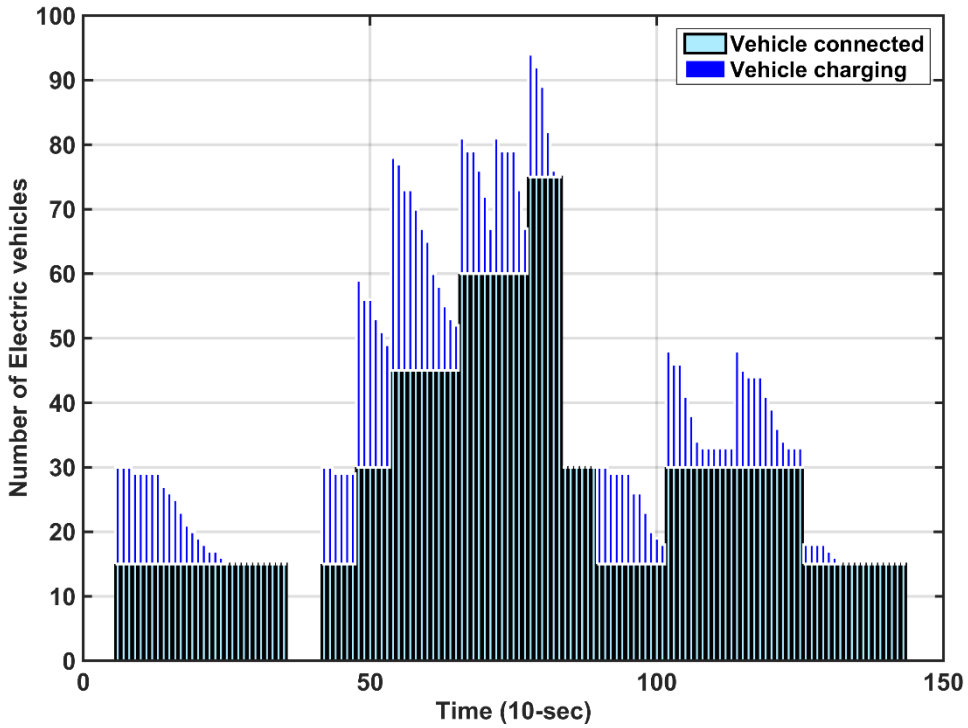

Figure 5-15: Number of vehicles connected vs. number of vehicles that do charge at a specific time

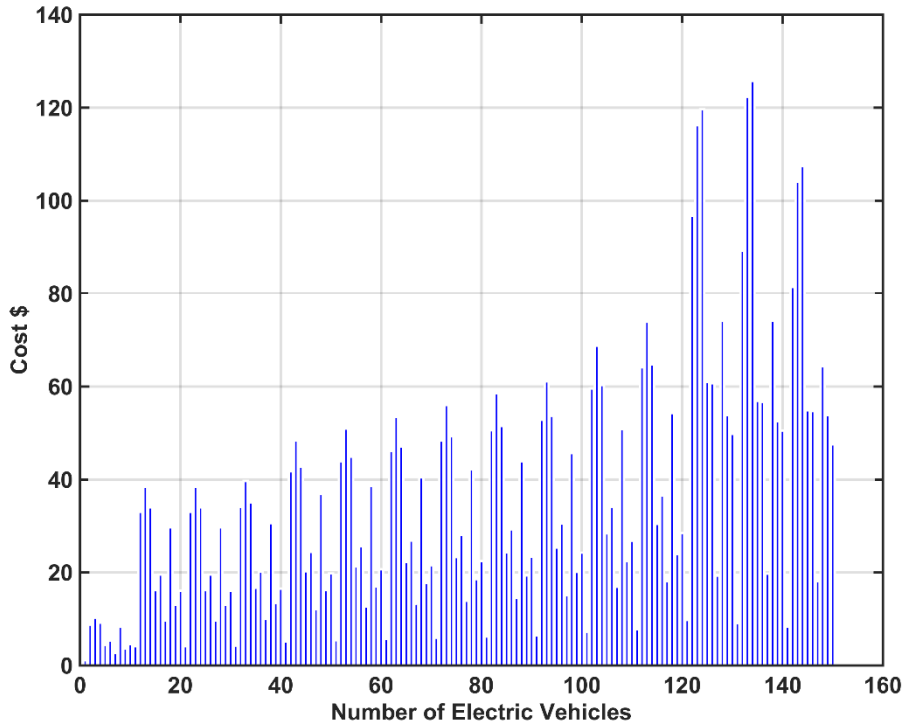

Figure 5-16: The cost of power charging for each vehicle

5.8.2 Scenario two

This senario seeking for objective function of finding minimum charging cost of EVs by applying the optimisation algorithm. The full demand of the CSO is coverd by MGO, whereas the CSO predicts the optimum slots of charging each EV. The CSO analyses the state of each EV periodically to predict the optimum slots to charge the EVs based on the objective function at equation 5-1. The performance of each EV over a day in terms of the state of charge and power consumed is depicted in Figure 5-17 and Figure 5-18 respectively where the curves show the response of initial SoC of EVs at connected time and zero at disconnected time. The results clearly show that all EVs reached the desired state of charge before leaving the CSS. Figure 5-17 shows that not all EVs charged at the instant connection to the microgrid, whereas the charging EVs fall into to three groups. In the first group, the EV charges instantaneously after connection, as shown in parts A and B of Figure 5-17, other EVs in the second group charge before leaving as shown in parts H, I and J, of Figure 5-17 whereas the rest of the EVs which belong to the third group distribute charging between the start time of connection and before leaving, as shown in parts C, D, E and F of Figure 5-17. The diversity of charging behaviour is dependent on the power availability and the optimisation algorithm, which distribute charging slots at minimum cost of power. Figure 5-18 shows the charging power of the three groups above based on the permission slots of the CSO agency. The current at the first group flow continues at the beginning of connection, whereas the second group draws zero current at the beginning of the connection. The current flows before leaving time for the second group. In contrast to the first and second groups, the charging current flow is distributed between the beginning of connection and before leaving time, whereas the period between them is zero current flowing. The converter carries a rated current for all EVs at charging time.

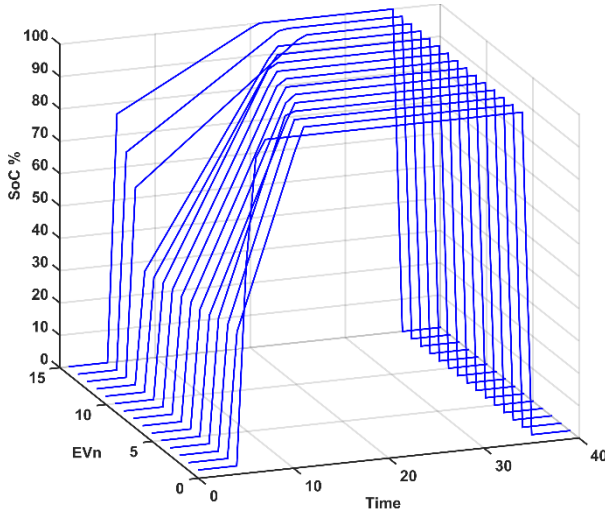

A- State of charge for vehicles number 1-15

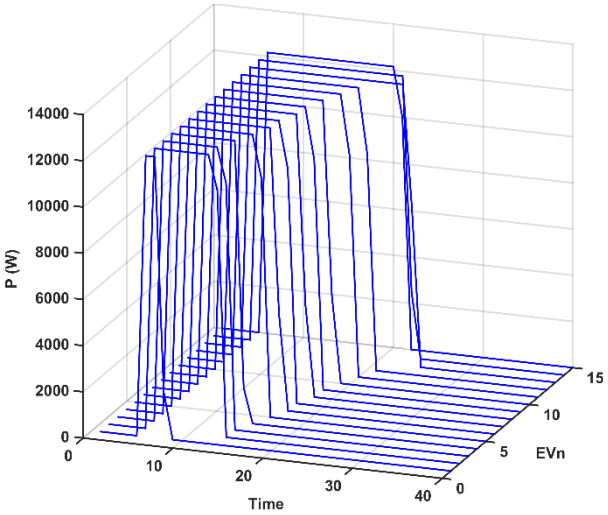

A- Power consumed for vehicles number 1-15

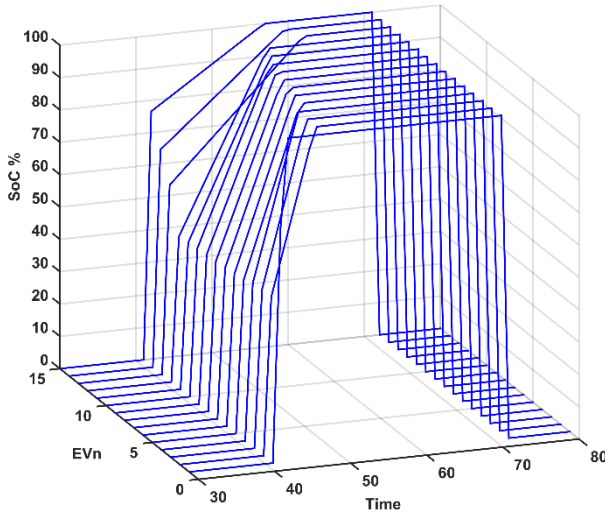

B- State of charge for vehicles number 16-30

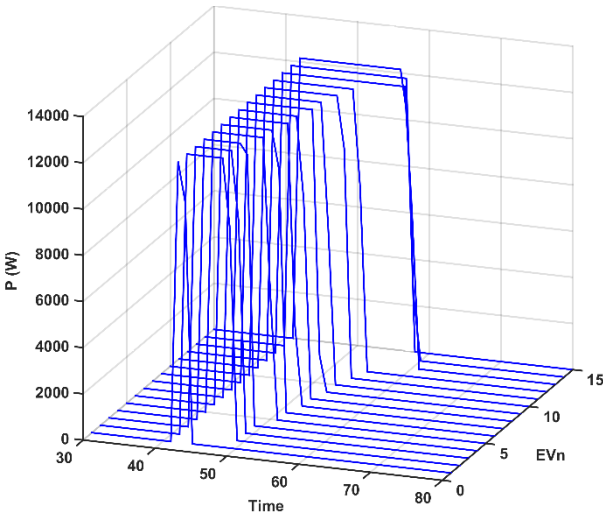

B- Power consumed for vehicles number 16-30

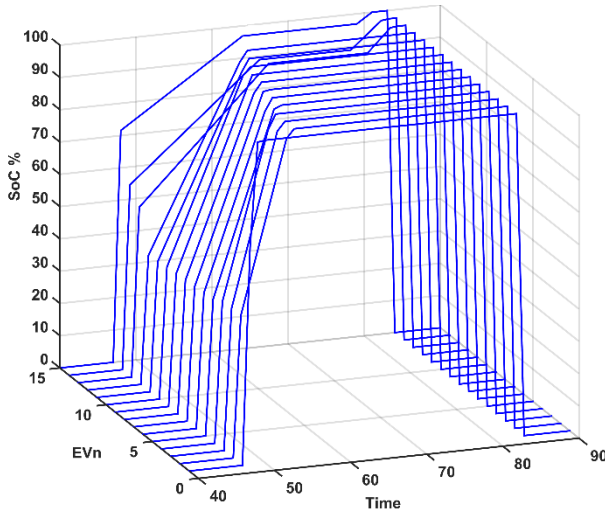

C- State of charge for vehicles number 31-45

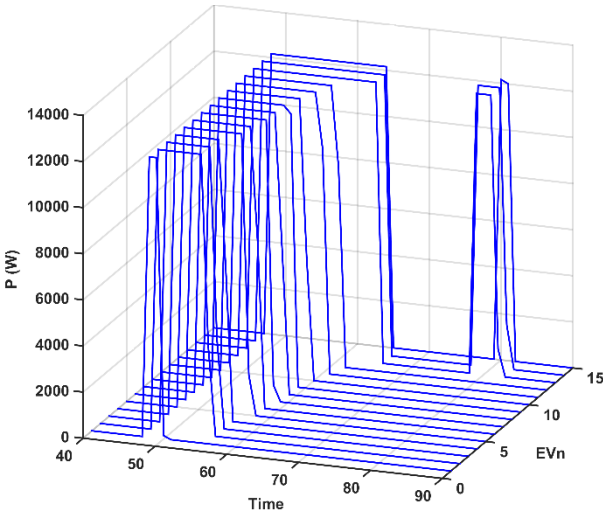

C- Power consumed for vehicles number 31-45

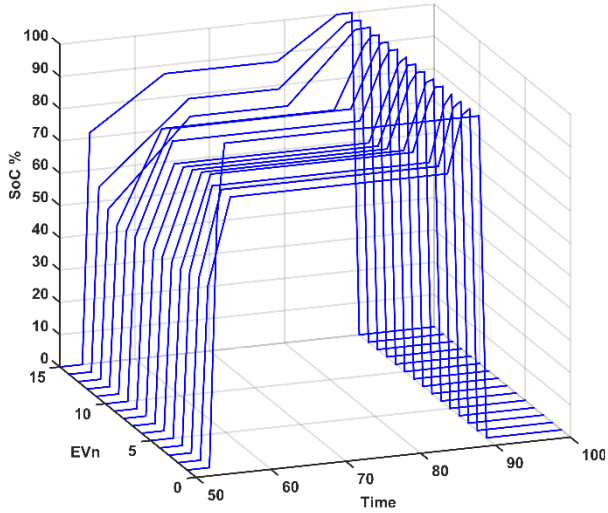

D- State of charge for vehicles number 46-60

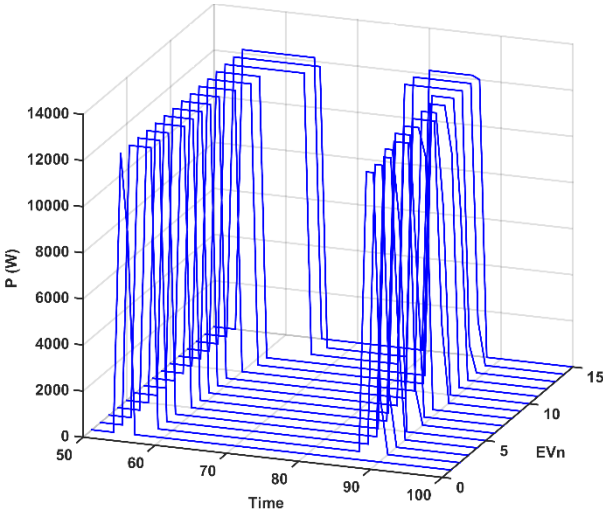

D- Power consumed for vehicles number 46-60

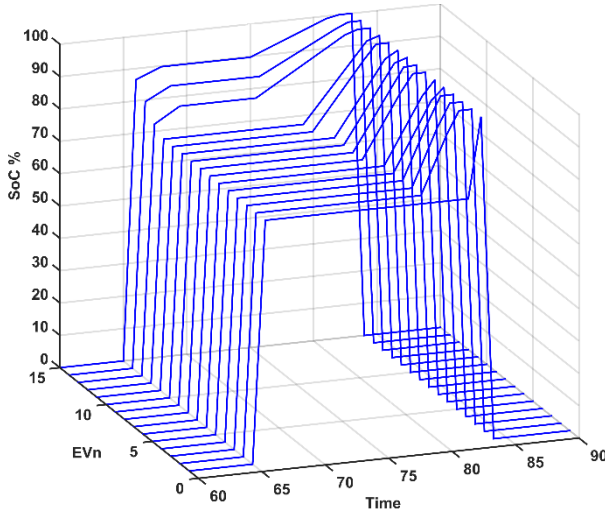

E- State of charge for vehicles number 61-75

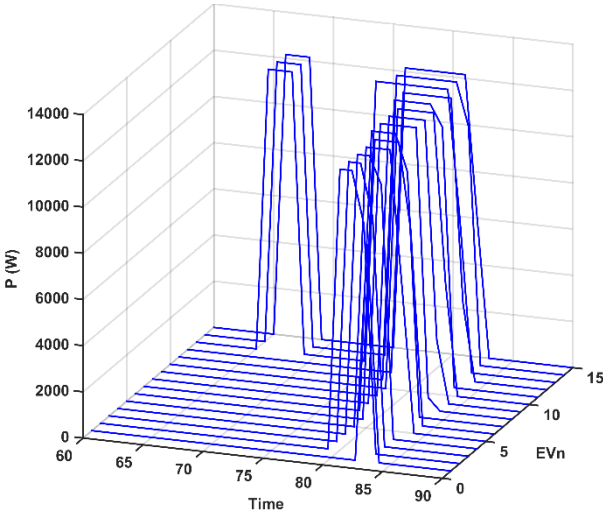

E- Power consumed for vehicles number 61-75

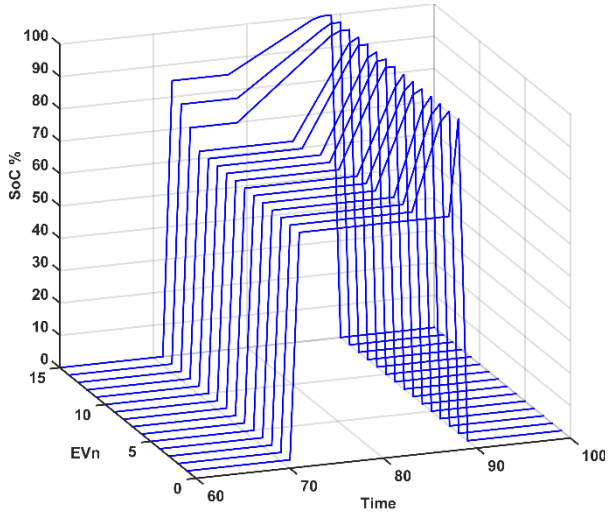

F- State of charge for vehicles number 76-90

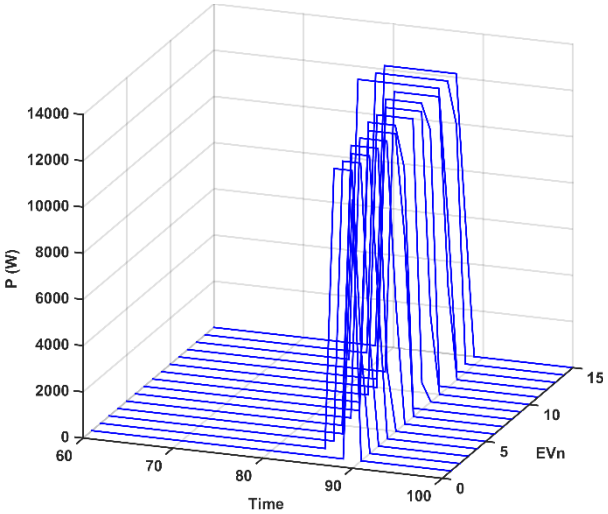

F- Power consumed for vehicles number 76-90

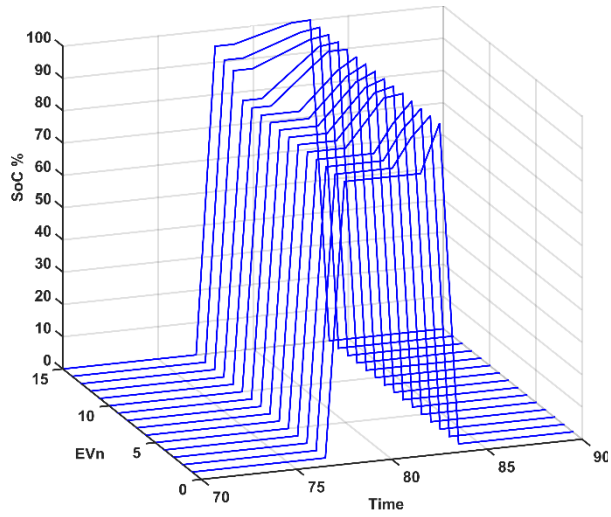

G- State of charge for vehicles number 91-105

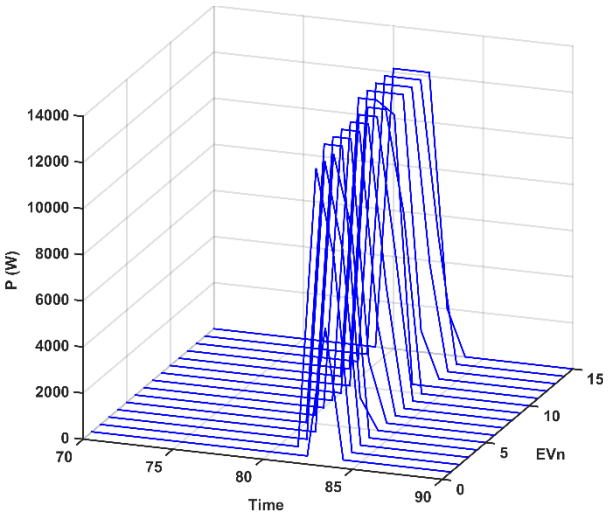

G- Power consumed for vehicles number 91-105

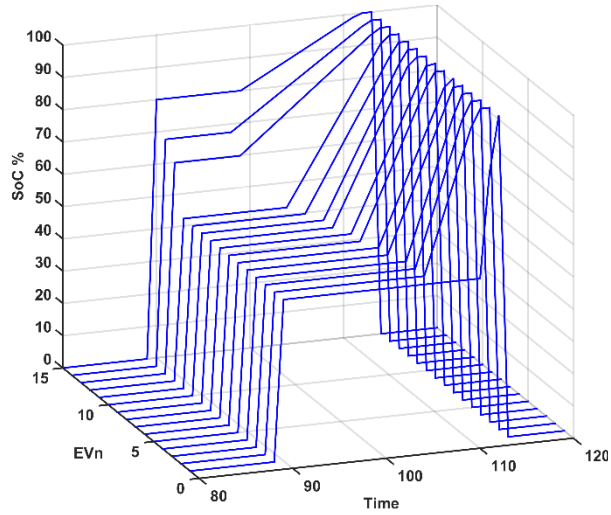

H- State of charge for vehicles number 106-120

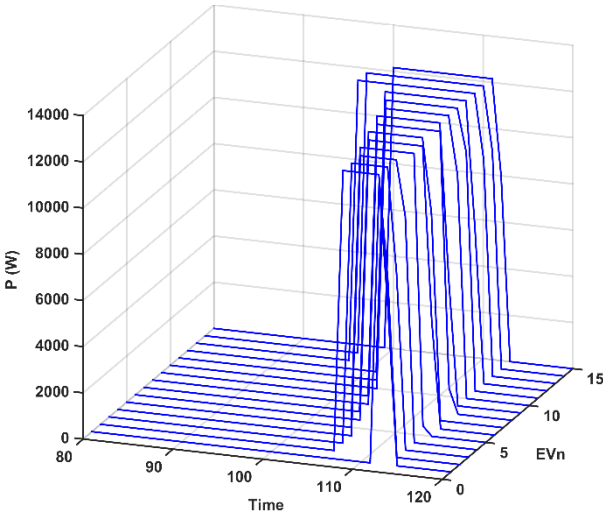

H- Power consumed for vehicles number 106-120

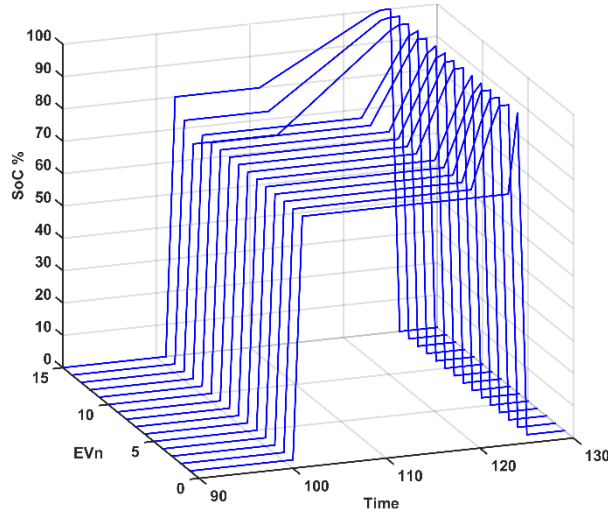

I- State of charge for vehicles number 121-135

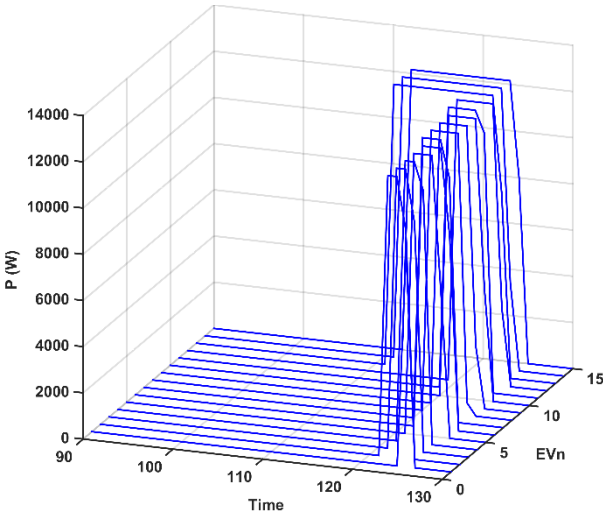

I- Power consumed for vehicles number 121-135

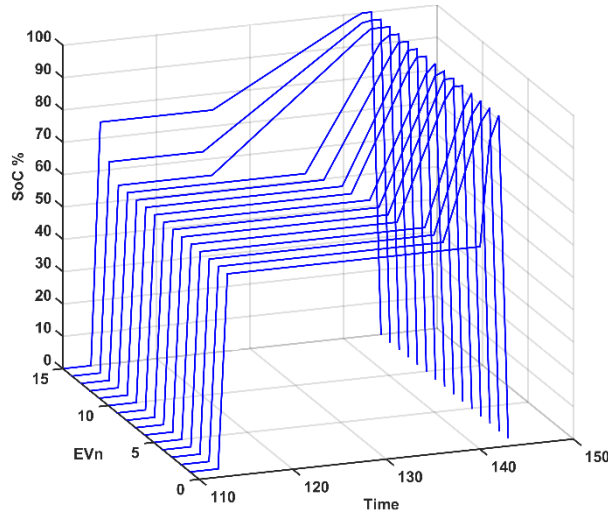

J- State of charge for vehicles number 136-150

Figure 5-17: SoC from charging EVs with power demand 100%

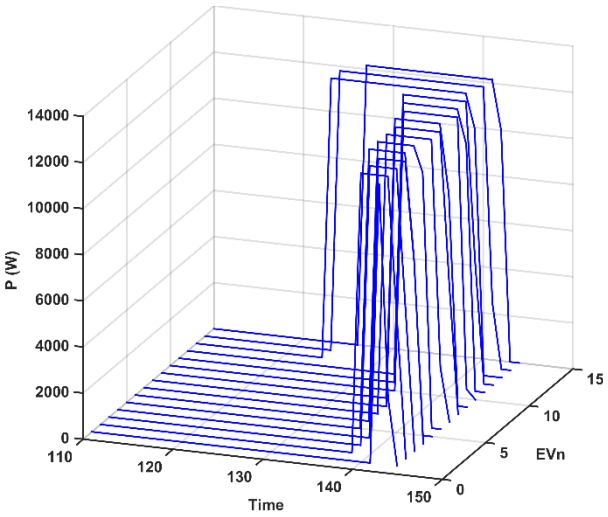

J- Power consumed for vehicles number 136-150

Figure 5-18: Power consumed from charging EVs with power demand 100%

Figure 5-19 shows the comparison between the numbers of EVs connected to the charging station at time t to the number of EVs that do not reach the desired state of charge at the same time. The number of EVs not fully charged are still until a short time before leaving, as shown by the dark blue bars, whereas the charging EVs are distributed among all the periods of EVs' connection, as shown by the light blue bars. Furthermore, the vehicles that fully reached the desired state of charge are shown in Figure 5-20, where the light blue bars refer to the connected vehicle to the CSS and the dark blue bars refer to the vehicles still charging towards the desired level of state of charge. The dark blue bars show that the EVs still charged during all the periods of connection based on the group classification. The cost of charging power for each EV is provided in Figure 5-21 which recorded less cost than the first scenario.

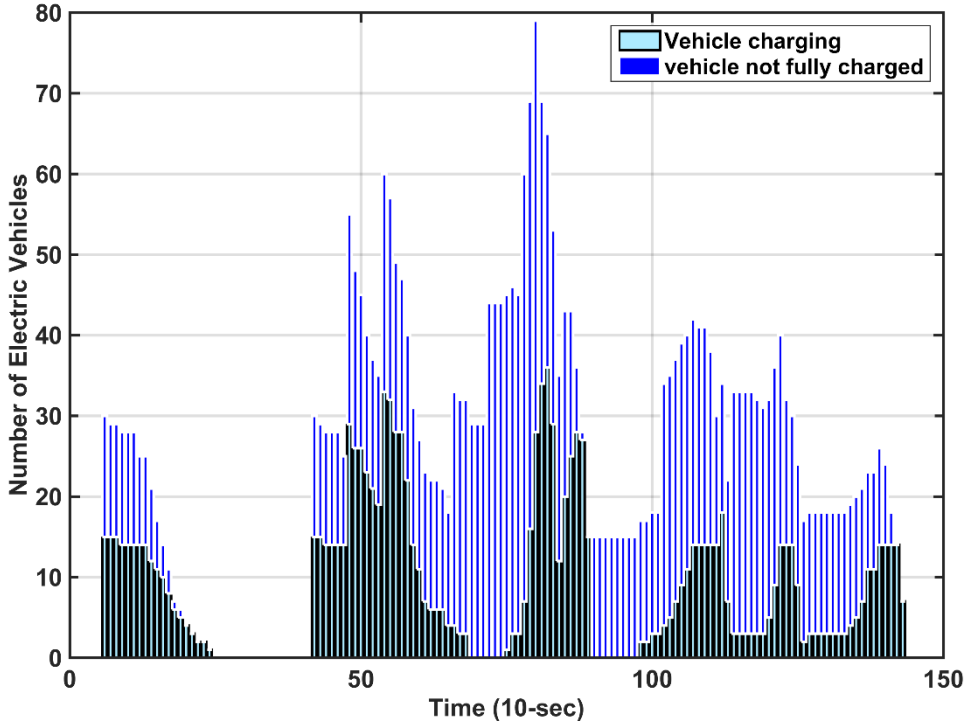

Figure 5-19: Number of vehicles connected vs. number of vehicles that do not achieve the desired SoC at a specific time

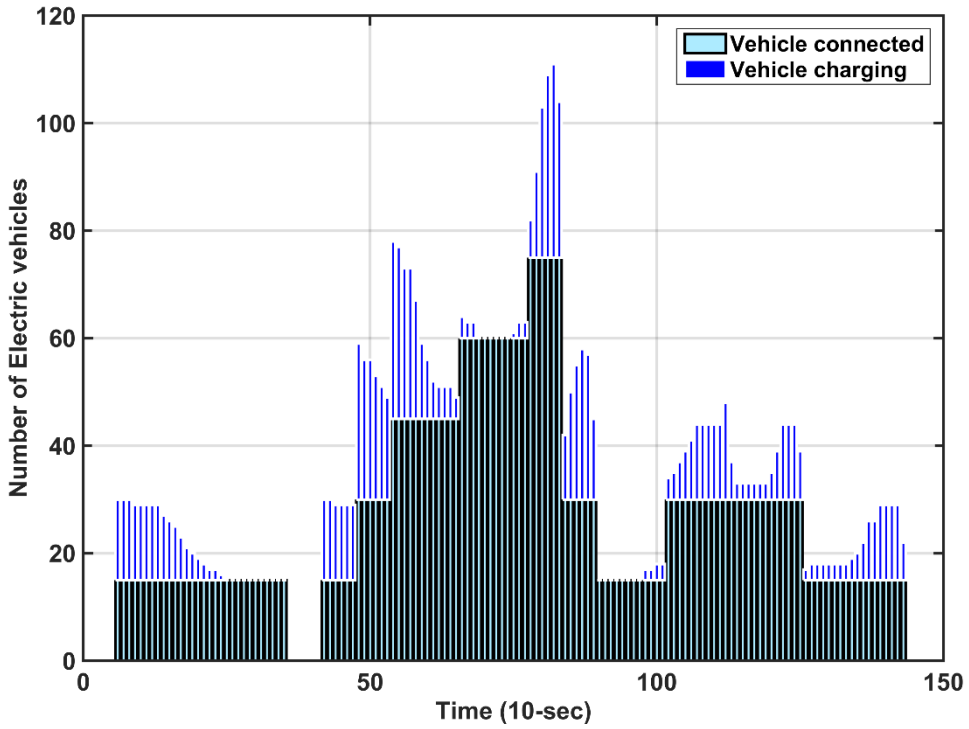

Figure 5-20: Number of vehicles connected vs. number of vehicles not charging at a specific time

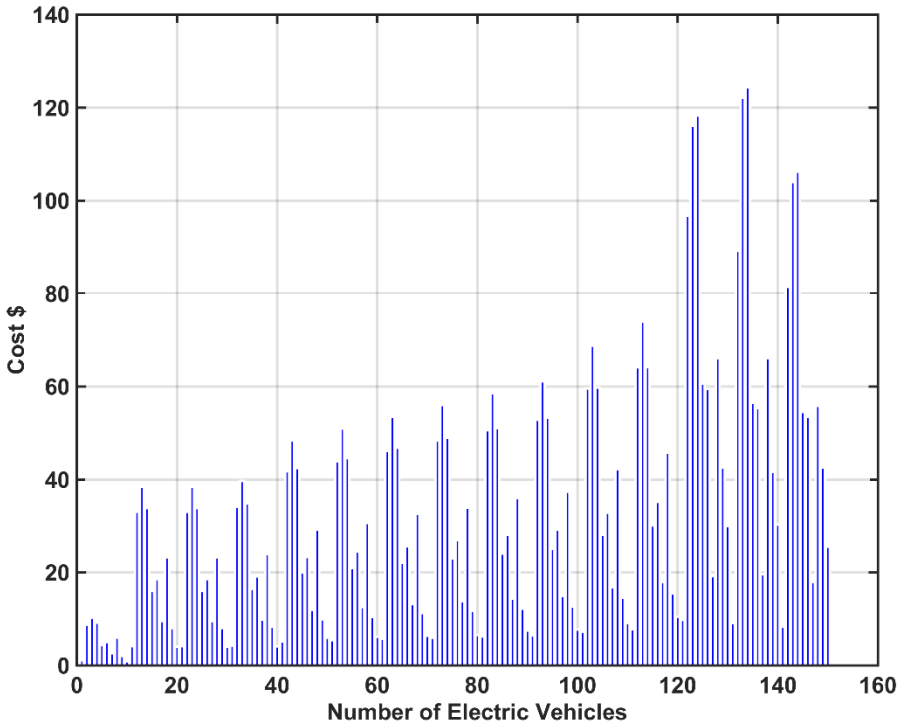

Figure 5-21: The cost of power charging for each vehicle

5.8.3 Scenario three

The difference between scenarios 3 and 2 is in applying the schedule charging and priority charging methodology to charge the EVs due to leaks in power provided by the MGO, whereas the MGO feeds 75% of the CSS total demand. Hence with scenario 3 it is possible to explore further based on Figures 5-24 to 5-31 during the following concepts. Sometimes the MGO cannot cover all the demands of the CSO. In this case, it is supposed that the MGO could cover about 75% of the load of the CSS. The CSO should charge all EVs, reaching the desired state of charge based on two functions, which are achieving the objective function at equation 5-1 and applying the schedule charging at equation 5-3. The priority procedure analyses the level of the state of charge of each EV at the departure time based on the limit of the converter and the demand of the MGO.

The performance of each EV in terms of the state of charge and consumed power is depicted in Figure 5-22 and Figure 5-23 respectively where the curves show the response of initial SoC of EVs at connected time and zero at disconnected time. Figure 5-22 shows that in addition to classifying the charging EVs to three groups, as in scenario two, there is fluctuation in charging, whereas some EVs have the opportunity to charge at the lowest price. However, it does not always take a charge due to the lack of electricity demand, as shown in all EVs especially in vehicles 12, 13, 14, and 15 of all groups. Figure 5-23 shows the charging power of the EVs, whereas the current flow through the converter of the EV is based on the permission slots of the charging optimisation function, schedule charging algorithm, and priority permission. Therefore, the current of EVs is not always at the rated value of the converter; it could be in the range of the minimum to maximum value of the converter range, in contrast to the previous

scenarios, whereas the current flow is always at the rated level of converters until achieving a full charge.

The results showed that not all EVs reached the desired state of charge before leaving the CSS, as shown in Figure 5-24. The priority charging strategy is applied to make either all the EVs or most of them reach the desired level of state of charge in case not all the EVs reached it, as shown in Figure 5-25. Vehicle number 143 reached 85% of the desired state of charge. Therefore, the CSO informs the owner via the EVA to change the desired state of charge to a new calculation value. The alternative way to reach the desired state of charge is by giving permission to the CSO to ignore the optimisation function and return to the case one by applying an extra charging cost. Mathematically this is applied by changing the factor ρ of equation 5-1 from the nominal value of 1 to 1.5, to inform the CSA of exceeding the optimisation function and charging the EV at the rated power of the converter by increasing the price of the UG tariff to 1.5.

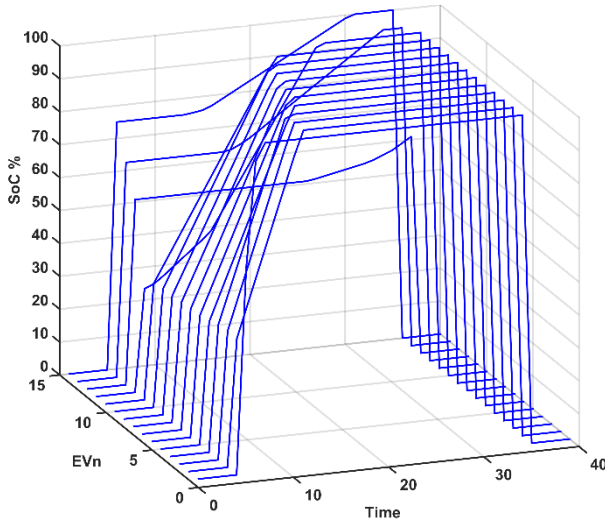

A- State of charge for vehicles number 1-15

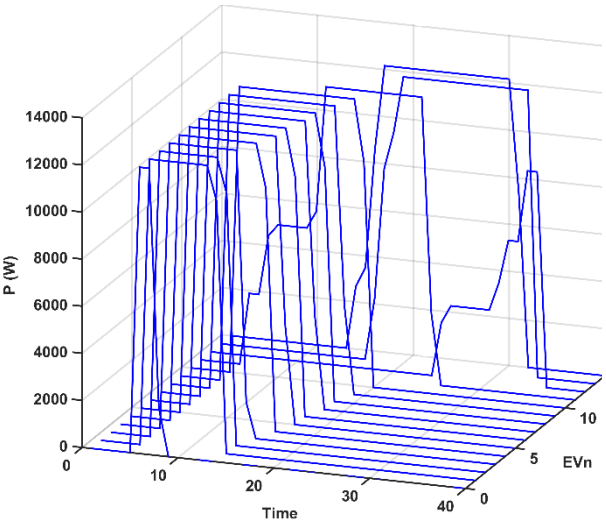

A- Power consumed for vehicles number 1-15

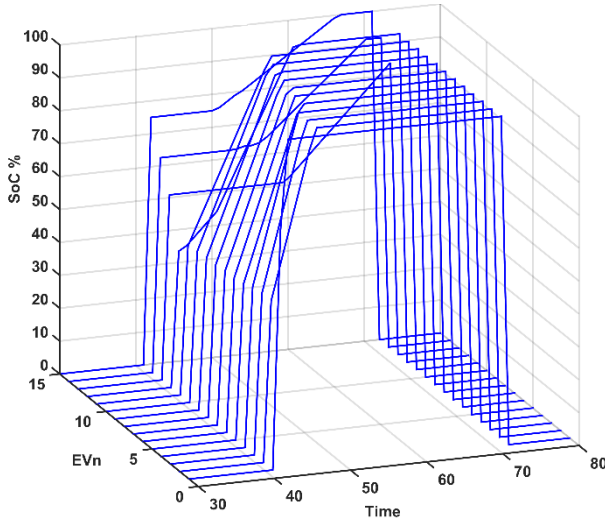

B- State of charge for vehicles number 15-30

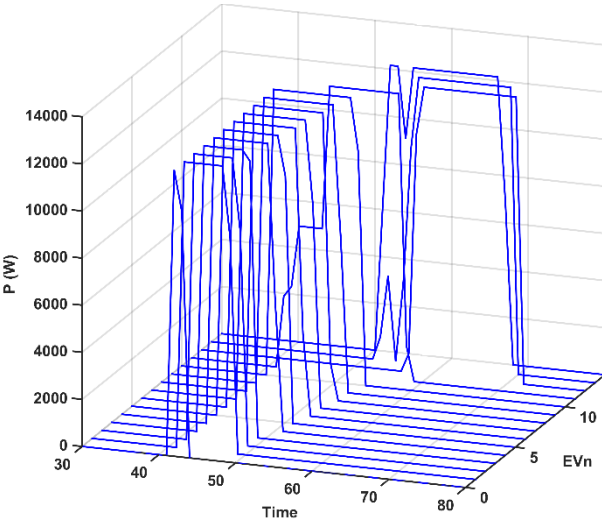

B- Power consumed for vehicles number 15-30

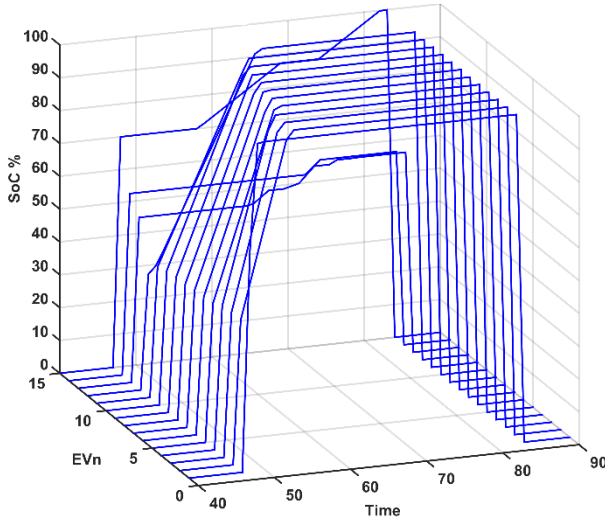

C- State of charge for vehicles number 16-45

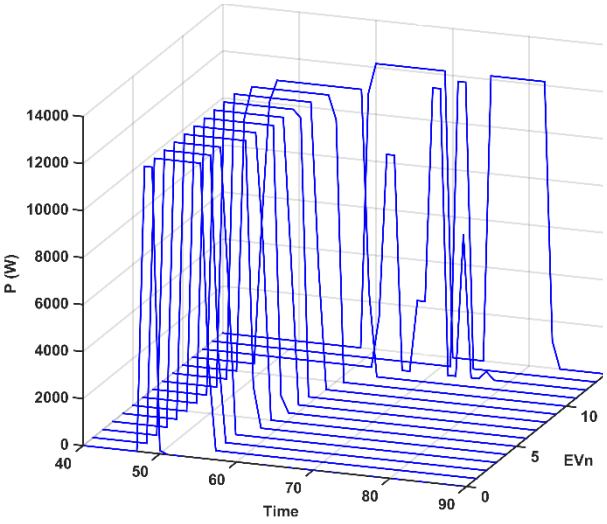

C- Power consumed for vehicles number 16-45

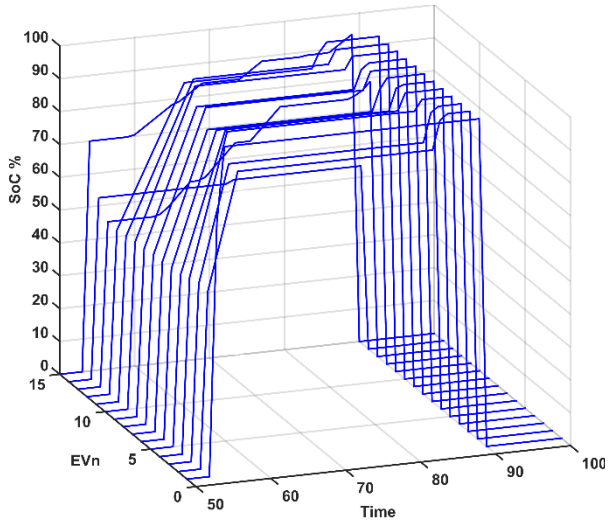

D- State of charge for vehicles number 46-60

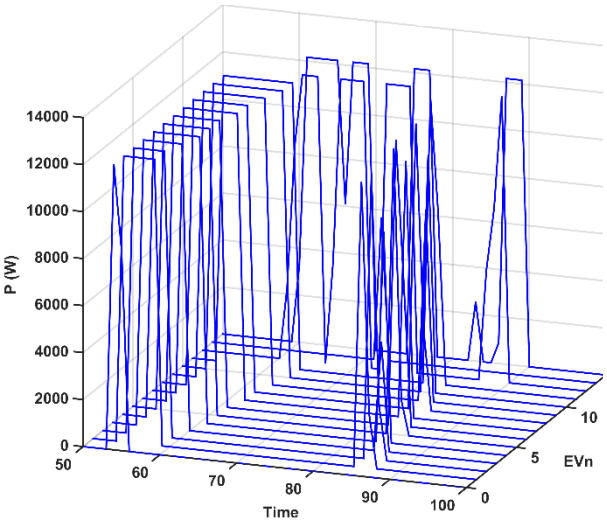

D- Power consumed for vehicles number 46-60

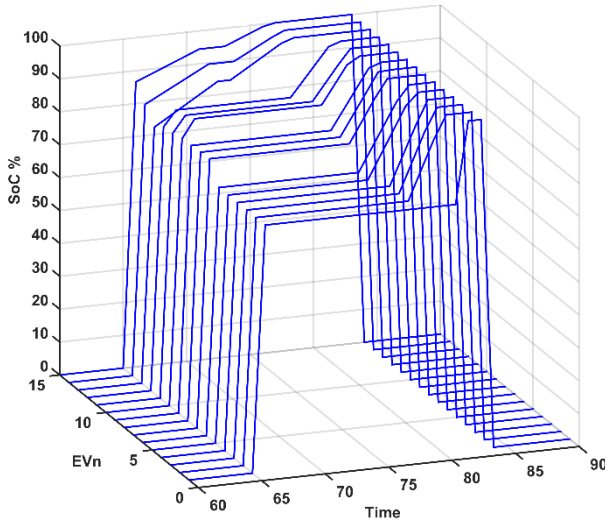

E- State of charge for vehicles number 61-75

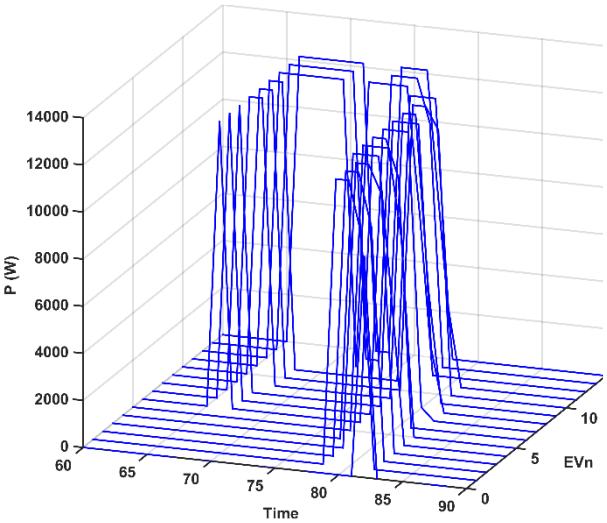

E- Power consumed for vehicles number 61-75

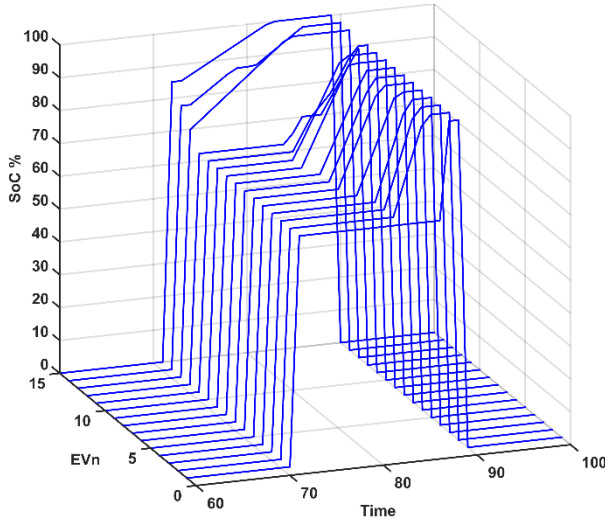

F- State of charge for vehicles number 76-90

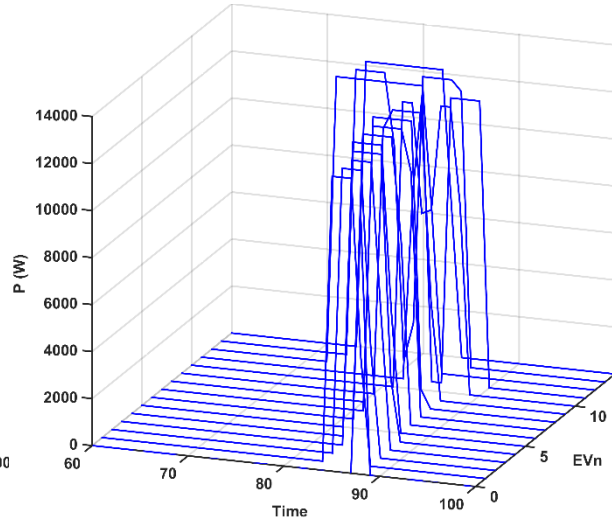

F- Power consumed for vehicles number 76-90

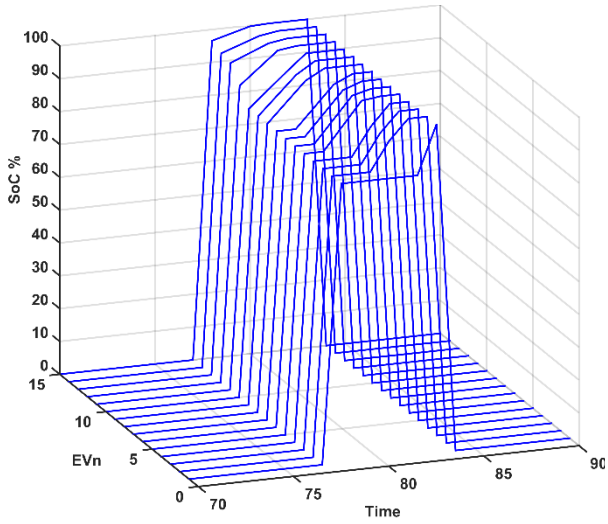

G- State of charge for vehicles number 91-105

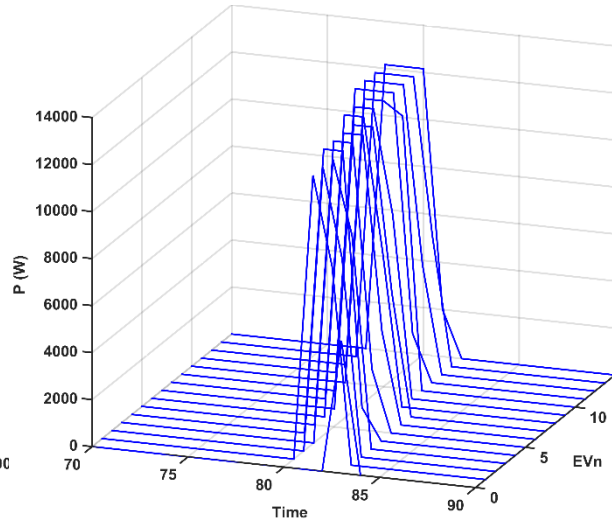

G- Power consumed for vehicles number 91-105

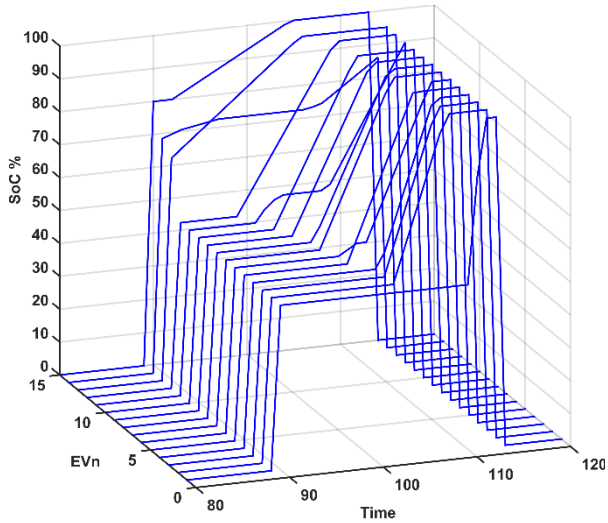

H- State of charge for vehicles number 106-120

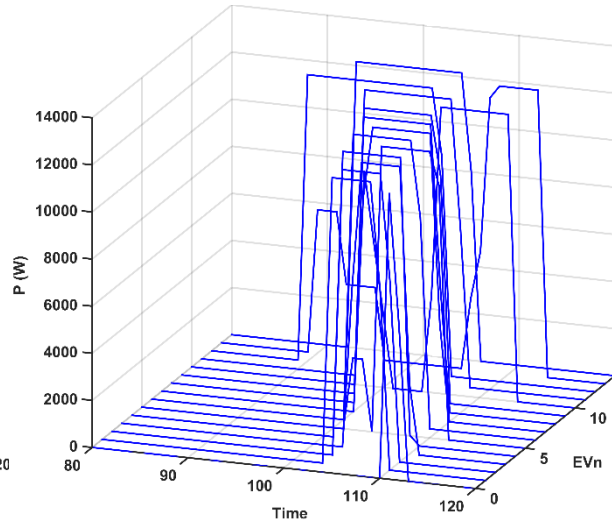

H- Power consumed for vehicles number 106-120

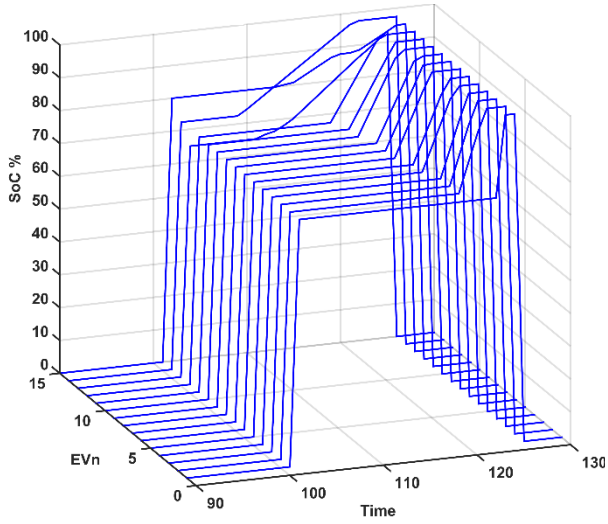

I- State of charge for vehicles number 121-135

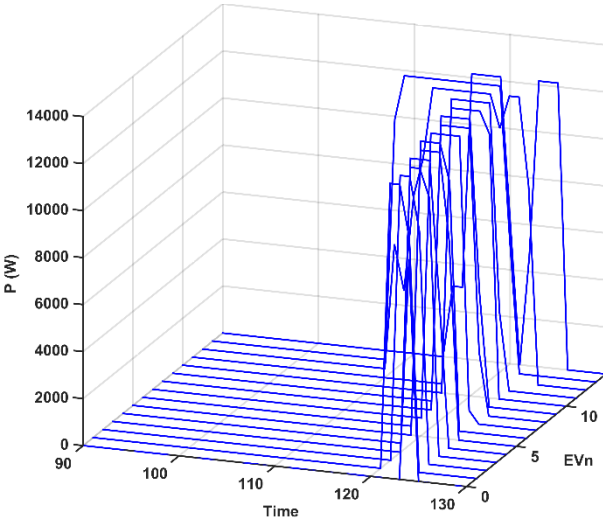

I- Power consumed for vehicles number 121-135

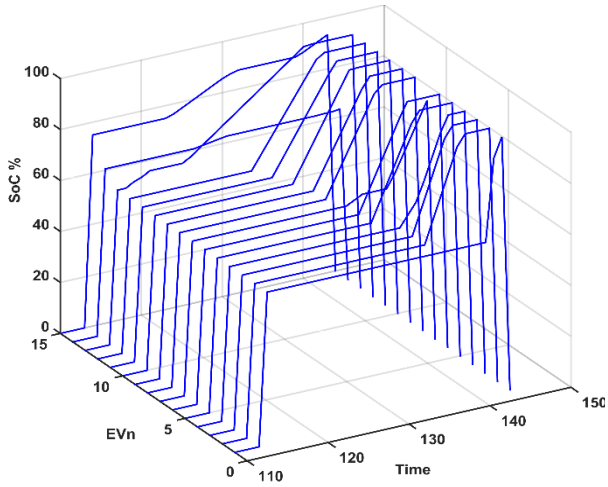

J- State of charge for vehicles number 136-150

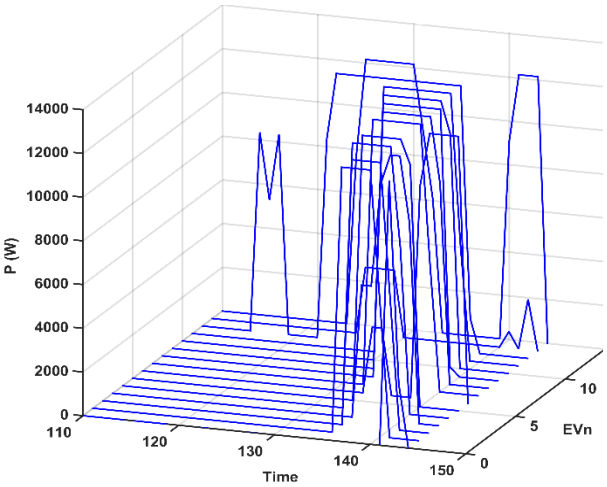

J- Power consumed for vehicles number 136-150

Figure 5-22: SoC of charging EVs with power demand at 75%

Figure 5-23: Power consumed of charging EVs with power demand at 75%

Figure 5-26 shows the comparison between the number of EVs connected to the CSS at time *t* and the number of vehicles that do not reach the desire to leave state of charge at the same time. It is clear that the mathematical operation of the CSO becomes more complicated than scenarios 1 and 2, whereas the number of EVs are not fully occupied for most of the period on the connection and at the various values of the current. Therefore, the CSS still charges vehicles until the leaving time. However, the input information by the owners should be accurate enough to make an accurate calculation by the CSO for achieving a full charge before leaving. Furthermore, the vehicles fully reaching the desired state of charge are shown in Figure 5-27 where the light blue bars refer to the vehicle connected to the charging station and the dark blue bars refer to the vehicles still charging towards the desire to leave state of charge. The dark blue bars show that the EVs still charged during all the period on the connection. The cost of power charging for each vehicle and applying a priority strategy of charging is shown in Figure 5-28 and Figure 5-29 respectively. The cost of the priority

charging strategy could be a little bit higher than the cost of normal schedule charging strategy. However, the total charging cost of EVs at the third scenario is higher than at the second scenario and lower than the first scenario.

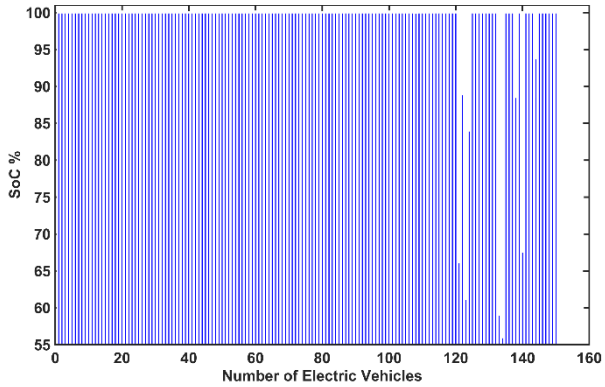

Figure 5-24: The state of charge of each vehicle at departure time at the optimisation function

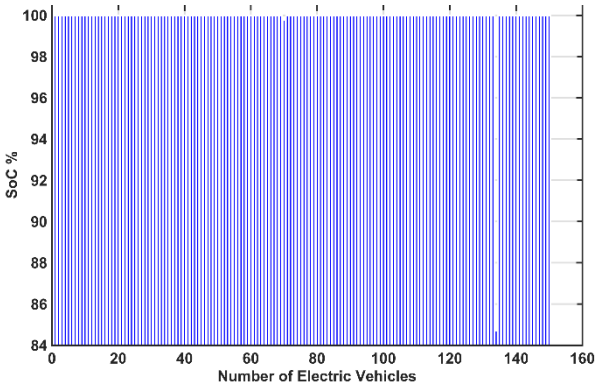

Figure 5-25: The state of charge of each vehicle at departure time after applying the priority strategy

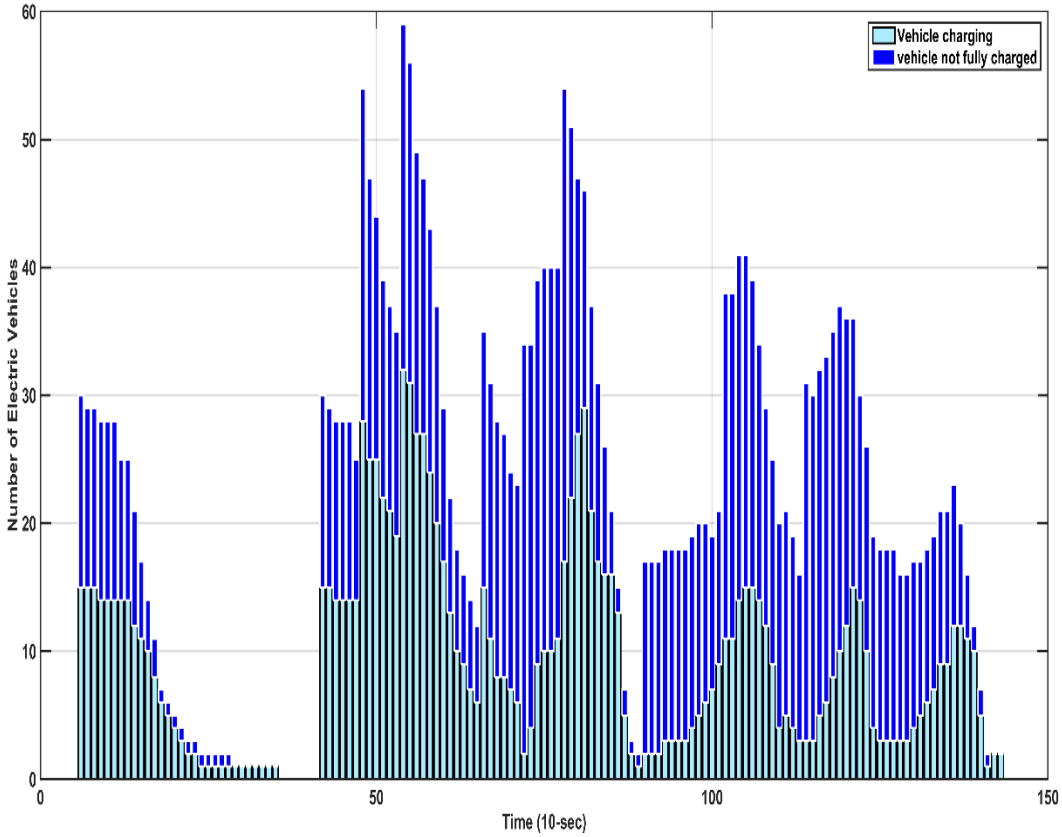

Figure 5-26: Number of EVs connected vs. number of EVs that do not achieve the desired SoC

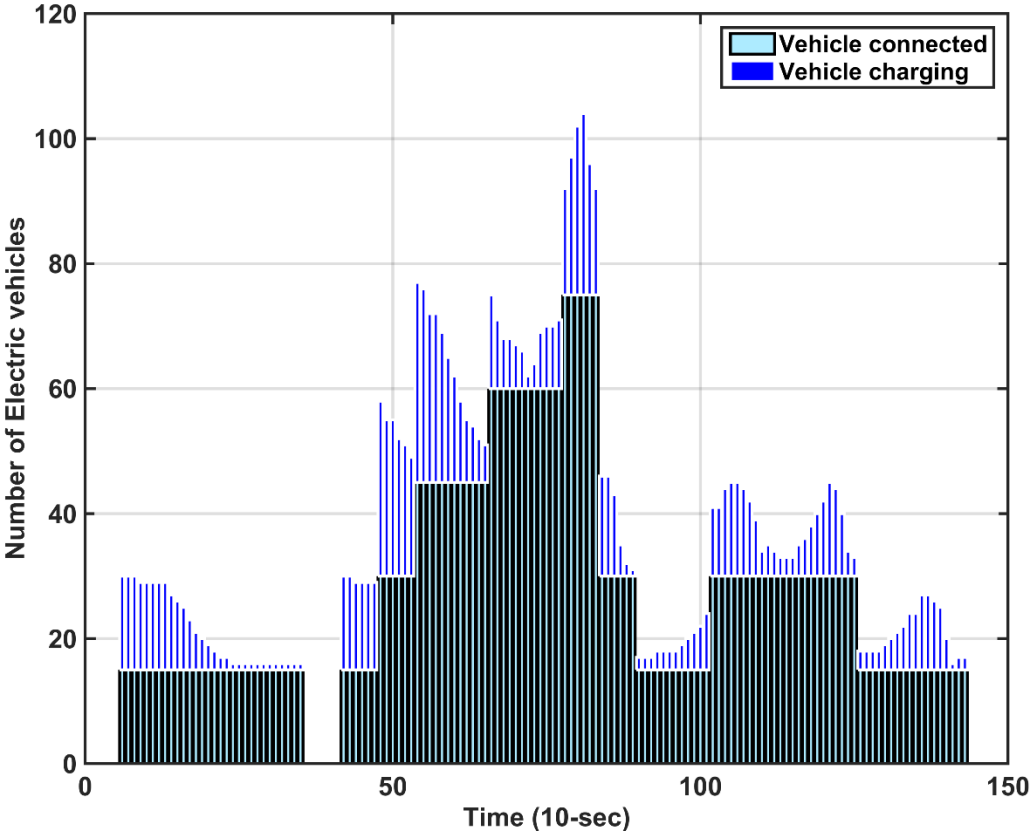

Figure 5-27: Number of vehicles connected vs. number of vehicles do charge at time

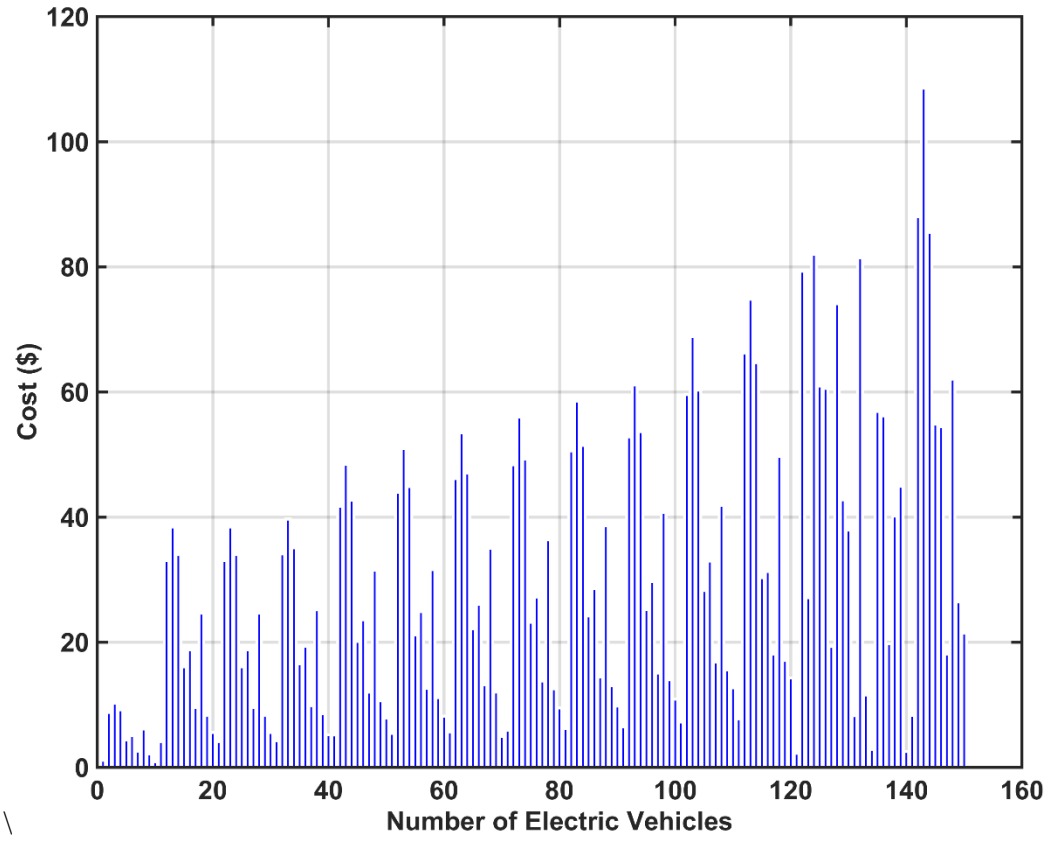

Figure 5-28: The total charging cost of each vehicle at the optimisation function

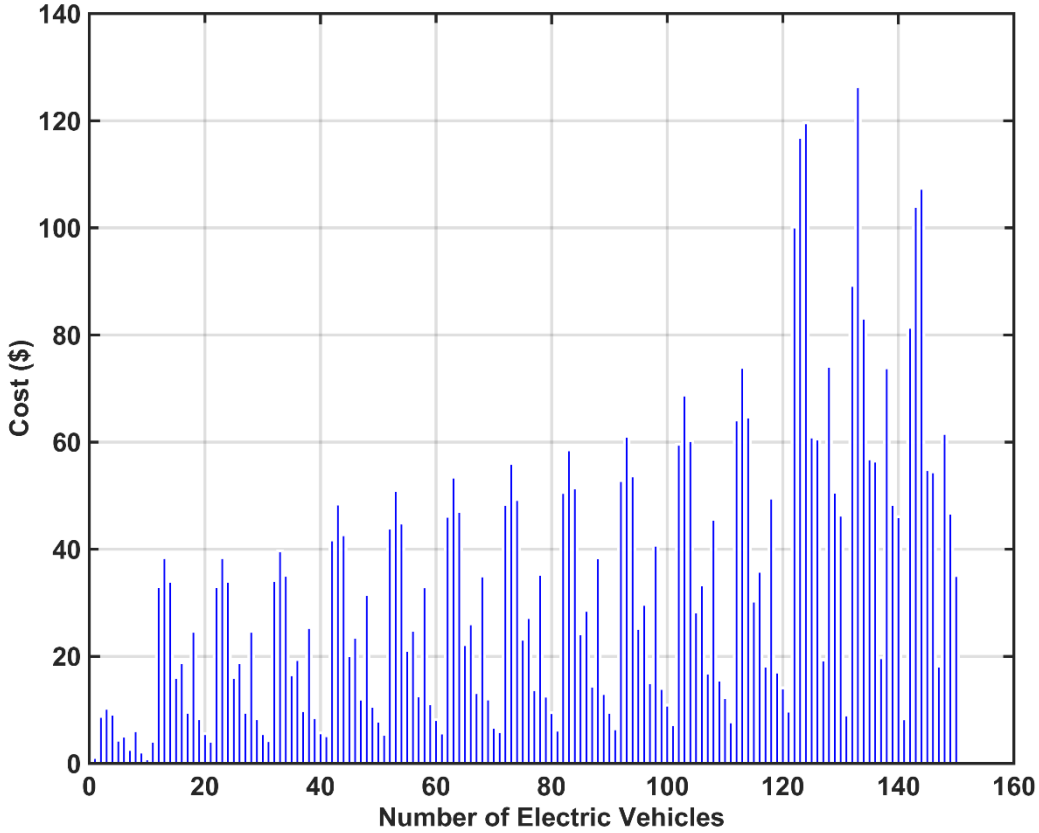

Figure 5-29: The total charging cost of each vehicle after applying the priority strategy

5.8.4 Scenario four

The states of scenario 4 are similar those of scenario 2 except for the discharging option of EVs with owner agreement to discharge those vehicles which are implemented by binary input D. Hence with scenario 4, it is possiable to explore further based on Figures 5-32 to 5-37 during the following concepts.

The EVs can be represented as a resource for the microgrid in a congested electricity market, such as generator outage or a sudden increase in demand. Moreover, the reference for discharging the EVs is VBN, VOBN, FBN or FOBN. The CSO receives the discharging references from the MGO to start discharging all qualified EVs, either with scheduled discharging by applying equations 5-2 and 5-4 when the reference is VBN or FBN, or at the maximum converter rating power of the EV by applying equation 5-2 only when the reference is VOBN or FOBN. The CSA applies the selling tariff to the discharging EV.

The performance of each EV regarding the state of charge and power consumed is depicted in Figure 5-30 and Figure 5-31 respectively where the curves show the response of initial SoC of EVs at connected time and zero at disconnected time. Figure 5-30 shows normal charging as in scenario 2. However, at midday, a variation in voltage happens that requires discharging qualified EVs. Therefore, the EVs in group two, which is shown in C, D, E, F, and G, respond to the MGO to discharge the resources to feed power to the microgrid, which is seen as reducing the state of charge of the battery for those vehicles. Figure 5-31 shows a similarly positive power flow to charge the battery of EVs as shown in scenario 2 except for the discharging

period, whereas the negative power starts feeding current to the microgrid of the discharging EVs group.

Figure 5-32 shows that some EVs are slightly different from the leaving state of charge at leaving time because they are discharging some power from their resources.

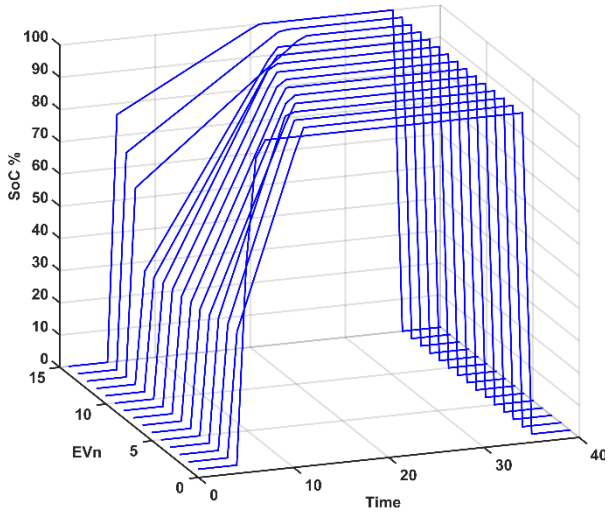

A- State of charge for vehicles number 1-15

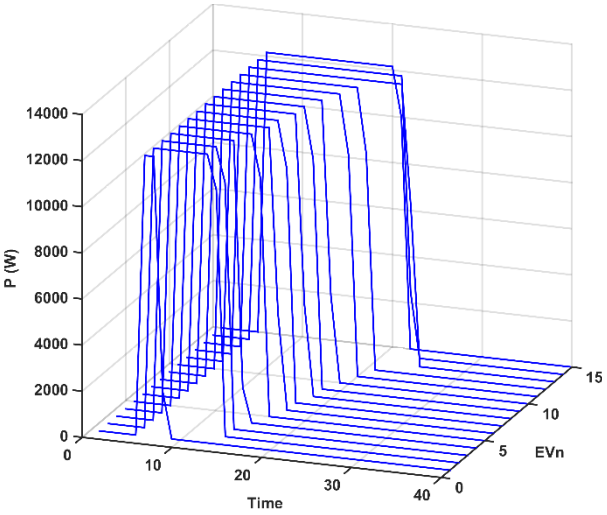

A- Power consumed for vehicles number 1-15

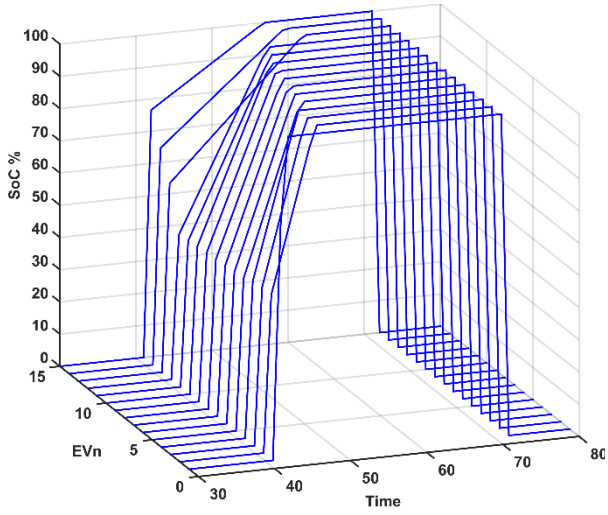

B- State of charge for vehicles number 15-30

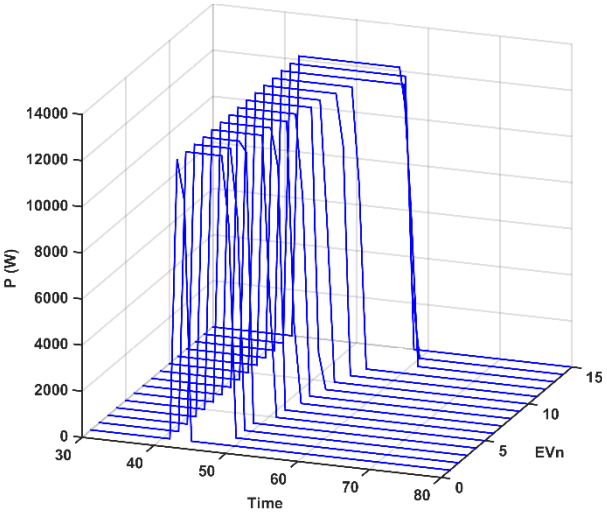

B- Power consumed for vehicles number 15-30

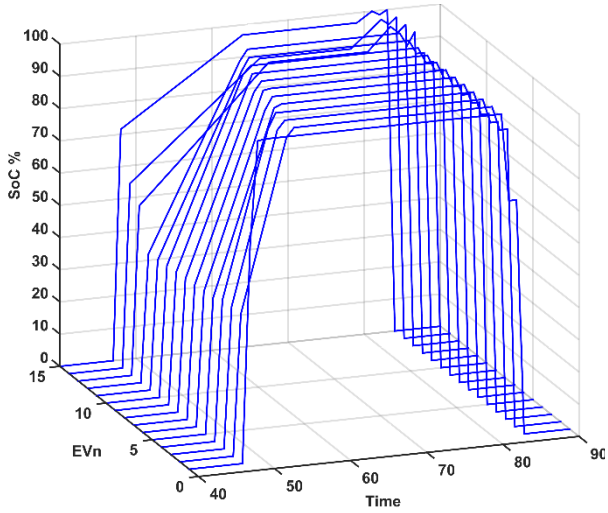

C- State of charge for vehicles number 16-45

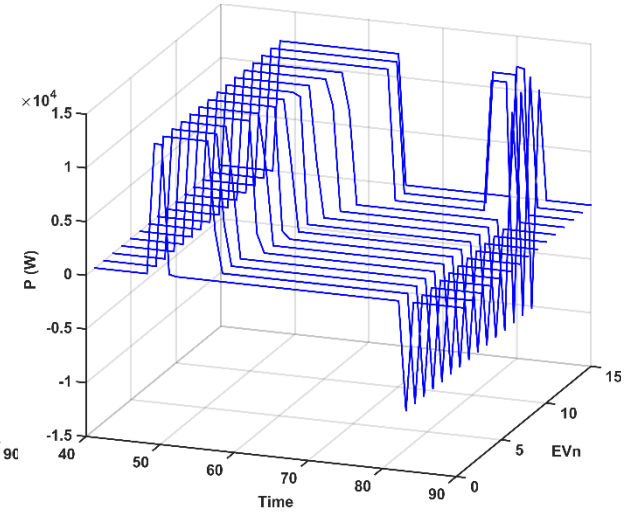

C- Power consumed for vehicles number 16-45

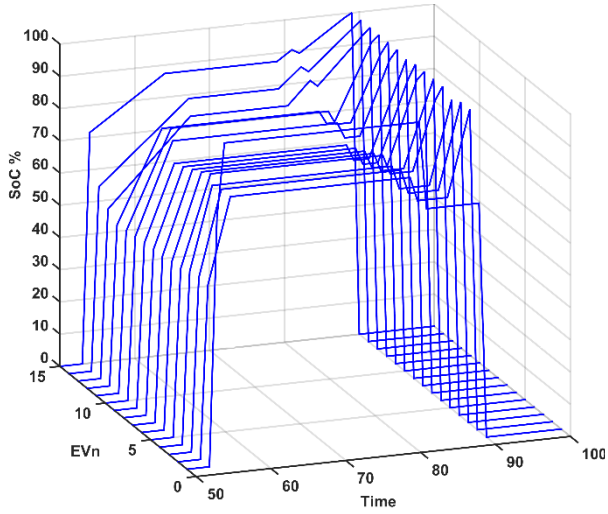

D- State of charge for vehicles number 46-60

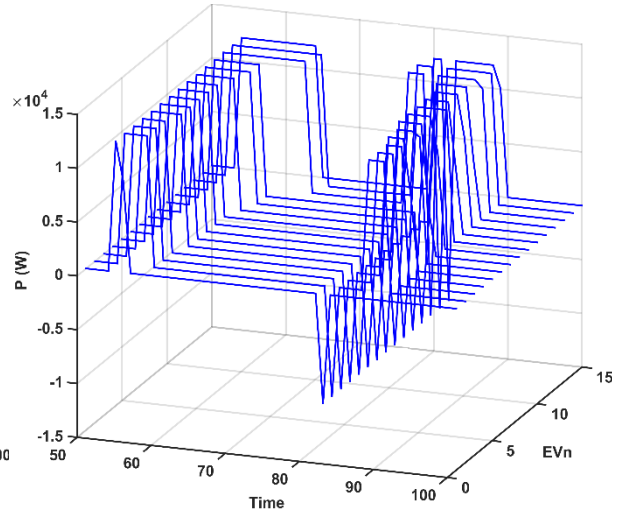

D- Power consumed for vehicles number 46-60

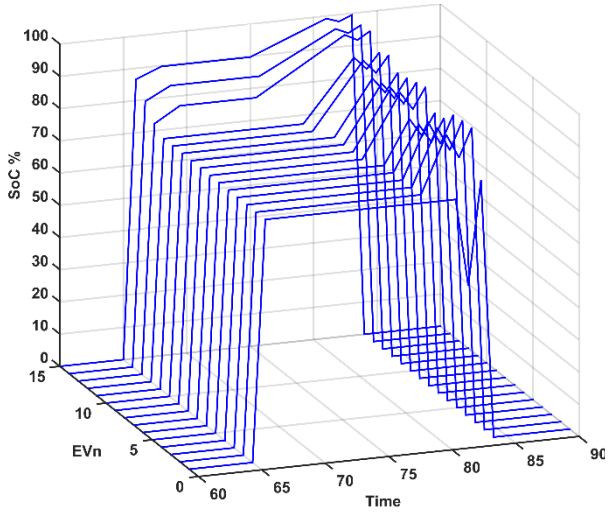

E- State of charge for vehicles number 61-75

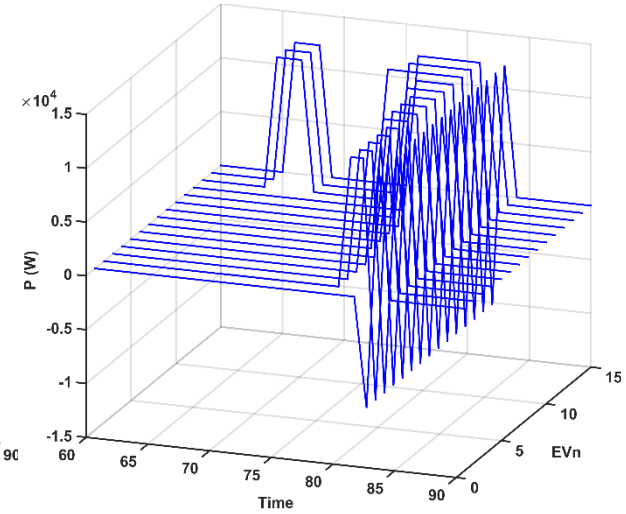

E- Power consumed for vehicles number 61-75

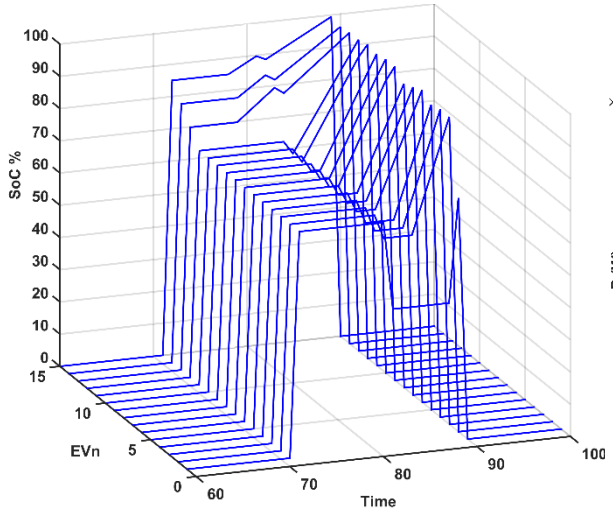

F- State of charge for vehicles number 76-90

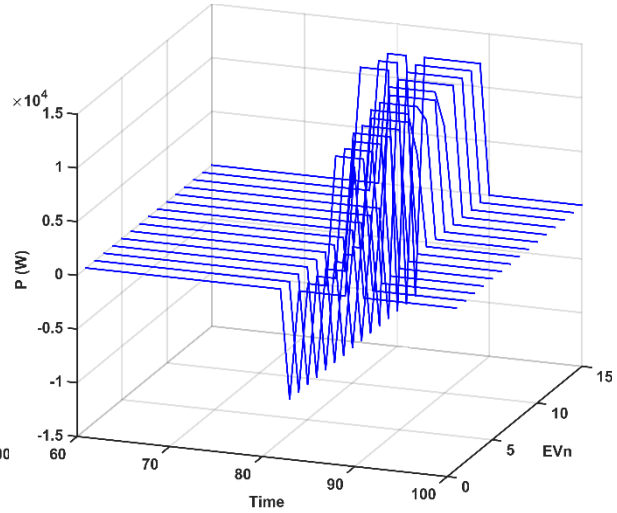

F- Power consumed for vehicles number 76-90

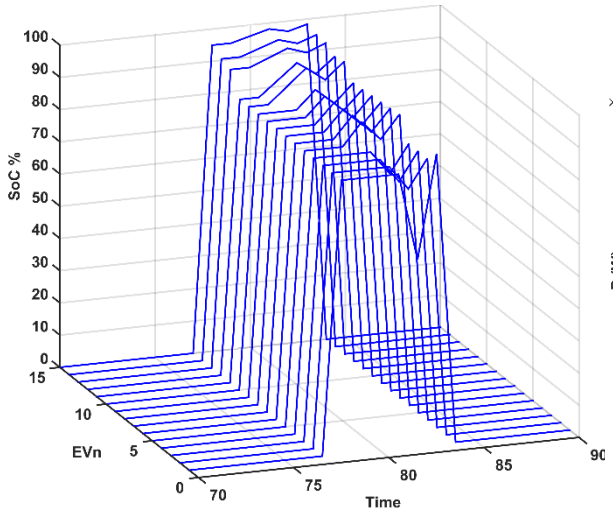

G- State of charge for vehicles number 91-105

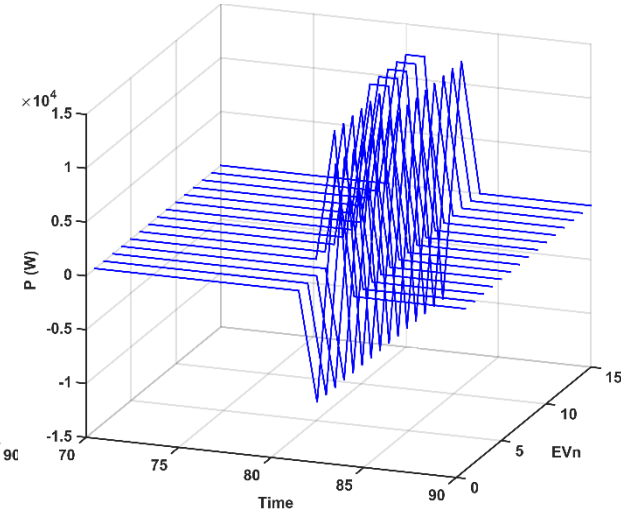

G- Power consumed for vehicles number 91-105

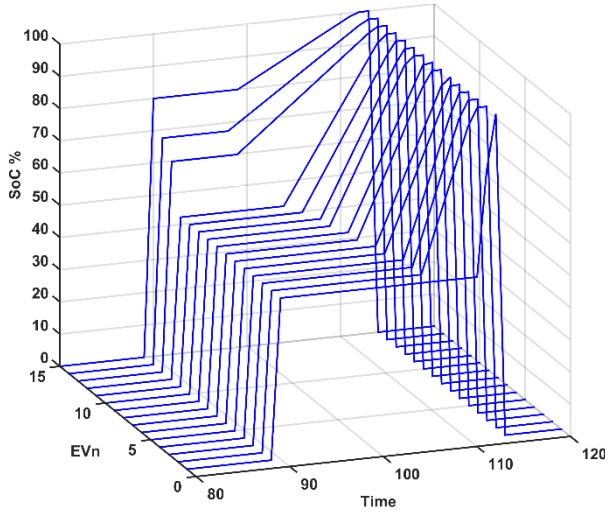

H- State of charge for vehicles number 106-120

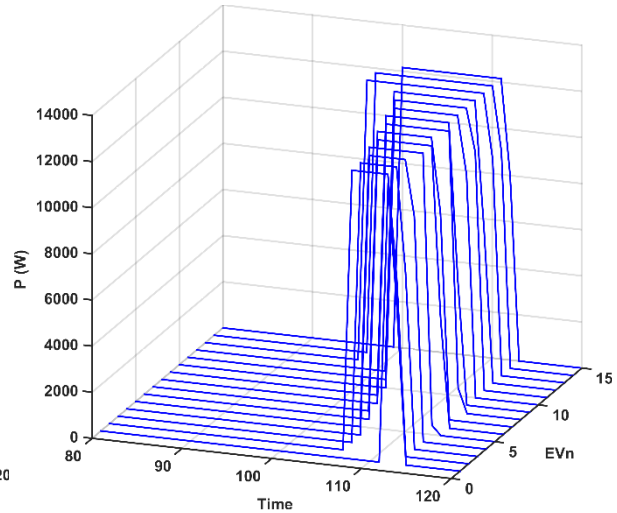

H- Power consumed for vehicles number 106-120

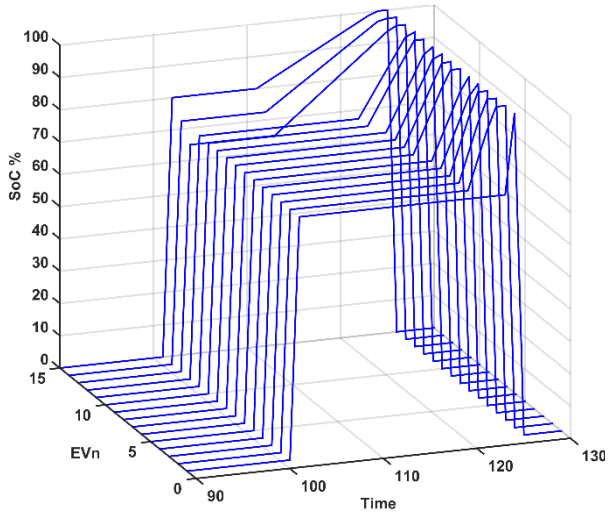

I- State of charge for vehicles number 121-135

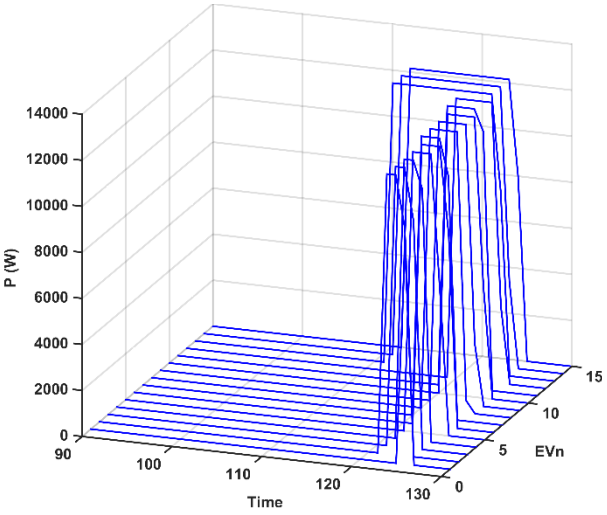

I- Power consumed for vehicles number 121-135

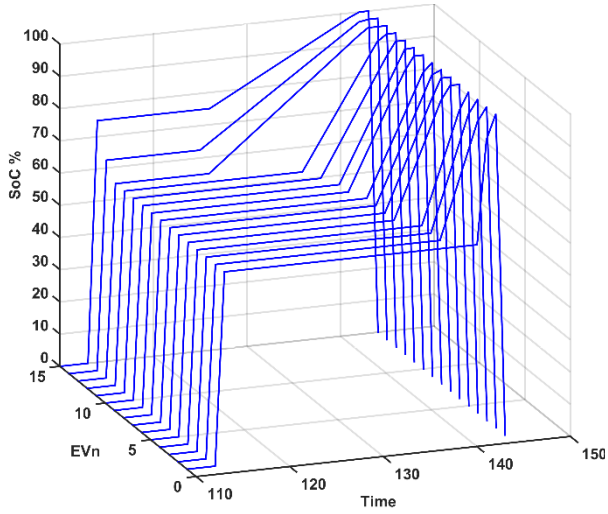

J- State of charge for vehicles number 136-150

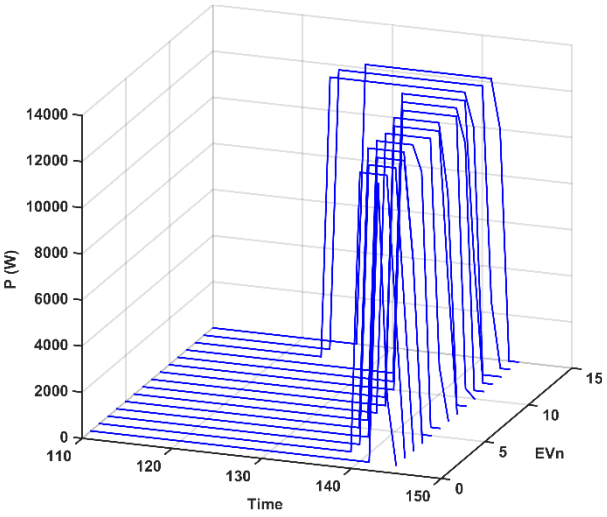

J- Power consumed for vehicles number 136-150

Figure 5-30: SoC of charging EVs with power demand

Figure 5-31: Power consumed of charging EVs with power demand

Figure 5-33 shows the comparison between the numbers of EVs connected to the CSS at time t to the number of vehicles that do not reach the desired state of charge at the same time. The operating of the CSS becomes more effective than in previous scenarios due to applying the discharging option, whereas the EVs that discharged their power reduced the state of charge of the battery that makes charging them more frequent than in previous scenarios. Furthermore, the vehicles that fully reach the desired state of charge are shown in Figure 5-34, where the light blue bars refer to the connected vehicle to the CSS and the dark blue bars refer to the EVs still charging towards the desire to leave the state of charge. The number of vehicles charging is increased compared with scenario 2 due to the discharging option. The net cost of power charging and discharging for each EV is shown in Figure 5-35 which records a lower charging cost than in the previous scenarios.

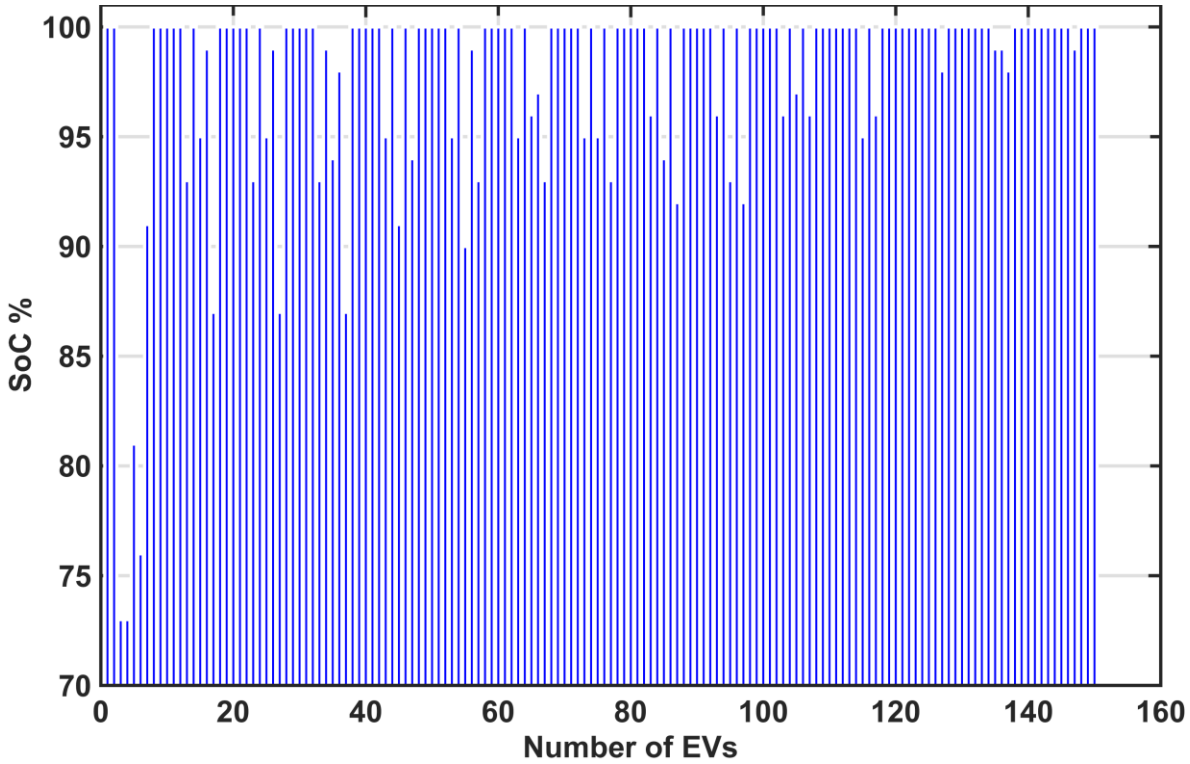

Figure 5-32: The state of charge of each vehicle at departure time

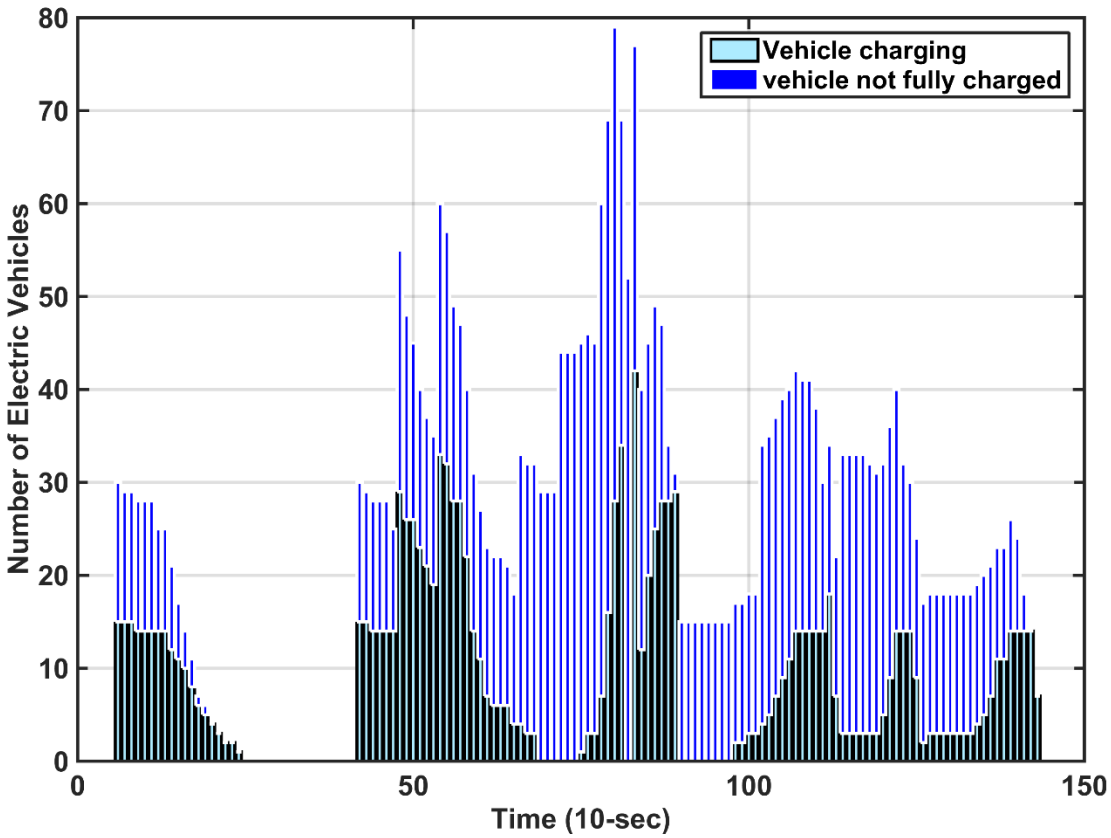

Figure 5-33: Number of vehicles connected vs. number of vehicles that do not achieve the desired SoC at a specific time

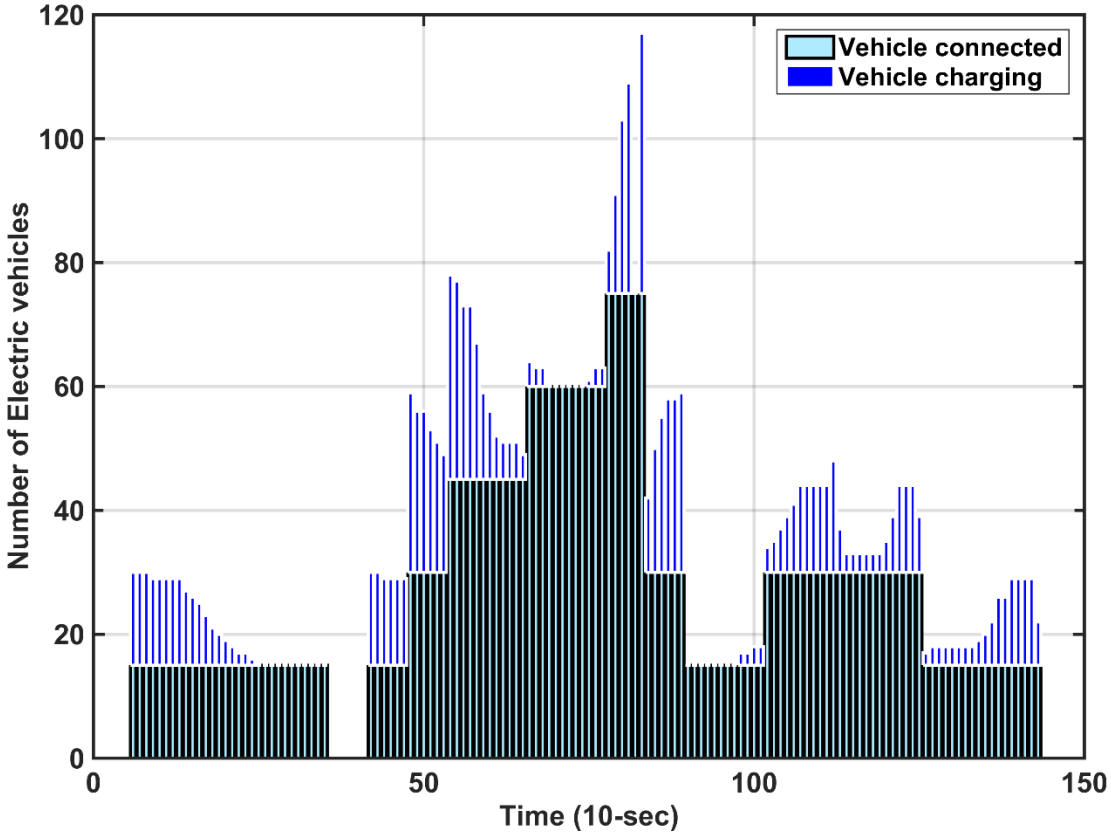

Figure 5-34: Number of vehicles connected vs. number of vehicles do charge at specific time

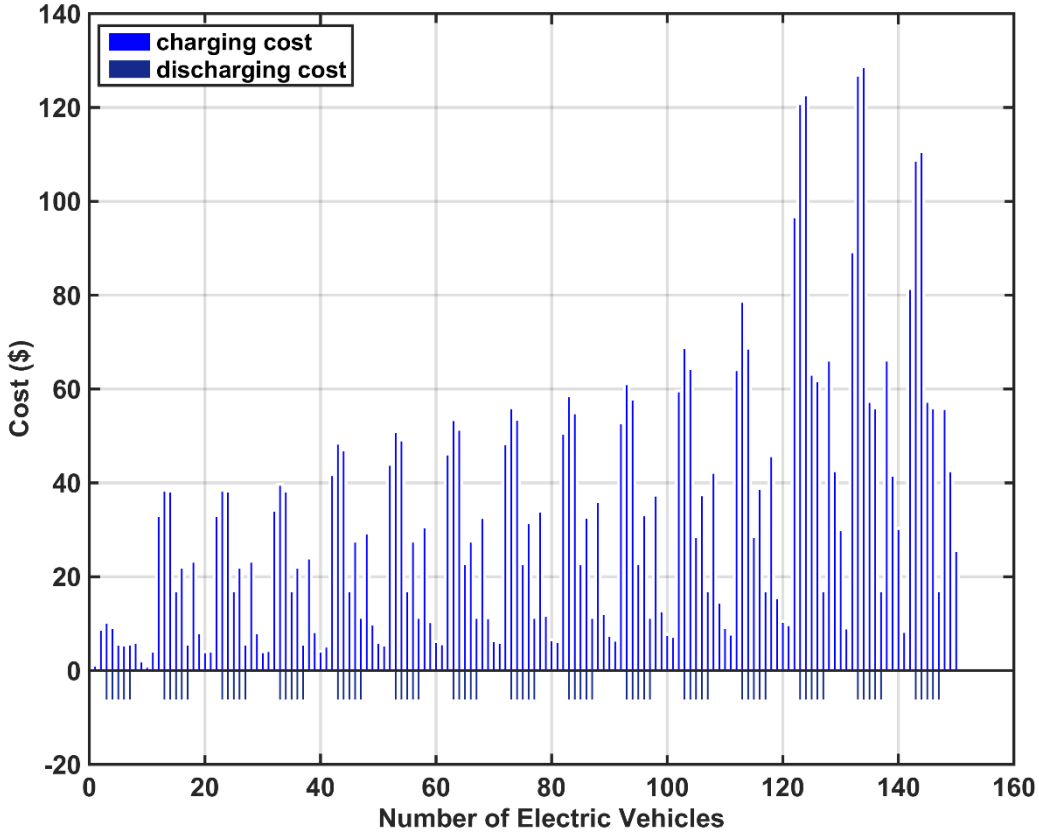

Figure 5-35: The cost of power charging of each vehicle

5.8.5 Cost comparison of the previous four senarios

The CSO should charge all EVs connected to the CSS to the desired level of state of charge with minimum cost. There are four successful strategies proposed in this dissertation. A comparison of the cost of power charging for each case is shown in Figure 5-36. A first connect first charge strategy recorded the highest price of charging the battery of the EV (red bars in the figure). Applying schedule charging on the CSO are divided into two modes. In the first mode, the CSO has a penalty of power to cover all connected demand, whereas the CSO could cover part of the connected demand in the second mode. The first scenario records a better power charging cost than the second one even when applying the priority charging strategy. The blue bars refer to the charging cost of the first scenario, whereas the pink bars refer to the charging cost of the second scenario. The best charging cost for the owner stated is when the vehicle starts discharging power to the microgrid (green bars in the figure). The discharging cost is assumed to be higher than the charging cost by 10% from the daily tariff at the time of discharge. In discharging mode, some EVs could not reach the desired leaving state of charge. However, they could increase revenue cost rather than paying to the CSO.

The charging tariff of the EVs was increased after 6:00 sinusoidal until reaching the top at 12:00 when it was starting to reduce a shown in Figure 4-11. For those vehicles connected around 12:00, the algorithm booked slots away from the midday at the beginning of the connection period or at the end of the connection period until reaching the desire to leave state of charge. This strategy made the microgrid cover the heavy demand at midday with high tariff and used the CSO as a resources node. The period of the connection of the EVs was divided into three groups before midday, around midday, and after midday. EVs 1-30 belong to the first group, 31-75 to the second group, and 76-150 to the third group. In the first case, all EVs started charging directly after connection, regardless of the cost of the electricity unit. Therefore, the first group of the EVs had a similar charging cost to the applied optimisation algorithm. However, the other groups had higher charging costs than the other cases. The second case expressed the optimum solution of operation by the CSO. It provided diverse slots for charging the EVs. The first and second group are charged as normal, as the first case is due to low charging cost in the early morning. The charging slot of the second group was diverted between the early and late connection periods. The CSO booked slots for charging some EVs at the second group at the early connection rather than late due to the lower price, as shown in vehicles number 31-42 and 61-72 Figure 5-18 parts C and E respectively, whereas vehicles number 46-60 in part D diverted between the beginning and end of the connection period. The third group was shifted to the late period of connection time. Case three had less flexibility than the other cases where the objective algorithm was applied to provide minimum charging cost. However, the demand was not available for all the EVs. Therefore, the CSO looked for charging slot to satisfy the limited demand of the MGO and reached the desire to leave state of charge at minimum charging cost. Thus, some EVs from the first group were still charging at the late time of the connection period which was at a higher cost than the early time of connection, as explained in Figure 5-23 parts A and B. Some EVs in the second group were charging at the mid-term of connection, which is the highest rate of charging cost, as shown in Figure 5-23 parts C, D, and E. The same behaviour was recorded for the third group where some vehicles were charging at the beginning term of the connection period, as illustrated in

Figure 5-23 parts H and J. However, case three had a lower charging cost than the first case and a higher cost than the second case. In the fourth case, the MGO informed the CSO to discharge qualified EVs connected at midday. Therefore, the second group and part of the third group responded to the CSO discharging option, as shown in Figure 5-31 parts C, D and E from the second group and parts F and G from the third group. Those vehicles sold the power stored at energy storage system at the highest tariff rate of the microgrid with 10% extra for the discharging option. Therefore, the revenue of discharging power was higher than paying for charging power at the same rate as the state of charge. Thus, the charging cost of case four recorded the lowest amount, as shown in Figure 5-36.

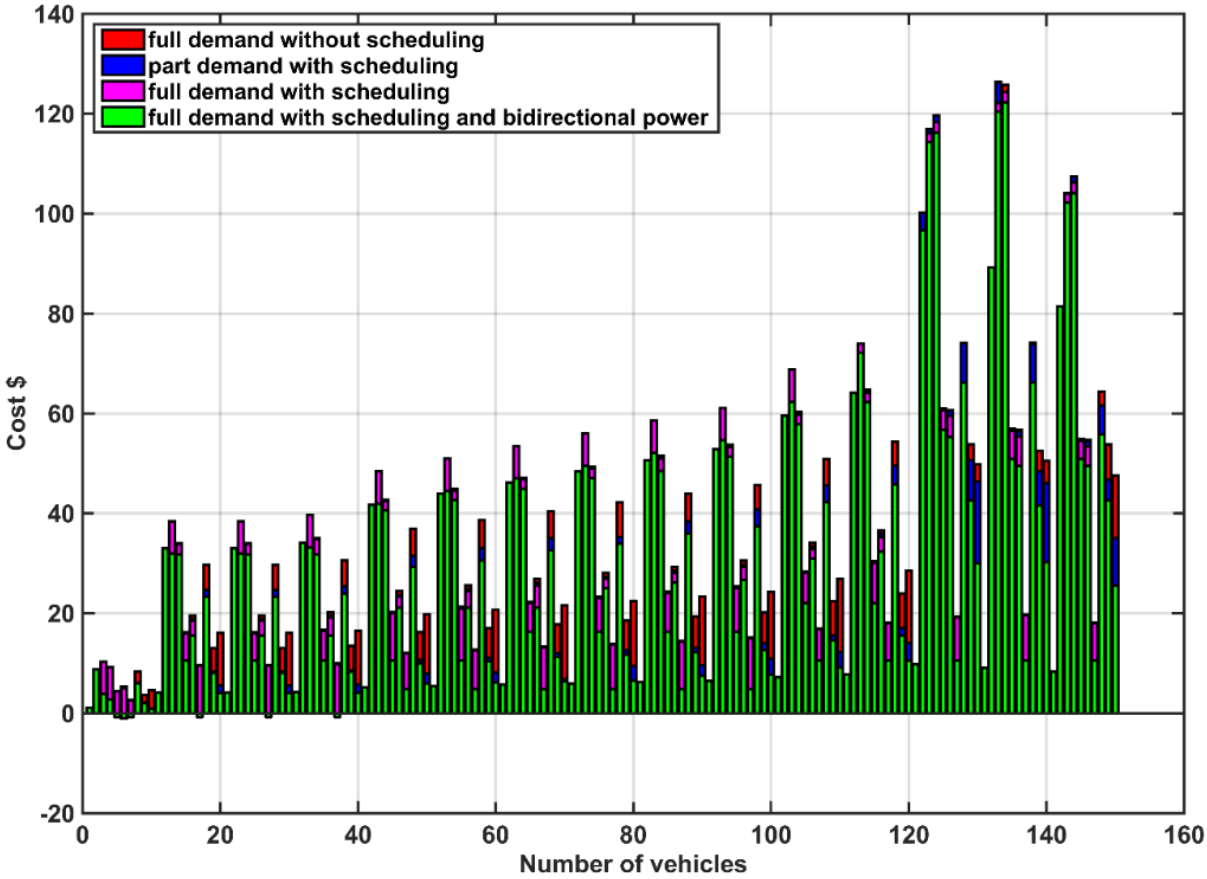

Figure 5-36: Cost compression for all cases

5.8.6 Scenario five

The difference between scenario 5 and previous scenarios is in applying the optimisation methodology on charging and discharging the supercapacitors of EVs, whereas the MGO feed all demands of the CSS. Hence with scenario 5, it is possible to explore further based on Figures 5-29 to 5-41 within the following concepts. The supercapacitor charging characteristics are similar to the electrochemical battery except that the supercapacitor can charge and discharge a virtually unlimited number of times. The charging supercapacitor is very fast which takes a much faster time than the battery at about 1-10 seconds. However, the rated of the converter limits the charging supercapacitor. In this study, the first minutes of the connection are reserved

to charge the supercapacitor of the EV fully by applying equation 5-1, whereas the discharging of the supercapacitor strategy is the same as the discharging battery strategy as in case four. A fuzzy interference programmatic solution is employed as a solution to make a logical decision for discharging the battery and supercapacitor within the EVO level. The fuzzy rule antecedents are the frequency of the microgrid, the voltage of the microgrid, the state of charge of the battery, and the state of charge of the supercapacitors, whereas the fuzzy rule consequence is the battery reference trajectory and the supercapacitor reference trajectory. The fuzzy power management for the battery and supercapacitor is the subject of the next chapter at section 6.7.2 within PMS shell of management duel resources strategy.

The performance of each EV regarding the state of charge and consumed power is depicted in Figure 5-37 and Figure 5-38 respectively where the curves show the response of initial SoC of EVs at connected time and zero at disconnected time. Figure 5-37 shows that the supercapacitors are very fast, fully charging within a couple of minutes of connection. Therefore, most of the potential of the CSS is directed to operate the batteries of EVs. The supercapacitors synergize the batteries of EVs to deliver the required power in discharging mode. The supercapacitor consumes the rated power of the converter to achieve full charging, as shown in Figure 5-38. The results clearly show that all EVs reached the full charge in the early minutes of connection and remained fully charged before leaving the CSS. All the supercapacitors connected at midday have discharged power to the microgrid at the heavy load when the MGO treats the CSO as a resource node, as shown in Figure 5-38 parts C, D, E, F and G. The results clearly show that all EVs reached the desired state of charge before leaving the CSS even after discharging power at midday. The cost of power charging for each EV is shown in Figure 5-39. It refers to EVs having a higher capacity of the supercapacitor could bring more money from the discharging power. Therefore, the revenue of the discharging power increased as the capacity of the supercapacitor increased.

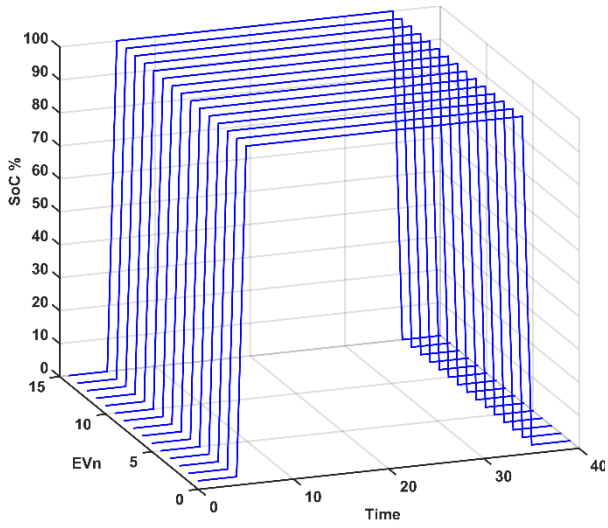

A- State of charge for vehicles number 1-15

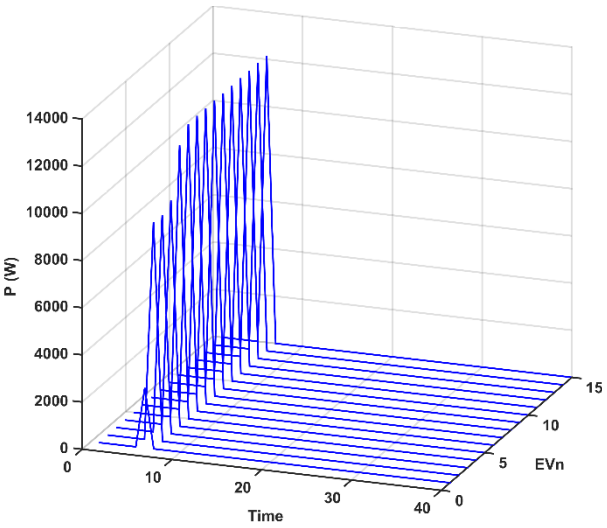

A- Power consumed for vehicles number 1-15

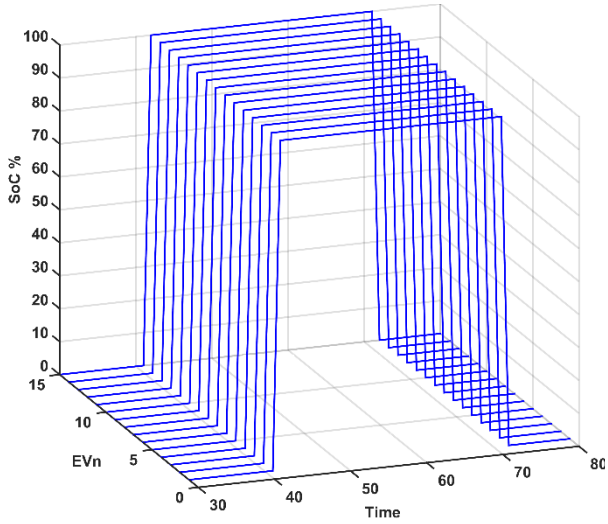

B- State of charge for vehicles number 15-30

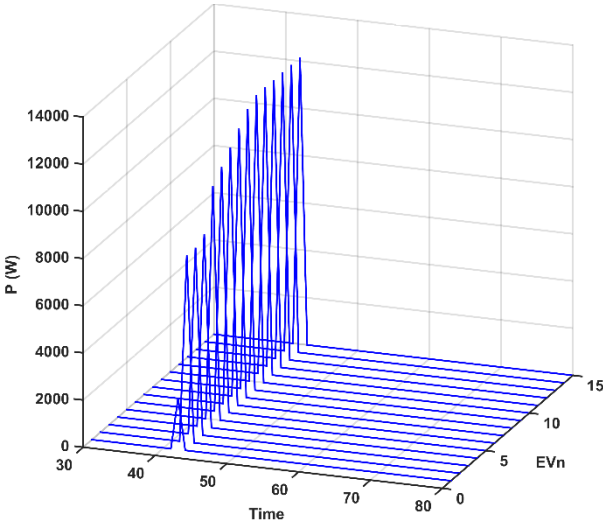

B- Power consumed for vehicles number 15-30

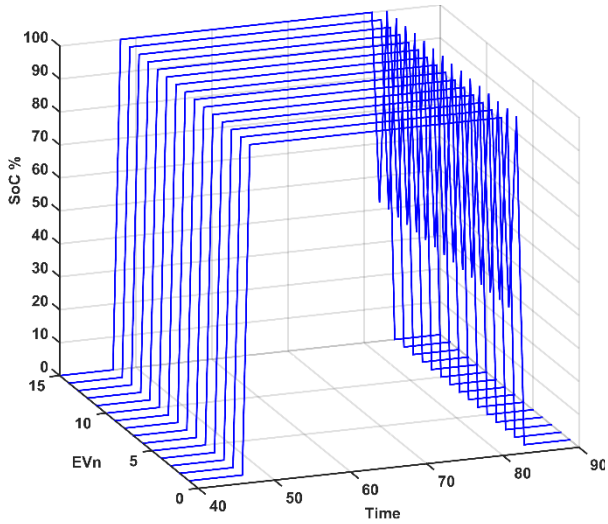

C- State of charge for vehicles number 16-45

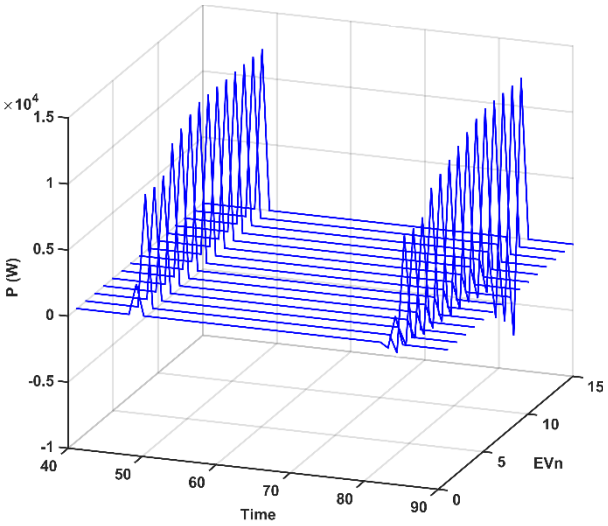

C- Power consumed for vehicles number 16-45

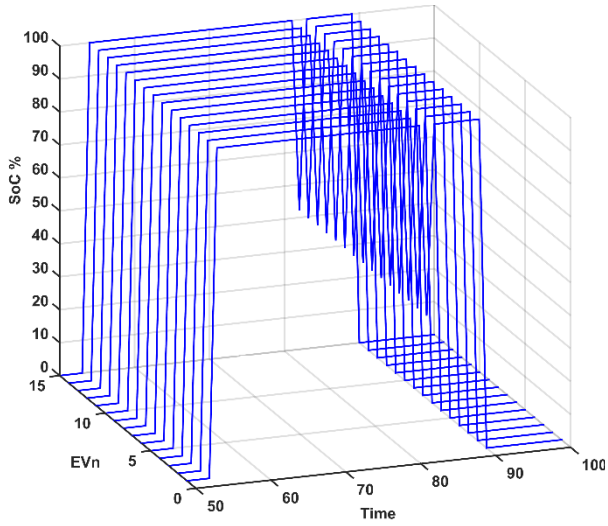

D- State of charge for vehicles number 46-60

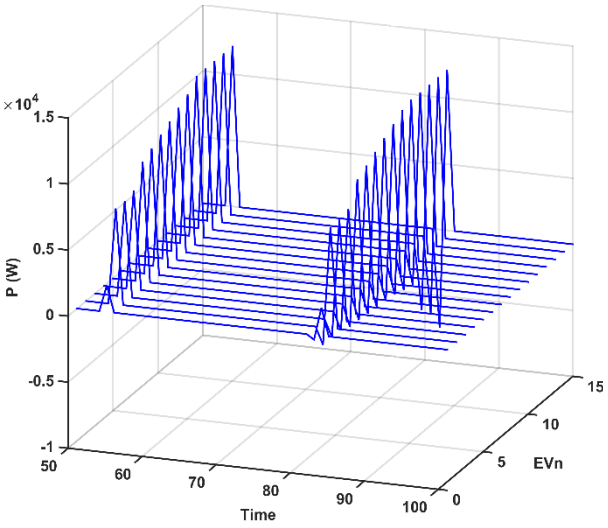

D- Power consumed for vehicles number 46-60

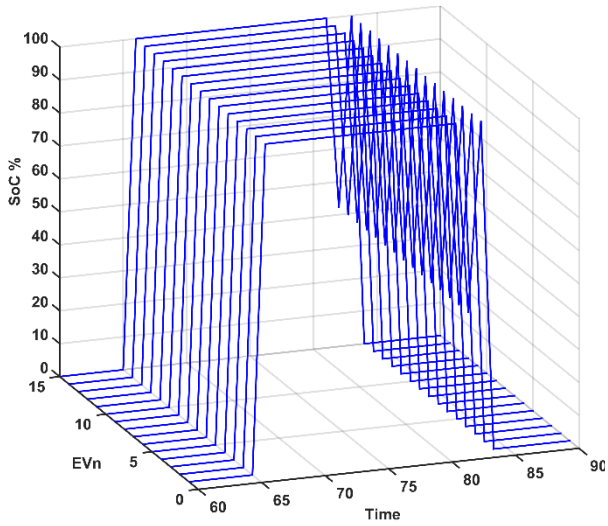

E- State of charge for vehicles number 61-75

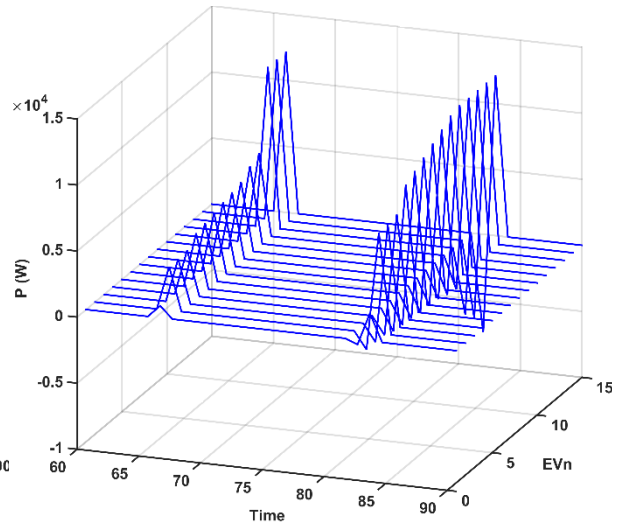

E- Power consumed for vehicles number 61-75

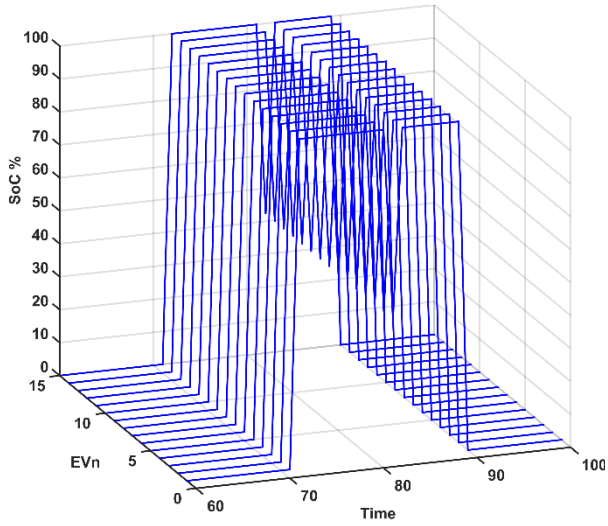

F- State of charge for vehicles number 76-90

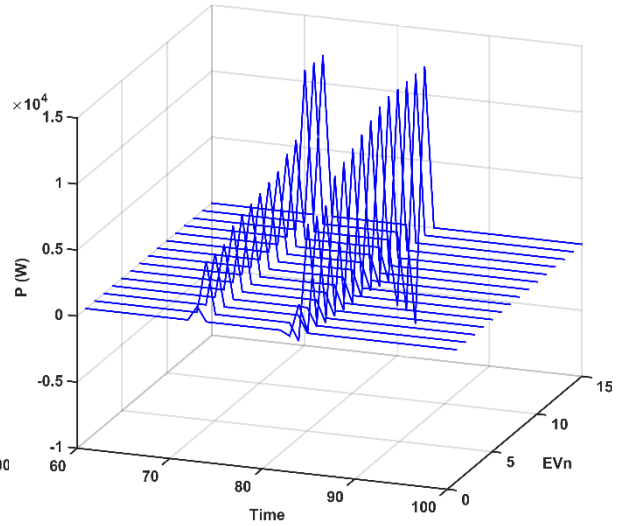

F- Power consumed for vehicles number 76-90

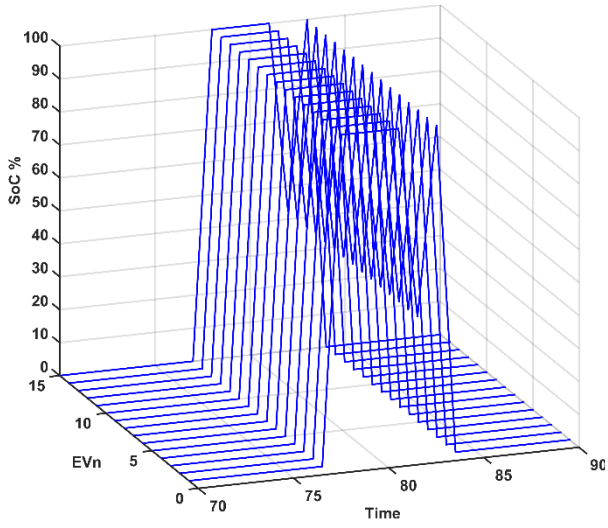

G- State of charge for vehicles number 91-105

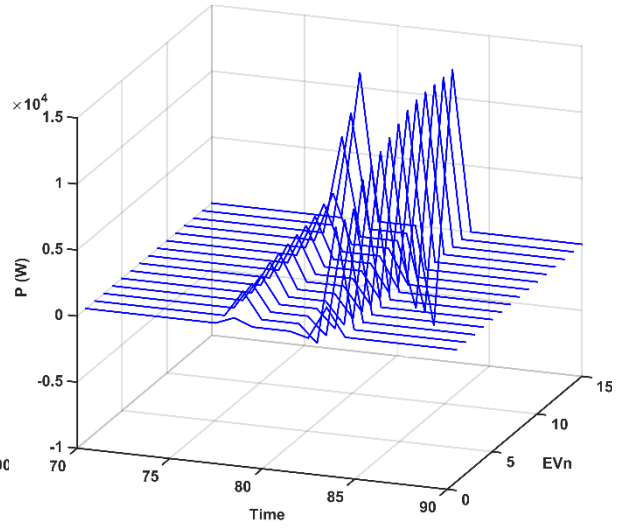

G- Power consumed for vehicles number 91-105

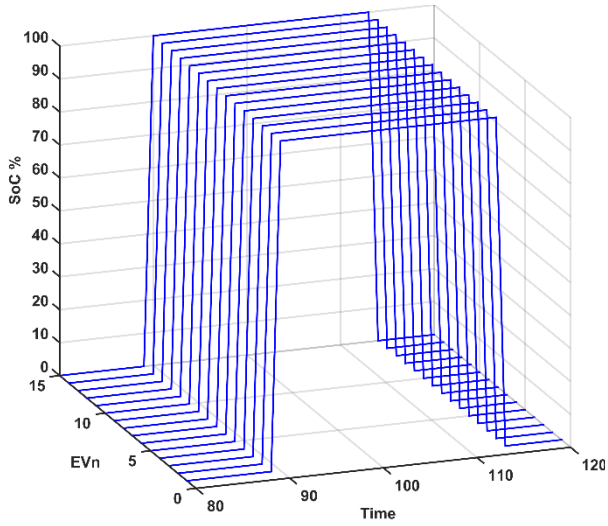

H- State of charge for vehicles number 106-120

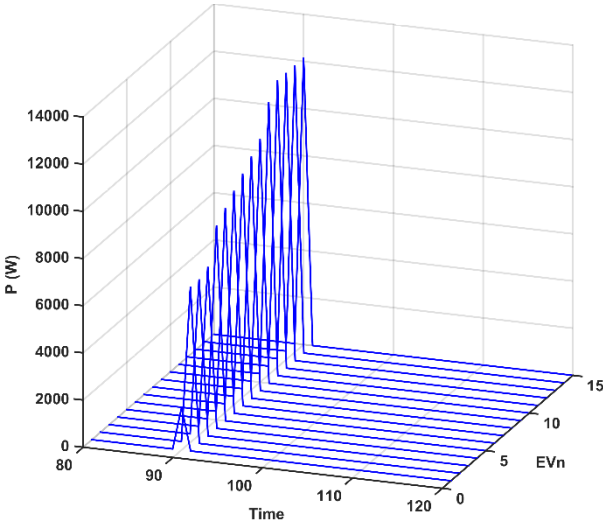

H- Power consumed for vehicles number 106-120

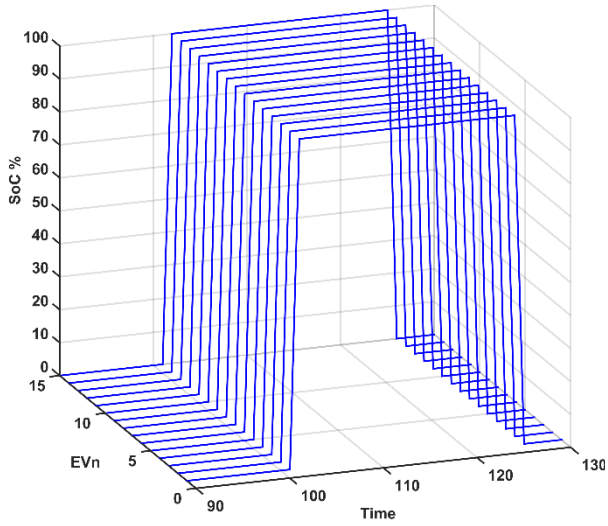

I- State of charge for vehicles number 121-135

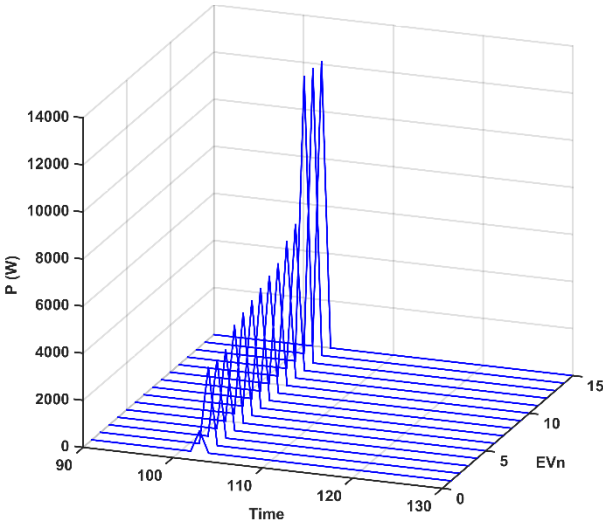

I- Power consumed for vehicles number 121-135

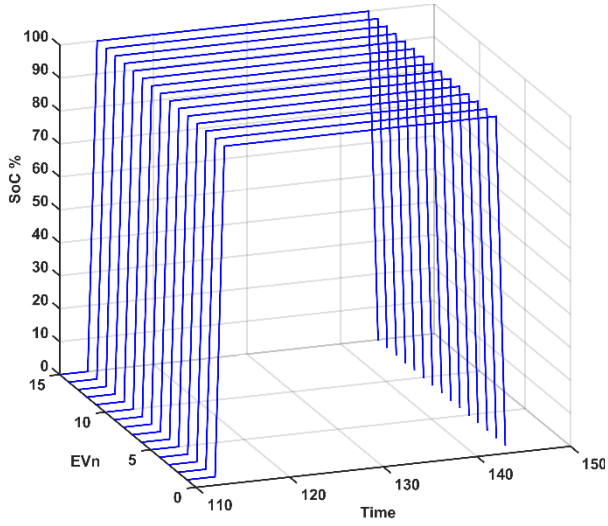

J- State of charge for vehicles number 136-150

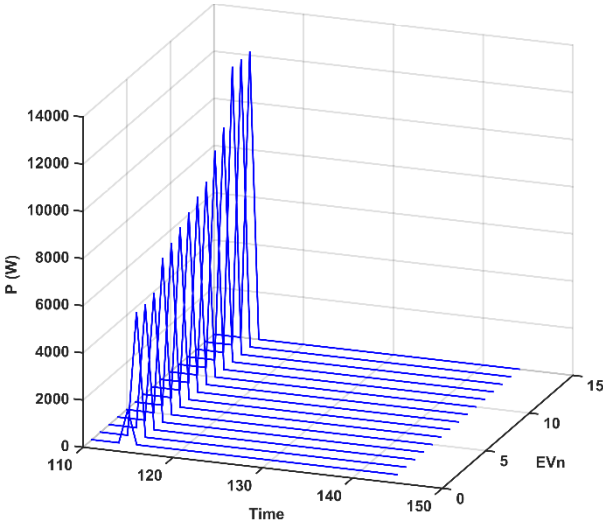

J- Power consumed for vehicles number 136-150

Figure 5-37: SoC of each vehicle along connected time

Figure 5-38: Power of each vehicle along connected time

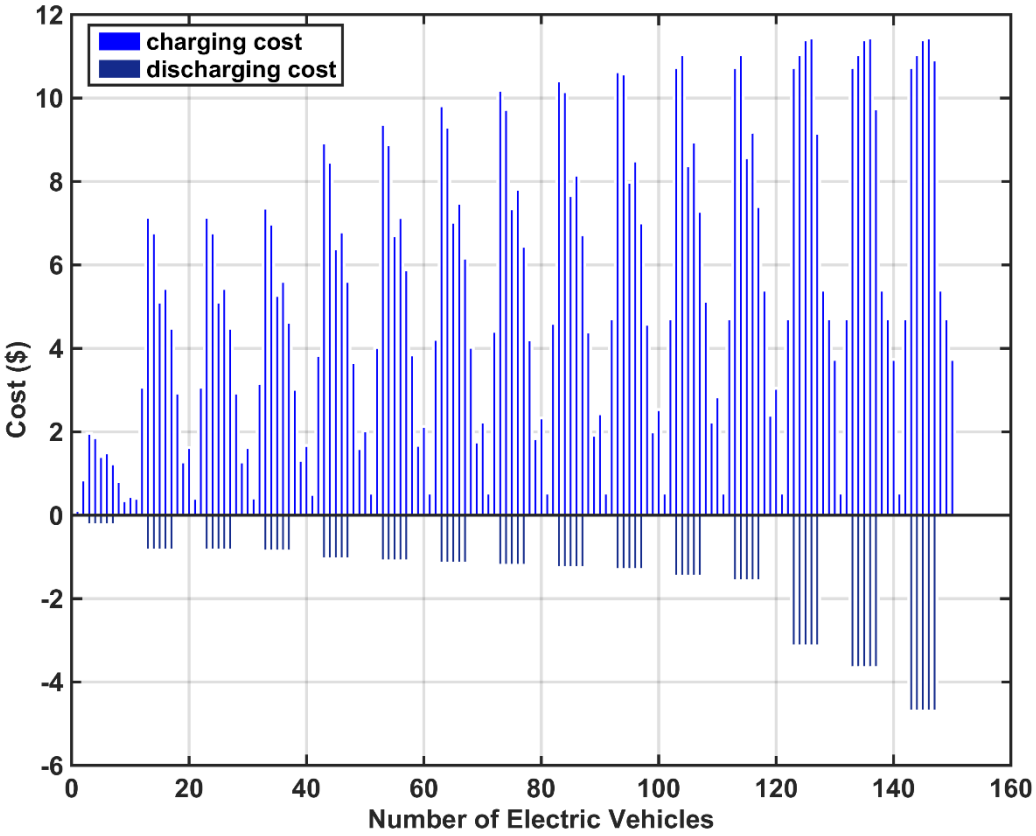

Figure 5-39: The cost of power charging for each vehicle

5.9 Conclusion

This chapter has illustrated the infrastructure of the charging station system, problem definition, and management layout of the CSO to manage the charging and discharging power for Many EVs from different brands connected at charging station system for avoiding congestion in the microgrid and satisfying the owners of the EVs.

Charging the EVs depend on many variables, such as time of connection, period of connection, desire to leave state of charge, capacity of the energy storage system, rated power of the inverter, frequency and voltage level of the microgrid, the power availability that the CSO is allowed to consume from the MGO, and the tariff of the electricity unit at a specific time. According to the input, the MILP optimisation function is used to decide the power level of each vehicle and either charging all EVs or scheduling the charging of EVs. Generally, the charging decision of the CSO depends on the frequency and voltage level. The CSO starts to charge all the EVs normally at FN and VN, whereas the scheduled charging takes place at FAN, FOA, VAN, and/or VOA, as described in Table 5-3. If the frequency and voltage levels are at FBN, FOB, VBN, or VOB, the CSO could not charge all the connected EVs, therefore, curtail strategy should apply starting from the nearest to leaving the state of charge vehicle. The curtail strategy iterates until satisfying the available power from the MGO.

The objective function of the optimisation algorithm is either achieving minimum charging cost or maximum discharging cost of the electricity unit. The electricity cost is chosen to be variable over a day. The scheduled charging is implemented according to the proposed nonlinear function which depends on the state of the charge level of the energy storage system. If the CSO predicts that it could not reach the desired state of charge at leaving time, then the priority charging should apply. The priority charging applies based on increasing the charging slots of the EV that leaves early without reaching the desired state of charge over the vehicles that stay longer. The priority charging could increase the cost charging of some EVs slightly. If the priority charging does not achieve the desired leaving state of charge, the CSO suggests a new level of leaving state of charge to the owner of the vehicle. The role of the CSO is flexible to allow the EVs to charge directly at the rated power of the inverter with the extra cost of the normal tariff.

Discharging the EVs is a feature that makes them work bidirectionally with the microgrid. It helps the microgrid to balance the load in a stable condition. The discharging EVs provide the owners with revenue from selling the power of the resources to the microgrid. It encourages the owners of the EVs to charge those vehicles at a low rate tariff and make them ready to discharge at a high rate tariff which is normally the highest demand time on the network. The discharging EV depends on the acceptance of the owner, predefined limit of the state of charge, frequency deviation, and voltage deviation. The minimum limit of discharging the battery and supercapacitor has been chosen as 70% and 40% respectively. The frequency and voltage deviation of discharging EVs have been chosen within the range of FBN, FOB, VBN, and VOB, as described in Table 5-3. The MILP optimisation function using the MATLAB environment and Cplex software is chosen to manage the discharging EVs during the frequency and voltage deviation according to the power required from the MGO. The objective function of the optimisation algorithm is achieving the maximum power discharging cost of the EVs.

A case study of 150 EVs from 15 brands connected at different times of a day is chosen to focus on the snapshot operation of charging and discharging the EVs. To offer useful insight when studying the operation of EVs, the case study is divided into four cases of charging the battery of the EVs. The first and second cases studied stable microgrid operation where the MGO had provided the full demand from the EVs. The first case discussed charging the EVs directly after connecting to the microgrid, whereas the second case applied the proposed optimisation algorithm. The third and fourth cases studied fluctuation in the microgrid where the MGO had provided part of the EVs' demand. The third case discussed applying the optimisation algorithm and priority charging strategy to the vehicles that could not reach the desired leaving state of charge, whereas the fourth case applied the discharging algorithm to the qualified EVs. All the EVs in case one reached the desired to leave state of charge as in case two. However, the cost of electricity units for some EVs, which are still charged at the high tariff rate, in case one is higher than charging in case two.

The optimisation algorithm shifted all the vehicles charging at high rate tariff to lower cost whereas other vehicles still charge normally as in case one. Not all vehicles reached the desire to leave state of charge in case three, therefore applying priority charging of most of the vehicles to the desired leaving state of charge except one vehicle, which is number 134, where the CSO informed the owner of the applicable level that can be reached. The cost of charging EVs at case three after applying the priority strategy is almost the same as the cost of charging EVs in case two. Some EVs started discharging the energy of the battery at a specific time, which is midday, in case four. The MGO informed the CSO to manage the discharge of qualified EVs at midday to synergize the distributed generator in order to balance the load. The discharged battery of many EVs could not reach the desire to leave state of charge at leaving time. However, all the vehicles discharged power has revenue from the cost of discharging, which is higher than the charging cost tariff by 10%. For vehicles having a high battery capacity, this could generate high revenues from discharging the energy of the battery, reaching 70% of the state of charge of the battery. This offers a benefit from charging vehicles at the low rate of charging, such as after midnight and making them ready to discharge at a high rate tariff such as midday to generate money from the microgrid rather than paying it at same charging and discharging level of state of charge.

Case five observed how fast charging and discharging the supercapacitor compares with battery. However, the rated capacity of the supercapacitor is much less than the rated capacity of the battery, and the charging and discharging rate of the supercapacitors are much higher than the battery at the same rate of capacity.

The CSS is vital to ensure deployment of EVs in society and management of the operation of the EVs within the microgrid. The appropriate rules are the supreme of operating the CSS to avoid congestion in the microgrid operation.

6. Chapter Six: Mangment of Multiple Resources in Electric Vehicles

6.1 Introduction

The previous chapter describes the middle tier policy planning of the modular management structure to handle the centralised charging and discharging aggregated EVs connected to the specific bus bar on the network to achieve either minimum charging cost or maximum discharging cost for each EV. The system has been designed as a unified systematic framework where the power management decomposes into modular blocks in chronological executions.

Smart charging of EV allows cooperation between the vehicle and the microgrid regarding scheduling charging and discharging profiles to achieve technical and economical benefits. The previous chapter discussed the centralised smart charger of aggregated EVs that connected to the CSS. The most important part of the centralised smart charger collects and circulates a large amount of data from the vehicles to the CSO and from MGO to CSO. The EVA is the responsible equipment to supply the information of the EVs to the CSO whereas the MGO agent is responsible for providing the information of the microgrid to the CSO. Therefore, congestion of information may happen that delays the reference signal for each vehicle regarding charging or discharging. A significant negative impact happenes when the MGO requires power to maintain the stability of the system, whereas the CSO continous to activate the charging mode. On the other hand, the decentralised smart charger fuelled each vehicle collaborates between the smart controller and the EVA. The EVA in the previous chapter is displayed as a buffer equipment to inform the microgrid about the states of the EV at each period of operation and to control the power flow between the microgrid and the storage energy system of the EVs. The cooperation between the centralised smart charger topology and decentralised smart charger topology increases the reliability and sustainability of the system. It is possible to merge the smart controller and the EVA into one part, as the main controller of the vehicle in running mode and assistant controller for the CSO in connected mode. The emerging system is called smart controller agent (SCA). Therefore, each vehicle should ensure the SCA controls and manages the EV when it is running or connected to the CSS to synergize the centralised charger under fluctuation operation conditions. Typically, both battery and supercapacitor of the EV supplies direct current (DC) mode. On the other hand, both the motor, which runs the vehicle and the microgrid works in Alternating Current (AC) mode. A converter is a very efficient electronic device that is used to connect the vehicle resources to the motor or the microgrid to alternate between DC and AC with specific waveform characteristics regarding the input voltage, output voltage, frequency, and power capacity.

This chapter describes the lower tier of the modular management structure which decides appropriate actions of the process planning or short-term process of either applying the instruction to the middle tier (CSO) or the decentralised charging/discharging aggregated EV in order to manage synchronising the waveform of the resources with the network, arbitrate the required energy between the battery and supercapacitors, and apply the switching modulation to operate the inverter. The integration is between the EV and the microgrid across the modified cascade multilevel inverter and set of controller processes through the Electric Vehicle

Operator (EVO). The EVO involves a holistic modular process from three shells which operate at different execution times. The controller target of the EVO is achieved by linking three sub processes which involve the management energy shell (MES) to regulate the energy management of the resources, the power management shell (PMS) to advise the arbitrating power of the resources, and the power electronic shell (PES) to instruct the modulation strategy of the switches. The controllers of the shells apply several processes which include detecting the positive sequence of waveform, droop controller, and vector controller at EMS, heuristic fuzzy logic at PMS, and modified Space Vector Pulse Width Modulation (SVPWM) at PES.

6.2 Algorithm Design of Hierarchical Management Concept to Power and Energy Management of the EVO

As the complete process to obtain the desired results for charging or discharging the EV, it should simplify the system to manage the charging and the discharging power of the resources and control the waveform characteristics. It is clear that the system has many resources, which are the battery, the three supercapacitors, and the microgrid. The direction of required power is either from microgrid to battery and/or supercapacitors in charging mode or from supercapacitors and/or battery to microgrid in discharging mode. The management of the system focuses on utilising all available resources to achieve the desired power from each one in a specific direction with maximum efficiency. The control focuses on implementing and executing the management strategy to achieve the standard waveform of the system. The management process requires identifying a strategic vision, setting an objective, and identifying a strategy.

The management organisation consists of three perspectives: long-, middle- and short-term; each one executes a different task at a different time. The long-term period involves the decision of energy expenditure from the resources. The middle-term period involves the decision of the power management to define the power split decisions of the battery and the supercapacitors. To control the switching function of 18 switches, the short-term period is responsible for decomposing the reference power trajectory into multilevel space vector pulse width modulation. The long-term period takes places within an energy management shell (EMS). The EMS period has a lower time segment which is seconds as it has slower dynamic parameters. The EMS provides control parameters to the middle-term period to implement power management strategy. The middle term takes places within a power management shell. The power management shell (PMS) time segment is milliseconds where it compares four parameters, which are voltage and frequency of the microgrid, the state of charge of the battery and the supercapacitors to handle the direction, and the amount of power of the resources.The PMS provides control parameters to the short-term period to implement space vector pulse width modulation. The short-term takes place within a power electronic shell. The power electronic shell (PES) has a faster time segment, i.e. microseconds, as it treats the frequency modulation signal, which is very high frequency compared with a fundamental frequency of the microgrid. The PES provides a signal to the switching devices to process the voltage and current of the battery and the supercapacitors. The three shells of the PEMS implementation requirement, described as a hierarchical decision, are illustrated in Figure 6-1.

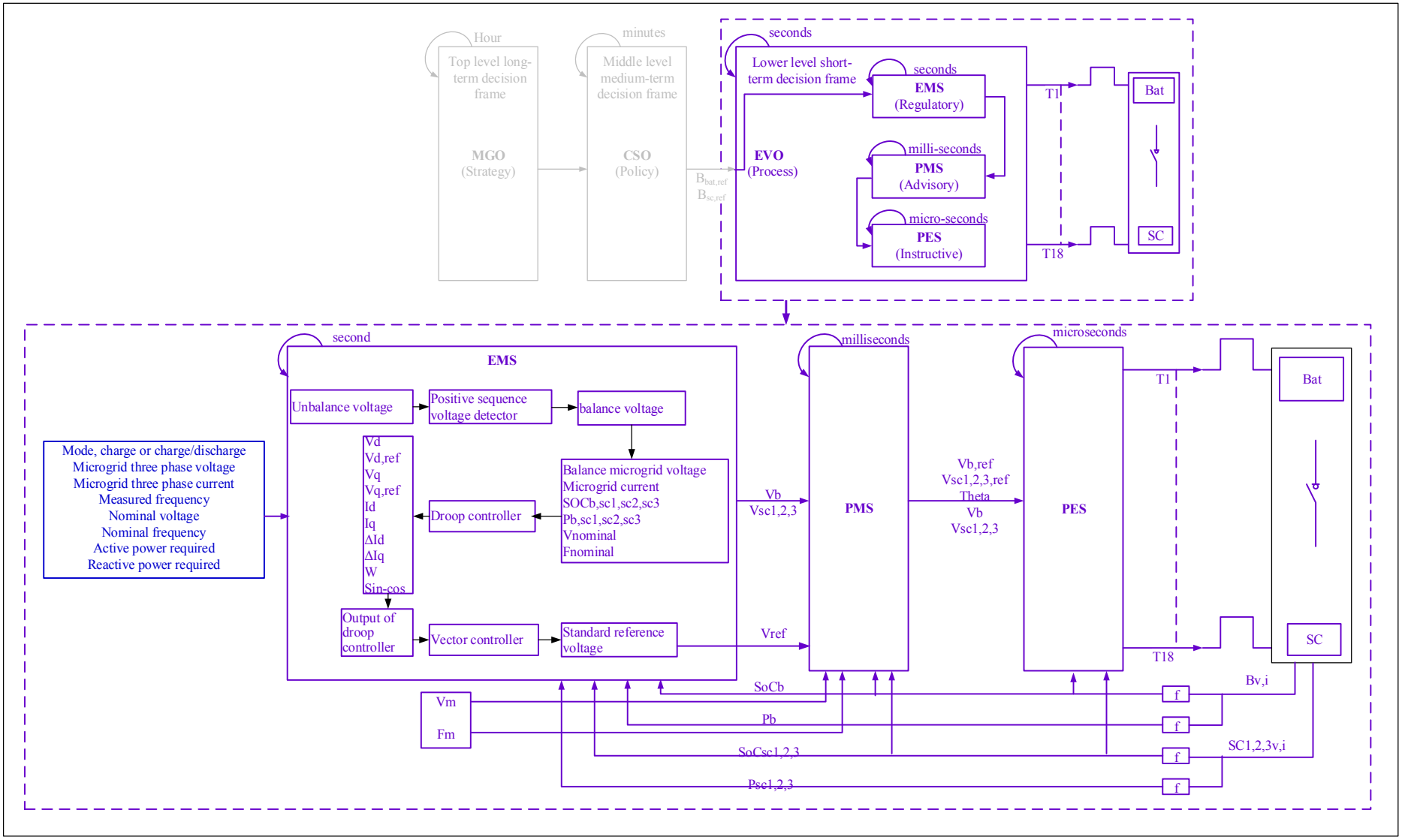

Figure 6-1: EVO optimisation algorithm

6.3 Modelling and Application of Energy Storage Systems

The stored energy and the rate of extracting this energy are important characteristics for the application of the EV's energy storage system. The stored energy refers to the energy capacity of the device, whereas the rate of extraction relates to the power rating of the device. In order to engage the EVs' storage devices with a microgrid, the operating constraint for the energy storages need to be considered; in addition, the energy and power management must be studied.

The battery is considered to be the main resource to power the EV. The battery produces the electric charge through a chemical process. Therefore, it could store high energy as a capacity to do work. However, due to the chemical process, the battery may not be fast enough to deliver the stored energy. On the other hand, the supercapacitor stores the energy in a static charge form. Therefore, the supercapacitor stores less energy than a battery. However, it is much higher to deliver the power to the application than the battery [322]. In relation to the hybridization, the battery and supercapacitor in an EV complement each other to deliver energy strategically to meet transient demand. This dissertation expresses the battery as the main source of the EV and the supercapacitor as an auxiliary source of the EV.

6.3.1 Battery system of electric vehicles

In EVs' application, the battery is considered to be a key component of the EVs to store electrical energy, which has the highest cost, weight and volume of the equipment of the EV; desirable parameters of the battery system are the higher number of life cycles and a large amount of energy and power consumption. Most technologies of EVs are using the harsh bidirectional environment rechargeable battery to meet the subjected operation of the EV.

The battery in the EV consists of many electric cells connected in series or parallel to reach the desired voltage and increase the total capacity. The cells contain positive and negative electrodes that are joined by an electrolyte. There are different types and sizes of batteries for EV purposes which have different characteristics. However, the lead acid battery is the most well-known rechargeable battery. On the other hand, the battery technology of EVs is still under researched. However, the same battery capacity of lithium-ion and lead acid results in the less weight and volume of the lithium-ion than the lead acid. Therefore, most of the companies used lithium-ion technology in EVs application. According to research the lead acid battery is cheaper and has better known parameters than the lithium-ion battery. Thus, the lead acid battery is used in this research. Therefore, it is considered in this work that the current flows through a battery when the external circuit is completed. Thévenin's model equivalent circuit of the battery and the corresponding voltage characteristics of the battery's stored charge capacity are shown in Figure 6-2; the battery has been represented as a resistance connected in series with an ideal open circuit voltage. This basic model does not represent the dynamic behaviour of the battery. However, it gives a good voltage prediction of the battery [323, Sec. 3.12].

The terminal voltage can be found using Kirchhoff's voltage law as follows:

$$V = E_o - IR_{in} \tag{6-1}$$

The open circuit voltage and internal resistance depend upon the state of charge at the instantaneous state of the battery and temperature. Empirical methods could find the open circuit voltage. The internal resistance is preferable to be low as possible to keep the voltage droop remarkably small when the current is drawn by the circuit. The internal resistance of the battery for charging mode is different from a discharging mode, where the internal resistance for discharging mode is normally higher than the charging mode. One of the most important features of the lead acid battery is having extremely lower internal resistance than other types of batteries. A good estimation of the internal resistance of the lead acid battery can be calculated by

$$R_{in} = N \times \frac{0.022}{C} \qquad 6\text{-}2$$

whereas the open circuit voltage of the lead acid battery can be written as [323, Sec. 3.12].

$$E = N \times (2.15 - DoD \times (2.15 - 2)) \qquad 6\text{-}3$$

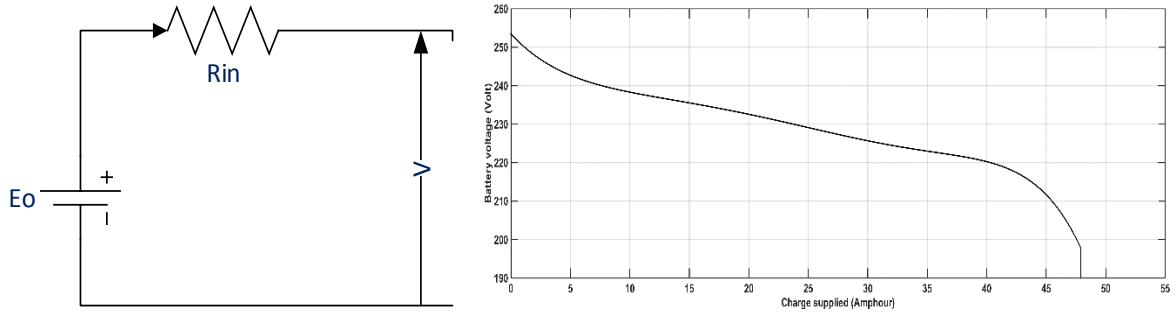

A- Modelling Battery equivalent circuit

B- Terminal voltage supply as a function of charge capacity

Figure 6-2: Battery basic equivalent circuit and voltage characteristic

In the EV application, the current drawn from the battery is high. It is important to predict the effect of current on the capacity of the battery as the capacity of the battery is reduced when the current is drawn quickly from the battery. The best way to determine the empirical relationship between capacity, current, and time is by using Peukert's model of battery behaviour, even though it is not very accurate at low current drawn from the battery. The method supposes a constant Peukert capacity that is given by

$$C_p = I^k \times T \qquad 6\text{-}4$$

k is suggested empirically according to the kind of battery. It reaches 1 for a small current and 2 for a large current. However, practically it has a range between 1.05 and 2. Typically, it is equal to 1.2 for a lead acid battery. Equation 6-4 assumes that the battery discharges at constant current till flat and last T hours [323, Sec. 3.12].

The state of charge (SoC) of the battery represents the ratio of actual battery capacity to the nominal capacity. The SoC indicates the amount of energy that charges or discharges from the battery; the SoC is formulated as follows [324, Sec. 3.12]:

$$\mathrm{SoC} = \frac{\text{actual battery charge}}{\text{total battery charge}} \qquad 6\text{-}5$$

The accuracy in estimating the SoC is necessary to give precise information regarding the amount of energy that could be used in the energy management scheme of the system. Various methods are used to estimate the SoC, such as an analytical method based on Peukert's equation [323, Sec. 3.12], [325], heuristic method modelling [326], and a combined approach using a empirically obtained look-up table [327, Sec. 7.2.1].

In most SoC estimation methods, the battery current is integrated over time and related to the nominal battery capacity. The charge removed from or supplied to the battery can be calculated based on the integrated Peukert's current and normal current over time, by the following forms[323, p. 69,70]:

$$\mathrm{CR}(n+1) = \mathrm{CR}(n) + \frac{\int_{t0}^{t1} I^{k}(t)dt}{3600} \qquad 6\text{-}6$$

$$\mathrm{CS}(n+1) = \mathrm{CS}(n) + \frac{\int_{t0}^{t1} I(t)}{3600} \qquad 6\text{-}7$$

The depth of discharge for the battery is calculated from the charge removed related to Peukert's capacity, as stated in equation 6-8, whereas the state of charge can be calculated from the charge supply related to the nominal capacity by the following forms [323, p. 70]:

$$\mathrm{DoD}_n = \frac{\mathrm{CR}_n}{C_p} \qquad 6\text{-}8$$

$$\mathrm{SoC}_n = \frac{\mathrm{CS}_n}{C_n} \qquad 6\text{-}9$$

The battery model equations can be calculated in discrete time steps of real-time control application, as shown in the folloing forms [323, p. 70], [324, Sec. 3.12]:

$$\mathrm{DoD}_{(n+1)} = \mathrm{DoD}_n + \frac{I^{k} \times \Delta t}{C_p \times 3600} \qquad 6\text{-}10$$

$$\mathrm{SoC}_{(n+1)} = \mathrm{SoC}_n + \frac{I \times \Delta t}{C_n \times 3600} \qquad 6\text{-}11$$

Δt is the sampling period between n and n+1. The sampling time has been kept small to ensure that the current of the battery remains constant during the time steps [323, Sec. 3.12].

The power and current of the battery can be calculated by

$$P = VI = EI - RI^{2} \qquad 6\text{-}12$$

$$\mathrm{I} = \frac{\mathrm{E} - \sqrt{\mathrm{E}^2 - 4\mathrm{R_{in}} \times \mathrm{P}}}{2\mathrm{R_{in}}} \quad 6\text{-}13$$

If the current is flowing into the battery, then the voltage and current equations can be calculated by

$$\mathrm{V} = \mathrm{E} + \mathrm{I} \times \mathrm{R_{in}} \quad 6\text{-}14$$

$$\mathrm{I} = \frac{-\mathrm{E} + \sqrt{\mathrm{E}^2 + 4 * \mathrm{R_{in}} * \mathrm{P}}}{2 * \mathrm{R_{in}}} \quad 6\text{-}15$$

The charging is removed, and the state of charge can be described by

$$\mathrm{CR(n+1)} = \mathrm{CR(n)} - \frac{\mathrm{I^k} \times \Delta\mathrm{t}}{3600} \quad 6\text{-}16$$

$$\mathrm{CS(n+1)} = \mathrm{CS(n)} - \frac{\mathrm{I} \times \Delta\mathrm{t}}{3600} \quad 6\text{-}17$$

Figure 6-3 explains the implementation of a battery state of charge estimation, including all required parameters.

At high charging current, the Peukert correction will be removed as it does not have a proportionately effective impact at a small current.

The maximum charging or discharging power of the battery is limited by the maximum allowable charging or discharging current, minimum terminal voltage, and temperature. The maximum charging current is less than the maximum discharging current because the charge acceptance rate is always less than the charge release rate [323, Sec. 3.12]. The maximum charging and discharging power can be formulated by

$$P_{ch,max} = I_{b,max} \times V_{oc,SoC} + I_{b,max}^2 \times R_{i,SoC} \quad 6\text{-}18$$

$$P_{dis,max} = I_{b,max} \times V_{oc,SoC} - I_{b,max}^2 \times R_{i,SoC} \quad 6\text{-}19$$

where $V_{oc,SoC}$ and $R_{i,SoC}$ are the battery state of charge dependent upon the circuit voltage and internal resistance respectively.

The maximum charging and discharging power are also limited by the maximum charging voltage, as stated in the following:

$$P_{ch,max} = V_{b,max} \times \left[\frac{V_{b,max} - V_{oc,SoC}}{R_{i,SoC}}\right] \quad 6\text{-}20$$

$$P_{dis,max} = V_{b,min} \times \left[\frac{V_{oc,SoC} - V_{b,min}}{R_{i,SoC}}\right] \quad 6\text{-}21$$

where $V_{b,max}$ and $V_{b,min}$ are the maximum and minimum allowable voltage that can be applied to the battery

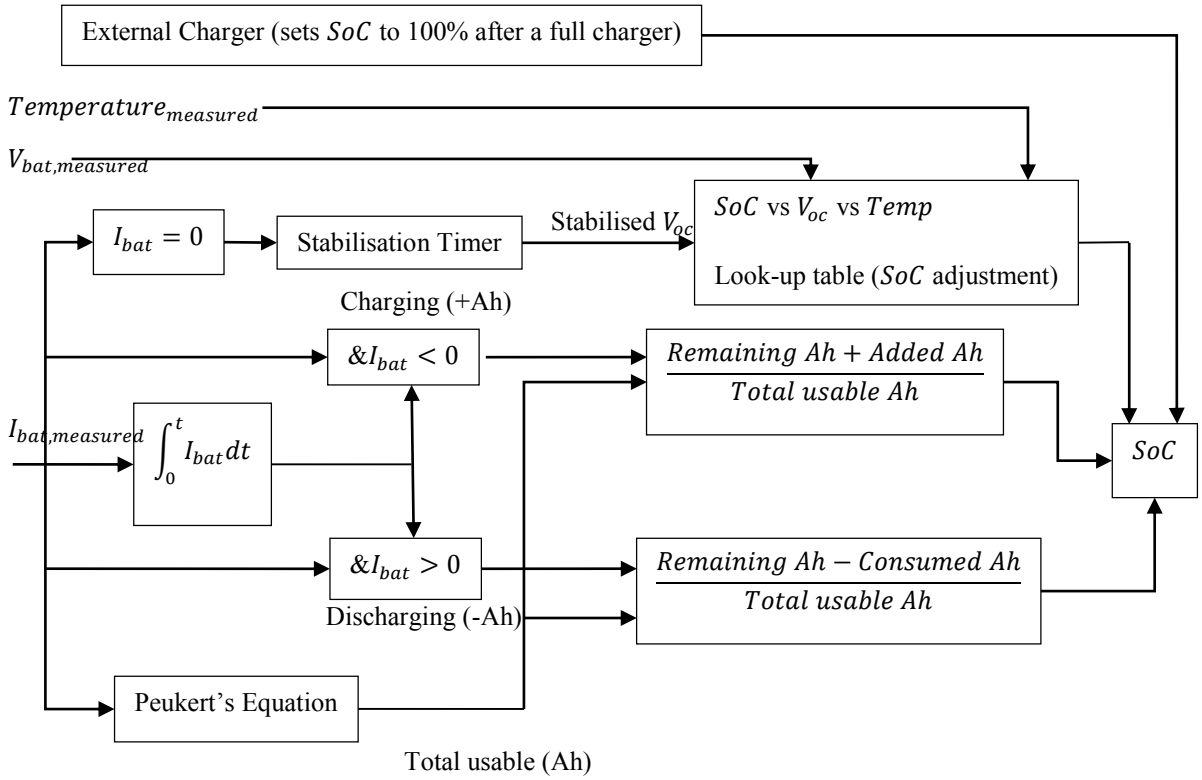

Figure 6-3: Combined method for practical implementation of SoC estimation (adapted from [324, Sec. 3.12], [327, Sec. 7.2.1])

6.3.2 Supercapacitor system of electric vehicles

A supercapacitor is another resource for the energy storage system. It has higher capacitance than the regular capacitor. The supercapacitor stores energy as a static charge as opposed to an electrochemical reaction. Therefore, it has higher specific power stored than a battery with lower energy, which enables the supercapacitor to work in a complementary manner to the battery, as shown in the Ragone plot of Figure 6-5, in addition to using lower toxicity of material than the electrochemical battery. A time constant for the supercapacitor is very fast compared with a battery. The ESR effects are on the time constant of the supercapacitor where the transient response time = 5T = 5(ESR (ohm).C (farad)), which is around 0.1-20 seconds, whereas the battery is much slower than the supercapacitor. There are many parameter effects on the time constant of the battery such as internal resistance, temperature, vibration due to chemical reaction, and uniform chemical reaction. A supercapacitor is a potentially versatile solution to a variety of emerging energy applications based on the ability to achieve a wide range of energy and power density. The charging characteristics of the supercapacitor are similar to the charging characteristics of an electrochemical battery; however, the storage mechanism itself is very different. Consequently, the charging or discharging time of the supercapacitor is much faster (about 10 times faster) than the charging or discharging time of the battery at a similar capacity. Unlike the electrochemical battery, the age of the supercapacitor is longer than the battery; in addition, the supercapacitor could be charged or discharged at a much higher cycle rate than the battery even though in low temperature

conditions [328, Sec. 10.2]. A high load current could be drawn from the supercapacitor due to the low internal resistance. A supercapacitor is located in between the battery and a conventional capacitor for balancing energy and power density. Many cells are connected in series and parallel with a voltage balancing to achieve specific voltage and capacity, where each cell has a low voltage.

There are many representations of a supercapacitor model; the simplest model could be represented as lumped capacitance, equivalent series resistance (ESR), and equivalent parallel resistance (EPR), as shown in Figure 6-4. Estimating the state of charge of the supercapacitor is easier than for the battery.

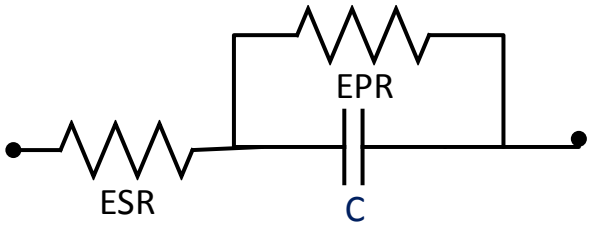

Figure 6-4: Modelling of supercapacitor

EPR represents the current leakage; it has an influence on the long-term energy storage. EPR effects on the cell voltage distribution are due to the resistor divider effect. Experimentally, EPR could be neglected due to transient discharge calculation. However, EPR is important for considering the cell balancing of the series connection of supercapacitors. The ESR is considered to be a non-time dependent parameter whereas the EPR which relates to the voltage decay ratio can be calculated by [329]

$$\mathrm{EPR} = \frac{-\mathrm{t}}{\ln(\frac{\mathrm{V_2}}{\mathrm{V_1}})\mathrm{C}} \qquad 6\text{-}22$$

where $\mathrm{V_1}$,$\mathrm{V_2}$, and C are the initial voltage, the final voltage, and the rated capacitance respectively.

Power and energy transfer requirements specify the sizing of the supercapacitor where the power constraint determines how fast the extracted energy could be.

The fundamental voltage and current equations of the supercapacitor can be described as follows:

$$\mathrm{i} = \mathrm{C}\frac{\mathrm{dv}}{\mathrm{dt}} \qquad 6\text{-}23$$

$$\mathrm{E} = \frac{1}{2}\mathrm{CV}^2 \qquad 6\text{-}24$$

The available energy for the supercapacitor during discharging can be calculated by.

$$\mathrm{E_n^{n+1}} = \frac{1}{2}\mathrm{C}(\mathrm{V_n^2} - \mathrm{V_{n+1}^2}) \qquad 6\text{-}25$$

The usable energy of the supercapacitor, depending on a minimum to a maximum allowable voltage ratio, is shown in equation 6-26. Therefore, the state of charge of the supercapacitor

could be calculated from the ratio of initial voltage to maximum voltage, as shown the following [330]:

$$E_u = \frac{1}{2}CV_{max}^2 - \frac{1}{2}CV_{min}^2 = E_{max}\left[1 - \frac{v_d}{100}\right] \quad 6\text{-}26$$

$$E_{max} = \frac{1}{2}CV_{max}^2 \quad 6\text{-}27$$

$$v_d = \frac{V_{min}}{V_{max}} \times 100 \quad 6\text{-}28$$

$$SoC = \frac{V_{s,0(t)}^2}{V_{max}^2} \quad 6\text{-}29$$

$$V_{s,0(t)}^2 = V_s(t) - 2R_s \times I_s(t) \quad 6\text{-}30$$

where V_{max} and V_{min} are the maximum and minimum terminal voltage respectively.

E_u and E_{max} are the usable and maximum stored energy respectively and v_d is the voltage discharge ratio.

The maximum power of supercapacitor can be calculated by

$$\mathrm{P_{scap,max}} = \frac{\mathrm{V_{scap}^2}}{4\mathrm{ESR}} \quad 6\text{-}31$$

A general comparison between the supercapacitor and Lithium-ion battery could be found in Table 6-1.

Table 6-1: Performance comparison between supercapacitor and Lithium-ion [331].

Function	**Supercapacitor**	**Lithium-ion (general)**
Charge time	1–10 seconds	10–60 minutes
Cycle life	1 million or 30,000h	500 and higher
Cell voltage	2.3 to 2.75V	3.6V nominal
Specific energy (Wh/kg)	5 (typical)	120–240
Specific power (W/kg)	Up to 10,000	1,000–3,000
Service life (industrial)	10-15 years	5 to 10 years
Charge temperature	–40 to 65°C (–40 to 149°F)	0 to 45°C (32°to 113°F)
Discharge temperature	–40 to 65°C (–40 to 149°F)	–20 to 60°C (–4 to 140°F)

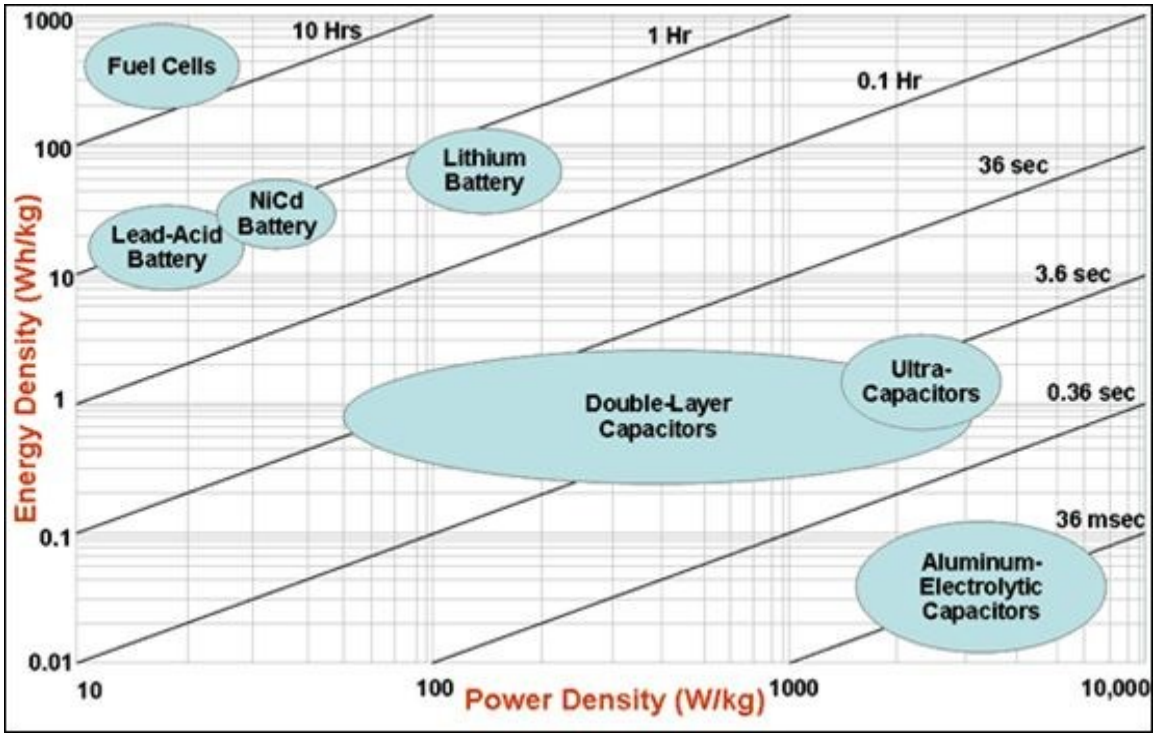

Figure 6-5: Ragone plot of energy storage system [332]

6.4 Power Arbitration of Dual Resources in Electric Vehicles

The main challenge in designing an electric system to integrate the EV into the microgrid is finding a way to fill short-term power as well as long-term energy. Combining the battery and supercapacitor into a hybrid system satisfies short-term power from the supercapacitor and long-term energy from the battery; this combination increases the longer service life of the battery by reducing battery stress. The supercapacitor is very effective in supplying a power gap lasting from a few seconds to a few minutes to reduce peak power usage from the battery. The supercapacitor can be recharged very quickly even during regenerative braking, whereas regenerating the kinetic energy to electric energy could improve the energy storage capability of the EV, due to recovered energy, by converting the braking torque into energy-based saving [333]. However, this kind of charging is not sustainable. On the other hand, it could charge the supercapacitor rather than waste the braking energy within a short time, about 0.1-20 seconds, based on the capacity of the supercapacitor.

The supercapacitor interfaces combined usages of the energy resources in a synergistic way to strategies and attribute power flow, which is working ideally as a peak load enhancer to deliver high current on acceleration. Using the supercapacitor prevents building the voltage sag during the acceleration of the EV. Another function of the supercapacitor is to back up the battery and to provide power until the battery stabilises. However, hybridization of the EV energy storage systems makes the energy management problem more complicated, where reasonable energy management strategy is required to:

- Manage the energy and power expenditure to meet the proportional vehicle demand without harming the resources and shortening its longevity.
- Manage the charging of energy storage systems as the main control unit in a decentralised charging strategy or assistant control unit in a centralised charging strategy.
- Establish a method of power split between the energy resources to interface the power discharging requirement of the EV into the microgrid.

The strategy of sharing power and energy management between the battery and the supercapacitor, presented in [334], is academically implemented on a small vehicle based on its journey on the New York driving cycle in order to estimate the instantaneous traction power and the capability of the power delivery of resources, as shown in Figure 6-6 A-D. The parameters for a typical, small EV are assumed as shown in Table 6-2 [335]. The figures show that the required power of the motor increases when the speed of the vehicle is increased. Therefore, the motor is accelerated within 36 seconds from zero to 93.5 kph for the first three patterns and within 68 seconds from zero to 87 kph for the fourth pattern of the journey, as shown in Figure 6-6-A. The power required from the motor is 7.7 kw at 93.5 kph and 16.2 kw at 87 kph, as shown in Figure 6-6-B.

The supercapacitor delivers power at an instant until the motor builds its power to feed the motor with the rated power of the battery. At the same time, the power of the supercapacitor reduces proportionally with the increasing power of the motor to feed the rest of the net power, as shown in Figure 6-6 C and D. The braking regenerative power from the motor charges the supercapacitor four times at seconds (64, 124, 184, and 346) at different amounts of power, as shown in Figure 6-6-D

Table 6-2: Parameters for a typical small EV.

Aerodynamic drag coefficient	0.19
The vehicle equivalent frontal area	1.8 m^2
The coefficient of rolling resistance	0.015
Mass of vehicle with two passengers	820 Kg
Tyre radius	0.261 m
Estimated gear efficiency	0.91
Density of air	1.25 Kgm^{-3}
Road gradient	0

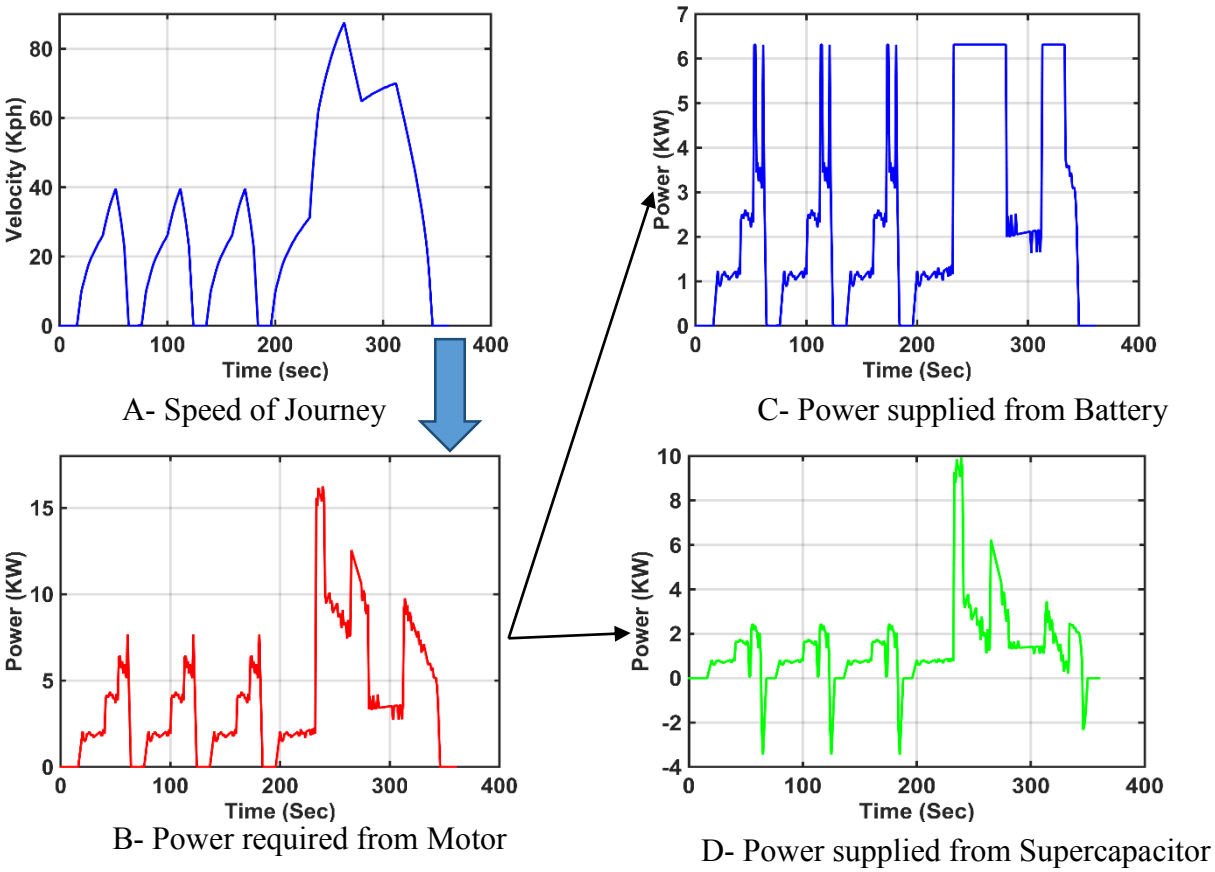

Figure 6-6: The capability of the power delivery of the battery and supercapacitor for a small vehicle based on NYCC driving cycle.

The strategic power and energy management requires an efficient bidirectional converter to control the power flow of resources of the EV at maximum efficiency.

6.5 Traditional Converter Topology versus Multi-Level Converter Topology

Multilevel inverter technology is a very important alternative in the area of high-power medium-voltage energy control. The multilevel inverter performs the power conversion in small voltage steps by utilising a higher number of active semiconductor switches, whereas the traditional topology obtains a controllable voltage in two levels. The main difference between them is explained in the next two sections.

6.5.1 Traditional converter topology

A DC-DC voltage conversion topology is a variation of the standard buck and boost converters, as shown in Figure 6-7. The switching device with the parallel diode of the converter operates at the switching frequency and duty cycle to achieve a specific DC output voltage. It consists of two switching devices, which are alternately gated, and an inductor connected in series with a DC source, in addition to shunt capacitors to filter the waveform. The switching gate works synchronously to rectify power in a bidirectional mode that functions as a buck converter in

one direction and boost converter in the other direction. The duty cycle directs the voltage conversion ratio in both directions that makes one switch on whereas the other is off in a time cycle. Current flows through the circuit according to the voltage difference and series impedance between the resources. Furthermore, the current flows through the inductor in either direction at all times. Therefore, the inductor just works in a continuous mode. However, this topology is not capable of providing large voltage conversion ratios. In the other words, this topology is not efficient enough to provide a duty cycle less than 10% in the case of a high voltage ratio required, such as 200V:10V where the duty cycle is 5%; in addition to a high voltage ratio, it requires uneconomical switches that should operate at high peak voltage and high peak current [336, Sec. 2.1].

This topology works with various conversion ratios; however, the circuit should perform over a varied range of voltages. To achieve efficient performance, keep magnetic flux within limits, and handle a high voltage conversion ratio, the input and output of the circuit should be isolated. By adding a transformer as an isolator the duty cycle could reduce the voltage and current rating by lowering the voltage at the low voltage side and lowering the current at the high voltage side.

The inductor, which is the main magnetic energy storage component of the traditional converter topology, could add a ripple to the circuit. The ripple should be reduced by adding a shunt capacitor to filter the waveform. The more ripple that is produced, the larger the capacitor that should be used, which is a nonlinear phenomenon; however, the capacitor slows the control system response to variations in the output voltage. The higher the capacitor is integrated, the slower the response achieved, as shown in the follows: [336, Sec. 2.1].

$$C = \frac{I_L \times D}{V_{pp} \times f_s \times (1 - D)} \qquad 6\text{-}32$$

The capacitor has dissipative equivalent series resistance (ESR). This resistance causes a voltage droop that increases the actual voltage ripple in addition to creating power dissipation problems in the circuit. Figure 6-8, Figure 6-9 and Figure 6-10 show the ripple that adds to the DC circuit inductor, capacitor, and both of them, respectively.

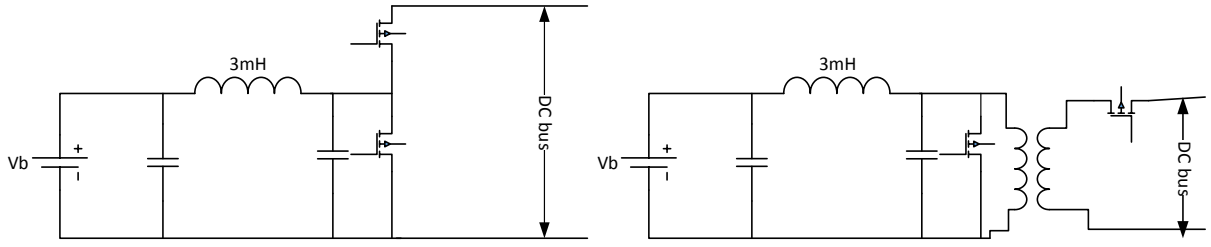

Figure 6-7: Bidirectional converter topology

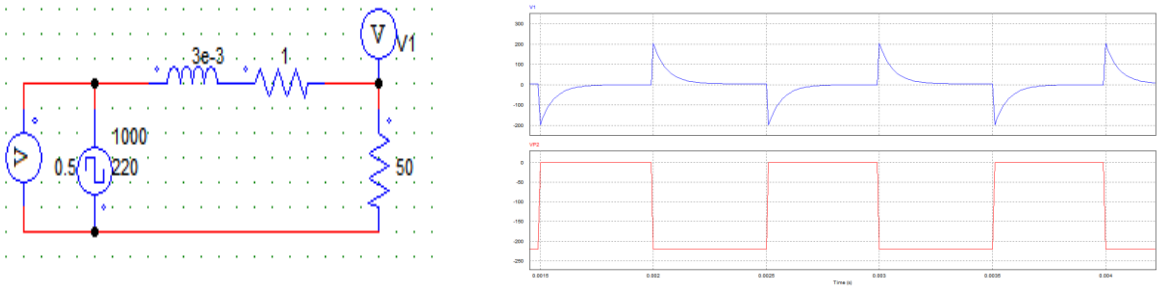

Figure 6-8: Voltage ripple due to inductor

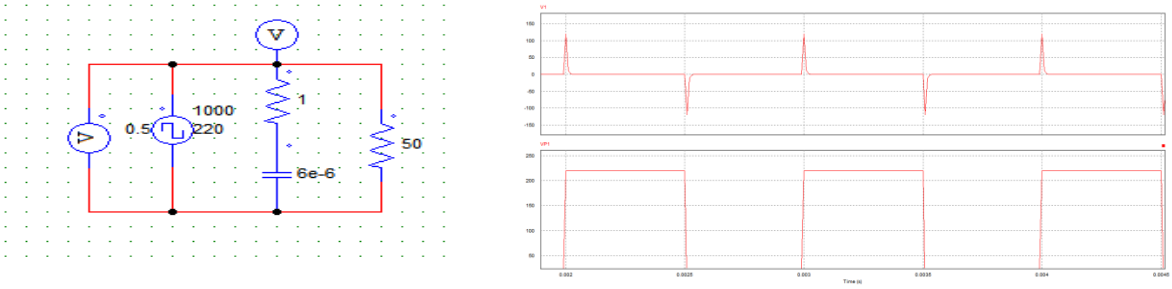

Figure 6-9: Voltage ripple due to capacitor

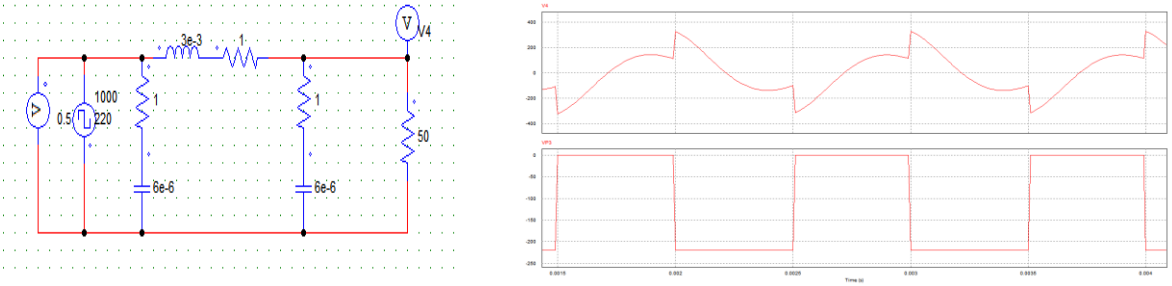

Figure 6-10: Voltage ripple due to both inductor and capacitor

Ripple on the circuit could increase the harmonics of the system by increasing the nonlinearity. Fewer ripples produce less edge of continuous inductor current mode, and less RMS switch current. Therefore, large inductance is integrated with the circuit to reduce the ripple's effect. However, large inductance increases physical size, weight, cost, and complicated of the controller to the application based on the required voltage rating and flux. The effect of various magnetic flux currents (magnetisation effect) could be observed in the switching devices. The magnetisation effect adds large RMS current and more losses on the switches; in addition, a current saturation spike could happen. On the other hand, connecting many EVs to the microgrid with a large sized inductor could increase the inductive characteristics of the microgrid which then causes a negative impact on the power factor.

Due to the resistivity of the inductive materials, which are made of one long wound piece of wire, high parasitic resistances are likely to be included in the circuit. Therefore, a fraction of the dissipated power is produced by the converter, as formulated by [337].

$$\frac{V_0}{V_i} = \frac{-D}{\frac{R_L}{R(1-D)} + 1 - D} \qquad 6\text{-}33$$

If the inductor resistance is zero, the equation above becomes equal to that of the ideal case; however, when the RL increases, the voltage gain of the converter decreases compared with the ideal case. Furthermore, the influence of RL increases with the duty cycle. This is summarised in Figure 6-11.

Integrating the inductor of the converter with the distribution line of the network makes the line characteristically more inductive, which reduces both the voltage of the line and the power factor of the network. Therefore, a large bank of capacitors should be connected to the distribution network to handle the effect of the inductor.

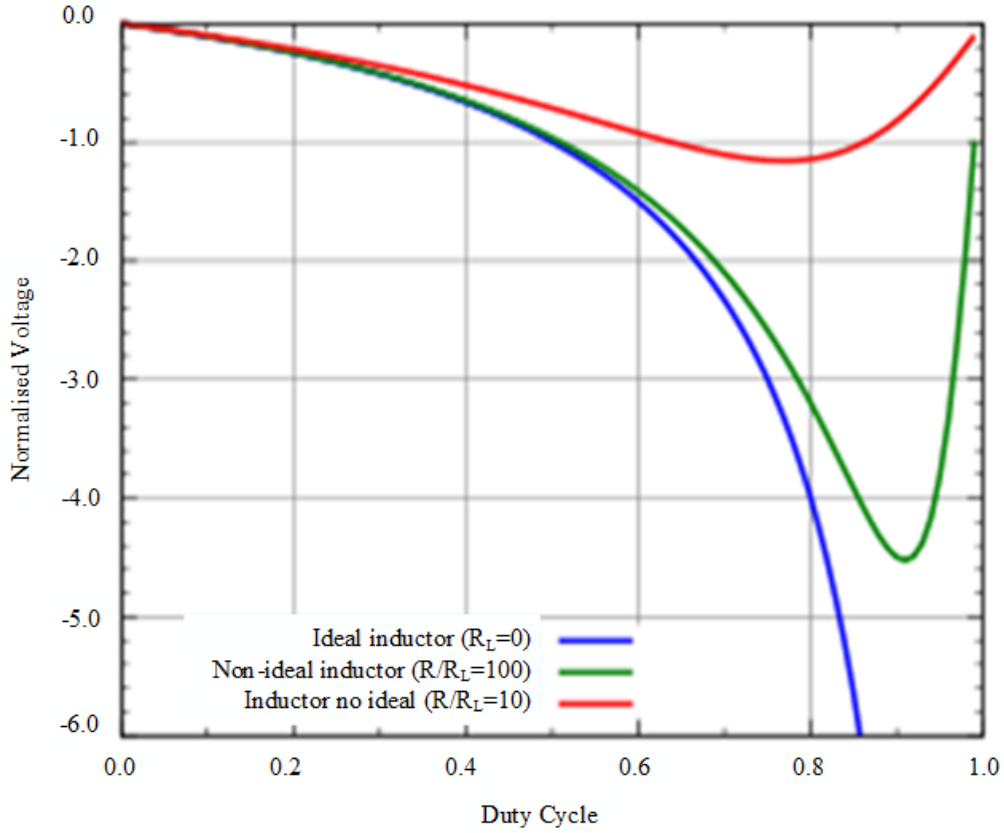

Figure 6-11: Evolution of the output voltage of a buck–boost converter with the duty cycle when the parasitic resistance of the inductor increases [337].

There are two common types of closed loop controller used in bidirectional traditional topology: voltage mode and current mode. The voltage mode controller uses the output voltage feedback compared with a DC reference voltage to adjust the duty cycle of voltage regulation, whereas the current mode controller uses the inductor current feedback compared with output voltage to adjust similar voltage regulation, as shown in Figure 6-12. The literature by researchers provides a good design for the current mode control technique that provides distinct

advantages over the voltage mode control technique. The main advantage of the current mode control technique is limited inductor current by clamping the signal through current protection. However, the current mode controller has a complicated way of working. There are current measuring difficulties with enough bandwidth and stability issues, such as operating the duty cycle above 70%, with peak current control that requires using another technique, such as ramp compensation technique.

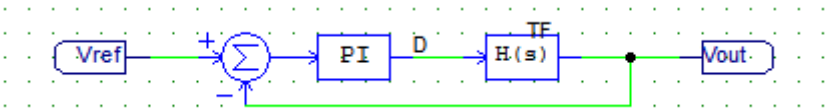

a- Voltage closed loop controller mode

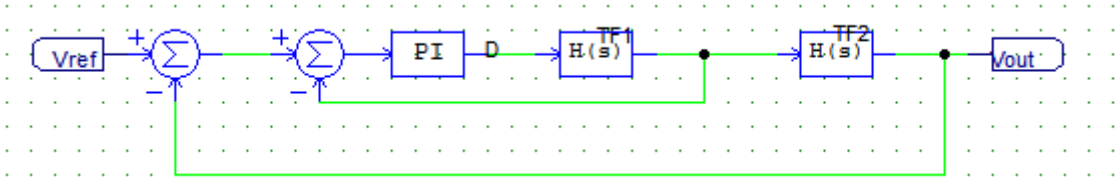

b- Voltage and current loop controller mode

Figure 6-12: Closed loop controller

6.5.2 Multi-Level converter topology

Since there is no need to add an inductor to boost voltage in a modified cascade H-bridge inverter, all the disadvantages listed for the traditional topology are avoided. The modified H-bridge converter works in optimum solution when compared with the traditional topology, where harmonic distortions and EMI can be significantly reduced in addition to the possibility of instantaneous energy transfer. The modified H-bridge converter has a low number of components, modularized circuit layout and packaging, and the variety of switches manage and control the batteries and supercapacitors in a synergistic way. It provides the separation of DC sources, which allows batteries and supercapacitors to be easily accommodated into this multilevel structure; in addition, the inverter works as an isolator between the resources and load. The modified H-bridge converter concept is found to be a most appropriate approach to replace three single cells with one three-phase bridge to apply to the proposed drive train.

The above topology allows using a single battery bank and multi-supercapacitors that can operate as an active filter. The number of switches required to assemble this set is smaller than three single cells and also smaller than a typical five-level cascade, which is made up of six cells or 24 switches, whereas the set at hand only has 18 switches, which can reduce up to 25% of inverter cost. Therefore, the modified cascade H-bridge converter has been chosen according to those advantages.

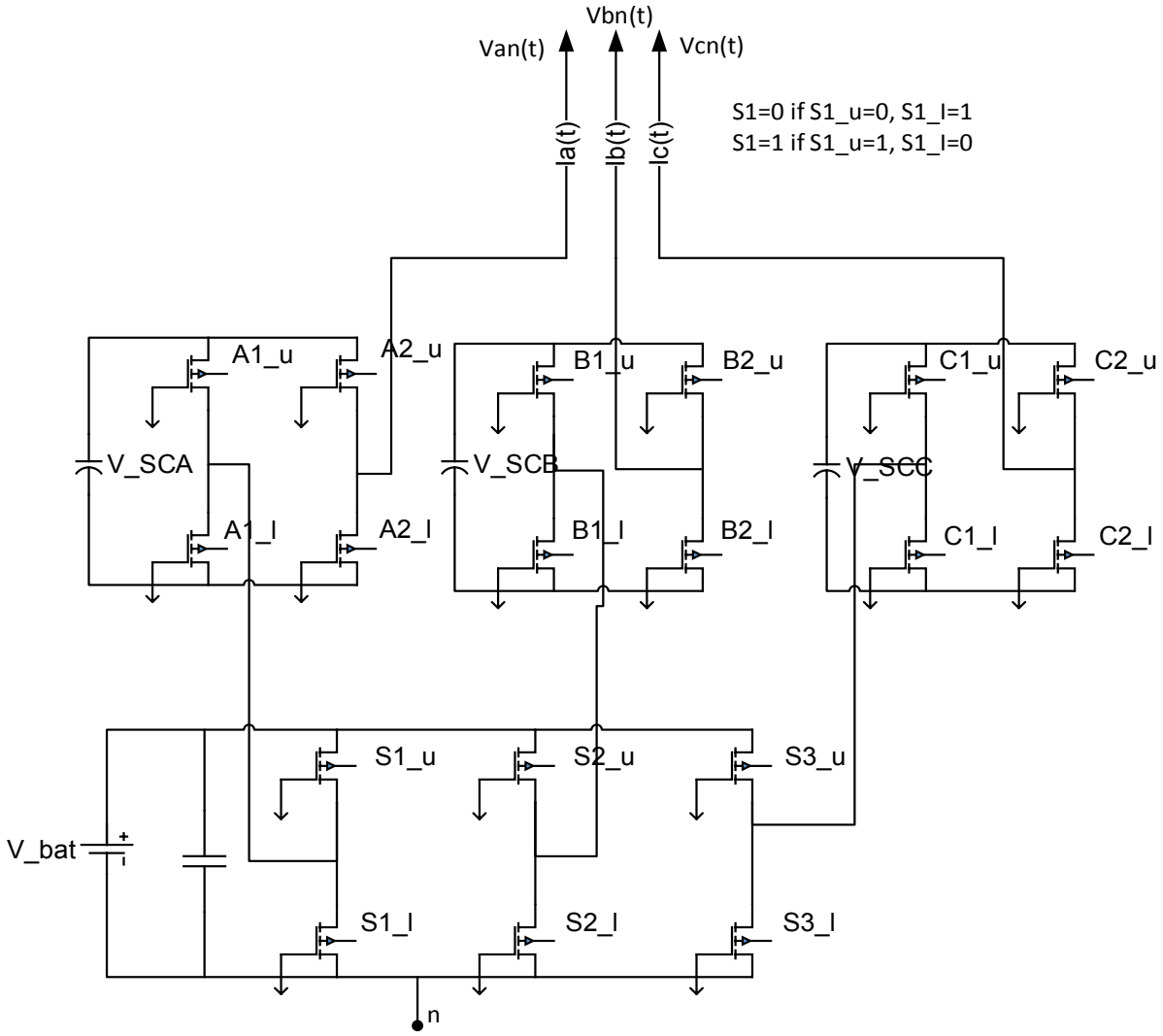

Figure 6-13: Schematic diagram of a modified H-bridge multi-level converter

6.6 Charging Station Systems Infrastructure

A Charging Station System (CSS) is an essential part of the integration of EVs into the microgrid. The CSS requires regulating the active and reactive power exchange between the EV and the microgrid. The active and reactive power exchange is associated directly with the frequency and voltage of the system. The charging station controller is responsible for regulating the integration between the EV and the microgrid to keep the frequency and voltage under certain limits based on the network characteristics. The charging station manages to charge the different dynamic response resources until reaching the desired charging limit state. The CSS is the main interface between the microgrid and mobile energy storage of the EV to improve the response of both.

A modified cascade multi-level H-bridge inverter without inductors has been chosen for this study to achieve good performance both of high power and high efficiency. This topology is supported by the Oak Ridge National Laboratory, which presented at 23-27 September 2007 [338]. It consists of a three-phase bridge with the main DC link fed by a single DC resource

(battery), and each phase series-connected respectively to an H-bridge fed by a floating DC resource (supercapacitor) where the voltage is allowed to vary depending on the energy stored, as shown in Figure 6-13. This type of modified cascade multilevel inverter is selected since the structure is known to deliver a high number of output voltage levels for a relatively low number of switches, and the DC sources are isolated [339], [340].

The output voltage waveform depends on the correlation between the voltages of isolated DC resources $V_{bat}, V_{ca}, V_{cb}, V_{cc}$. The three-phase bridge can generate eight voltage vectors and each single H-bridge can generate four voltage vectors, as illustrated in Table 6-3 and Table 6-4 respectively. The inverter can modify the phase voltage waveform based on the ratio of $\left(\frac{V_{bat}}{V_{sc}}\right)$. The inverter could be treated as one inverter when the voltage ratio is an integer number and the voltages of the supercapacitors are balanced, or separate inverters when the voltage ratio is a fraction number. For a voltage ratio equal to two, the inverter operates in five levels (4/3 V_{dc}, 2/3 V_{dc}, 0, -2/3 V_{dc}, -4/3 V_{dc}). The output phase voltage (V_{an}, V_{bn}, V_{cn}) of the inverter, in reference to the point 'n' of the main voltage resource, can be described as a function of battery voltage (V_{bat}), supercapacitor voltages $(V_{SCA}, V_{SCB}, V_{SCC})$, and switch combinations $(S1, S2, S3, A1, A2, B1, B2, C1, C2)$ as summarised by the following:

$$\mathrm{V_{an}} = \mathrm{V_{bat}}(2.\mathrm{S1} - 1) + \mathrm{V_{SCA}}(\mathrm{A2} - \mathrm{A1}) \quad 6\text{-}34$$

$$\mathrm{V_{bn}} = \mathrm{V_{bat}}(2.\mathrm{S2} - 1) + \mathrm{V_{SCB}}(\mathrm{B2} - \mathrm{B1}) \quad 6\text{-}35$$

$$\mathrm{V_{cn}} = \mathrm{V_{bat}}(2.\mathrm{S3} - 1) + \mathrm{V_{SCC}}(\mathrm{C2} - \mathrm{C1}) \quad 6\text{-}36$$

Converting those three-phase voltages in the time domain by Clark alpha-beta transformation into stationary space vectors two-phase plane $\left(V_{alpha}, V_{beta}\right)$ as formulatd by

$$\mathrm{V_{alpha}} = \frac{2}{3}\left(V_{an} - \frac{1}{2}V_{bn} - \frac{1}{2}V_{cn}\right) \quad 6\text{-}37$$

$$\mathrm{V_{beta}} = \frac{\sqrt{3}}{3}(V_{bn} - V_{cn}) \quad 6\text{-}38$$

,t becomes possible to generate 512 voltage vectors; this is because with nine top and bottom switches there are 2^9 combinations.

Since there is no need to add an inductor to boost voltage in a modified H-bridge converter, all the disadvantages listed for the traditional topology are ignored [341]–[345]. The modified H-bridge converter is working in optimum solution compared with a traditional topology where immediate energy transfer is possible. Furthermore, harmonic distortions and EMI can be significantly reduced [346]. The modified H-bridge converter was chosen because it has many advantages. It has a low number of components, modularized circuit layout and packaging, and a variety of switching states that control the battery and supercapacitors. It also provides separation between DC resources, which allows the battery and supercapacitors to be easily accommodated.

This inverter is suitable for EV application as it has two kinds of resources based on criteria such as:

- using fewer components to reduce the cost and weight of the EV.
- engaging the resources of EV in converter topology.
- easier and more flexible in control than other existing topologies for the same purpose.
- provides a variety of switching states to emerge a variety of discharging active and reactive power from the resources.
- converts the waveforms of two types of resources with different dynamic effect – DC and AC directly, without the intermediary device.
- emerges between symmetrical waveforms of the battery with three separate supercapacitors to deal with balanced and unbalanced systems, whereas the battery connected to the three phase bridge inverter and each supercapacitor is connected to the H-bridge converter.
- the possibility to operate the inverter as a synchroniser to synchronise the EV with the microgrid.

The net power to run the motor at different speeds along the journey results from the collaboration between the power of the battery and the supercapacitors. The regenerative braking power from the motor is saved in the supercapacitors [334], [347]. Moreover, the converter is suitable to connect the EV to the microgrid for charging the resources or discharging the required power from the resources in an emergency situation [348]. The converter has a low distortion effect on the microgrid due to the absence of the inductor. Therefore, this topology of the converter could build high waveform quality in addition to using the supercapacitor to enhance the power factor of the microgrid [331]. Such a system is very complicated to switch. The best way to analyse this complexity is by using a multi-level space vector modulation of the multilevel inverter.

Table 6-3: Standard three-leg inverter generation pattern

Space vector	Switching state (Sx_u)	On-state switch	Vector definition	Alpha definition	Beta Definition	Vector
$\vec{V_0}$	[000]	S_4, S_6, S_2	$V_1 = 0$	0	0	0
$\vec{V_1}$	[100]	S_1, S_6, S_2	$V_1 = \frac{2}{3}V_{dc}e^{j0}$	$\frac{2}{3}V_{dc}$	0	V_{0°
$\vec{V_2}$	[110]	S_1, S_3, S_2	$V_2 = \frac{2}{3}V_{dc}e^{j\frac{\pi}{3}}$	$\frac{1}{3}V_{dc}$	$\frac{1}{\sqrt{3}}V_{dc}$	V_{60°
$\vec{V_3}$	[010]	S_4, S_3, S_2	$V_3 = \frac{2}{3}V_{dc}e^{j\frac{2\pi}{3}}$	$-\frac{1}{3}V_{dc}$	$\frac{1}{\sqrt{3}}V_{dc}$	V_{120°
$\vec{V_4}$	[011]	S_4, S_3, S_5	$V_4 = \frac{2}{3}V_{dc}e^{j\frac{3\pi}{3}}$	$-\frac{2}{3}V_{dc}$	0	V_{180°
$\vec{V_5}$	[001]	S_4, S_6, S_5	$V_5 = \frac{2}{3}V_{dc}e^{j\frac{4\pi}{3}}$	$-\frac{1}{3}V_{dc}$	$-\frac{1}{\sqrt{3}}V_{dc}$	V_{240°
$\vec{V_6}$	[101]	S_1, S_6, S_5	$V_6 = \frac{2}{3}V_{dc}e^{j\frac{5\pi}{3}}$	$\frac{1}{3}V_{dc}$	$-\frac{1}{\sqrt{3}}V_{dc}$	V_{300°
$\vec{V_7}$	[111]	S_1, S_3, S_5	$V_7 = \frac{2}{3}V_{dc}e^{j0}$	0	0	0

Table 6-4: H-bridge generation pattern

Space vector	Switching state (Ax_u)	On-state switch	Vector definition	Vector
$\overrightarrow{V_0}$	[00]	S_{A3}, S_{A4} $B3 \quad B4$ $C3 \quad C4$	$V_0 = 0$	$V_{0^\circ}, V_{180^\circ}$ $V_{60^\circ}, V_{240^\circ}$ $V_{120^\circ}, V_{300^\circ}$
$\overrightarrow{V_1}$	[01]	S_{A3}, S_{A2} $B3 \quad B2$ $C3 \quad C2$	$V_1 = V_{dc}$	$V_{0^\circ}, V_{180^\circ}$ $V_{60^\circ}, V_{240^\circ}$ $V_{120^\circ}, V_{300^\circ}$
$\overrightarrow{V_2}$	[10]	S_{A1}, S_{A4} $B1 \quad B4$ $C1 \quad C4$	$V_2 = -V_{dc}$	$V_{0^\circ}, V_{180^\circ}$ $V_{60^\circ}, V_{240^\circ}$ $V_{120^\circ}, V_{300^\circ}$
$\overrightarrow{V_3}$	[11]	S_{A1}, S_{A2} $B1 \quad B2$ $C1 \quad C2$	$V_3 = 0$	$V_{0^\circ}, V_{180^\circ}$ $V_{60^\circ}, V_{240^\circ}$ $V_{120^\circ}, V_{300^\circ}$

6.7 Adoption of Hierarchical Management Concept for Power and Energy Management

The following sections details the operation of each shell in hierarchical management concept to power and energy management of the EVO. The following sections describe the operation of each shell in hierarchical management concept to power and energy management of the EVO within EMS, PMS, and PES respectively.

6.7.1 Energy management shell (EMS)

The EMS is intended to satisfy the power balance of the battery and supercapacitors. The operation of the EMS is responsible for a long-term decision due to the slower dynamic parameters, such as the power and SoC of the battery and supercapacitors in addition to the process step of control operation. Decisions are taken by the EMS based on the parameters with a time constant that is expressed in seconds. These parameters are the frequency, voltage and current of the microgrid, and the state of charge and power limit of the battery and supercapacitors.

An important control issue related to the resources voltage of the converter is switching the reference signal. The reference signal must be provided from a positive sequence component to reduce the harmonic effect on the switching controller. However, the distribution network is likely to work in an unbalanced condition. Therefore, the network measurement signal contains positive, negative, and zero sequence components at the fundamental frequency. The first part of the controller focuses on measuring the positive signal using a positive sequence voltage detector.

The operation of the inverter must be identified according to the power direction either charging or discharging. The battery and supercapacitors are connected in series. Therefore, one kind of the resources could be charged at the same time by either the battery or the supercapacitors. Charging the battery switches the H-bridge off whereas charging the

supercapacitors switches the three-phase bridge inverter off. The smart charger is responsible for identifying the priority of working mode of the inverter whereas the EVA is responsible for applying the operation of working mode of the inverter. The priority of charging is considered to be charging the supercapacitors to full state of charge and the battery to the desired state of charge respectively.

The EVA collaborates with the smart charger to determine the priority of operation and the required time to reach the desired state of charge for both resources at the rated power of the inverter. The smart charger, which knows the tariff of the microgrid from the microgrid market, collects the information about the period of connection and how much power is needed to reach the desired state of charge from the EVA. It also selects the cheapest tariff time to charge the supercapacitors and the battery. The smart charger sends an order to the EVA to activate the charging mode and the amount of power that it should use. The EVA sets the references to the control agent of the inverter to start the stages of the controller. The strategy of the controller can be classified according to their dependency on the frequency deviation and voltage deviation into either charging or discharging power.

Several casual control methods of the positive sequence voltage detector, droop controller, and vector controller are applied which are investigated extensively below:

6.7.1.1 Positive sequence voltage detector

Normally the distribution system works in the unbalanced condition. The unbalance waveform contains three parts which are positive, negative and zero sequences at the fundamental frequency in addition to the harmonics from any sequence components at a different frequency. One of the most important aspects of a power electronic controller is measuring the fundamental positive sequence voltage component. Quicker and more accurate responses detect the phase and amplitude of the positive sequence component; the fastest response that can be achieved by the converter controller. However, the dynamic response of the PLL of the voltage unbalanced signal becomes slower than the voltage balanced signal [349]. That is determined by using the positive sequence voltage detector in control steps, which increases control accuracy. However, it slows the operation of the system.

The primary voltage detector works based on instantaneous power calculation to filter the fundamental positive sequence from the unbalanced input waveform; the power is calculated from transferring the input V_{abc}voltage waveform to the $V_{\alpha\beta0}$ and $i_{\alpha\beta0}$ current waveform using a phase lock loop.

The three phase voltage is detecting from the grid bus bar. Then, the detecting signal transfers to the alpha beta axes voltage waveform using Clarke's transformation. It is used together with $\bar{i_\alpha}$ and $\bar{i_\beta}$ that are produced by PLL to calculate p and q. The $\bar{i_\alpha}$ and $\bar{i_\beta}$ that are produced by PLL derive only from the positive current sequence at the fundamental frequency. The general equation of alpha-beta-zero current waveforms of accurate fundamental frequency (ω_1) is revealed by

$$i_\alpha = \sqrt{3} I_{+1} \sin(\omega_1 t + \delta_{+1}) \quad 6\text{-}39$$

$$i_\beta = -\sqrt{3} I_{+1} \cos(\omega_1 t + \delta_{+1}) \quad 6\text{-}40$$

For simplicity, just the accurate fundamental frequency (ω_1) should be calculated by PLL from the equations above because the magnitude and angle of i_α and i_β are not important and can be chosen arbitrarily. Therefore, the alpha-beta-zero current waveforms can be reconstructed as

$$\bar{i_\alpha} = \sin(\omega_1 t) \quad 6\text{-}41$$

$$\bar{i_\beta} = \cos(\omega_1 t) \quad 6\text{-}42$$

The power is calculated based on dual p-q theory with the following form.

$$\begin{bmatrix} p \\ q \end{bmatrix} = \begin{bmatrix} i_\alpha & i_\beta \\ -i_\beta & i_\alpha \end{bmatrix} \begin{bmatrix} v_\alpha \\ v_\beta \end{bmatrix} \quad 6\text{-}43$$

The average power is obtained from the power signal using a second-order low-pass filter with a cut-off frequency of 50 Hz.

The instantaneous voltages $\overline{V_\alpha}$ and $\overline{V_\beta}$ are calculated by

$$\begin{bmatrix} \overline{v_\alpha} \\ \overline{v_\beta} \end{bmatrix} = \frac{1}{\overline{i_\alpha^2} + \overline{i_\beta^2}} \begin{bmatrix} \overline{i_\alpha} & -\overline{i_\beta} \\ \overline{i_\beta} & \overline{i_\alpha} \end{bmatrix} \begin{bmatrix} \bar{p} \\ \bar{q} \end{bmatrix} \quad 6\text{-}44$$

In the steady state $\overline{i_\alpha^2} + \overline{i_\beta^2} = \sin^2(\omega_1 t) + \cos^2(\omega_1 t) = 1$

The inverse Clark's transformation is applied to calculate $\overline{V_a}$, $\overline{V_b}$, and $\overline{V_c}$ as follows:

$$\begin{bmatrix} \overline{V_a} \\ \overline{V_b} \\ \overline{V_c} \end{bmatrix} = \sqrt{\frac{2}{3}} \begin{bmatrix} 1 & 0 \\ -\frac{1}{2} & \frac{\sqrt{3}}{2} \\ -\frac{1}{2} & -\frac{\sqrt{3}}{2} \end{bmatrix} \begin{bmatrix} \overline{V_\alpha} \\ \overline{V_\beta} \end{bmatrix} \quad 6\text{-}45$$

The most important part of the detector circuit is the PLL circuit, which is supposed to track the fundamental frequency waveform continuously under distorted and unbalanced voltage waveforms. An effective synchronising circuit to detect the system frequency and phase angle of the positive component is described in [350, Sec. 4.2.2], whereas the block diagram is shown in Figure 6-15. Figure 6-14 shows the control block diagram to detect the fundamental voltage positive sequence waveform.

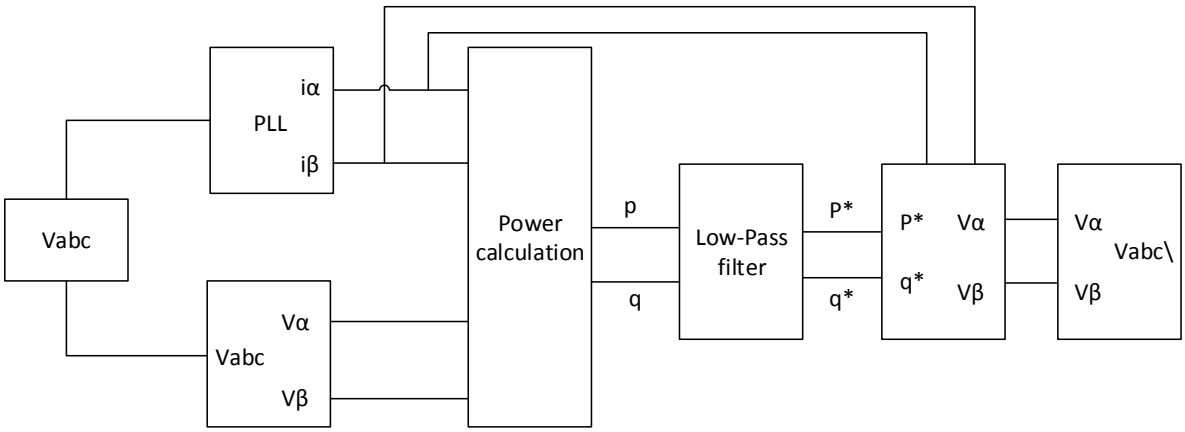

Figure 6-14: Block diagram to detect the fundamental voltage positive sequence.

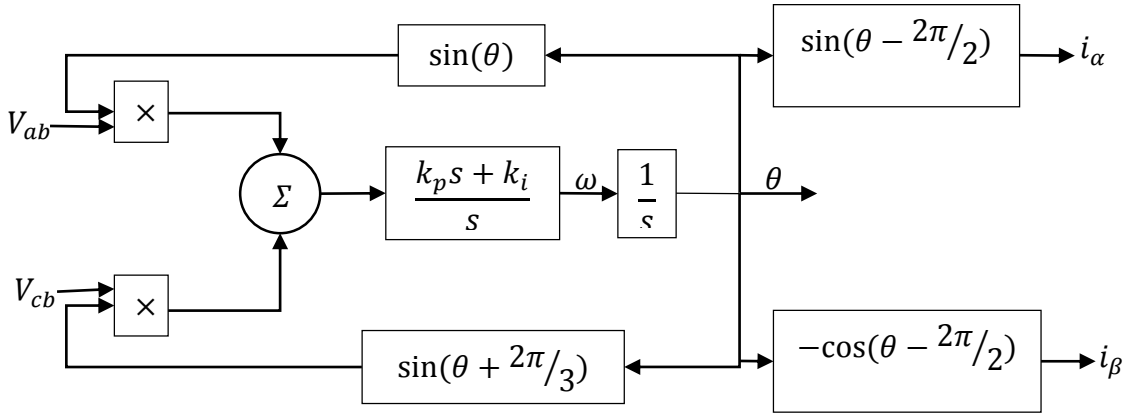

Figure 6-15: Block diagram of the PLL circuit [350, p. 142]

6.7.1.2 Droop controller

The frequency and voltage that are produced by the inverter must be in equilibrium with the microgrid in the discharging mode. The unbalance between them causes a frequency deviation and voltage deviation of the system from a set point value. The purpose of the droop controller is to make sure that the value of the frequency and the voltage of the system keep around the set point values by adjusting the active and reactive power of the inverter.

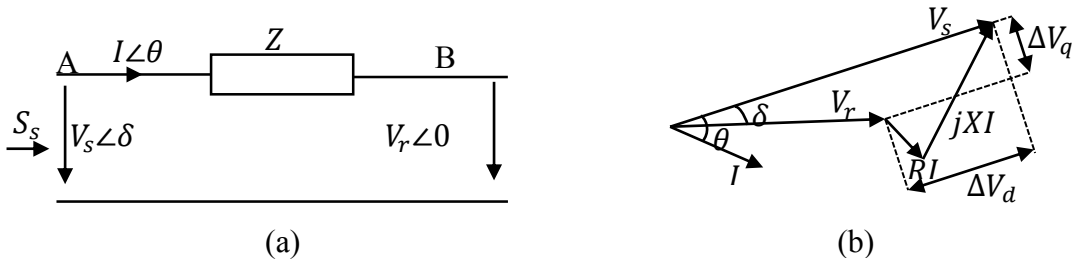

Figure 6-16: (a) Represents power flow through a line. (b) Represents the phasors diagram

Power transfer between two nodes in the distribution line are represented in Figure 6-16. The power transfer between two nodes in the steady state based on the short line model and complex phasors of the distribution network is derived in the following [283, Sec. 2.6], [351, Sec. 6.3].

$$S_r = P_r + jQ_r = V_r I^* = V_r \left(\frac{V_s \angle \delta - V_r}{Z}\right)^* \quad 6\text{-}46$$

$$P_r + jQ_r = V_r \left(\frac{V_s e^{-j\delta} - V_r}{Z e^{-j\theta}}\right) \quad 6\text{-}47$$

where δ refers to the load angle and θ refers to the power factor angle at point A. The active and reactive power flowing in the line is expressed by

$$P_r + jQ_r = \frac{V_s V_r}{Z} e^{j(\theta-\delta)} - \frac{V_r^2}{Z} e^{j\theta} \quad 6\text{-}48$$

$$P_r = \frac{V_s V_r}{Z}\cos(\theta - \delta) - \frac{V_r^2}{Z}\cos(\theta) \quad 6\text{-}49$$

$$Q_r = \frac{V_s V_r}{Z}\sin(\theta - \delta) - \frac{V_r^2}{Z}\sin(\theta) \quad 6\text{-}50$$

where $R = Z\cos\theta$ and $X = Z\sin\theta$

$$P_r = \frac{V_r}{R^2 + X^2}(RV_s\cos\delta + XV_s\sin\delta - RV_r) \quad 6\text{-}51$$

$$Q_r = \frac{V_r}{R^2 + X^2}(XV_s\cos\delta - RV_s\sin\delta - XV_r) \quad 6\text{-}52$$

Hence

$$\Delta V_d = V_s cos\delta - V_r = \frac{RP_r + XQ_r}{V_r} \quad 6\text{-}53$$

$$\Delta V_q = V_r sin\delta = \frac{XP_r - RQ_r}{V_r} \quad 6\text{-}54$$

$$\Delta V = \sqrt{{\Delta V_d}^2 + {\Delta V_q}^2} \quad 6\text{-}55$$

$$\Delta V = \sqrt{\frac{(R^2 + X^2)(P_r^2 + Q_r^2)}{V_r^2}} \quad 6\text{-}56$$

In contrast to the transmission line, the distribution network is more likely to be of a resistive than reactive nature. Therefore, in the distribution network, both R and X should be considered in distribution line parameters.

The active and reactive powers are modified by using an orthogonal linear, rotational transformation matrix T form, as shown by [269].

$$\begin{bmatrix}\overline{P}\\ \overline{Q}\end{bmatrix} = T\begin{bmatrix}P\\ Q\end{bmatrix} = \begin{bmatrix}\cos\varphi & -\sin\varphi\\ \sin\varphi & \cos\varphi\end{bmatrix}\begin{bmatrix}P\\ Q\end{bmatrix} = \begin{bmatrix}\frac{X}{Z} & -\frac{R}{Z}\\ \frac{R}{Z} & \frac{X}{Z}\end{bmatrix}\begin{bmatrix}P\\ Q\end{bmatrix} \quad 6\text{-}57$$

where

$$\varphi = {}^{\pi}/_{2} - \theta = \tan^{-1}\left(\frac{R}{X}\right)$$

From 6-51, 6-52 and 6-57, it is possible to conclude the following:

$$\sin\delta = \frac{Z\overline{P_r}}{V_s V_r} \quad 6\text{-}58$$

$$V_s\cos\delta - V_r = \frac{Z\overline{Q_r}}{V_r} \quad 6\text{-}59$$

At a small power angle and small voltage difference, equations 6-58 and 6-59 show that the power angle and voltage difference depend mainly on the active power $\overline{P}$ and the reactive power $\overline{Q}$ respectively. Control of frequency dynamically depends on the power angle control. Thus, the frequency and voltage of the inverter could be controlled by adjusting the active power P and reactive power Q respectively.

The optimal frequency and voltage droop regulation become as in the following equations:

$$f - f_0 = -m(\overline{P} - \overline{P_0}) = -m\frac{X}{Z}(P - P_0) + m\frac{R}{Z}(Q - Q_0) \quad 6\text{-}60$$

$$V - V_0 = -q(\overline{Q} - \overline{Q_0}) = -q\frac{R}{Z}(P - P_0) - q\frac{X}{Z}(Q - Q_0) \quad 6\text{-}61$$

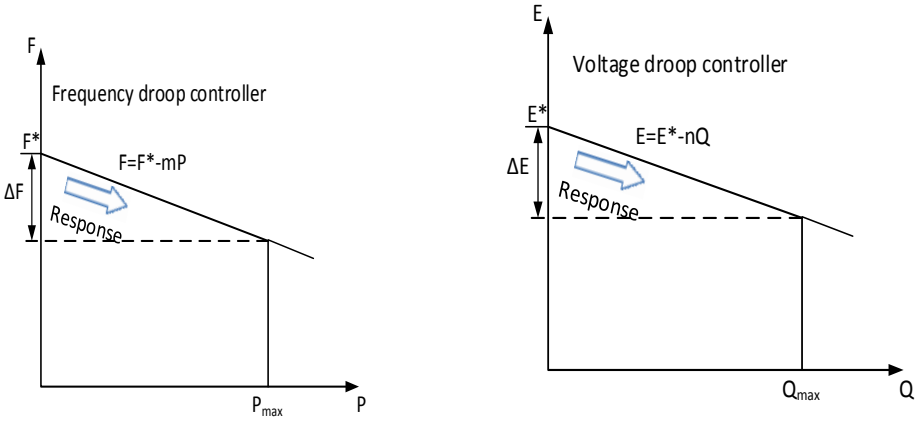

Figure 6-17: Frequency and voltage droop characteristics

The active and reactive current drawing from the inverter can be calculated by

$$I_a = \frac{P_r}{V_r} = \frac{(RV_s\cos\delta + XV_s\sin\delta - RV_r)}{R^2 + X^2} \quad 6\text{-}62$$

$$I_a = \frac{P_s}{V_s} = \frac{(RV_s - RV_r\cos\delta + XV_r\sin\delta)}{R^2 + X^2} \quad 6\text{-}63$$

$$I_r = \frac{Q_r}{V_r} = \frac{(XV_s\cos\delta - RV_s\sin\delta - XV_r)}{R^2 + X^2} \quad 6\text{-}64$$

$$I_r = \frac{Q_s}{V_s} = \frac{(XV_s - XV_r\cos\delta - RV_r\sin\delta)}{R^2 + X^2} \quad 6\text{-}65$$

$$I = \sqrt{I_a^2 + I_r^2} \quad 6\text{-}66$$

Following the active and reactive power, the active and reactive current is modified as follows.

$$\begin{bmatrix}\overline{I_a}\\ \overline{I_r}\end{bmatrix} = T\begin{bmatrix}I_a\\ I_r\end{bmatrix} \quad 6\text{-}67$$

Thus

$$\bar{I_a} = \frac{\bar{P_r}}{V_r} = \frac{V_s \sin\delta}{Z} \quad 6\text{-}68$$

$$\bar{I_r} = \frac{\overline{Q_r}}{V_r} = \frac{V_s \cos\delta - V_r}{Z} \quad 6\text{-}69$$

The equations to obtain the nominal power are discussed in the next section.

6.7.1.2.1 Reference of droop controller

Various kinds of EVs from different brands will be connected to the microgrid at different times with different resources capacity and state of charge. Consequently, it is not wise to apply the same discharging reference to all of them. Therefore, the reference of power controller has been chosen based on the integration of the EV with the distribution line and the rate of the energy storage device. The virtual natural load is given by equation 6-70.

$$\bar{P_0} = P_0\sqrt{1 + K_d} \quad 6\text{-}70$$

The parameter K_d is useful to measure the required reactive power rating of the compensating equipment. Shunt capacitive compensation increases the virtual natural load of the line. The generalised circuit constants of the distribution line with EV compensation can be calculated by:

$$A_0 = \cosh(j\bar{\theta}) - j\sinh(j\bar{\theta}).K_d\bar{\theta} \quad 6\text{-}71$$

$$B_0 = \sinh(j\bar{\theta}).Z_0R \quad 6\text{-}72$$

$$C_0 = \sinh(j\bar{\theta}).\left(\frac{1}{Z_0R}\right) - j\cosh(j\bar{\theta}).\frac{K_d\theta}{Z_0} \quad 6\text{-}73$$

$$D_0 = \cosh(j\bar{\theta}) \quad 6\text{-}74$$

The sending end voltage at the EV socket is:

$$v_s = A_0 v_r + B_0 i_r \quad 6\text{-}75$$

$$i_r = \frac{V_s\angle\delta - A_0 V_r}{B_0} \quad 6\text{-}76$$

$$i_r^* = \frac{V_s(b_1 + jb_2)(\cos\delta - j\sin\delta) - v_r(b_1 + jb_2)(a_1 - ja_2)}{b_1^2 + b_2^2} \quad 6\text{-}77$$

$$i_r^* v_r = \frac{V_s v_r(b_1\cos\delta + b_2\sin\delta) - v_r^2(a_1b_1 + a_2b_2)}{b_1^2 + b_2^2} + j\frac{V_s v_r(b_2\cos\delta - b_1\sin\delta) - v_r^2(a_1b_2 - a_2b_1)}{b_1^2 + b_2^2} \quad 6\text{-}78$$

$$S_r = P_r + jQ_r = v_r \times i_r^* \quad 6\text{-}79$$

$$P_r = \frac{V_s v_r(b_1\cos\delta + b_2\sin\delta) - v_r^2(a_1b_1 + a_2b_2)}{b_1^2 + b_2^2} \quad 6\text{-}80$$

$$Q_r = \frac{V_s v_r(b_2\cos\delta - b_1\sin\delta) - v_r^2(a_1b_2 - a_2b_1)}{b_1^2 + b_2^2} \quad 6\text{-}81$$

where $A_0 = a_1 + ja_2$ and $B_0 = b_1 + jb_2$ are the generalised line constants for the compensated distribution line.

The maximum power transfer criterion is determined by considering the singularity of the Jacobian matrix. For stable operation, the singularity of the Jacobian matrix can be rearranged as follows:

$$\begin{bmatrix} P_r \\ Q_r \end{bmatrix} = \begin{bmatrix} \frac{\partial P_r}{\partial \delta} & \frac{\partial P_r}{\partial v_r} \\ \frac{\partial Q_r}{\partial \delta} & \frac{\partial Q_r}{\partial v_r} \end{bmatrix} \times \begin{bmatrix} \delta \\ v_r \end{bmatrix} \quad 6\text{-}82$$

$$\frac{\partial P_r}{\partial \delta}\frac{\partial Q_r}{\partial v_r} - \frac{\partial P_r}{\partial v_r}\frac{\partial Q_r}{\partial \delta} = 0 \quad 6\text{-}83$$

$$\frac{\partial P_r}{\partial \delta} = \frac{v_s v_r(b_2 cos\delta - b_1 sin\delta)}{b_1^2 + b_2^2} \quad 6\text{-}84$$

$$\frac{\partial Q_r}{\partial v_r} = \frac{v_s(b_2 cos\delta - b_1 sin\delta) - 2v_r(a_1 b_2 - a_2 b_1)}{b_1^2 + b_2^2} \quad 6\text{-}85$$

$$\frac{\partial P_r}{\partial v_r} = \frac{v_s(b_1 cos\delta + b_2 sin\delta) - 2v_r(a_1 b_1 + a_2 b_2)}{b_1^2 + b_2^2} \quad 6\text{-}86$$

$$\frac{\partial Q_r}{\partial \delta} = \frac{v_s v_r(-b_1 cos\delta - b_2 sin\delta)}{b_1^2 + b_2^2} \quad 6\text{-}87$$

$$v_{rc} = \frac{v_s}{2(a_1 cos\delta + a_2 sin\delta)} \quad 6\text{-}88$$

$$P_r = \frac{2v_s^2(a_1 cos\delta + a_2 sin\delta)(b_1 cos\delta + b_2 sin\delta) - v_s^2(a_1 b_1 + a_2 b_2)}{4(a_1 cos\delta + a_2 sin\delta)^2(b_1^2 + b_2^2)} \quad 6\text{-}89$$

$$Q_r = \frac{2v_s^2(a_1 cos\delta + a_2 sin\delta)(b_2 cos\delta - b_1 sin\delta) - v_s^2(a_1 b_2 - a_2 b_1)}{4(a_1 cos\delta + a_2 sin\delta)^2(b_1^2 + b_2^2)} \quad 6\text{-}90$$

Determination of critical angular separation δ, which is very difficult to measure, to make the reference signal, depends mainly on the characteristic equation of the distribution line of the CSO and the power factor of the microgrid. the relationship between the active and reactive power with power factor angle can be written as:

$$P_r tan\theta = Q_r \quad 6\text{-}91$$

based on equation 6-91, it is possible to derive the following equations.

$$\frac{P_r}{Q_r} = \frac{(a_1 b_1 - a_2 b_2) + (a_1 b_2 + a_2 b_1)\tan(2\delta)}{(a_1 b_1 - a_2 b_2)\tan(2\delta) - (a_1 b_2 + a_2 b_1)} \quad 6\text{-}92$$

$$\delta = \frac{1}{2}\tan^{-1}\left(\frac{a_1(b_1 tan\theta + b_2) + a_2(b_1 - b_2 tan\theta)}{a_1(b_1 - b_2 tan\theta) - a_2(b_1 tan\theta + b_2)}\right) \quad 6\text{-}93$$

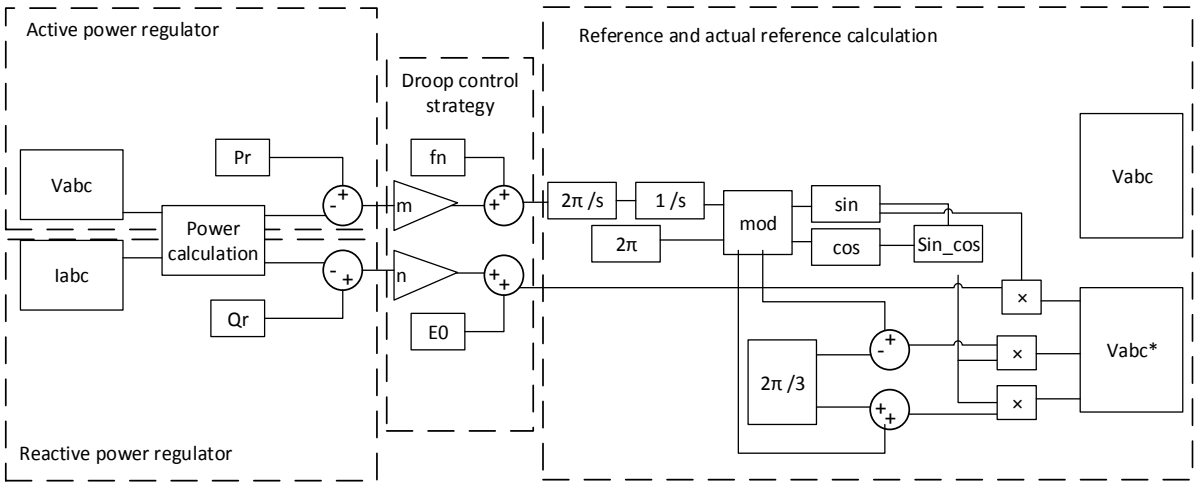

Figure 6-18: Schematic diagram of droop controller

The voltage and frequency restoration from 209.2 V and 49.864 Hz to nominal value 220V and 50 Hz are shown in Figure 6-19 and Figure 6-20 respectively. The duration time of responding the droop controller to restore the voltage from the beginning of disturbance at 0.495 to the nominal voltage at 0.525 took 0.03 seconds whereas the duration time to restore the frequency from the beginning of disturbance at 0.495 to the nominal frequency at 0.528 took 0.033 seconds.

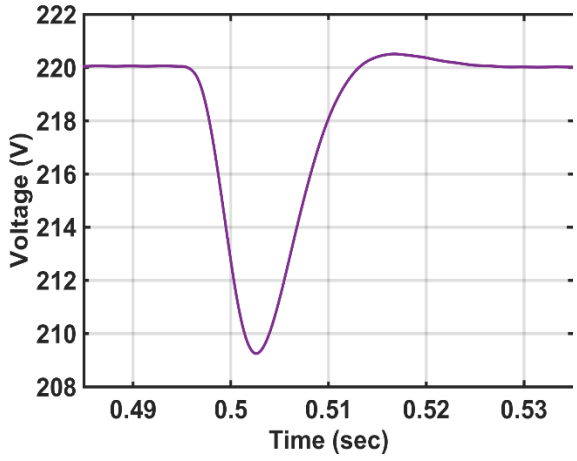

Figure 6-19: Voltage restoration

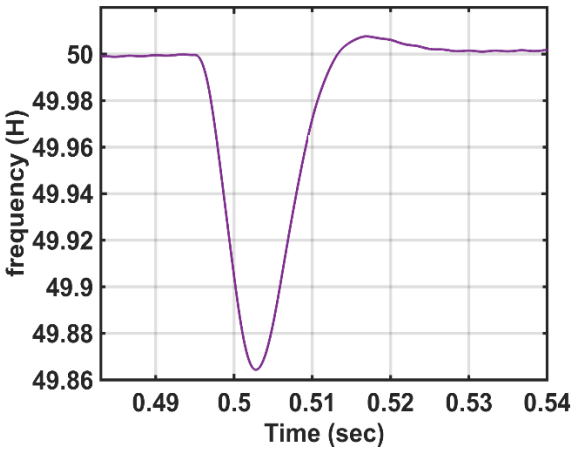

Figure 6-20: Frequency restoration

6.7.1.3 Vector controller

The droop controller restores the frequency and voltage of the system to the set point value. The direct and quadrature voltage stationary frame can be found from the voltage and frequency restoration after the droop controller as well as the rotation angle of the grid. The vector controller is part of the EMS to feed a reference signal of the PMS and configures the synchronisation operation of EV within the microgrid to equalise the line voltage, frequency, phase sequence, and phase angle. On the other hand, the EMS is responsible for interacting the EVO with the CSO at the centralised operation of the EV or interact the

smart charger and EVA with the connected bus bar of the microgrid to measure the voltage and frequency at the decentralised operation of the EV.

$$\theta = \int \omega(t)dt + \theta_{int} \quad 6\text{-}94$$

The three-phase voltage is found using the following equations:

$$V_a^* = Esin(wt) \quad 6\text{-}95$$

$$V_b^* = Esin(\omega t - {}^{2\pi}/_{3}) \quad 6\text{-}96$$

$$V_c^* = Esin(\omega t + {}^{2\pi}/_{3}) \quad 6\text{-}97$$

The instantaneous stationary reference of the three-phase voltage is calculated and transformed to the time invariant $d-q-0$ synchronous rotating reference frame with the angular velocity ω by using Park's transformation, as follows:

$$\begin{bmatrix} V_d \\ V_q \\ V_0 \end{bmatrix} = \begin{bmatrix} \cos(\omega t) & \sin(\omega t) & 0 \\ -\sin(\omega t) & \cos(\omega t) & 0 \\ 0 & 0 & 1 \end{bmatrix} \begin{bmatrix} V_a \\ V_b \\ V_c \end{bmatrix} \quad 6\text{-}98$$

The vector controller is the primary controller of the EMS shell which is divided into three parts: power, voltage, and current controller. The main objective of the power controller is controlling the active and reactive currents that are drawn from the EV independently at the connected terminal. Thus, the active and reactive power injected from the EV to the microgrid are used to enhance the angle stability or voltage stability of the system. It is possible to depend on the d-q rotating frame to control the active current (i_d) and reactive current (i_q) injection from the EV independently. The function of the active and reactive current controllers is finding the change in injection of i_d and i_q in the d-q rotating frame. The objective of the frequency and voltage controllers is changing the active and reactive power of the resources of the EV based on the frequency deviation and voltage deviation respectively, as represented in equations 6-99 and 6-100. The change of the active power and the reactive power that are drawn from the resources of the EV follow from the d-q component of the V_m, ΔI_d, and ΔI_qas represented in equations 6-101 to 6-104. This controller is implemented within the vector controller, as shown in Figure 6-21.

The voltage controller compares the voltage references d-axis and q-axis from the droop controller block (secondary controller) with microgrid voltage d-axis and q-axis respectively. Then, the comparison value is entered to the PI controller which is used to achieve a zero steady-state error and stabilise the output voltage. The corresponding state equations of the voltage block controller are given in equations 6-105 and 6-106.

The current controller compares the voltage block controller using the PI controller to achieve the output current. The corresponding state equations of the current block controller are given in equations 6-107 and 6-108. The response of the primary controller is fast because it uses local measurement only without needing any communication medium. The block diagram of the primary controller is shown in the following:

$$\Delta P = m\Delta f \quad 6\text{-}99$$

$$\Delta Q = n\Delta V \tag{6-100}$$

$$\Delta P = \sqrt{\frac{3}{2}} V_m \Delta I_d \tag{6-101}$$

$$\Delta I_d = \frac{m}{\sqrt{\frac{3}{2}} V_m} \Delta f \tag{6-102}$$

$$\Delta Q = \sqrt{\frac{3}{2}} V_m \Delta I_q \tag{6-103}$$

$$\Delta I_q = \frac{n}{\sqrt{\frac{3}{2}} V_m} \Delta V \tag{6-104}$$

$$I_{d,ref} = \Delta I_d - \omega_n C_f V_q + K_{pv}\left(V_{d,ref} - V_d\right) + \int K_{iv}(V_{d,ref} - V_d)\, dt \tag{6-105}$$

$$I_{q,ref} = \Delta I_q + \omega_n C_f V_d + K_{pv}\left(V_{q,ref} - V_q\right) + \int K_{iv}(V_{q,ref} - V_q) dt \tag{6-106}$$

$$V_{Id,ref} = -\omega_n L_f I_q + K_{pc}\left(I_{d,ref} - I_d\right) + \int K_{ic}(I_{d,ref} - I_d)\, dt \tag{6-107}$$

$$V_{Iq,ref} = \omega_n L_f I_d + K_{pc}\left(I_{q,ref} - I_q\right) + \int K_{ic}(I_{q,ref} - I_q) dt \tag{6-108}$$

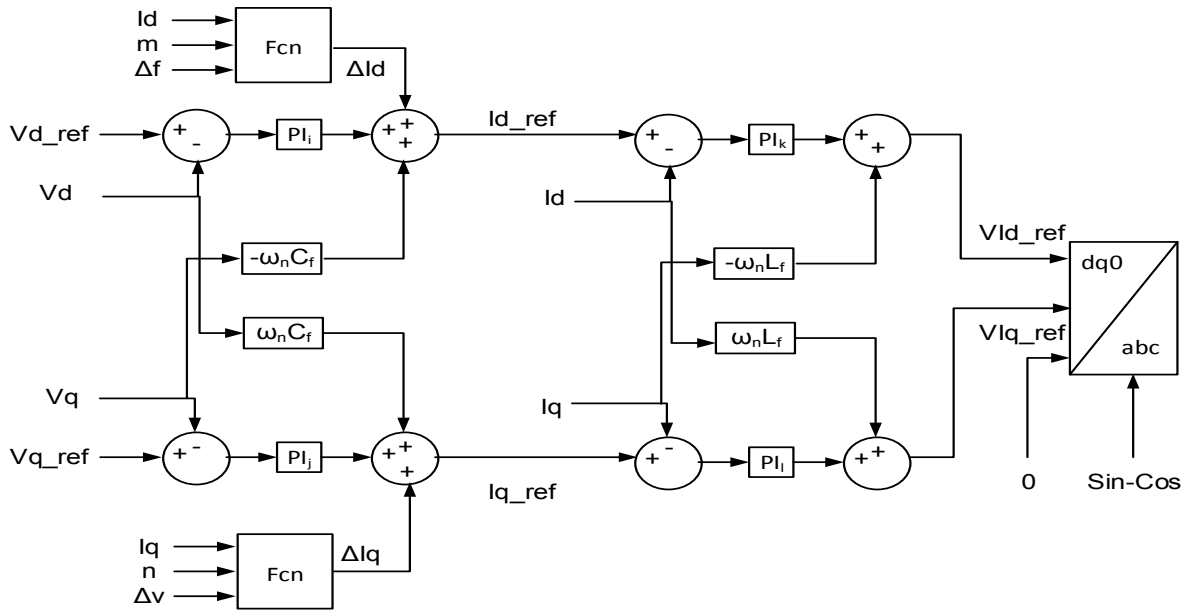

Figure 6-21: Vector controller

6.7.2 Power management shell (PMS)

The objective function of the PMS is to make a decision on either charging or discharging the resources of the EV. The discharging decision is activated in case the mode input by the owner accepts discharging the resources of the EV to a prior definition of the state of charge. The decision made depends on the comparison between the state of the four variables: the frequency of the microgrid, the voltage of the microgrid, the state of charge of the battery, and the state of charge of the supercapacitor. It is assumed that all supercapacitors have a balanced condition and therefore, all of them have the same voltage and state of charge.

The primary goal of PMS is considered in two points. The first point is full charging of the resources of EV but preventing overcharging in a healthy microgrid situation. The second point is discharging the resources of the EV in an emergency situation of the microgrid without exceeding the under-charging limit. The undercharging limit is an acceptable limit of the state of charge of resources to make them capable of delivering power for the next journey of the EV. The benefit to the owner of the vehicle is the discharging power tariff, which is normally higher than the charging power tariff. Heuristic system approaches representation is a candidate for PMS strategy implementation.

A fuzzy inference solution is utilised as a solution to make a logical decision to charge or discharge resources. Measured variables are mapped into fuzzy sets through a fuzzification process. Then, a fuzzy inference engine evaluates the fuzzy sets according to prior defined control rules in the fuzzy logic rule base. Finally, an output set is produced based upon the rule base evaluation. The output of the fuzzy controller represents the power control reference of the battery and the supercapacitors.

The heuristic reasoning is written in a logical way, such as:

Heuristic Reasoning-1

If the frequency of the microgrid is higher than $0.9998F_n$ and the voltage of the microgrid is higher than $0.97V_n$ and the supercapacitor is fully charged, whereas the battery is not fully charged, then the PMS will activate the charging vector's trajectory in PES towards the stored microgrid energy inside the battery, thus the state of charge of the battery increases until reaching 100%.

Heuristic Reasoning-2

If the frequency of the microgrid is less than $0.9998F_n$ and the voltage of the microgrid is higher than $0.97V_n$ and the state of charge of the supercapacitor range is between 40-70%, whereas the state of charge of battery range is between 90-100%, then the PMS will activate the discharging vector's trajectory in PES towards discharging 90% of reference power from the battery and 10% of reference power from the supercapacitors, thus the EV helps the microgrid to stabilize the frequency within standard limits.

The FIS is represented as four inputs, and two outputs in the generic form of conjunctive rules as follows:

$$\underbrace{\text{IF } x_1 \text{ is } A_{i1} \text{AND } x_2 \text{ is } A_{i2} \text{ AND } x_3 \text{ is } A_{i3} \text{ AND } x_4 \text{ is } A_{i4}}_{\text{Fuzzy Rule Antecedent}} \underbrace{THEN\ y_1 = \Psi_i(x_1, x_2, x_3, x_4) \text{ AND } y_2 = 1 - y_1}_{\text{Fuzzy Rule Consequent}} \quad (6\text{-}109)$$

The fuzzy rule antecedents are the frequency of the microgrid, the voltage of the microgrid, the state of charge of the battery, and the state of charge of the supercapacitors, whereas the fuzzy rule consequently is the battery reference trajectory and the supercapacitor reference trajectory. The identification of a rule statement to construct the fuzzy rule base is as follows:

$$\underbrace{FIS \rightarrow \boldsymbol{IF} F_m = FC\ \boldsymbol{AND}\ V_m = VD\ \boldsymbol{AND}\ SoC_b = B9.1\ \boldsymbol{AND}\ SoC_{sc} = S4.7}_{\text{Fuzzy Rule Antecedent}} \underbrace{THEN\ P_b = 0.9P_m\ AND\ P_{sc} = 0.1P_m}_{\text{Fuzzy Rule Consequent}} \quad (6\text{-}110)$$

For the four antecedent fuzzy rule, the firing strength for the i[th] rule is given by [326]

$$\beta_i = \prod_{j=1}^{j_{max}} A_{ij}\,(x_j) \quad (6\text{-}111)$$

where j_{max} corresponds to the maximum number of sensors which are four. The firing strength combines all the fuzzy sets A_{ij} which are associated with the i rule. The fuzzy logic output variable (defuzzication includes all i rules) is evaluated by the following:

$$\mathrm{y}^* = \frac{\sum_{i=1}^{i_{max}} \left(\prod_{j=1}^{j_{max}} A_{ij}(x_j)\right)_i . \mathrm{y}_i}{\sum_{i=1}^{i_{max}} \left(\prod_{j=1}^{j_{max}} A_{ij}(x_j)\right)_i} \quad (6\text{-}112)$$

The graphical illustration of the fuzzy inference system and the range of input values are shown in Figure 6-22. The output regulation parameters, which are the vector trajectory corresponding to the battery and the supercapacitors, feed to the PES to control the switching function. The FIS decision surfaces that are composed of 77 rules are shown in Figure 6-23 to Figure 6-28 which explain the rules of fuzzy logic, whereas at the discharging mode, the battery and supercapacitors respond when the $SoC_b \geq 70\%$ and $SoC_{sc} \geq 40\%$ respectively. Meanwhile, the battery is more responsible for frequency variation, whereas the supercapacitors are more responsible for the voltage variation. However, the battery and supercapacitors exchange roles when one of them fades. The input and output membership functions of the fuzzy system are shown in Figure 6-29 to Figure 6-34.

The base of a fuzzy rule is linked between the frequency deviation of the battery power discharge and the voltage variation with the supercapacitors' power discharge. Therefore, at frequency deviation and if the state of charge of the battery is stronger than the state of charge of the supercapacitor, the battery provides higher power than the supercapacitor. At the low state of charge of the battery, the power provided from the battery and the supercapacitors is a rapprochement.

Any resources which reach the limit of the state of charge-discharge then produce zero power. At voltage deviation, the priority of discharging the supercapacitors is higher than discharging the battery unless the state of charge of the battery is higher than the state of charge of the supercapacitors. Any resources which reach the limit of the state of charge-discharge produce

zero power. The frequency deviation response has a higher priority than the voltage deviation response, due to the sensitivity of the microgrid to frequency deviation. Therefore, the discharging focuses on restoring the frequency first at frequency (angle) stability issue.

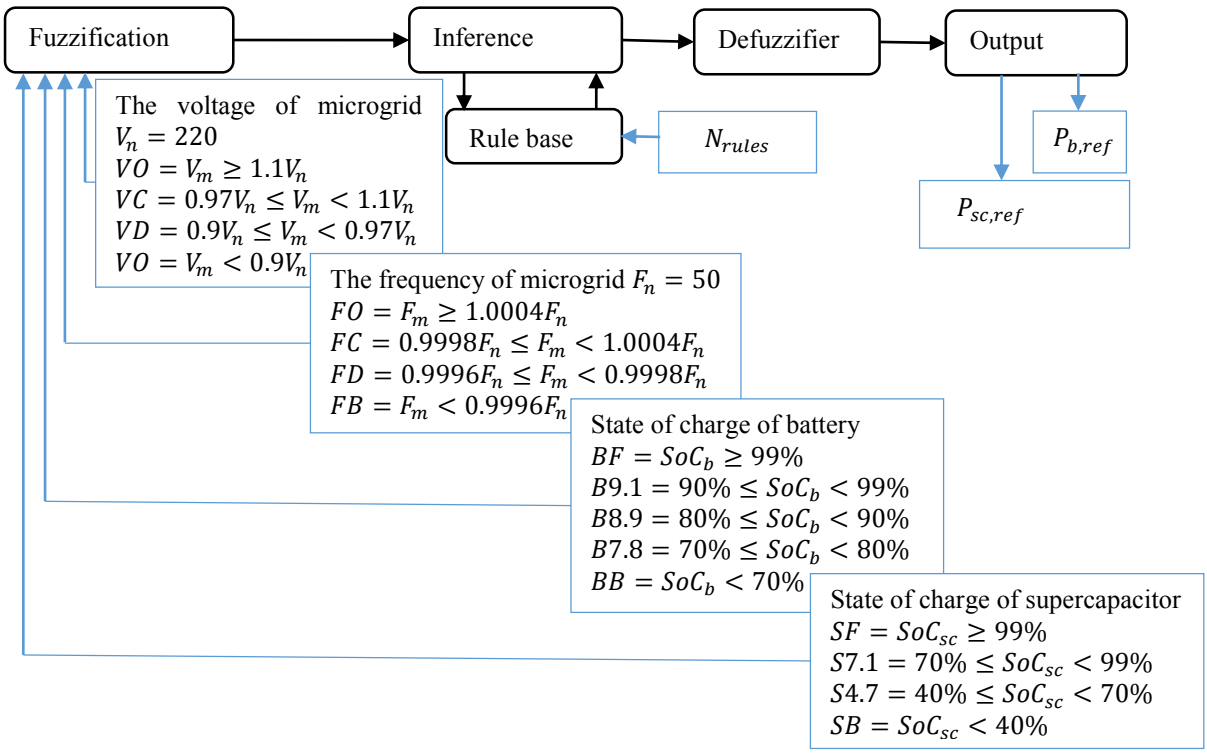

Figure 6-22: PMS fuzzy inference system block diagram

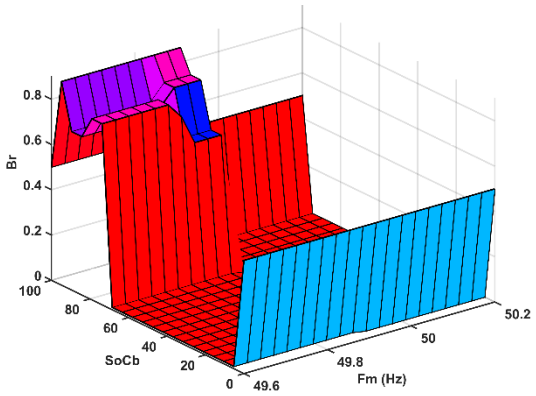

Figure 6-23: Fuzzy rule of battery reference at Vm = 227V and SoCsc = 50%

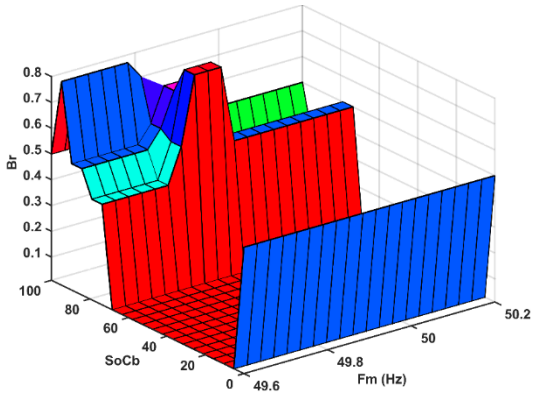

Figure 6-24: Fuzzy rule of battery reference at Vm = 205V and SoCsc = 50%

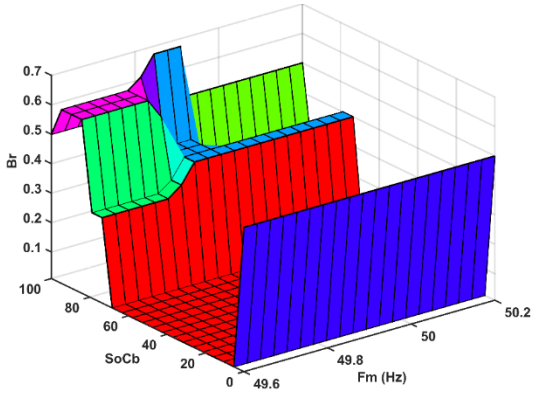

Figure 6-25: Fuzzy rule of battery reference at Vm = 194 and SoCsc = 50%

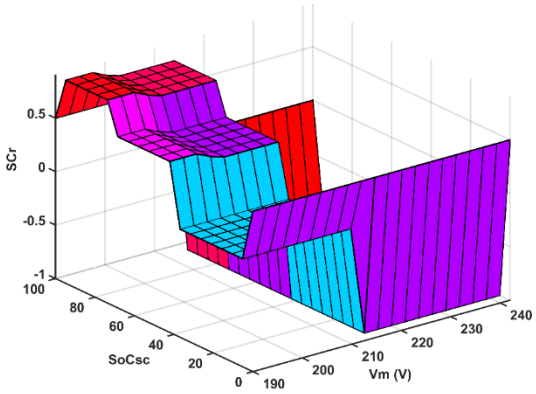

Figure 6-26: Fuzzy rule of supercapacitor reference at Fm = 50Hz and SoCb = 75%

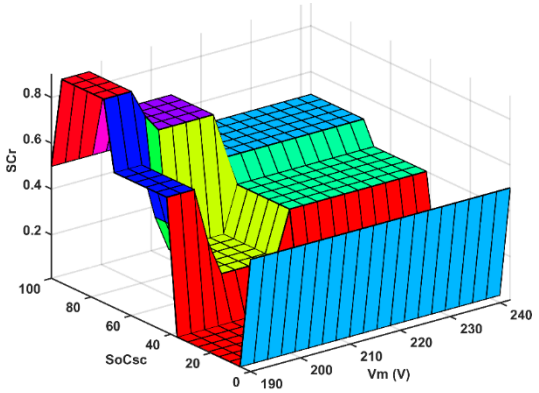

Figure 6-27: Fuzzy rule of supercapacitor reference at Fm = 49.85Hz and SoCb = 75%

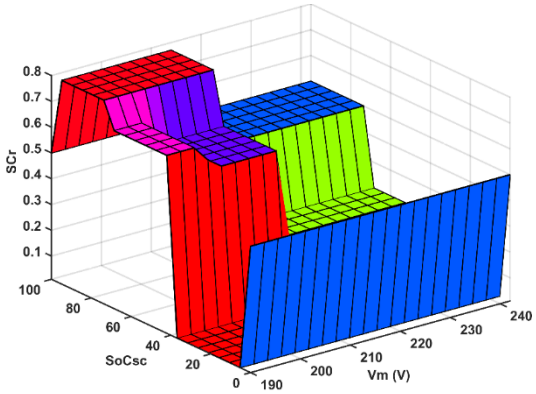

Figure 6-28: Fuzzy rule of supercapacitor reference at Fm = 49.7Hz and SoCb = 75%

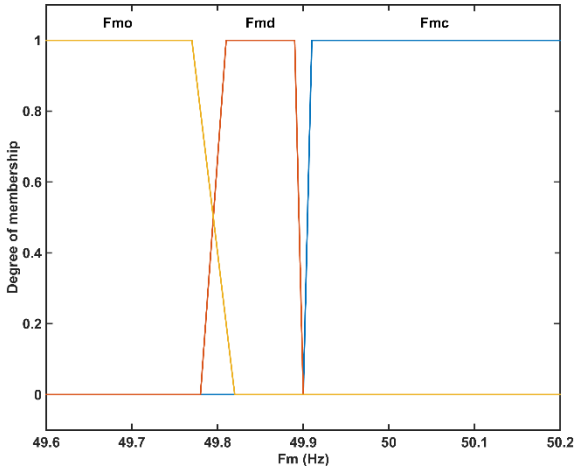

Figure 6-29: Fuzzy Sugeno input membership functions' plots of frequency

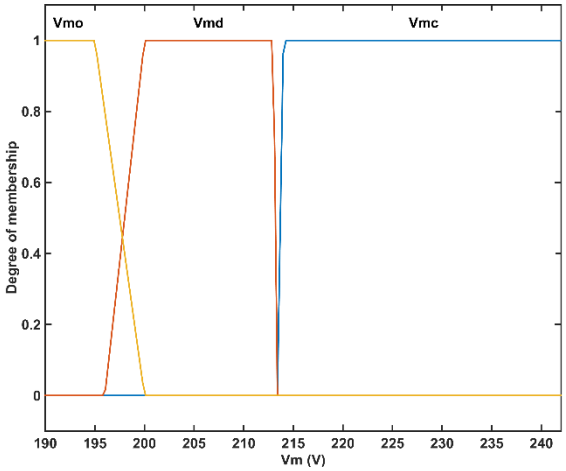

Figure 6-30: Fuzzy Sugeno input membership functions' plots of voltage

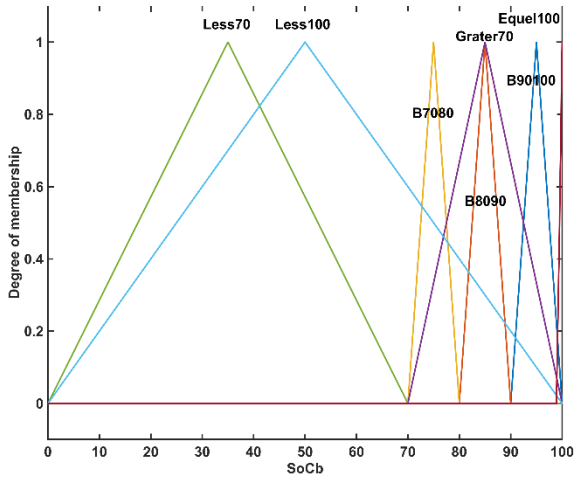

Figure 6-31: Fuzzy Sugeno input membership functions' plots of SoCb

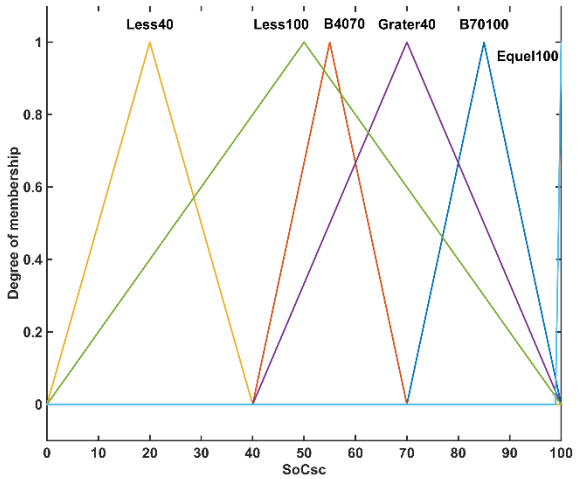

Figure 6-32: Fuzzy Sugeno input membership functions plots' of SoCsc

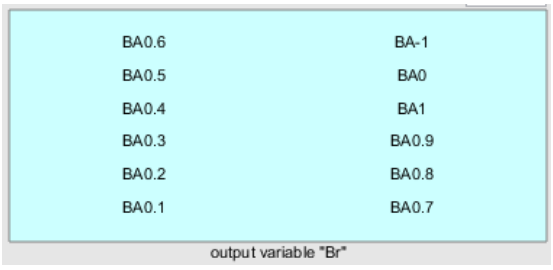

Figure 6-33: Fuzzy Sugeno output weight functions' plots of battery reference

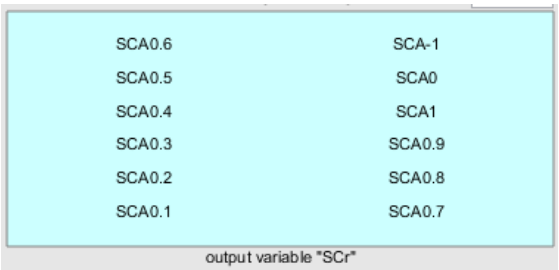

Figure 6-34: Fuzzy Sugeno output weight functions' plots of supercapacitor reference

6.7.3 Power electronic shell (PES)

The PES handles the switching modulation to operate the switches of the inverter ON and OFF. The PMS feeds the PES the reference of battery and supercapacitors, whereas the PES operates the three-phase bridge inverter to achieve the battery reference and the three H-bridges to achieve supercapacitors, reference. The strategy of the switching modulation is explained in the following sections.

6.7.3.1 Space vector PWM algorithm

PES is the downstream process in the hierarchy strategy of the PMS. The PMS sends two reference vectors trajectories in addition to the actual voltage of resources to PES to generate the signal commands. The PES performs the SVPWM form of an actual summation power from multiple energy resources connected to the multilevel inverter. The SVPWM represents the required control of the switching function to transfer DC form to AC form or vice versa. The relationship between the fuzzy logic algorithm and the switching modulation strategy is explained as the priority of operation, whereas the fuzzy belongs to PMS and the space vector algorithm belongs to PES. The PMS priority is higher than the PES. Therefore, the PMS feeds the reference signals to the PES. The configured surface diagram of the fuzzy rule consumes time, whereas the implementation of the fuzzy algorithm has a very fast response, which is

compatible with the execution time of the SVPWM strategy. Therefore, the heuristic fuzzy logic algorithm is preferred to any other heuristic method.

SVPWM has been an active research for many years. It has better performance benefits than other switching techniques such as SPWM, random switching, and hysterics switching. It has acceptable performance for the two-level inverter; however, it is hardly studied with regard to a uniform multi-level converter such as the H-bridge converter. Furthermore, it is much harder studied for modified multi-level inverter such as the topology under study. Most of the SVPWM of a multi-level inverter deals with specific switching states of operation or a particular number of levels because the number of switching increases significantly with increasing the number of levels.

This work deals with M-SVPWM of converters that have an active hybridization of multiple electrical energy storage systems with a different level of voltages. The M-SVPWM for the multi-level inverter is mainly an extension for the two-level SVPWM. The algorithm is formulated based on numerical analysis; it reduces the complexity of the SVPWM of the multilevel converter.

6.7.3.2 State matrix

The states of the modified H-bridge converter, which contains nine legs, are represented as a binary value of nine bits for upper switches. The first three bits b1, b2, b3 represent battery states whereas the other six bits b4, b5, b6, b7, b8, and b9 represent the three phase supercapacitors' states as two bits for each phase. The total number of states is $2^9 = 512$; b=1 when the switch is turned on and b=0 when it is turned off. The lower switches are complementary to the upper switches of inverter legs $b_{lower} = 1 - b_{upper}$. The details of switching states are illustrated in Table 6-5.

The space vector diagram is represented in two phase axes ($\alpha - \beta$ axis) to avoid working on a stationary reference frame. The reference voltage performance is defined as the time integral function that draws a hexagonal locus. The hexagonal diagram contains six sectors to allow an immediate identification of the nearest three vectors. Each sector is divided into the equilateral triangles which are equal to $(number\ of\ levels - 1)^2$. The leg of the triangle represents the DC resource voltage. The tip of the reference voltage could be located in any triangle. The vertices of the triangle that contains the tip of reference voltage represents the switching vectors. The performance waveform of the inverter depends mainly on the selection of these switching states. The detail of switching states for the first sextant is shown in Figure 6-35.

An example provides a good insight for generation reference point A with fewer switching states as shown below:

Point A

1- 000 00 00 00 100 00 00 00 110 00 00 00 111 00 00 00
2- 000 01 00 00 000 01 00 10 000 01 10 10 000 00 10 10
3- 000 00 00 10 000 01 00 10 000 01 00 00 000 01 01 00

4- 000 00 00 10 000 01 00 10 000 01 01 10 000 01 01 00

The other switching is redundant, whereas the state to provide reference B with less switching is given below:

Point B

1- 100 00 00 10 100 01 00 10 100 01 00 00 100 01 01 00

The reference voltage is distributed between the battery and the supercapacitors based on the state of charge of both the voltage level, and the frequency level of the bus bar. The amplitude of the highest voltage vector that could be provided from Clark's transformation is 2/3 of the total supply voltage ($^2/_3 \times (V_{bat} + 2V_{SC})$).

The switching states of the three-phase bridge and H-bridges must be selected with the minimum transition during the sample period to reduce losses, ripples, and harmonics effects. High switching losses and big ripples in output voltage occur in the case of a required high number of switching states. A higher level chooses the lower states available. The sum of the bits chooses either one bit higher or one bit lower to provide optimum switching states. For example, the sum of bits to provide point B is 2, 3, 2 and 3.

Table 6-5: Switching state

		Battery	**Supercapacitor phase-A**	**Supercapacitor phase-B**	**Supercapacitor phase-C**
		$2^0 2^0 2^0$ A B C	$2^0 2^0$ A	$2^0 2^0$ B	$2^0 2^0$ C
1.	Phase A^+	$2^1 2^0 2^0$	$2^0 2^1$		
2.	Phase A^-	$2^0 2^1 2^1$	$2^1 2^0$		
3.	Phase B^+	$2^0 2^1 2^0$		$2^0 2^1$	
4.	Phase B^-	$2^1 2^0 2^1$		$2^1 2^0$	
5.	Phase C^+	$2^0 2^0 2^1$			$2^0 2^1$
6.	Phase C^-	$2^1 2^1 2^0$			$2^1 2^0$
	Total number of states = $2^9 = 512$				

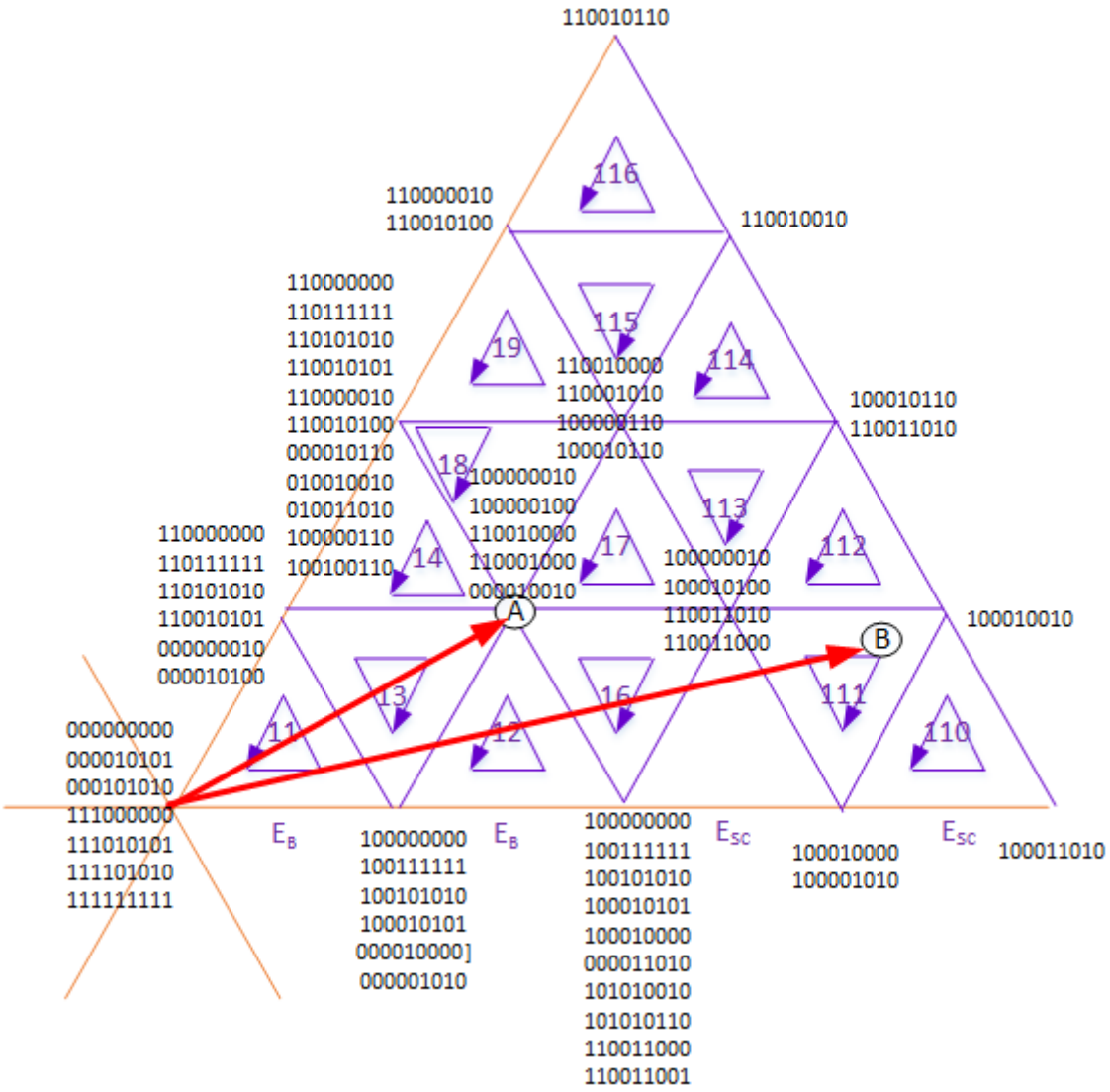

Figure 6-35: Switching state for the first sextant

6.7.3.3 Space vector location

The identification of the nearest three vectors in a multilevel hexagon map depends on the magnitude and angle of the reference voltage. The reference voltage is distributed among the DC resources based on the fuzzy rules. Normally, the hexagonal diagram is divided into six sectors based on the angle of the reference voltage. Each sector is divided into triangles depending on the number of levels $(number\ of\ levels - 1)^2$. The modified H-bridge inverter could operate in four levels or more, based on the voltage ratio between the battery and supercapacitor $(\frac{E_{bat}}{E_{sc}})$. Since the ratio difference is proposed twice in this study, the inverter works in a five-level mode. First of all, it should find the sector number and region number of the reference voltage.

Clarke's transformation is used to obtain the voltage magnitude in the $(\alpha - \beta - 0)$ frame, as follows:

$$\begin{bmatrix} V_\alpha \\ V_\beta \\ V_0 \end{bmatrix} = \frac{2}{3}\begin{bmatrix} 1 & -\frac{1}{2} & -\frac{1}{2} \\ 0 & \frac{\sqrt{3}}{2} & -\frac{\sqrt{3}}{2} \\ \frac{1}{2} & \frac{1}{2} & \frac{1}{2} \end{bmatrix}\begin{bmatrix} V_a \\ V_b \\ V_c \end{bmatrix} \quad 6\text{-}113$$

The vector magnitude and vector angle can be obtained by

$$V_m = \sqrt{V_\alpha^2 + V_\beta^2} \quad 6\text{-}114$$

$$\theta = \tan^{-1}\left(\frac{V_\beta}{V_\alpha}\right) \quad 6\text{-}115$$

The sector of operation and the angle within the sector on the α axis can be determined by

$$S = ceil\left(\frac{\theta}{\pi/3}\right) \quad 6\text{-}116$$

$$\theta_s = rem(\frac{\theta}{\pi/3}) \quad 6\text{-}117$$

where ceil and rem represent the standard function rounded to the high number and reminder respectively.

Based on the parameters of the voltage magnitude and the angle of a sector, the region number is determined based on three parameters k_1, k_2, and k_3, whereas the first, second, and third parameters (k_1, k_2, and k_3) represent the part of the sector inclined at 60, 120 and zero degrees respectively with respect to the α axis. Furthermore, the maximum value that could be obtained for k_1, k_2, and k_3 is one less than the number of the level $(n-1)$.

The numerical analysis to specify the region number from these three parameters is illustrated in the following equations based on the triangle vertices leg length, as shown in Figure 6-36.

$$regionNumber = k_2^2 - k_2 - k_1 + k_3 + 1 \quad 6\text{-}118$$

$$k_1 = ceil(V_\alpha/\sqrt{3}E) \quad 6\text{-}119$$

$$k_2 = ceil\,(\frac{V_\alpha + V_\beta/\sqrt{3}}{E}) \quad 6\text{-}120$$

$$k_3 = ceil(\frac{2V_\beta}{\sqrt{3}E}) \quad 6\text{-}121$$

For example to generate the voltage reference $V_m = 226.716\angle 48.576^\circ$ and $V_m = 265.754\angle 41.186^\circ$, the k_1, k_2, and $k_3$magnitude is as shown in Figure 6-37 and

Table 6-6.

Table 6-6: Example

$V_m = 226.716\angle 48.576^\circ$	$V_m = 265.754\angle 41.186^\circ$
$V_\alpha = 150$	$V_\alpha = 200$
$V_\beta = 170$	$V_\beta = 175$
$E = 100$	$E = 100$
$k_1 = 1$	$k_1 = 2$
$k_2 = 3$	$k_2 = 4$
$k_3 = 2$	$k_3 = 3$
The vector located in triangle eight	The vector located in triangle 14

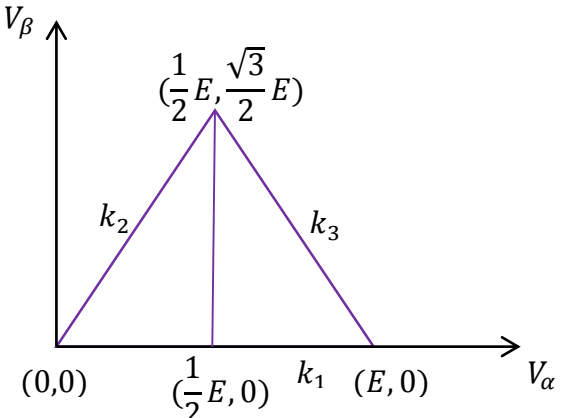

Figure 6-36: Triangle coordinate

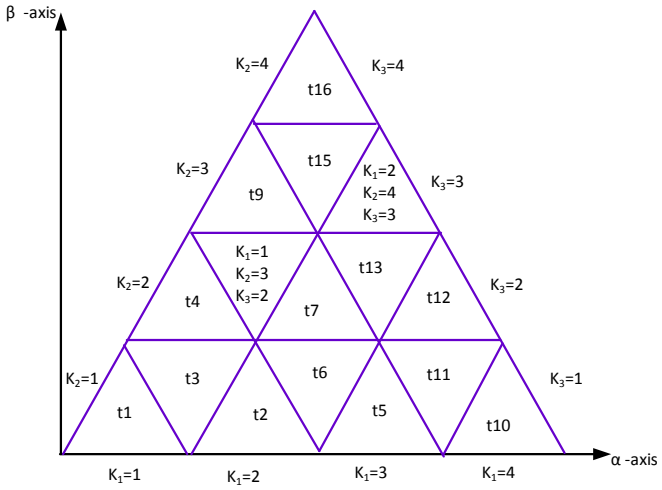

Figure 6-37: The region number according to k_1, k_2, k_3

The modulation index for the modified H-bridge multilevel inverter configuration can be generalised as

$$m_a = \frac{\sqrt{3}V_m}{(n-1)E} \qquad 6\text{-}122$$

The maximum magnitude of the reference vector $V_{m,max}$ corresponding to the radius of the largest circle enclosed inside hexagon diagram can be obtained as follows

$$V_{ref,max} = \frac{2}{3}(n-1)E \times \frac{\sqrt{3}}{2} = \frac{(n-1)E}{\sqrt{3}} \quad 6\text{-}123$$

Substituting 6-123 in 6-122 gives the maximum modulation index

$$m_{a,max} = 1$$

6.7.3.4 Distributing sampling time

After finding the sector number and the triangle number for the reference voltage, three stationary vectors could synthesise the reference voltage. The sampling time for the stationary vectors represents the duty cycle time of the switching states during the whole sampling time (T_s) of the modulation. The dwell time is distributed based on the volt-second integral principle between the chosen states of three vertices of the triangle, as shown in following equations

$$\overrightarrow{V_{ref}}T_s = \overrightarrow{V_1}T_a + \overrightarrow{V_2}T_b + \overrightarrow{V_3}T_0 \quad 6\text{-}124$$

$$T_s = T_a + T_b + T_0 \quad 6\text{-}125$$

where T_a, T_b, and T_0 are the dwell times of the vectors $\overrightarrow{V_1}$, $\overrightarrow{V_2}$, and $\overrightarrow{V_0}$ respectively.

The dwell times are distributed based on the location of V_{ref} as shown below:

If the V_{ref} lies on $\theta = 0^{\circ}$, then $T_b = 0$

If the V_{ref} lies on $\theta = 60^{\circ}$, then $T_a = 0$

If the V_{ref} lies on $\theta = 30^{\circ}$, then $T_a = T_b$

If the V_{ref} lies on $0^{\circ} < \theta < 30^{\circ}$, then $T_a > T_b$

If the V_{ref} lies on $30^{\circ} < \theta < 60^{\circ}$, then $T_a < T_b$

The rotation sequence for each triangle of odd sectors is illustrated in Figure 6-35, whereas the rotation sequence is reversed for even sectors.

A generalised equation of the dwell times can be determined using numerical analysis based on k_1, k_2, and k_3 parameters, as follows

$$\begin{bmatrix} T_s\cos(\theta) \\ T_s\sin(\theta) \\ T_s \end{bmatrix} = \begin{bmatrix} \left(\frac{2k_1 - 1 - k_3}{2}\right)E & \left(\frac{3k_1 - k_2 - 2 + 2k_3}{2}\right)E & \left(\frac{2k_2 - k_3}{2}\right)E \\ (k_3 - 1)E & (k_2 - k_1)E & k_3E \\ 1 & 1 & 1 \end{bmatrix} \begin{bmatrix} t_0 \\ t_1 \\ t_2 \end{bmatrix} \quad 6\text{-}126$$

Solving equation regarding t_0, t_1,and t_2 gives:

$$\begin{bmatrix} t_0 \\ t_1 \\ t_2 \end{bmatrix} = \frac{1}{aE^2} \begin{bmatrix} a_{11}E & a_{12}E & a_{13}E^2 \\ a_{21}E & a_{22}E & a_{23}E^2 \\ a_{31}E & a_{32}E & E^2 \end{bmatrix} \begin{bmatrix} T_s\cos(\theta) \\ T_s\sin(\theta) \\ T_s \end{bmatrix} \quad 6\text{-}127$$

$$a = (2k_1 - 2k_2 + 2k_3 - 1) \quad 6\text{-}128$$

$$a_{11} = (k_2 - k_1 - k_3) \quad 6\text{-}129$$

$$a_{12} = (\frac{3k_2 - 3k_1 - 3k_3 + 2}{2}) \quad 6\text{-}130$$

$$a_{13} = (k_1k_3 + {k_3}^2 - k_3 + k_1k_2 - {k_2}^2)a_{11} = (k_2 - k_1 - k_3) \quad 6\text{-}131$$

$$a_{21} = 1 \quad 6\text{-}132$$

$$a_{22} = -\frac{1}{2} \quad 6\text{-}133$$

$$a_{23} = (k_3 - k_2) \quad 6\text{-}134$$

$$a_{31} = (k_1 - k_2 + k_3 - 1) \quad 6\text{-}135$$

$$a_{32} = (\frac{3k_1 - 3k_2 + 3k_3 - 1}{2}) \quad 6\text{-}136$$

$$a_{33} = ({k_2}^2 - k_1k_2 - k_2 + 2k_1 - k_1k_3 + 2k_3 - 1 - {k_3}^2) \quad 6\text{-}137$$

6.7.3.5 Overmodulation

Normally overmodulation occurs when the modulation index is greater than unity. The operation of overmodulation causes minimum number of line to line voltage pulses, which lead to increasing the nonlinearity of the inverter and the emergence of low order harmonics, such as the 5^{th} and 11^{th}. Furthermore, overmodulation could cause a mismatch between the magnitude of the reference voltage and the angle. Therefore, the magnitude of the reference voltage could change, whereas the angle could transmit without any change. This mismatch gives an unrealistic duration of the zero vectors. All researchers try to avoid working in the overmodulation region due to the difficulty in eliminating the low order harmonics and nonlinearity of power switch characteristics in addition to zero vectors not being used in the overmodulation.

The SVPWM operates based on finding the vertex of the triangle of the hexagon diagram that the reference voltage lies on; then the duty cycle is applied on the three-voltage vector. The trajectory of the reference voltage is circulated and located inside the hexagon diagram until the modulation index reaches the maximum value. At maximum value point, the on the duration of zero vector becomes zero and a negative vector beyond it. The reference voltage trajectory exceeds the hexagon boundary at angle $\frac{k\pi}{3} + \alpha$ to $\frac{k\pi}{3} - \alpha$ where $k = 0, 1, 2, 3, 4, and\ 5$. The overmodulation strategy is based on reprogramming the magnitude of the reference voltage if it reaches the limit of the hexagon boundary, as shown in Figure 6-38, for the first sextant of the space vector modulation. The dashed circle refers to the reference voltage trajectory outside the hexagon boundary. When the reference voltage trajectory passes the hexagon boundary b c, the space vector modulation should modify the duty cycle and locus the reference vector trajectory to make it work in the hexagon boundary based on the region number; it means, moving the reference vector trajectory from dashed line V_{ref} to solid line V_{ref}^{*}.

Following the [352] approach, the equation to reduce locus of V_{ref} to V_{ref}^{*} along the bc line becomes.

$$y = \cos(\frac{\pi}{6})(8E - 2x) \quad 6\text{-}138$$

The equation of line oa is:

$$y = x\tan(\theta_0) \quad 6\text{-}139$$

where $\alpha < \theta_0 < \frac{\pi}{3} - \alpha$

Solving equations 6-138 and 6-139 gives

$$x = \frac{8E\cos(\pi/6)}{\tan(\theta_0) + 2\cos(\pi/6)} \quad 6\text{-}140$$

The limited voltage V_{ref}^{*} can be expressed as a function of x, as follows

$$V_{ref}^{*} = \frac{x}{\cos(\theta_0)} \quad 6\text{-}141$$

From equations 6-140 and 6-141 V_{ref}^{*} becomes as follows

$$V_{ref}^{*} = \frac{8E\cos(\pi/6)}{\sin\left(\theta_0 + \frac{\pi}{3}\right)} \quad 6\text{-}142$$

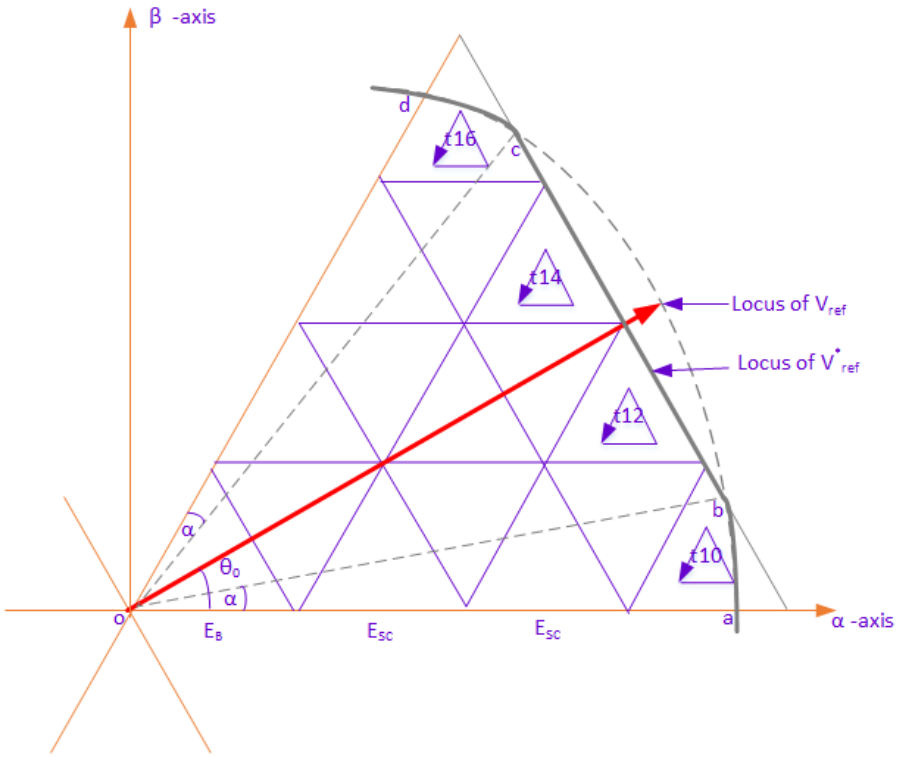

Figure 6-38: Overmodulation of SVPWM method

Figure 6-39 shows the flow chart diagram of applied modified SVPWM algorithm. Figure 6-40 to Figure 6-51 show the phase and line voltage waveforms of the battery, supercapacitors, and inverter at the bus bar connected to the microgrid.

6.7.3.6 Limitations of the modified space vector modulation

The battery is expressed as the main energy storage system of the inverter whereas the supercapacitors assist with the transient power delivery. Thus, the battery is compensated, and the synergy leads to superior dynamic behaviour. In running mode, the function of the supercapacitors is either to provide power at the acceleration mode of the vehicle or recuperate energy at the braking mode of the vehicle. In connecting mode, the function of the supercapacitors is either to provide power in discharging mode or recuperate energy at the charging mode. The voltages of the battery and supercapacitors are varied according to the state of charge of the resources. Using three separate supercapacitors with variable voltage in the topology increases the complexity to implement the proposed space vector modulation where the triangle in the hexagon diagram becomes unequal. Furthermore, the asymmetrically connected resources are highly likely to circulate current between them due to the difference in voltage magnitude. When this occurs, it is much better to simplify the analysis to two separate inverters connected in series. The power of the inverter is the accumulated power of these two inverters, and the voltage of the inverter is the vectored sum of the voltage of these two inverters. It is assumed that the voltage of the supercapacitors is equal following the operation. Therefore, the supercapacitors deliver the same power and charge the same energy during operation.

Another parameter affecting the proposed space vector modulation is the ratio of voltage between the battery and the supercapacitors ($^{V_b}/_{V_{sc}}$). For a non-integer ratio, the state of the H-bridges is unique for each vector, which could be generated by only one switching combination. Therefore, there is no redundant switching vector. For the integer ratio, increasing the ratio raises the number of levels of the space vector modulation. Therefore, the redundant switching vector modification increases. For a voltage ratio equal to two, the number of levels that could be achieved is five as shown in Figure 6-35. It is assumed that the voltage ratio between the battery and the supercapacitors is equal to two in this dissertation.

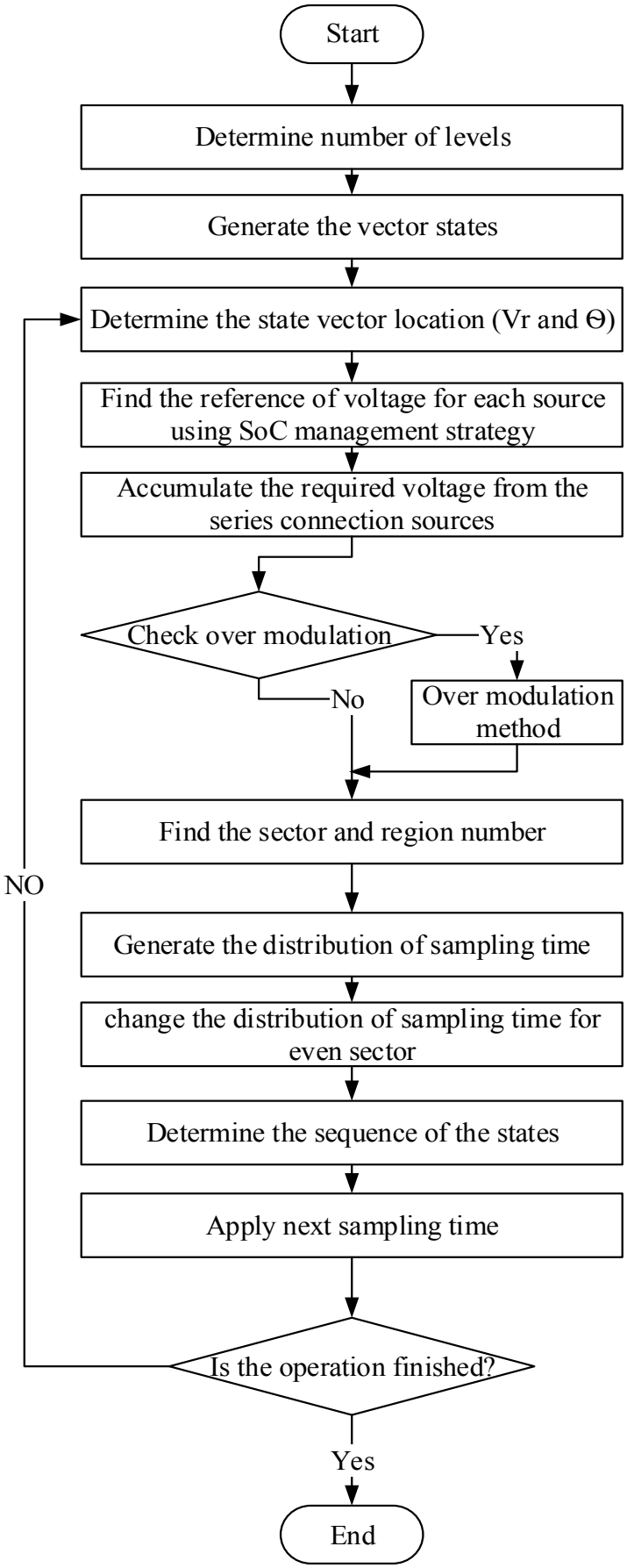

Figure 6-39: Flow chart space vector pulse width modulation algorithm

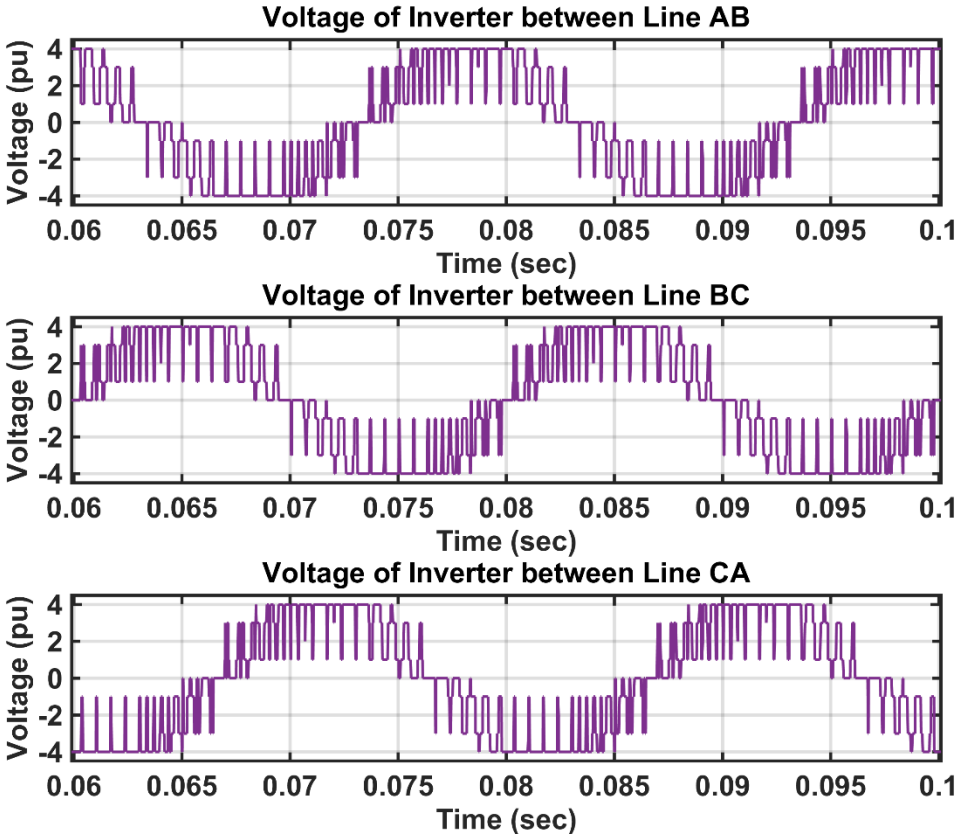

Figure 6-40: Line voltage waveforms of inverter (simulated results)

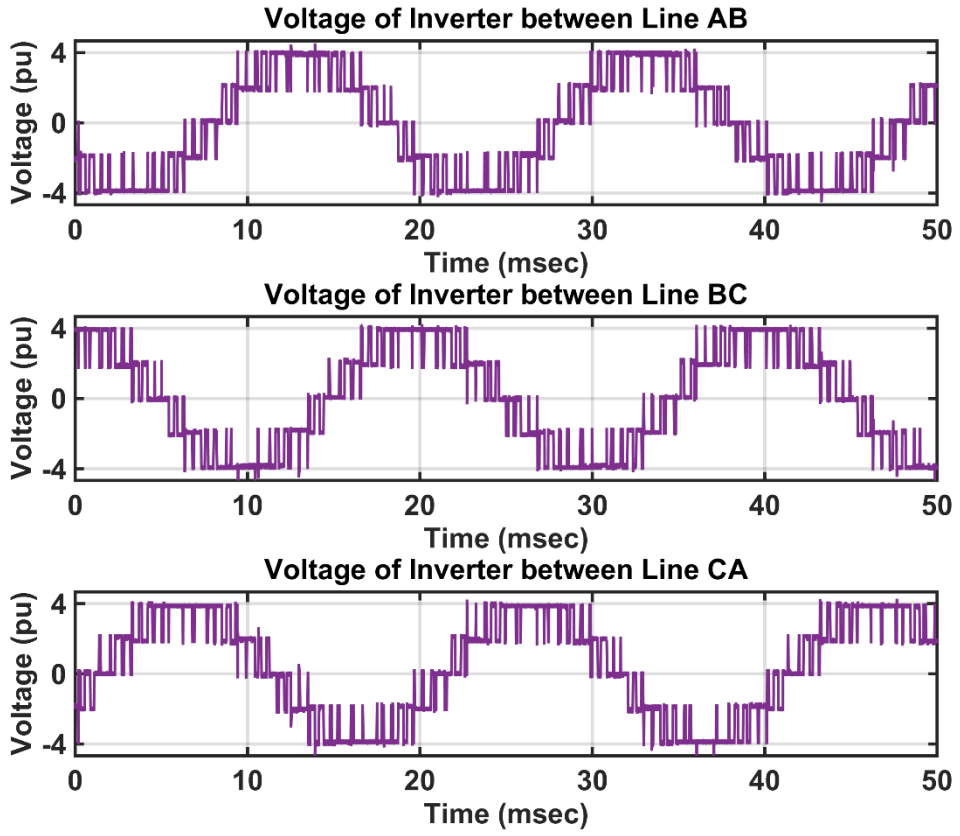

Figure 6-41: Line voltage waveforms of inverter (experimental results)

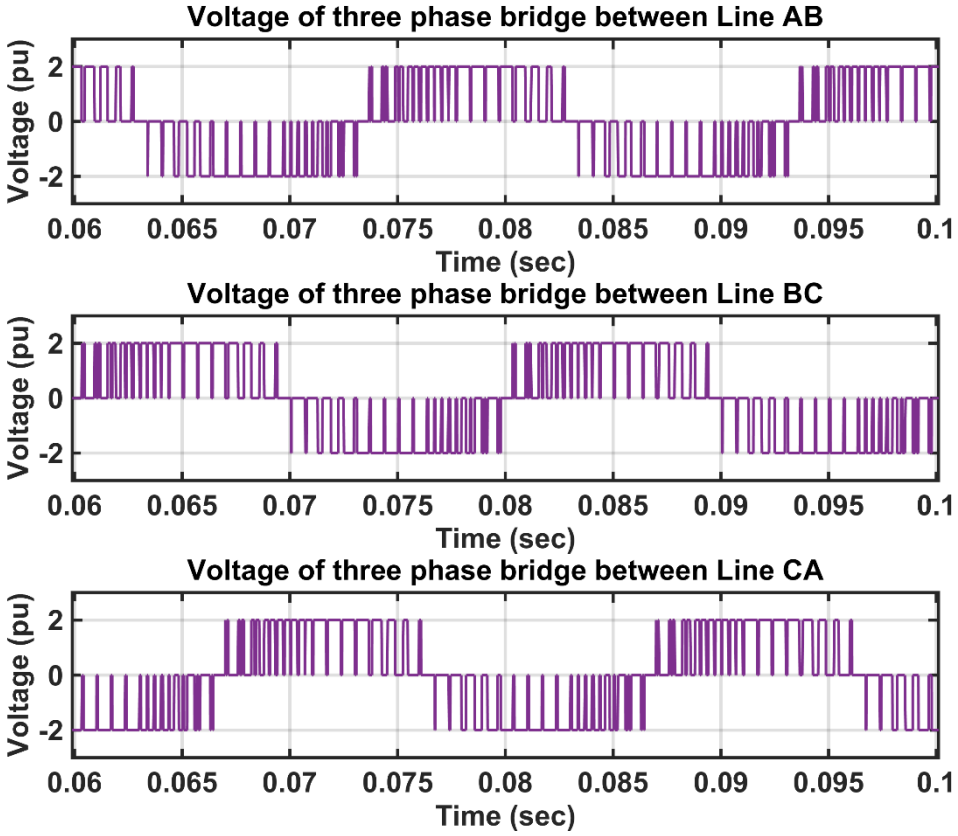

Figure 6-42: Line voltage waveforms of three-phase bridge (simulated results)

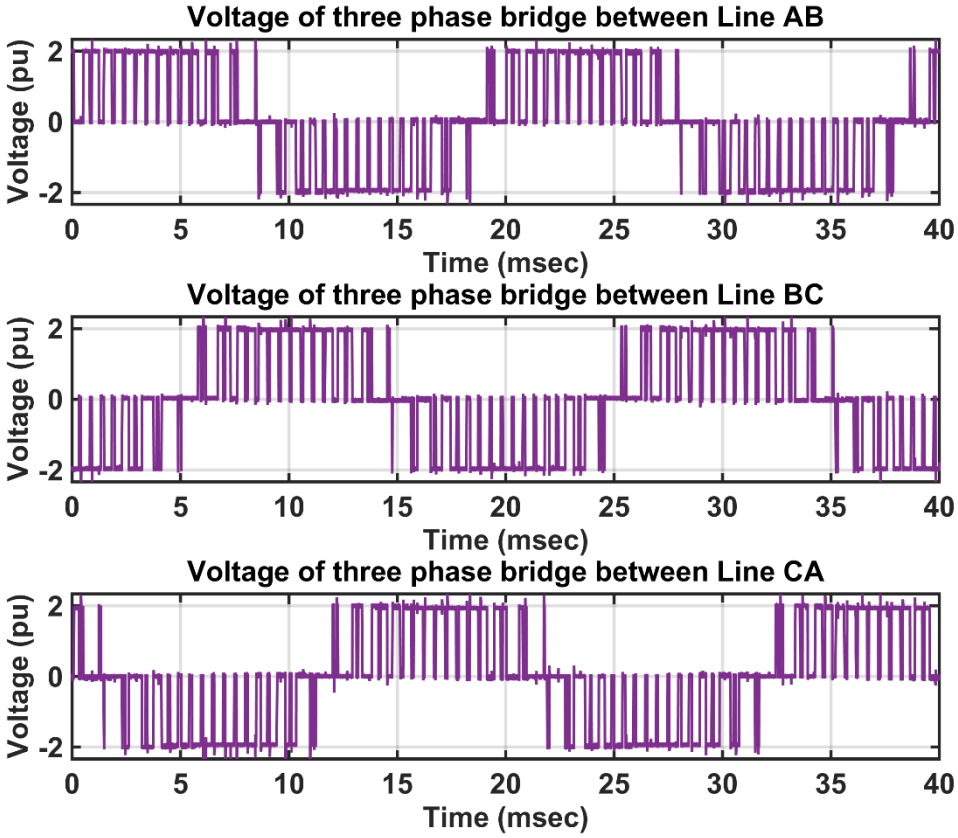

Figure 6-43: Line voltage waveforms of three-phase bridge (experimental results)

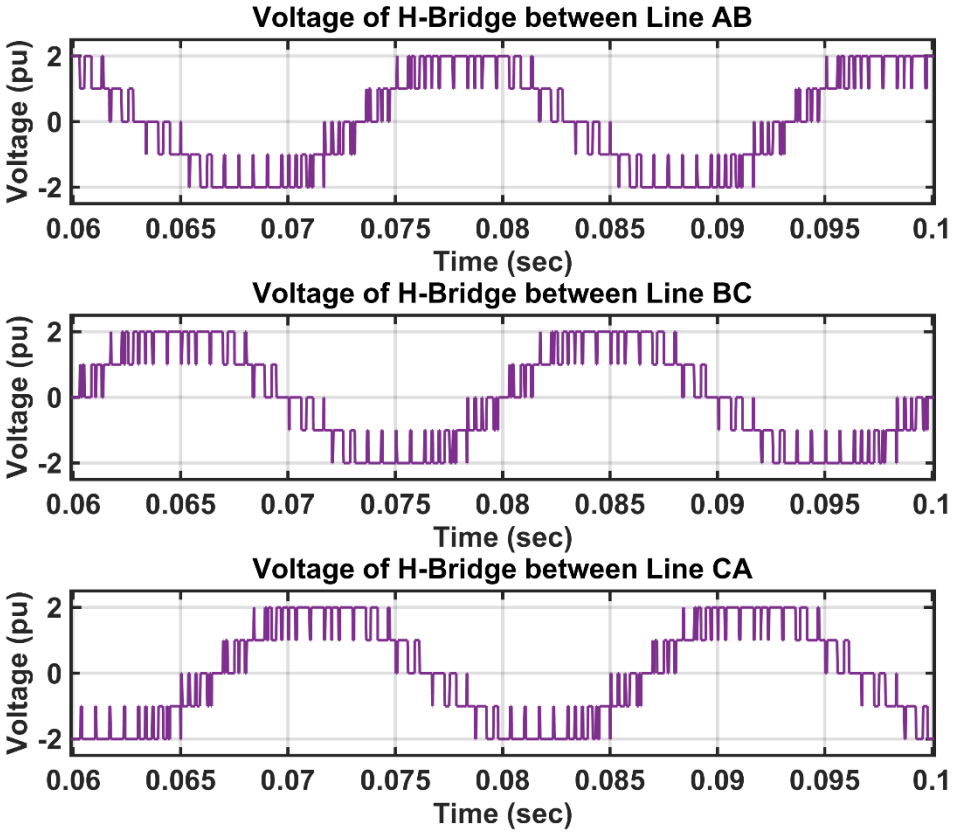

Figure 6-44: Line voltage waveforms of H-bridge (simulated results)

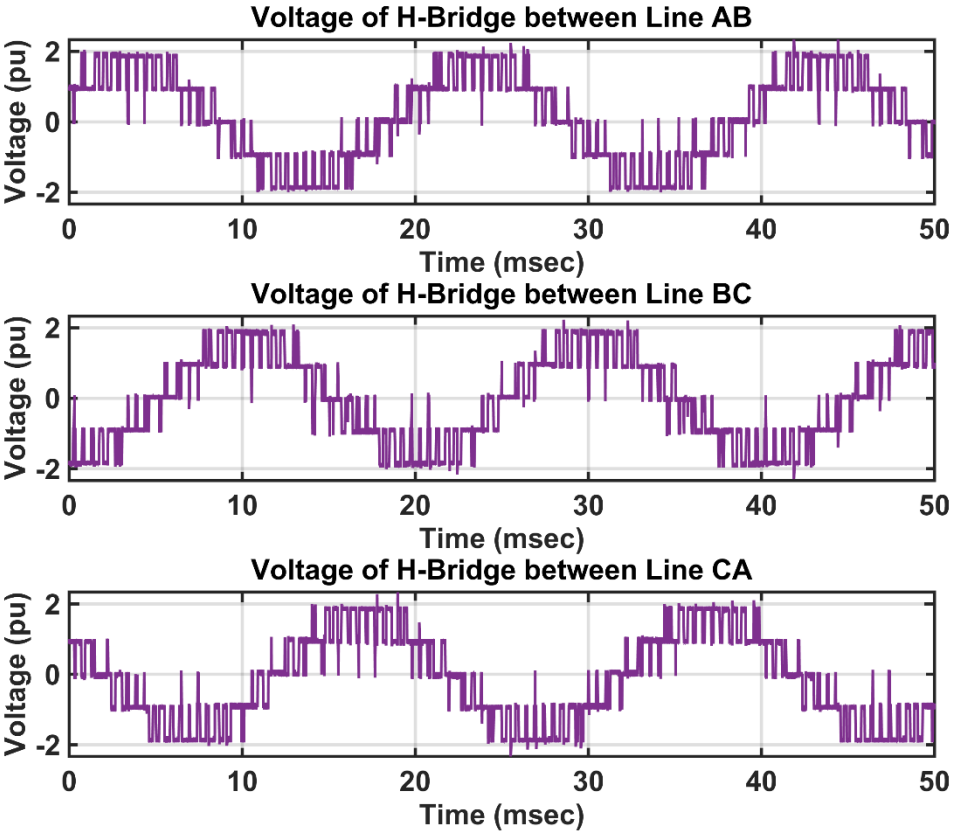

Figure 6-45: Line voltage waveforms of H-bridge (experimental results)

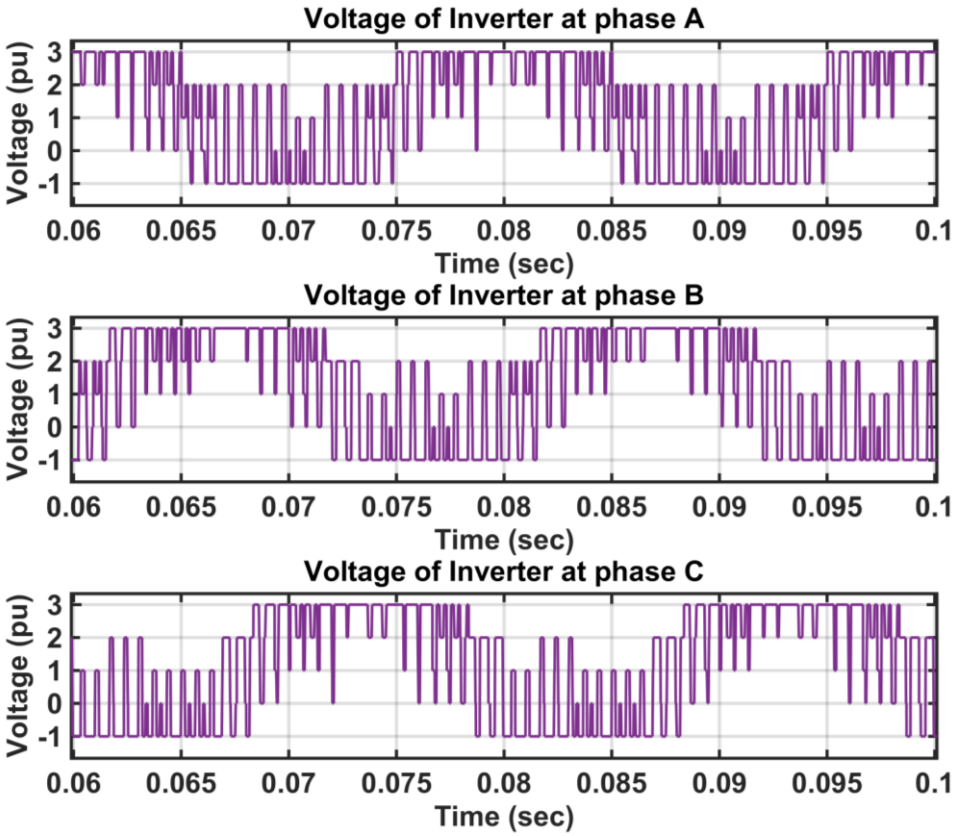

Figure 6-46: Phase voltage waveforms of Inverter (simulated results)

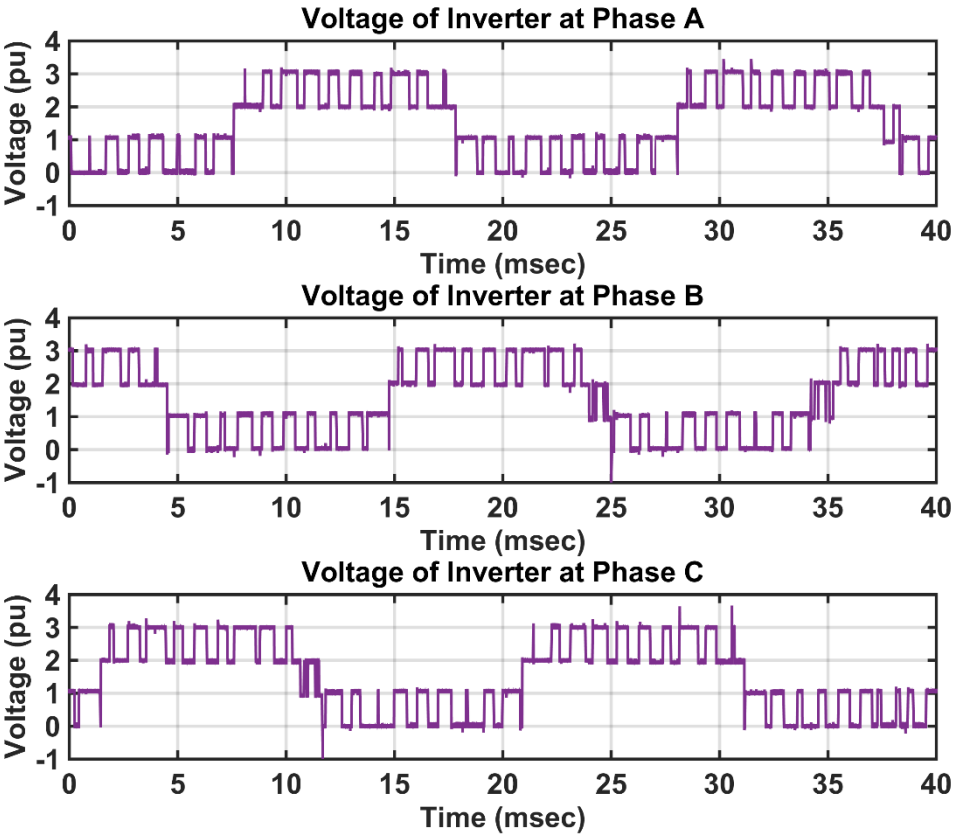

Figure 6-47: Phase voltage waveforms of Inverter (experimental results)

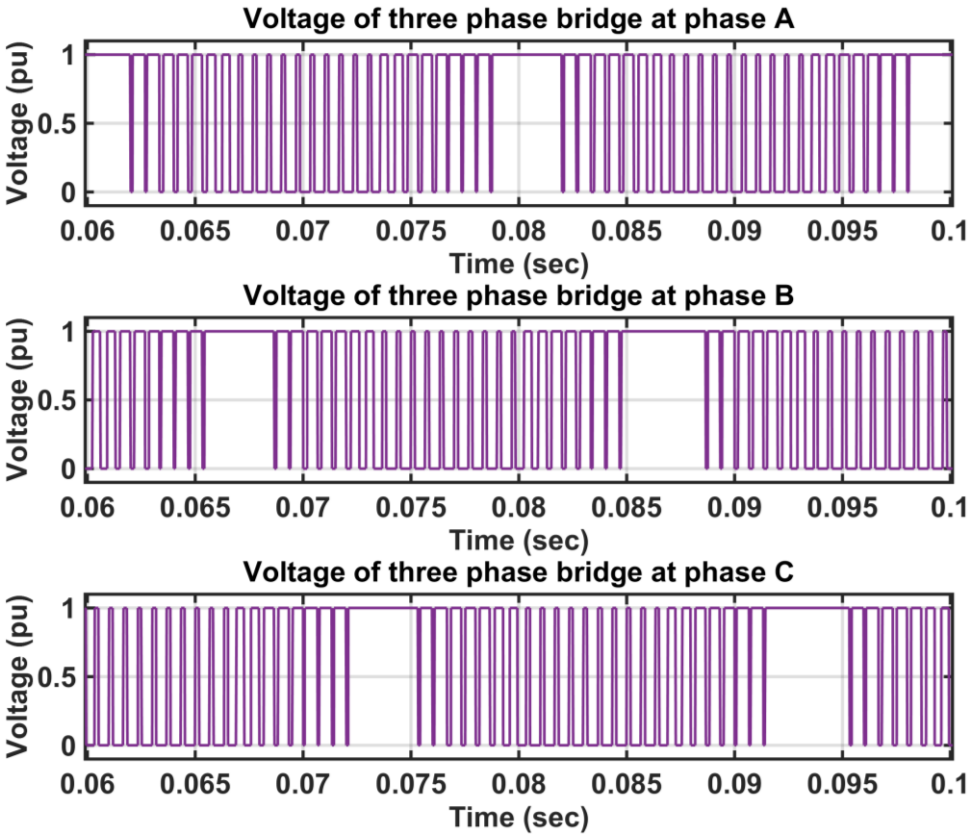

Figure 6-48: Phase voltage waveforms of three-phase bridge (simulated results)

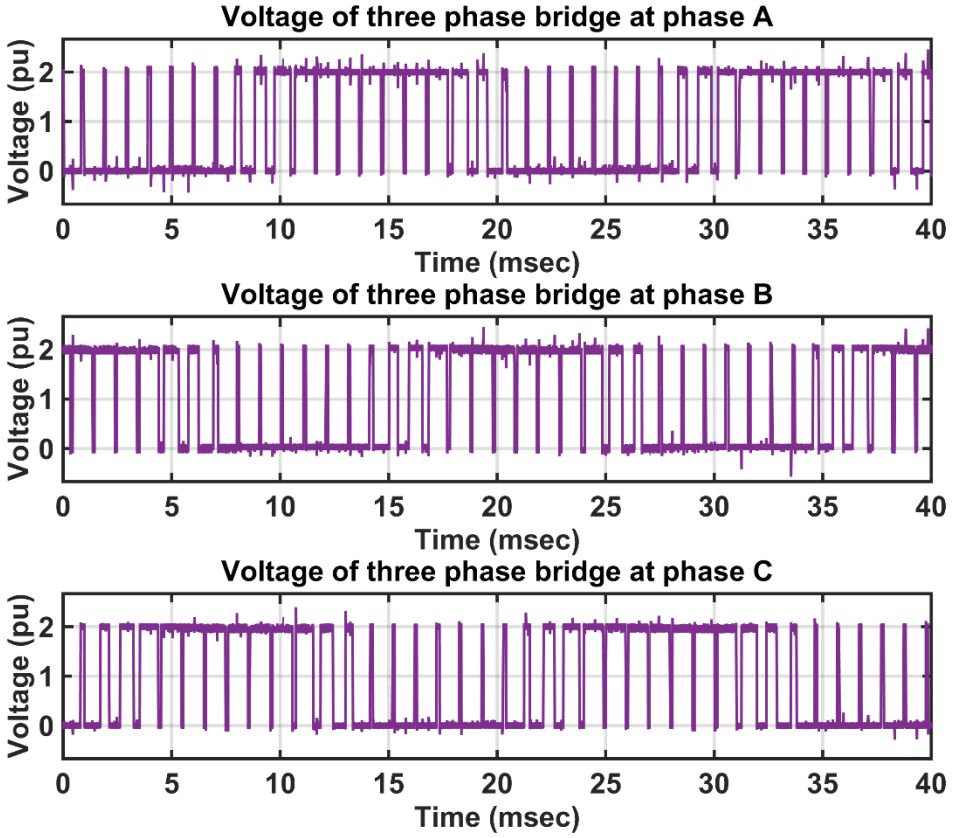

Figure 6-49: Phase voltage waveforms of three-phase Bridge (experimental results)

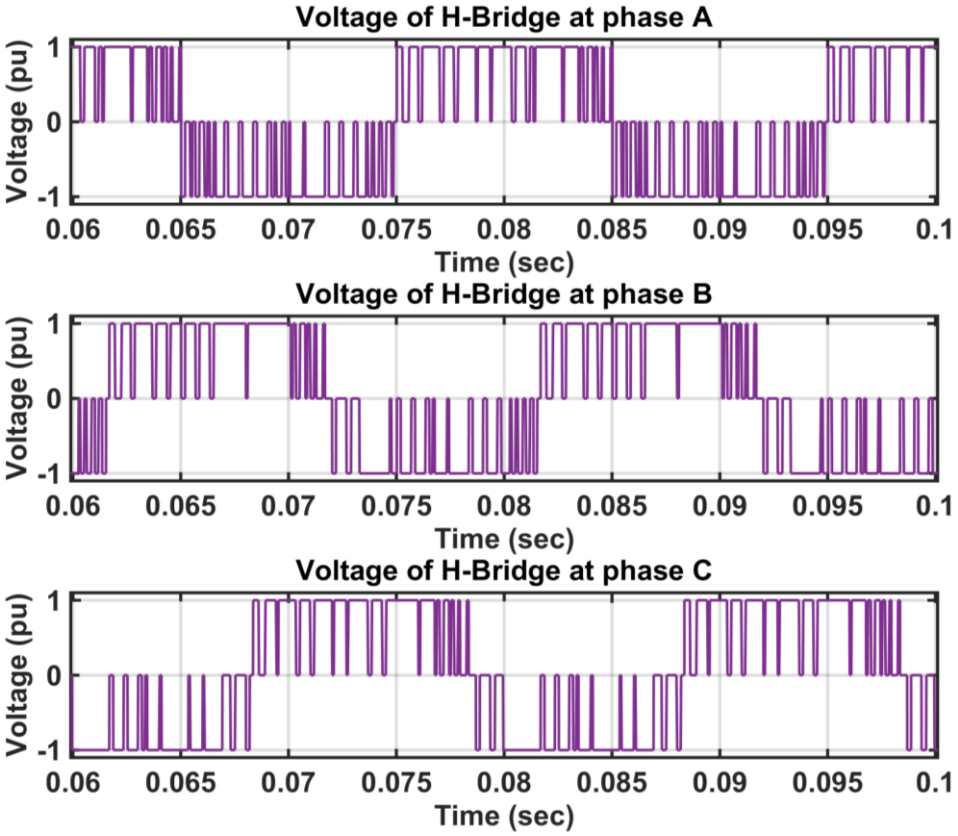

Figure 6-50: Phase voltage waveforms of H-bridge (simulated results)

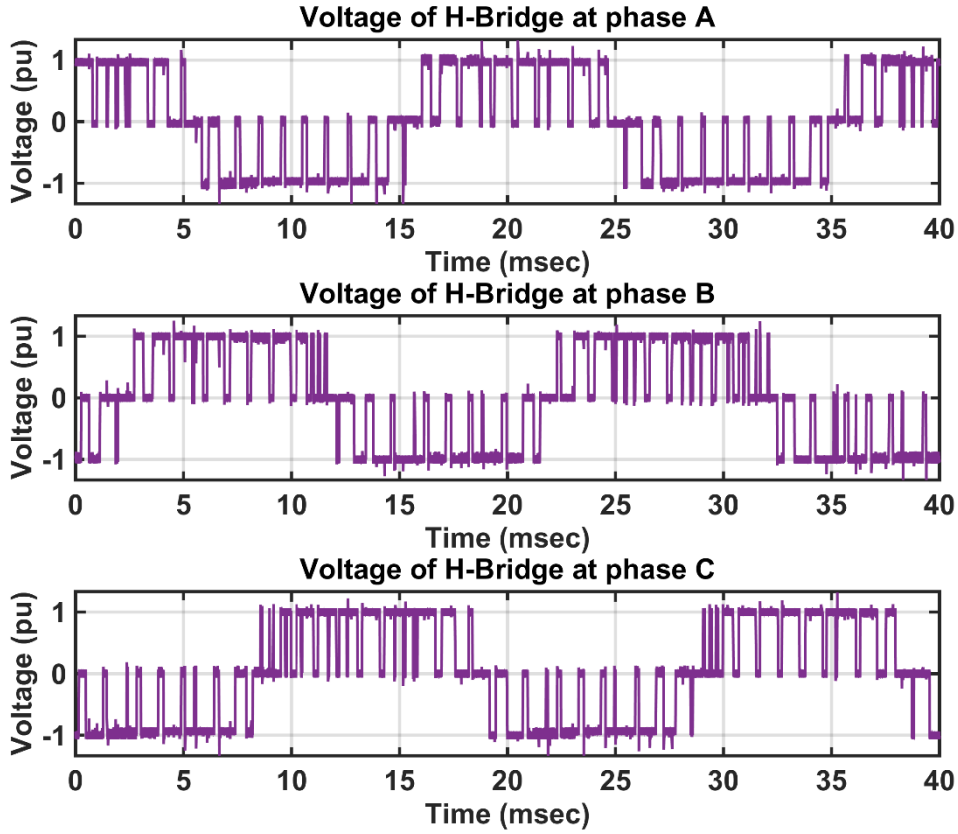

Figure 6-51: Phase voltage waveforms of H-bridge (experimental results)

6.8 Voltage Vectors Modulation Strategy Controller

The control signal which is provided to this stage is assumed to be a sinusoidal signal in addition to the modulated vector which has a circular trajectory. According to a signal received from the EVA, the real-time simulator starts switching the switches either on or off according to the switching strategy. The state of switching strategy can be classified, as stated below:

6.8.1.1 Charging battery mode

In this configuration, only one resource can be charged at a time, which is the battery where the three-phase bridge inverter is operating. The supercapacitors should switch off at charging battery mode. The H-bridge converters provide zero output from the supercapacitors by switching all lower switches off. The upper switches of the H-bridge converters connect the microgrid network to the battery through the three-phase inverter; it is operated with normal modulation as the standard three-phase voltage source inverter. The real-time simulator provides a xxx010101 signal to the switches where xxx are the upper switches of the three-phase inverter; the rest of the bits are the upper switches of the H-bridge converter. All the lower switches are complementary to the same leg upper switch, as presented in Figure 6-53. The switching strategy activates eight vectors as three variables exist 2^3 where six of them are active vectors, and the other two are zero vectors, as presented in Figure 6-52. The output voltage amplitude of the active vectors in the stationary $(\alpha - \beta)$ coordinate axis is equal to $\frac{2}{3}\mathrm{V_{bat}}$ based on the following equations:

$$V_\alpha = \frac{2}{3}\left(V_{an} - \frac{1}{2}V_{bn} + \frac{1}{2}V_{cn}\right) \quad 6\text{-}143$$

$$V_\beta = \frac{\sqrt{3}}{3}\left(V_{bn} - V_{cn}\right) \quad 6\text{-}144$$

$$V_{an} = \frac{V_{bat}}{2}\left(2S_{1\_u} - 1\right) + V_{SCA}(A_{2\_u} - A_{1\_u}) \quad 6\text{-}145$$

$$V_{bn} = \frac{V_{bat}}{2}\left(2S_{2\_u} - 1\right) + V_{SCB}(B_{2\_u} - B_{1\_u}) \quad 6\text{-}146$$

$$V_{cn} = \frac{V_{bat}}{2}\left(2S_{3\_u} - 1\right) + V_{SCC}(C_{2\_u} - C_{1\_u}) \quad 6\text{-}147$$

as shown in Table 6-3 and Figure 6-52. The charging current could be any amount less than the rating of the inverter based on the reference of the vector controller.

In such a configuration, the power is consumed from the microgrid by the battery only follows:

$$P_{bat} = V_{bat}I_{bat} = \sqrt{3}V_l I_l cos\emptyset \quad 6\text{-}148$$

$$P_{SCA} = P_{SCB} = P_{SCC} = 0$$

The voltage level is the same as a standard microgrid voltage, whereas the current flow depends on the rated capacity of the inverter, which is 32A in this study. The state of charge of the battery starts charging with the optimum current provided from the smart charger until it reaches the desired departure state of charge. The power consumed from the supercapacitors is zero. Therefore, the state of charge of the supercapacitors remains unchanged.

The above equations facilitate the PES of EVO to operate the inverter with the right amount of power from the resources of the EV.

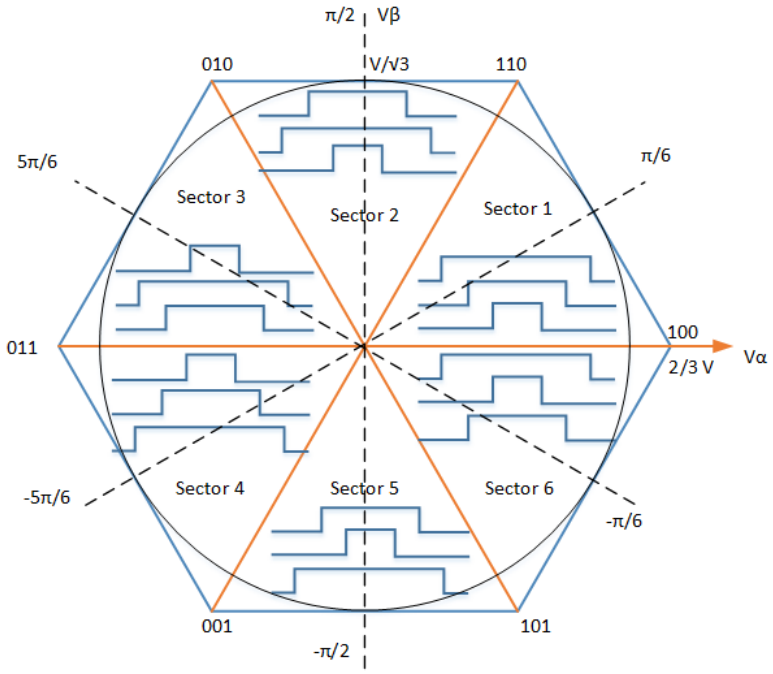

Figure 6-52: Standard three-leg inverter hexagon diagram

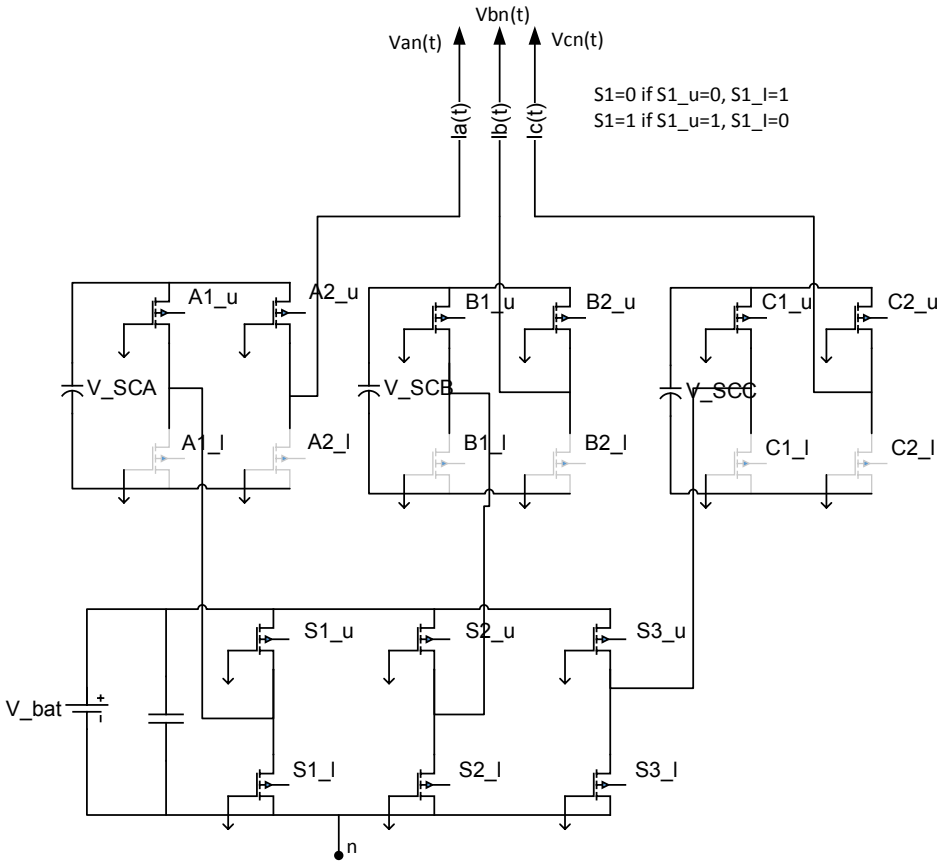

Figure 6-53: Modified H-bridge multi-level inverter at battery charging mode.

The state of charge (top plot), the current (middle plot), and the voltage (bottom plot) response of the battery at three charging current steps of the charging battery mode are shown in Figure 6-54. The battery charging is at ten amperes for a period of 0-0.3 seconds, 20A for a period of 0.3-0.6 seconds, and 30A for a period of 0.6-1 seconds. The effect of charging the current appears in an increase of the voltage level of the battery and increasing the state of charge of the battery. Increasing the state of a charge is related to the amount of current flow through the battery, where high current flows through the battery, a low time of fully charged is required. The rate of the state of charge increased by 1.7% and 2.4% at 20A and 30A respectively compared with 10A. At the instant of charging, the high transient effect applied to the battery can have an acute impact on the current signal due to the internal resistance of the battery. Furthermore, increasing the input reference of the charging current at PES shows the charging current settling down at a new current value of three cycles of the fundamental frequency.

The current of the battery (top plot), current of the supercapacitor (middle plot), and current of the inverter (bottom plot) response at three charging current steps of the charging battery mode are shown in Figure 6-55. The figure shows the supercapacitor charged at zero current where the H-bridges converter is connected to the battery directly from the microgrid. The drawn current from the microgrid increases as the reference of the charging current of the battery increases.

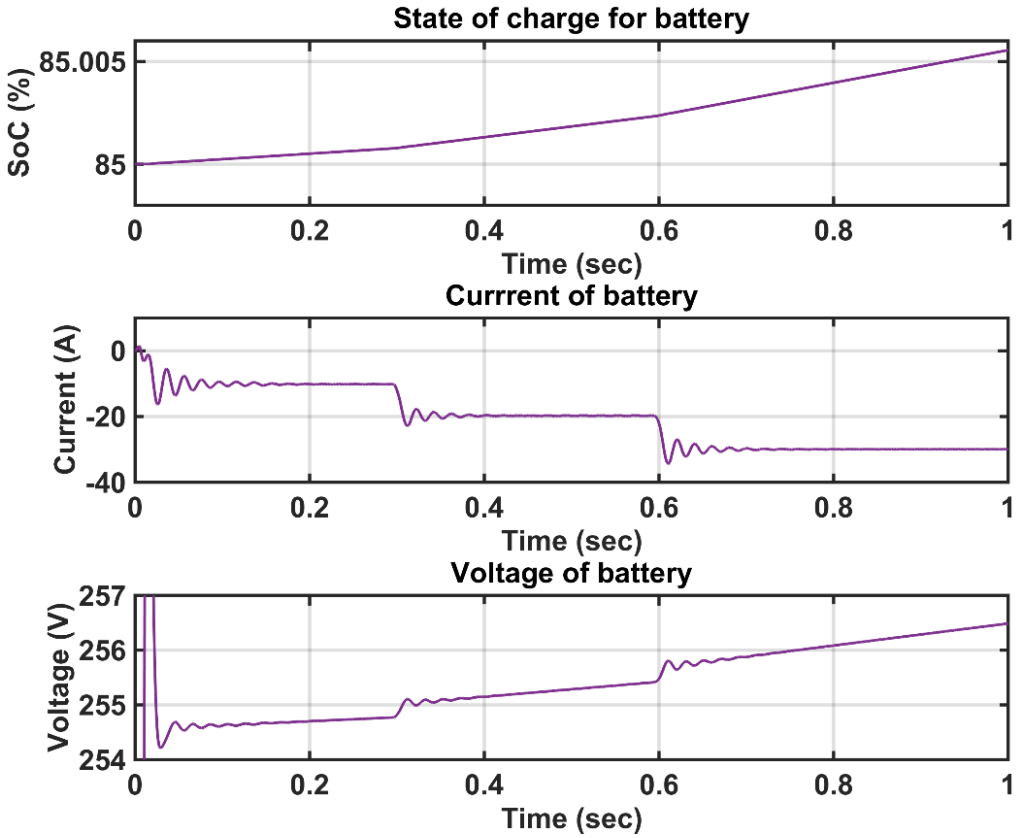

Figure 6-54: States of charge, current, and voltage waveforms of battery (simulated results)

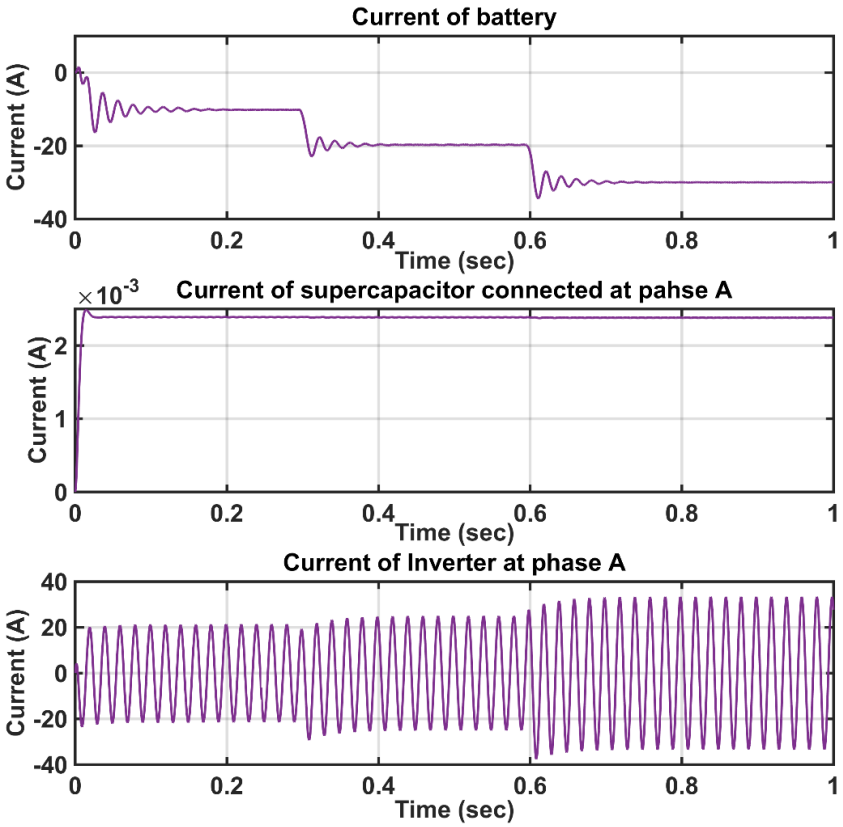

Figure 6-55: Battery, supercapacitor, and inverter current waveforms (simulated results)

6.8.1.2 Charging supercapacitor mode

In this configuration, only the resources connected to the H-bridge converters are assumed to be charged at a specific time, which are the supercapacitors. To charge the supercapacitors, the battery should switch off. The three-phase bridge provides zero output from the battery by switching all upper switches of the inverter off. The lower switches of the three-phase inverter connect the H-bridges converters together, as shown in Figure 6-56.

The H-bridge is operated at normal modulation as the standard H-bridge voltage source inverter. The real-time simulator provides a 000xxxxxx signal to the switches where xxxxxx are the upper switches of the three H-bridge converters whereas the rest of the zero bits are the upper switches of the three-phase bridge inverter, as shown in Figure 6-57. All the lower switches are complementary to the same leg upper switches. The switching strategy activates 64 vectors for the H-bridge converter where six switches pair combinations exist (2^6). It is possible to produce a combination of four zero vectors and 24 active vectors. Two of the zero vectors combinations which are 010101 and 101010 are used to circulate the energy between cells, depending on the phase currents.

The output voltage amplitude in the stationary ($\alpha - \beta$) coordinate system of the active vectors is equal to $\frac{2}{3}V_{sc}$ for a one cell activate, $\frac{2}{\sqrt{3}}V_{sc}$ for a two cell activate, and $\frac{4}{3}V_{sc}$ for a three cell activate. The switching activation of the two cells and three cells supply voltage can be

produced from a unique switching configuration. The charging current could be any amount less than the rated current of the inverter based on the reference of the vector controller.

The power produced from the microgrid is consumed by supercapacitors where the battery is in an isolated condition. The maximum power of this configuration is related to the state of charge of the supercapacitors and the rated power of the inverters. It is necessary to keep all the voltage levels of the supercapacitors at the same amount to keep them operating in a balanced condition.

For normal operation, the switching algorithm provides a balanced voltage vector to the supercapacitors. However, the normal behaviour of the distribution network provides an unbalanced voltage among the phases. The switching strategy tries to select an adequate switching combination to control the current vector direction and to keep the amount of charging power to an adequate state of charge for the supercapacitors. The switching combination is controlled either by reducing or increasing the dwell time of the phases switching combination to decide the current flowing through each supercapacitor.

For example, to provide $V = \frac{4}{3}V_{dc}e^{j0}$ vector 011010 is applied, as shown in Figure 6-57. Two combinations could be applied starting from either vector combination 010000 to let the current of phase A flow during all duty cycle of switching combination or vector combination 001010 to reduce the dwell time switching combination of the current at phase A, as presented below.

$010000 \rightarrow 010010 \rightarrow 011010 \rightarrow 001010$

$001010 \rightarrow 011010 \rightarrow 010010 \rightarrow 010000$

To provide $V = \frac{2}{3}V_{dc}e^{j0}$, there are three combinations that could be used either using a positive phase, a vector combination, or using another negative phase combination that makes the current of phase A flow in the opposite direction as explained below and depicted in Figure 6-57.

$000000 \rightarrow 010000 \rightarrow 010100 \rightarrow 000000$

$000000 \rightarrow 000010 \rightarrow 001010 \rightarrow 000000$

$000000 \rightarrow 001000 \rightarrow 001010 \rightarrow 000000$

The same strategy could be applied to other phases that need to reduce the dwell time of the switching combination. The total power of the converter can be calculated by

$$P_t = V_{SCA}I_{SCA} + V_{SCB}I_{SCB} + V_{SCC}I_{SCC} = \sqrt{3}V_l I_l cos\emptyset \qquad 6\text{-}149$$
$$P_{bat} = 0$$

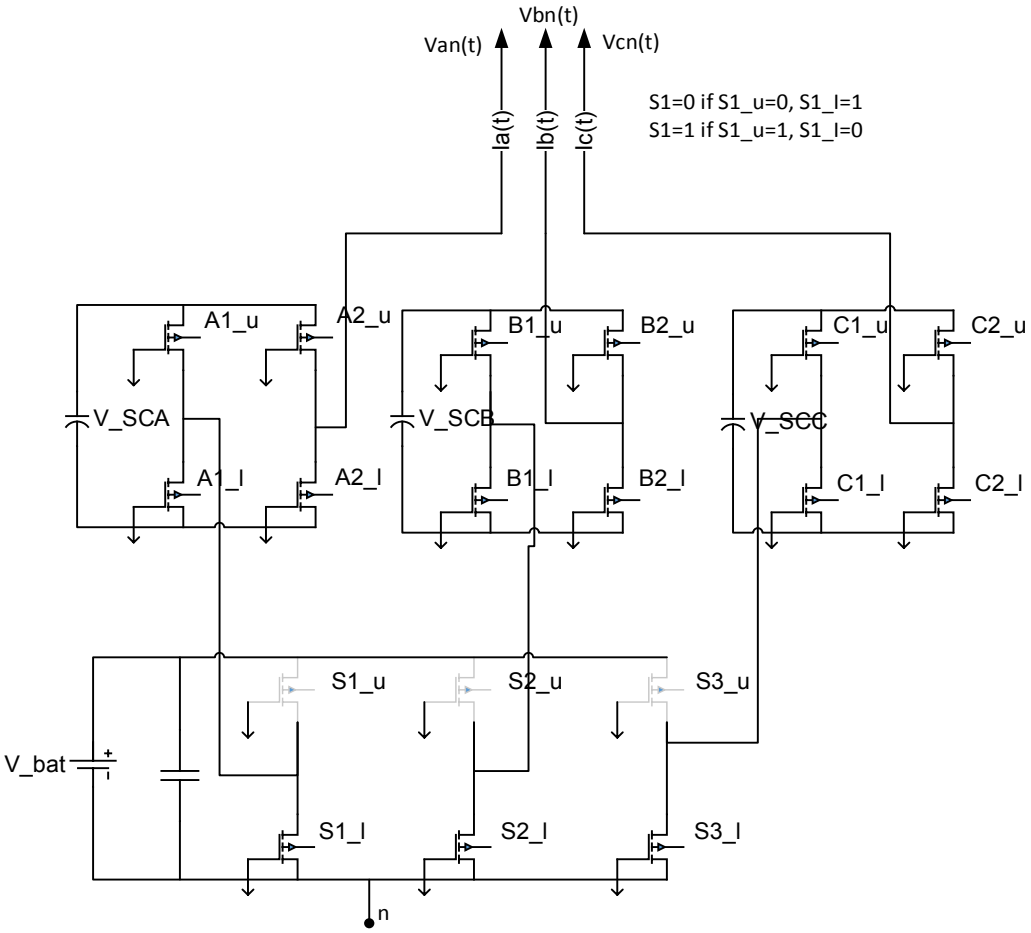

Figure 6-56: Modified H-bridge multi-level inverter at supercapacitors charging mode (the semiconductor switches).

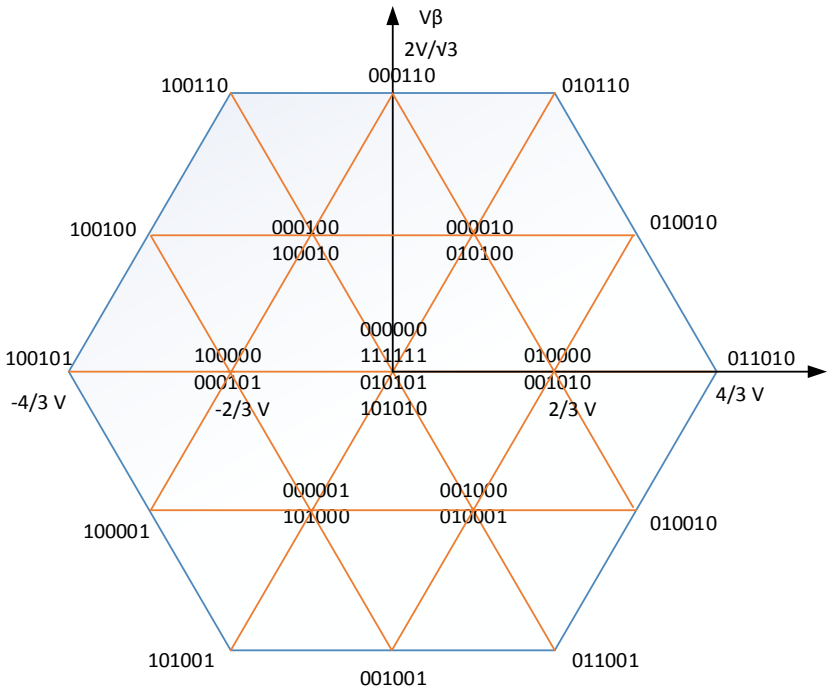

Figure 6-57: H-bridge hexagon diagram

The state of charge (top plot), the current (middle plot), and the voltage (bottom plot) response of the supercapacitors at two charging current steps of the charging supercapacitors mode are shown in Figure 6-58. The supercapacitors are charging at 10A for a period of 0-0.5 seconds and 16A for a period of 0.5-1.0 seconds. The effect of the charging current appears in an increasing of the voltage level of the supercapacitors and increasing the state of charge of the supercapacitors. The state of charge increases at the charging current increase where high current passes on to the supercapacitors, low time of full required charge. The rate of the state of charge increased by 1.9% at 16A compared with 10A.

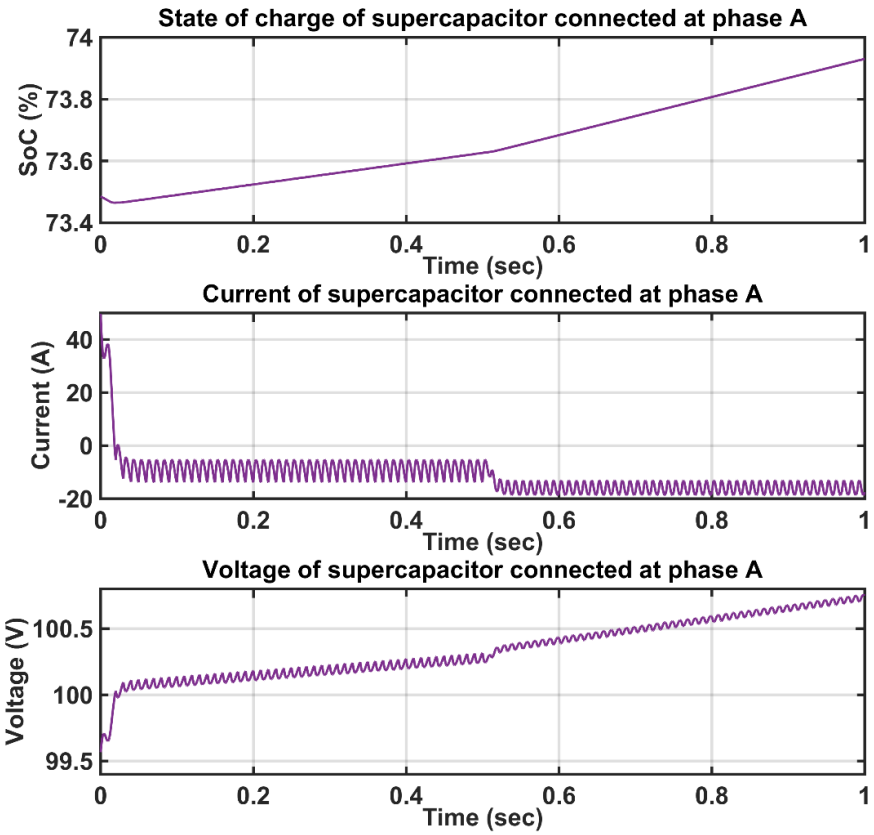

Figure 6-58: State of charge, current, and voltage waveforms of supercapacitor connected at phase A (simulated results)

The current of the battery (top plot), current of the supercapacitor (middle plot), and current of the inverter (bottom plot) responses at two charging current steps of the charging supercapacitor mode are shown in Figure 6-59. The figure shows the battery charged at zero current where the H-bridges converter connects the supercapacitors directly to the microgrid at the positive plate, whereas the negative plate of the supercapacitors is connected by the three-phase bridge inverter. The current drawn from the microgrid increases as the reference of charging current of the supercapacitor increases.

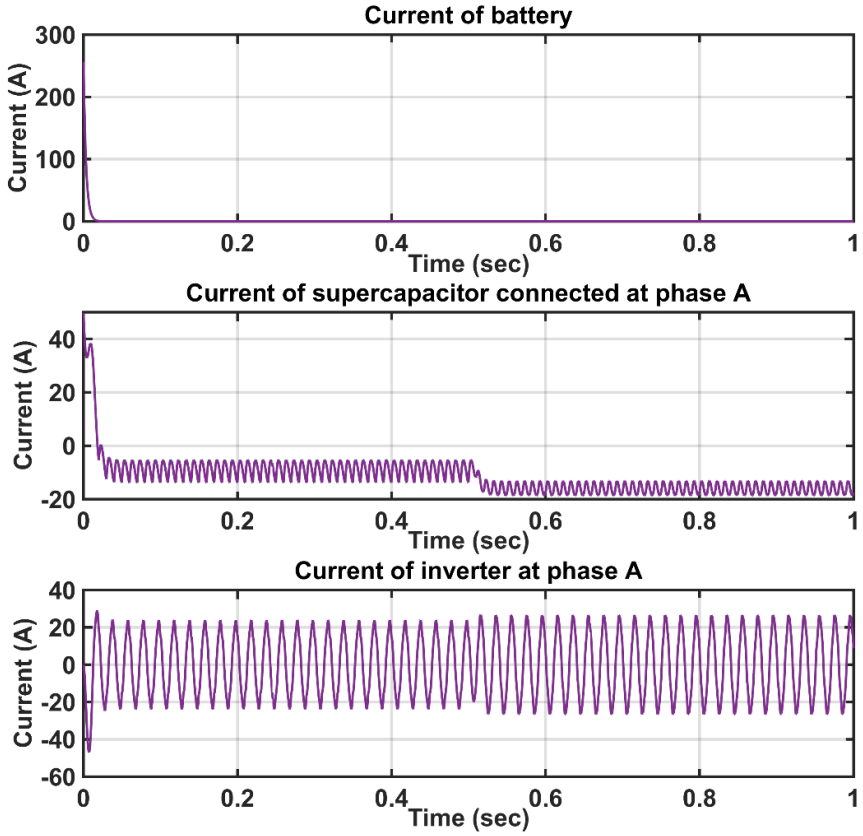

Figure 6-59: Battery, supercapacitor, and inverter current waveforms at supercapacitors charging mode (simulated results)

The balance currents of the supercapacitors at two charging current steps of the charging supercapacitor mode are shown in Figure 6-60. The top plot refers to the current of the supercapacitors connected at phase A; the middle plot refers to the current of the supercapacitors connected at phase B; and the bottom plot refers to the current of the supercapacitors connected at phase C. The figure shows that the currents drawn from the supercapacitors are exactly the same. It could draw unbalanced currents, as shown in Figure 6-61, where different currents passed through the supercapacitors at the same reference control signal of Figure 6-60 and different switching combinations. The inverter waveform is similar to the H-bridge waveform as the standard three-phase bridge inverter droop zero current.

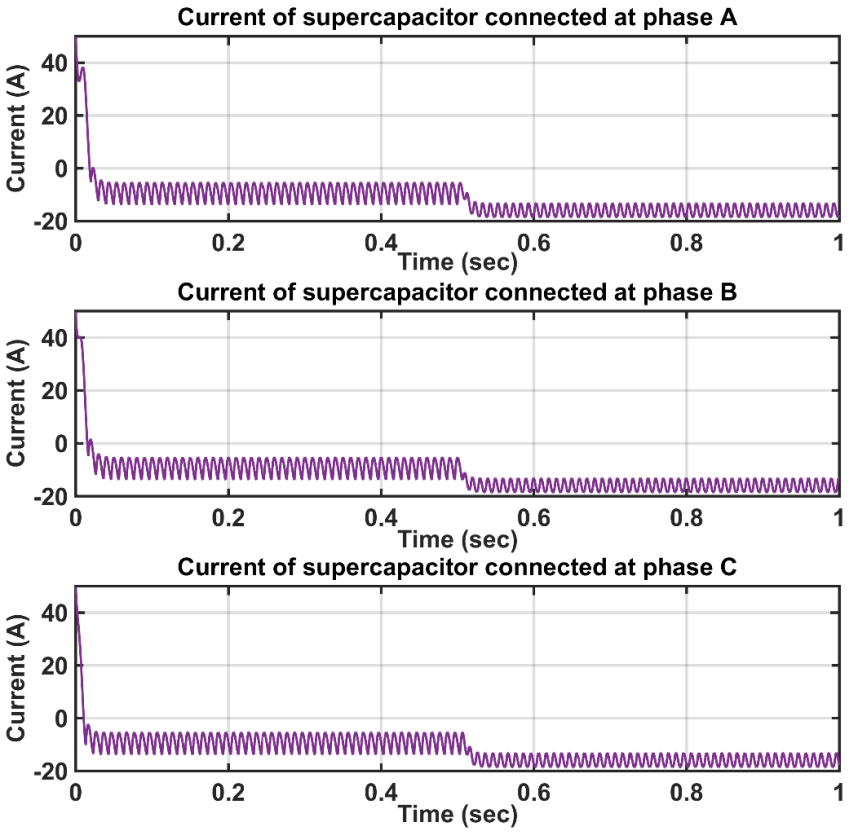

Figure 6-60: Balance current waveforms of supercapacitors (simulated results)

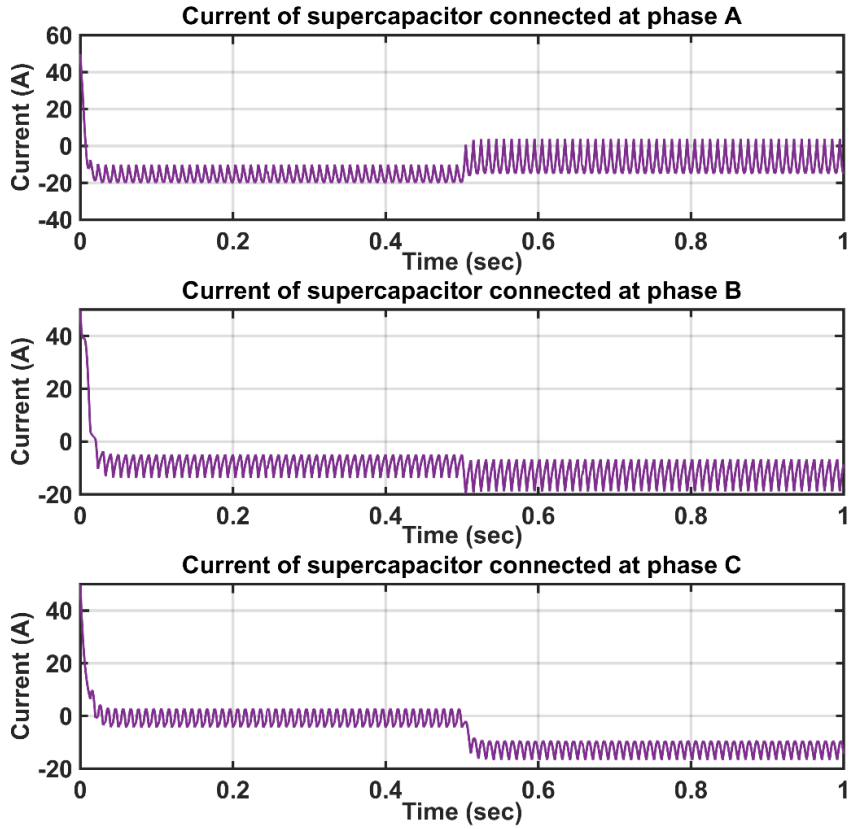

Figure 6-61: Unbalanced current waveforms of supercapacitors (simulated results)

6.8.1.3 Discharging battery priority mode

The priority strategy interacts the CSO with EVO accurately by determining the response of the resources. In this mode, both the three-phase bridge inverter and three H-bridge converters collaborate to supply the required voltage to the microgrid. The modulation strategy in this mode is based on activating the three-phase bridge inverter at the fundamental frequency of the microgrid and compensates the remaining voltage of the standard microgrid voltage level from operating the H-bridge converters. The real-time simulator of the hybrid inverter provides a xxxxxxxxx signal to the upper switches of the inverter, as shown in Figure 6-13. All the lower switches are complementary to the same leg upper switch. The switching strategy activates 512 vectors as nine switches pairs combinations existing of (2^9). It is possible to produce a seven zero vectors combination and 192 active vectors combination. The maximum and minimum output voltage vectors which can be achieved by this modulation are $V_I = \frac{2}{3}(V_{bat} + 2V_{sc})$ and $V_I = \frac{2}{3}(V_{bat} - 2V_{sc})$ respectively. The discharging or charging current could be any amount of current less than the rated current of the inverter based on the reference of the vector control.

The output voltage amplitude in the stationary $(\alpha - \beta)$ coordinate system of the active vectors is equal to $\frac{2}{3}V_{sc}$ for a one cell activate, $\frac{2}{\sqrt{3}}V_{sc}$ for a two cell activate, and $\frac{4}{3}V_{sc}$ for a three cell activate. The switching activation of the two and three cells to supply voltage can be produced from a unique switching configuration.

6.8.1.4 Discharging supercapacitor priority mode

In this mode, the same strategy applied in mode III is activated except that the three H-bridge converters switch first at the fundamental frequency of the microgrid and the three-phase bridge inverter can supply the remaining standard voltage level of the microgrid. Mode III activates at frequency deviation whereas mode IV activates at voltage deviation.

The power supplied in discharging mode is a shared power between all resources of the inverter with figuring out using a minimum switching combination transition to reduce the losses, harmonics, voltage ripple, and current ripple of the waveform. During discharge modes, there is one inverter operating at a fundamental frequency of the microgrid whereas other parts compensate the voltage to reach the standard voltage level of the microgrid.

The three-phase bridge inverter can switch one bit in each transition during the dwell time of the vector combination. The vector repeats uniformly every one-sixth of the frequency period for the asymmetrical transition of the three phase waveforms. Therefore, the inverter could produce a sinusoidal voltage waveform and pure DC current flow through the battery. The peak output voltage magnitude is $\frac{2}{3}V_b$. The three H-bridge converters connect to the three supercapacitors; each one works in single phase mode. For collaborating between two supercapacitors, more than one bit transition may be required to apply the vector combination, in addition to the difficulty of keeping the voltage level of all supercapacitors at the same level practically. That increases the losses, harmonics, voltage ripple and current ripple of the inverter. Therefore, the output voltage waveform has some distortion and ripple.

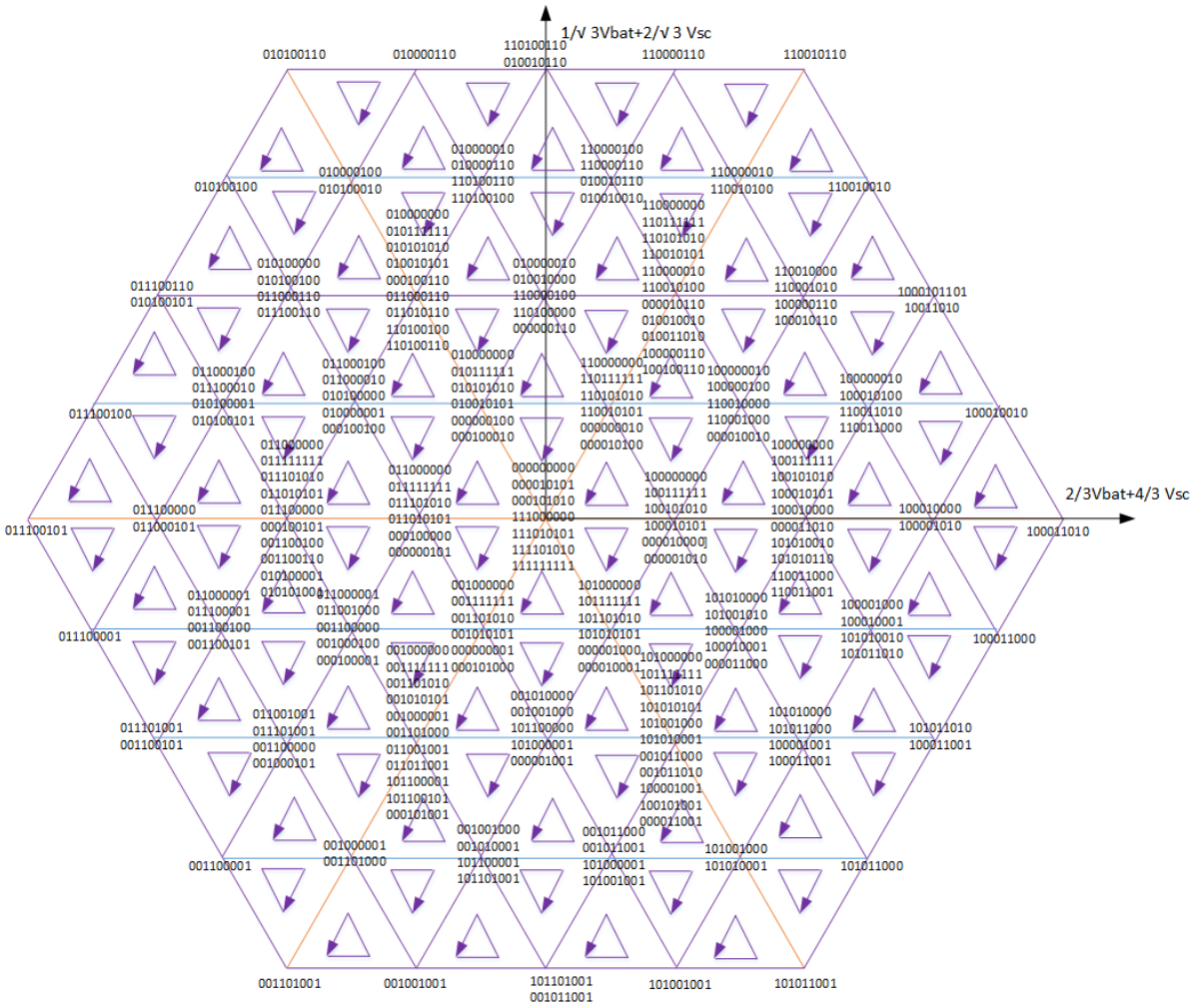

Figure 6-62: Hexagon diagram of modified H-bridge multi-level inverter.

For operation mode III, the three-phase bridge inverter operates at a fundamental frequency of the microgrid and the H-bridge converters compensate the voltage level of the inverter. In contrast to operation mode IV, where the three H-bridge converters operate at the fundamental frequency of the microgrid and the three-phase bridge inverter compensates the voltage level of the inverter, the inverter is likely to have distortion in the mode IV operation more than in the mode III operation due to the bits transition in the vector combination.

The state of charge (top plot), current (middle plot), and voltage (bottom plot) response of the battery at two current steps of the discharging mode are shown in Figure 6-63. The battery discharged at 15A for a period of 0.3-0.6 seconds and 30A for a period of 0.6-1.0 seconds. The effect of the discharging current appeared to decrease the state of charge and the voltage level of the supercapacitor. The state of charge decreases rapidly at increased discharge current, where high current is drawn from the battery, low time of full discharge is required.

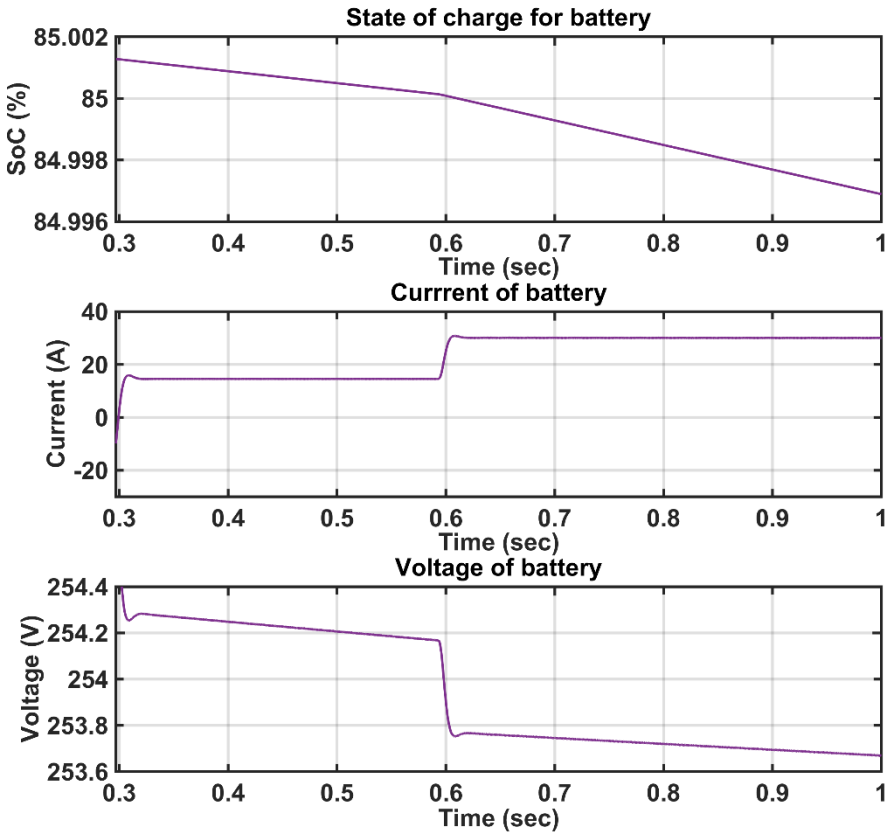

Figure 6-63: States of charge current and voltage waveforms of battery (simulated results)

The state of charge (top plot), current (middle plot), and voltage (bottom plot) response of the supercapacitors at two current steps of the discharging mode are shown in Figure 6-64. The supercapacitor discharged at 10A for a period of 0.3-0.6 seconds and 20A for a period of 0.6-1.0 seconds. The effect of the discharging current appeared to decrease the state of charge and the voltage level of the supercapacitor. The state of charge decreased rapidly at increased discharging current, in the same way as the behaviour of battery states.

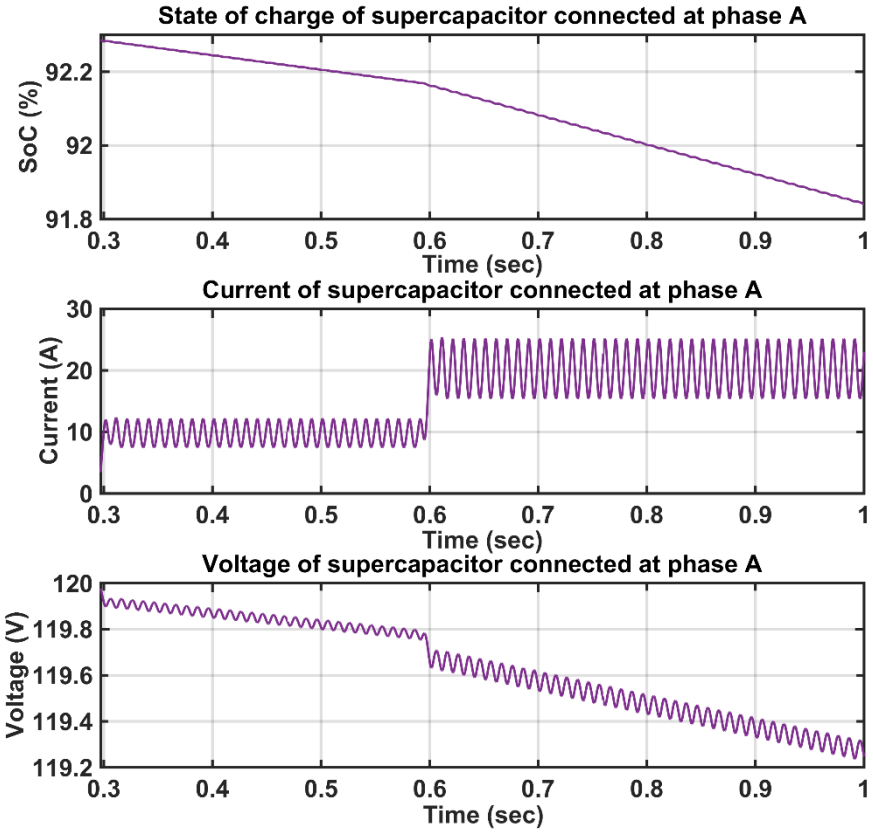

Figure 6-64: States of charge, current, and voltage of supercapacitor at discharging mode (simulated results)

The current of the battery (top plot), current of the supercapacitor (middle plot), and current of the inverter (bottom plot) response at two current steps of the discharging mode are shown in Figure 6-65. The figure shows that the inverter current is the sum of the battery current and the supercapacitors' current. The reference of discharging current of the battery and supercapacitor increase when the current drawn from the microgrid increased.

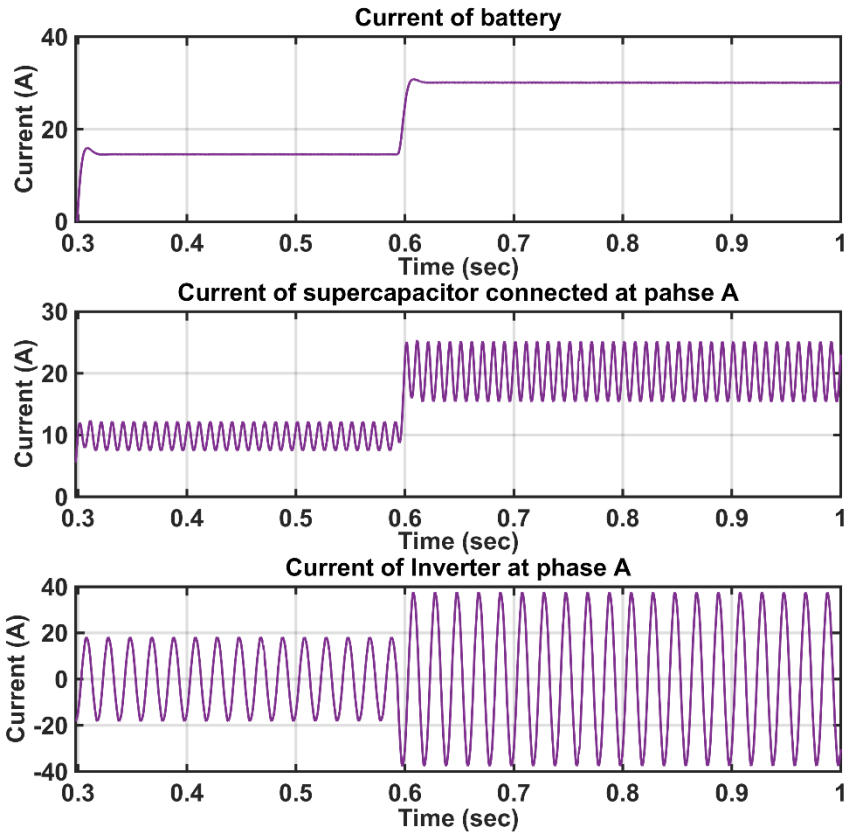

Figure 6-65: Battery, supercapacitor, and inverter current waveforms (simulated results)

The voltage waveform of the standard three-leg inverter (top plot), the voltage waveform of the H-bridge converter (middle plot), and the voltage waveform of the inverter (bottom plot) response at two current steps of discharging mode are shown in

Figure 6-66. The inverter waveform is the sum of the battery waveform and the supercapacitors waveform because they are connected in series.

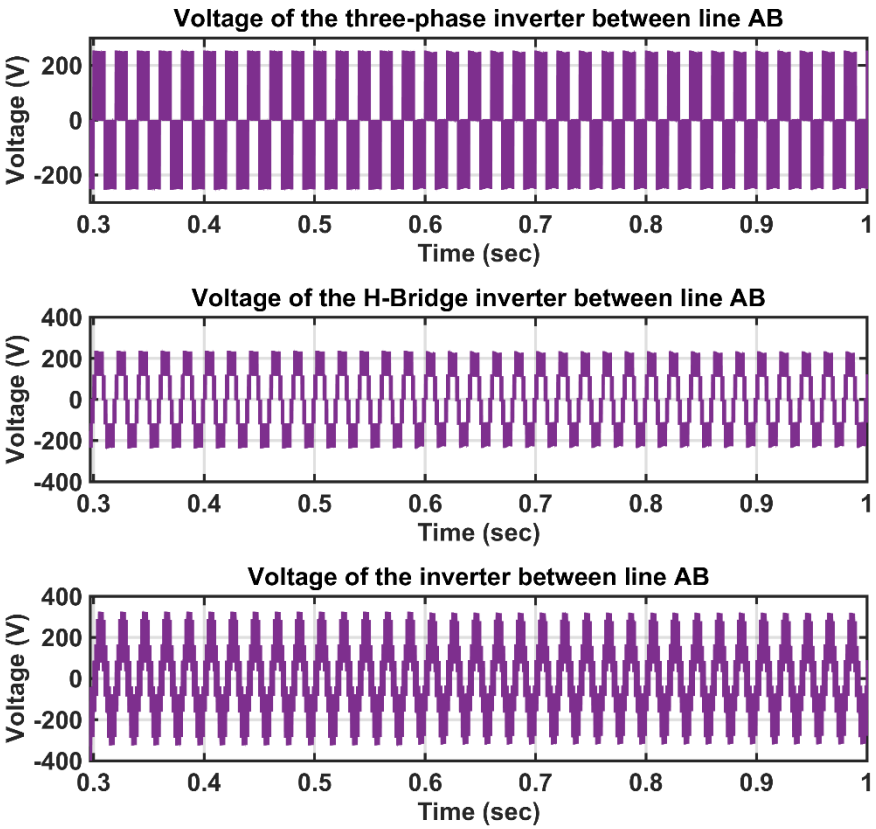

Figure 6-66: Battery, supercapacitor, and inverter voltage waveforms (simulated results)

The three-phase voltage (top plot) and three-phase current (bottom plot) of the inverter are shown in Figure 6-67.

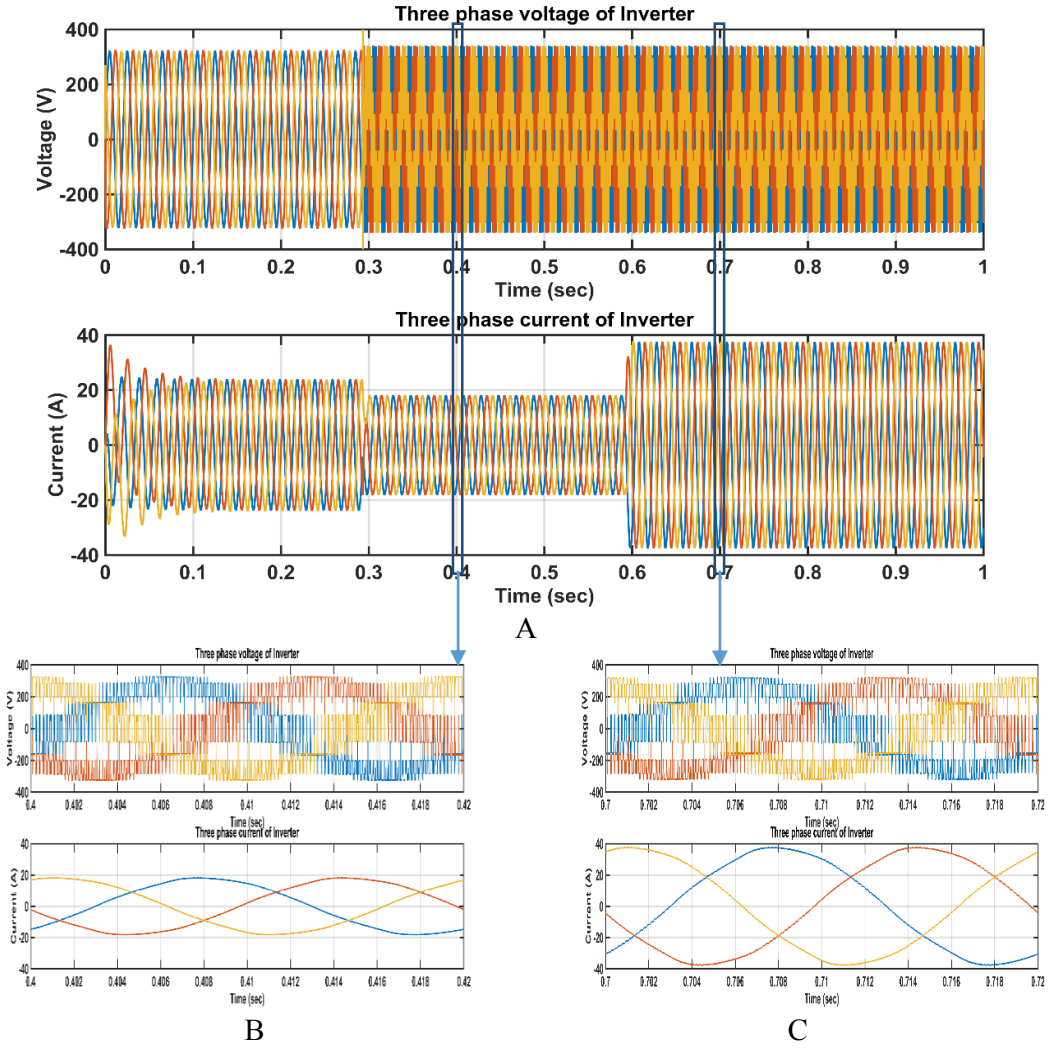

Figure 6-67: Three-phase currents and voltages of the inverter (simulated results)

6.8.2 Real and reactive power from electric vehicles

The active power and reactive power injection in the microgrid from the EV are controlled using the primary control of the EMS. The total power of the inverter is the sum of the power of the battery and the supercapacitors. Therefore, there is a range to generate the power from the battery and the supercapacitors based on their state of charge. Investigation of the proposed method of control shows that the active power and reactive power can be controlled independently, as explained in the next three approaches.

The first approach is that the EV injects a very small reactive power to the microgrid. Figure 6-68 shows the real power that is generated from the EV at two levels, which were 4.5 kW for the period of 0.2-0.6 seconds and 4 kW for the period of 0.6-1.0 seconds. The active power of the inverter is sharing the power of the battery and the supercapacitors. Normally, generating active power from the battery is higher than generating active power from the supercapacitors. The figure shows two ranges of the battery and supercapacitors in producing active power. The 4.5 kW could be generated as either 2.45 kW from the battery and 2.05 kW

from the supercapacitors or the battery generated 2.4 kW whereas the supercapacitors generated 2.1 kW, as shown in the periods of 0.2-0.4 seconds and 0.4-0.6 seconds of Figure 6-68 respectively. The 4.0 kW could be generated as either 2.2 kW from the battery, and 1.8 kW from the supercapacitor or the battery generated 2.1kW, and the supercapacitors generated 1.9 kW, as shown in the periods of 0.6-0.7 seconds and 0.7-1.0 seconds of Figure 6-68 respectively.

The second approach is that the EV injects a very small active power to the microgrid. During voltage stability issues, the EV operates as reactive power injection to the microgrid with very low active power generated from the resources of the EV. The reactive power generated from the EV at two levels, i.e. 4.5 kVAR for a period of 0.2-0.6 seconds and 4 kVAR for a period of 0.6-1.0 seconds, as shown in Figure 6-69. To generate 4.5 kVAR, the inverter generated two different reactive power levels of the battery and supercapacitors where the battery supplied 2.5 kVAR and the supercapacitors supplied 2 kVAR during 0.2-0.4 seconds or the battery and the supercapacitors supplied 2.25 kVAR during 0.4-0.6 seconds, as shown in Figure 6-69. Another level of 4 kVAR was applied. The battery supplied either 2.2 kVAR during 0.6-0.8 seconds or 2 kVAR during 0.8-1.0 seconds. The rest of the power was generated by the supercapacitors.

The third approach is that the EV generates active and reactive power simultaneously. In this case, the EV supplied 3 kW and 1.5 kVAR for 0.2-0.6 seconds and 3.6 kW and 1.8 kVAR for the rest of the time. The generation of power from the battery and supercapacitors is shown in Figure 6-70 and Figure 6-71. It is clear that the battery and supercapacitors are sharing generating both active and reactive power. The battery supplied 1.9kW+0.5kVAR for a period of 0.2-0.4 seconds whereas the supercapacitors supplied the rest of the power of the inverter. The reference power had changed to produce 1.2kW+1.5kVAR from the battery for the period of 0.4-0.6 seconds, whereas the supercapacitor successfully produced the rest of the power of the inverter. The same behaviour of battery and supercapacitors is noticed when increasing the inverter power injection to 3.6kW+1.8kVAR.

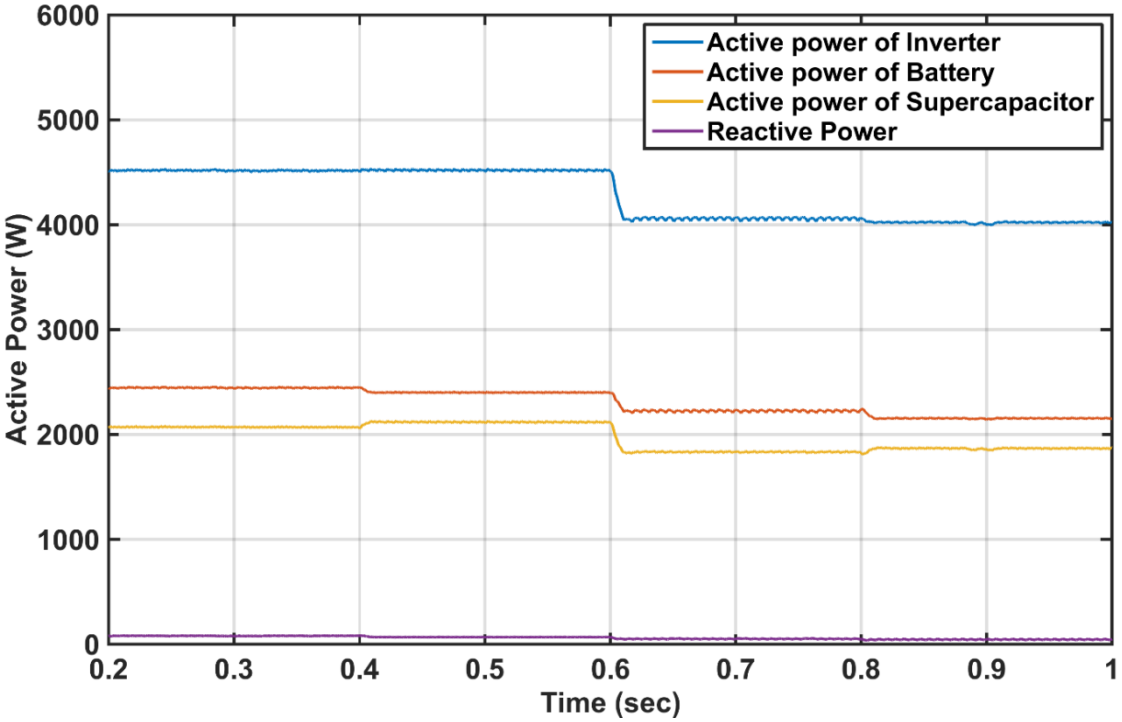

Figure 6-68: Active power of inverter, battery, and supercapacitor of EV at different ranges of injection of active power to the microgrid (simulated results)

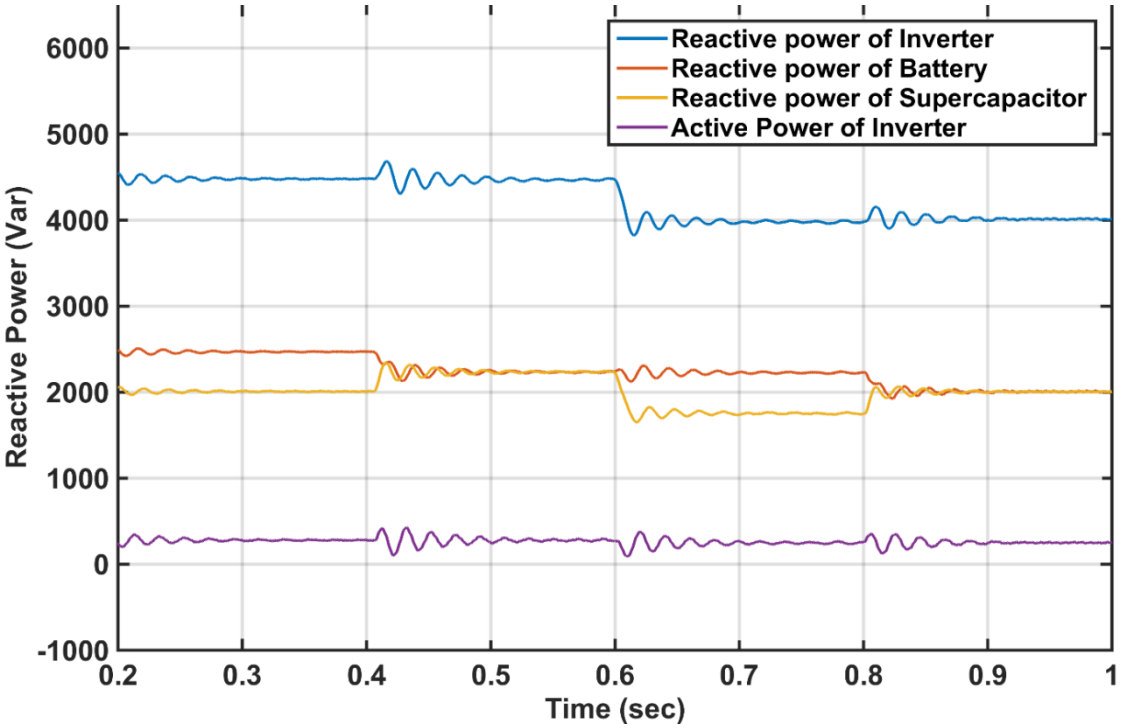

Figure 6-69: Reactive power of inverter, battery, and supercapacitor of EV at different ranges of injection of reactive power to the microgrid (simulated results)

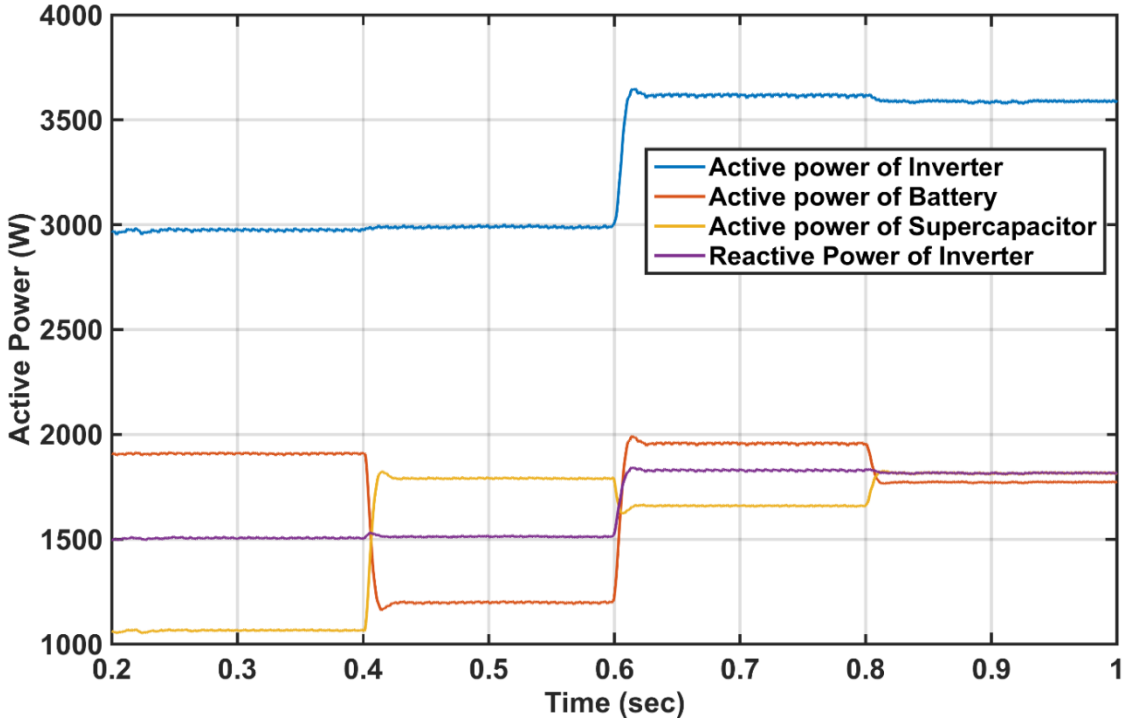

Figure 6-70: Active power of inverter, battery, and supercapacitor of EV at different ranges of injection of active and reactive power to the microgrid (simulated results)

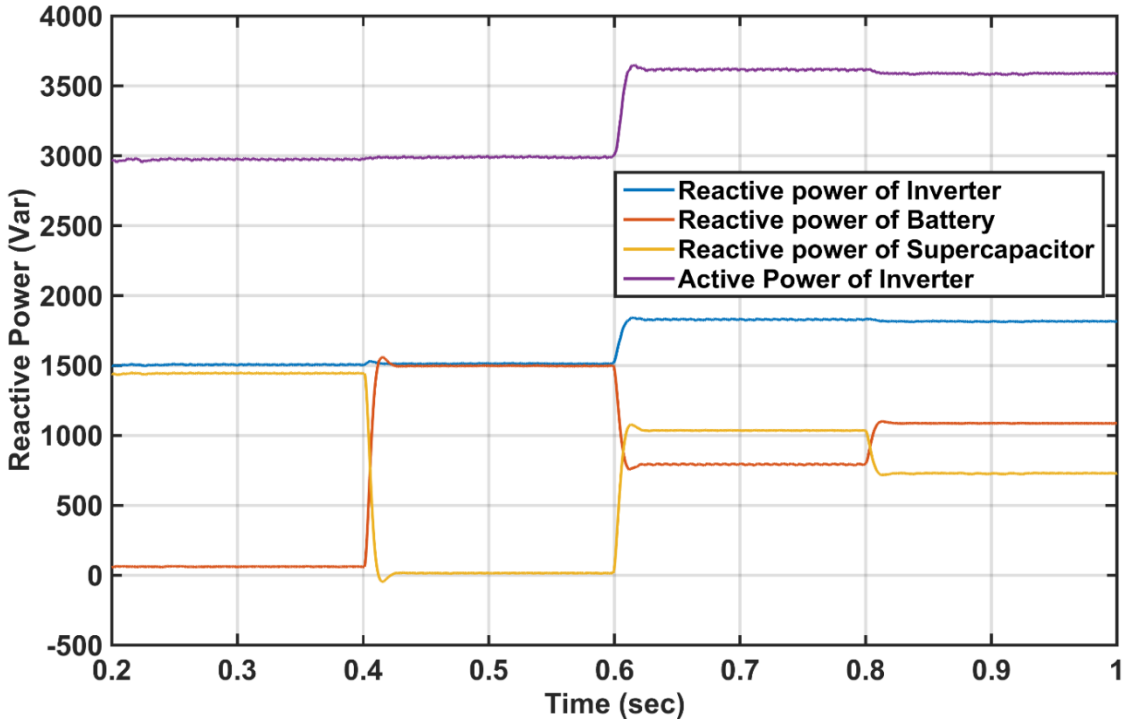

Figure 6-71: Reactive power of inverter, battery, and supercapacitor of EV at different ranges of injection of active and reactive power to the microgrid (simulated results)

6.9 Conclusion

This chapter introducs the mathematical formulae of the lead acid battery and the double layer supercapacitor. The modified H-bridge multilevel inverter has been chosen to operate the battery and the supercapacitors with load or microgrid connection. A comprehensive and systematic framework is implemented to address the power and energy management of the battery and the supercapacitors' energy storage system of the EV. The power and energy management framework operates in a chronological way from high-level to low-level shells. The high-level shell, medium level shell, and low-level shell are represented by Energy Management Shell (EMS), the Power Management Shell (PMS), and the Power Electronic Shell (PES) respectively.

The EMS is intended to control the voltage and frequency of the waveform to a standard level and balance the power of the battery and supercapacitors. All the operations within EMS apply at a positive sequence waveform within the fundamental frequency. Droop controller adjusts the voltage and frequency of the waveform to the standard level of the network which is 50 Hz and 220 V in this study. The droop controller should set the amount of power that the energy storage systems could provide. The discharging reference power of the energy storage systems is changeable according to the capacity and state of charge of the resources. Each EV has discharging reference power. A set of mathematical equations of integrating EV to the distribution line of the microgrid at CSO node are derived to calculate the suitable power reference for each EV based on the characteristic equation, the voltage of the CSO, and the power factor of the microgrid to automate the operation of the EMS. The results of the droop controller section showed the fast-tracking response of the fundamental frequency and standard voltage at the point of disturbance, which took about 1.5 cycles. The vector controller used Park's transformation to transform the three-phase instantaneous stationary reference frame into a time-invariant synchronous rotating reference frame to control the active and reactive current drawn from the energy storages of the EV. The advantage of using this method has resulted in constructing a perfect orientation of the frame dq0 axis to coincide with the axis d with the rotor flux vector, whereas in most control cases the quadrature component of flux and its derivative will be cancelled. Therefore, this kind of controller is very useful for control purposes, which is a vector controller to simplify the electromagnetic equations to deal with DC value rather than time varying AC rotating value. Furthermore, the alfa-beta controller is used for the observer design to cancel the stator torque pulsation. Therefore, the PID controller could be used directly with dq0 or alpha-beta controller, whereas it is not possible to use it directly with the time varying ABC model. The amount of active power or reactive power drawn from the battery or supercapacitors depends on the state of charge, frequency variation, and voltage variation of the resources. For example, at frequency variation, the microgrid should draw active power from the battery, whereas at voltage variation the supercapacitors supply reactive power to the microgrid. In case one kind of resource fades the other one generates the required power. The response of the vector controller to sharing power from the battery and the supercapacitors at different references of active and reactive power are depicted in Figure 6-68 to Figure 6-71.

The PMS is responsible for managing the power split between the battery and supercapacitors based on the state of charge of the energy storage systems, frequency deviation, and voltage deviation. The fuzzy heuristic derivation is used to balance the variables of the system and to decide the reference consuming power from the battery and the supercapacitors. The rules for the PMS to choose the most suitable consuming power from the battery and supercapacitors are shown in Figure 6-23 to Figure 6-28. The dissection made a rollover to the PES within milliseconds.

The PES is the downstream process in the modular hierarchy power and energy management strategy. The PES performs the SVPWM modular to operate the switches of the inverter. The modified multi-level H-bridge inverter proposed in this study consists of 18 switches to control the battery and the three supercapacitors. The topology of the inverter consists of the three-phase bridge inverter to control battery operation and three H-bridge converters to control the supercapacitors' operation where each H-bridge converter connects in series with one leg of the three-phase bridge inverter. The modified SVPWM approach is proposed as an extension of the two-level SVPWM to hybridize the operation of multiple energy storage systems. State matrix, space vector location, distribution of the sampling time, and overmodulation are represented mathematically in the study. The results show an asymmetrical trigger with a phase shift of 120^0.

Results are demonstrated for operating the system at two modes: charging and discharging; at charging mode, either the battery or the supercapacitors are charging at a single time because they are connected in series. Furthermore, the energy flow from the microgrid to one of them until reaching the desire to leave state of charge, then, the other resources start charging. Charging supercapacitors is much faster than charging the battery due to its characteristics and the rated capacity of the supercapacitor, where the rated capacity of the supercapacitor has been chosen as it is much lower than the battery. At discharging mode, both the battery and the supercapacitors are synergized to provide the required power.

7. Chapter Seven: Experimental Validation

7.1 Introduction

The physical design and implementation of the proposed system under research validate and support the achievement of a mathematical model. There is no mathematical model compact with physical model unless doing comparison between the results of the mathematical model with the physical model. However, some researchers are very difficult to implement physically such as the one under research whereas building a physical model as in Figure 1-12 is very complicated and very expensive due to the range of the system which starts from the power system level to the power electronic level.

The research starts by applying power flow analysis at a system consisting of 86 bus bars with a variety of loads that balanced by ten centralised generators and connected by 97 lines and transformers to figure out the benefits of reconstructing the system to microgrid based on the eigenvalue and eigenvector analysis. Then, the analysis of integrating EVs into microgrid network of 49 bus bars with a variety of distributed load balanced by 13 of four types distributed generators connected by 48 distribution lines studied deeply.

Three operators of the controller were proposed to provide resilient operation to the microgrid which are MGO, CSO, and EVO. The MGO has applied by multi-objective optimisation algorithm using MIQP model of Cplex program based on MATLAB environment to manage minimum cost operation of the microgrid. The CSO has applied by objective optimisation function using MILP model of Cplex program based on the MATLAB environment to achieve either minimum charging cost or maximum discharging cost of EVs operation. The EVO applied real time snapshot of interconnecting EV within microgrid through three sub-process which are EMS, PME, and PES to manage and control the proposed model of providing acceptable waveforms characteristics, arbitrating power between resources, and applying switching modulation strategy. Therefore, a couple of researcher through years should help each other to prepare platform rig of such system. However, many mathematical models of the real component of the system validated by several researchers such as power flow analysis of the power system, the models of the distributed generators, the lead-acid battery and supercapacitor resources of the EVs. Therefore, based on the previous argument, this research is focused on validating the real-time operation of modified switching modulation at modified cascade multilevel inverter to provide a specific reference from the bank of batteries and three supercapacitors which applied the PES level of the research controller. The real-time simulator is implemented based on CompactRIO devices and LabVIEW software.

The proposed research consists of many threads which could be challenging to experiment. Hence parts of this research are experimentally validated which feed into the wider and higher level parts of the research.

In particular, this chapter describes the equipment that was employed experimentally to validate the energy management scheme proposed in PES in chapter six. For this part of the research, an experimental facility was developed with the aim of:

1. Demonstrating the voltage waveforms of the three-phase output at different modes.
2. Demonstrating the current waveforms of the battery, supercapacitor, and the AC side of the inverter
3. Showing the response of the supercapacitors to synergize the battery.
4. Validate the modulation of modified space vector pulse width modulation to generate the voltage waveforms.
5. Comparing the experimental results with the results of PES from the simulation studies carried out in 6.7.3.

The design considerations of the experimental rig which is presented in this chapter is extended of modification and design of Maciej Bendyk [353].

7.2 Experimental Rig Description

The overall layout of the experimental rig can be shown in Figure 7-1. The experimental rig designed to run a motor drive consisting of 0.37 kW induction motor using a modified cascade multilevel inverter. The inverter is powered by a bank of the battery to generate 60 V and three supercapacitors each one supply 30 V. The real-time simulator used is CompactRio from National Instrument company supported by FPGA technology; it is used to control the rig. The overall applied layout of the experimental rig is shown in Figure 7-2 and Figure 7-3. The details of the experimental rig are described in following sections.

7.2.1 Three phase induction motor

KAPAK induction motor built by English Electric Machines AEI was used in this research as shown in the Figure 7-3. The winding of the motor is connected in delta configuration to match the voltage available from the resources of the inverter. The three-phase terminal of the motor is connected to the output of the inverter through simple LC filter to minimise switching noise as shown in Apx_Figure K-16 in the Appendix K. The parameters of the motor are shown in Table 7-1.

Table 7-1: Induction motor parameter

	Parameter	**Value**
1.	Power	0.37 kW
2.	Voltage	220/250 V, Delta configuration 380/440 V, Star configuration
3.	Current	1.5 A, Delta configuration 0.9 A, Star configuration
4.	Number of phases	Three
5.	Frequency	50 Hz
6.	Speed	2840 rev/min
7.	Regime	Continuous work
8.	Winding resistance	21 Ω, Delta configuration 30 Ω, Star configuration

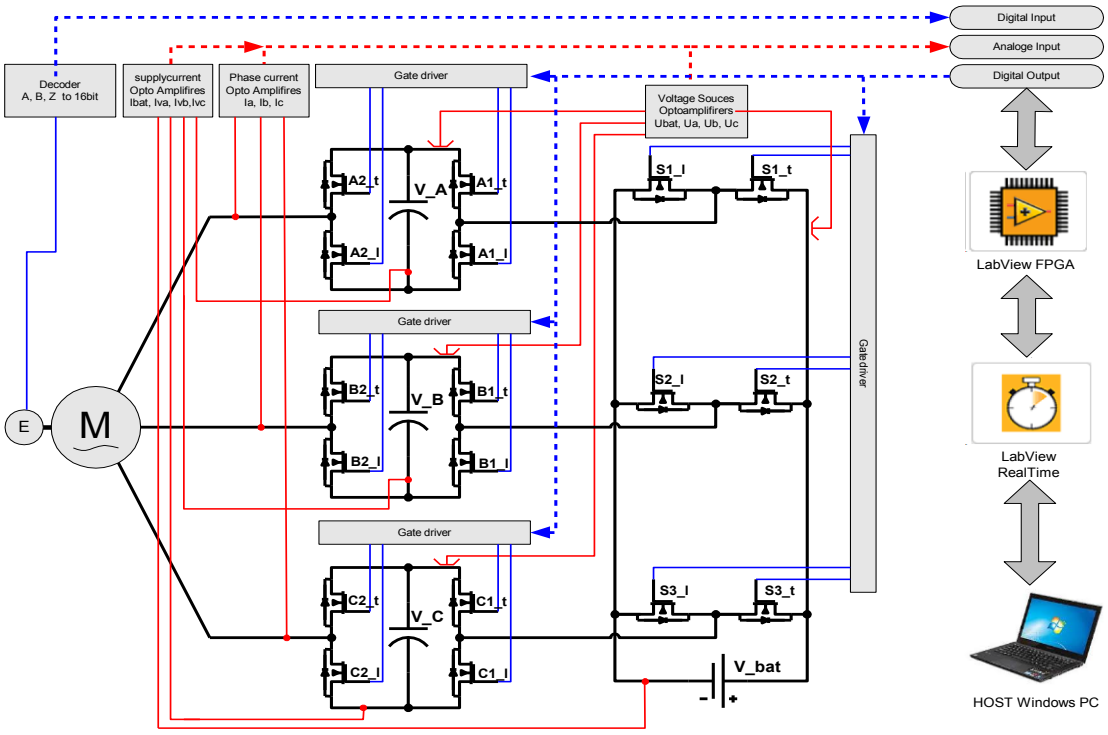

Figure 7-1: Overall layout of experimental rig

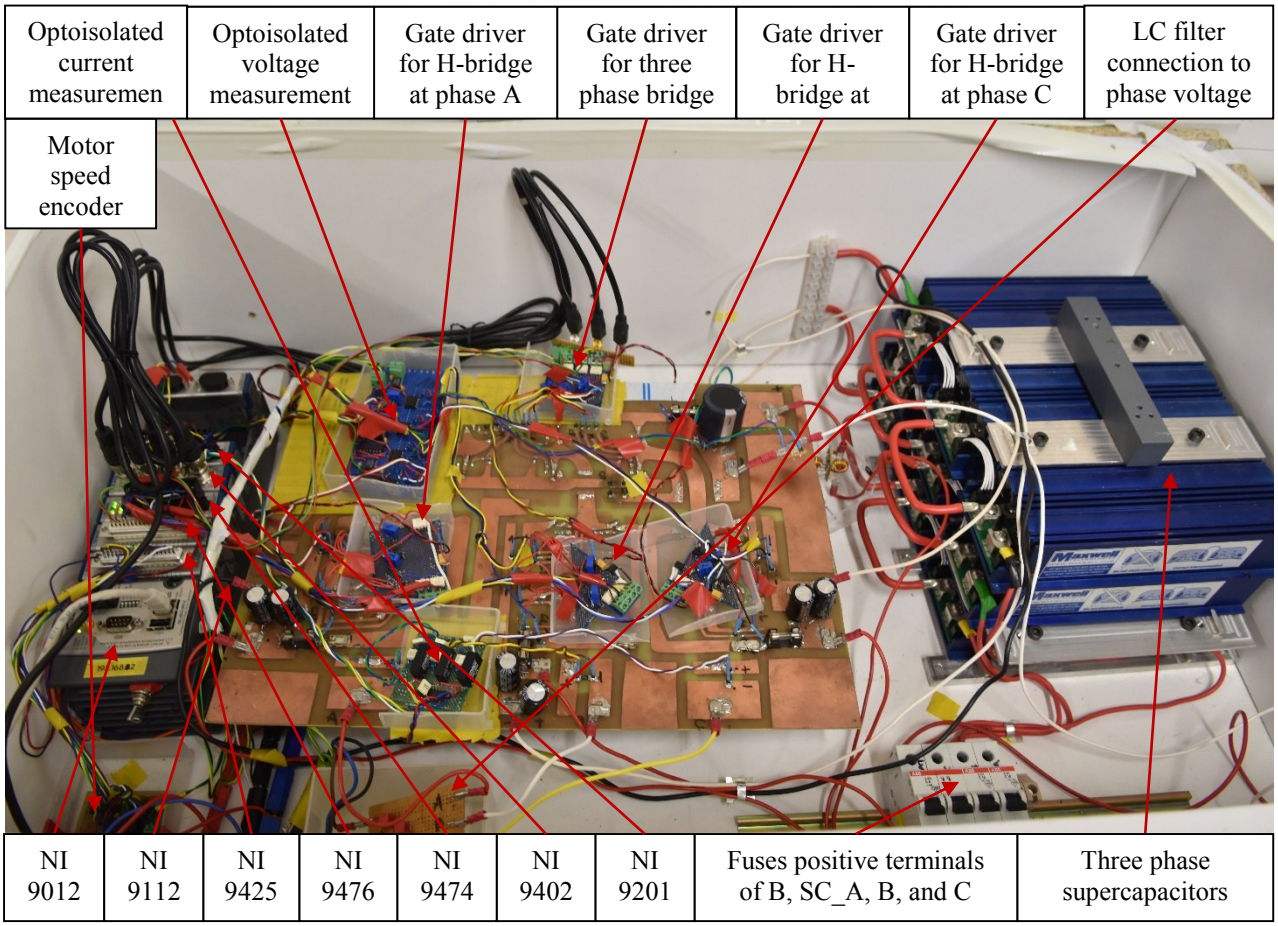

Figure 7-2: Inverter overview

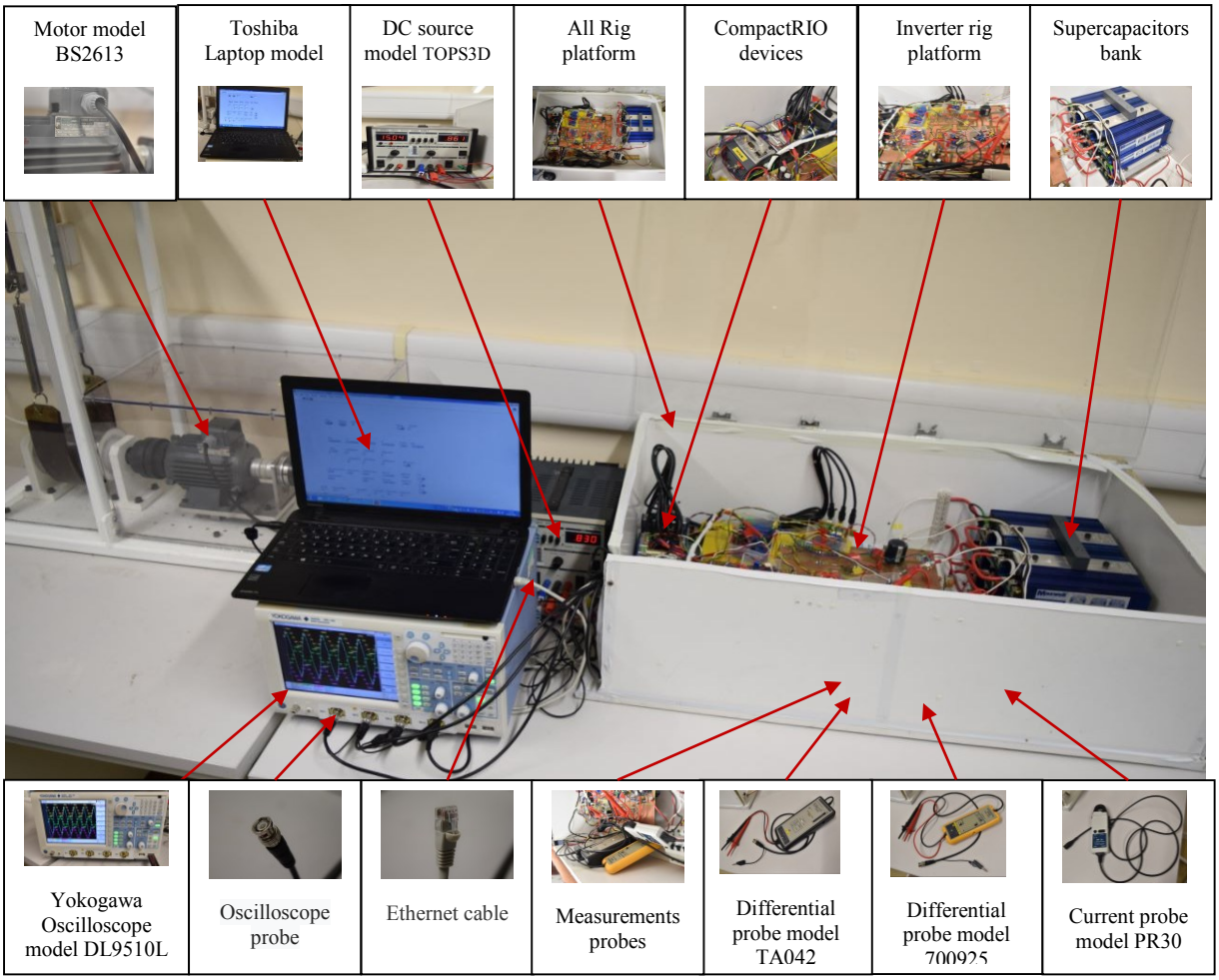

Figure 7-3: Rig overview

7.2.2 Modified cascade multilevel inverter

It consists of four resources and four converters. The schematic diagram is explained as three phase bridge inverter supplied by a battery connected in series to three H-Bridge converters, each one supplied by supercapacitor as described in Apx_Figure K-10 in the appendix K.

7.2.3 National instruments CompactRIO real time simulator

The National Instruments CompactRIO controller has been chosen. The architecture of the typical NI CompactRIO system is shown in Figure 7-4. The configuration of the CompactRIO that is used to implement the experimental rig reveals below:

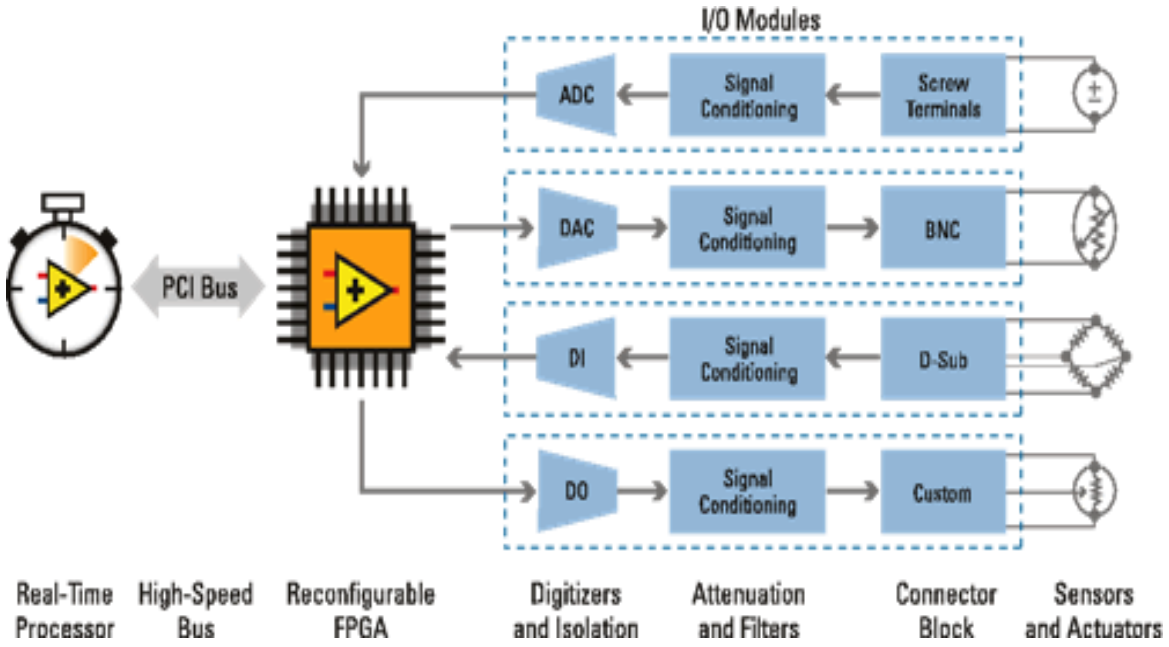

Figure 7-4: Architecture of the CompactRIO system

NI CRIO 9012: it is an embedded real-time controller that is suitable for advanced control and monitoring the operation of proposed inverter. The specification of this device is 400 MHz CPU, 64 MB DRAM, and 128 MB of storage. This controller features accept one Ethernet, one USB, and one serial connectivity ports. The configuration of the cRIO-9012 is shown in Apx_Figure K-1 in the Appendix K.

NI CRIO 9112: it is a rugged programmable FPGA CRIO chassis that can be used to add C series I/O modules to the controller. It consists of eight Xilinx Virtex 5 LX30 FPGA slots with 19200 flip-flops and 1152 kbit embedded RAM. It operates at an internal clock frequency of 40 MHz. The chassis is connected to the compatible CRIO controller to communicate with the modules installed in the chassis as shown in Apx_Figure K-2 in the Appendix K.

NI 9425: it is input series digital model with 32 channels and 7 µs resolution. It works to read decoded information from position encoder. The configuration of the model NI 9425 is shown in Apx_Figure K-3 in the Appendix K.

NI 9476: it is a source of low-speed digital output model with 500µs resolution. It is used to control shutdown function of gate drivers. D01 to D0 4 that are used to enable switching of the manual switch, three phase bridge, H-bridge phase A, H-bridge phase B, and H-bridge phase C respectively. The configuration of the model NI 9476 is shown in Apx_Figure K-4 in the Appendix K.

NI 9474: it is eight high-speed digital output channels module with 1 µs resolution. Six channels outputs are used to control H- bridge converters in each phase. D02 and D03 control gate signals of H-bridge converter connected at phase A. D04 and D05 control gates signals of H-bridge converter connected at phase B. D06 and D07 control gates signals of H-bridge converter connected at phase C. The configuration of the model NI 9474 is shown in Apx_Figure K-5 in the Appendix K.

NI 9402: it is high speed four bidirectional channels model with 4 µs resolution. The first three channels (DIO0-DIO2) are used to control gate signals of the three-phase bridge while digital input DIO3 is used to detect full rotation from the encoder. The signal level of DIO0 to DIO2 is amplified from 5V to 15V for the optoisolated circuit. The configuration of the model NI 9402 is shown in Apx_Figure K-6 in the Appendix K.

NI 9201: it is the eight analogue input channels model with ±10 V input range, 12-Bit resolution, and 500 kS/s sampling frequency. It is used to measure voltage and current feedback signals. The channel is distributed as below:

AI0 is occupied to measure three phase bridge inverter supply current (Ibat)

AI1 is occupied to measure H-bridge converter supply voltage connected to phase C (SCc)

AI2 is occupied to measure H-bridge converter supply voltage connected to phase B (SCb)

AI3 is occupied to measure H-bridge converter supply voltage connected to phase A (SCa)

AI4 is occupied to measure inverter current at phase A (Ia)

AI5 is occupied to measure inverter current at phase C (Ic)

AI6 is occupied to measure inverter current at phase B (Ib)

AI7 is occupied to measure three phase bridge inverter supply voltage (Vbat).

The current in AI0, AI4, AI5, and AI6, the voltage in AI1, AI2, and AI3, and the voltage in AI7are converted by external hardware from ±6 A to ±10 V, from floating 0-65 V to 0-10 V, and from floating 0-160 V to 0-10 V respectively. The configuration of the model NI 9201 is shown in Apx_Figure K-7 in the Appendix K.

7.2.4 Gate drivers circuit for inverter

Providing galvanic isolation between the resources of the inverter and control system is the most important part of the design. NCS6S4815C and astec ASA00CC36-L are used as universal galvanic isolated DC/DC converters PSU1, PSU2, PSU3, and PSU4 deliver stable 15 V to gate drivers in each bridge in addition to optoisolated all the ports (analogue and digital) of the NI CRIO as shown in Apx_Figure K-8. The L6390 gate driver is chosen to switch the gate of the MOSFET. The schematic diagram of the upper and lower pair MOSFET gate drive is shown in Apx_Figure K-9 in the Appendix K. There are nine circuits used to trigger the 18 switches of Inverter.

7.2.5 Optoisolated digital signal interface

The high-speed logic optocoupler HCPL2601 device is used as galvanic isolation between control signals from NI CRIO system and converter gate drivers. The speed and common mode rejection of this device are 10 kV/us and 10 Mbit/s. The schematic diagram of digital optoisolator is shown in Apx_Figure K-11 in the Appendix K.

7.2.6 Optoisolated voltage and current sensing circuit

Accurate voltage and current measurement of the resources are required to provide many features such as:

- Estimated maximum available energy of resources to decide the amount of discharging or charging power.
- Stabilise the supercapacitors voltage and current between phases to make it balance.
- Implementing the space modulation strategy.

Shunt resistance of 0.05 ohm is used to measure the voltage drop across the resistors that are connected with each resource. The separate circuit has been built for each current sense depending on isolation amplifiers HCPL-7840 as shown in Apx_Figure K-12.

The voltage measurement has two features which are measuring the voltage of resources and providing isolation between each floating resource and CRIO control system. Therefore, high linear analogue optocoupler HCNR201 is used. The schematic diagram of the voltage sense is shown in Apx_Figure K-13. The schematic diagram to connect the current and voltage measurement is shown in Apx_Figure K-14 in the Appendix K.

7.2.7 Voltage sources

There are two kinds of measuring used as the voltage supplied to the inverter. The main voltage resource is a bank of batteries that supply the three-phase bridge inverter. The bank of batteries consists of seven Leoch LP12-4.0 Sealed Lead Acid Batteries (LAB). Each one has a capacity of 4.0 Ah and operates at 12 V (SLA 12 V 4.0 Ah). The internal resistance for each one is 0.4 ohm. The batteries are connected to the three-phase bridge inverter through LC filter to reduce the stress on the batteries by minimising the current ripples. The filter consists of 80 uH inductor connected in series with the batteries and set of two 1 mF electrolytic capacitors connected in parallel with the batteries. The current is measured across the batteries through 0.05-ohm shunt resistor that is connected in series with the batteries.

The assistance voltage resource is three banks of supercapacitors that supply three H-Bridge converters. Each supercapacitor is connected in series with the battery through the legs of the three-phase bridge inverter. The electric double layer boost cap supercapacitor from Maxwell Technologies (BMOD0350-15) with individual balanced cells has been selected. Three supercapacitors are connected in series for each phase to provide 45 V from total capacitance 19.333 F where each one has a capacitance of 58 F and supply 15 V. The maximum energy that can be stored in each phase is 19.6 kJ while the total energy of the three phases is 58.7 kJ. The schematic diagram of the connected resources is shown in Apx_Figure K-15 in the Appendix K.

7.3 Results Description

To generate clear waveforms, the results were printed from the oscilloscope as a wdf extension. It was converted to csv extension using X viewer program from Yokogawa company; then it is drawn by MATLAB. The MATLAB figures show the real axis of the waveforms. Figure 7-5A and B show the waveforms of three-phase bridge inverter at output voltage 40 V in wdf extension while C shows the same waveforms in MATLAB figures. The rest of the results treat same as the previous waveforms. Figure 7-6 to Figure 7-8 show the waveforms of three-phase bridge inverter at 50, 60, and 65 V. Figure 7-9 to Figure 7-12 show the waveforms of H-Bridge converters operation at 40, 50, 60, 65 V respectively. Figure 7-13 to Figure 7-22 show the waveforms of sharing power between the three-phase bridge inverter and H-bridge converters at 40, 50, 60, 70, 80, 90, 100, 110, 120, and 128 respectively. The Figure 7-8, Figure 7-12, and Figure 7-22 operate in overmodulation area. Therefore, the nonlinearity of the waveforms increased. Figure 7-23 to Figure 7-26 show the phase voltage waveforms of the three-phase bridge inverter at reference voltage 40, 50, 60, and 65 V respectively. Figure 7-27 to Figure 7-30 show the phase voltage waveforms of the H-Bridges at reference voltage 40, 50, 60, and 65 V respectively. Figure 7-31 to Figure 7-40 show the phase voltage waveforms of operation of both bridges at the reference voltage of 40, 50, 60, 70, 80, 90, 100, 110, 120, and 128 V respectively.

7.3.1 Measurement devices

The results of this dissertation are based on the instruments, shown below:

- TA042 100 MHz 1400 V Differential Probe (three probes)
- 700925 15 MHz 1000 V Differential Probe (one probe)
- LEM PR30 Oscilloscope AC/DC Current Probe (one probe)
- DL9510L - Yokogawa mixed signal oscilloscopes (one oscilloscope)

7.3.2 Discussion of experimental results

The inverter is proposed to operate mainly in three modes. The first mode is the battery that supplied the load through three-phase bridge inverter. The second mode is the supercapacitors supplied the load through the three H-Bridge converters. The third mode is both the battery and the supercapacitors supplied the load through the three-phase bridge inverter and the H-Bridge converters respectively. The maximum voltage could supply the inverter depending on the voltage of the battery and the supercapacitors.

During the first mode, the amplitude of active voltage vector in stationary alpha-beta coordinate system is represented as two third of battery voltage while the maximum amplitude of the rotary voltage vector is equal to $\frac{V_{bat}}{\sqrt{3}}$ which represented the radius of the circle inscribed inside the hexagon diagram. Therefore, the nonlinearity increased at maximum voltage operation as increasing voltage reference of the load due to operation in overmodulation area. Increasing nonlinearity distorted the waveforms and increased the harmonics of the waveforms as noticed

in Figure 7-8. The system within mode one operates in two level waveforms. Therefore, the system does not benefit from the inverter structure to supply high voltage amplitude to reduce switching ripples and losses of covering high demand. However, operating the inverter based on the three-phase bridge inverter provides symmetrical voltage waveforms with phase shift 120^{o} . Thus, the output voltage from the inverter would be balanced without depending on the state of charge of the supercapacitors.

The second mode has covered the operation of the H-Bridge converters only. Therefore, the supercapacitors supply the load at three levels of vectors which are 0, V_{sc}, and $2V_{sc}$ where the operation voltage of the supercapacitors is 30 V. The maximum amplitude of the rotary output vector voltage is limited to $\frac{2V_{sc}}{\sqrt{3}}$. It is easy to notice that the supercapacitors respond very quickly to the demand required from

Figure 7-9 to Figure 7-12. However, practically it is very difficult to keep the supercapacitors at the same level of state of charge and same level of voltage. The nonlinearity of the waveforms increased as the demand voltage reference increased due to operation of the H-Bridge converters in overmodulation area as shown clearly in Figure 7-12. Therefore, the ripples and the harmonics of the waveforms increased. The supercapacitors discharge power very quickly. Therefore, it is difficult to maintain the demand for long time at same voltage level of supercapacitors without sharing the demand power with the three-phase bridge inverter. It is worth to operate this mode as a filter, power factor correction, accelerating the vehicle, recapture of the braking energy or maintaining angle or voltage stability of the system for short period.

The maximum benefits that can be achieved from the proposed inverter topology are operating all converters to supply the demand from the battery and the supercapacitors. The operation of this mode depends on the requirement as either supercapacitor synergies the battery, or the battery synergies the supercapacitors. The inverter could modulate to generate vector voltage as sum of three phase bridge inverter and H-Bridge converters which are equal to $\frac{2}{3}(V_{bat} + 2V_{sc})$ whereas the maximum output voltage could be generated from this mode is $\frac{1}{\sqrt{3}}(V_{bat} + 2V_{sc})$. Therefore, this mode could supply much higher voltage than previous modes. The number of voltage level tolerates between two to five levels as the reference of demand, which increased due to sharing power from both the battery and the supercapacitors. The direction of power could be discharging both resources, charging both resources or circulating the current between resources to discharge one and charge the other resources based on the phase shift angle of the generated waveforms, where the smallest output voltage vector could be supplied from this mode is $\frac{2}{3}(V_{bat} - 2V_{sc})$. By noticing Figure 7-14 to Figure 7-22, it could be obviously seen that the response of the supercapacitor is quicker than the battery; the supercapacitors filtered the current waveforms of the battery by reducing the current ripples even at high voltage vector requirement which is shown at Figure 7-40. Therefore, the switching losses within the inverter are expected to be small where the transition between the switches would be smooth and the switching current would be small. Therefore, the switching losses are reduced and the harmonic measurement is expected to be at minimum level.

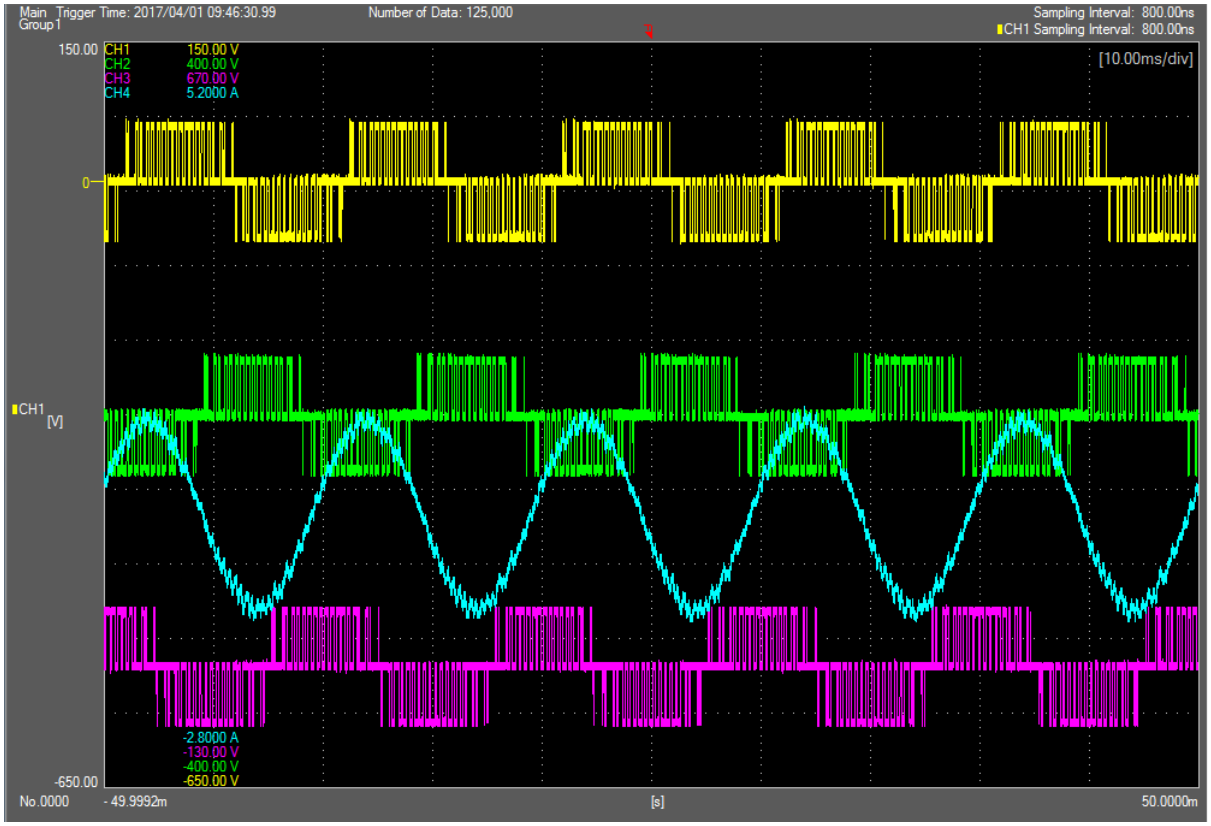

A- waveforms of the three-phase bridge at output voltage 40 V in wdf extension

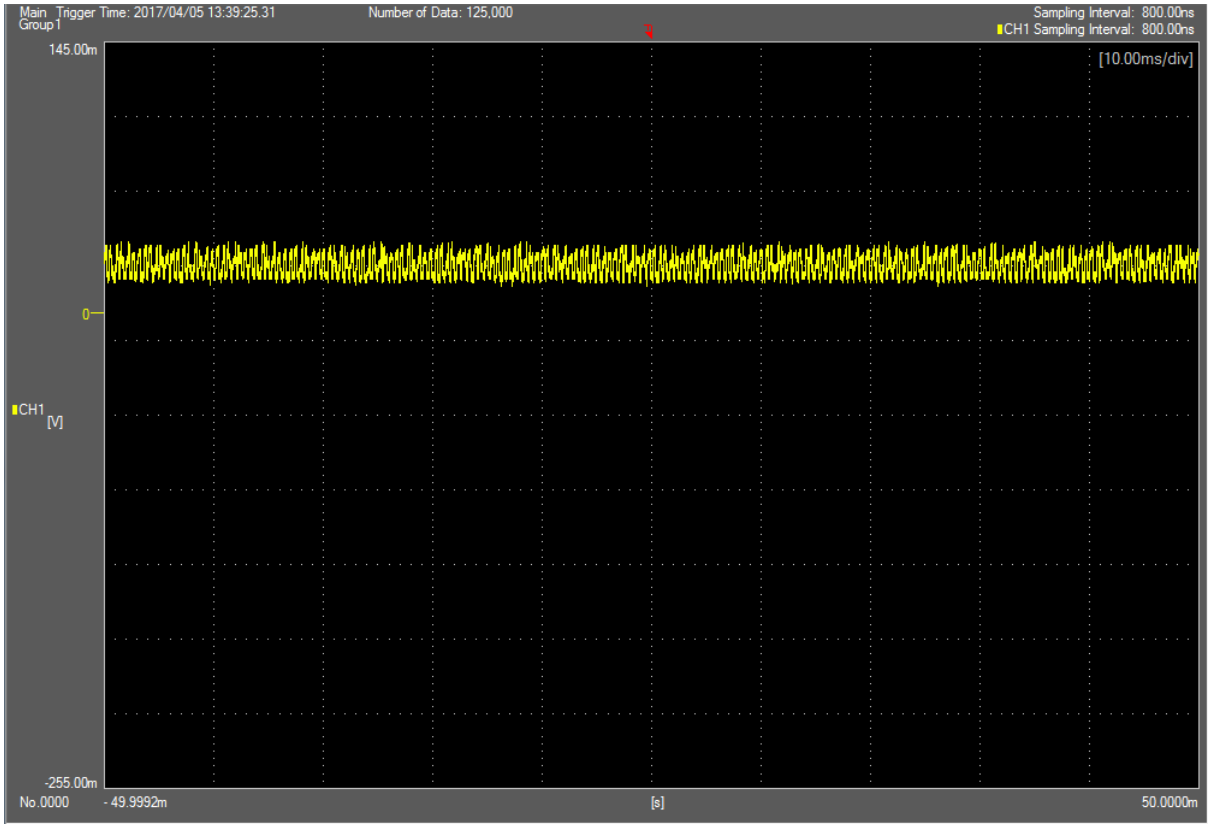

B – Battery current waveform of three Phase Bridge at output voltage 40 V in wdf extension

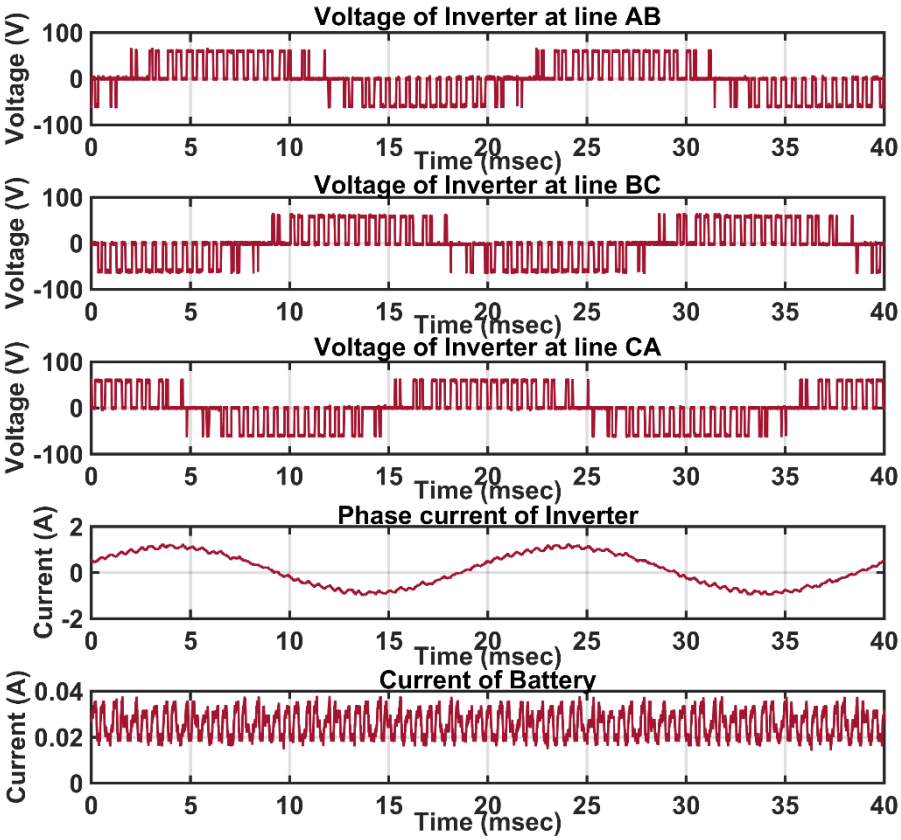

C - Waveforms of three-phase bridge at output voltage 40 V in MATLAB figure

Figure 7-5: Waveforms of the three-phase bridge at output voltage 40 V

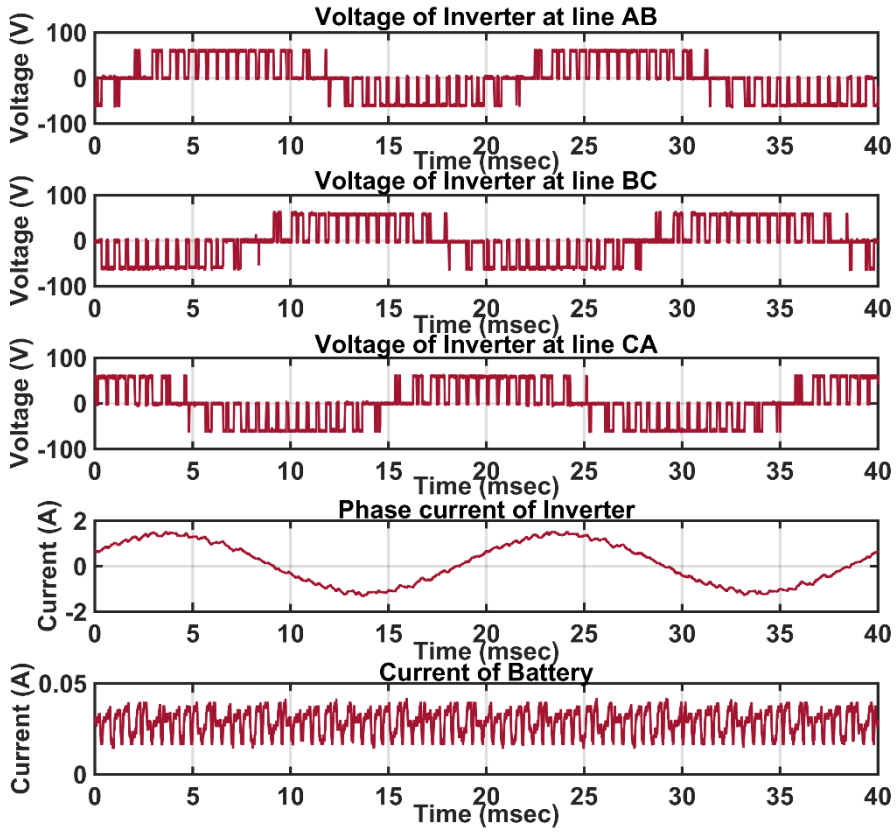

Figure 7-6: Waveforms of three-phase bridge at output voltage 50 V

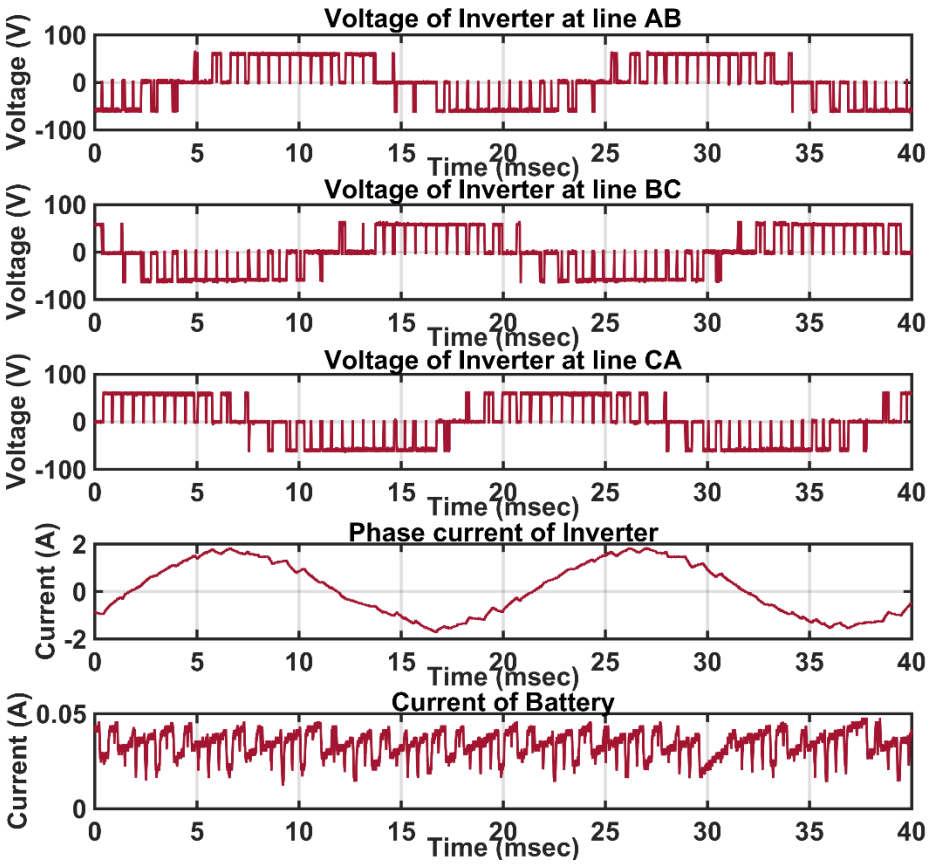

Figure 7-7: Waveforms of three-phase bridge at output voltage 60 V

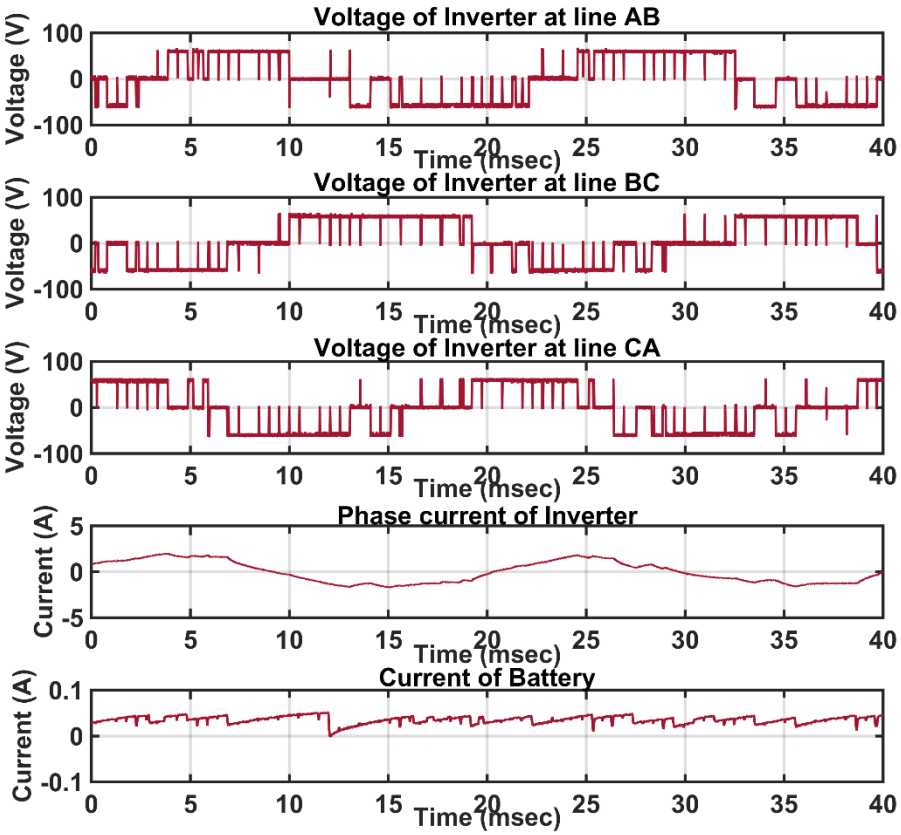

Figure 7-8: Waveforms of three-phase bridge at output voltage 65 V

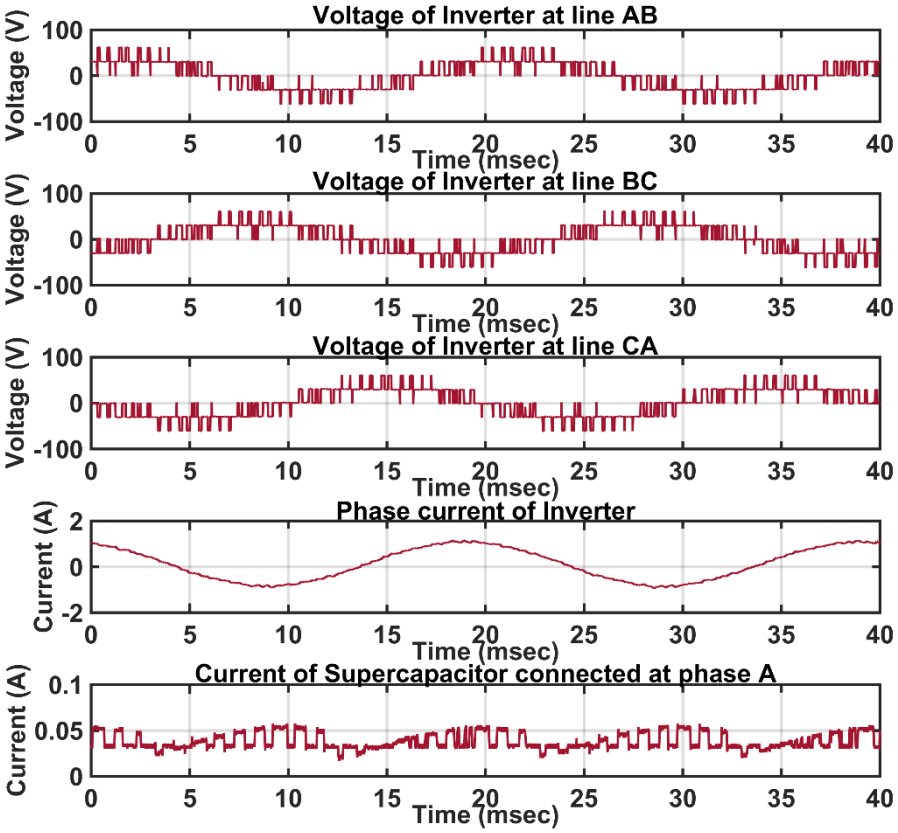

Figure 7-9: Waveforms of H-Bridge at output voltage 40 V

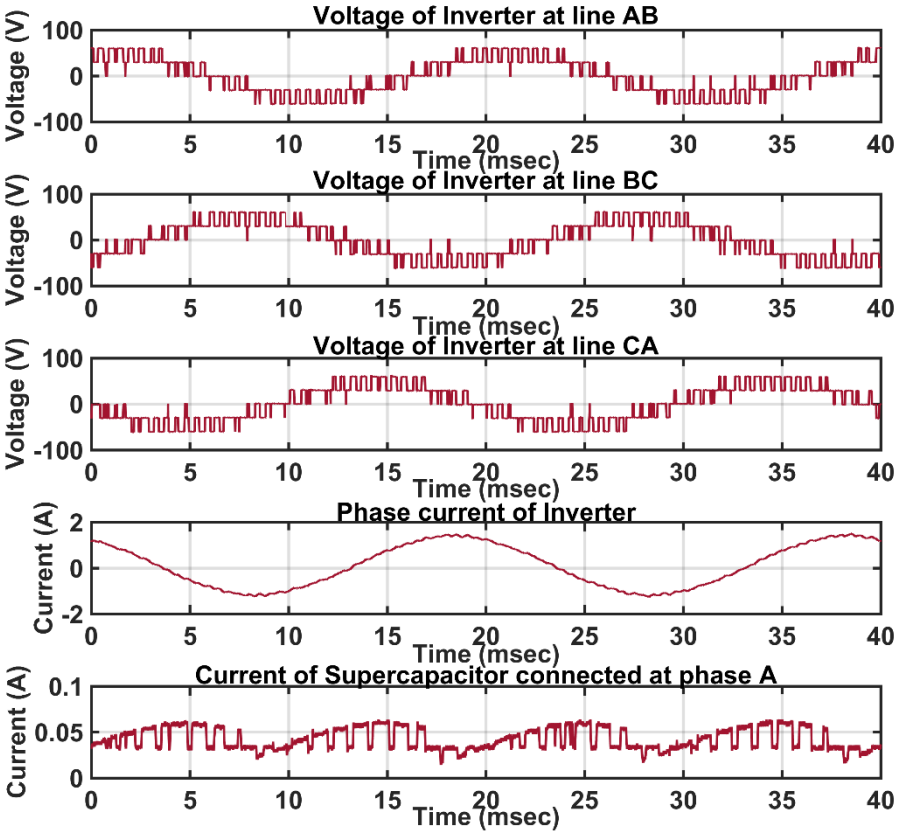

Figure 7-10: Waveforms of H-Bridge at output voltage 50 V

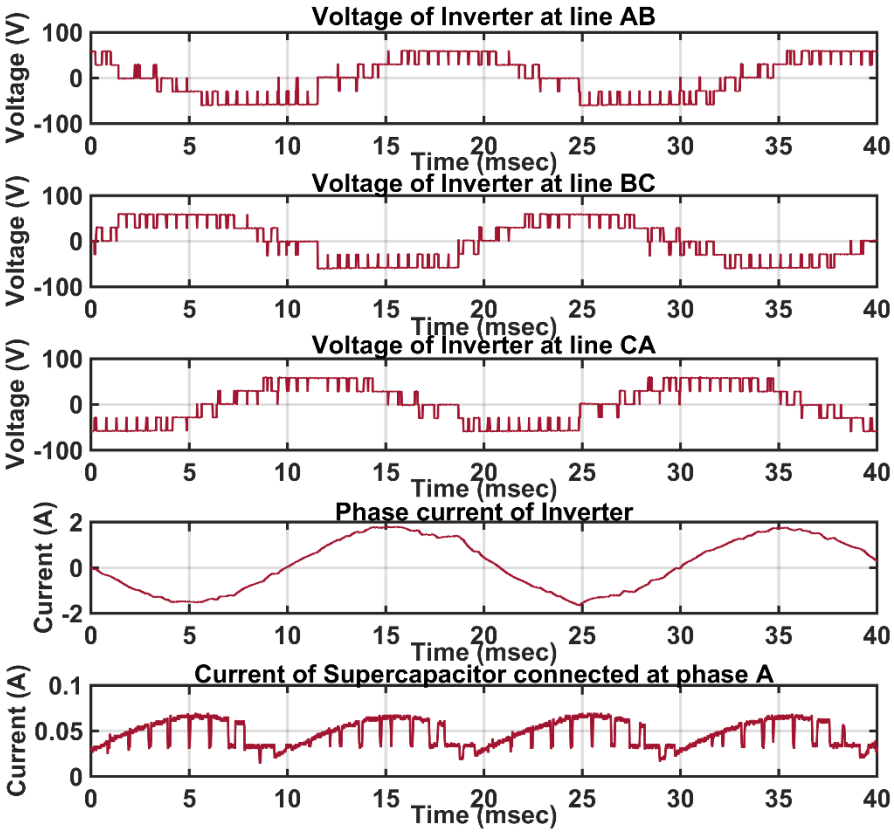

Figure 7-11: Waveforms of H-Bridge at output voltage 60 V

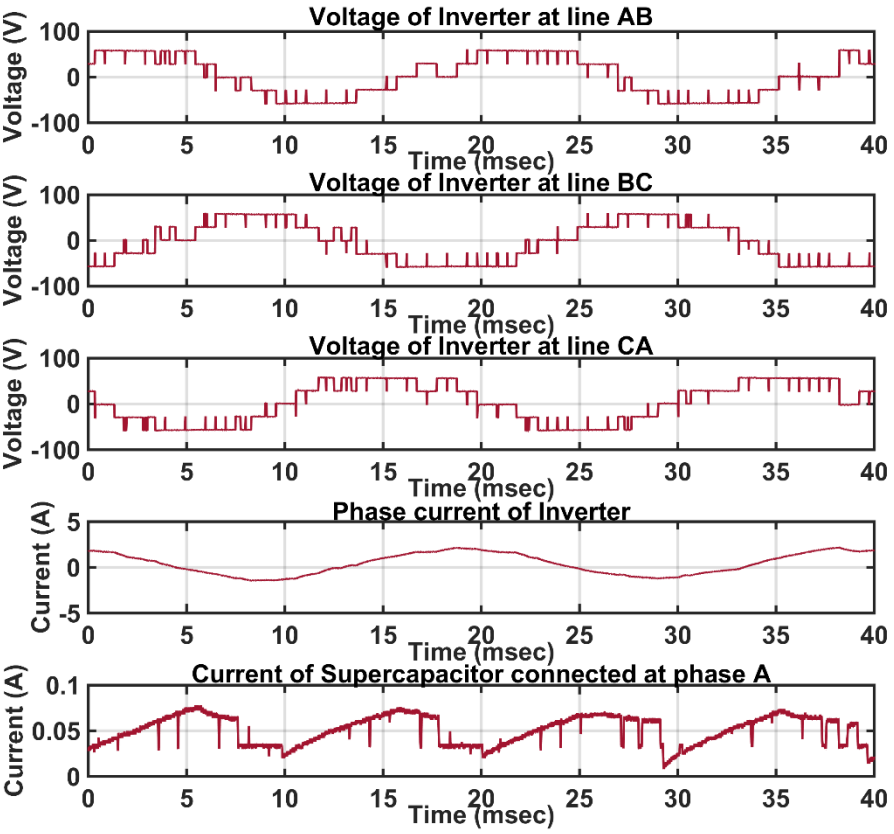

Figure 7-12: Waveforms of H-Bridge at output voltage 65 V

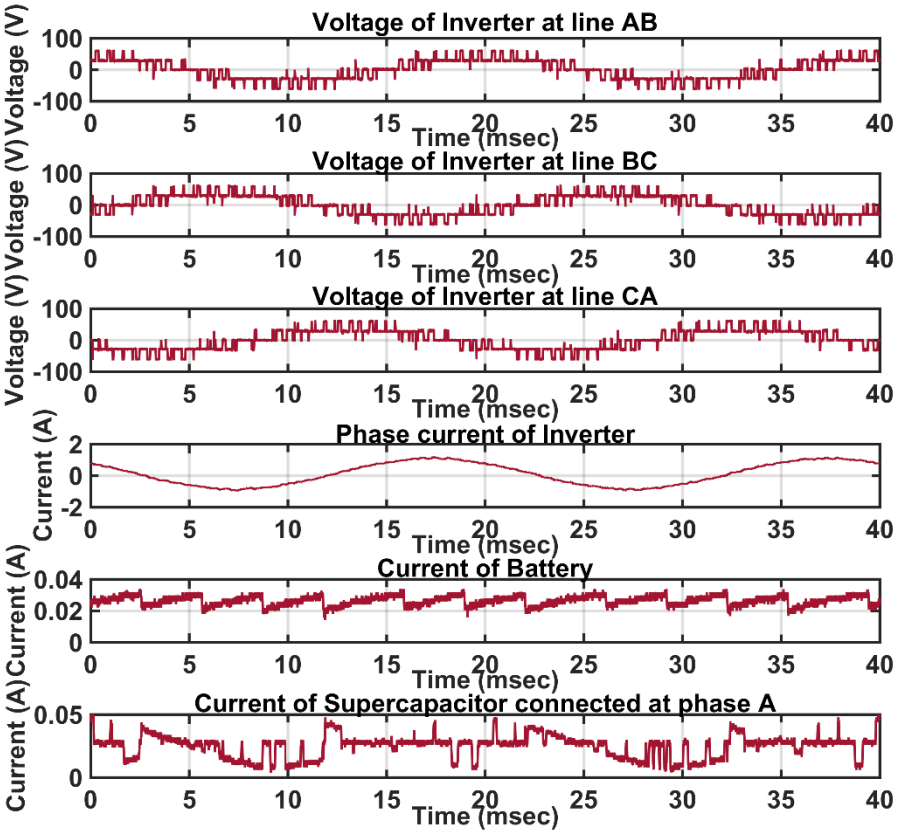

Figure 7-13: Waveforms of Inverter at output voltage 40 V

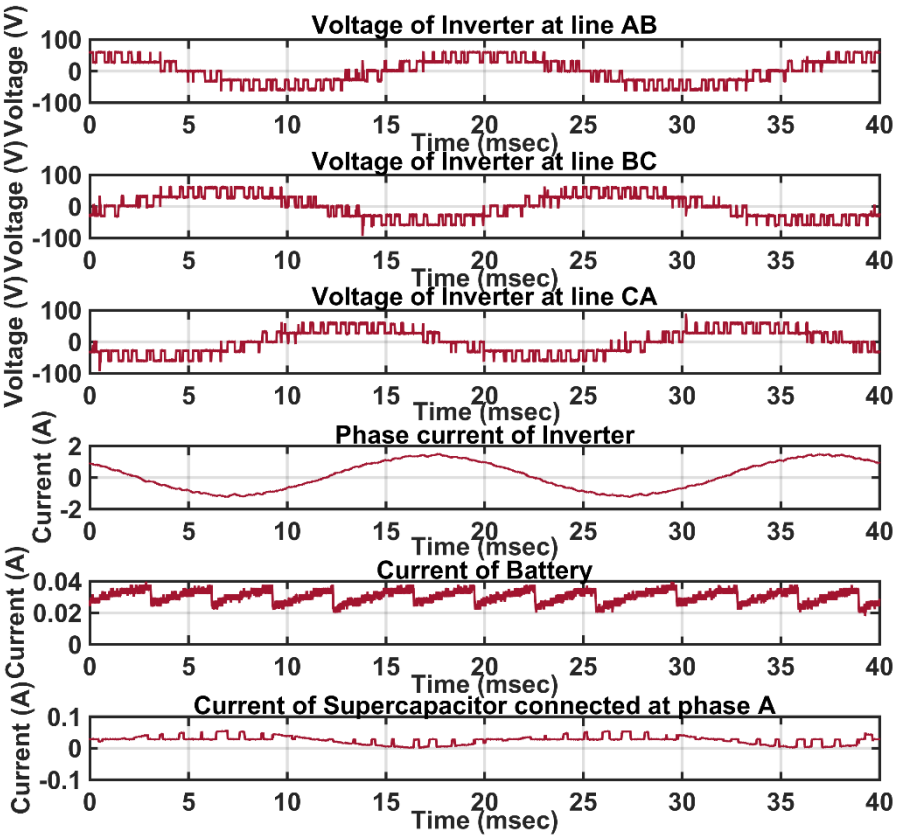

Figure 7-14: Waveforms of Inverter at output voltage 50 V

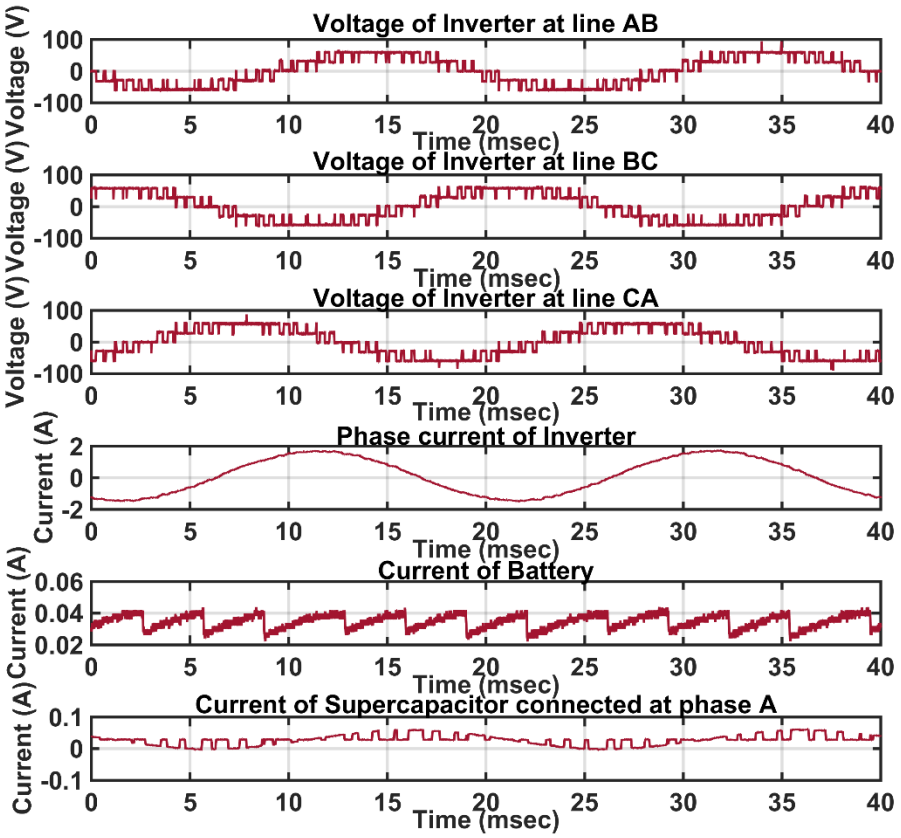

Figure 7-15: Waveforms of Inverter at output voltage 60 V

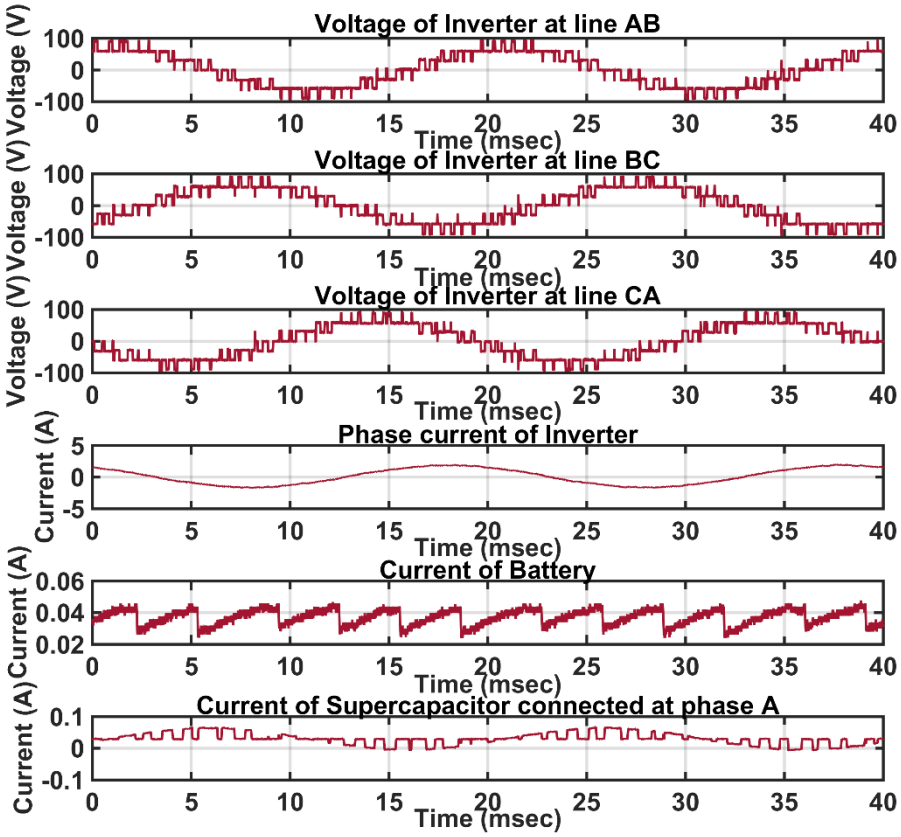

Figure 7-16: Waveforms of Inverter at output voltage 70 V

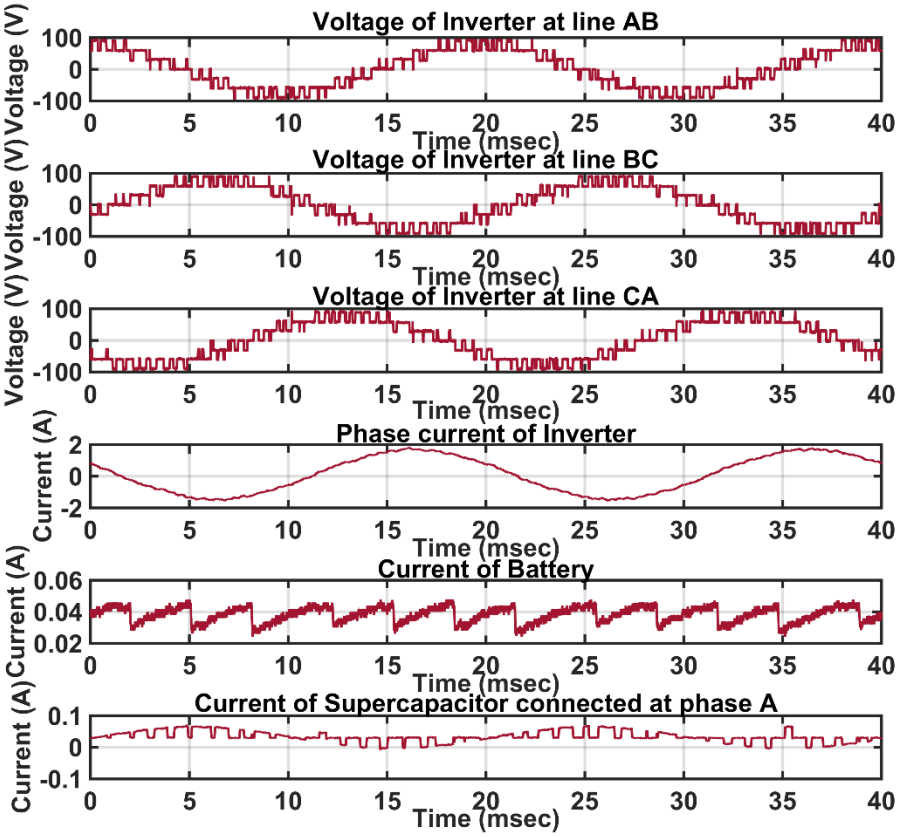

Figure 7-17: Waveforms of Inverter at output voltage 80 V

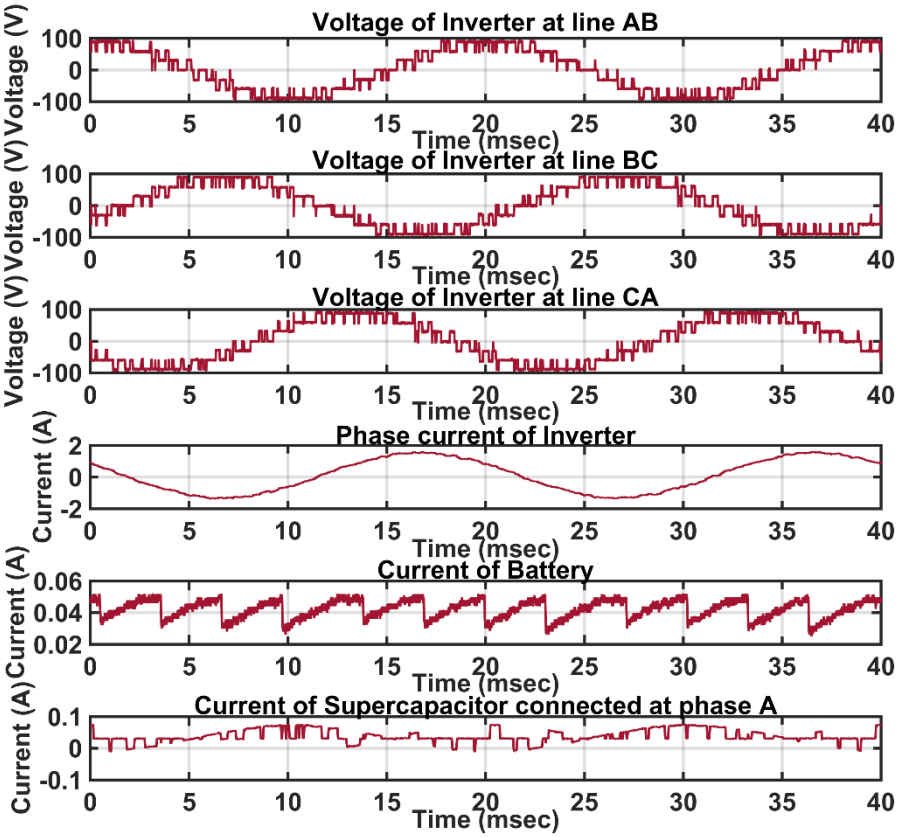

Figure 7-18: Waveforms of Inverter at output voltage 90 V

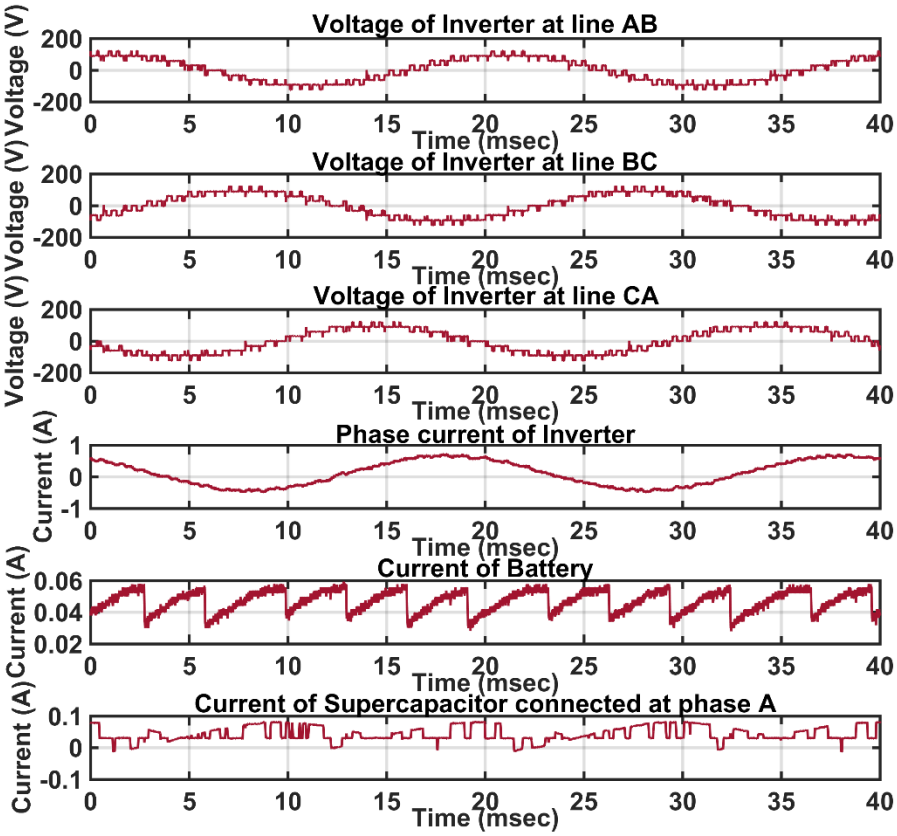

Figure 7-19: Waveforms of Inverter at output voltage 100 V

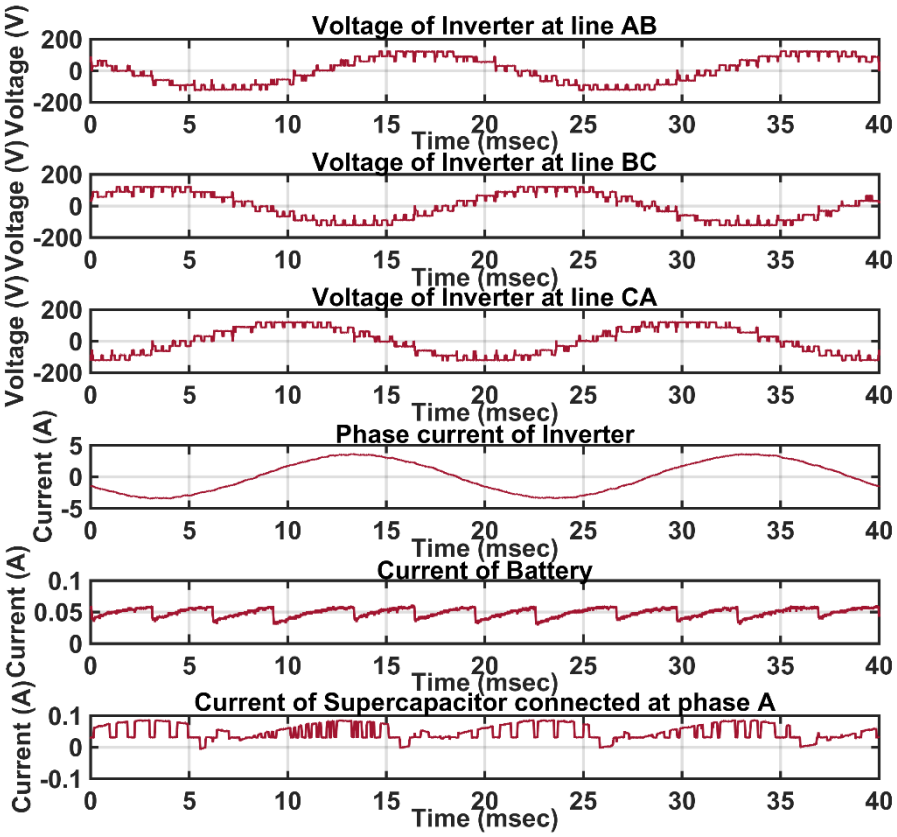

Figure 7-20: Waveforms of Inverter at output voltage 110 V

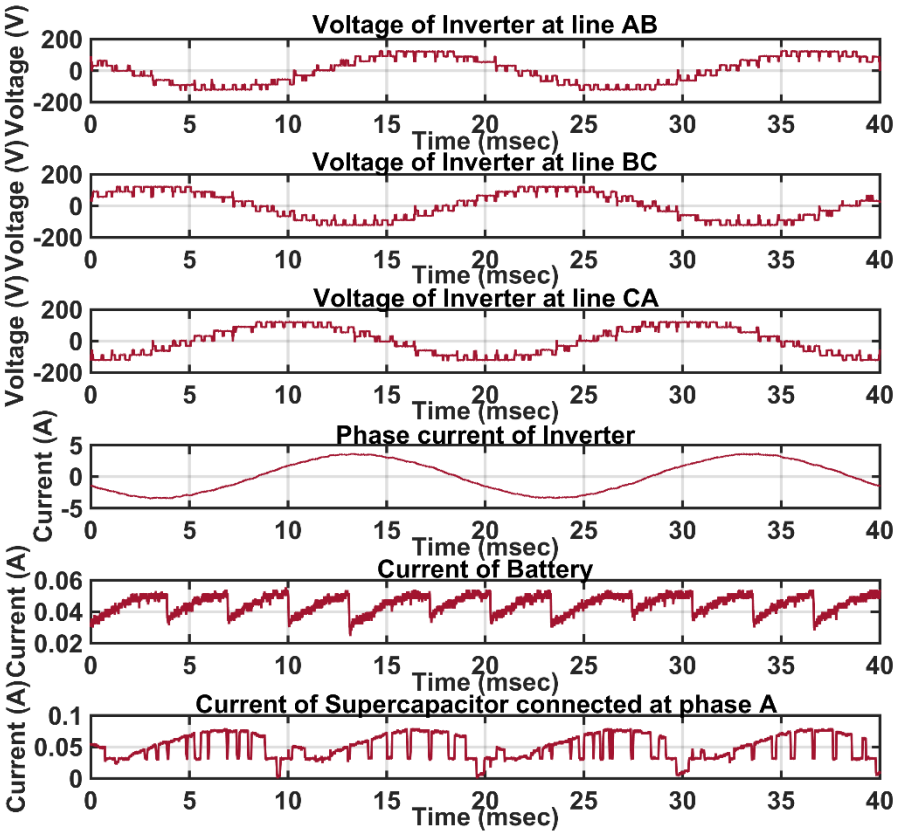

Figure 7-21: Waveforms of Inverter at output voltage 120 V

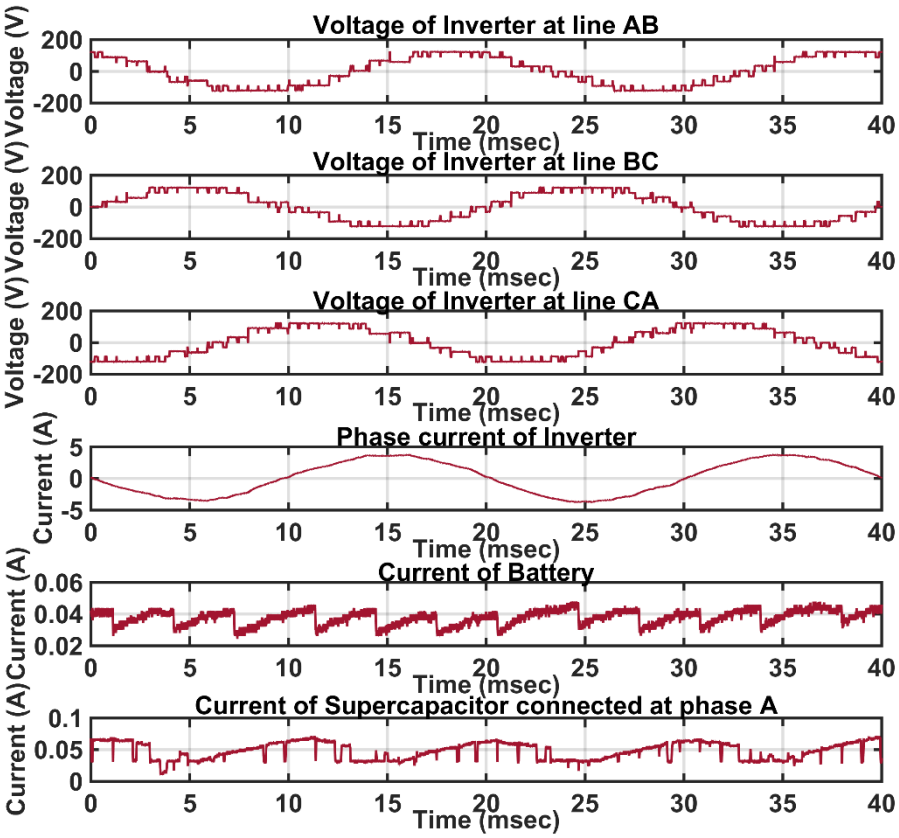

Figure 7-22: Waveforms of Inverter at output voltage 128 V

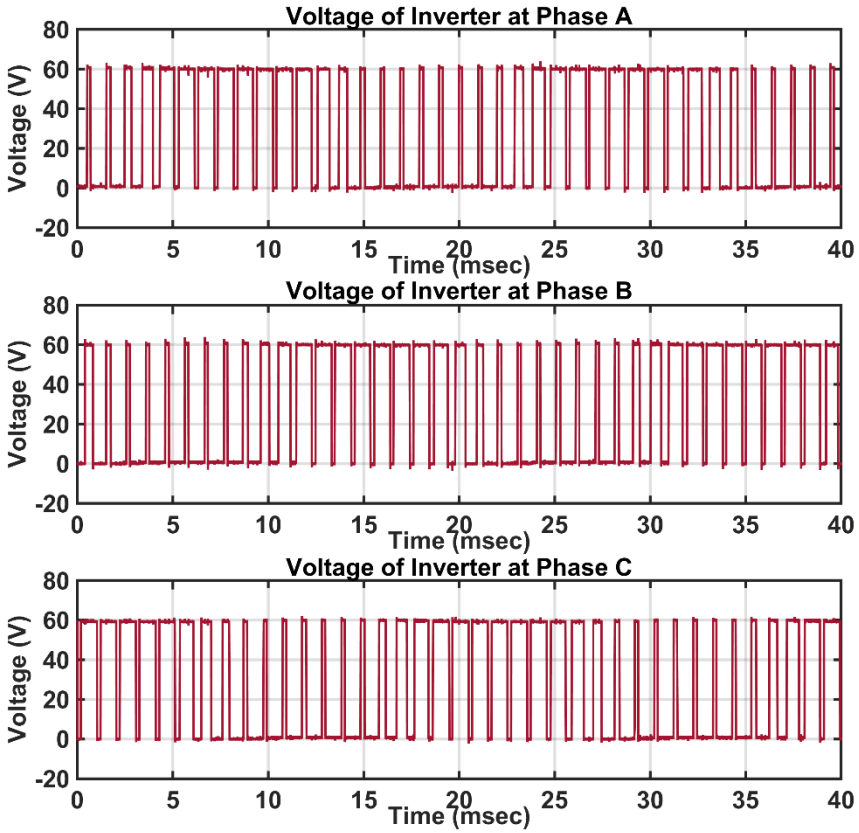

Figure 7-23: Phase waveforms of three-phase bridge at output voltage 40 V

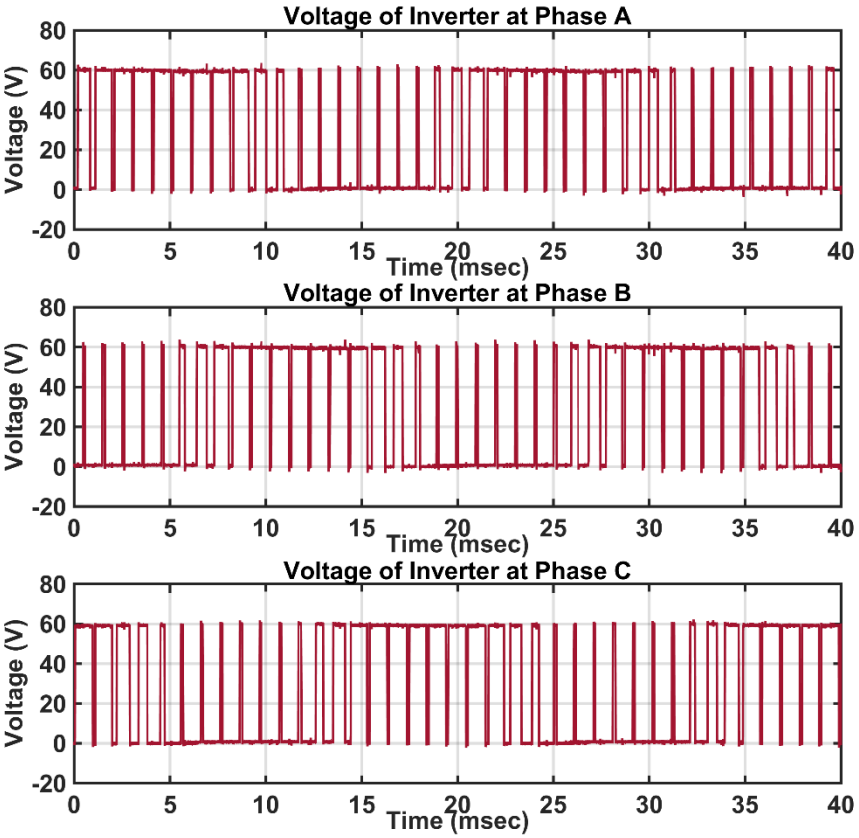

Figure 7-24: Phase waveforms of three-phase bridge at output voltage 50 V

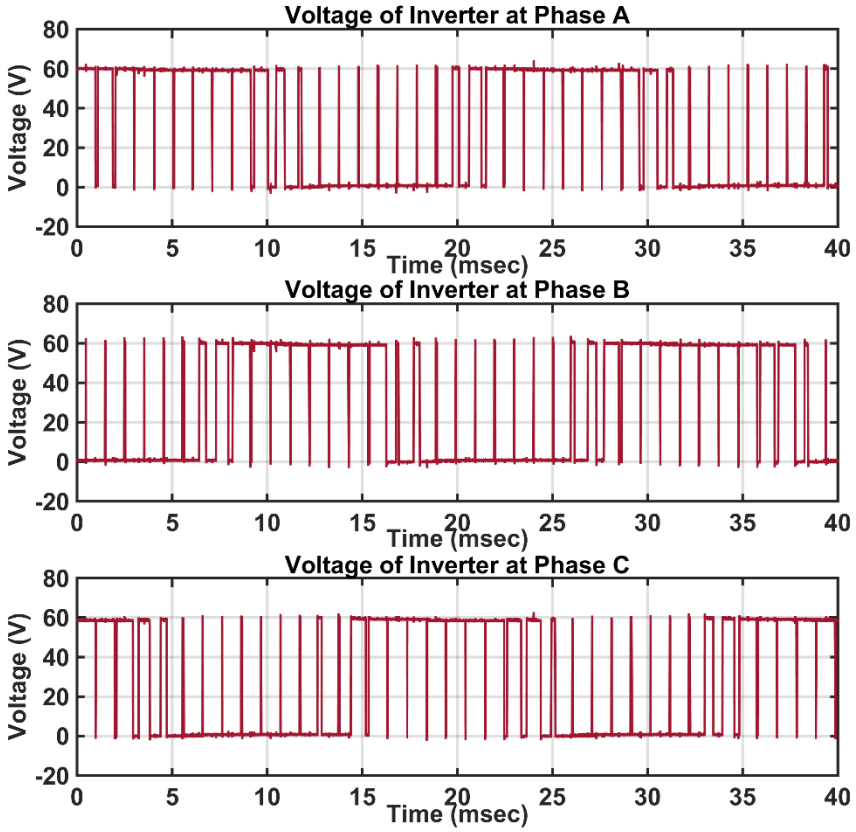

Figure 7-25: Phase waveforms of three-phase bridge at output voltage 60 V

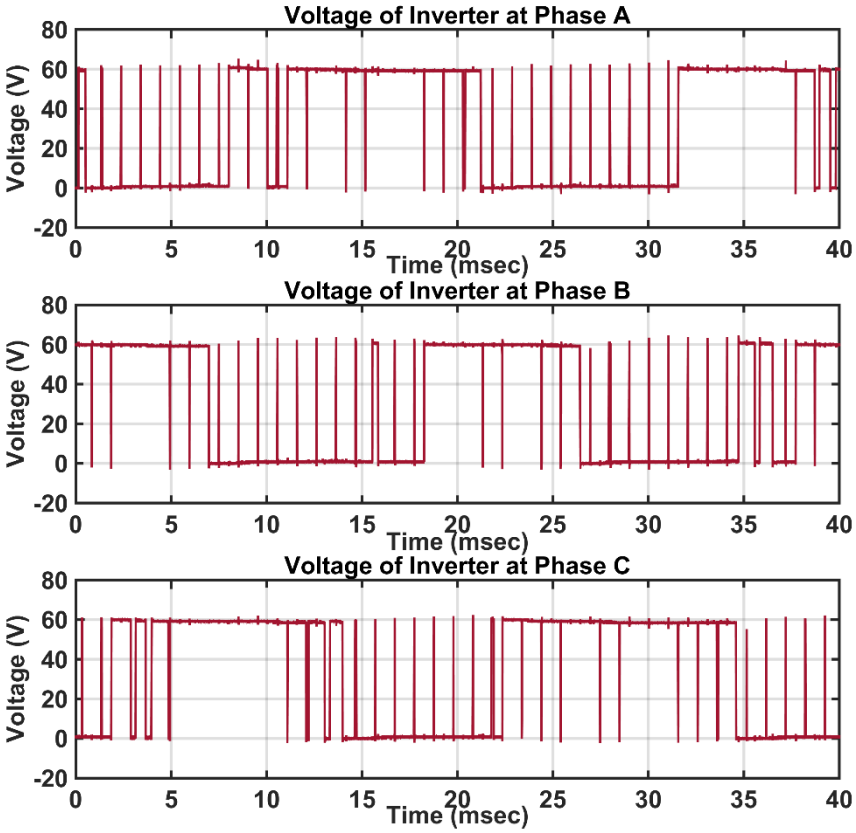

Figure 7-26: Phase waveforms of three-phase bridge at output voltage 65 V

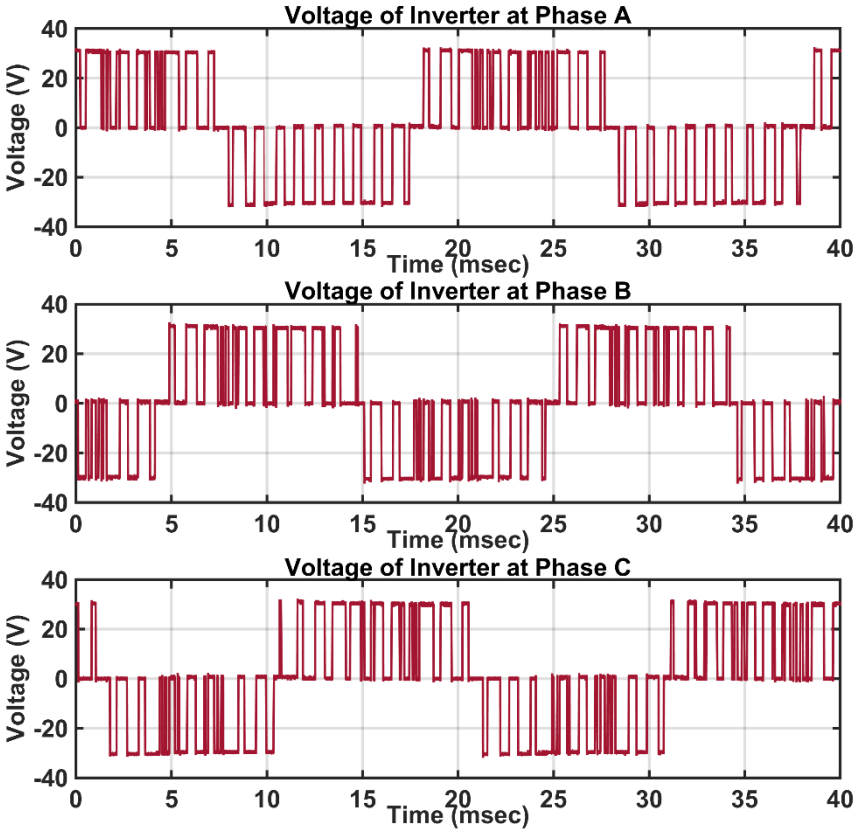

Figure 7-27: Phase waveforms of H-bridge at output voltage 40 V

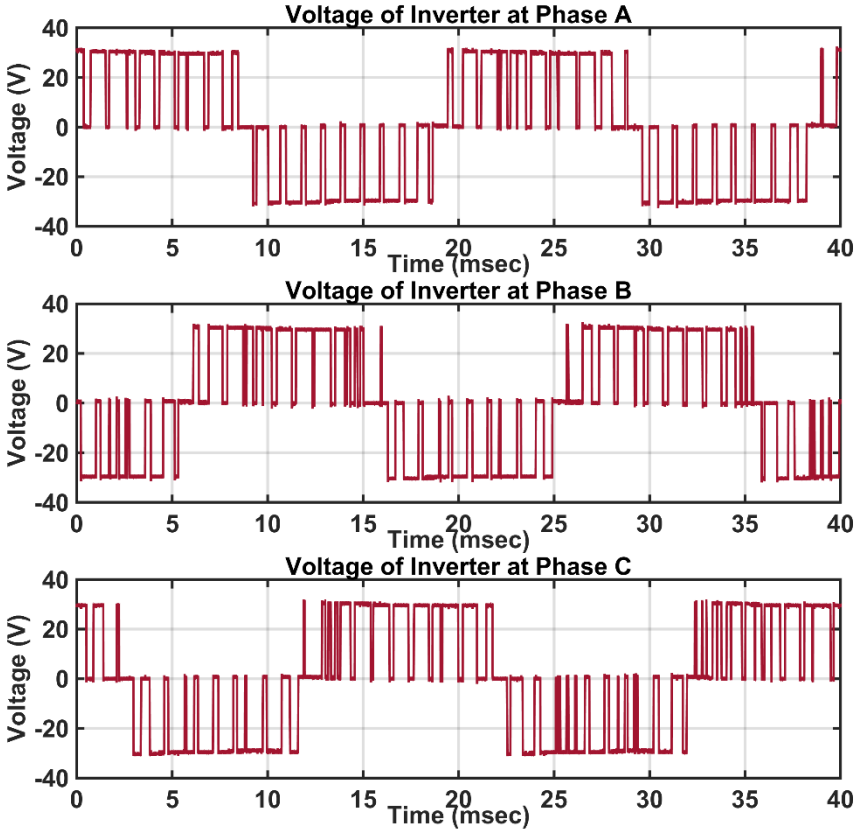

Figure 7-28: Phase waveforms of H-bridge at output voltage 50 V

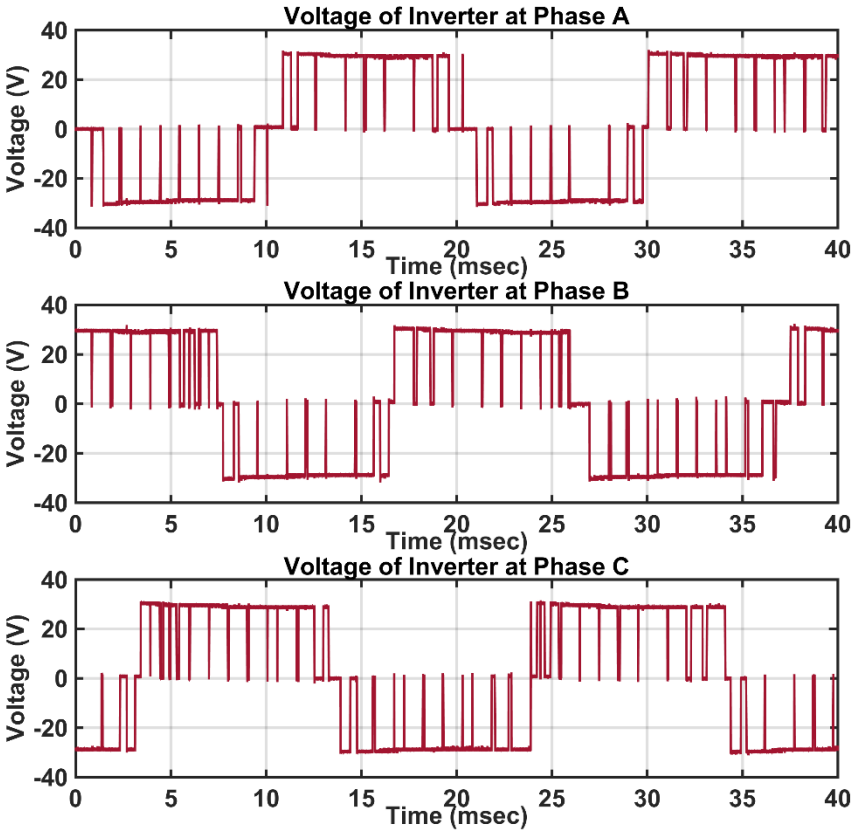

Figure 7-29: Phase waveforms of H-bridge at output voltage 60 V

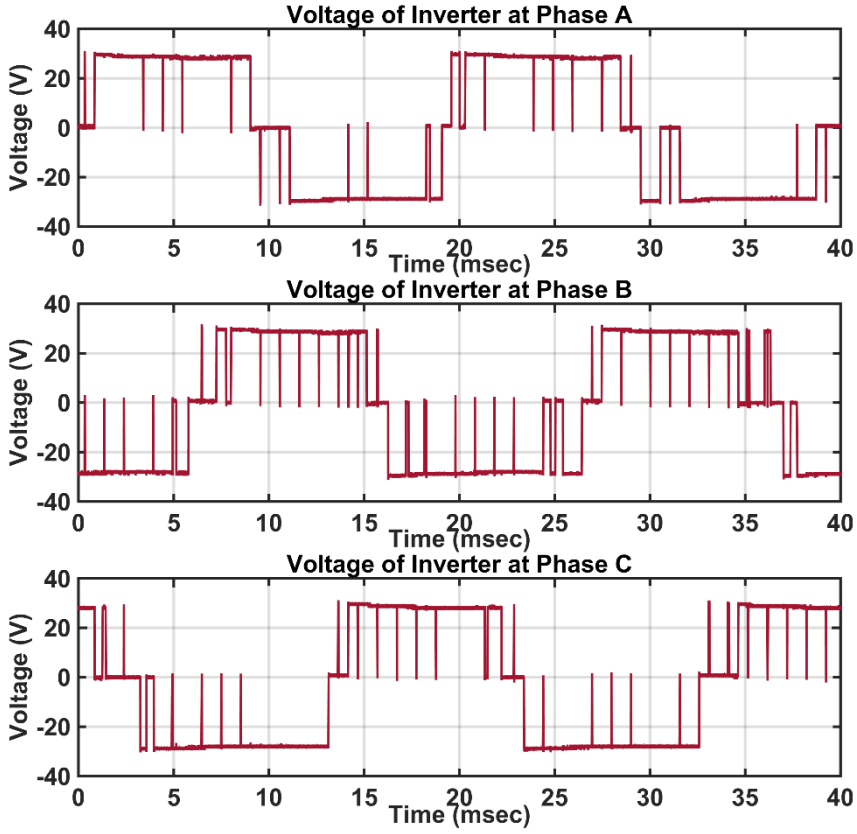

Figure 7-30: Phase waveforms of H-bridge at output voltage 65 V

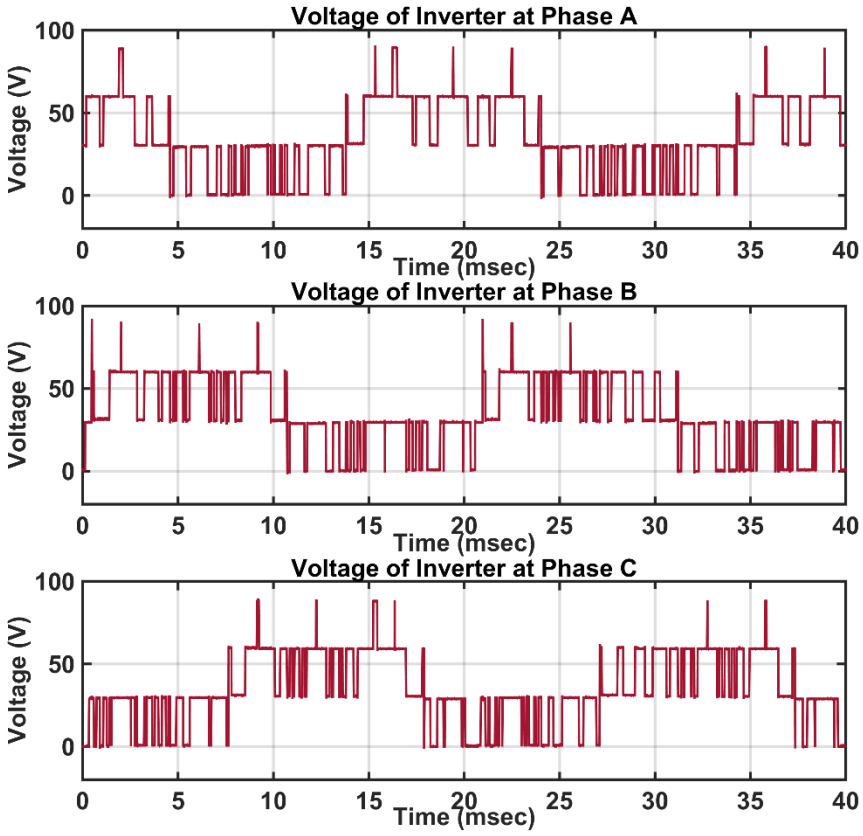

Figure 7-31: Phase waveforms of Inverter at output voltage 40 V

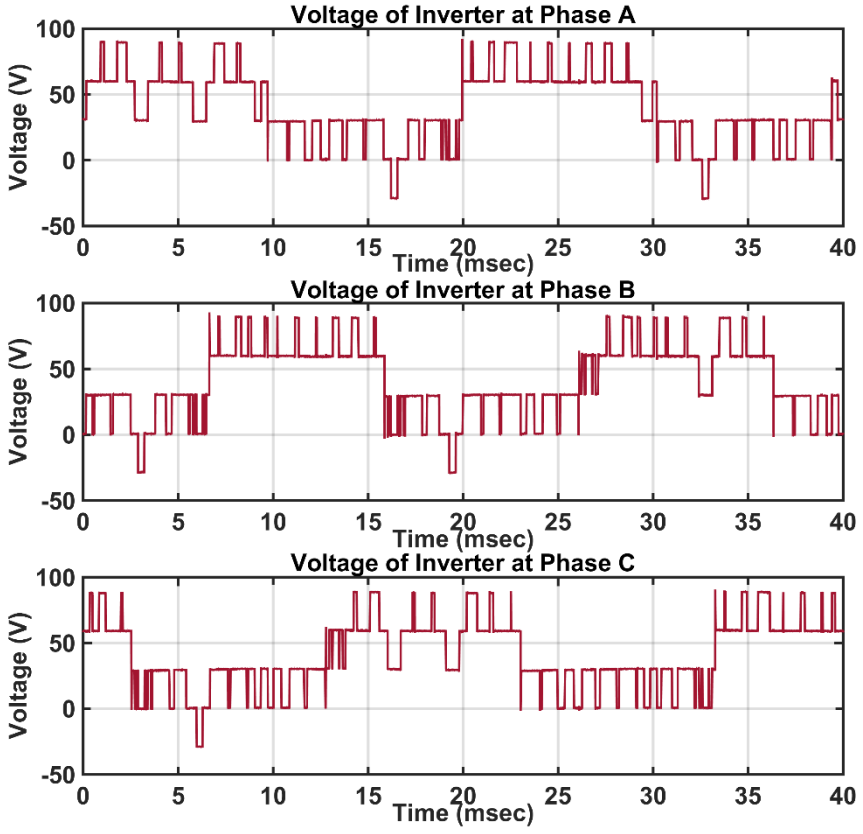

Figure 7-32: Phase waveforms of Inverter at output voltage 50 V

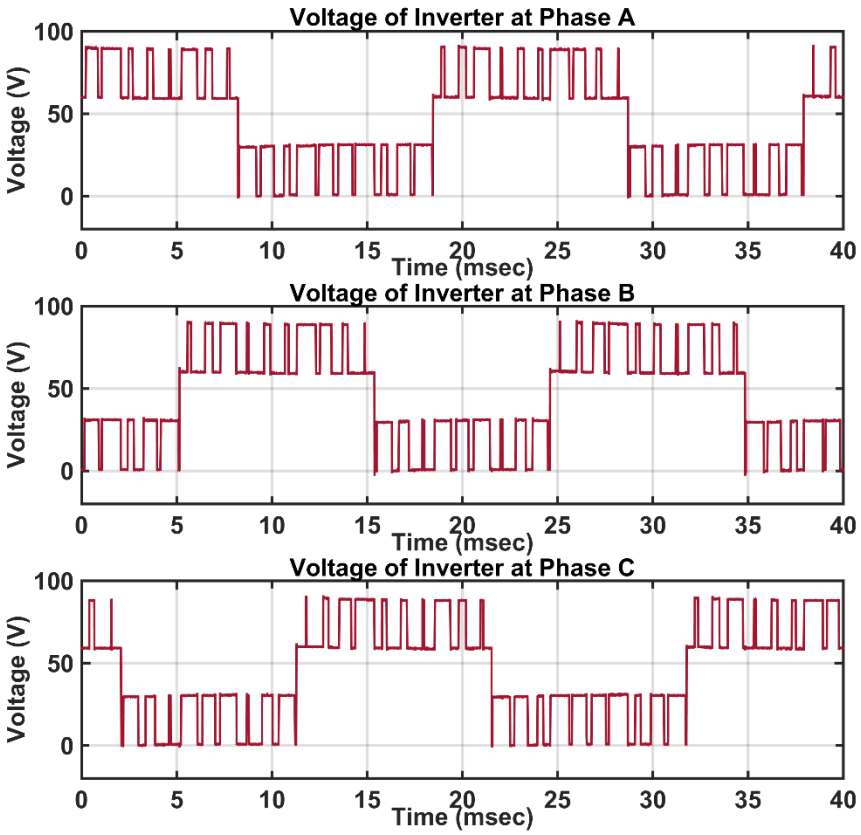

Figure 7-33: Phase waveforms of Inverter at output voltage 60 V

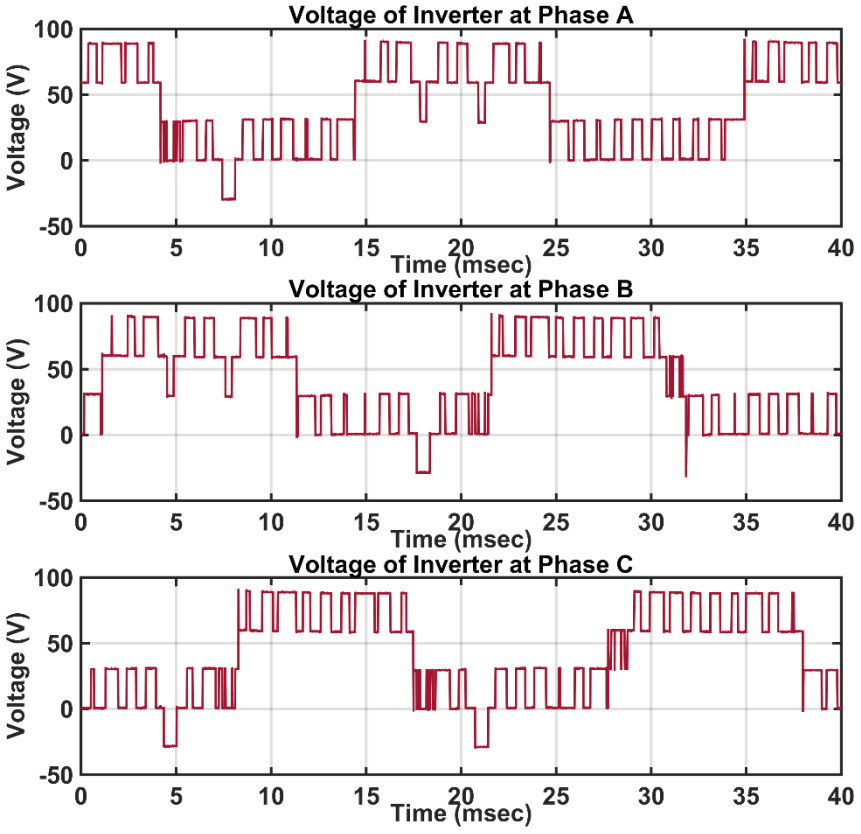

Figure 7-34: Phase waveforms of Inverter at output voltage 70 V

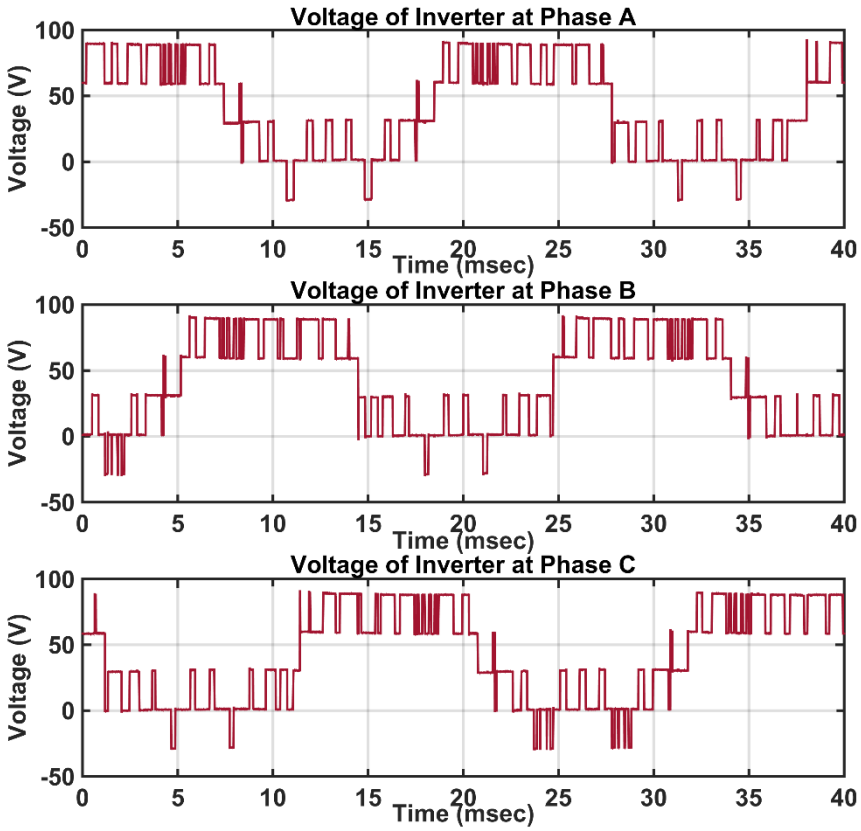

Figure 7-35: Phase waveforms of Inverter at output voltage 80 V

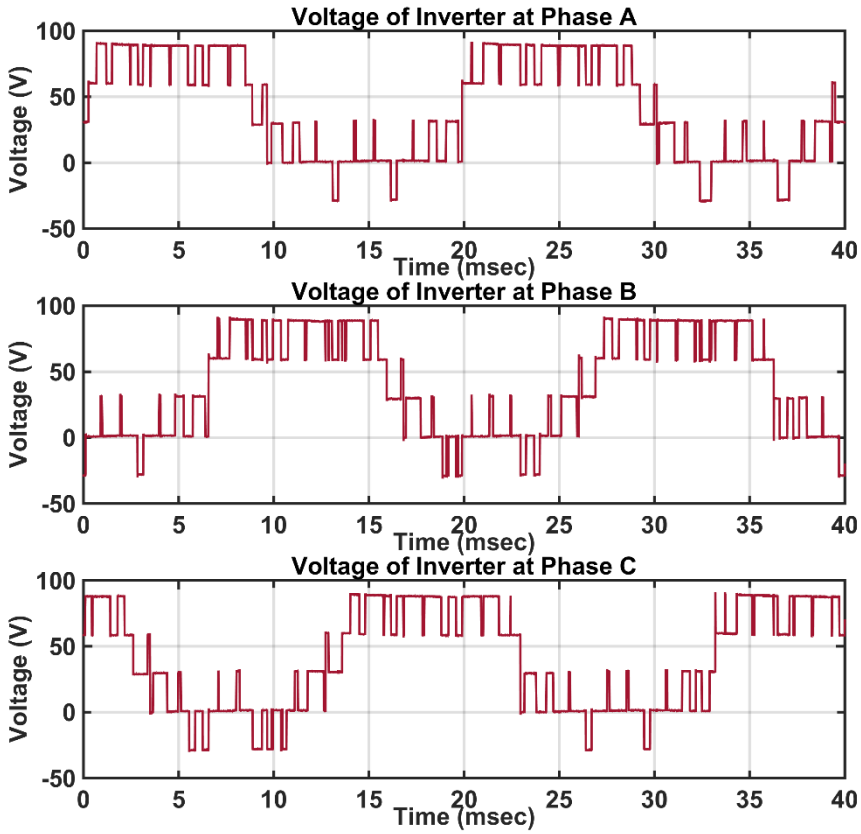

Figure 7-36: Phase waveforms of Inverter at output voltage 90 V

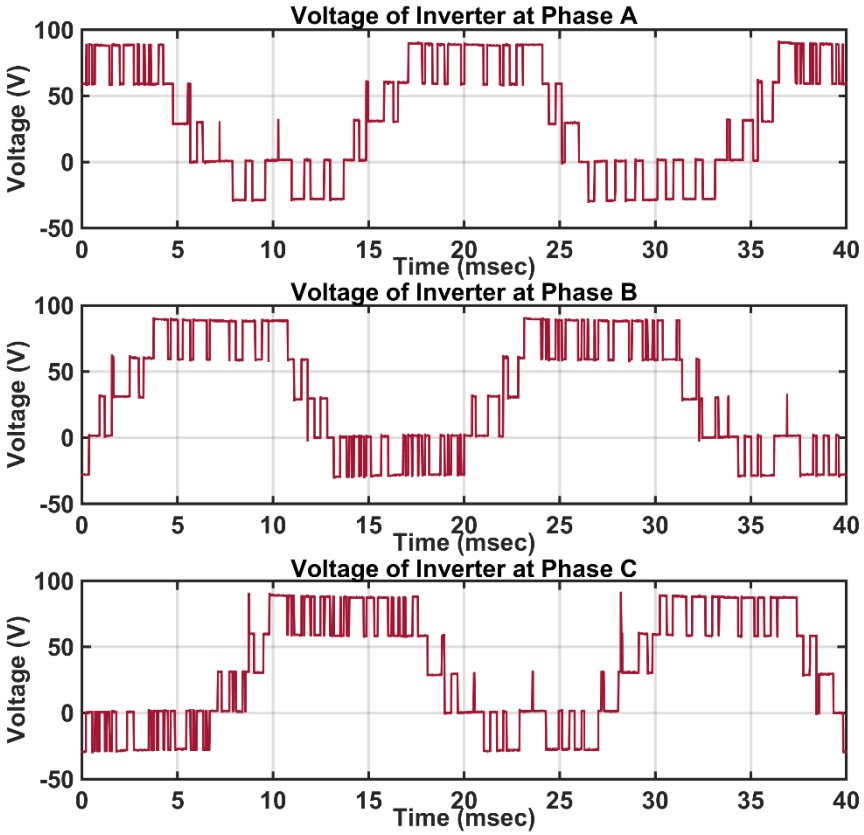

Figure 7-37: Phase waveforms of Inverter at output voltage 100 V

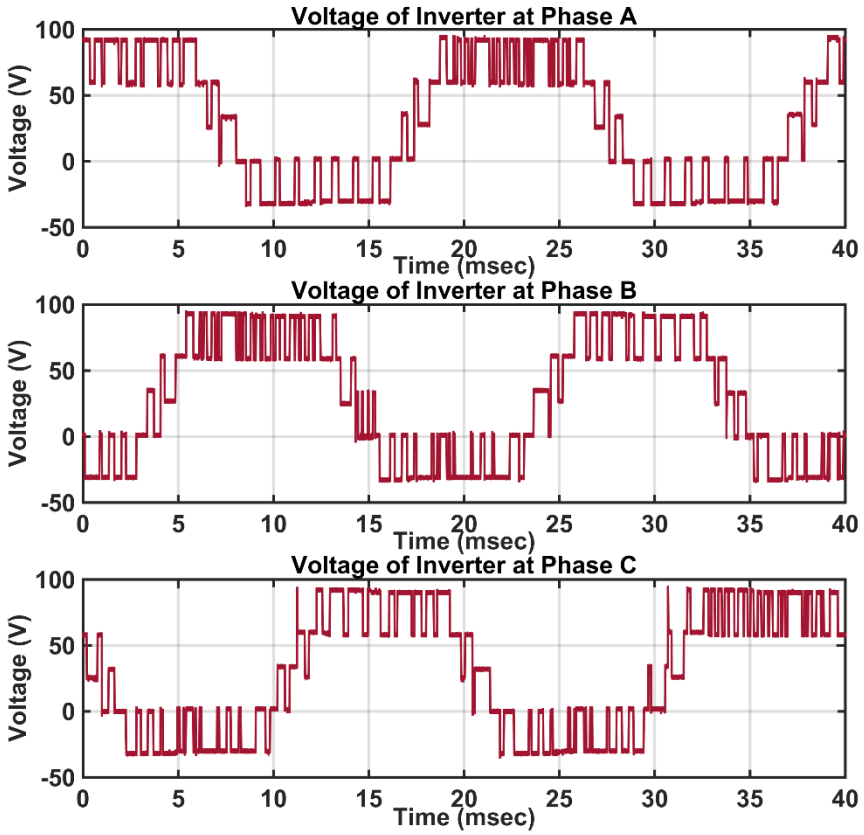

Figure 7-38: Phase waveforms of Inverter at output voltage 110 V

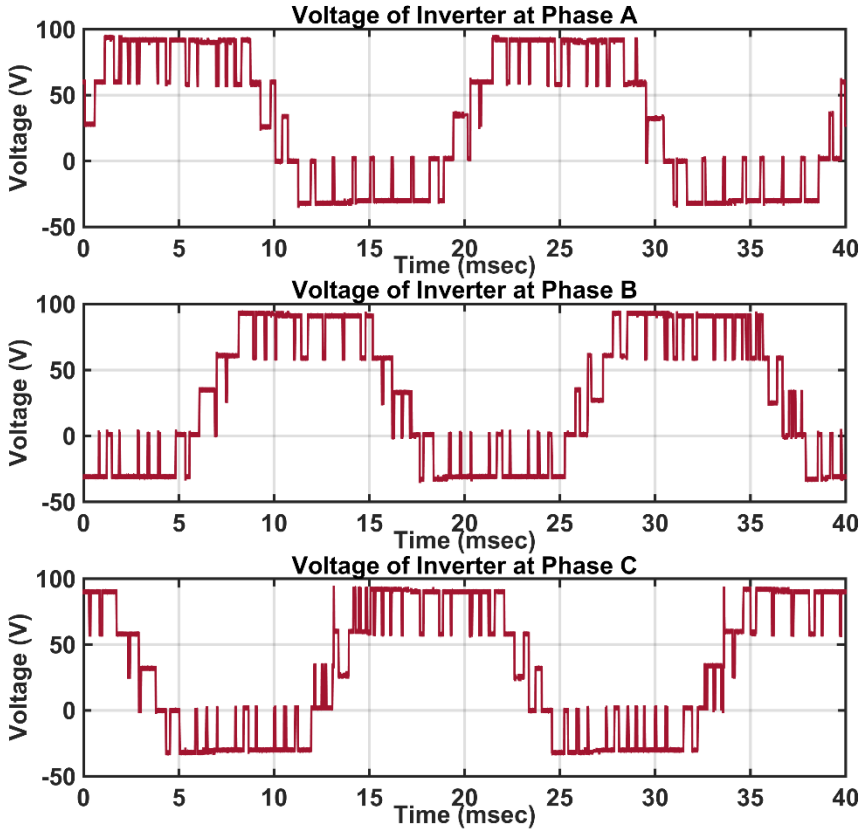

Figure 7-39: Phase waveforms of Inverter at output voltage 120 V

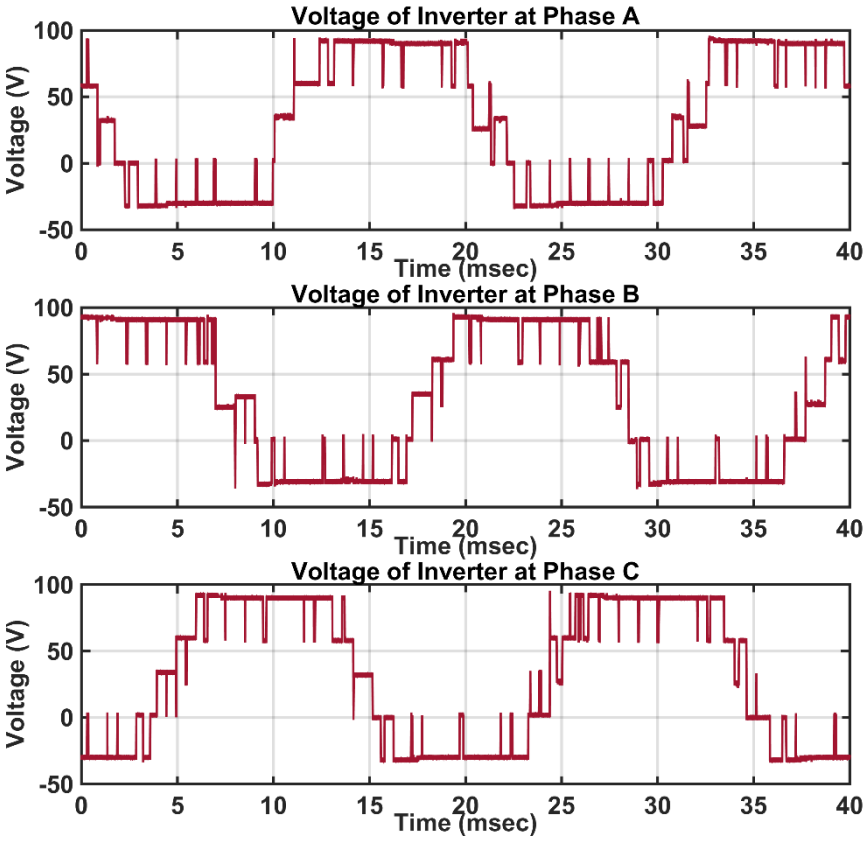

Figure 7-40: Phase waveforms of Inverter at output voltage 128 V

7.4 Conclusion

Building physical model to represent microgrid as shown in Figure 1-12 is very complicated and very expensive due to the higher number of elements spread in wide geographical area that have different dynamic response and nature of operation, which distribute between power system elements response down to the power electronic elements response. Therfore, the micorgrid research consists of many threads which could be challenging to experiment. Hence part of EVO is experimentally validated which represents particularly faster domain in the research.

To validate the proposed strategy of switching multi-level inverter, the experimental platform has been developed from discrete components which connected to CompactRio devices that support FPGA technology and control by LabVIEW Program. Several scenarios have been demonstrated based on battery and supercapacitors priority operation whereas the battery and the bank of supercapacitors are the main and the assistance resources respectively. The inverter and controller utilize flexibility regarding supply voltage reference from the resources at their state of charge limitation, achieve optimum voltage quality, and utilize full capacity of resources with minimum ripples and switching losses. They even flexible to override the overmodulation issue returning the voltage reference to maximum level based on the state of charge of resources. However, the nonlinearity of voltage waveform increased at operation near the voltage limitation boundary of resources.

In general, the inverter topology and control strategy could provide an effective method of power flow management and control for resources of EV at connected mode or even running mode. Therefore, this scheme of hardware and controller demonstrate feasible solution for hardware implementation with minimum components which gives opportunity for further commercial applications.

8. Chapter Eight: Conclusions and Suggestions for Future Work

8.1 Conclusions

Electricity has become essential in our life and the electricity network has a major impact on our lifestyle. Therefore, maintaining an electricity system is extremely important for the resilient operation of an electricity system with high reliability and stability, to reduce or even prevent any disturbance effect on feeding electricity to loads. However, generating electricity is a very complex process and has very expensive components. Moreover, delivering electricity to the load has a very complicated network spread around a large geographical area. Due to several changes, in the nature of the elements of the electricity network, such as integrating renewable energy and distributed generators in distribution network near the load, electrifying the transportation sector, and changing the nature of load from a single direction to a bidirectional element brings many challenges to the existing electrical system and increases the possibility of electricity congestion and loss to the system. Therefore, development of the existing electricity system to an automated system focusing on reconstruction of the distribution network to a microgrid network becomes important to ensure electricity is available to the end users. The study presented a holistic approach from three levels, which are MGO, CSO, and EVO, to manage and control the power flow of a microgrid network with regard to balancing the supply of the distributed generators and aggregated EVs with electricity demand. The EVs are powered both by battery and supercapacitors. The thesis has demonstrated the multidisciplinary problem of managing and control energy and power indecomposable in such a way that three major processes and the links between them can be identified.

This thesis illustrated the modular structure of managing the power flow of a microgrid that consists of various distributed generators, loads, and EVs. Each EV is connected to the microgrid and has multiple energy resources; these are one battery pack and three supercapacitors. The EV power train is connected to the microgrid through a modified H-bridge multilevel inverter that also consists of a three-phase bridge inverter for controlling the battery and three H-bridge converters connected in series, with a three-phase bridge inverter for controlling the supercapacitors. The thesis described two optimisation formulations to manage the microgrid and EV's operation respectively. The objective function of the microgrid management used MIQP optimisation formulation to control and schedule the operation of the distributed generators, EVs and the electrical demand to avoid possible overloading or network degradation. The objective function of the EV's management used a MILP optimisation formulation to control the power flow from the battery and supercapacitors of the EV to the microgrid. The formulations were derived by adopting a fresh perspective of the management integrating dual resources of EVs to the microgrid problem. The analogies presented in this thesis explicate and demonstrate the problem as a chronological systematic implementation framework. Based on the conducted investigations, the following conclusions can be drawn from this study:

Chapter one gave a general introduction, basis of the hierarchical management and control strategy, and the research novelty and contributions of the thesis.. The connotation of research which applied to the next chapters are illustrated in the optimisation model of the microgrid and the modular power management of the microgrid structure sections to pave the way for the next chapters to design the tier of a modular structure framework for each section of the microgrid. The general intentions of the research emphasise the points that should be accomplished, and address the long-term project outcomes established in the aims section, whereas the subsidiary to the aims is formulated in the objectives section.

This chapter brings attention that reconstructing the electrical system into a smart grid is very difficult and very expensive; also, delivering electricity from the generation units to the electrical demand happens through a very complex process and large network. Much extra equipment, as well as management and control operators, and communication protocols should be built into a smart grid to automate the system. It is difficult to anticipate the direction of power flow within the smart grid whereas more stable parts could deliver power to less stable parts of the system. The stability of the system is not underestimated, whereas some parts of the system could have high stability at one time and less stability at a different time based on the available electricity sources and nature of the load. Communication protocols, accurate measurements, and management operators are at the heart of the smart grid to communicate and control the states of each element in the smart grid with operators for accurate decisions on balancing load with generation. The distribution network of the smart grid will reconstruct to the many small areas based on the nature of the load called the microgrid.

Each microgrid which could be one building or a couple of buildings is a single controllable system. Many distributed generators that generate electricity based on renewable energy will integrate within microgrid areas to cover the local demands of the electricity network. The microgrid has two modes of operation – either isolated or connected. The isolated mode is activated by the isolated point of common coupling device when a major disturbance happens to the electrical system that threatens the stability of the system, whereas the generation units balance the load locally. It is possible to reconnect the microgrid to the electrical system in case the distributed generators of the microgrid are not able to balance the load. The microgrid could deliver the surplus power to the adjacent networks or absorb power from them in case the distributed generators of the microgrid are not capable of covering the local load requirement. The major difference between the existing passive distribution network and the future active microgrids is the bidirectional power flow behaviour of the microgrid elements which could cause electricity congestion. Therefore, the microgrid should manage and control, probably by adding an intelligent controller. It consists of many operators, which are DNO, MGO, CSO, PHO, and EVO, that handle many elements of different dynamic responses, whereas each element has its own local controller. Therefore, the execution operating time will be different between operators. Small period operation and less scheduled time between the operators could achieve a more resilient operation of the microgrid; however, operating the distribution network as microgrids is very complicated and expensive, as mentioned in Figure 1.7. Therefore, timing the operators of the microgrid should be applied in a realistic way based on the response of the communication link, measurements, and dynamics of the elements.

The interconnection between operators is a key to the continued operation of the microgrid; however, delay to or even disconnecting the interconnection between the operators could blind the management and controller system, leaving the balancing power flow between the distributed generation and loads in chaos. Therefore, flexibility between the centralised and decentralised operation of the operators in the interconnection process or disconnecting them respectively are required to guarantee the resilient operation of the microgrid. The operators are spread across a geographical area of the microgrid and operate autonomously, whereas the control unit to manage the operators is located at a distribution network operator, which includes a demand management system and market operator sections. Higher delay of execution between operators could cause instability due to holding the reference of slower operators for many executions of the faster operator without measuring the new, related parameters.

Chapter two identified the literature review related to the subjects of the thesis. The research has a wide range of topics such as power system infrastructure, power system analysis, power electronic devices, control strategy, and EV technology. Therefore, this research implicates different survey views of knowledge. The research view of distributing management, control operators, and an electrical conversation about connecting EVs to the microgrid are presented briefly.

The available statistical analysis, which presented in this chapter, informs the electricity community of the importance of finding an electrical solution to cope with the rapidly increasing demand and reduce the environmental pollutants. The solution should cover all parts of the power system infrastructure to implement the smart grid and microgrid concepts. The literature review reflects the spread of the microgrid among the misalliance sectors of science to cover the operation of different elements that have different dynamic response operations. The general architecture of the microgrid could be as small as a building or as large as being spread through a large geographical area. Therefore, physical elements, protection devices, measurement systems, communication links, and controller operators should cover all parts of the microgrid, whatever its difficulty and size, to make its operation viable as a single controllable system.

Some sorts of elements in a microgrid could treat as a source in a time and load at a different time such as EVs, which could provide mobile energy storage to save the system in emergency cases. The range of execution in the operating time of elements within the microgrid has a range between minutes in distribution generators to microseconds in power electronic devices. Therefore, the timing of the operators should cover the operation delay of different elements. There is no exact map or dependable prediction for the number, location, time and size of connecting EVs to the microgrid. Therefore, promotion of a charging station system, either public or private, will help to spread EVs and control distributing them in a specific location which makes it easier to predict the required power needed for them as well as control discharging them as a mobile energy storage system. Moreover, the MGO will treat the point of the charging station system as an aggregated load in charging mode or a resource in discharging mode, rather than treating many points on the system as loads or resources.

missing large indicator of the DC-DC converter in modified multi-level inverter bring attention to use the inverter as a suitable inverter to cope with different resources of EVs with less cost and weight due to easier management and controller, and a variety of available switching modulation.

Chapter three displayed the construction of the microgrid network from a realistic distribution network and distinction of the enhancement of voltage stability on the system at functions of the microgrid. The voltage stability measurement is enhanced in the microgrid operation much more than in a traditional operation. The thesis described the formulation of integrated EVs within the microgrid. The EV adds a capacitive effect characteristic of the distribution line of the microgrid. It increases the critical voltage and critical power limit of the distribution line. Therefore, integrating EVs into microgrids demonstrates a positive impact on microgrids in enhancement of the power factor of the network and discharges the power of the energy storage system to balance the load in case of power flow congestion.

The voltage stability analysis process much better operation of the electricity system at smart grid operation than conventional ones whereas the voltage stability of both transmission system and microgrid enhanced further than collapse point at the conventional grid. Therefore, this chapter draws attention to the value of reconstructing the electricity system from the view of voltage stability analysis which domesticates the connotation of the benefits of the microgrid concept and hierarchical management structure in other chapters. The main idea behind constructing a microgrid is to allocate the distributed generators in an effective way in a specific location. Therefore, allocating the weakest bus strategy to integrate the distributed generators within the microgrid provide better voltage stability for the microgrid than a minimum voltage bus strategy. The effectiveness of renewable energy resources is different from others based on the environment; for example, photovoltaic cells have a very efficient output in the Iraq environment due to the high level of solar radiation, whereas wind turbines are not effective in the same area due to the naturally low wind speed movement.

Finding mathematical equations to implement integrating the EVs within the distribution line of the microgrid is the key to placing EVs within the power flow analysis to be integrated into the system. Therefore, the MGO will incorporate the aggregated EVs that are connected to the charging station system as mobile energy resources, considering the electrical characteristics of EVs. Normally, the main resources of EVs are the battery and supercapacitor which have capacitive element characteristics. Therefore, increasing deployment of the EVs within the microgrid will help to compensate for the inductive characteristic of the microgrid, which has a positive impact on the power factor correction of the network. Connecting EVs with a high state of change could increase the critical voltage and critical power at the user end bus bars. It is not necessary for the weakest bus bar on the microgrid to be the same minimum voltage bus bar on the network. Therefore, by allocating the distribution generators, EVs could allocate the weakest and the minimum voltage bus bars on the network.

Generally, an instalment charging station system at both bus bars could ameliorate the voltage stability and voltage profile of the microgrid. The market operator provides the price of

electricity at each time of operation during a day to operators. Therefore, the interconnection between the operators and market operator should be maintained carefully.

Chapter four discussed the operation of the MGO level of hierarchical management and control system by identifying the overall challenge and the research problem, which includes the available capacity of all distributed generators, all electrical demands, the state of all EVs, and the capacity of all energy storage systems of connected EVs for the microgrid. The chapter presented the physical, electrical, and dynamic response prosperities which includes the operating constraint of all distributed generators, the total demand and losses of the power flow analysis, the operating constraints of the EVs, and the operating constraints of the energy storage systems of the EV. Subsequently, a problem classification was identified which includes calculating the optimisation power of all distributed generators, serving each load demand either shaving or curtailing, and the EV charging demand available or discharging power required.

Optimal operation of distributed generators determines the positive impact of using renewable energy resources related to the cost of operation, and reduces emission pollutants. However, the intermittent nature of the renewable energy could cause the unstable operation of the microgrid. Therefore, the energy storage system compensates the intermittent nature of the renewable energy to maintain the stable operation of the microgrid with minimum cost and minimum emissions. EVs have the characteristic of a mobile energy storage system that discharges power from the EVs based on owner acceptance and a predefined limited state of charge of energy storage system. Using EV as a mobile energy storage system instead of a fixed energy storage system reduces the maintenance cost in addition to no space being required to allocate a fixed storage system. However, intelligent management and control should apply to ensure the flexible operation of the EVs within the microgrid. The optimisation management of the MGO formulation was based on the MIQP for the optimal cost and minimum pollution of the distributed generators operation, to balance the load. The optimisation model had been implemented in the case study, with a participant of EVs. The results presented show that priority of generation should be given to the renewable energy sources and this is compensated by the energy storage system, whereas the diesel generator used to balance the electric demands at losing the renewable energy due to weather conditions. The power transfer between the microgrid and the utility grid depends on the reserve power and tariff that has a variable cost per electricity unit over a day.

The MGO manages the strategic operation of the microgrid to balance the electricity generation load by using a variety of distributed generators and storage devices such as EVs that are combined within charging station system. The renewable energy sources are reliable to cover all the loads of the microgrid due to their intermittency. Furthermore, generation of electricity from EVs is not reliable due to the difficult prediction of the number, location, size, time and period of connection, and the level of state of charge of EVs as well as the owner acceptance to discharge those EVs. Therefore, the distributed generators should be ready at any time of the day to recoup the intermittency of the renewable sources and mis-prediction of EVs availability. It is not necessary that EVs provide cheaper electricity than distributed generators,

whereas the cost electricity curve of the diesel generator has a quadratic shape. Therefore, delivering low electricity from the diesel generator could be cheaper than EVs, whereas increasing the generation of the diesel generator increases the price of electricity quadratically to make it more expensive than other sources. The EVs and renewable energy sources produce electricity free of pollutants emission. However, the manufacturing, recycling or disposal of the EVs and renewable energy produce a different kind of pollutant emission. Therefore, the pollutant emissions of manufacturing and free emissions of operations should be balanced to find the actual impact of renewable energy and EVs on the biodiversity of the Earth. The execution time of the MGO is relatively higher than other operators due to the dynamic operation of elements within the MGO. Building on the priority of the judgment matrix to process multiobjective functions has a direct effect on the operation of the MIQP of the Cplex program, whereas changing the value of weighting function could change the output decision of the MGO. The mathematical model of the microgrid operation has different parameters from logical controller parameters, constraints parameters, mathematical model parameters, and multi-objective function parameters. Therefore, the hardware of the MGO should be chosen correctly to be able to cope with the data of elements and execute the operation within a predefined time execution. Increasing the size of the microgrid would increase the cost and delay the execution time of the MGO. On the other hand, increasing the number of microgrids would increase the difficulty of interconnection between MGOs and communication links between them, which will increase the cost of installation and operation. Therefore, the size of the microgrid should be chosen accurately to balance the advantages and disadvantages of the operating MGOs. Generally, operating a microgrid with a unit commitment strategy is cheaper than without applying a unit commitment strategy. Furthermore, operating a microgrid in the connected mode is cheaper than in the isolated mode.

Chapter five discussed the operation of the CSO level of hierarchical management and control system. It explained the CSO as being an essential part to distribute the EVs' spatiotemporally to optimise the charging operation of aggregated EVs and avoid microgrid congestion. The CSO facilitates the required electrical demand and available electrical demand to implement a pricing policy for the microgrid to charge the energy storage system of each EV reaching to desire to leave state of charge. The optimisation formulation was applied to the CSO based on MILP, to predict optimum slots of charging each energy storage system of the EV. The decision of the CSO was taken according to the time of connection, a period of parking, the initial state of charge for energy resources, the capacity of energy resources, and a desire to leave state of charge of energy resources. Some EVs could discharge power to help the microgrid balance the loads and keep the system stable. The decision of the discharging EVs was initiated based on the frequency deviation, voltage deviation, owner of the vehicle acceptance, and predefined limit of the state of charge of energy storage systems. The thesis determined that the EVs charge at low tariff (at night) and discharge at high tariff (mid-day) could save revenue money, rather than paying at the same ratio of the state of charge. Some of those EVs could not reach the desired leaving state of charge for the rest of the connection period. Therefore, the priority charging strategy could balance charging the EVs reaching or nearly leaving the state of charge with a little extra payment rather than optimum slots of charging. The supercapacitor has much

faster charging and discharging characteristics than the battery. Thus, the supercapacitors could charge during braking energy or the first couple of minutes of connected EV to the microgrid. The CSO strategy is flexible enough to charge the energy storage system of the EV at the rated power of the converter out the optimum slots calculation by paying extra money to the normal tariff.

The size of the microgrid specifies the number of charging station systems that could be installed within a microgrid. More charging station systems provide flexibility in generating electricity using EVs. Each charging station system is controlled by a CSO to do centralised charging or discharging for connected EVs. The CSO connects hierarchically with the MGO, therefore, it is not necessary to connect many CSOs together, whereas the MGO controls all CSOs within a microgrid. The size of the charging station system and the hardware memory capacity, processor speed, and complicated operation of CSO depend on the number of platforms. The CSO manages centralised charging or discharging aggregated EVs according to the objective function of the minimum cost of charging EVs or maximum cost of discharging EVs based on the MILP of Cplex program. Therefore, the complexity and time processing increased when the number of connected EVs increased. MGO provides voltage variation, frequency variation, and available or required power to charge or discharge EVs respectively. The execution time of CSO is faster than MGO. Therefore, CSO holds the output of the MGO and processes it repeatedly until the next execution of the MGO. Therefore, disturbance or unpredicted load case changes the parameters of the microgrid without updating it by MGO, making the wrong decision by the CSO. To deal with these kinds of fault operation, the watch dog timer should receive interrupted signals from MGO to restart the process of the CSO to deal with an exact reading of the microgrid. The charging station system will accommodate different brands of EVs that have different converter topologies, different resources capacity, and register plate. Furthermore, the charging station system should respond to the owner's requirement regarding the period of connection, desire to leave the state of charge of resources, and the ability to discharge the EV. Therefore, the measurements and hardware component capability should cope with these changeable parameters to achieve the target of CSO. The mathematical model of EVs includes the reference of either charging or discharging at normal, scheduled, and maximum capacity based on the voltage variation and frequency variation of the MGO. Furthermore, the mathematical model of EVs applied logical control, required or available power, and the current of each EV to apply the objective function of the optimisation model. Therefore, the CSO should maintain a strong connection with the electric vehicle agency of each vehicle to achieve the objective function of each EV precisely within the execution period. Generally, discharging EVs could offer revenue to the owner of the EV by charging those vehicles at a low rate tariff and preparing them to discharge at a high rate tariff to income the discharging rate and time rate, whereas the discharging income is higher than the charging pay by 10%. The greatest complexity of operating is that of the CSO equipped with a battery of EV, whereas the supercapacitor has a very fast charging characteristic and less capacity than the battery.

Chapter six discussed the operation of the EVO level of hierarchical management and control system. It presented the analogy of organisational management and control philosophy in a modular hierarchical system. The management and control of the discharging operation used a heuristic derivation of split power between the energy storage systems, modulation SVPWM to control the modulation of switching devices, and control steps of waveform characteristics for power quality purposes. The power conversion to connect the dual energy storage system to motor or microgrid is required to unify the operation of the DC waveform of the energy storage system and the AC waveform of the motor or microgrid with specific characteristics. A modified H-bridge multilevel inverter has been used in this study due to the advantages of this topology over traditional bidirectional converters since there is no need to add an inductor to boost voltage. Thus, all the disadvantages listed for the traditional topology due to the inductor are ignored, such as high ripple of the circuit, the slow response of the control system, high voltage droop, nonlinearity of the system, and physical size, weight, and cost. In contrast to traditional topology, the modified H-bridge converter has a low number of components, various states of control switches, low harmonic distortion and EMI interface, and easily accommodates multiple DC resources.

The modular structure explicated three main processes that added a holistic approach to the power and energy management of energy storage systems' problem description. The process is split into the three chronological shells. The timely contributions of the EVO began from seconds at EMS to milliseconds at PMS then microseconds at PES. The thesis demonstrated the cooperation of using battery and supercapacitors as dispersed, discharging power based on the state of charge level to reduce the losses of the system and to increase the lifecycle of energy storage systems.

The first shell (EMS) is responsible for controlling the waveform power quality, which includes zero sequence detectors to split the imbalance component from the waveform, the droop controller to maintain the frequency and voltage to the standard level, and the vector controller to change the rotating reference frame to the stationary reference frame. The filtered reference waveform provides the second process in the structure, which is PMS. The PMS uses the fuzzy heuristic approach to split the power between the battery and the supercapacitors based on the state of charge of energy storage systems, frequency deviation, and voltage deviation of the microgrid.

The third shell of the process is PES, which is responsible for implementing the MSVPWM to trigger the 18 switches of the converter topology to implement the PMS power reference of the battery and the supercapacitors. The battery operates at three-phase waveform for charging and discharging. Therefore, the DC waveform of the battery had low harmonic distortion and low ripple. The supercapacitors operate at single phase waveform for charging and discharging. Therefore, the DC waveform of the battery had higher harmonic and higher ripple than battery waveform. The ripple increased as the current of the supercapacitor increased. Normally, the microgrid operates at the unbalanced condition. The supercapacitors could assist balancing the microgrid by providing an unsymmetrical switching modulation for operating different values of current through the phases of supercapacitors. The switching modulation of the proposed inverter topology provided a sinusoidal three-phase waveform at 120^0 phase shift at the

discharging operation. The total power of the inverter was the sum of the power of the battery and the supercapacitors. The modulation switching strategy could supply a range of power by cooperation between the battery and the supercapacitors to synergise the microgrid operation.

The hierarchical organisation management philosophy of MGO, CSO, and EVO presented a cogent argument to the stable and reliable operation of EVs within the microgrid. It provided not only a very different perspective to the management of the microgrid problem but also an implementation of a modular structure that addresses all aspects of managing the optimum operation of distributed generators and EVs to balance the electrical demand of the microgrid network. This approach unified the management of EVs within the microgrid as a comprehensive description including aspects of the research problem, rather than isolated the research into subproblems without fitting it into a whole picture, as taken from many publications.

The time response of the supercapacitor is much faster than that of the battery. Therefore, the supercapacitor could deliver power in acceleration or discharge to the microgrid to cover the fast response until the battery recaptures the main load. The kinetic energy of braking could be saved as electrical energy in a supercapacitor rather than waste it. Therefore, the hybridized battery-supercapacitor are complementary resources to achieve better performance for EV operation, increase the efficiency of both, extend the life of both, and reduce THD. The multi-level inverter has many advantages over the conventional converter, such as less weight and cost due to the missing main inductor, flexibility in control, better response due to using fewer components, lower harmonic and EMI effect, can easily accommodate two resources into it, and handling the unbalanced phases by using three separate supercapacitors. However, controlling such a converter is complex. Therefore, this kind of inverter is suitable for EV application either in running mode or connected mode. EVO could carry out the CSO instruction as the centralised operation of EV or collaborate with the electric vehicle agency and smart charger controller of EV as a decentralised operation. This flexibility provides the continuous operation of EV within the microgrid without interruption, whereas the execution time of the EVO is much faster than the execution time of the CSO. Therefore, the EVO does not interrupt operating the EV even when the fault happens at CSO. EVO is responsible for synchronising, managing and controlling the resources waveforms with the microgrid in connected mode as well as running mode in the charging or discharging operation. Therefore, it is divided into different dynamic shells, whereas the response of EMS is lower in response than PMS and PES, and the PES has a faster response to the controller system. Furthermore, the PMS and PES are responsible for power arbitrating and switching modulation respectively. Therefore, the reference of the PMS and PES is feeding on EMS which makes the system respond in seconds. The EMS is more active in discharging mode than in charging mode. Therefore, the system in charging mode operates faster than in discharging mode which can catch the PMS execution period which is in milliseconds. The fuzzy controller is a very active toolbox to implement the arbitrating power between resources of EV in a synergizing, rigid, and fast way, based on four parameters, two of them belonging to microgrid and the others to the resources of EV. The switching modulation strategy of the inverter must switch between either controlling all switches together or spread switching control of the three-phase bridge and H bridges at integer and non-integer ratios between battery and supercapacitor respectively.

It is difficult to generalise the states of switching in one form due to the non-uniform conversion type of battery and supercapacitors. Therefore, each state of battery and supercapacitors has the main solution with minimum switching transition and redundancy, except the non-integer ratio which has a special solution. Each EV should generate its discharging reference based on the capacity and state of charge of resources to help controllers decide the most suitable discharging power, as it is not adequate to provide the same reference discharging power for an EV that has a different capacity and state of charge resources.

Chapter seven presented the details of the experimental rig and the results to validate the PES shell in the EVO level. The simulation results of the mathematical model match the practical results of the inverter operation at PES. Therefore, the mathematical model proposed a good approach to extend over the research. A different mode of operation is applied based on the switching and resources states. Therefore, the control voltage of resources maximises recaptured energy or achieves a maximum number of levels of the inverter. Increasing the voltage reference near the limit of resources provides less pulse width modulation, which increases the nonlinearity at the waveform. Even when the reference voltage exceeds the limit of resources, the overmodulation technique recaptures the voltage reference inside the hexagon diagram to make the system stable. However, the nonlinearity of the waveform would be maximum. The developed hardware together with its control algorithm supported by CompactRIO devices, and LabVIEW software, can fully utilise the resources and control algorithms to control the system instantaneous in real time simulation. It presents the capability to increase output voltage using hybridization resources and maintain a balanced voltage at supercapacitors as well as the ability to provide a stable output from the resources. Therefore, the proposed configuration enhances the performance of inverters to connect the resources of EVs to microgrids as well as enhancing the drivetrain. Furthermore, the proposed modulation strategy operates the inverter in a robust way with a minimum size of FPGA hardware resources. Therefore, the proposed inverter and control strategy could be a feasible solution for the hardware implementation of commercial applications.

8.2 Future work

The major objective of this thesis has been accomplished. However, there are several avenues that warrant further immediate investigation in short time scale such as:

1- The distribution network will facilitate many microgrids depending on the nature of the load. Therefore, another level of the operator is required to control the management and control the power flow between the microgrids. This level is not included in this dissertation. It could be called distribution network operator (DNO). Therefore, more investigation of the nature of the load and types of the microgrid should be considered to apply the distributed management system to manage and control the circulating power of many microgrids within the distribution network and the utility grid.
2- The thesis contributes charging and discharging aggregated EVs that connected to many platforms in charging station system using centralised and decentralised strategy

whereas the single platform at home or private charging station does not include. Therefore, the hierarchical management should include management and control charging and discharging the single EV to cover all kind of charging station system within microgrid. The individual strategy should be applied to manage and control many EVs spread in a geographical place that have different characteristics such as either treat each EV as single CSO or connected single EV by a communication link to the nearest CSO. It could be suggested another operator for this kind of charging station system called Private Home Station Operator (PHO) and proposed some rules to operate it.

3- It can be noticed that the equation of the microgrid represents the mixed integer quadratic optimisation problem. Therefore, many numerical methods proposed to simplify the implementation of the optimisation algorithm to provide a rapid solution. However, there are many open issues to implement these solvers such as the dynamic behaviour of the devices that include in the management problem, the spatiotemporal spread of the EVs around the microgrid, the communication delay between the layers of the microgrid implanting in a different time. All of these issues present difficulty to implement the centralised management and control the power flow and optimisation algorithm in real time. Therefore, it is a big challenge to implement the proposed algorithm in reality with instant time at the physical component implementation.

4- Such complicated system that implements centralised solvers in geographically spread components population and scalability of the solution is required intelligent communication system to deal with the decisions of the solvers between the operators. The communication network is essential to collect data and respond to the solvers every time some changes occur. Any delays or interference in the electrical signal could cause a negative response from the operators that lead to a fault in the system then congestion may happen. Therefore, unqualified communication system could cause a blackout of the microgrid network.

5- Each equipment within microgrid has a microcontroller. A function of the microcontroller is to synchronise and connect the equipment to the microgrid. Therefore, fast response of the microcontroller helps the microgrid to exceed the congestion of the system. In addition, the micro controllers should contact each other to simulate the behaviour of the network as the microgrid operates as one block where any fault happening could lead to losing all the network. Therefore, unify controller design that applies to all applications is required to make the equipment operation synergize each other to produce healthy network and mitigate the harmonics to provide pure sinusoidal waveforms. The dynamic effect of the connecting or disconnecting the microgrid from the utility grid at the point of common coupling could cause a surpluses power that leads to isolate the frequency and voltage of the microgrid. Therefore, there is a specific strategy that should be applied to prevent the continuous variation/oscillation of the grid frequency and voltage during bidirectional power flow (between the microgrid and the utility grid).

6- The most expensive equipment and the highest weight in the EVs is the battery. There is still many research in battery technology to reduce the price and weight and increase the efficiency. The other challenge of the battery technology is finding the electrical

effect of chemical reaction at battery operation to find the exact effect of integration many batteries within microgrid and to find the economic evaluation of hybridization the supercapacitors within the battery. Monitoring the state of charge of the energy storage system is very important where the underestimation can occur within the application of the Peukert's equation leading to inaccurate measurement [354]. Therefore, further research on the estimation of the accurate state of charge of the energy storage systems at real time is essential to include and analyse the effect and controllability of most or all parameters of energy storage system.

7- Normally, the distribution network has an unbalanced nature. Therefore, the load flow analysis and modulation analysis should include the unsymmetrical behaviour of the distribution network within the formulation algorithms. Including the unsymmetrical behaviour of the electricity waveform could change the distributed power among the distributed generators where unbalance phases are applied. Therefore, the optimisation algorithm becomes more complicated and require large size to implement in addition to not all brands of the EVs apply the same topology of the inverter.

8- Therefore, the effect of different topologies requires more investigation to balance the charging and discharging the energy storage system of the proposed topology. This study has been used the equal triangle in the modulation the M-SVPWM whereas at unbalance condition the unequal triangle should include in the modulation analysis, in addition, the ratio of the voltage between the battery and supercapacitors become unequal. Therefore, a unique vector should be applied for each case which may be required. It is possible to use three separate supercapacitors in the EV to mitigate the unbalancing effect of the microgrid waveform.

9- The main feature of the EV is covering owner purposes. Therefore, the research should consider the propulsion load of the EV on studying proposed topology and switching modulation to figure out the feasible applicability of the managing power and energy of multiple energy resources for EV applications.

10- The thesis discussed three levels of operators that work based on different functions at different time scale in addition to the suggestion of the DNO to control different microgrids. Therefore, studying the stability analysis of the chronological framework of the DNO, MGO, CSO, PHO, and EVO and the sensitive dependency on component variations become necessary to figure out the effect of the interconnected operation of the operators that have a different response of component on the stability issue.

11- The PHO could include more than two resources such as photovoltaic cell in private parking. Therfore, the multilevel inverter topology in single charging station system may be extended to higher than five levels to cover another kind or electrical sources which then complecates sychronising the inverter with microgrid, the mangment of resources, and control switching modulation strategy. .

References

[1] F. Appavou *et al.*, “Renewables 2016: Global Status Report,” 2016.

[2] O. Zinaman *et al.*, “Power Systems of the Future: A 21st Century Power Partnership Thought Leadership Report,” 2015.

[3] R. R. Bowker *et al.*, “Annual report: board of directors to the stockholders,” New York, NY, 1891.

[4] D. P. Tuttle *et al.*, “The history and evolution of the U.S . electricity industry,” Texas, 2016.

[5] British Petroleum company, “BP energy: outlook to 2035,” 2016.

[6] U. Sultana, A. B. Khairuddin, M. M. Aman, A. S. Mokhtar, and N. Zareen, “A review of optimum DG placement based on minimization of power losses and voltage stability enhancement of distribution system,” *Renew. Sustain. Energy Rev.*, vol. 63, pp. 363–378, 2016.

[7] The word bank company, “Report WB: World bank development indicator 2016.,” *Available at: http://data.worldbank.org/indicator/EG.ELC.LOSS.ZS*, 2016. .

[8] A. Larocque, D. Nadeau, and M. Landry, “Comprehensive Planning for Electric Power Supply in Haiti – Expansion of the Supply for Electricity Generation,” 2014.

[9] T. S. Ustun, C. Ozansoy, and A. Zayegh, “Recent developments in microgrids and example cases around the world: A review,” *Renew. Sustain. Energy Rev.*, vol. 15, no. 8, pp. 4030–4041, Oct. 2011.

[10] G. G. Mendes, C. Ioakimidis, and P. Ferrão, “On the planning and analysis of Integrated Community Energy Systems: A review and survey of available tools,” *Renew. Sustain. Energy Rev.*, vol. 15, no. 9, pp. 4836–4854, Dec. 2011.

[11] S. A. Gopalan, V. Sreeram, and H. H. C. Iu, “A review of coordination strategies and protection schemes for microgrids,” *Renew. Sustain. Energy Rev.*, vol. 32, pp. 222–228, 2014.

[12] X. Fang, S. Misra, G. Xue, and D. Yang, “Smart Grid — The New and Improved Power Grid: A Survey,” *IEEE Commun. Surv. Tutorials*, vol. 14, no. 4, pp. 944–980, 2012.

[13] M. E. El-hawary, “The Smart Grid: State of the art and future trends,” *Electr. Power Components Syst.*, vol. 42, no. 3–4, pp. 239–250, 2014.

[14] C. Gouveia *et al.*, “Experimental validation of smart distribution grids: Development of a microgrid and electric mobility laboratory,” *Int. J. Electr. Power Energy Syst.*, vol. 78, pp. 765–775, 2016.

[15] United States Environmental Protection Agency, “Climate Change 2014: Mitigation of Climate Change,” *Available at: https://www.epa.gov/ghgemissions/global-greenhouse-gas-emissions-data*, 2014. [Online]. Available: https://www.epa.gov/ghgemissions/global-greenhouse-gas-emissions-data. [Accessed: 16-Jan-2017].

[16] The shift project, “Breakdown of Electricity Generation by Energy Source,” *Available At: http://www.tsp-data-portal.org/Breakdown-of-Electricity-Generation-by-Energy-*

Source#tspQvChart, 2016. [Online]. Available: http://www.tsp-data-portal.org/Breakdown-of-Electricity-Generation-by-Energy-Source#tspQvChart. [Accessed: 16-Jan-2017].

[17] S. Abraham, "National Transmission Grid Study," U.S., 2002.

[18] National Grid company, "Undergrounding high voltage electricity transmission lines: The technical issues," 2015.

[19] T. Hague, "Iraq Electricity Masterplan," Baghdad, Iraq, 2010.

[20] A. Mohamed and O. Mohammed, "Real-time energy management scheme for hybrid renewable energy systems in smart grid applications," *Electr. Power Syst. Res.*, vol. 96, pp. 133–143, 2013.

[21] M. Kolhe, K. Agbossou, J. Hamelin, and T. Bose, "Analytical model for predicting the performance of photovoltaic array coupled with a wind turbine in a stand-alone renewable energy system based on," *Renew. Energy*, vol. 28, pp. 727–742, 2003.

[22] L. Xie and M. D. Ilic, "Model Predictive Dispatch in Electric Energy Systems with," *IEEE Int. Conf. Syst. Man Cybern.*, pp. 42–47, 2008.

[23] M. K. Deshmukh and S. S. Deshmukh, "Modeling of hybrid renewable energy systems," *Renew. Sustain. Energy Rev.*, vol. 12, no. 1, pp. 235–249, 2008.

[24] P. Nema, R. K. Nema, and S. Rangnekar, "A current and future state of art development of hybrid energy system using wind and PV-solar: A review," *Renew. Sustain. Energy Rev.*, vol. 13, no. 8, pp. 2096–2103, 2009.

[25] W. Zhou, C. Lou, Z. Li, L. Lu, and H. Yang, "Current status of research on optimum sizing of stand-alone hybrid solar-wind power generation systems," *Appl. Energy*, vol. 87, no. 2, pp. 380–389, 2010.

[26] R. H. H. Lasseter, "MicroGrids," *IEEE Power Eng. Soc. Winter Meet. Conf. Proc. (Cat. No.02CH37309)*, vol. 1, pp. 305–308, 2002.

[27] P. Asmus, "Why Microgrids Are Moving into the Mainstream," *Electrif. Mag. IEEE*, vol. 2, no. 1, pp. 12–19, 2014.

[28] J. M. Guerrero, J. C. Vasquez, J. Matas, L. G. De Vicuña, and M. Castilla, "Hierarchical Control of Droop-Controlled AC and DC Microgrids — A General Approach Toward Standardization," *IEEE Trans. Ind. Electron.*, vol. 58, no. 1, pp. 158–172, 2011.

[29] A. Bidram and A. Davoudi, "Hierarchical structure of microgrids control system," *IEEE Trans. Smart Grid*, vol. 3, no. 4, pp. 1963–1976, 2012.

[30] D. E. Olivares *et al.*, "Trends in microgrid control," *IEEE Trans. Smart Grid*, vol. 5, no. 4, pp. 1905–1919, 2014.

[31] The United States Congress, "Energy Independence and Security Act of 2007," U.S., 2007.

[32] V. C. Güngör *et al.*, "Smart grid technologies: Communication technologies and standards," *IEEE Trans. Ind. Informatics*, vol. 7, no. 4, pp. 529–539, 2011.

[33] D. Coll-Mayor, M. Paget, and E. Lightner, "Future intelligent power grids: Analysis of the vision in the European Union and the United States," *Energy Policy*, vol. 35, no. 4,

pp. 2453–2465, Apr. 2007.

[34] J. Fan and S. Borlase, “The evolution of distribution,” *IEEE Power Energy Mag.*, vol. 7, no. 2, pp. 63–68, 2009.

[35] H. Liang, A. K. Tamang, W. Zhuang, and X. S. Shen, “Stochastic Information Management in Smart Grid,” *IEEE Commun. Surv. Tutorials*, vol. 16, no. 3, pp. 1746–1770, 2014.

[36] S. Galli, A. Scaglione, and Z. Wang, “For the Grid and Through the Grid: The Role of Power Line Communications in the Smart Grid,” *Proc. IEEE*, vol. 99, no. 6, pp. 998–1027, 2011.

[37] J. A. P. Lopes, C. L. Moreira, and A. G. Madureira, “Defining Control Strategies for MicroGrids Islanded Operation,” *IEEE Trans. Power Syst.*, vol. 21, no. 2, pp. 916–924, 2006.

[38] F. Nejabatkhah and Y. W. Li, “Overview of Power Management Strategies of Hybrid AC/DC Microgrid,” *IEEE Trans. Power Electron.*, vol. 30, no. 12, pp. 7072–7089, 2015.

[39] A. Kaur, J. Kaushal, and P. Basak, “A review on microgrid central controller,” *Renew. Sustain. Energy Rev.*, vol. 55, pp. 338–345, 2016.

[40] A. R. Metke and R. L. Ekl, “Security technology for smart grid networks,” *IEEE Trans. Smart Grid*, vol. 1, no. 1, pp. 99–107, 2010.

[41] F. F. Wu, K. Moslehi, and A. Bose, “Power System Control Centers: Past, Present, and Future,” *Proc. IEEE*, vol. 93, no. 11, pp. 1890–1908, 2005.

[42] F. Rahimi and A. Ipakchi, “Demand response as a market resource under the smart grid paradigm,” *IEEE Trans. Smart Grid*, vol. 1, no. 1, pp. 82–88, 2010.

[43] P. Basak, S. P. Chowdhury, S. Halder nee Dey, and S. P. Chowdhury, “A literature review on integration of distributed energy resources in the perspective of control, protection and stability of microgrid,” *Renew. Sustain. Energy Rev.*, vol. 16, no. 8, pp. 5545–5556, Oct. 2012.

[44] R. H. Lasseter and P. Paigi, “Microgrid: a conceptual solution,” in *IEEE 35th Annual Power Electronics Specialists Conference, Germany*, 2004, pp. 4285–4290.

[45] Robert H. Lasseter, “Smart Distribution: Coupled Microgrids,” *Proc. IEEE*, vol. 99, no. 6, 2011.

[46] L. Y. Wang, M. Polis, C. Wang, and F. Lin, “Voltage Stability and Robustness for Microgrid Systems,” *Eur. Control Conf. (ECC), Zürich, Switzerland.*, pp. 2038–2043, 2013.

[47] M. Ettehadi, H. Ghasemi, and S. Vaez-Zadeh, “Voltage stability-based DG placement in distribution networks,” *IEEE Trans. Power Deliv.*, vol. 28, no. 1, pp. 171–178, 2013.

[48] M. Parol and Ł. Rokicki, “Voltage stability in low voltage microgrids in aspects of active and reactive power demand,” *Arch. Electr. Eng.*, vol. 65, no. 1, pp. 19–32, 2016.

[49] S. Abu-Sharkh *et al.*, “Can microgrids make a major contribution to UK energy supply?,” *Renew. Sustain. Energy Rev.*, vol. 10, no. 2, pp. 78–127, Apr. 2006.

[50] S. Parhizi, H. Lotfi, A. Khodaei, and S. Bahramirad, “State of the art in research on

microgrids: A review," *IEEE Access*, vol. 3, pp. 890–925, 2015.

[51] R. Majumder, "Some Aspects of Stability in Microgrids," *IEEE Trans. Power Syst.*, vol. 28, no. 3, pp. 3243–3252, Aug. 2013.

[52] M. Soshinskaya, W. H. J. Crijns-Graus, J. M. Guerrero, and J. C. Vasquez, "Microgrids: Experiences, barriers and success factors," *Renew. Sustain. Energy Rev.*, vol. 40, pp. 659–672, 2014.

[53] S. F. Tie and C. W. Tan, "A review of energy sources and energy management system in electric vehicles," *Renew. Sustain. Energy Rev.*, vol. 20, pp. 82–102, 2013.

[54] P. Gaur and S. Singh, "Investigations on Issues in Microgrids," *J. Clean Energy Technol.*, vol. 5, no. 1, pp. 47–51, 2017.

[55] O. P. R. van Vliet, T. Kruithof, W. C. Turkenburg, and A. P. C. Faaij, "Techno-economic comparison of series hybrid, plug-in hybrid, fuel cell and regular cars," *J. Power Sources*, vol. 195, no. 19, pp. 6570–6585, 2010.

[56] Department for Business Energy and industrial strategy, "UK Greenhouse Gas Emissions – 3 rd Quarter 2015 Provisional Figures Statistical Release : Official statistics," London, United Kingdom, 2015.

[57] International Energy Agency group (IEA), "Global EV Outlook 2016 Electric," Paris, France, 2016.

[58] Tennessee Valley Authority., "Types of Electric Vehicles," 2015. [Online]. Available: http://www.tva.com/environment/technology/car_vehicles.htm. [Accessed: 15-Jul-2015].

[59] N. Rahbari-Asr and M. Y. Chow, "Cooperative distributed demand management for community charging of PHEV/PEVs based on KKT conditions and consensus networks," *IEEE Trans. Ind. Informatics*, vol. 10, no. 3, pp. 1907–1916, 2014.

[60] C. Battistelli, L. Baringo, and A. J. Conejo, "Optimal energy management of small electric energy systems including V2G facilities and renewable energy sources," *Electr. Power Syst. Res.*, vol. 92, pp. 50–59, 2012.

[61] B. Khorramdel, H. Khorramdel, J. Aghaei, A. Heidari, and V. G. Agelidis, "Voltage Security Considerations in Optimal Operation of BEVs/PHEVs Integrated Microgrids," *IEEE Trans. Smart Grid*, vol. 6, no. 4, pp. 1575–1587, 2015.

[62] S. Beer, T. Gómez, D. Dallinger, C. Marnay, M. Stadler, and J. Lai, "An Economic Analysis of Used Electric Vehicle Batteries Integrated Into Commercial Building Microgrids," *IEEE Trans. Smart Grid*, vol. 3, no. 1, pp. 517–525, 2012.

[63] IEC company, "Electrical Energy Storage: White Paper Report," 2009.

[64] M. Alkhafaji, P. Luk, and J. Economuo, "A holistic modular power management framework to achieve resilience operation of microgrid including electric vehicles," in *Cranfield Science for a Circular Economy. How to tackle the Water, Energy, Food nexus Conference Proceedings, Cranfield, United Kingdom*, 2017.

[65] M. Alkhafaji, P. C. K. Luk, and J. Economou, "A new modular power management framework for operating bidirectional vehicle to grid system within microgrid," in *Cranfield Science for a Circular Economy. How to tackle the Water, Energy, Food nexus*

Conference Proceedings, Cranfield, United Kingdom, 2017, no. June.

[66] M. H. Alkhafaji, P. C. K. Luk, and A. F. Bati, "Integration of electric vehicles within microgrid," in *UKACC 11th International Conference on Control, Belfast, United Kingdom*, 2016.

[67] M. Alkhafaji, P. C. K. Luk, J. Economou, and J. Economuo, "Optimizing the location of distributed generators in microgrid based on voltage stability," in *Cranfield Science for a Circular Economy. How to tackle the Water, Energy, Food nexus Conference Proceedings, Cranfield, United Kingdom*, 2017.

[68] M. Alkhafaji, P. C. K. Luk, J. Economuo, and J. Economou, "Impact of integration electric vehicles to the microgrid," in *Cranfield Science for a Circular Economy. How to tackle the Water, Energy, Food nexus Conference Proceedings, Cranfield, United Kingdom*, 2017.

[69] M. Alkhafaji, P. Luk, and J. Economou, "Optimal Design and Planning of Electric Vehicles Within Microgrid," in *Advanced Computational Methods in Energy, Power, Electric Vehicles, and Their Integration: LSMS and ICSEE 2017 Proceedings, Nanjing, China*, 2017, pp. 677–690.

[70] M. Alkhafaji, P. Luk, and J. Economou, "Charging and Discharging Strategy of Electric Vehicles Within a Hierarchical Energy Management Framework," in *Advanced Computational Methods in Energy, Power, Electric Vehicles, and Their Integration: LSMS and ICSEE 2017 Proceedings, Nanjing, China*, 2017, pp. 704–718.

[71] European Environment Agency, "Monitoring the CO2 emissions from new passenger cars in the EU: summary of data for 2010." [Online]. Available: http://www.gperi.moptc.pt/tempfiles/20110811154608moptc.pdf. [Accessed: 15-Jul-2015].

[72] P. European Federation for Transport and Environment, "How clean are Europe's cars? An analysis of carmaker progress towards EU CO2 targets Report in 2012," 2012.

[73] Department of energy and climate change in UK, "Energy Trends Report," United Kingdom, 2014.

[74] UK and Chinese Collabrators project team (iGIVE), "Intelligent Grid Interfaced Vehicle Eco-charging (iGIVE) Project," 2013.

[75] Department for Business Enterprise and Regulatory Reform (BERR): Department for Transport, "Investigation into the Scope for the Transport Sector to Switch to Electric Vehicles and Plug- in Hybrid Vehicles," London / United Kingdom, 2008.

[76] W. Kempton and J. Tomić, "Vehicle-to-grid power implementation: From stabilizing the grid to supporting large-scale renewable energy," *J. Power Sources*, vol. 144, no. 1, pp. 280–294, Jun. 2005.

[77] Amish Pleasures Inc., "The History of Electric Vehicles," *EllectricVehiclesNews.com*, 1998. [Online]. Available: http://www.electricvehiclesnews.com/History/historyV.htm. [Accessed: 27-Jun-2017].

[78] P. Kundur, *Power System Stability and Control*, First Edit. McGraw-Hill, 1994.

[79] Distribution Network Operators of Great Britain, "The distribuation code and the guide to the distribution code of licensed distribution network operators of great Britain,"

2014.

[80] I. MacLeay, K. Harris, and A. Annut, “Digest of United Kingdom Energy Statistics 2014,” London / United Kingdom, 2014.

[81] S. Butler, “The nature of UK electricity transmission and distribution networks in an intermittent renewable and embedded electricity generation future,” University of London: Imperial College, 2001.

[82] Distribution Network Operators of Great Britain, “The distribuation code and the guide to the distribution code of licensed distribution network operators of great Britain,” 2017.

[83] Department of Energy and Climate Change (DECC), “Developing our future electricity networks,” London / United Kingdom, 2011.

[84] M. Tritschler and W. Mackay, “UK Smart Grid Cyber Security,” 2011.

[85] U.S. Department of Energy, “The Smart Grid: An Introduction,” 2010.

[86] Independent Electricity System Operator, “Enabling Tomorrow’s Electricity System: Report of the Ontario Smart Grid Forum,” 2010.

[87] M. Keogh, “The Smart Grid: Frequently Asked Questions for State Commissions,” 2009.

[88] IEEE Std 2030-2011, *IEEE Guide for Smart Grid Interoperability of Energy Technology and Information Technology Operation with the Electric Power System (EPS), End-Use Applications, and Loads*, no. September. 2011.

[89] M. C. Chandorkar, M. D. Deepakraj, and R. Adapa, “Control of Parallel Connected Inverters in Standalone ac Supply Systems,” *IEEE Trans. Ind. Appl.*, vol. 29, no. 1, pp. 136–143, 1993.

[90] C. Marnay and R. Firestone, “Microgrids : An emerging paradigm for meeting building electricity and heat requirements efficiently and with appropriate energy quality,” *Eur. Counc. an Energy Effic. Econ. 2007*, vol. Summer Stu, no. April, pp. 4–9, 2007.

[91] R. Lasseter *et al.*, “The CERTS microgrid concept. White Paper on Integration of distributed energy resources,” California / U.S., 2002.

[92] D. T. Ton and M. A. Smith, “The U.S. Department of Energy’s Microgrid Initiative,” *Electr. J.*, vol. 25, no. 8, pp. 84–94, 2012.

[93] C. Marnay and S. Chatzivasileiadis, “Microgrid Evolution Roadmap,” in *International Symposium on Smart Electric Distribution Systems and Technologies conference (EDST)*, 2015, pp. 139–144.

[94] T. Funabashi and R. Yokoyama, “Microgrid Field Test Experiences in Japan,” in *Power Engineering Society General Meeting, 2006. IEEE, Montreal, Que., Canada*, 2006, vol. 2, pp. 1–2.

[95] Electric power research Institute EPRI, “Smart Grid Resource Center,” *EPRI Smart Grid Resource Center*. [Online]. Available: http://smartgrid.epri.com/. [Accessed: 19-May-2014].

[96] M. E. El-hawary, “The Smart Grid—State-of-the-art and Future Trends,” *Electr. Power*

Components Syst., vol. 42, no. 3–4, pp. 239–250, Mar. 2014.

[97] SMB Smart Grid Strategic Group (SG3), "Smart Grid Standardization Roadmap," 2010.

[98] U.S.-Argentina Binational Energy Working Group (BEWG), "Smart Grid," Buenos Aires / Argentina, 2012.

[99] S. Surbhi, "Difference Between Centralization and Decentralization," *key differences*, 2015. [Online]. Available: http://keydifferences.com/difference-between-centralization-and-decentralization.html. [Accessed: 27-Jun-2017].

[100] P. Stluka, D. Godbole, and T. Samad, "Energy Management for Buildings and Microgrids," in *IEEE Conference on Decision and Control and European Control Conference (CDC-ECC), Orlando, FL, USA*, 2011, pp. 5150–5157.

[101] G. C. Liao, "Solve environmental economic dispatch of Smart MicroGrid containing distributed generation system - Using chaotic quantum genetic algorithm," *Electr. Power Energy Syst.*, vol. 43, no. 1, pp. 779–787, 2012.

[102] A. Takeuchi, T. Hayashi, Y. Nozaki, and T. Shimakage, "Optimal scheduling using metaheuristics for energy networks," *IEEE Trans. Smart Grid*, vol. 3, no. 2, pp. 968–974, 2012.

[103] M. L. Di Silvestre, G. Graditi, and E. Riva Sanseverino, "A generalized framework for optimal sizing of distributed energy resources in micro-grids using an indicator-based swarm approach," *IEEE Trans. Ind. Informatics*, vol. 10, no. 1, pp. 152–162, 2014.

[104] H. Wu, X. Liu, and M. Ding, "Dynamic economic dispatch of a microgrid: Mathematical models and solution algorithm," *Electr. Power Energy Syst.*, vol. 63, pp. 336–346, 2014.

[105] R. Rigo-Mariani, B. Sareni, X. Roboam, and C. Turpin, "Optimal power dispatching strategies in smart-microgrids with storage," *Renew. Sustain. Energy Rev.*, vol. 40, pp. 649–658, 2014.

[106] J. Radosavljević, M. Jevtić, and D. Klimenta, "Energy and operation management of a microgrid using particle swarm optimization," *Eng. Optim.*, vol. 48, no. 5, pp. 811–830, 2015.

[107] F. A. Mohamed and H. N. Koivo, "System modelling and online optimal management of MicroGrid using Mesh Adaptive Direct Search," *Electr. Power Energy Syst.*, vol. 32, no. 5, pp. 398–407, 2010.

[108] M. Haghshenas and H. Falaghi, "Environmental/Economic Operation Management of a Renewable Microgrid with Wind/PV/FC/MT and Battery Energy Storage Based on MSFLA," *J. Electr. Syst.*, vol. 1, pp. 85–101, 2016.

[109] S. Ali, Y. A. I. Mohamed, S. Member, and T. H. M. El-fouly, "Optimum Microgrid Design for Enhancing Reliability," *IEEE Trans. Smart Grid*, vol. 4, no. 3, pp. 1567–1575, 2013.

[110] S. A. Arefifar, Y. A. I. Mohamed, and T. El-fouly, "Optimized Multiple Microgrid-Based Clustering of Active Distribution Systems Considering Communication and Control Requirements," *IEEE Trans. Ind. Electron.*, vol. 62, no. 2, pp. 711–723, 2015.

[111] R. Firestone and C. Marnay, "Energy Manager Design for Microgrids," California, 2005.

[112] G. Pepermans, J. Driesen, D. Haeseldonckx, R. Belmans, and W. D'haeseleer, "Distributed generation: Definition, benefits and issues," *Energy Policy*, vol. 33, no. 6, pp. 787–798, 2005.

[113] A. S. Siddiqui, C. Marnay, R. M. Firestone, and N. Zhou, "Distributed Generation with Heat Recovery and Storage," in *The 7th Annual International Association for Energy Economics European Energy Conference at the Norwegian School of Economics and Business Administration, Bergen, Norway*, 2005, vol. 133, no. 3, pp. 181–210.

[114] N. Hatziargyriou, H. Asano, R. Iravani, and C. Marnay, "Microgrids," *IEEE power energy Mag.*, no. July/august, pp. 78–94, 2007.

[115] E. D. Mehleri, H. Sarimveis, N. C. Markatos, and L. G. Papageorgiou, "Optimal design and operation of distributed energy systems: Application to Greek residential sector," *Renew. Energy*, vol. 51, pp. 331–342, 2013.

[116] D. Zhang, N. Shah, and L. G. Papageorgiou, "Efficient energy consumption and operation management in a smart building with microgrid," *Energy Convers. Manag.*, vol. 74, pp. 209–222, 2013.

[117] A. Parisio, E. Rikos, and L. Glielmo, "Stochastic model predictive control for economic/environmental operation management of microgrids: An experimental case study," *J. Process Control*, vol. 43, pp. 24–37, 2016.

[118] P. Malysz, S. Sirouspour, and A. Emadi, "An Optimal Energy Storage Control Strategy for Grid-connected Microgrids," *IEEE Trans. Smart Grid*, vol. 5, no. 4, pp. 1785–1796, 2014.

[119] A. Parisio, E. Rikos, and L. Glielmo, "A model predictive control approach to microgrid operation optimization," *IEEE Trans. Control Syst. Technol.*, vol. 22, no. 5, pp. 1813–1827, 2014.

[120] M. Falahi, K. Butler-Purry, and M. Ehsani, "Dynamic Reactive Power Control of Islanded Microgrid Using IPFC," *IEEE Trans. Power Syst.*, vol. 28, no. 4, pp. 3649–3657, 2013.

[121] P. O. Kriett and M. Salani, "Optimal control of a residential microgrid," *Energy*, vol. 42, no. 1, pp. 321–330, Jun. 2012.

[122] R. Palma-Behnke *et al.*, "A microgrid energy management system based on the rolling horizon strategy," *IEEE Trans. Smart Grid*, vol. 4, no. 2, pp. 996–1006, 2013.

[123] A. Parisio, C. Wiezorek, T. Kyntäjä, J. Elo, and K. H. Johansson, "An MPC-based Energy Management System for Multiple Residential Microgrids," in *IEEE International Conference on Automation Science and Engineering (CASE), Gothenburg, Sweden*, 2015.

[124] V. Jouanne and B. Banerjee, "assessment of voltage unbalance," *IEEE Trans. Power Deliv.*, vol. 16, no. 4, pp. 1176–1177, 2001.

[125] K. Sarwagya and P. K. Nayak, "An Extensive Review on the State of Art on Microgrid Protection," in *IEEE Power, Communication and Information Technology Conference (PCITC), Siksha "O" AnusandhanAnusandhan University, Bhubaneswar, India*, 2015.

[126] G. T. Heydt, "The Impact of Electric Vehicle Deployment on Load Management Straregies," *IEEE Trans. Power Appar. Syst.*, vol. PAS-102, no. 5, 1983.

[127] P. Denholm, E. Ela, B. Kirby, and M. Milligan, "The Role of Energy Storage with Renewable Electricity Generation," Colorado, U.S., 2010.

[128] B. Nyamdash, E. Denny, and M. O'Malley, "The viability of balancing wind generation with large scale energy storage," *Energy Policy*, vol. 38, no. 11, pp. 7200–7208, 2010.

[129] A. Testa, S. De Caro, R. La Torre, and T. Scimone, "Optimal Design of Energy Storage Systems for Stand-Alone Hybrid Wind / PV Generators," in *International Symposium on Power Electronics Electrical Drives Automation and Motion (SPEEDAM), Pisa, Italy*, 2010, pp. 1291–1296.

[130] H. Oh, "Optimal planning to include storage devices in power systems," *IEEE Trans. Power Syst.*, vol. 26, no. 3, pp. 1118–1128, 2011.

[131] T. M. Masaud, K. L. K. Lee, and P. K. Sen, "An overview of energy storage technologies in electric power systems: What is the future?," in *IEEE: North American Power Symposium (NAPS), Arlington, TX, USA*, 2010, vol. 80401, pp. 1–6.

[132] D. Pozo, J. Contreras, and E. E. Sauma, "Unit Commitment With Ideal and Generic Energy Storage Units," *IEEE Trans. Power Syst.*, vol. 29, no. 6, pp. 1–11, 2014.

[133] S. J. Park, J. H. Shin, J. H. Park, and H. J. Jeon, "Dynamic analysis and controller design for standalone operation of photovoltaic power conditioners with energy storage," *J. Electr. Eng. Technol.*, vol. 9, no. 6, pp. 2004–2012, 2014.

[134] W. El-Khattam and M. M. A. Salama, "Distributed generation technologies, definitions and benefits," *Electr. Power Syst. Res.*, vol. 71, no. 2, pp. 119–128, 2004.

[135] K. Shivarama Krishna and K. Sathish Kumar, "A review on hybrid renewable energy systems," *Renew. Sustain. Energy Rev.*, vol. 52, pp. 907–916, 2015.

[136] M. E. Khodayar, L. Wu, and M. Shahidehpour, "Hourly coordination of electric vehicle operation and volatile wind power generation in SCUC," *IEEE Trans. Smart Grid*, vol. 3, no. 3, pp. 1271–1279, 2012.

[137] A. Y. Saber and G. K. Venayagamoorthy, "Resource scheduling under uncertainty in a smart grid with renewables and plug-in vehicles," *IEEE Syst. J.*, vol. 6, no. 1, pp. 103–109, 2012.

[138] S. S. Hosseini, A. Badri, and M. Parvania, "The plug-in electric vehicles for power system applications: The vehicle to grid (V2G) concept," in *IEEE International Energy Conference and Exhibition, (ENERGYCON), Florence, Italy*, 2012, pp. 1101–1106.

[139] S. S. Hosseini, A. Badri, and M. Parvania, "A survey on mobile energy storage systems (MESS): Applications, challenges and solutions," *Renew. Sustain. Energy Rev.*, vol. 40, pp. 161–170, 2014.

[140] E. Talebizadeh, M. Rashidinejad, and A. Abdollahi, "Evaluation of plug-in electric vehicles impact on cost-based unit commitment," *J. Power Sources*, vol. 248, pp. 545–552, 2014.

[141] J. Taylor, A. Maitra, M. Alexander, D. Brooks, and M. Duvall, "Evaluation of the impact of plug-in electric vehicle loading on distribution system operations," in *IEEE Power and Energy Society General Meeting, PES '09, Calgary, AB, Canada*, 2009.

[142] M. D. Galus and G. Andersson, "Demand Management of Grid Connected Plug-In

Hybrid Electric Vehicles (PHEV)," in *IEEE Energy 2030 Conference, Atlanta, GA, USA*, 2008, pp. 1–8.

[143] R. C. Green, L. Wang, and M. Alam, "The impact of plug-in hybrid electric vehicles on distribution networks: A review and outlook," *Renew. Sustain. Energy Rev.*, vol. 15, no. 1, pp. 544–553, 2011.

[144] R. A. Verzijlbergh, M. O. W. Grond, Z. Lukszo, J. G. Slootweg, and M. D. Ilic, "Network impacts and cost savings of controlled EV charging," *IEEE Trans. Smart Grid*, vol. 3, no. 3, pp. 1203–1212, 2012.

[145] S. S. Williamson and P. D. Ziogas, "Electric Drive Train Efficiency Analysis Based on Varied Energy Storage System Usage for Plug-In Hybrid Electric Vehicle Applications," in *IEEE Power Electronics Specialists Conference, Orlando, FL, USA*, 2007, pp. 1515–1520.

[146] M. Stadler *et al.*, "Optimal Planning and Operation of Smart Grids with Electric Vehicle Interconnection," *J. Energy Eng. Am. Soc. Civ. Eng. (ASCE), Spec. Issue Challenges Oppor. 21st century energy Infrastruct.*, p. 26, 2012.

[147] S. Acha, T. C. Green, and N. Shah, "Effects of optimised plug-in hybrid vehicle charging strategies on electric distribution network losses," in *IEEE PES Transmission and Distribution Conference and Exposition: Smart Solutions for a Changing World, New Orleans, LA, USA*, 2010, pp. 1–6.

[148] S. Acha, T. C. Green, and N. Shah, "Optimal charging strategies of electric vehicles in the UK power market," in *IEEE PES: Innovative Smart Grid Technologies Conference (ISGT), Anaheim, CA, USA*, 2011, pp. 1–8.

[149] Z. Wang and S. Wang, "Grid power peak shaving and valley filling using vehicle-to-grid systems," *IEEE Trans. Power Deliv.*, vol. 28, no. 3, pp. 1822–1829, 2013.

[150] C. Pang, P. Dutta, and M. Kezunovic, "BEVs/PHEVs as dispersed energy storage for V2B uses in the smart grid," *IEEE Trans. Smart Grid*, vol. 3, no. 1, pp. 473–482, 2012.

[151] C. Pang, M. Kezunovic, and M. Ehsani, "Demand side management by using electric vehicles as Distributed Energy Resources," in *IEEE International Electric Vehicle Conference (IEVC), Greenville, SC, USA*, 2012, pp. 1–7.

[152] O. C. Onar, J. Kobayashi, D. C. Erb, and A. Khaligh, "A bidirectional high-power-quality grid interface with a novel bidirectional noninverted buck-boost converter for PHEVs," *IEEE Trans. Veh. Technol.*, vol. 61, no. 5, pp. 2018–2032, 2012.

[153] U. K. Madawala and D. J. Thrimawithana, "A bidirectional inductive power interface for electric vehicles in V2G systems," *IEEE Trans. Ind. Electron.*, vol. 58, no. 10, pp. 4789–4796, 2011.

[154] A. H. Hajimiragha, C. a. Cañizares, M. W. Fowler, S. Moazeni, and A. Elkamel, "A robust optimization approach for planning the transition to plug-in hybrid electric vehicles," *IEEE Trans. Power Syst.*, vol. 26, no. 4, pp. 2264–2274, 2011.

[155] Y. Mu, J. Wu, N. Jenkins, H. Jia, and C. Wang, "A Spatial-Temporal model for grid impact analysis of plug-in electric vehicles," *Appl. Energy*, vol. 114, pp. 456–465, 2014.

[156] M. Tabari and A. Yazdani, "A mathmatical model for stability analysis of a DC Distribution System for Power System Integration of Plug-In Hybrid Electric Vehicles,"

IEEE Trans. Veh. Technol., vol. 64, no. 5, pp. 1–5, 2013.

[157] P. M. R. Almeida, F. J. Soares, and J. a. P. Lopes, "Electric vehicles contribution for frequency control with inertial emulation," *Electr. Power Syst. Res.*, vol. 127, pp. 141–150, 2015.

[158] J. Zhong *et al.*, "Coordinated control for large-scale EV charging facilities and energy storage devices participating in frequency regulation," *Appl. Energy*, vol. 123, pp. 253–262, 2014.

[159] H. Liu, Z. Hu, Y. Song, and J. Lin, "Decentralized vehicle-to-grid control for primary frequency regulation considering charging demands," *IEEE Trans. Power Syst.*, vol. 28, no. 3, pp. 3480–3489, 2013.

[160] F. Kennel, D. Görges, and S. Liu, "Energy Management for Smart Grids With Electric Vehicles Based on Hierarchical MPC," *IEEE Trans. Ind. informatics*, vol. 9, no. 3, pp. 1528–1537, 2013.

[161] D. Sbordone, I. Bertini, B. Di Pietra, M. C. Falvo, A. Genovese, and L. Martirano, "EV fast charging stations and energy storage technologies: A real implementation in the smart micro grid paradigm," *Electr. Power Syst. Res.*, vol. 120, pp. 96–108, 2015.

[162] O. Veneri, C. Capasso, and D. Iannuzzi, "Experimental evaluation of DC charging architecture for fully-electrified low-power two-wheeler," *Appl. Energy*, vol. 162, pp. 1428–1438, 2016.

[163] C. Capasso and O. Veneri, "Experimental study of a DC charging station for full electric and plug in hybrid vehicles," *Appl. Energy*, vol. 152, pp. 131–142, 2015.

[164] J. a. Peças Lopes, S. a. Polenz, C. L. Moreira, and R. Cherkaoui, "Identification of control and management strategies for LV unbalanced microgrids with plugged-in electric vehicles," *Electr. Power Syst. Res.*, vol. 80, no. 8, pp. 898–906, 2010.

[165] Divya K. C, Jacob Østergaard, Esben Larsen, Claus Kern, T. Wittmann, and W. Michael, "Integration of electric drive vehicles in the Danish electricity network with high wind power penetration," *Eur. Trans. Electr. Power*, vol. 20, no. 2, pp. 1–6, 2009.

[166] J. a P. Lopes, F. J. Soares, and P. M. R. Almeida, "Integration of Electric Vehicles in the Electric Power System," *Proc. IEEE*, vol. 99, no. 1, 2010.

[167] D. Dallinger, S. Gerda, and M. Wietschel, "Integration of intermittent renewable power supply using grid-connected vehicles - A 2030 case study for California and Germany," *Appl. Energy*, vol. 104, pp. 666–682, 2013.

[168] A. Nagarajan and W. Shireen, "Integration of plug-in hybrid electric vehicles (PHEV) with grid connected residential photovoltaic energy systems," *Cent. Eur. J. Eng.*, vol. 3, no. 2, pp. 233–242, 2013.

[169] K. Valentine, W. G. Temple, and K. M. Zhang, "Intelligent electric vehicle charging: Rethinking the valley-fill," *J. Power Sources*, vol. 196, no. 24, pp. 10717–10726, 2011.

[170] C. Chen and S. Duan, "Microgrid economic operation considering plug-in hybrid electric vehicles integration," *J. Mod. Power Syst. Clean Energy*, vol. 3, no. 2, pp. 221–231, 2015.

[171] J. Traube *et al.*, "Mitigation of solar irradiance intermittency in photovoltaic power

systems with integrated electric-vehicle charging functionality," *IEEE Trans. Power Electron.*, vol. 28, no. 6, pp. 3058–3067, 2013.

[172] M. Ghofrani, A. Arabali, and M. Ghayekhloo, "Optimal charging/discharging of grid-enabled electric vehicles for predictability enhancement of PV generation," *Electr. Power Syst. Res.*, vol. 117, pp. 134–142, 2014.

[173] S. Jung, H. Lee, C. S. Song, J. H. Han, W. K. Han, and G. Jang, "Optimal operation plan of the online electric vehicle system through establishment of a dc distribution system," *IEEE Trans. Power Electron.*, vol. 28, no. 12, pp. 5878–5889, 2013.

[174] C. H. Dharmakeerthi, N. Mithulananthan, and T. K. Saha, "Impact of electric vehicle fast charging on power system voltage stability," *Electr. Power Energy Syst.*, vol. 57, pp. 241–249, 2014.

[175] H. Xu, S. Miao, C. Zhang, and D. Shi, "Optimal placement of charging infrastructures for large-scale integration of pure electric vehicles into grid," *Electr. Power Energy Syst.*, vol. 53, no. 1, pp. 159–165, 2013.

[176] J. M. Foster and M. C. Caramanis, "Optimal power market participation of plug-in electric vehicles pooled by distribution feeder," *IEEE Trans. Power Syst.*, vol. 28, no. 3, pp. 2065–2076, 2013.

[177] C. Jin, X. Sheng, and P. Ghosh, "Optimized Electric Vehicle Charging With Intermittent Renewable Energy Sources," *IEEE J. Sel. Top. Signal Process.*, vol. 8, no. 6, pp. 1063–1072, 2014.

[178] F. Sanchez-Sutil, J. C. Hernández, and C. Tobajas, "Overview of electrical protection requirements for integration of a smart DC node with bidirectional electric vehicle charging stations into existing AC and DC railway grids," *Electr. Power Syst. Res.*, vol. 122, pp. 104–118, 2015.

[179] J. M. Foster, G. Trevino, M. Kuss, and M. C. Caramanis, "Plug-in electric vehicle and voltage support for distributed solar: Theory and application," *IEEE Syst. J.*, vol. 7, no. 4, pp. 881–888, 2013.

[180] Z. Liu, D. Wang, H. Jia, and N. Djilali, "Power system operation risk analysis considering charging load self-management of plug-in hybrid electric vehicles," *Appl. Energy*, vol. 136, pp. 662–670, 2014.

[181] J. G. Vlachogiannis, "Probabilistic constrained load flow considering integration of wind power generation and electric vehicles," *IEEE Trans. Power Syst.*, vol. 24, no. 4, pp. 1808–1817, 2009.

[182] M. S. ElNozahy, T. K. Abdel-Galil, and M. M. a. Salama, "Probabilistic ESS sizing and scheduling for improved integration of PHEVs and PV systems in residential distribution systems," *Electr. Power Syst. Res.*, vol. 125, pp. 55–66, 2015.

[183] A. O'Connell, D. Flynn, and A. Keane, "Rolling Multi-Period Optimization to Control Electric Vehicle Charging in Distribution Networks," *IEEE Trans. Power Syst.*, vol. 29, no. 1, pp. 340–348, 2014.

[184] D. Jayaweera, "Security Enhancement With Nodal Criticality-Based Integration of Strategic Micro Grids," *IEEE Trans. Power Syst.*, vol. 30, no. 1, pp. 337–345, 2015.

[185] C. T. Li, C. Ahn, H. Peng, and J. Sun, "Synergistic control of plug-in vehicle charging

and wind power scheduling," *IEEE Trans. Power Syst.*, vol. 28, no. 2, pp. 1113–1121, 2013.

[186] B. Tarroja, J. D. Eichman, L. Zhang, T. M. Brown, and S. Samuelsen, "The effectiveness of plug-in hybrid electric vehicles and renewable power in support of holistic environmental goals: Part 1 - Evaluation of aggregate energy and greenhouse gas performance," *J. Power Sources*, vol. 257, pp. 461–470, 2014.

[187] P. Mitra and G. K. Venayagamoorthy, "Wide area control for improving stability of a power system with plug-in electric vehicles," *IET Gener. Transm. Distrib.*, vol. 4, no. 10, p. 1151, 2010.

[188] F. Marra, C. Traholt, and E. Larsen, "Planning future electric vehicle central charging stations connected to low-voltage distribution networks," in *3rd IEEE International Symposium on Power Electronics for Distributed Generation Systems conference Proceedings, PEDG, Aalborg, Denmark*, 2012, no. 81216, pp. 636–641.

[189] P. Reid, C. Mittelstadt, and T. Faber, "Electric Vehicle Conductive Charge Couplers," in *IEEE 60th Conference on Electrical Contacts (Holm), New Orleans, LA, USA*, 2014, pp. 776–790.

[190] M. Duvall *et al.*, "Transportation Electrification: A Technology Overview," 2011.

[191] P. F. Ribeiro, B. K. Johnson, M. L. Crow, A. Arsoy, and Y. Liu, "Energy Storage Systems for Advanced Power Applications," *Proc. IEEE*, vol. 89, no. 12, pp. 1744–1756, 2001.

[192] H. Matsuo, W. Lin, F. Kurokawa, T. Shigemizu, and N. Watanabe, "Characteristics of the Multiple-Input DC–DC Converter," *IEEE Trans. Ind. Electron.*, vol. 51, no. 3, pp. 625–631, 2004.

[193] I.-D. Kim, S.-H. Paeng, J.-W. Ahn, E.-C. Nho, and J.-S. Ko, "New Bidirectional ZVS PWM Sepic/Zeta DC-DC Converter," in *IEEE International Symposium on Industrial Electronics (ISIE), Vigo, Spain*, 2007, vol. 9, no. 3, pp. 555–560.

[194] P. Jose and N. Mohan, "A novel bidirectional DC-DC converter with ZVS and interleaving for dual voltage systems in automobiles," in *The IEEE Industry Applications Conference. 37th IAS Annual Meeting, Pittsburgh, PA, USA, USA*, 2002, vol. 2, pp. 1311–1314.

[195] G. Chen, D. Xu, and Y. Lee, "A novel fully zero-voltage-switching phase-shift bidirectional DC-DC converter," in *Sixteenth Annual IEEE Applied Power Electronics Conference and Exposition (APEC), Anaheim, CA, USA*, 2001, vol. 2, pp. 974–979.

[196] D. P. Urciuoli and C. W. Tipton, "Development of a 90 kW Bi-Directional DC-DC Converter for Power Dense Applications," in *Twenty-First Annual IEEE Applied Power Electronics Conference and Exposition (APEC '06), Dallas, TX, USA*, 2006, pp. 1375–1378.

[197] F. Caricchi, F. Crescimbini, G. Noia, and D. Pirolo, "Experimental study of a bidirectional DC-DC converter for the DC link voltage control and the regenerative braking in PM motor drives devoted to electrical vehicles," in *Ninth Annual IEEE Applied Power Electronics Conference and Exposition, APEC '94 Conference Proceedings, Orlando, FL, USA, USA*, 1994, pp. 381–386.

[198] K. ASANO, Y. INAGUMA, H. OHTANI, E. SATO, M. OKAMURA, and S. SASAKI,

"High Performance Motor Drive Technologies for Hybrid Vehicles," in *Power Conversion Conference - Nagoya, PCC '07, Nagoya, Japan*, 2007, pp. 1584–1589.

[199] S. Aso, M. Kizaki, and Y. Nonobe, "Development of Fuel Cell Hybrid Vehicles in TOYOTA," in *Power Conversion Conference - Nagoya, 2007. PCC '07, Nagoya, Japan*, 2007, pp. 1606–1611.

[200] X. Huang, X. Wang, T. Nergaard, J. J. Lai, X. Xu, and L. Zhu, "Parasitic Ringing and Design Issues of Digitally Controlled High Power Interleaved Boost Converters," *IEEE Trans. Power Electron.*, vol. 19, no. 5, pp. 1341–1352, 2004.

[201] N. Mohan, T. M. Undeland, and W. P. Robbins, *Power Electronics: Converters, Applications, and Design*, Thired edi. John Wiley and Sons, INC., 2003.

[202] M. H. Rashid, *Power Electronics: circuits, devices and applications*, Third edit. New Jersey: Prentice Hall, 2004.

[203] W. Chen, G. Wang, and X. Zhu, "A family of bidirectional DC/DC converters suitable for asymmetrical power flow requirement," in *IEEE Energy Conversion Congress and Exposition, Denver, CO, USA*, 2013, pp. 4878–4881.

[204] H. Xiao and S. Xie, "A ZVS Bidirectional DC–DC Converter With Phase-Shift Plus PWM Control Scheme," *IEEE Trans. Power Electron.*, vol. 23, no. 2, pp. 813–823, Mar. 2008.

[205] R. W. A. A. De Doncker, D. M. Divan, and M. H. Kheraluwala, "A Three-phase Soft-Switched High-Power-Density dc /dc Converter for High-Power Applications," *IEEE Trans. Ind. Appl.*, vol. 27, no. 1, pp. 63–73, 1991.

[206] H. Tao, A. Kotsopoulos, J. L. Duarte, and M. A. M. Hendrix, "Family of multiport bidirectional DC – DC converters," *IEE Proc. - Electr. Power Appl.*, vol. 153, no. 3, pp. 451–458, 2006.

[207] Z. Zhang, Z. Ouyang, O. C. Thomsen, and M. A. E. Andersen, "Analysis and Design of a Bidirectional Isolated DC-DC Converter for Fuel Cells and Super- Capacitors Hybrid System," *IEEE Trans. Power Electron.*, vol. 27, no. 2, 2012.

[208] S. Dutta and S. Bhattacharya, "Predictive current mode control of single phase dual active bridge DC to DC converter," in *IEEE Energy Conversion Congress and Exposition (ECCE), Denver, CO, USA*, 2013, vol. 8, pp. 5526–5533.

[209] S.-J. Jang, T.-W. Lee, Won-Cbul, and C.-Y. Won, "Bi-directional DC-DC Converter for Fuel Cell Generation System," in *351h Annual IEEE Power Elecrronics Specialisrs Conference, Aachen. Germany*, 2004, pp. 4722–4728.

[210] M. T. Zhang, M. M. Jovanovi, and F. C. Y. Lee, "Design Considerations and Performance Evaluations of Synchronous Rectification in Flyback Converters," *IEEE Trans. Power Electron.*, vol. 13, no. 3, pp. 538–546, 1998.

[211] T. Wu, S. Member, Y. Chang, C. Chang, and J. Yang, "Soft-Switching Boost Converter With a Flyback Snubber for High Power Applications," *IEEE Trans. Power Electron.*, vol. 27, no. 3, pp. 1108–1119, 2012.

[212] D. Segaran, B. P. McGrath, and D. G. Holmes, "Adaptive dynamic control of a bi-directional DC-DC converter," in *IEEE Energy Conversion Congress and Exposition, Atlanta, GA, USA, USA*, 2010, pp. 1442–1449.

[213] M. Cacciato, F. Caricchi, F. G. Capponi, and E. Santini, "A critical evaluation and design of bi-directional DC/DC converters for super-capacitors interfacing in fuel cell applications," in *IEEE Industry Applications Conference, 39th IAS Annual Meeting, Seattle, WA, USA, USA*, 2004, vol. 2, pp. 1127–1133.

[214] F. Zhang, L. Xiao, and Y. Yan, "Bi-directional Forward-Flyback DC-DC Converter," in *35th Annual IEEE Power Electronics Specialisls Conference, Aachen, Germany, Germany*, 2004, pp. 4058–4061.

[215] M. Jain, M. Daniele, P. K. Jain, and S. Member, "A Bidirectional DC – DC Converter Topology for Low Power Application," *IEEE Trans. Power Electron.*, vol. 15, no. 4, pp. 595–606, 2000.

[216] A. I. Pressman, K. Billings, and T. Morey, *Switching Power Supply Design*, Third edit. McGraw-Hill Companies, 2009.

[217] R. García-gil, J. M. Espí, E. J. Dede, and E. Sanchis-kilders, "A Bidirectional and Isolated Three-Phase Rectifier With Soft-Switching Operation," *IEEE Trans. Ind. Electron.*, vol. 52, no. 3, pp. 765–773, 2005.

[218] T. Mishima and E. Hiraki, "ZVS-SR Bidirectional DC-DC Converter for Supercapacitor-Applied Automotive Electric Energy Storage Systems," in *IEEE Vehicle Power and Propulsion Conference, Chicago, IL, USA*, 2005, vol. 9, pp. 731–736.

[219] B. Singh, B. N. Singh, A. Chandra, K. Al-haddad, A. Pandey, and D. P. Kothari, "A Review of Single-Phase Improved Power Quality AC – DC Converters," *IEEE Trans. Ind. Electron.*, vol. 50, no. 5, pp. 962–981, 2003.

[220] B. Singh *et al.*, "A Review of Three-Phase Improved Power Quality AC – DC Converters," *IEEE Trans. Ind. Electron.*, vol. 51, no. 3, pp. 641–660, 2004.

[221] D. Segaran, D. G. Holmes, and B. P. McGrath, "Comparative Analysis of Single and Three-phase Dual Active Bridge Bidirectional DC-DC Converters," in *Power Engineering Conference, AUPEC '08. Australasian Universities, Sydney, NSW, Australia*, 2008, vol. 1, pp. 1–6.

[222] J. Xue, F. Wang, D. Boroyevich, and Z. Shen, "Single-phase vs. three-phase high density power transformers," in *IEEE Energy Conversion Congress and Exposition (ECCE), Atlanta, GA, USA, USA*, 2010, pp. 4368–4375.

[223] J. A. F. M. Pavlovsky, S.W.H. de Haan, "Concept of50kW DC/DC converter based on ZVS, Quasi-ZCS topology and integrated thermal and electromagnetic design," *EPE-Dresden*, pp. 1–9, 2005.

[224] B. Singh *et al.*, "Multi-level Inverter: A Literature Survey on Topologies and Control Strategies," *Int. J. Rev. Comput.*, vol. 10, no. 1, pp. 1–16, 2012.

[225] A. H. Bhat and P. Agarwal, "Three-phase, power quality improvement ac/dc converters," *Electr. Power Syst. Res.*, vol. 78, no. 2, pp. 276–289, Feb. 2008.

[226] J. T. Economou, A. Tsourdos, B. A. White, and P. C. K. Luk, "Takagi-Sugeno model synthesis of a quasi-linear multiwheeled mobile robot," in *International Conference on Intelligent Robots and Systems, IEEE/RSJ*, 2003, pp. 805–818.

[227] F. Krismer and J. W. Kolar, "Accurate Small-Signal Model for the Digital Control of an Automotive Bidirectional Dual Active Bridge," *IEEE Trans. Power Electron.*, vol. 24,

no. 12, pp. 2756–2768, 2009.

[228] Bimal K. Bose, *Modern power electronics and AC drives*, First edit. Prentice Hall PTR, 2002.

[229] T. Lipo and D. G. Holmes, *Pulse Width Modulation for Power Converters*. A John Wiley & Sons, 2003.

[230] N. S. Ting, Y. Yasa, I. Aksoy, and Y. Sahin, "Comparison of SVPWM, SPWM and HCC control techniques in power control of PMSG used in wind turbine systems," in *International Aegean Conference on Electrical Machines & Power Electronics (ACEMP), International Conference on Optimization of Electrical & Electronic Equipment (OPTIM) & International Symposium on Advanced Electromechanical Motion Systems, Side, Turkey*, 2015, pp. 69–74.

[231] J. H. Seo, C. H. Choi, and D. S. Hyun, "A New Simplified Space – Vector PWM Method for Three-Level Inverters," *IEEE Trans. Power Electron.*, vol. 16, no. 4, pp. 545–550, 2001.

[232] Ó. López, J. Álvarez, J. Doval-Gandoy, and F. Freijedo, "Multilevel multiphase space vector PWM algorithm applied to three-phase converters," *IEEE Trans. Ind. Electron.*, vol. 55, no. 5, pp. 3290–3295, 2008.

[233] Y. Y. Tzou and H. J. Hsu, "FPGA realization of space-vector PWM control IC for three-phase PWM inverters," *IEEE Trans. Power Electron.*, vol. 12, no. 6, pp. 953–963, 1997.

[234] C. B. Jacobina, A. M. N. Lima, E. R. C. da Silva, R. N. C. Alves, and P. F. Seixas, "Digital scalar pulse-width modulation: A simple approach to introduce non-sinusoidal modulating waveforms," *IEEE Trans. Power Electron.*, vol. 16, no. 3, pp. 351–359, 2001.

[235] Q. Zeng and L. Chang, "An advanced SVPWM-based predictive current controller for three-phase inverters in distributed generation systems," *IEEE Trans. Ind. Electron.*, vol. 55, no. 3, pp. 1235–1246, 2008.

[236] A. R. Beig, G. Narayanan, and V. T. Ranganathan, "Modified SVPWM algorithm for three level VSI with synchronized and symmetrical waveforms," *IEEE Trans. Ind. Electron.*, vol. 54, no. 1, pp. 486–494, 2007.

[237] A. K. Gupta and A. M. Khambadkone, "A general space vector PWM algorithm for multilevel inverters, including operation in overmodulation range," *IEEE Trans. Power Electron.*, vol. 22, no. 2, pp. 517–526, 2007.

[238] H. M. Ryu, J. H. Kim, and S. K. Sul, "Analysis of multiphase space vector pulse-width modulation based on multiple d-q spaces concept," *IEEE Trans. Power Electron.*, vol. 20, no. 6, pp. 1364–1371, 2005.

[239] J. Sabarad and G. H. Kulkarni, "Comparative analysis of SVPWM and SPWM techniques for multilevel inverter," in *International Conference on Power and Advanced Control Engineering (ICPACE), Bangalore, India*, 2015, pp. 232–237.

[240] G. Waltrich, J. L. Duarte, and M. a. M. Hendrix, "Multiport converters for fast chargers of electrical vehicles - Focus on high-frequency coaxial transformers," in *The International Power Electronics Conference (IPEC), Sapporo, Japan*, 2010, pp. 3151–3157.

[241] L. Heinemann, “An Actively Cooled High Power, High Frequency Transformer with High Insulation Capability,” in *Seventeenth Annual IEEE Applied Power Electronics Conference and Exposition, APEC, Dallas, TX, USA*, 2002, pp. 352–357.

[242] A. M. Hava, R. J. Kerkman, and T. A. Lipo, “Carrier-Based PWM-VSI Overmodulation,” *IEEE Trans. Power Electron.*, vol. 13, no. 4, pp. 674–689, 1998.

[243] S. Fukuda and T. Yoda, “A Novel Current-Tracking Method for Active Filters Based on a Sinusoidal Internal Model,” *IEEE Trans. Ind. Appl.*, vol. 37, no. 3, pp. 888–895, 2001.

[244] J. F. SULTANI, “Modelling, Design and Implementation of D-Q Control in ingle-Phase Grid-Connected Inverters for Photovoltaic SSystems used in Domestic Dwellings.,” De Montfort University, 2013.

[245] G. H. Bode and D. G. Holmes, “Implementation of Three Level Hysteresis Current Control for a Single Phase Voltage Source Inverter,” in *IEEE 31st Annual Power Electronics Specialists Conference, PESC 00, Galway, Ireland, Ireland*, 2000, pp. 33–38.

[246] T. Grote, F. Schafmeister, H. Figge, N. Fröhleke, P. Ide, and J. Böcker, “Adaptive Digital Slope Compensation for Peak Current Mode Control,” in *IEEE Energy Conversion Congress and Exposition, ECCE, San Jose, CA, USA*, 2009, pp. 3523–3529.

[247] M. Aimé, G. Gateau, and T. A. Meynard, “Implementation of a Peak-Current-Control Algorithm Within a Field-Programmable Gate Array,” *IEEE Trans. Power Electron.*, vol. 54, no. 1, pp. 406–418, 2007.

[248] G. Xiaoqiang, Z. Qinglin, and W. Weiyang, “A Single-Phase Grid-Connected Inverter System With Zero Steady-State Error,” in *5th International Power Electronics and Motion Control Conference (CES/IEEE), Shanghai, China*, 2006, pp. 1–5.

[249] A. G. Yepes, “Digital Resonant Current Controllers for Voltage Source Converters,” University of Vigo, 2011.

[250] P. Mattavelli, “Synchronous-frame harmonic control for high-performance AC power supplies,” *IEEE Trans. Ind. Appl.*, vol. 37, no. 3, pp. 864–872, 2001.

[251] P. C. Krause, O. Wasynczuk, and S. D. Sudhoff, *Analysis of Electric Machinery and Drive Systems*, Second edi. A John Wiley & Sons, 2002.

[252] A. Maknouninejad, M. G. Simoes, and M. Zolot, “Single phase and three phase P+Resonant based grid connected inverters with reactive power and harmonic compensation capabilities,” in *IEEE International on Electric Machines and Drives Conference, (IEMDC ’09), Miami, FL, USA*, 2009, pp. 385–391.

[253] D. N. Zmood and D. G. Holmes, “Stationary Frame Current Regulation of PWM Inverters With Zero Steady-State Error,” *IEEE Trans. Power Electron.*, vol. 18, no. 3, pp. 814–822, 2003.

[254] D. N. Zmood, D. G. Holmes, and G. H. Bode, “Frequency-Domain Analysis of Three-Phase Linear Current Regulators,” *IEEE Trans. Ind. Appl.*, vol. 37, no. 2, pp. 601–610, 2001.

[255] L. Zhang, W. Kang, L. Jia, M. Zhao, and R. Xu, “Control of Bidirectional Current Source SVPWM Converter in the Power Accumulator Battery Testing System,” in *Asia-Pacific Power and Energy Engineering Conference (APPEEC), Chengdu, China*, 2010,

pp. 1–4.

[256] J. J. W. D. S. Grainger., *Power System Analysis*. Printed i1' Singapore: McGraw-Hill, 1994.

[257] Q. Zhong and G. Weiss, "Synchronverters : Inverters That Mimic Synchronous Generators," *IEEE Trans. Ind. Electron.*, vol. 58, no. 4, pp. 1259–1267, 2011.

[258] C. Schauder and H. Mehta, "Vector analysis and control of advanced static VAR compensators," *IEE Proc. C Gener. Transm. Distrib.*, vol. 140, no. 4, p. 299, 1993.

[259] R. Teodorescu, M. Liserre, and P. Rodrıguez, *Grid Converters for Photovoltaic and Wind Power Systems*, First edit. John Wiley & Sons, 2011.

[260] G. Kohlrusz and D. Fodor, "Comparison of Scalar and Vector Control Strategies of Induction Motors," *Hungarian J. Ind. Chem. Veszprém*, vol. 39, no. 2, pp. 265–270, 2011.

[261] W. Chang and K. Yeh, "Design of D-STATCOM for fast load compensation of unbalanced distribution systems," in *4th IEEE International Conference on Power Electronics and Drive Systems, (PEDS / IEEE), Denpasar, Indonesia, Indonesia*, 2001, vol. 2, pp. 801–806.

[262] A. B. ARSOY, Y. LIU, P. F. R. BEIRO, and F. . WANG, "Static-Synchronous Compensators and Superconducting Magnetic Energy Storage Systems in Controling Power System Dynamic," *IEEE Ind. Appl.*, pp. 21–28, 2003.

[263] a. Arulampalam, J. B. Ekanayake, and N. Jenkins, "Application study of a STATCOM with energy storage," *IEE Proc. - Gener. Transm. Distrib.*, vol. 150, no. 3, pp. 373–384, 2003.

[264] A. Jain, K. Joshi, A. Behal, and N. Mohan, "Voltage Regulation With STATCOMs: Modeling, Control and Results," *IEEE Trans. Power Deliv.*, vol. 21, no. 2, pp. 726–735, 2006.

[265] Z. Yang, C. Shen, L. Zhang, M. L. Crow, and S. Atcitty, "Integration of a StatCom and Battery Energy Storage," *IEEE Trans. Power Syst.*, vol. 16, no. 2, pp. 254–260, 2001.

[266] R. Majumder, G. Ledwich, A. Ghosh, S. Chakrabarti, and F. Zare, "Droop Control of Converter-Interfaced Microsources in Rural Distributed Generation," *IEEE Trans. Power Deliv.*, vol. 25, no. 4, pp. 2768–2778, 2010.

[267] J.-J. Seo, H.-J. Lee, W.-W. Jung, and D.-J. Won, "Voltage control method using modified voltage droop control in LV distribution system," in *Transmission & Distribution Conference & Exposition: Asia and Pacific, Seoul, South Korea*, 2009, pp. 1–4.

[268] R. R. Majumder, B. Chaudhuri, A. Ghosh, R. R. Majumder, G. Ledwich, and F. Zare, "Improvement of Stability and Load Sharing in an Autonomous Microgrid Using Supplementary Droop Control Loop," *IEEE Trans. Power Syst.*, vol. 25, no. 2, pp. 796–808, May 2010.

[269] K. De Brabandere, B. Bolsens, J. Van den Keybus, AchimWoyte, J. Driesen, and R. Belmans, "A voltage and frequency droop control method for parallel inverters," *IEEE Trans. Power Electron.*, vol. 22, no. 4, pp. 1107–1115, 2007.

[270] B. Gao, G. K. Morison, and P. Kundur, "Voltage Stability Evaluation Using Modal Analysis," *Transsctions power Syst.*, vol. 7, no. 4, pp. 1529–1542, Nov. 1992.

[271] P. Tschirhart, A. Sussman, and E. H. Abed, "Using participation factors to improve the consistency and accuracy of Prony analysis for voltage stability monitoring applications," in *IEEE Conference on Innovative Smart Grid Technologies (ISGT), Washington, DC, USA*, 2014, pp. 1–5.

[272] H.Hedayati, S.A.Nabaviniaki, and A.Akbarimajd, "A new method for placement of DG units in distribution networks," in *IEEE Conference on Power Systems Conference and Exposition (PSCE '06), Atlanta, GA, USA*, 2006.

[273] C. Wang and M. H. Nehrir, "Analytical approaches for optimal placement of distributed generation sources in power systems," *IEEE Trans. Power Syst.*, vol. 19, no. 4, pp. 2068–2076, 2004.

[274] C. L. T. Borges and D. M. Falcão, "Optimal distributed generation allocation for reliability, losses, and voltage improvement," *Electr. Power Energy Syst.*, vol. 28, no. 6, pp. 413–420, 2006.

[275] G. Celli, E. Ghiani, S. Mocci, and F. Pilo, "A multiobjective evolutionary algorithm for the sizing and siting of distributed generation," *IEEE Trans. Power Syst.*, vol. 20, no. 2, pp. 750–757, 2005.

[276] R. K. Singh and S. K. Goswami, "Optimum allocation of distributed generations based on nodal pricing for profit, loss reduction, and voltage improvement including voltage rise issue," *Electr. Power Energy Syst.*, vol. 32, no. 6, pp. 637–644, 2010.

[277] A. Keane and M. O'Malley, "Optimal allocation of embedded generation on distribution networks," *IEEE Trans. Power Syst.*, vol. 20, no. 3, pp. 1640–1646, 2005.

[278] M. A. Kashem, A. D. T. Le, M. Negnevitsky, and G. Ledwich, "Distributed generation for minimization of power losses in distribution systems," in *2006 IEEE Power Engineering Society General Meeting, Montreal, Que., Canada*, 2006.

[279] T. Ackermann, G. Andersson, and L. Söder, "Distributed generation: A definition," *Electr. Power Syst. Res.*, vol. 57, no. 3, pp. 195–204, 2001.

[280] J. D. Glover, M. S. Arma, and T. J. Overbye, *Power System Analysis and Design*, Fifth edit. Thomson, 2011.

[281] R. D. Zimmerman, C. E. Murillo-Sanchez, and R. J. Thomas, "Matpower: Steady- State Operations, Planning and Analysis Tools for Power Systems Research and Education," *IEEE Trans. Power Syst.*, vol. 26, no. 1, pp. 12–19, 2011.

[282] T. J. E. Miller, *Reactive power control in electric systems*, First edit. John Wiley & Sons, 1982.

[283] H. Saadat, *Power System Analysis*, First edit. WCB McGraw-Hill, 1999.

[284] C. S. Indulkar, B. Viswanathan, and S. S. Venkata, "Maximum power transfer limited by voltage stability in series and shunt compensated schemes for A.C. transmission systems," *IEEE Trans. Power Deliv.*, vol. 4, no. 2, pp. 1246–1252, 1989.

[285] S. Papathanassiou, H. Nikos, and S. Kai, "A benchmark low voltage microgrid network," in *Proceedings of the CIGRE symposium: power systems with dispersed*

generation: technologies, impacts on development, operation and performances, Athens, Greece, 2005, no. April, pp. 1–8.

[286] . Weather Undeground, "Historical Weather," 2016. [Online]. Available: https://www.wunderground.com/history. [Accessed: 25-Dec-2016].

[287] F. A. Mohamed and H. N. Koivo, "Multiobjective optimization using modified game theory for online management of microgrid," *Eouropean Trans. Electr. Power*, no. 21, pp. 839–854, 2010.

[288] S. Mohammadi, B. Mozafari, S. Solimani, and T. Niknam, "An Adaptive Modified Firefly Optimisation Algorithm based on Hong's Point Estimate Method to optimal operation management in a microgrid with consideration of uncertainties," *Energy*, vol. 51, pp. 339–348, 2013.

[289] B. Zhao, Y. Shi, X. Dong, W. Luan, and J. Bornemann, "Short-term operation scheduling in renewable-powered microgrids: A duality-based approach," *IEEE Trans. Sustain. Energy*, vol. 5, no. 1, pp. 209–217, 2014.

[290] B. Zhao, X. Zhang, J. Chen, C. Wang, and L. Guo, "Operation optimization of standalone microgrids considering lifetime characteristics of battery energy storage system," *IEEE Trans. Sustain. Energy*, vol. 4, no. 4, pp. 934–943, 2013.

[291] M. H. Moradi, M. Abedini, and S. M. Hosseinian, "Improving operation constraints of microgrid using PHEVs and renewable energy sources," *Renew. Energy*, vol. 83, pp. 543–552, 2015.

[292] Weather Underground, "Weather History for Baghdad - July, 2015," 2015. [Online]. Available: https://www.wunderground.com/history/airport/KQTZ/2015/7/26/DailyHistory.html?req_city=Baghdad&req_state=&req_statename=Iraq&reqdb.zip=00000&reqdb.magic=1&reqdb.wmo=40650o Title. [Accessed: 23-Nov-2016].

[293] F. González-Longatt, "Model of photovoltaic module in Matlab," in *Proceedings in conference 2DO Congreso Iberoamericanode Estudiantes De Ingenieria Electrica, Electronica Y Computacion (II CIBELEC)*, 2005, pp. 1–5.

[294] C.-T. Chiang, T.-S. Chiang, and H.-S. Hunang, "Modeling a Photovltaic Power System by CMAC_GBF," in *3rd World Conference on Phoiovolfoic Enera Conversion, Osaka, Japan*, 2003, pp. 2431–2434.

[295] F. a. Mohamed and H. N. Koivo, "Online Management of MicroGrid with Battery Storage Using Multiobjective Optimization," in *International Conference on Power Engineering, Energy and Electrical Drives, Setubal, Portugal*, 2007, pp. 231–236.

[296] M. Honarmand, A. Zakariazadeh, and S. Jadid, "Integrated scheduling of renewable generation and electric vehicles parking lot in a smart microgrid," *Energy Convers. Manag.*, vol. 86, pp. 745–755, 2014.

[297] Y. M. A. Welaya, M. M. El Gohary, and N. R. Ammar, "A comparison between fuel cells and other alternatives for marine electric power generation," *Int. J. Nav. Archit. Ocean Eng.*, vol. 3, no. 2, pp. 141–149, 2011.

[298] S. Alkaner and P. Zhou, "A comparative study on life cycle analysis of molten carbon fuel cells and diesel engines for marine application," *J. Power Sources*, vol. 158, no. 1, pp. 188–199, 2006.

[299] HILTech Developments group, “The use of Micro Turbine Generators in Hybrid Electric Vehicles,” 2000.

[300] R. K. Agrawal and K. K. Khatri, “Comparison of Technological Options for Distributed Generation-Combined Heat and Power in Rajasthan State of India,” *Hindawi Publ. Corp. J. Energy*, pp. 1–8, 2013.

[301] A. Zakariazadeh, S. Jadid, and P. Siano, “Multi-objective scheduling of electric vehicles in smart distribution system,” *Energy Convers. Manag.*, vol. 79, no. March, pp. 43–53, 2014.

[302] H. Wu, H. Zhuang, W. Zhang, and M. Ding, “Optimal allocation of microgrid considering economic dispatch based on hybrid weighted bilevel planning method and algorithm improvement,” *Electr. Power Energy Syst.*, vol. 75, pp. 28–37, 2016.

[303] H. Liu, Y. Ji, H. Zhuang, and H. Wu, “Multi-objective dynamic economic dispatch of microgrid systems including vehicle-to-grid,” *Energies*, vol. 8, no. 5, pp. 4476–4495, 2015.

[304] T. L. Saaty, “Decision making with the analytic hierarchy process,” *Int. J. Serv. Sci.*, vol. 1, no. 1, p. 83, 2008.

[305] T. Niknam, F. Golestaneh, and A. Malekpour, “Probabilistic energy and operation management of a microgrid containing wind/photovoltaic/fuel cell generation and energy storage devices based on point estimate method and self-adaptive gravitational search algorithm,” *Energy*, vol. 43, no. 1, pp. 427–437, 2012.

[306] Energy Transition Group, “Local Energy: The paradox of simultaneous upscaling and downscaling,” 2016. [Online]. Available: www.energytransitiongroup.com/vision/localenergy.html. [Accessed: 25-Dec-2016].

[307] R. A. Waraich, M. D. Galus, C. Dobler, M. Balmer, G. Andersson, and K. W. Axhausen, “Plug-in hybrid electric vehicles and smart grids: Investigations based on a microsimulation,” *Transp. Res. Part C*, vol. 28, pp. 74–86, 2013.

[308] S. Acha, S. Member, T. C. Green, S. Member, and N. Shah, “IEEE Xplore - Effects of optimised plug-in hybrid vehicle charging strategies on electric distribution network los...,” in *IEEE conferece on Transmission and Distribution Conference and Exposition, New Orleans, LA, USA*, 2010, pp. 1–6.

[309] M. D. Galus *et al.*, “Integrating power systems, transport systems and vehicle technology for electric mobility impact analysis and efficient control,” *IEEE Trans. Smart Grid*, vol. 3, no. 2, pp. 934–949, 2012.

[310] K. Clement, E. Haesen, and J. Driesen, “Coordinated charging of multiple plug-in hybrid electric vehicles in residential distribution grids,” in *IEEE/PES Power Systems Conference and Exposition, (PSCE’09), Seattle, WA, USA*, 2009, pp. 1–7.

[311] H. Liu, Z. Hu, Y. Song, J. Wang, and X. Xie, “Vehicle-to-Grid Control for Supplementary Frequency Regulation Considering Charging Demands,” *IEEE Trans. Power Syst.*, vol. 30, no. 6, pp. 3110–3119, 2015.

[312] H. Turker, A. Radu, S. Bacha, D. Frey, J. Richer, and P. Lebrusq, “Optimal charge control of electric vehicles in parking stations for cost minimization in V2G concept,” in *3rd International Conference on Renewable Energy Research and Applications, (ICRERA ’14), Milwakuee, USA*, 2014, pp. 945–951.

[313] J. Hu, H. Morais, T. Sousa, and M. Lind, "Electric vehicle fleet management in smart grids: A review of services, optimization and control aspects," *Renew. Sustain. Energy Rev.*, vol. 56, pp. 1207–1226, 2016.

[314] W. Yao, J. Zhao, F. Wen, Y. Xue, and G. Ledwich, "A hierarchical decomposition approach for coordinated dispatch of plug-in electric vehicles," *IEEE Trans. Power Syst.*, vol. 28, no. 3, pp. 2768–2778, 2013.

[315] Z. Xu, W. Su, Z. Hu, Y. Song, and H. Zhang, "A hierarchical framework for coordinated charging of plug-in electric vehicles in China," *IEEE Trans. Smart Grid*, vol. 7, no. 1, pp. 428–438, 2016.

[316] J. A. Peças Lopes, F. J. Soares, and P. M. Rocha Almeida, "Identifying management procedures to deal with connection of electric vehicles in the grid," in *PowerTech Conference,, IEEE Bucharest, Bucharest, Romania*, 2009, pp. 1–8.

[317] C. Ahn, C. T. Li, and H. Peng, "Optimal decentralized charging control algorithm for electrified vehicles connected to smart grid," *J. Power Sources*, vol. 196, no. 23, pp. 10369–10379, 2011.

[318] O. Beaude, Y. He, and M. Hennebel, "Introducing decentralized EV charging coordination for the voltage regulation," in *4th IEEE/PES Innovative Smart Grid Technologies Europe, ISGT Europe, Copenhagen, Denmark*, 2013, pp. 1–5.

[319] Sustainable Energy Authority of Ireland, "A Guide to Electric Vehicle Infrastructure," 2012.

[320] R. NeWberry, "United States Reissued Patent," US RE43,619 E, 2012.

[321] C. D. White and K. M. Zhang, "Using vehicle-to-grid technology for frequency regulation and peak-load reduction," *J. Power Sources*, vol. 196, no. 8, pp. 3972–3980, 2011.

[322] V. Musolino and E. Tironi, "A comparison of supercapacitor and high power lithium batteries," in *Electrical Systems for Aircraft, Railway and Ship Propulsion (ESARS), Bologna, Italy*, 2010, pp. 1–6.

[323] J. Larminie and J. Lowry, *Electric Vehicle Technology Explained*, Second edi. A John Wiley & Sons, 2012.

[324] L. Rosario, "Power and energy management of multiple energy storage systems in electric vehicles," Cranfield University, DCMT Shrivenham, 2007.

[325] J. Van Mierlo, P. Van den Bossche, and G. Maggetto, "Models of energy sources for EV and HEV: Fuel cells, batteries, ultracapacitors, flywheels and engine-generators," *J. Power Sources*, vol. 128, no. 1, pp. 76–89, 2004.

[326] J. T. Economou, "Intelligent Energy Source SoC Modelling for a Hybrid Electric Vehicle," in *Proceedings of the IEEE International Symposium on Industrial Electronics (ISIE), Dubrovnik, Croatia*, 2005, vol. 1, pp. 325–330.

[327] C. C. Chan and K. T. Chau, *Modern Electric Vehicle Technology*, First edit. Oxford university press, 2001.

[328] J. M. Miller, *Propulsion Systems for Hybrid Vehicles, 2nd Edition*, Second edi. The Institution of Engineering and Technology, London, United Kingdom, 2010.

[329] R. L. Spyker and R. M. Nelms, “Double Layer Capacitor/DC-DC Converter System Applied to Constant Power Loads,” in *Proceedings of the 31st Intersociety on Energy Conversion Engineering Conference (IECEC 96), Washington, DC, USA*, 1996, pp. 255–259.

[330] M. G. SIMÕES, B. BLUNIER, and A. MIRAOUI, “Fuzzy-Based Energy Management Control,” *IEEE Ind. Applcations Mag.*, pp. 41–49, 2014.

[331] Isidor Buchmann, “Battery University,” *Cadex Electronics Inc.*, 2016. [Online]. Available: http://batteryuniversity.com. [Accessed: 25-Dec-2015].

[332] Barrie Lawson, “Battery Performance Characteristics,” *Woodbank Communications Ltd,* 2012. [Online]. Available: http://www.mpoweruk.com/performance.htm. [Accessed: 20-Feb-2017].

[333] P. Suntharalingam, J. T. Economou, and K. Knowles, “Kinetic energy storage using a dual-braking system for an unmanned parallel hybrid electric vehicle,” *Proc. Inst. Mech. Eng. Part D J. Automob. Eng.*, 2016.

[334] L. C. Rosario and P. C. K. Luk, “Implementation of a Modular Power and Energy Management Structure for Battery-Ultracapacitor Powered Electric Vehicles,” in *Hybrid Vehicle Conference, IET The Institution of Engineering and Technology, Coventry, UK*, 2006, pp. 141–156.

[335] T. J. Barlow, S. Latham, I. S. Mccrae, and P. G. Boulter, “A reference book of driving cycles for use in the measurement of road vehicle emissions: Version 3,” 2009.

[336] A. D. Swingler, “A new DSP contrlled bi-directonal DC-DC converter system for inverter/charger applications,” The University of British Columbia, 1999.

[337] Wikiwand authers, “Buck–boost converter,” *Wikimedia Foundation, Inc.*, 2016. [Online]. Available: http://www.wikiwand.com/en/Buck–boost_converter. [Accessed: 25-Dec-2015].

[338] H. Liu, L. M. Tolbert, B. Ozpineci, and Z. Du, “Comparison of fundamental frequency and PWM methods applied on a hybrid cascaded multilevel inverter,” in *34th Annual Conference Proceedings of the IEEE Industrial Electronics Society, (IECON ’08), Orlando, FL, USA*, 2008, pp. 3233–3237.

[339] S. Khomfoi and N. Praisuwanna, “A hybrid cascaded multilevel inverter for interfacing with renewable energy resources,” in *The 2010 International Power Electronics Conference (ECCE’10), Sapporo, Japan*, 2010, pp. 2912–2917.

[340] A. L. Batschauer, S. A. Mussa, and M. L. Heldwein, “Three-phase hybrid multilevel inverter based on half-bridge modules,” *IEEE Trans. Ind. Electron.*, vol. 59, no. 2, pp. 668–678, 2012.

[341] S. S. Williamson, A. K. Rathore, and F. Musavi, “Industrial Electronics for Electric Transportation: Current State-of-the-Art and Future Challenges,” *IEEE Trans. Ind. Electron.*, vol. 62, no. 5, pp. 3021–3032, 2015.

[342] M. C. Kisacikoglu, M. Kesler, and L. M. Tolbert, “Single-phase on-board bidirectional PEV charger for V2G reactive power operation,” *IEEE Trans. Smart Grid*, vol. 6, no. 2, pp. 767–775, 2015.

[343] R. Alishah, D. Nazarpour, S. H. Hosseini, and M. Sabahi, “Novel topologies for

symmetric, asymmetric, and cascade switched-diode multilevel converter with minimum number of power electronic components," *IEEE Trans. Ind. Electron.*, vol. 61, no. 10, pp. 5300–5310, 2014.

[344] Y. Cheng, C. Qian, M. L. Crow, S. Pekarek, and S. Atcitty, "A comparison of diode-clamped and cascaded multilevel converters for a STATCOM with energy storage," *IEEE Trans. Ind. Electron.*, vol. 53, no. 5, pp. 1512–1521, 2006.

[345] K. W. Hu, P. H. Yi, and C. M. Liaw, "An EV SRM Drive Powered by Battery/Supercapacitor with G2V and V2H/V2G Capabilities," *IEEE Trans. Ind. Electron.*, vol. 62, no. 8, pp. 4714–4727, 2015.

[346] Z. Du, B. Ozpineci, L. M. Tolbert, and J. N. Chiasson, "DC-AC Cascaded H-Bridge Multilevel Boost Inverter with No Inductors for Electric / Hybrid Electric Vehicle Applications," *IEEE Trans. Ind. Appl.*, vol. 45, no. 3, pp. 963–970, 2009.

[347] R. T. Meyer, R. A. Decarlo, and S. Pekarek, "Hybrid Model Predictive Power Management of a Battery-Supercapacitor Electric Vehicle," *Asian J. Control*, vol. 18, no. 1, pp. 150–165, 2016.

[348] K.-W. Hu and C.-M. Liaw, "Incorporated Operation Control of DC Microgrid and Electric Vehicle," *IEEE Trans. Ind. Electron.*, vol. 63, no. 1, pp. 202–215, 2016.

[349] E. Robles, J. Pou, S. Ceballos, J. Zaragoza, J. L. Martín, and P. Ibañez, "Frequency-Adaptive Stationary-Reference-Frame Generation Systems," *IEEE Trans. Ind. Electron.*, vol. 58, no. 9, pp. 4275–4287, 2011.

[350] H. Akagi, E. H. Watanabe, and M. Aredes, *Instantaneous power theory and applications to power conditioning*, First edit. Hoboken, New Jersey.: John Wiley & Sons, 2007.

[351] P. Kundur, *Power System Stability and Control*, First edit. McGraw-Hill, Inc., 1994.

[352] A. . Massoud, S. J. Finney, and B. . Williams, "Systematic analytical-based generalised algorithm for multilevel space vector modulation with a fixed execution time," *IET Power Electron.*, vol. 1, no. 2, pp. 175–193, 2008.

[353] M. Bendyk, "Advanced Control of a Multi-sourced Multi- level Voltage Source Inverter System for High Performance Electric Vehicles," Cranfield University, 2017.

[354] D. Doerffel and S. A. Sharkh, "A critical review of using the Peukert equation for determining the remaining capacity of lead-acid and lithium-ion batteries," *J. Power Sources*, vol. 155, no. 2, pp. 395–400, 2006.

Appendices

Appendix A

Determination of critical voltage$V_{r,critical}$

$$v_s = A_0 \times v_r + B_0 \times i_r \quad \text{A-1}$$

where v_s and v_r are the sending end and receiving end voltage.
i_r is the receiving end current.
A_0, B_0 are the generalized line constant.

$$i_r = \frac{v_s \angle\delta - A_0 \times v_r}{B_0} \quad \text{A-2}$$

$$i_r{}^* = \frac{v_s \times (b_1 + jb_2) \times (cos\delta - jsin\delta) - v_r \times (b_1 + jb_2) \times (a_1 - ja_2)}{\left(b_1{}^2 + b_2{}^2\right)} \quad \text{A-3}$$

$$i_r{}^* v_r = \left[\frac{v_s v_r (b_1 cos\delta + b_2 sin\delta) - v_r (a_1 b_1 + a_2 b_2)}{\left(b_1{}^2 + b_2{}^2\right)} - j\frac{v_s v_r (b_1 sin\delta - b_2 cos\delta) + v_r{}^2 (a_1 b_2 - a_2 b_1)}{\left(b_1{}^2 + b_2{}^2\right)}\right] \quad \text{A-4}$$

$$S_r = P_r + jQ_r = v_r \times i_r{}^* \quad \text{A-5}$$

$$P_r = \frac{v_s v_r (b_1 cos\delta + b_2 sin\delta) - v_r{}^2 (a_1 b_1 + a_2 b_2)}{\left(b_1{}^2 + b_2{}^2\right)} \quad \text{A-6}$$

$$Q_r = \frac{v_s v_r (b_2 cos\delta - b_1 sin\delta) - v_r{}^2 (a_1 b_2 - a_2 b_1)}{\left(b_1{}^2 + b_2{}^2\right)} \quad \text{A-7}$$

where $A_0 = a_1 + ja_2$ and $B_0 = b_1 + jb_2$ are the generalized line constant for the compensated transmission system.
Hence the power balance equations at the receiving end of the transmission system are:

$$f_1(V_S, V_R, \delta) = P_R - \frac{v_s v_r (b_1 cos\delta + b_2 sin\delta) - v_r{}^2 (a_1 b_1 + a_2 b_2)}{\left(b_1{}^2 + b_2{}^2\right)} \quad \text{A-8}$$

$$f_2(V_S, V_R, \delta) = Q_R - \frac{v_s v_r (b_2 cos\delta - b_1 sin\delta) - v_r{}^2 (a_1 b_2 - a_2 b_1)}{\left(b_1{}^2 + b_2{}^2\right)} \quad \text{A-9}$$

From Jacobian matrix, it can be written:

$$\begin{bmatrix} P_R \\ Q_R \end{bmatrix} = \begin{bmatrix} \frac{\partial P_R}{\partial \delta} & \frac{\partial P_R}{\partial v_r} \\ \frac{\partial Q_R}{\partial \delta} & \frac{\partial Q_R}{\partial v_r} \end{bmatrix} \times \begin{bmatrix} \delta \\ v_r \end{bmatrix} \quad \text{A-10}$$

where P_R and Q_R are the real and reactive power.
δ and v_r are the load angle and the receiving voltage.
The maximum power transfer criterion is determined by considering the singularity of the Jacobian.
This leads to the following condition for stable operation

$$\frac{\partial P_R}{\partial \delta} \times \frac{\partial Q_R}{\partial v_r} - \frac{\partial P_R}{\partial v_r} \times \frac{\partial Q_R}{\partial \delta} \quad \text{A-11}$$

Then

$$\frac{\partial P_R}{\partial \delta} = \frac{v_s v_r (b_2 cos\delta - b_1 sin\delta)}{\left({b_1}^2 + {b_2}^2\right)} \quad \text{A-12}$$

$$\frac{\partial P_R}{\partial v_r} = \frac{v_s (b_1 cos\delta + b_2 sin\delta) - 2v_r (a_1 b_1 + a_2 b_2)}{\left({b_1}^2 + {b_2}^2\right)} \quad \text{A-13}$$

$$\frac{\partial Q_R}{\partial \delta} = \frac{v_s v_r (b_2 sin\delta - b_1 cos\delta)}{\left({b_1}^2 + {b_2}^2\right)} \quad \text{A-14}$$

$$\frac{\partial Q_R}{\partial v_r} = \frac{v_s (b_2 cos\delta - b_1 sin\delta) - 2v_r (a_1 b_2 - a_2 b_1)}{\left({b_1}^2 + {b_2}^2\right)} \quad \text{A-15}$$

it is possible to write equation A-15 as in equation A-16:

$$\frac{v_s v_r [v_s - 2v_r (a_1 cos\delta + a_2 sin\delta)]}{\left({b_1}^2 + {b_2}^2\right)} = 0 \quad \text{A-16}$$

Either

$$v_s v_r = 0 \quad \text{A-17}$$

Or

$$\frac{[v_s - 2v_r (a_1 cos\delta + a_2 sin\delta)]}{\left({b_1}^2 + {b_2}^2\right)} = 0 \quad \text{A-18}$$

At substituting $\delta_{critical}$ then

$$V_{r,critical} = \frac{v_s}{2(a_1 cos\delta_{critical} + a_2 sin\delta_{critical})} \quad \text{A-19}$$

Appendix B

Determination of critical angular separation $\delta_{critical}$

$$P_r \times tan\emptyset = Q_r \quad \text{B-1}$$

where $P_r \& Q_r$ are the real and reactive power.

$\emptyset$ is the power factor angle of the load

From appendix (A)

$$\frac{P_r}{Q_r} = \frac{(a_1b_1 - a_2b_2) + (a_1b_2 + a_2b_1) \times tan(2\delta_{critical})}{(a_1b_1 - a_2b_2) \times tan(2\delta_{critical}) - (a_1b_2 + a_2b_1)} \quad \text{B-2}$$

Equation B-3 formed by substituting equation B-2 in equation B-1:

$$\frac{(a_1b_1 - a_2b_2) + (a_1b_2 + a_2b_1) \times tan(2\delta_{critical})}{(a_1b_1 - a_2b_2) \times tan(2\delta_{critical}) - (a_1b_2 + a_2b_1)} tan\emptyset = 1 \quad \text{B-3}$$

$$tan(2\delta_{critical}) = \frac{a_1(b_1 tan\emptyset + b_2) + a_2(b_1 - b_2 tan\emptyset)}{a_1(b_1 - b_2 tan\emptyset) - a_2(b_1 tan\emptyset + b_2)} = \frac{K_1}{K_2} \quad \text{B-4}$$

$$\delta_{critical} = \frac{1}{2} tan^{-1}\left(\frac{K_1}{K_2}\right) \quad \text{B-5}$$

$$K_1 = a_1(b_1 tan\emptyset + b_2) + a_2(b_1 - b_2 tan\emptyset) \quad \text{B-6}$$

$$K_2 = a_1(b_1 - b_2 tan\emptyset) - a_2(b_1 tan\emptyset + b_2) \quad \text{B-7}$$

Appendix C

Determination of the ratio of the critical power transfer $P_{R\,critical}$ and the surge impedance loading.

The surge impedance loading (SIL) of a lossy line is given by:

$$SIL = \frac{{V_S}^2 z_1}{Z_0} \quad \text{C-1}$$

where $\overline{Z_0} = z_1 + jz_2$ is the surge impedance of the lossy line

$$\overline{Z_0} = Z_0\sqrt{1 - j\alpha} \quad \text{C-2}$$

where Z_0 is the surge impedance of a lossless line.

α is the line loss factor of the lossy line i.e. $\alpha = \frac{R}{\omega L}$

$where\ R$ and ωL are the resistance and inductive reactance of the lossy line.

Using equation (C-2), equation (C-1) may be written as:

$$SIL = \frac{{V_S}^2\sqrt{1 + \sqrt{1 + \alpha^2}}}{Z_0\sqrt{\sqrt{2(1 + \alpha^2)}}} \quad \text{C-3}$$

The critical limit of power transfer $P_{R\,critical}$ is obtained from equation (A-1) of appendix A by replacing V_R and δ by their critical values. Finally, $P_{R\,critical}$ in terms of SIL of a lossy line is expressed as:

$$P_{R,critical} = \frac{K_3K_4\sqrt{\sqrt{2(1 + \alpha^2)}} - (a_1b_1 + a_2b_2)}{\sqrt{1 + \sqrt{1 + \alpha^2}} \times {K_4}^2\left({b_1}^2 + {b_2}^2\right)} \quad \text{C-4}$$

where

$$K_3 = b_1 cos\delta_{critical} + b_2 sin\delta_{critical} \quad \text{C-5}$$

$$K_4 = a_1 cos\delta_{critical} + a_2 sin\delta_{critical} \quad \text{C-6}$$

Appendix D

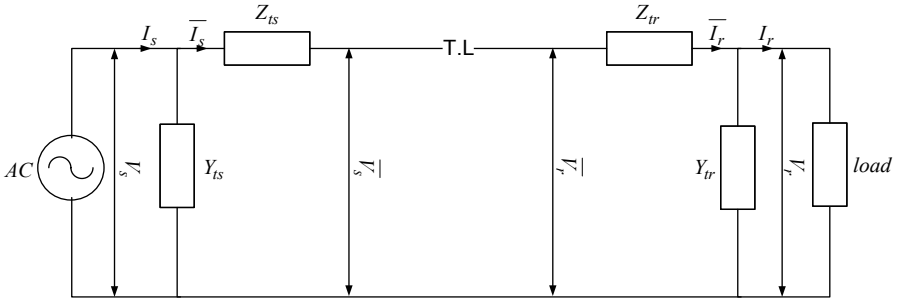

Apx_Figure D-1: Schematic diagram of the equivalent π model with load

$$\overline{V_s} = A\overline{V_r} + B\overline{I_r} \quad \text{D-1}$$

$$\overline{I_r} = I_r + Y_{tr}V_r \quad \text{D-2}$$

$$\overline{V_r} = V_r + Z_{tr}\overline{I_r} \quad \text{D-3}$$

$$\overline{V_r} = (1 + Z_{tr}Y_{tr})V_r + Z_{tr}I_r \quad \text{D-4}$$

$$\overline{V_s} = (A + AZ_{tr}Y_{tr} + BY_{tr})V_r + (AZ_{tr} + B)I_r \quad \text{D-5}$$

$$\overline{I_s} = C\overline{V_r} + D\overline{I_r} \quad \text{D-6}$$

$$\overline{I_s} = (C + CZ_{tr}Y_{tr} + DY_{tr})V_r + (CZ_{tr} + D)I_r \quad \text{D-7}$$

$$V_s = \overline{V_s} + Y_{ts}\overline{I_s} \quad \text{D-8}$$

$$V_s = (A + AZ_{tr}Y_{tr} + BY_{tr} + CZ_{ts} + CZ_{ts}Z_{tr}Y_{tr} + DZ_{ts}Y_{tr})V_r + (AZ_{tr} + B + CZ_{ts}Z_{tr} + DZ_{ts})I_r \quad \text{D-9}$$

$$I_s = \overline{I_s} + Y_{ts}V_s \quad \text{D-10}$$

$$I_s = \big(A(Y_{tr} + Y_{ts} + Y_{ts}Z_{tr}Y_{tr} + Z_{ts}Y_{ts}Y_{tr}) + BY_{ts}Y_{tr} + C(1 + Z_{tr}Y_{tr} + Z_{ts}Y_{ts} + Z_{ts}Y_{ts}Z_{tr}Y_{tr})\big)V_r + (A(Y_{ts}Z_{tr} + Z_{ts}Y_{ts}) + BY_{ts} + C(Z_{ts}Y_{ts}Z_{tr} + Z_{tr}) + D)I_r \quad \text{D-11}$$

$$A_0 = A(1 + Z_{tr}Y_{tr} + Z_{ts}Y_{tr}) + BY_{tr} + C(Z_{ts} + Z_{ts}Z_{tr}Y_{tr}) \quad \text{D-12}$$

$$B_0 = A(Z_{tr} + Z_{ts}) + B + CZ_{ts}Z_{tr} \quad \text{D-13}$$

$$C_0 = A(Y_{tr} + Y_{ts} + Y_{ts}Z_{tr}Y_{tr} + Z_{ts}Y_{ts}Y_{tr}) + BY_{ts}Y_{tr} + C(1 + Z_{tr}Y_{tr} + Z_{ts}Y_{ts} + Z_{ts}Y_{ts}Z_{tr}Y_{tr}) \quad \text{D-14}$$

$$D_0 = A(1 + Y_{ts}Z_{tr} + Z_{ts}Y_{ts}) + BY_{ts} + C(Z_{ts}Y_{ts}Z_{tr} + Z_{tr}) \quad \text{D-15}$$

Appendix E

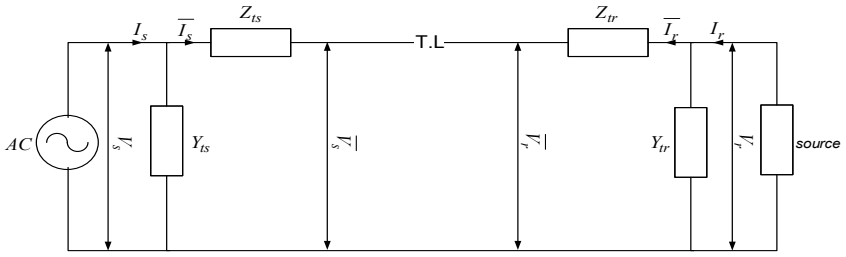

Apx_Figure E-1: Schematic diagram of the equivalent π model with source

$$\overline{V_s} = A\overline{V_r} + B\overline{I_r} \quad \text{E-1}$$

$$\overline{I_r} = -I_r + Y_{tr}V_r \quad \text{E-2}$$

$$\overline{V_r} = V_r + Z_{tr}\overline{I_r} \quad \text{E-3}$$

$$\overline{V_r} = (1 + Z_{tr}Y_{tr})V_r - Z_{tr}I_r \quad \text{E-4}$$

$$\overline{V_s} = (A + AZ_{tr}Y_{tr} + BY_{tr})V_r - (AZ_{tr} + B)I_r \quad \text{E-5}$$

$$\overline{I_s} = C\overline{V_r} + D\overline{I_r} \quad \text{E-6}$$

$$\overline{I_s} = (C + CZ_{tr}Y_{tr} + DY_{tr})V_r - (CZ_{tr} + D)I_r \quad \text{E-7}$$

$$V_s = \overline{V_s} + Y_{ts}\overline{I_s} \quad \text{E-8}$$

$$V_s = (A + AZ_{tr}Y_{tr} + BY_{tr} + CZ_{ts} + CZ_{ts}Z_{tr}Y_{tr} + DZ_{ts}Y_{tr})V_r - (AZ_{tr} + B + CZ_{ts}Z_{tr} + DZ_{ts})I_r \quad \text{E-9}$$

$$I_s = \overline{I_s} + Y_{ts}V_s \quad \text{E-10}$$

$$I_s = \big(A(Y_{tr} + Y_{ts} + Y_{ts}Z_{tr}Y_{tr} + Z_{ts}Y_{ts}Y_{tr}) + BY_{ts}Y_{tr} + C(1 + Z_{tr}Y_{tr} + Z_{ts}Y_{ts} + Z_{ts}Y_{ts}Z_{tr}Y_{tr})\big)V_r - (A(Y_{ts}Z_{tr} + Z_{ts}Y_{ts}) + BY_{ts} + C(Z_{ts}Y_{ts}Z_{tr} + Z_{tr}) + D)I_r \quad \text{E-11}$$

$$A_0 = A(1 + Z_{tr}Y_{tr} + Z_{ts}Y_{tr}) + BY_{tr} + C(Z_{ts} + Z_{ts}Z_{tr}Y_{tr}) \quad \text{E-12}$$

$$B_0 = -A(Z_{tr} + Z_{ts}) - B - CZ_{ts}Z_{tr} \quad \text{E-13}$$

$$C_0 = A(Y_{tr} + Y_{ts} + Y_{ts}Z_{tr}Y_{tr} + Z_{ts}Y_{ts}Y_{tr}) + BY_{ts}Y_{tr} + C(1 + Z_{tr}Y_{tr} + Z_{ts}Y_{ts} + Z_{ts}Y_{ts}Z_{tr}Y_{tr}) \quad \text{E-14}$$

$$D_0 = -A(1 + Y_{ts}Z_{tr} + Z_{ts}Y_{ts}) - BY_{ts} - C(Z_{ts}Y_{ts}Z_{tr} + Z_{tr}) \quad \text{E-15}$$

Definition

$$k_d = \text{Degree of shunt compensation} = \frac{b}{\omega C} = \frac{bZ_0}{\theta} \quad \text{E-16}$$

$$\alpha = \text{Line loss factor} = \frac{r}{\omega L} \quad \text{E-17}$$

$$\beta = \text{Phase shift constant of a loss less line} = \omega\sqrt{LC} \quad \text{E-18}$$

$$\theta = \text{Line angle of a loss less line} = \beta\ell \quad \text{E-19}$$

$$\ell = \text{Line length} \quad \text{E-20}$$

$$\overline{\theta} = \text{Line angle of a lossy line} = \theta\sqrt{1 - j\alpha} \quad \text{E-21}$$

$$Z_0 = \text{Surge impedance of a loss less line} = \sqrt{\frac{L}{C}} \quad \text{E-22}$$

$$R = \sqrt{1 - j\alpha} \quad \text{E-23}$$

Appendix F

From the characteristics of long transmission line, the equation in terms of the *ABCD* constants for transmission line is

$$\begin{bmatrix} V_S \\ I_S \end{bmatrix} = \begin{bmatrix} A & B \\ C & D \end{bmatrix} \begin{bmatrix} V_R \\ I_R \end{bmatrix} \quad \text{F-1}$$

where V_S&V_R are the voltage at the sending and the receiving end of the line.
I_s&I_R are the current at the sending and the receiving end of the line.
$ABCD$ parameter is the generalized circuit constant of the line,

$$A = cosh(\gamma\ell) \quad \text{F-2}$$

$$B = Z_c sinh(\gamma\ell) \quad \text{F-3}$$

$$C = \frac{1}{Z_c} sinh(\gamma\ell) \quad \text{F-4}$$

$$D = cosh(\gamma\ell) \quad \text{F-5}$$

Note that $A = D$ and $AD - BC = 1$.

It is now possible to find an accurate equivalent π model, shown in figure (E-1) to replace the *ABCD* constants of the two-port network.

$$\begin{bmatrix} V_R \\ I_R \end{bmatrix} = \begin{bmatrix} D & -B \\ -C & A \end{bmatrix} \begin{bmatrix} V_S \\ I_S \end{bmatrix} \quad \text{F-6}$$

$$A = 1 + \frac{ZY}{2} = D \quad \text{F-7}$$

$$B = Z \quad \text{F-8}$$

$$C = Y\left(1 + \frac{ZY}{4}\right) \quad \text{F-9}$$

$$\tanh\left(\frac{\gamma\ell}{2}\right) = \frac{\cosh(\gamma\ell) - 1}{\sinh(\gamma\ell)} \quad \text{F-10}$$

The parameters of the equivalent π model are obtained in Equations F-11 and F-12 respectively.

$$\overline{Z} = Z_c \sinh(\gamma\ell) = Z\frac{\sinh(\gamma\ell)}{\gamma\ell} \quad \text{F-11}$$

$$\frac{\overline{Y}}{2} = \frac{1}{Z_c}\tanh\left(\frac{\gamma\ell}{2}\right) = \frac{Y}{2}\frac{\tanh\left(\frac{\gamma\ell}{2}\right)}{\frac{\gamma\ell}{2}} \quad \text{F-12}$$

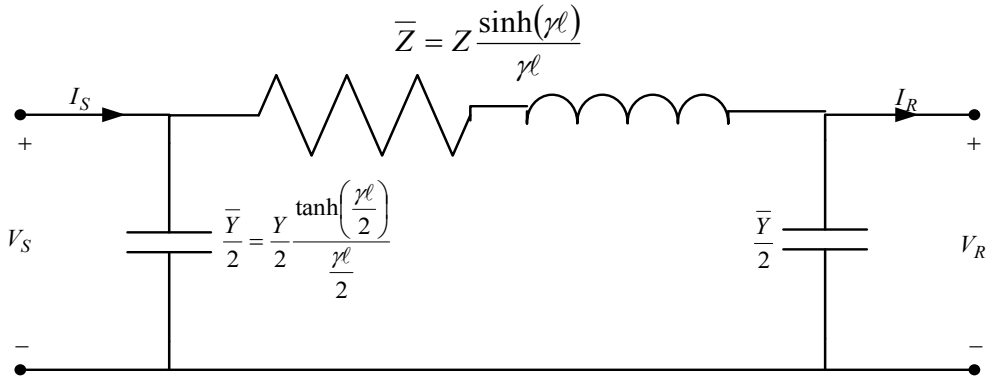

Apx_Figure F-1: Equivalent π model for long length line

Appendix G

From equation (D-1), (D-2), (D-3) and (D-4) then

$$A_0 = \cosh(j\overline{\theta}) - j\sinh(j\overline{\theta}) \times k_d\overline{\theta} \quad \text{G-1}$$

$$B_0 = \sinh(j\overline{\theta})\, Z_0 R \quad \text{G-2}$$

$$C_0 = \sinh(j\overline{\theta}) \times \left(\frac{1}{Z_0 R}\right) - j\cosh(j\overline{\theta}) \times \frac{k_d\theta}{Z_0} \quad \text{G-3}$$

$$A_0 = \cosh(j\overline{\theta}) \quad \text{G-4}$$

Appendix H

Multi-level inverter state space equations

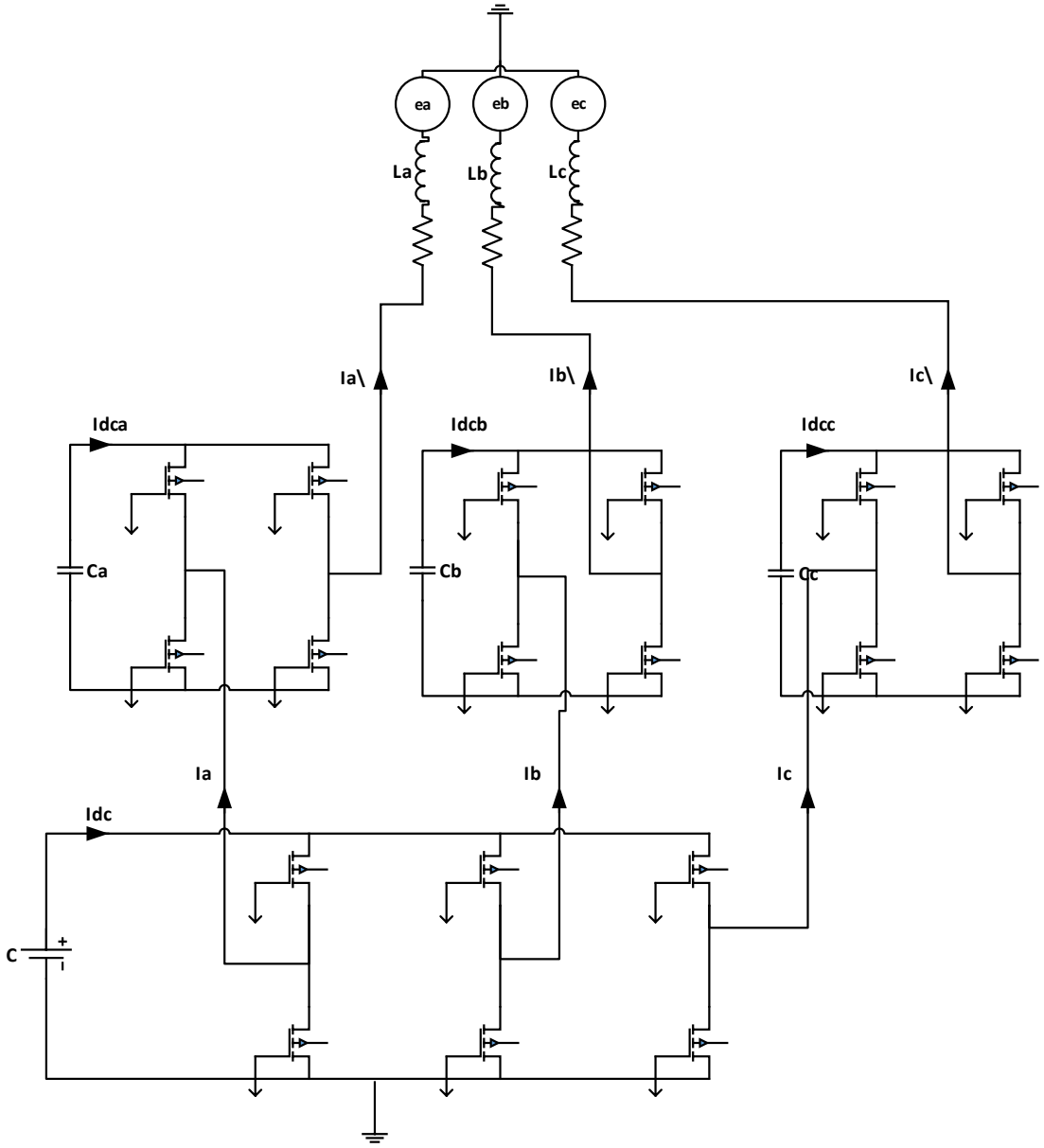

Apx_Figure H-1: Schematic diagram of inverter topology

$$V_{ab}(t) = V_{dc}(t)[S_a - S_b] \quad \text{H-1}$$

$$V_{bc}(t) = V_{dc}(t)[S_b - S_c] \quad \text{H-2}$$

$$V_{ca}(t) = V_{dc}(t)[S_c - S_a] \quad \text{H-3}$$

$$V_{an}(t) = \frac{1}{3}[V_{ab}(t) - V_{ca}(t)] = \frac{1}{3}V_{dc}(t)[2S_a - S_b - S_c] \quad \text{H-4}$$

$$V_{bn}(t) = \frac{1}{3}[V_{bc}(t) - V_{ab}(t)] = \frac{1}{3}V_{dc}(t)[2S_b - S_a - S_c] \quad \text{H-5}$$

$$V_{cn}(t) = \frac{1}{3}[V_{ca}(t) - V_{bc}(t)] = \frac{1}{3}V_{dc}(t)[2S_c - S_a - S_b] \quad \text{H-6}$$

$$i_{dc}(t) = [2S_a - 1]i_a(t) + [2S_b - 1]i_b(t) + [2S_c - 1]i_c(t) \quad \text{H-7}$$

$$i_{dc}(t) = -C\frac{dv_{dc}(t)}{dt} \quad \text{H-8}$$

$$-C\frac{dv_{dc}(t)}{dt} = [2S_a - 1]i_a(t) + [2S_b - 1]i_b(t) + [2S_c - 1]i_c(t) \quad \text{H-9}$$

$$\overline{V_{ab}(t)} = V_{dca}(t)[S_{a1} - S_{a2}] - V_{dcb}(t)[S_{b1} - S_{b2}] \quad \text{H-10}$$

$$\overline{V_{bc}(t)} = V_{dcb}(t)[S_{b1} - S_{b2}] - V_{dcc}(t)[S_{c1} - S_{c2}] \quad \text{H-11}$$

$$\overline{V_{ca}(t)} = V_{dcc}(t)[S_{c1} - S_{c2}] - V_{dca}(t)[S_{a1} - S_{a2}] \quad \text{H-12}$$

$$\overline{V_{an}}(t) = \frac{1}{3}\big[2V_{dca}(t)[S_{a1} - S_{a2}] - V_{dcb}(t)[S_{b1} - S_{b2}] - V_{dcc}(t)[S_{c1} - S_{c2}]\big] \quad \text{H-13}$$

$$\overline{V_{bn}}(t) = \frac{1}{3}\big[2V_{dcb}(t)[S_{b1} - S_{b2}] - V_{dca}(t)[S_{a1} - S_{a2}] - V_{dcc}(t)[S_{c1} - S_{c2}]\big] \quad \text{H-14}$$

$$\overline{V_{cn}}(t) = \frac{1}{3}\big[2V_{dcc}(t)[S_{c1} - S_{c2}] - V_{dca}(t)[S_{a1} - S_{a2}] - V_{dcb}(t)[S_{b1} - S_{b2}]\big] \quad \text{H-15}$$

$$V_{\bar{a}a}(t) = \overline{V_{an}}(t) - V_{an}(t) \quad \text{H-16}$$

$$V_{\bar{a}a}(t) = \frac{1}{3}\big[2V_{dca}(t)[S_{a1} - S_{a2}] - V_{dcb}(t)[S_{b1} - S_{b2}] - V_{dcc}(t)[S_{c1} - S_{c2}] - V_{dc}(t)[2S_a - S_b - S_c]\big] \quad \text{H-17}$$

$$V_{\bar{b}b}(t) = \overline{V_{bn}}(t) - V_{bn}(t) \quad \text{H-18}$$

$$V_{\bar{b}b}(t) = \frac{1}{3}\big[2V_{dcb}(t)[S_{b1} - S_{b2}] - V_{dca}(t)[S_{a1} - S_{a2}] - V_{dcc}(t)[S_{c1} - S_{c2}] - V_{dc}(t)[2S_b - S_a - S_c]\big] \quad \text{H-19}$$

$$V_{\bar{c}c}(t) = \overline{V_{cn}}(t) - V_{cn}(t) \quad \text{H-20}$$

$$V_{\bar{c}c}(t) = \frac{1}{3}\big[2V_{dcc}(t)[S_{c1} - S_{c2}] - V_{dca}(t)[S_{a1} - S_{a2}] - V_{dcb}(t)[S_{b1} - S_{b2}] - V_{dc}(t)[2S_c - S_a - S_b]\big] \quad \text{H-21}$$

$$L\frac{\overline{di_a}(t)}{dt} = V_{\bar{a}a}(t) - e_a(t) \quad \text{H-22}$$

$$L\frac{\overline{di_a}(t)}{dt} = \frac{1}{3}\big[2V_{dca}(t)[S_{a1} - S_{a2}] - V_{dcb}(t)[S_{b1} - S_{b2}] - V_{dcc}(t)[S_{c1} - S_{c2}] - V_{dc}(t)[2S_a - S_b - S_c]\big] - e_a(t) \quad \text{H-23}$$

$$L\frac{\overline{di_b}(t)}{dt} = V_{\bar{b}b}(t) - e_b(t) \quad \text{H-24}$$

$$L\frac{\overline{di_b}(t)}{dt} = \frac{1}{3}\big[2V_{dcb}(t)[S_{b1} - S_{b2}] - V_{dca}(t)[S_{a1} - S_{a2}] - V_{dcc}(t)[S_{c1} - S_{c2}] - V_{dc}(t)[2S_b - S_a - S_c]\big] - e_b(t) \quad \text{H-25}$$

$$L\frac{\overline{di_c}(t)}{dt} = V_{\bar{c}c}(t) - e_c(t) \quad \text{H-26}$$

$$L\frac{\overline{di_c}(t)}{dt} = \frac{1}{3}\big[2V_{dcc}(t)[S_{c1} - S_{c2}] - V_{dca}(t)[S_{a1} - S_{a2}] - V_{dcb}(t)[S_{b1} - S_{b2}] - V_{dc}(t)[2S_c - S_a - S_b]\big] - e_c(t) \quad \text{H-27}$$

$$\overline{I_{dca}}(t) = [S_{a1} - S_{a2}][\overline{i_a}(t) - i_a(t)] \quad \text{H-28}$$

$$\overline{I_{dcb}}(t) = [S_{b1} - S_{b2}][\overline{i_b}(t) - i_b(t)] \quad \text{H-29}$$

$$\overline{I_{dcc}}(t) = [S_{c1} - S_{c2}][\overline{i_c}(t) - i_c(t)] \quad \text{H-30}$$

$$\overline{I_{dca}}(t) = -C_a\frac{d_{vca}(t)}{dt} \quad \text{H-31}$$

$$-C_a\frac{d_{vca}(t)}{dt} = [S_{a1} - S_{a2}][\overline{i_a}(t) - i_a(t)] \quad \text{H-32}$$

$$\overline{I_{dcb}}(t) = -C_b\frac{d_{vcb}(t)}{dt} \quad \text{H-33}$$

$$-C_b\frac{d_{vcb}(t)}{dt} = [S_{b1} - S_{b2}][\overline{i_b}(t) - i_b(t)] \quad \text{H-34}$$

$$\overline{I_{dcc}}(t) = -C_c\frac{d_{vcc}(t)}{dt} \quad \text{H-35}$$

$$-C_c\frac{d_{vcc}(t)}{dt} = [S_{c1} - S_{c2}][\overline{i_c}(t) - i_c(t)] \quad \text{H-36}$$

$$\dot{X} = A.X + B.U \quad \text{H-37}$$

$$X = \begin{bmatrix} \overline{i_a}(t) \\ \overline{i_b}(t) \\ \overline{i_c}(t) \\ V_{dca} \\ V_{dcb} \\ V_{dcc} \\ V_{dc} \end{bmatrix} \quad \text{H-38}$$

$$B = \begin{bmatrix} -1/L & 0 & 0 \\ 0 & -1/L & 0 \\ 0 & 0 & -1/L \\ 0 & 0 & 0 \\ 0 & 0 & 0 \\ 0 & 0 & 0 \end{bmatrix} \quad \text{H-39}$$

$$U = \begin{bmatrix} e_a \\ e_b \\ e_c \end{bmatrix} \quad \text{H-40}$$

$$A = \begin{bmatrix} 0 & 0 & 0 & 2[S_{a1} - S_{a2}]/3L & S_{b2} - S_{b1}/3L & S_{c2} - S_{c1}/3L & S_b + S_c - 2S_a/3L \\ 0 & 0 & 0 & S_{a2} - S_{a1}/3L & 2[S_{b1} - S_{b2}]/3L & S_{c2} - S_{c1}/3L & S_a + S_c - 2S_b/3L \\ 0 & 0 & 0 & S_{a2} - S_{a1}/3L & S_{b2} - S_{b1}/3L & 2[S_{c1} - S_{c2}]/3L & S_a + S_b - 2S_c/3L \\ S_{a2} - S_{a1}/C_a & 0 & 0 & 0 & 0 & 0 & 0 \\ 0 & S_{b2} - S_{b1}/C_b & 0 & 0 & 0 & 0 & 0 \\ 0 & 0 & S_{c2} - S_{c1}/C_c & 0 & 0 & 0 & 0 \end{bmatrix} \quad \text{H-41}$$

Appendix I

Apx_Table I-1: Distributed generators operation at unit commitment consideration of isolated mode optimisation including operation and pollutants treatment policy

Unit	Hours (1-24)																							
FC1	11	11	11	11	11	11	11	11	11	11	11	11	11	11	11	11	11	11	11	11	11	11	11	11
FC2	11	11	11	11	11	11	11	11	11	11	11	11	11	11	11	11	11	11	11	11	11	11	11	11
FC3	11	11	11	11	11	11	11	11	11	11	11	11	11	11	11	11	11	11	11	11	11	11	11	11
MT1	11	11	11	11	11	11	11	11	11	11	11	11	11	11	11	11	11	11	11	11	11	11	11	11
MT2	11	11	11	11	11	11	11	11	11	11	11	11	11	11	11	11	11	11	11	11	11	11	11	11
MT3	11	11	11	11	11	11	11	11	11	11	11	11	11	11	11	11	11	11	11	11	11	11	11	11
MT4	00	00	00	00	00	00	00	00	11	11	11	11	11	11	11	11	11	11	11	11	11	11	11	11
UG	00	00	00	00	00	00	00	00	00	00	00	00	00	00	00	00	00	00	00	00	00	00	00	00
DG1	00	00	00	00	00	00	00	00	00	00	00	00	11	00	00	11	11	11	11	11	11	11	00	00
EV	00	00	00	00	00	00	00	00	00	00	00	11	00	00	00	00	00	00	00	00	00	00	00	00
PV1	00	00	00	00	00	11	11	11	11	11	11	11	11	11	11	11	11	11	11	00	00	00	00	00
PV2	00	00	00	00	00	11	11	11	11	11	11	11	11	11	11	11	11	11	11	00	00	00	00	00
PV3	00	00	00	00	00	11	11	11	11	11	11	11	11	11	11	11	11	11	11	00	00	00	00	00
PV4	00	00	00	00	00	11	11	11	11	11	11	11	11	11	11	11	11	11	11	00	00	00	00	00
PV5	00	00	00	00	00	11	11	11	11	11	11	11	11	11	11	11	11	11	11	00	00	00	00	00

Apx_Table I-2: Distributed generators operation at unit commitment consideration of connected mode optimisation including operation and pollutants treatment policy

Unit	Hours (1-24)																							
FC1	11	01	10	11	01	10	11	11	11	11	11	11	11	11	11	11	11	11	11	11	11	01	11
FC2	10	11	01	10	11	01	11	11	11	11	11	11	11	11	11	11	11	11	11	11	11	11	10
FC3	01	10	11	01	10	11	11	11	11	11	11	11	11	11	11	11	11	11	11	11	11	10	11
MT1	11	01	10	11	01	10	11	11	11	11	11	11	11	11	11	11	11	11	11	11	11	11	11
MT2	10	11	01	10	11	01	11	11	11	11	11	11	11	11	11	11	11	11	11	11	11	11	11

MT3	01	10	11	01	10	11	11	11	11	11	11	11	11	11	11	11	11	11	11	11	11	11	11	11
MT4	00	00	00	00	00	00	11	11	11	11	11	11	11	11	11	11	11	11	11	11	11	11	11	11
UG	11	11	11	11	11	11	B	B	B	B	B	00	B	B	B	B	11	11	11	11	11	11	11	11
DG1	00	00	00	00	00	00	00	01	11	11	11	00	11	11	11	11	00	00	00	00	00	00	00	00
EV	00	00	00	00	00	00	00	00	00	00	00	11	00	00	00	00	00	00	00	00	00	00	00	00
PV1	00	00	00	00	00	11	11	11	11	11	11	11	11	11	11	11	11	11	11	00	00	00	00	00
PV2	00	00	00	00	00	11	11	11	11	11	11	11	11	11	11	11	11	11	11	00	00	00	00	00
PV3	00	00	00	00	00	11	11	11	11	11	11	11	11	11	11	11	11	11	11	00	00	00	00	00
PV4	00	00	00	00	00	11	11	11	11	11	11	11	11	11	11	11	11	11	11	00	00	00	00	00
PV5	00	00	00	00	00	11	11	11	11	11	11	11	11	11	11	11	11	11	11	00	00	00	00	00

Appendix J

Apx_Table J-1: Input data of case study

	EV make	**Energy_B (kWh)**	Q_{sc} **(kWh)**	$SoC_{min,ch/dis}$	SoC_{max}	SoC_{req}	SoC_t	t_a	t_d
1.	Toyota Prius PHEV	4.4	0.44	25/70	100	100	30	1	6
						100	40	7	12
						100	35	8	14
						100	45	9	15
						100	75	11	14
						100	70	12	15
						100	85	13	14
						100	50	15	19
						100	75	17	21
						100	60	19	24
2.	Chevy Volt PHEV	16	1.6	25/70	100	100	30	1	6
						100	40	7	12
						100	35	8	14
						100	45	9	15
						100	75	11	14
						100	70	12	15
						100	85	13	14
						100	50	15	19
						100	75	17	21
						100	60	19	24
3.	Mitsubishi iMiEV	16	1.6	25/70	100	100	30	1	6
						100	40	7	12
						100	35	8	14
						100	45	9	15
						100	75	11	14
						100	70	12	15
						100	85	13	14
						100	50	15	19
						100	75	17	21
						100	60	19	24
4.	Smart Fortwo ED	16.5	1.65	25/70	100	100	30	1	6
						100	40	7	12
						100	35	8	14
						100	45	9	15
						100	75	11	14
						100	70	12	15
						100	85	13	14

						100	50	15	19
						100	75	17	21
						100	60	19	24
5.	Honda Fit	20	2	25/70	100	100	30	1	6
						100	40	7	12
						100	35	8	14
						100	45	9	15
						100	75	11	14
						100	70	12	15
						100	85	13	14
						100	50	15	19
						100	75	17	21
						100	60	19	24
6.	GM Spark	21	2.1	25/70	100	100	30	1	6
						100	40	7	12
						100	35	8	14
						100	45	9	15
						100	75	11	14
						100	70	12	15
						100	85	13	14
						100	50	15	19
						100	75	17	21
						100	60	19	24
						100	50	15	19
						100	75	17	21
						100	60	19	24
7.	BMW i3	22	21	25/70	100	100	30	1	6
						100	40	7	12
						100	35	8	14
						100	75	11	14
						100	70	12	15
						100	85	13	14
						100	45	9	15
						100	50	15	19
						100	75	17	21
						100	60	19	24
8.	Ford Focus	23	2.3	25/70	100	100	30	1	6
						100	40	7	12
						100	35	8	14
						100	45	9	15
						100	75	11	14
						100	70	12	15

						100	85	13	14
						100	50	15	19
						100	75	17	21
						100	60	19	24
9.	Fiat 500e	24	2.4	25/70	100	100	30	1	6
						100	40	7	12
						100	35	8	14
						100	45	9	15
						100	75	11	14
						100	70	12	15
						100	85	13	14
						100	50	15	19
						100	75	17	21
						100	60	19	24
10.	Nissan Leaf	25	2.5	25/70	100	100	30	1	6
						100	40	7	12
						100	35	8	14
						100	45	9	15
						100	75	11	14
						100	70	12	15
						100	85	13	14
						100	50	15	19
						100	75	17	21
						100	60	19	24
11.	Mercedes B	28	2.8	25/70	100	100	30	1	6
						100	40	7	12
						100	35	8	14
						100	45	9	15
						100	75	11	14
						100	70	12	15
						100	85	13	14
						100	50	15	19
						100	75	17	21
						100	60	19	24
12.	Nissan Leaf	30	3.0	25/70	100	100	30	1	6
						100	40	7	12
						100	35	8	14
						100	45	9	15
						100	75	11	14
						100	70	12	15
						100	85	13	14
						100	50	15	19

						100	75	17	21
						100	60	19	24
13.	Tesla S 60	60	6	25/70	100	100	30	1	6
						100	40	7	12
						100	35	8	14
						100	45	9	15
						100	75	11	14
						100	70	12	15
						100	85	13	14
						100	50	15	19
						100	75	17	21
						100	60	19	24
14.	Tesla S70	70	7	25/70	100	100	30	1	6
						100	40	7	12
						100	35	8	14
						100	45	9	15
						100	75	11	14
						100	70	12	15
						100	85	13	14
						100	50	15	19
						100	75	17	21
						100	60	19	24
15.	Tesla S85	90	9	25/70	100	100	30	1	6
						100	40	7	12
						100	35	8	14
						100	45	9	15
						100	75	11	14
						100	70	12	15
						100	85	13	14
						100	50	15	19
						100	75	17	21
						100	60	19	24

Appendix K

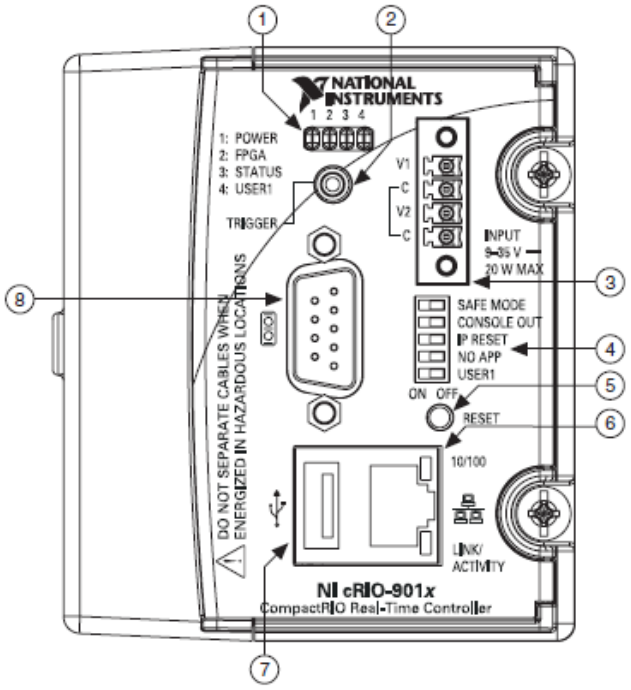

1	LEDs	5	Reset Button
2	SMB Connector	6	RJ-45 Ethernet Port
3	Power Connector	7	USB Port
4	DIP Switches	8	RS-232 Serial Port

Apx_Figure K-1: CompactRIO cRIO-9012 configuration[353]

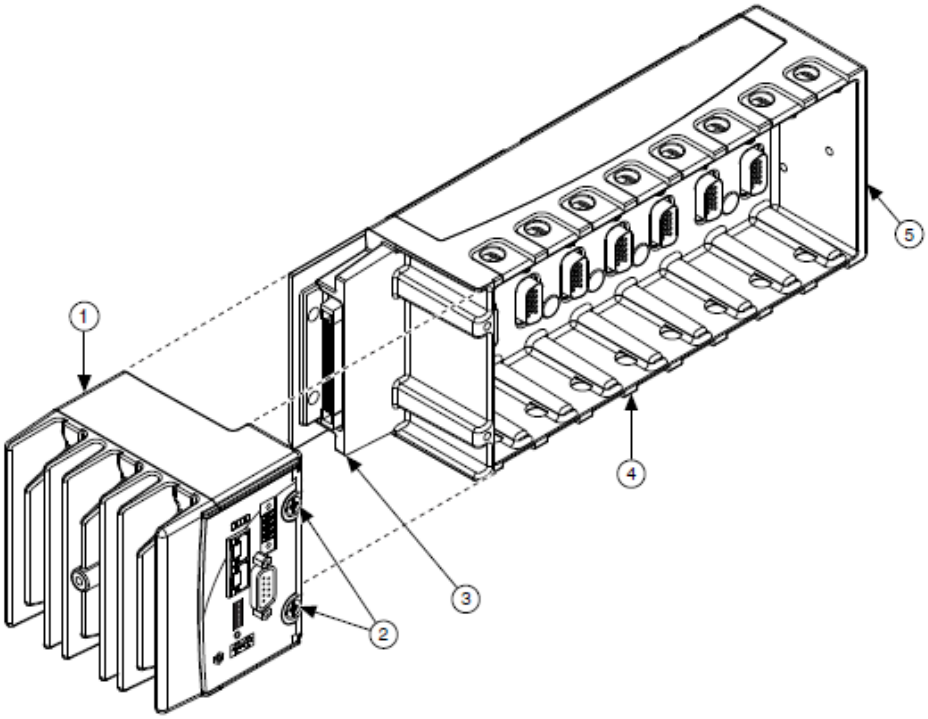

1. Controller
2. Captive Screws
3. Controller Slot
4. Reconfigurable Embedded Chassis
5. Grounding Screw

Apx_Figure K-2: CRIO chassis connection to CRIO controller

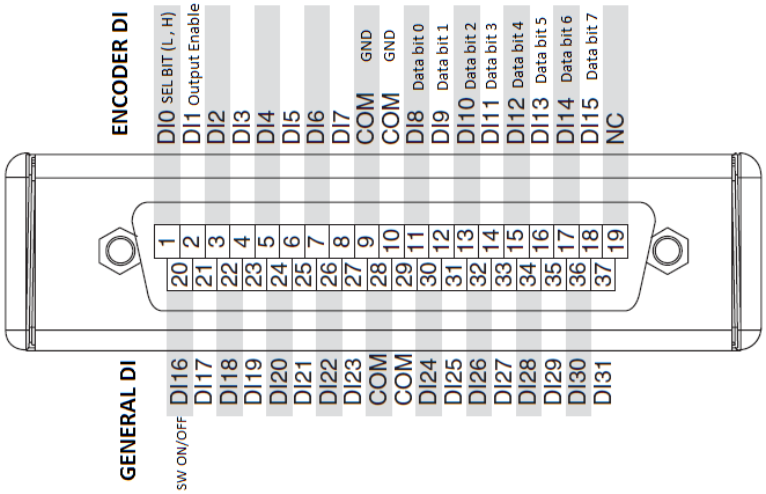

Apx_Figure K-3: NI 9425 model configuration

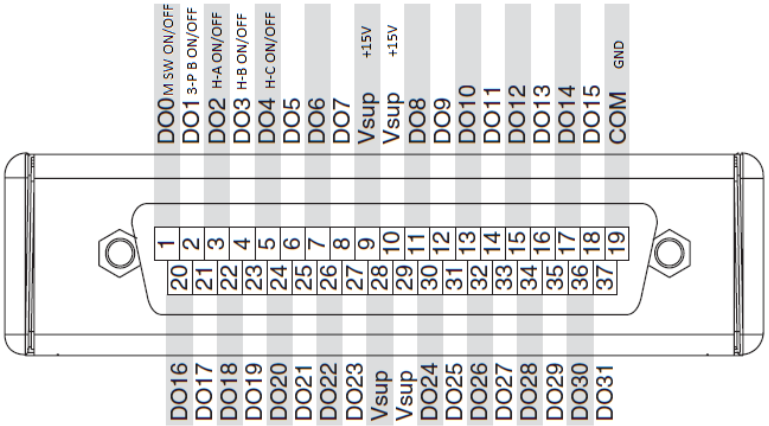

Apx_Figure K-4: NI 9476 model configuration

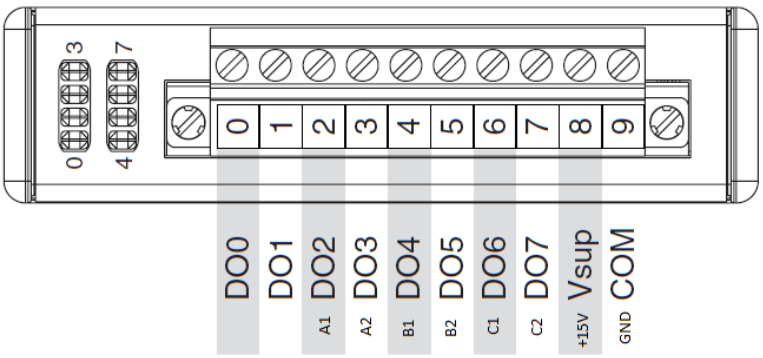

Apx_Figure K-5: NI 9474 model configuration

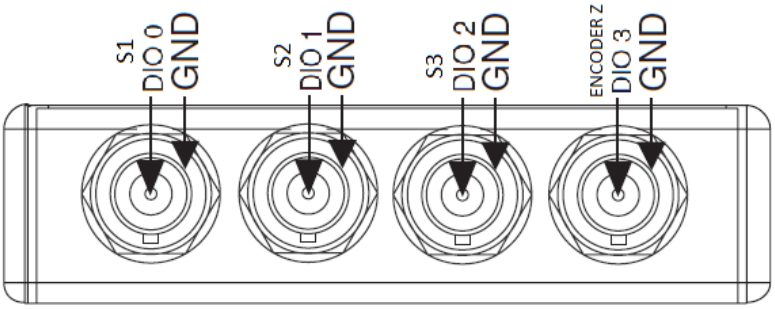

Apx_Figure K-6: NI 9402 model configuration

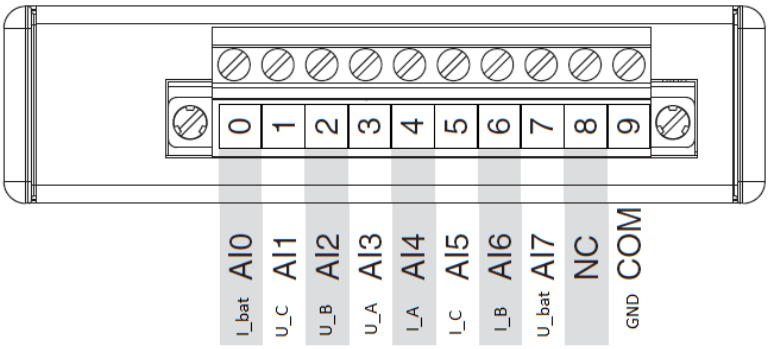

Apx_Figure K-7: NI 9201 model configuration

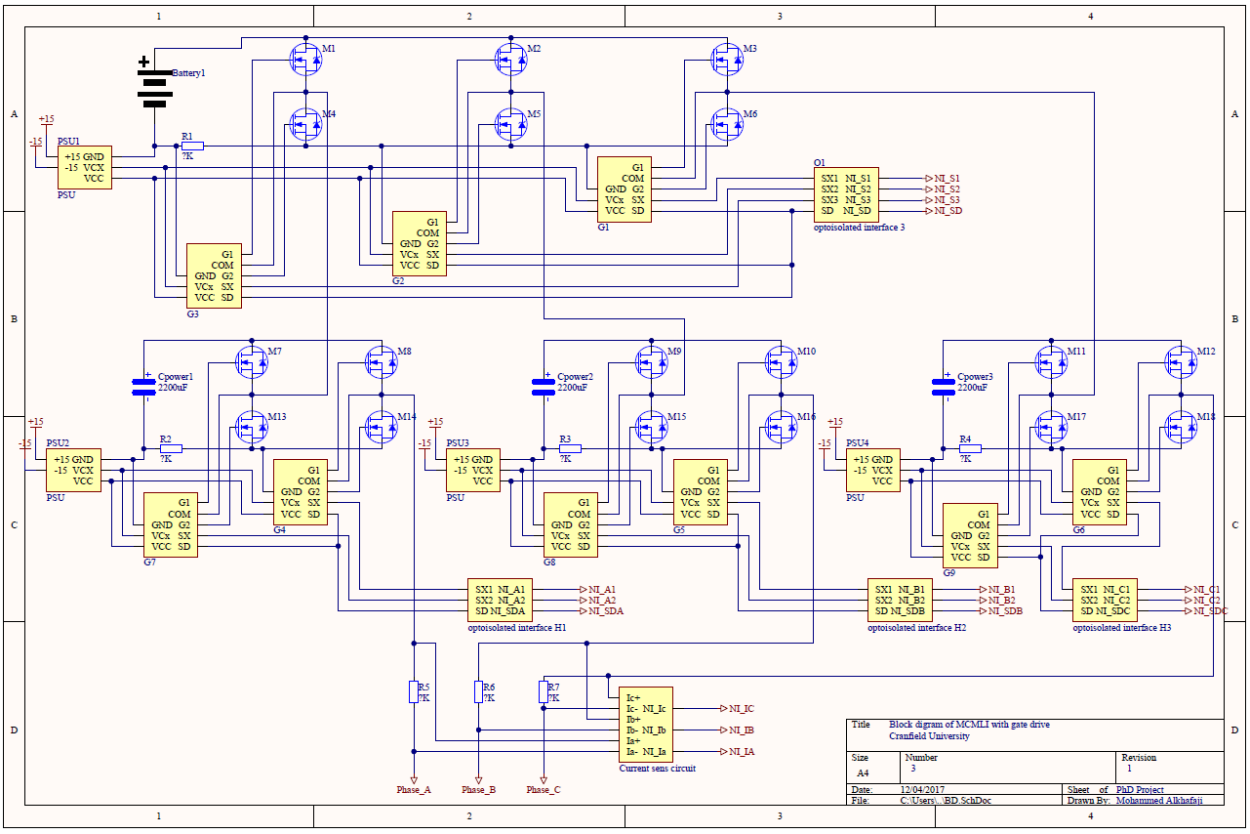

Apx_Figure K-8: Schematic diagram of Modified Cascade Multi-Level Inverter (MCMLI) with gate drive [Extended design of [353]]

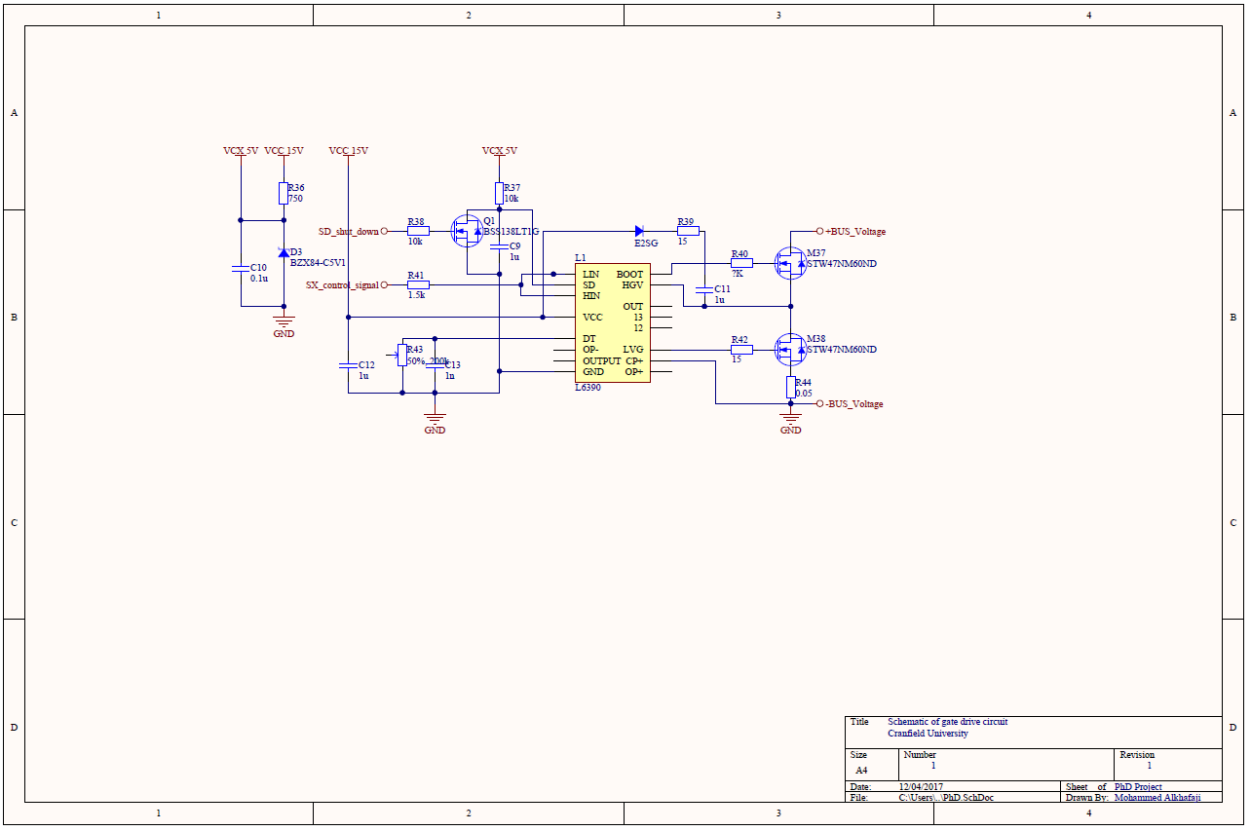

Apx_Figure K-9: Schematic diagram of gate drive circuit [Extended design of [353]]

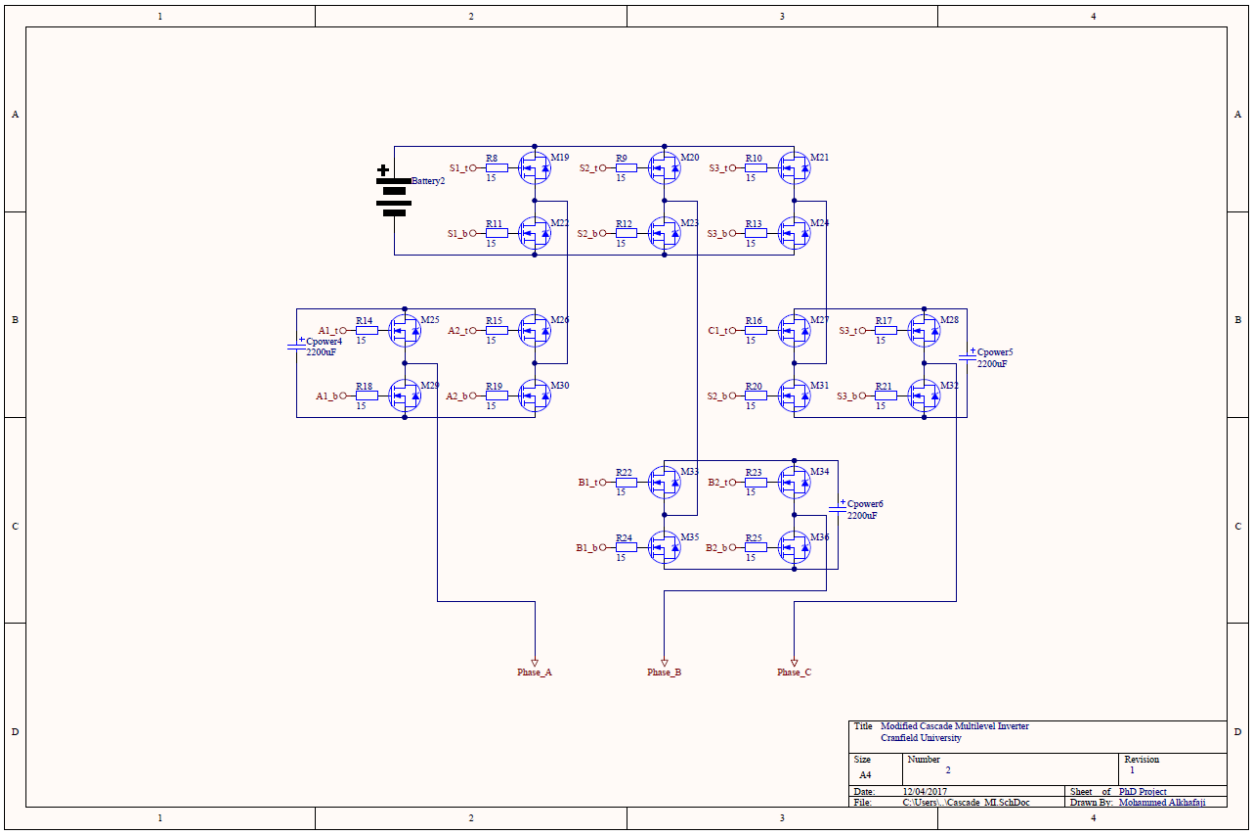

Apx_Figure K-10: Schematic diagram of Modified Cascade Multi-Level Inverter (MCMLI) [Extended design of [353]]

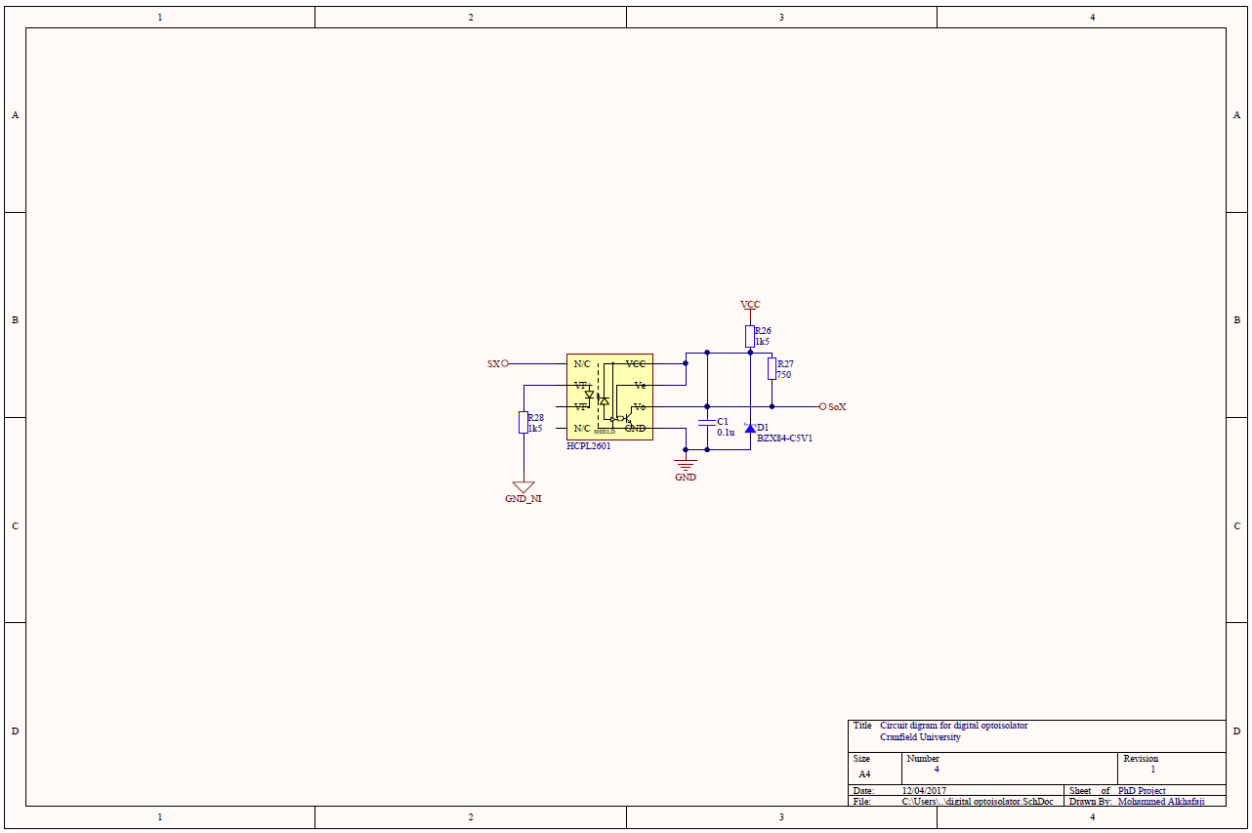

Apx_Figure K-11: Schematic diagram of digital optoisolator [Extended design of [353]]

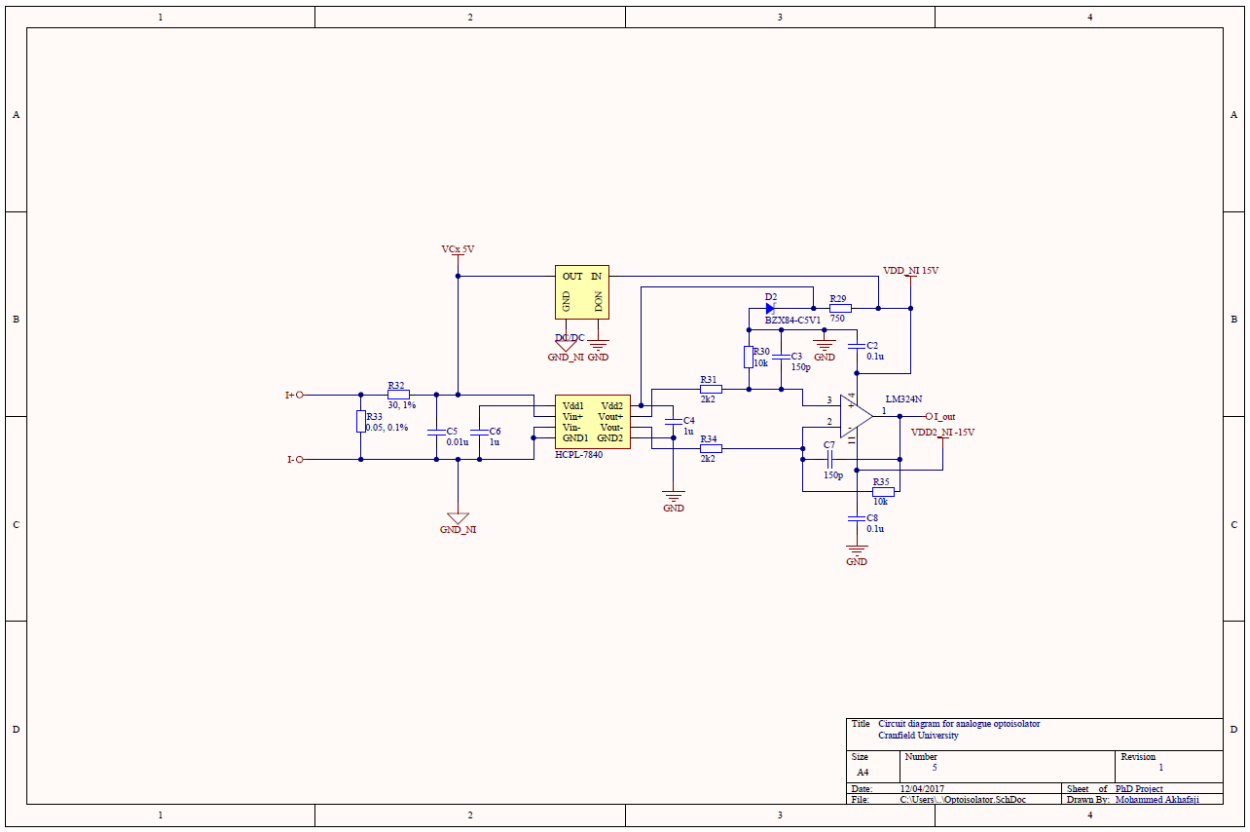

Apx_Figure K-12: Schematic diagram of analogue optoisolator [Extended design of [353]]

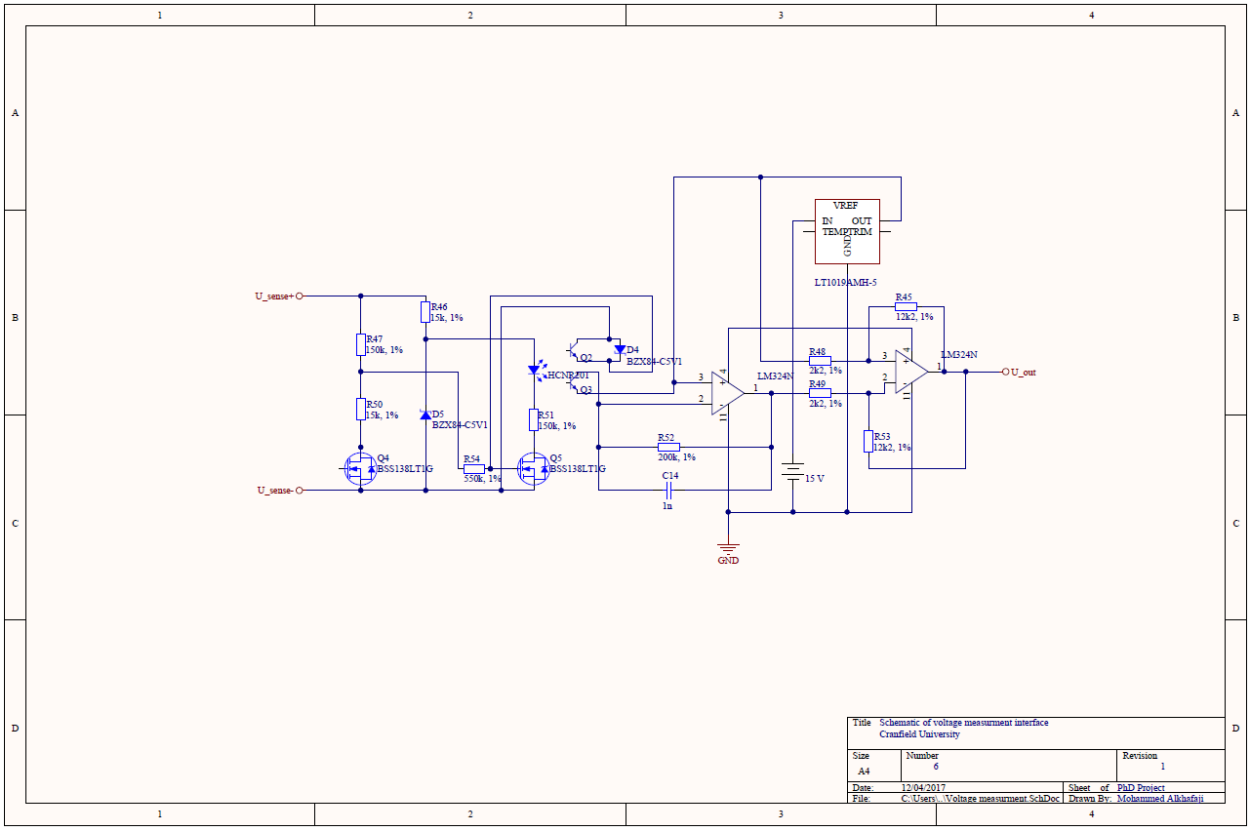

Apx_Figure K-13: Schematic diagram of voltage measurement interface [Extended design of [353]]

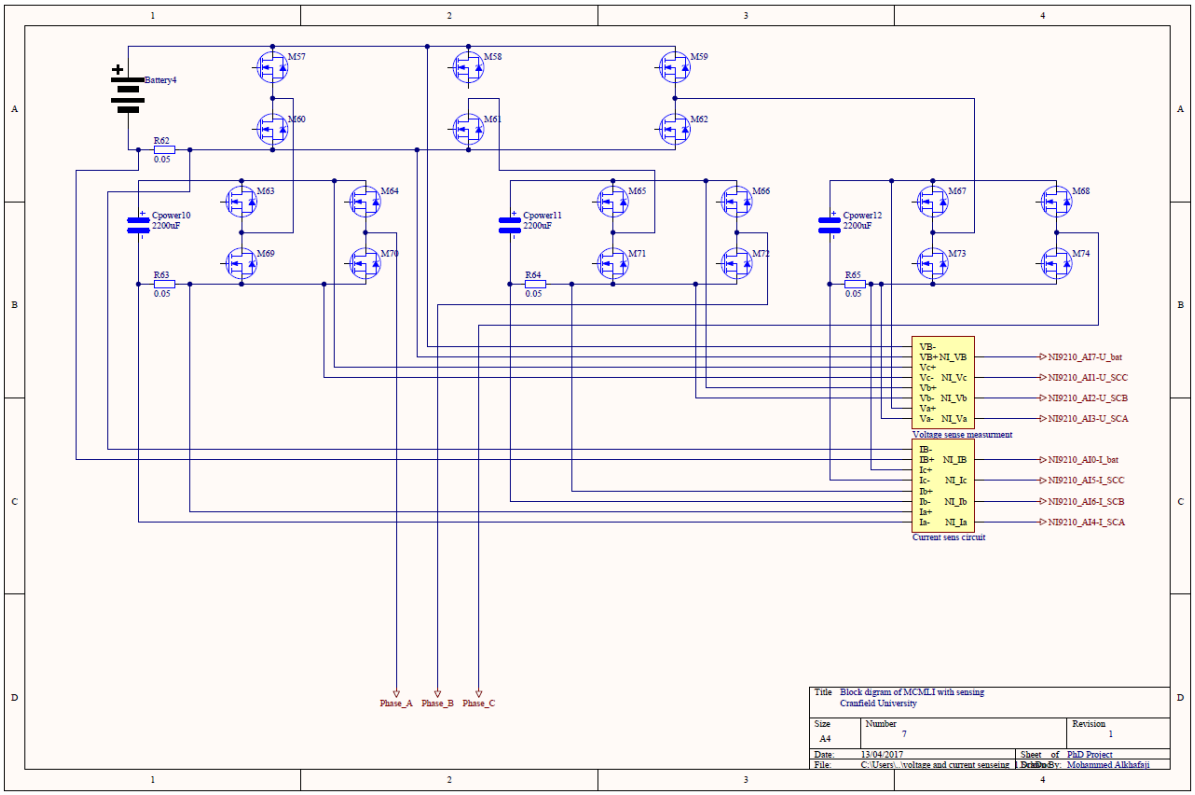

Apx_Figure K-14: Schematic diagram of MCMLI including voltage and current sensing [Extended design of [353]]

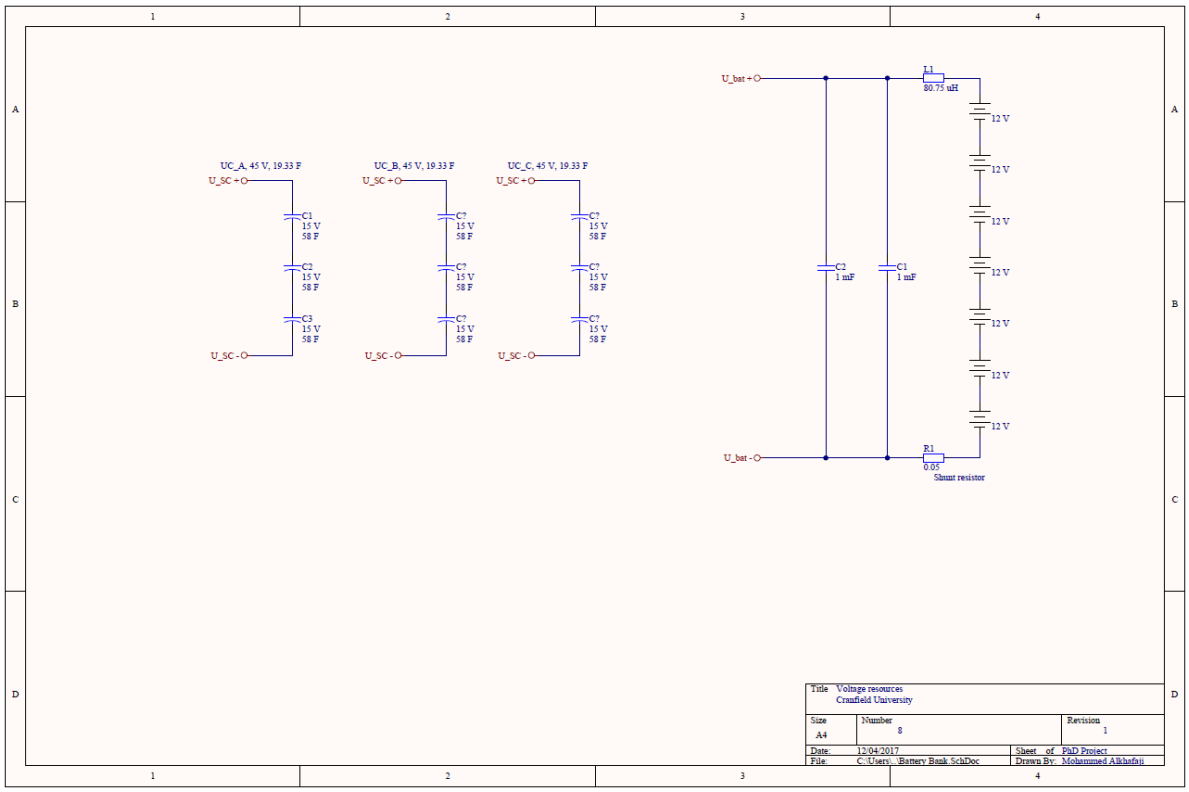

Apx_Figure K-15: Schematic diagram of battery bank and supercapacitor bank [Extended design of [353]]

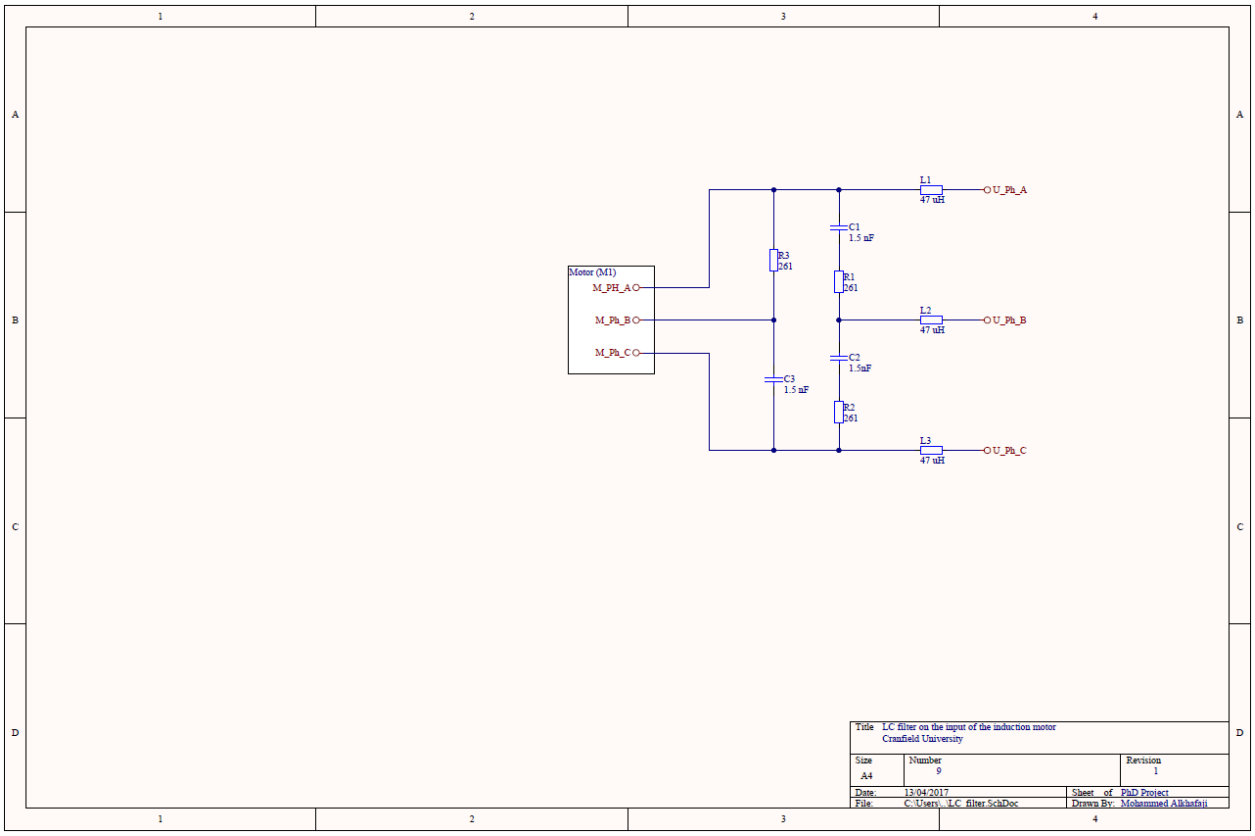

Apx_Figure K-16: Schematic diagram of input LC_filter for induction motor [Extended design of [353]]

Appendix L

Programing model

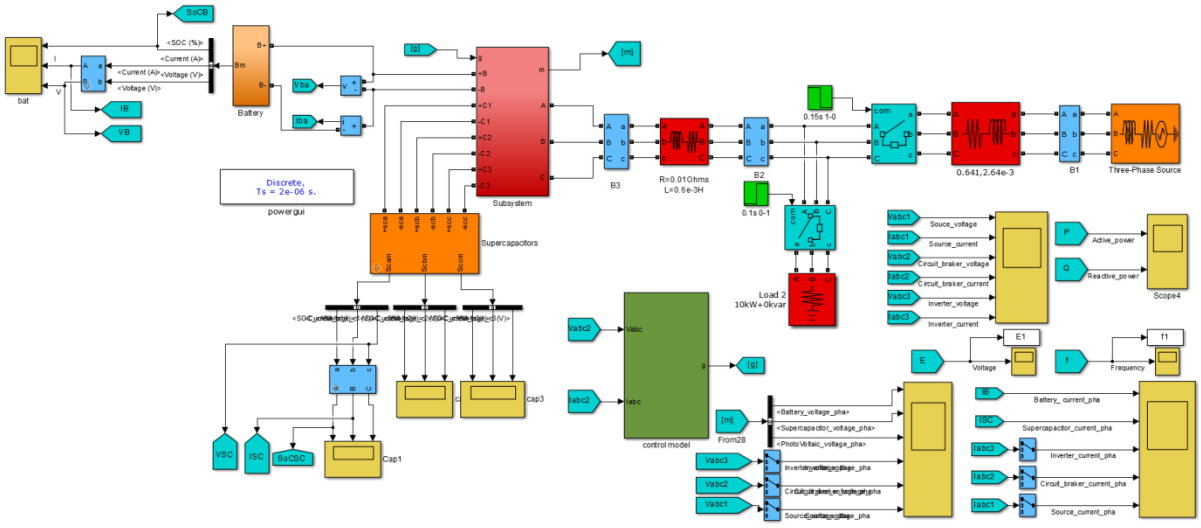

A

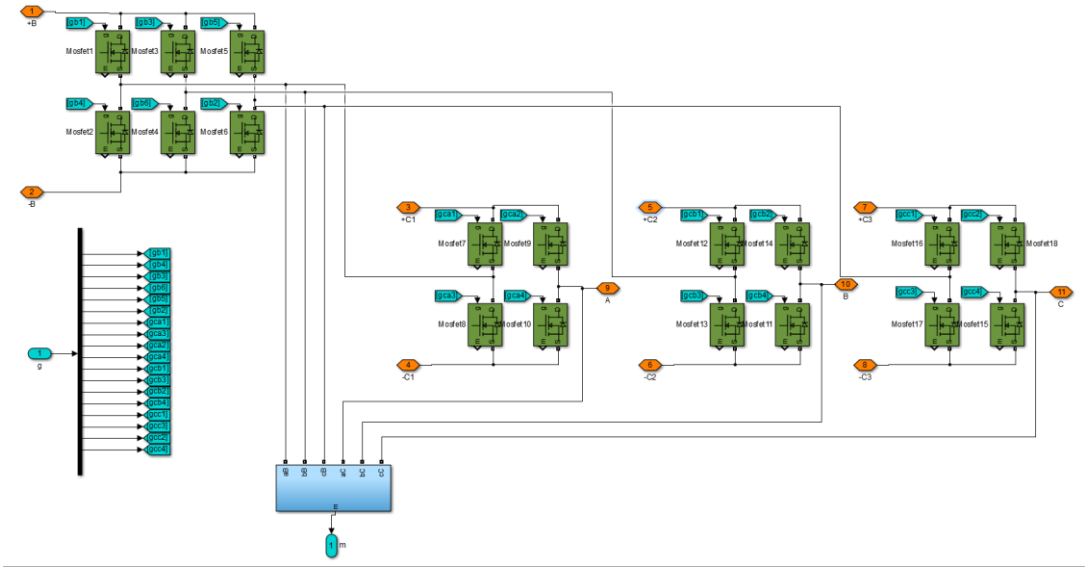

B

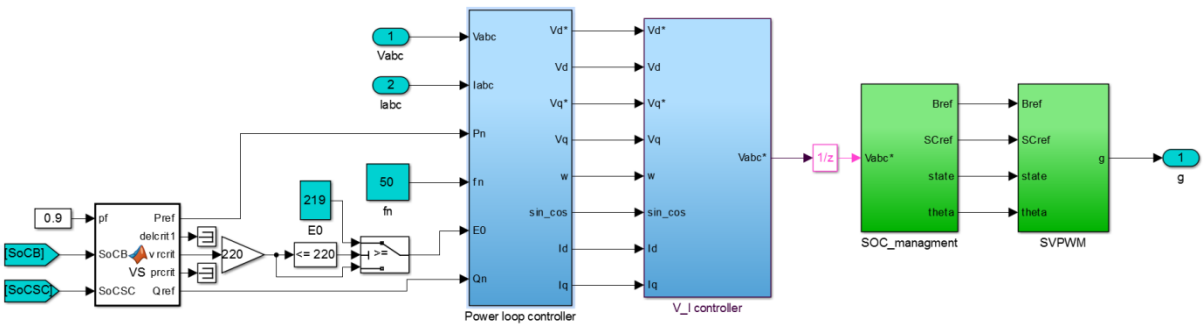

C

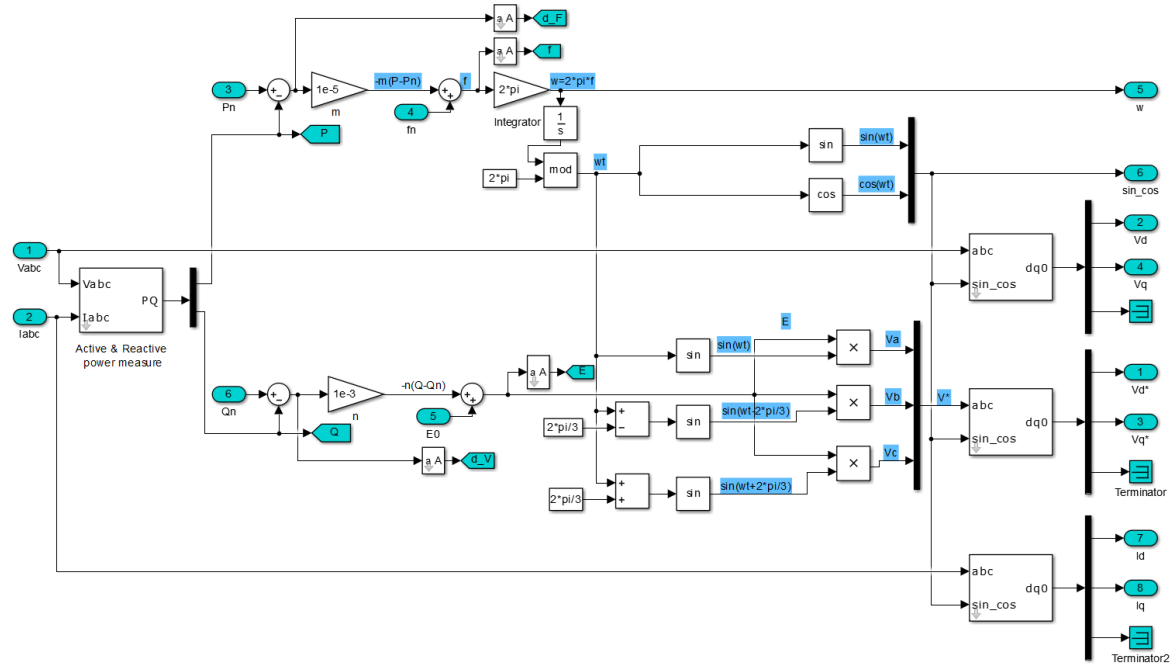
Pn
Qn
fn
m
n
E0
Integrator
w=2*pi*f
mod
sin
cos
sin(wt)
cos(wt)
Vabc
Iabc
Vabc
Iabc
PQ
Active & Reactive power measure
abc
dq0
sin_cos
Va
Vb
Vc
V*
E
d_F
d_V
Vd
Vq
Vd*
Vq*
Id
Iq
w
sin_cos
Terminator
Terminator2

D

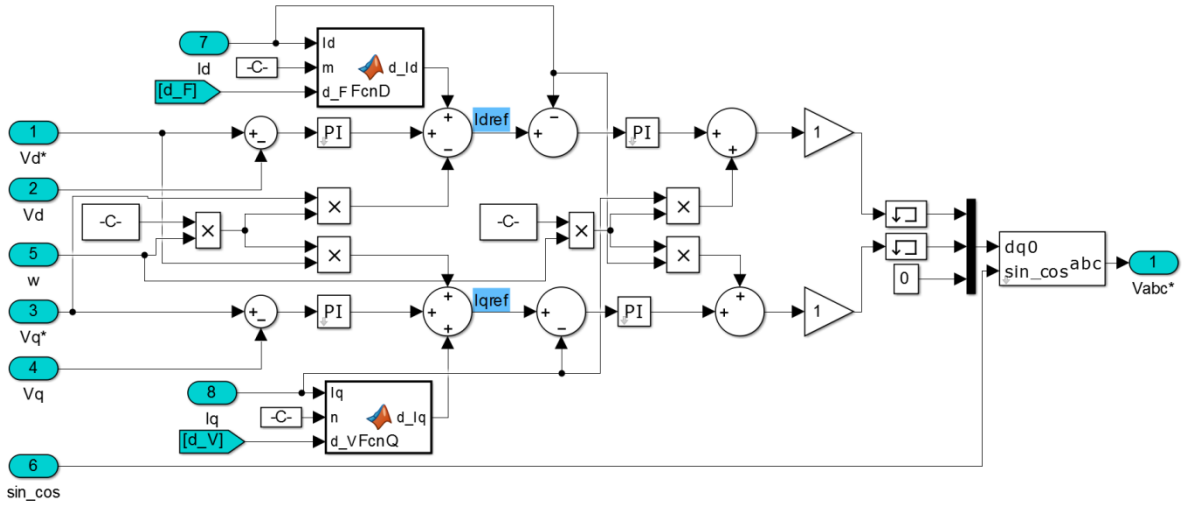
Id
[d_F]
d_Id
d_F FcnD
Idref
Iqref
PI
Vd*
Vd
w
Vq*
Vq
Iq
[d_V]
d_Iq
d_V FcnQ
sin_cos
dq0
sin_cos
abc
Vabc*

E

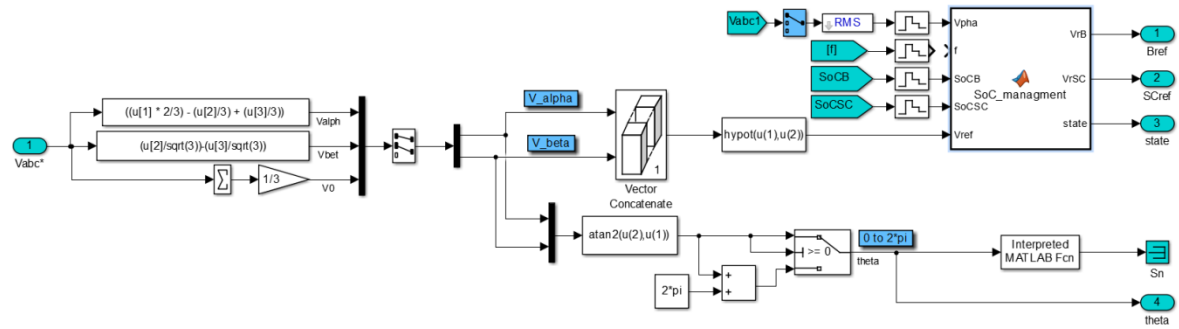
Vabc*
((u[1] * 2/3) - (u[2]/3) + (u[3]/3))
(u[2]/sqrt(3))-(u[3]/sqrt(3))
Valph
Vbet
V0
1/3
V_alpha
V_beta
Vector Concatenate
hypot(u(1),u(2))
atan2(u(2),u(1))
2*pi
0 to 2*pi
theta
Vabc1
RMS
[f]
SoCB
SoCSC
Vpha
f
SoCB
SoCSC
Vref
VrB
VrSC
state
SoC_managment
Bref
SCref
state
Interpreted MATLAB Fcn
Sn
theta

F

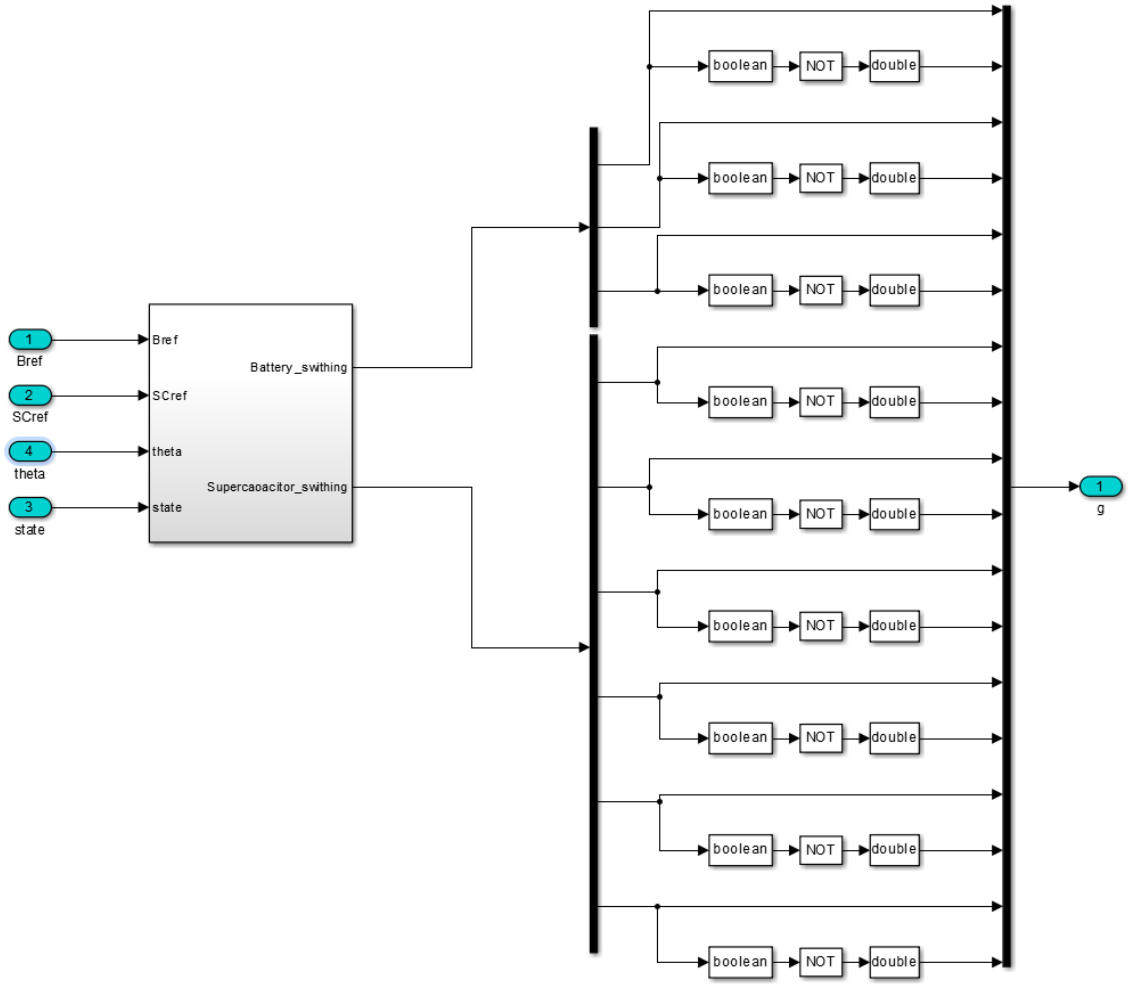

G

Apx_Figure L-1: MATLAB print screen programming

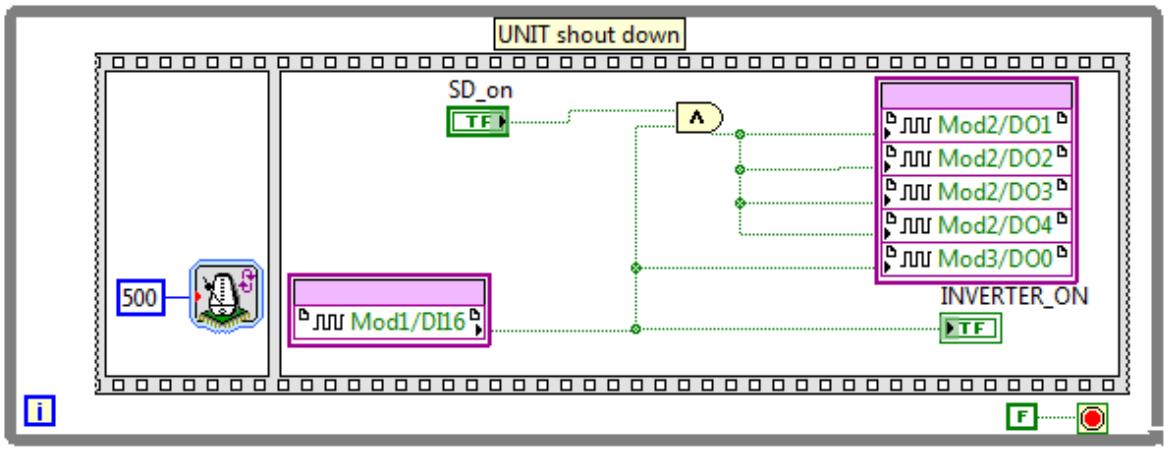

A

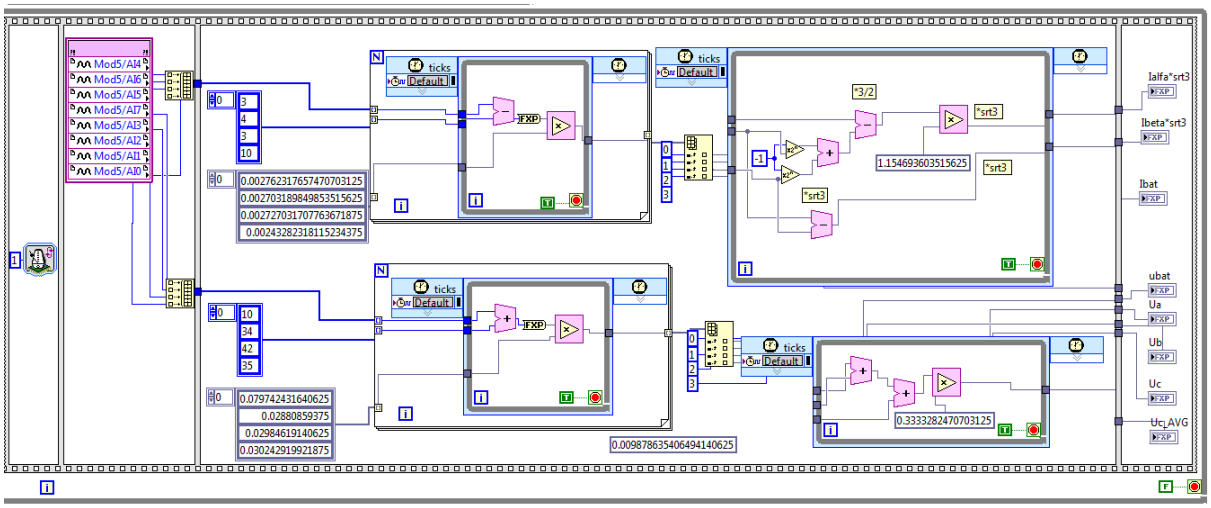
Mod5/AI4
Mod5/AI6
Mod5/AI5
Mod5/AI7
Mod5/AI3
Mod5/AI2
Mod5/AI1
Mod5/AI0
ticks
Default
FXP
*3/2
*srt3
1.154693603515625
Ialfa*srt3
Ibeta*srt3
Ibat
ubat
Ua
Ub
Uc
Uc_AVG
0.3333282470703125
0.009878635406494140625

B

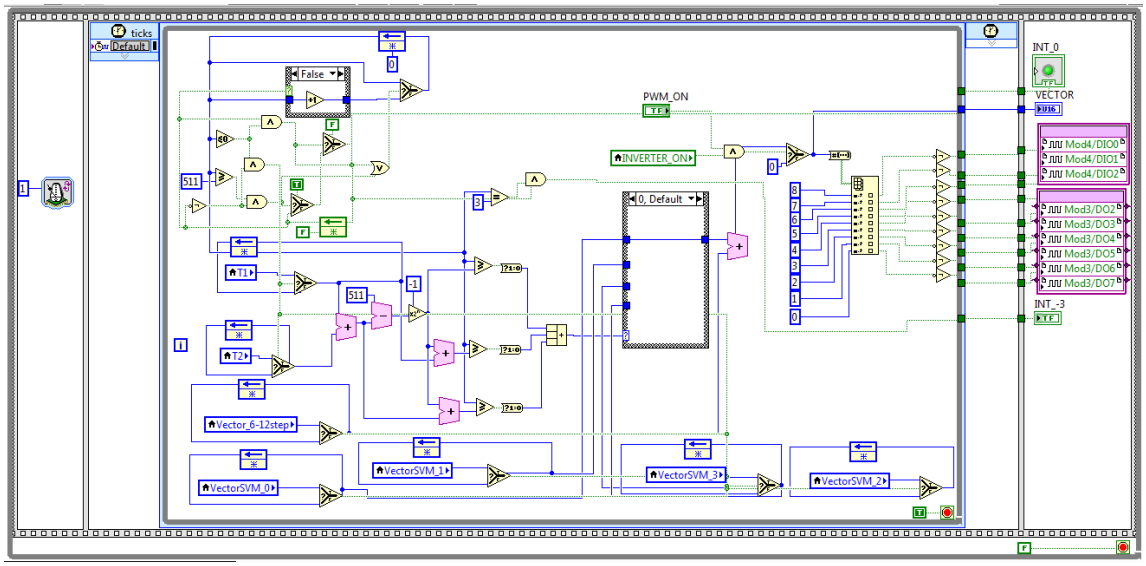
ticks
Default
False
PWM_ON
INVERTER_ON
0, Default
INT_0
VECTOR
U16
Mod4/DIO0
Mod4/DIO1
Mod4/DIO2
Mod3/DO2
Mod3/DO3
Mod3/DO4
Mod3/DO5
Mod3/DO6
Mod3/DO7
INT_-3
T1
T2
511
Vector_6-12step
VectorSVM_0
VectorSVM_1
VectorSVM_3
VectorSVM_2

C

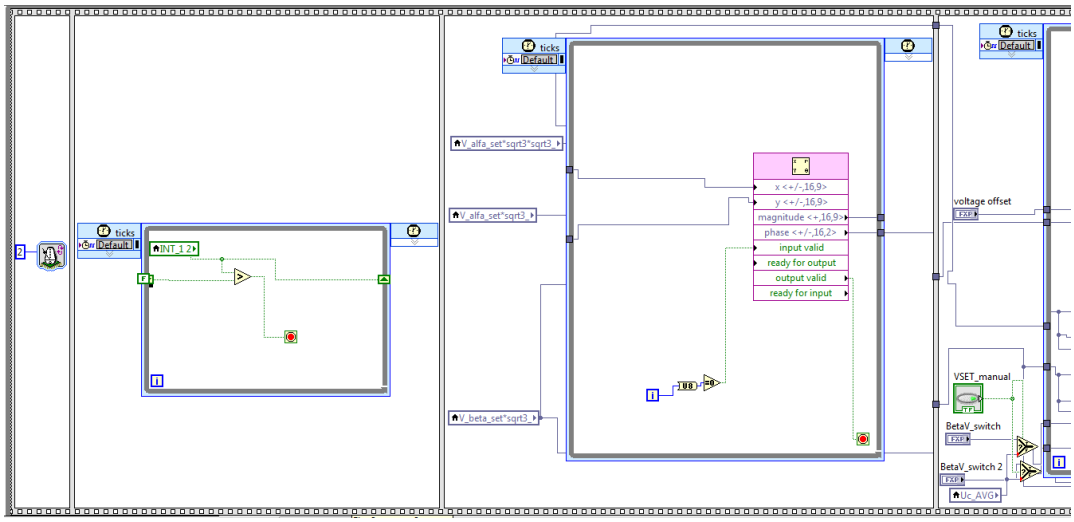
ticks
Default
INT_1 2
V_alfa_set*sqrt3*sqrt3_
V_alfa_set*sqrt3
V_beta_set*sqrt3_
x <+/-,16,9>
y <+/-,16,9>
magnitude <+,16,9>
phase <+/-,16,2>
input valid
ready for output
output valid
ready for input
voltage offset
VSET_manual
BetaV_switch
BetaV_switch 2
Uc_AVG

D

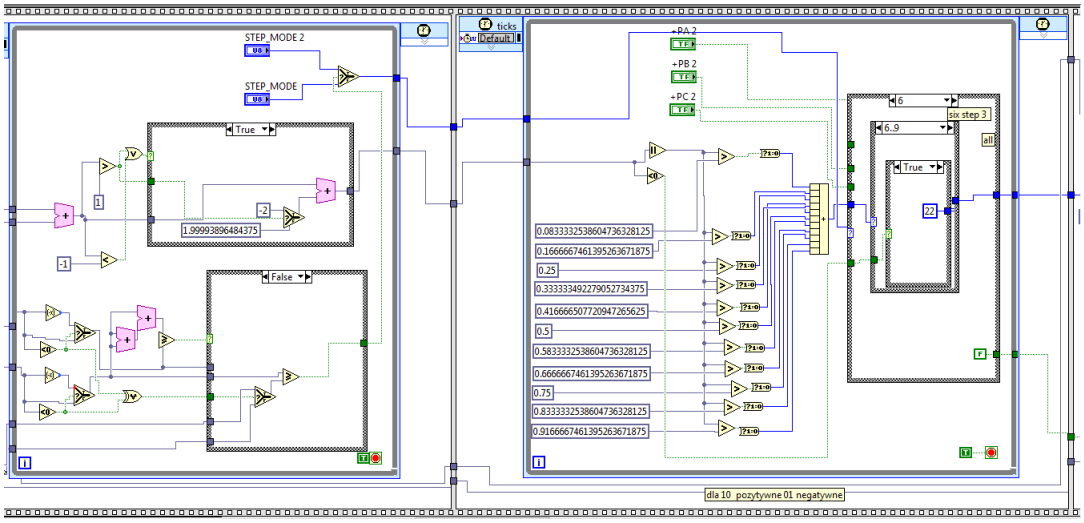
STEP_MODE 2
STEP_MODE
True
False
1.99993896484375
ticks
Default
+PA 2
+PB 2
+PC 2
six step 3
0.0833332538604736328125
0.166666746139526367187 5
0.25
0.333333492279052734375
0.416666507720947265625
0.5
0.583333253860473632812 5
0.666666746139526367187 5
0.75
0.833333253860473632812 5
0.916666746139526367187 5
dla 10 pozytywne 01 negatywne

E

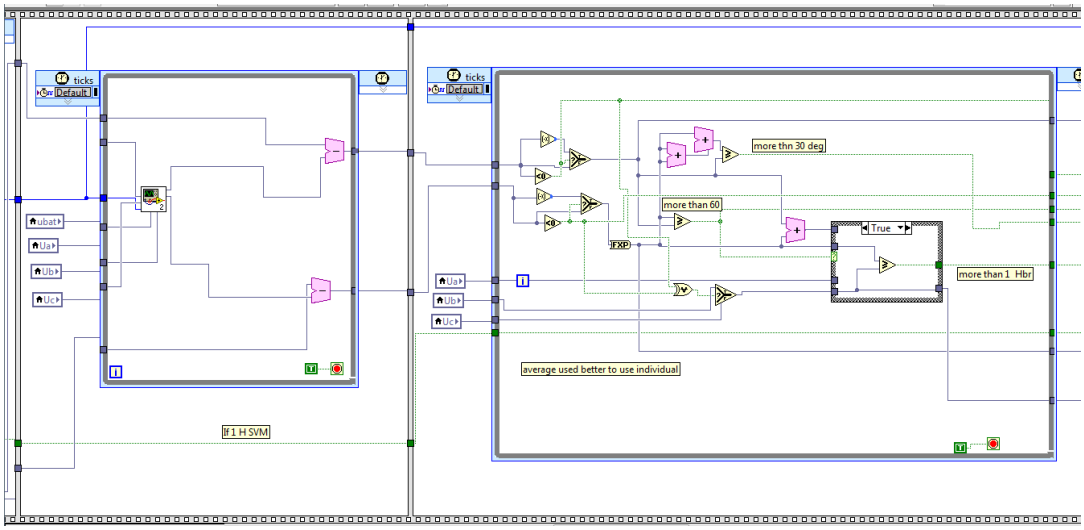
ticks
Default
ubat
Ua
Ub
Uc
If 1 H SVM
more thn 30 deg
more than 60
more than 1 Hbr
average used better to use individual

F

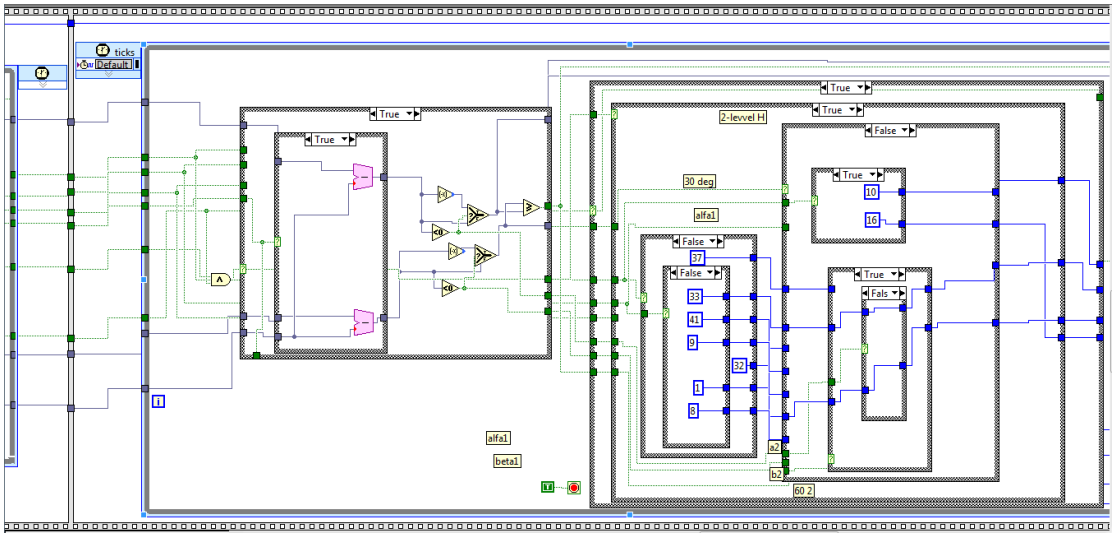
ticks
Default
True
2-leyvel H
30 deg
alfa1
beta1
60 2

G

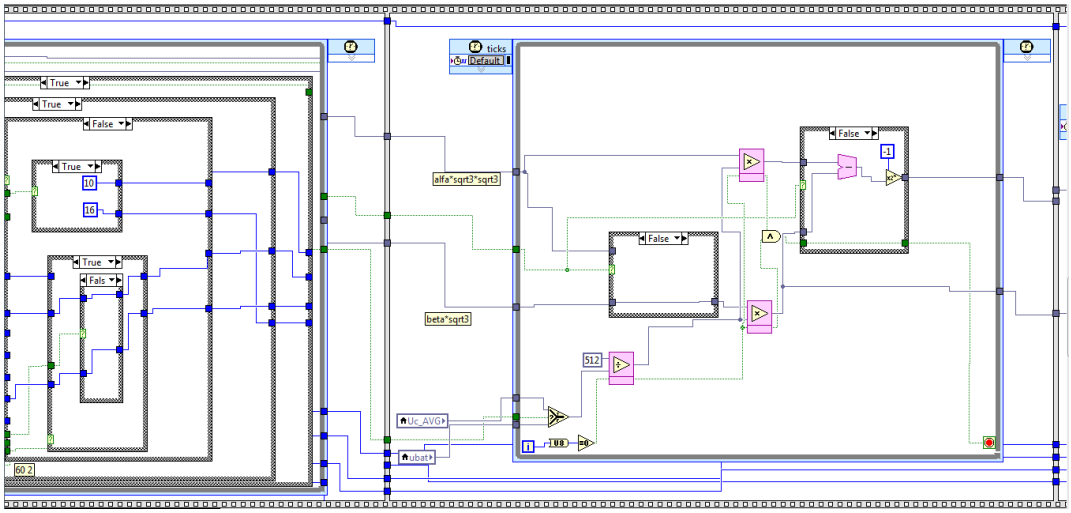
ticks
Default
True
False
alfa*sqrt3*sqrt3
beta*sqrt3
512
Uc_AVG
ubat

H

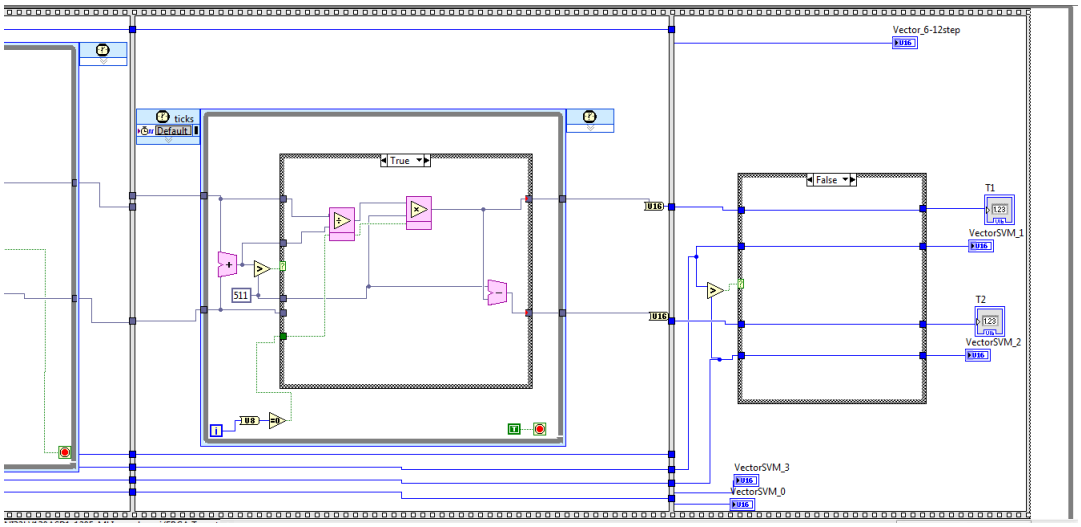
ticks
Default
True
False
511
Vector_6-12step
T1
VectorSVM_1
T2
VectorSVM_2
VectorSVM_3
VectorSVM_0

I

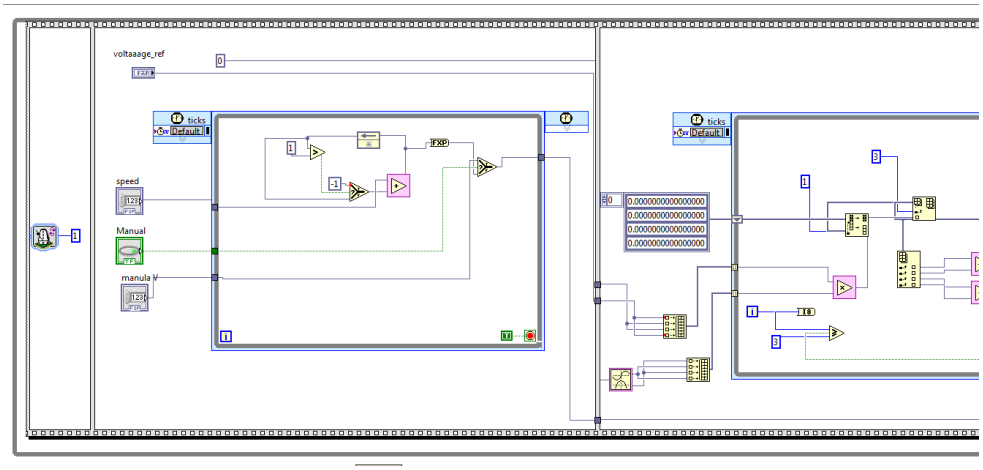
voltaaage_ref
ticks
Default
speed
Manual
manula

J

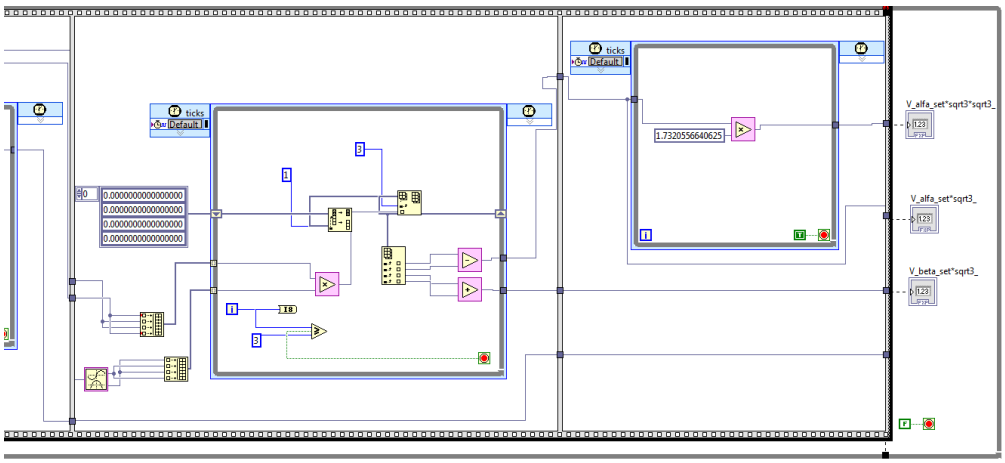

K

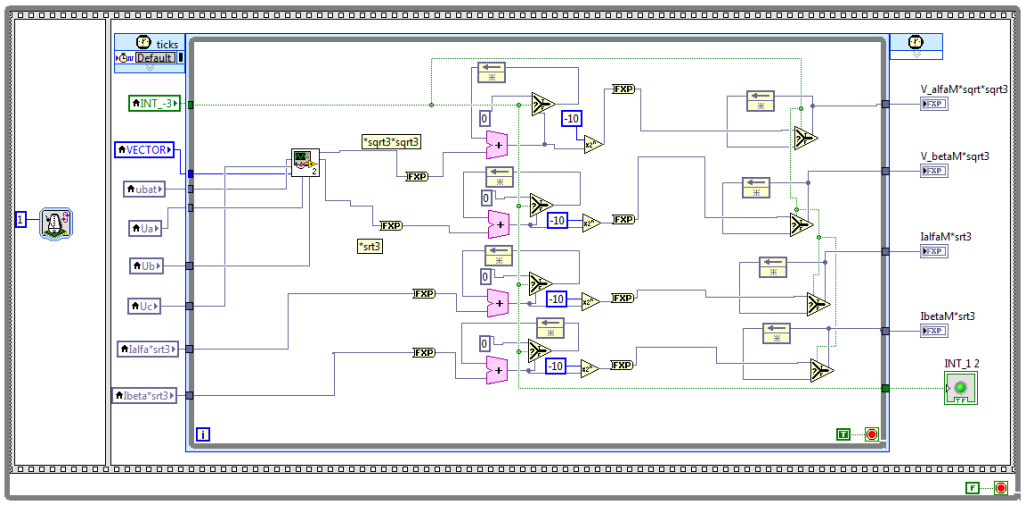

L

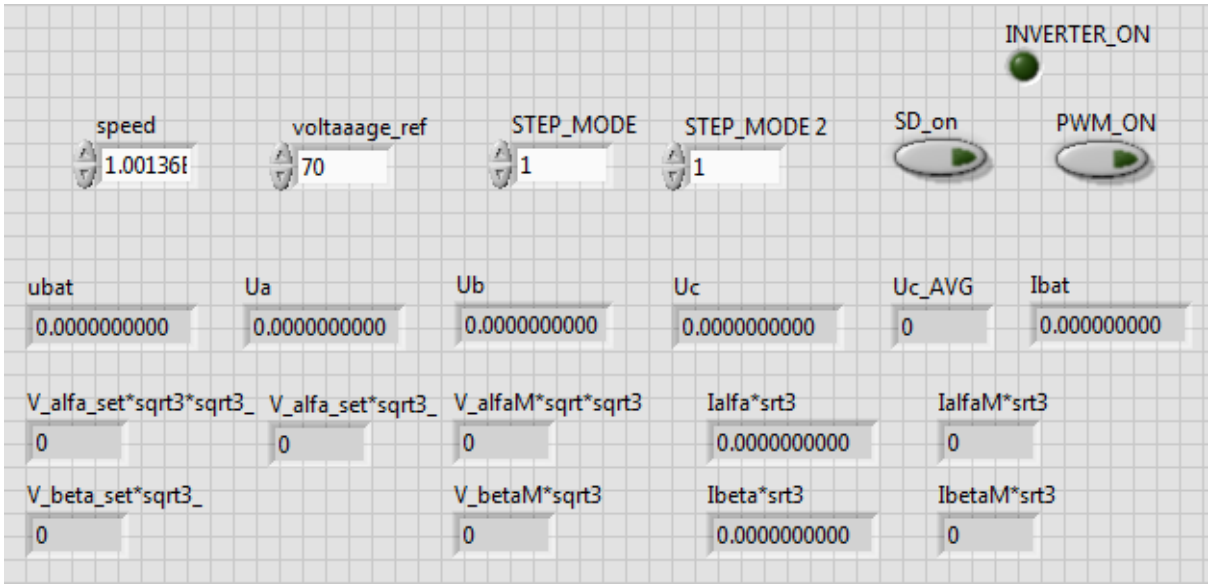

M

Apx_Figure L-2: Lab VIEW print screen programming [Extended design of [353]]